XA9848323 _39

Application of isotope techniques to investigate groundwater pollution

INTERNATIONAL ATOMIC ENERGY AGENCY IAEA

R 29-49

APPLICATION OF ISOTOPE TECHNIQUES
TO INVESTIGATE GROUNDWATER POLLUTION
IAEA, VIENNA, 1998
IAEA-TECDOC-1046
ISSN 1011-4289

FOREWORD

This publication is a compilation of scientific results from the Co-ordinated Research Project (CRP) on the Application of Isotope Techniques to Investigate Groundwater Pollution which was implemented from 1995 to 1997. The conclusions of the CRP were presented during the final Research Co-ordination Meeting held in Vienna from 2 to 5 December 1997 by scientists from the following participating Member States: Austria, Brazil, China, Czech Republic, France, Hungary, India, Israel, Italy, New Zealand, Pakistan, Poland, Senegal and the United Kingdom.

The CRP was initiated during an IAEA consultants meeting conducted in December 1993 on Isotope Techniques in Groundwater Pollution Studies, which identified the major causes of pollution as the concentration of toxic substances, bacteria from sewage, nitrates, pesticides from agricultural practices and radioactive materials from industries, as well as salinization from surface and seawater. The CRP was implemented in recognition of the importance of protecting groundwater resources, and promoting the role of isotope techniques when integrated to classical hydrological methods to identify the sources and mechanisms by which pollution takes place. It consisted of investigations of various field scenarios where different sources of pollution are encountered, prioritizing urban groundwater pollution due to domestic waste and sewage disposal; landfill performance and hazard assessment; as well as seawater intrusion and pollution from agricultural practices.

The results from this CRP are expected to find practical applications in tackling hydrological problems encountered in technical co-operation projects of the IAEA. This publication could also provide a contribution toward the continuing efforts of various sectors to investigate, mitigate and control the threat of groundwater pollution.

The IAEA is grateful to J. Chilton (United Kingdom), B. Robinson (New Zealand) and Y. Travi (France) who reviewed papers for publication. J. Gerardo-Abaya of the Division of Physical and Chemical Sciences, as the Scientific Secretary of the CRP, was responsible for the completion of this TECDOC.

EDITORIAL NOTE

CONTENTS

SUMMARY

The majority of the world's population relies on groundwater for drinking, agricultural or industrial requirements because it is widely available in good quality. However, in recent years, particularly with the advent of industrialization and population growth, the stresses on groundwater resources have increased. Current available water is only half of what it was some 30 years ago, and is projected by World Bank studies to drop by another half in the next 25 years. The problems associated with groundwater availability and deteriorating quality originates from intentional or inadvertent disposal of wastes in the ground. Tracing the source and movement of pollutants in a complex geological environment requires hydrological tools like isotopes.

The Co-ordinated Research Project (CRP) on the Application of Isotope Techniques to Investigate Groundwater Pollution aimed to investigate by isotope techniques various sources of pollution and to develop methodologies to encourage sound scientific input into decision and policy making for water resource utilization. The CRP resulted in the completion of 16 investigations dealing with the more traditional isotopes of ^{18}O, ^2H, ^3H, ^{13}C, ^{14}C as well as with applications of ^{34}S, ^{18}O in SO_4, ^{15}N and B which to some extent were integrated with the classical hydrological tools of investigation.

Isotopes of nitrogen, boron, sulphur and oxygen in dissolved sulphate were used in the CRP to distinguish pollutant sources and pathways. Nitrate-nitrogen and oxygen isotopes in an agricultural area were able to distinguish between fertilizer and waste as sources of pollutants. Several of the studies have indicated how important nitrate isotopes can be in densely populated urban areas, where there is increasing evidence of multiple sources of pollution and nitrate is one of the most widespread pollutants of groundwater.

Sulphate oxygen and sulphur isotopes in river water enable discrimination between natural (geological, sea water, geothermal and volcanic) and anthropogenic sources such as fertilizers.

The systematics of boron isotopes were well described with a good characterization of the isotope signatures of the sources. Because of its high solubility in aqueous solution and lack of effects from evaporation as well as oxidation-reduction reactions, boron can be used as a tracer in groundwater. Concentrations of boron in pristine groundwater are generally low while it is high in contaminant sources such as sea water and domestic waste.

^{131}I has demonstrated the efficiency of radiometric tracers for defining the hydrogeological characteristics and determining the effective velocity of the water during artificial recharge. The information derived from the investigation appears effective to control the evolution of a cone during artificial recharge of the aquifers.

Field studies that included stable and radioactive isotopes have been very useful to evaluate lake water, groundwater relationships and the hydrological dynamics in investigating fluoride contamination.

The component studies of the CRP have therefore broadly confirmed the use of isotope techniques in two main ways:

(a)   improving the understanding of groundwater flow systems; and

(b)   tracing the origin and pathways of a range of groundwater pollutants.

The CRP indicated that the use of isotopic techniques is moving from the realm of academic, research-oriented studies to take a more regular part in improving the understanding of applied groundwater problems. The investigations illustrated several important aspects:

-       Isotopic techniques have been used to confirm the results obtained by hydrochemical and other hydrogeological approaches. For example, they have been able to provide independent confirmation of travel times obtained by conventional modeling.

-       A reasonable conceptual model of the local or regional hydrogeology is a basic requirement prior to isotope interpretations. Where the isotopic results are in conflict with the current conceptual model, the model may have to be revised. This may particularly occur in coastal or inland situations where a correct model of salinity evolution is required for aquifer management purposes.

-       It is advisable not to rely on single isotopes, but to combine several where possible, particularly oxygen with nitrogen and sulphur.

-       It is essential to integrate isotope techniques with conventional hydrochemistry. While sometimes overlooked, trace elements, for example, have an important role to play in an integrated approach to the interpretation of contaminant sources and pathways.

This CRP should be regarded as a stepping stone, considering that the magnitude of groundwater pollution is enormous in global terms. In order to have an impact on the mitigation of groundwater pollution, the need is seen for follow-up by other investigations targeted at specific areas or problems. The magnitude and scope of problems associated with (a) urban waste, both human and industrial; (b) salinity in groundwater; and (c) nitrate in groundwater in both agricultural and urban areas, require well focused studies. While dating recent water is an essential concern in groundwater pollution studies, the IAEA has initiated alternative tools like CFC to replace environmental tritium which has become less useful. Further work is also required on the behaviour of tracers, their adsorption, fractionation and interaction with the rock matrix, as well as their chemical and biological stability.

2

ANALYTICAL DEVELOPMENTS IN THE MEASUREMENTS OF BORON, NITRATE, PHOSPHATE AND SULPHATE ISOTOPES AND CASE EXAMPLES OF DISCRIMINATION OF NITROGEN AND SULPHUR SOURCES IN POLLUTION STUDIES

J. AGGARWAL, D.S. SHEPPARD
Institute of Geological & Nuclear Sciences, Lower Hutt

B.W. ROBINSON
Wairakei Research Centre,
Institute of Geological & Nuclear Sciences, Taupo

New Zealand

Abstract - *Methods are documented for the analysis of B isotopes, O and N isotopes in nitrates. B isotopes can be measured by negative ion thermal ionisation mass spectrometry. Nitrate is recovered from groundwaters by ion exchange and the resulting silver nitrate combusted for stable isotope gas analysis. Oxygen isotope analysis of phosphates can be determined by generating and analysing CO_2 gas from the combustion of silver phosphate produced from aqueous samples. Sulphate in ground and surface waters can be separated and concentrated by ion exchange and precipitated as barium sulphate. This is reacted with graphite to yield CO_2 and CO, the latter being spark discharged to CO_2 and the total CO_2 measured for oxygen isotope analysis. Barium sulphide from this reaction is converted to silver sulphide which is reacted with cuprous oxide to give SO_2 gas for sulphur isotope measurements.*

A case study of the semi-rural Manakau area in New Zealand was conducted to see if nitrate isotopes could be used to detect the source of nitrate contamination (groundwater nitrate <0.5 to 11.3 mg/L NO_3^--N). Nitrogen isotope (+4 to +12‰) coupled with oxygen isotope measurements (+5 to +9‰) demonstrated that the nitrogen is not sourced from fertilisers but from some combination of septic tank and animal waste.

For the case study of sulphate isotope use, sulphur and oxygen isotopic compositions of sulphate in river and lake water from seven major catchments of New Zealand were determined. The isotope analyses have allowed the distinction between natural (geological, geothermal and volcanic) and anthropogenic (fertiliser) sulphur sources.

1.   INTRODUCTION

A study has been initiated using a suite of different isotopes in an attempt to be able to fingerprint and determine the source of contaminants into groundwater systems. Four different isotope systems have been examined, viz. B isotopes, O and N isotopes in nitrates O isotopes in phosphates and O and S isotopes in sulphates. B isotopes have the potential to identify not only seawater in groundwaters, but also boron bearing detergents commonly found in effluents [1]. Studies on phosphates have been used to show the discharge of sewage and fertilisers into groundwaters, [2,3] but no studies have been carried out on the use of O isotopes in phosphates to distinguish between these two sources. A combination of N and O

3

and O isotopes in nitrates have been used in a number of studies to identify sewage and fertiliser components in groundwaters [4,5]. Identification of sewage and fertiliser components in these systems is complicated by fractionation of N isotopes during denitrification processes which increases the $\delta^{15}N$ of the nitrate dissolved in water, as shown by Komor and Anderson [6]. The measurement of the O isotopes in nitrate assists in recognising such processes. Sulphate isotopic compositions may be useful as discriminats of S source except where redox reactions have altered original SO_4 isotopic ratios. In general, sulphur isotopic compositions are relatively robust and retain some information but sulphate oxygen isotopic compositions are often a product of soil zone and other redox processes.

2. ISOTOPIC TECHNIQUES

This study documents the development of appropriate techniques to enable these isotope measurements to be carried out with sufficient precision to identify contaminant sources. Two case examples of discrimination of nitrogen and sulphur sources in pollution studies are also given.

2.1 Boron

Boron concentrations of waters and wastes from a variety of different sources were determined by ICP-MS. In the case of the dairy shed effluent and Eketahuna sewage, samples were filtered through a sand bed, a 10μ filter followed by a 0.45μ filter. Results are shown in Table I.

Table I.   B concentration from different sources.

Sample	B concentration (ppb)
Dairy Shed	120
Eketahuna sewage	<10
Waiwhetu stream	640
Kaiwharawhara stream	47
Well water, Moore and Wilson, Wellington	75
Well water, Petone	25
Well water, Bartholomew, Manawatu	500
Persil Micro	15,000

The data show great variability in B concentrations in groundwaters and this may mask any variations as a consequence of anthropogenic discharges. Sewage from Eketahuna shows no B, and if this is compared to the dairy shed effluent, it may be suggested that cattle are fed with B rich supplements or that the sewage was collected at a time of day when most of the discharge would be water with little anthropogenically derived B.

The Waiwhetu stream from Seaview shows elevated B concentrations and this may reflect the discharge of an anthropogenically rich B source into the stream or the addition of marine B. Cl/B ratios of the stream water are different from those of seawater and even using a mixing model, the waters can not be related. B used to be a common component in detergents with B as high as 3%, however more recent detergent formulations contain significantly less, e.g. Persil Micro 15 ppm, (pers comms Paul Milson, Lever-Rexona). Industrial detergents contain more B than domestic ones, suggesting that the high B in Waiwhetu stream may be industrially sourced. B isotopic analysis of the water may confirm this.

2.2   B Isotope Measurements

A Micromass 30B at Lamont Doherty Earth Observatory (LDEO) in New York was used for the analysis of B isotope ratios by negative ion thermal ionisation mass spectrometry. A month was spent at LDEO developing a suitable technique that would be applicable to a wide range of samples.

<u>Method</u>

Sufficient aqueous sample for 5 ng B is taken and dropped onto a sheet of Parafilm. To this is added $1\mu L$ 1M HCl and $1\mu L$ boron free seawater to improve ionisation [7]. The B free seawater was prepared by passing seawater through a B specific ion exchange resin, which removes B from the water. Re filaments that had been outgassed at 4A at a vacuum better than 1×10^{-7} torr for 30 minutes and allowed to oxidise for at least 2 days were mounted into the mass spectrometer turret. The extraction plate of the turret was cleaned thoroughly with dilute nitric acid followed by methanol and placed on the turret. The filaments were aligned directly with extraction slits of the extraction plate. Samples were loaded onto the centre of the filaments at about 0.1-0.2 μL aliquots until the whole sample had been deposited. An infra-red lamp was used to assist in evaporating the samples to dryness. Once all of the samples had been loaded onto the filaments, the extraction plate was mounted on the turret.

The cold finger on the mass spectrometer was warmed up by the addition of hot water, and the source vented to atmosphere. The old turret was removed and the slit in the lens stack replaced with a clean one. The new turret was installed and the mass spectrometer was pumped down.

Once the vacuum had dropped to a pressure of better than 1×10^{-6} torr, the cold finger was filled with liquid nitrogen. At a vacuum of better than 1×10^{-7} torr, the filaments were heated to 950°C (as observed with an optical pyrometer) over a period of 10 mins and held at that temperature for a further 10 mins. The filament was then allowed to cool before the next filament was run.

After each of the filaments had been run, a period of 10 mins was allowed before the mass spectrometer was vented during which period the cold finger was warmed with hot water. The extraction plate on the turret was replaced with a clean one, as was the slit on the lens stack. The turret was placed back in the mass spectrometer and the instrument pumped down using the procedure described in the previous paragraph.

At a vacuum of better than 5 x 10^{-8} torr, the filaments were heated to 950°C ± 3°C over a period of 10 mins. The HT was switched on and the flight tube opened. Isotope ratios were continually measured until the ratios stopped climbing. At this point 5 ratios were measured to give the data point.

Samples containing substantially more than 5ng of B in 1 µl were diluted with sub-boiling distilled water. Where samples were more dilute than 5ppm, they were concentrated down from a larger volume on a hot plate (<40°C) in a class 100 filtered flow air chamber. Samples with a Si/B (wt/wt) ratio >2 had to be treated with HF. Sufficient sample was taken for 10 ng B and to this was added 2µL of B-free seawater and sufficient HF to digest all of the Si on a 1:1 mole ratio. The mixture was evaporated to dryness at <40°C in a class 100 filtered flow air chamber until the sample had reached dryness. The sample was then taken up in 2µL of sub-boiling distilled water before being loaded directly onto a Re filament.

Problems Encountered in Carrying out the Analyses.

1.   Optimum Filament Running Temperature.

It has been found that there is a very narrow optimal range in temperature in which to run filaments for B isotope analysis. At temperatures above 950°C B isotopes fractionate and no stable ratios are produced. At lower temperatures, the intensity of the ion beam is low resulting in poor data precision.

2.   Interference.

Much of the B literature shows problems with isobaric interference on mass 42($^{10}BO_2$-) by a species most likely to be CNO [8]. It was clearly shown that as the nitrogen cold finger warms up, the $^{11}B/^{10}B$ ratio starts to fall which is consistent with the release of CNO. The cold finger appears to provide a cold surface on which the CNO condenses. It was also found during these experiments that the effects of the CNO interference could be monitored by the examination of CN species at mass 26. An excellent vacuum (better than 5 x 10^{-8} torr) and a liquid nitrogen cold finger are essential to removing the isobaric interference.

3.   Unstable Emission

During many of the runs and analyses that were performed the ion beam emission appeared unstable. It was found that the cause of the instability was the build up of charge on salt that was being deposited on the extraction plate and the slit from the filament itself. This charge build-up resulted in the ion beam being deflected erratically and hence the unstable ratios. Regular cleaning of the extraction plate, slit and the whole lens stack assembly was found to be imperative. In addition, by pre-running each filament for 10 mins at 950°C the salt was evolved and deposited on the extraction plate and slit, which were replaced before data was collected.

6

Results

B isotope measurements were carried out on the Bartholomew (Manawatu) and Petone waters once they had been concentrated down, by evaporation at 40°C, and then loaded with boron free seawater onto outgassed Re filaments. Samples were analysed repeatedly until replicate analyses agreed to within 1 . B isotope ratios are shown relative to NBS 951 which has an $^{11}B/^{10}B$ of 4.0005. The results of the isotope analyses are shown in Table II.

Table II. Boron isotope ratios for groundwaters from New Zealand.
Seawater is shown for comparison.

	B (ppm)	Cl/B	$\delta^{11}B$ (‰)
Bartholomew	0.5	3680	18.9
Petone	0.047	510	11.9
Seawater	4.6	4130	39.5

The Cl/B ratio and the $\delta^{11}B$ of the water from Bartholomew may be interpreted as a consequence of mixing between a saline water and a fresh water. Seawater has a distinctly heavy B isotopic composition, relatively high B concentrations and a high Cl/B ratio, whereas the freshwater contains a variable B isotope ratio with a low B concentration and a much lower Cl/B ratio than the seawater. According to this model, approximately 30% of the B in the Bartholomew groundwater may be derived from a seawater source. Further modification of the groundwater post-mixing must have occurred to account for the B isotope ratio.

Interpretation of the Petone groundwater using the B isotopic data is problematic and can not be explained by a mixing model. Further data are required to allow a more complete interpretation of the B isotope ratios of groundwaters.

2.3   Nitrate Isotopes

There has been continued development of the nitrate isotope facility at the New Zealand Institute of Geological & Nuclear Sciences (GNS) and a number of improvements have been carried out to the technique and to the mass spectrometer. A method has been developed based on that of Silva and Chang [9].

The existing technique has been limited in its suitability for groundwaters as 35mg nitrate are required for an analysis and this effectively limits analysis to samples with a nitrate concentration greater than 3ppm. The sample cold finger has been cut on the Micromass 1202E mass spectrometer, to allow the analysis of smaller samples. Dial gauges have been installed on the mass spectrometer to ensure that the magnet can be moved between the optimum position for N isotopes and S isotopes quickly and reproducibly. Modification of the software for the 1202E, has allowed more automated analyses of samples and improved the precision of the data from the mass spectrometer. For example, 36 analyses of dry N_2 have yielded a $\delta^{15}N$ of 0.99± 0.2‰ .

An ion exchange resin has been employed to concentrate anions in water samples, and through careful elution control, sulphate and nitrate ions have been separated, with complete recovery of nitrate. This has reduced the amount of barium chloride that is required to separate the nitrate ion and should improve the overall precision of the data by reducing the amount of potential contamination from the barium chloride, and reduce the amount of interference that is introduced from sulphate oxygen.

During the course of some mass spectrometric analyses the ratios have been found to increase with time and this has been attributed to the presence of water in the samples. Fresh CaO has been prepared to reduce this potential loading of water, and in future experiments CuO will not be used as this has the potential to add further water.

The technique developed to date for N isotope analysis is as follows:

a) Preparation of Ion exchange columns:
   i)   Condition 2mL anion exchange (AG1 X8 200-400 mesh) columns by pumping 20mL water, 10mL 6M HCl, and 50 mL water at a rate of 1mL/min.
   ii)   Load sample at 1ml/min ensuring that capacity of resin is not exceeded.
   iii)   Elute sulphate by addition of 15mL 0.5M HCl.
   iv)   Collect nitrate by elution of 25mL 1M HCl.

b) Preparation of silver nitrate
   i)   Add silver oxide to sample until sample reaches pH 6
   ii)   Filter mixture through 0.45μ filters.
   iii)   Dry filtrate on a warm plate in a filtered-flow air chamber.

c) Combustion of silver nitrate
   i)   Take 35mg silver nitrate in an oven-dried 6mm quartz tube.
   ii)   Add 0.1g CaO and 1g Cu.
   iii)   Evacuated and seal tube.
   iv)   Place tube in a combustion furnace at 900°C for 1 hour to produce N_2 gas followed by an overnight cooling

d) Mass spectrometry
   i)   Attach sample to mass spectrometer via tube cracker.
   ii)   Cool sample tube in CO_2/ethanol slurry.
   iii)   Crack sample tube when cool and admit sample into mass spectrometer.

The method is continually being modified to suit an increasingly larger range of samples. Samples from Canterbury are currently being prepared for analysis, and these will comprise the first background level nitrate isotope analyses of New Zealand groundwaters.

The technique required for oxygen isotope analysis in nitrates is as follows:

a) Preparation of $AgNO_3$
   i)   take 20% of solution from bii) in nitrogen isotope preparation technique
   ii)   add 0.5mL 0.5M $BaCl_2$ solution and filter off precipitate

iii)	load filtrate onto 2mL of preconditioned AG50-X8 ion exchange resin
iv)	neutralise eluant with 1g Ag_2O and filter
v)	collect filtrate and evaporate down using freeze drier

b) Combustion of $AgNO_3$
i)	take 10mg of $AgNO_3$ into a quartz tube with equal amount of graphite
ii)	evacuate and seal tube
iii)	place tube in combustion furnace at 900°C for 1 hour followed by overnight cooling

c) Purification of combustion gases
i)	attach combustion tube purification line and evacuate
ii)	crack tube and freeze CO_2 in liquid N_2.
iii)	after 5 mins pump away non condensable gases.
iv)	allow CO_2 to warm up and refreeze in liquid N_2 on sample gas bottle.
v)	collect frozen CO_2

d) Analysis
| i) | attach sample tube to NAA mass spectrometer for automated isotope determination |

Analysis of synthetic nitrate samples showed $\delta^{18}O$ of 21.3, 21.8 and 22.2‰ , indicating that the technique is sensitive to variations of about 1 . With the arrival of the new Geo 20/20 mass spectrometer at GNS, much smaller samples for O isotope analysis will be sufficient, and samples should be able to be processed more quickly and with better accuracy.

2.4   Phosphate Isotopes

Oxygen isotope analysis in phosphates has been tried at GNS based on the technique of O'Neil et al [10]. Some modifications to the technique have been carried out, and the technique employed is as follows:

a) Precipitation of silver phosphate
i)	Take 25mg equivalent phosphate sample and mix with 15ml of a buffered silver amine solution.
ii)	Heat sample on a warm plate at ~ 50°C and precipitate yellow $AgPO_4$ crystals
iii)	Collect $AgPO_4$ on a filter paper and dry.

b) Combustion of silver phosphate
i)	Take 30 mg $AgPO_4$ into an oven-dried quartz tube with 0.4mg graphite sheet.
ii)	Place tube in combustion tube and evacuate.
iii)	Raise combustion tube temperature to 1000°C and place over sample.
iv)	Combust sample for 3 mins and purify any gases evolved on line.
v)	Freeze down CO_2 for transfer to mass spectrometer.

c) Analysis
| i) | Introduce sample to NAA for analysis. |

Two synthetic phosphate samples have been analysed for O isotopes and their $\delta^{18}O$ show values of 31.89 and 31.86‰ . This difference in $\delta^{18}O$ is at the limit of precision for the mass spectrometer and shows promise of a reproducible technique. The accuracy of the technique will be tested by the analysis of an international standard (NBS 120c), which has been prepared and awaits analysis.

2.5   Sulphate Isotopes

For sampling rivers, lakes and groundwater, five litre samples are required for the sulfate isotope measurements. Samples are preserved in the field by the addition of 1mL of $HgCl_2$ saturated solution. Where SO_4 concentrations are <20 mgL^{-1} separation and concentration of sulfate by ion exchange is required. For this, HCl - conditioned columns were used packed with 100 mL of wet AG1-X2 resin. The sample was run through a coarse filter paper and then through a 0.45µm membrane filter connected to the ion exchange column. A gravity flow rate of 150-200 mL min^{-1} was used. Samples were eluted with 300 mL of 1 M NaCl at a flow rate of about 1mL min^{-1} and the sulfate precipitated as $BaSO_4$ by addition of $BaCl_2$ solution. The efficiency of the ion exchange process is around 93% and the isotopic compositions remain unaffected within the overall error of the analytical techniques [11]. All the $BaSO_4$ samples were reacted with graphite (ratio1:1) at 1000°C [12] to yield CO_2 and CO; the latter being spark discharged to CO_2 and the total CO_2 measured on a NAA mass spectrometer for $\delta^{18}O_{VSMOW}$ values with a precision of ±0.4‰ for the overall method. BaS from the above reaction was converted to Ag_2S by washing through a 0.45 m filter into acidified $Ag(NO_3)_2$ solution. The Ag_2S was in turn reacted with Cu_2O [13] to give SO_2 gas for $\delta^{34}S_{CDT}$ measurements on a VG Micromass 1202 mass spectrometer with a precision for the whole method of ±0.2‰ . The S isotopic compositions of the major sedimentary and other rock types that have been measured were obtained by treatment with strong Kiba reagent to extract total S which is predominantly in the form of sulphide in most samples [14]. Total sulphur contents were determined gravimetrically from the Ag_2S precipitate with a maximum accuracy of ± 5% for the low sulphur concentrations.

3.   CASE STUDIES

3.1   Nitrate Isotopes: Manakau, New Zealand

A case study has been conducted on groundwaters from Manakau in the Manawatu-Wanganui Regional Council [15] where nitrate concentrations from bores sampling the groundwater, showed a range in concentration from <0.5mg/L to >30 mg/L (three times the allowable nitrate concentration for drinking waters). High nitrate concentrations in groundwaters in New Zealand are less likely than in other countries because the rainfalls are considerably higher allowing significant degrees of dilution of nitrate from an isolated point source.

The geology of the Manakau region is dominated by glacial and interglacial deposits comprising the Otaki sandstones of the last interglacial (80 - 12 kyr), and fluvial gravels of the last interglacial. The unconfined aquifer for Manakau is contained in these sandstones and gravels, and it is bounded laterally by the Tararua Ranges to the east and the Levin Fault to the west. Water flow in the Manakau aquifer is from the foothills of the Tararua range to the coast i.e. east-south-east to west-north-west. Unconformities are likely to exist between

the contacts of the gravels and the sandstones, and these provide controls on the flow paths through the aquifer.

Local streams in the Manakau area showed nitrate concentrations below 1mg/L and the bores showed a random spacial distribution of bores with high nitrate concentrations suggesting no single point source discharge of nitrate, nor a source of high nitrate originating from an upstream source. As a consequence of the high nitrate concentrations from these groundwaters, water from roof collection systems was utilised for domestic use, however these sources became liable to contamination from agricultural sprays.

Potential sources of nitrates in the groundwaters in this semi-rural area, comprise cattle manure, fertilisers and discharges from septic tanks. Manure and fertiliser sources produce diffuse sources of nitrates into groundwater systems, in contrast to that from septic tanks which give rise to point source discharges of nitrates.

Nitrate measurements of the groundwater were unable to distinguish between these different sources. However, as each of these sources has a distinctive nitrogen isotopic signature (see Figure 1), the use of nitrogen isotopes in the nitrates has the potential to identify the source of contamination. Nitrogen isotopes may be fractionated during their transport from source to the groundwater as a consequence of processes such as denitrification, nitrate reduction and volatilization of ammonia. Denitrification leads to the greatest range in nitrogen isotope ratios as a consequence of fractionation.

Nitrogen isotope ratios of groundwaters from Manakau have been measured in an attempt to determine the source of nitrates. The data are shown in Figure 2 (along with data from other New Zealand areas)and show a range in $\delta^{15}N$ from +4 to +12‰. These results overlap between the $\delta^{15}N$ values of both animal and septic tank wastes. Oxygen isotope data indicate that fertilisers can not provide a source of nitrate for the Manakau groundwaters. The combination of both $\delta^{15}N$ and $\delta^{18}O$ data indicate that the signatures observed in the groundwaters are the result of nitrification of ammonia originating from either animal wastes or septic tank wastes, with no significant influence from commercial fertilisers. Land-uses indicate that in Manakau village the source of nitrates are likely to be derived from septic tanks rather than animal wastes, and that where dairying practises occur outside the village the nitrates are likely to be derived from a combination of both animal wastes and septic tank discharges.

3.2   Sulphate Isotopes: New Zealand River Catchments

An analysis of the sulphur and oxygen isotopic compositions and concentrations of dissolved sulfate in river and lake water from seven major catchments of the North and South Islands, New Zealand, allows the distinction between natural (geological, geothermal and volcanic) and anthropogenic sulphur sources [16].

All the isotope data from this area are summarised in Fig. 3 and Fig. 4, where it can be seen in general terms, that most of the river sulfate isotopic compositions result from mixtures of particular end members.   The bedrock-derived sulfate is typified by relatively depleted isotopic compositions and the rain-water, fertilizer and crater lake sulfate by relatively enriched isotopic compositions. In particular the pristine rivers, such as the Buller
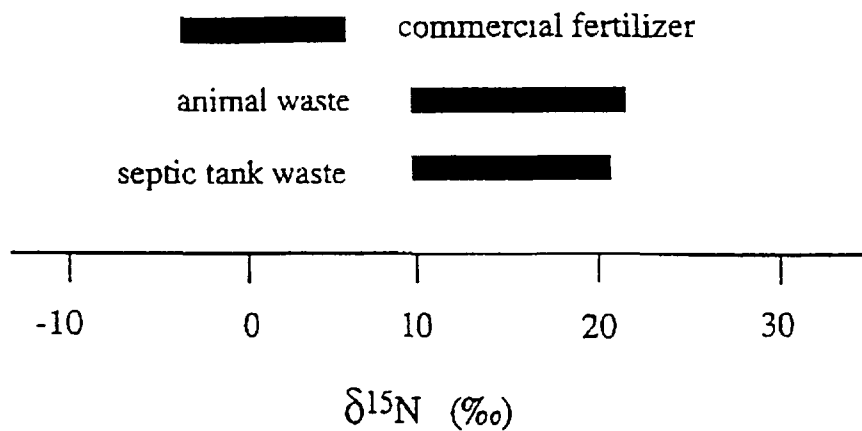
Figure 1   Range of $\delta^{15}N$ values for the major sources of nitrates into groundwaters, data from Wassenaar [5].
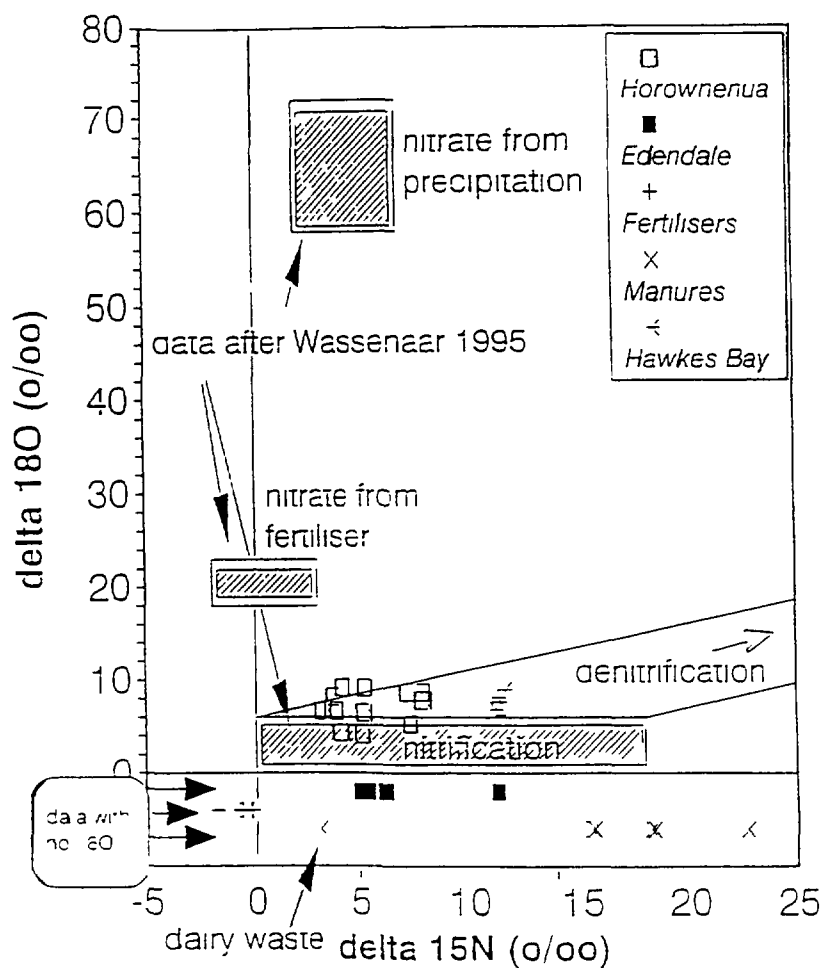
Figure 2:   Measured nitrate isotope compositions from New Zealand groundwaters from a Canterbury Regional Council report. The Horowhenua samples are shown as unshaded squares.

12
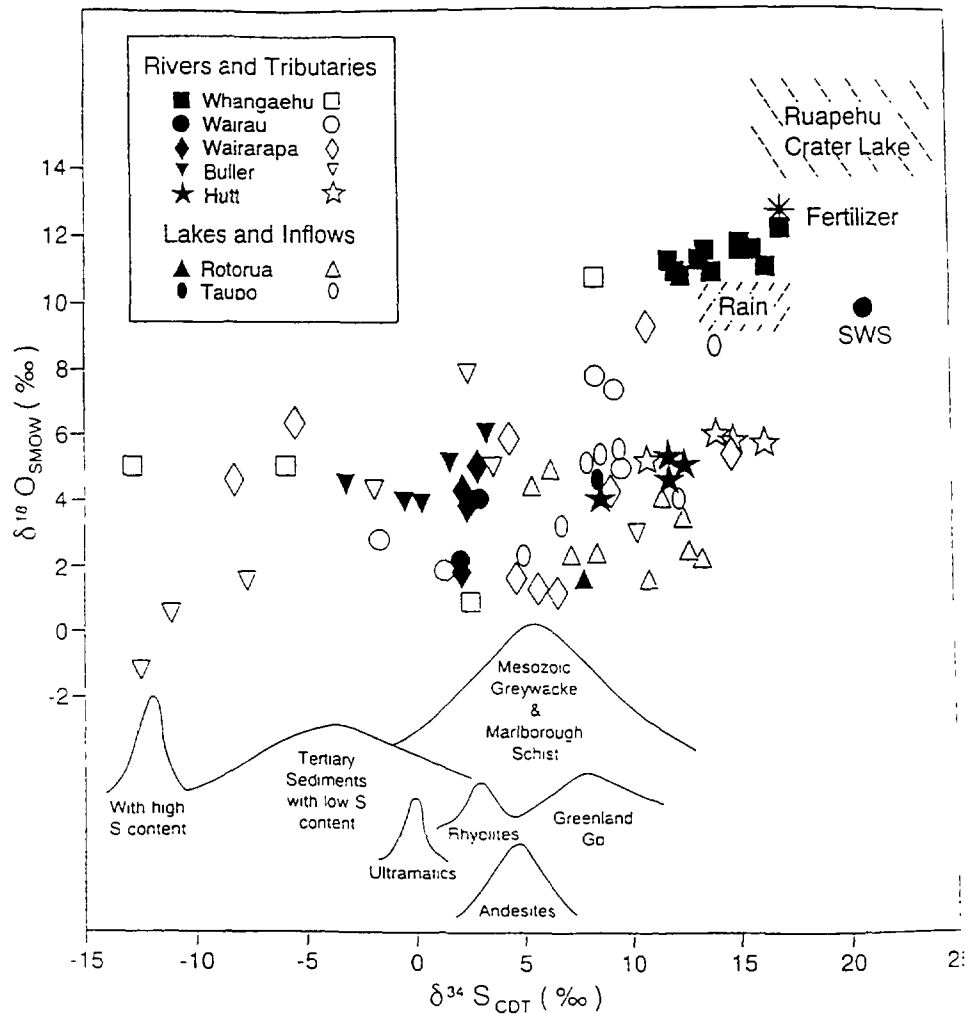
Figure 3:   New Zealand river and lake samples and main sulphur sources plotted as δ^{34}S vs δ^{18}O. SWS is sea water sulphate.
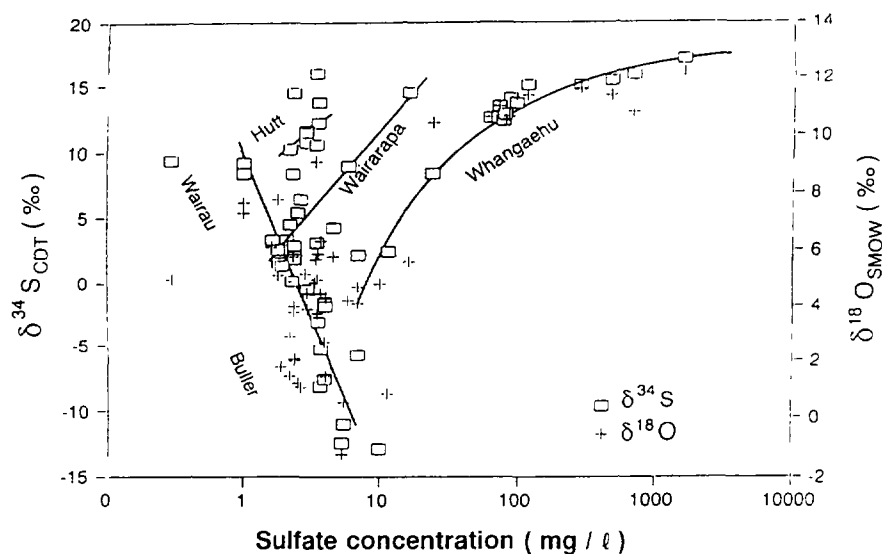
Figures 4:   New Zealand river water sulphate samples plotted as sulphate concentration vs isotopic composition. The main rivers are named.

and the Wairau, show relatively simple two end member mixing of rock - derived sulfate with rain-water sulfate. In these cases trends are also present on a plot of sulfate concentration versus isotopic composition (Fig. 4). The sedimentary rocks contribute sulfate in relatively high concentrations with $\delta^{34}S$ and $\delta^{18}O$ depleted isotope compositions (presumably through pyrite oxidation), which mixes with rainwater derived sulfate of low concentration and relatively enriched isotopic compositions. The Hutt River also demonstrates a simple mixing model shown in Fig. 3 but gives a trend with an opposite slope to the Wairau and Buller Rivers in Fig. 4. This is explained by the sulfate contribution from rainwater being greater (proximity to the sea) and the bedrock greywacke yielding less sulphur. Overall, the geologic inputs (see Fig. 3) have a relatively wide range of sulphur isotopic compositions from about +10 to -15‰, whereas their oxygen isotope range is much narrower (0 to +5‰) since sulfate is produced by broadly similar reactions in each case.

Natural geothermal and volcanic inputs of sulfate can be detected by their isotopic compositions and their concentrations. The Ruapehu Crater lake sulfate isotopic signature dominates the Whangaehu River (Fig. 3 and Fig. 4). Downstream, tributaries have a diluting effect supplying sulfate derived by oxidation of pyrite in the Tertiary sediments. Geothermally derived sulfate does not show up so clearly in the rivers flowing into and out of Lake Taupo. However it is clearly distinguishable in some of the Lake Rotorua and Lake Taupo inputs and particularly the outflow of Lake Rotorua which shows a major contribution from a geothermal source.

Anthropogenic sulphur inputs to the river systems have been identified mainly in the Wairarapa catchment. A combination of isotopic signatures, sulfate concentration and sulfate/sulfate+chloride ratios is required to distinguish the fertilizer source from rainwater sulfate. In the case of the Wairarapa, trends are apparent both in Fig. 3 and Fig. 4, whereby as sulfate concentration increases the sulphur and oxygen isotopic compositions become relatively enriched. Furthermore, if a baseline value is derived from the isotopic composition of "bedrock plus rainwater" for a particular rock type then, given the isotopic composition for fertilizer sulfate, the offset due to fertilizer loading in a river can be calculated. For the Ruamahanga River in the Wairarapa such a graphical offset suggests that about 20 ±5% of the sulfate in the river was derived from fertilizers. The amount of fertilizer sulfate lost to the river represents about 18% of the sulfate applied to the area as superphosphate and is much higher than figures for phosphorus loss.

4.   SUMMARY

Progress has been made to allow the determination of B isotopes, O and N isotopes in nitrates, O isotopes in phosphates and S and O isotopes in sulphates. Further work is required to ensure that the techniques are robust enough to produce data of sufficient precision accuracy. Using the current techniques it is possible in particular to use nitrogen oxygen and sulphur isotopes to discriminate between different sources of anthropogenic contamination into ground and surface water systems.

14

REFERENCES

[1] BARTH, S., HEMMING, N.G., HANSON, G.N. and GERCKEN, B. Tracing groundwater pollution by boron isotope systematics. Science (in press).

[2] LANCE, J.C., Phosphate removal from sewage water by soil columns. Journal of Environment Quality, 6, 279-284 (1977).

[3] HILL, D.E. AND SAWHNEY, B.L., Removal of phosphorus from waste water by soil under aerobic anaerobic conditions. Journal of environment quality, 10, (1981) 401-405.

[4] ARAVENA, R., EVANS, M.L. and CHERRY, J.A., Stable isotopes of oxygen and nitrogen in source identification of nitrate from septic systems. Groundwater 31, (1993) 180-186.

[5] WASSENAAR, L.I., Evaluation of the origin and fate of nitrate in the Abbotsford Aquifer using the isotopes of ^{15}N and ^{18}O in NO3-. Applied geochemistry, 10, (1995) 391-405.

[6] KOMOR, S.C. and ANDERSON, H.W., Nitrogen isotopes as indicators of nitrate sources in Minnesota sand-plain aquifers. Groundwater, 31, (1993) 260-270.

[7] AGGARWAL, J.K., PALMER, M.R., GIGGENBACH, W.F., ARNORSSON, S., GUNLAUGSSON, E.,RAGNARSDOTTIR, K.V. and KRISTMANNSDOTTIR, H., The Boron Isotope Systematics of Icelandic hydrothermal Systems (in prep).

[8 HEMMING, N.G. and HANSON, G.N., A procedure for the isotopic analysis of boron by negative thermal ionisation mass spectrometry. Chemical Geology, 114, (1004) 147-156.

[9 SILVA, R.R. and CHANG, C., Preliminary version on resin-column nitrate technique for $\delta^{15}N$ and $\delta^{18}O$ analysis (in press).

[10] O'NEIL, J.R., ROE, L.J., REINHARD, E., BLAKE, R.E., A rapid and precise method of oxygen isotope analysis of biogenic phosphate. Isr.J. Earth Sci., 43, (1994) 203-212.

[11] BOTTRELL, S.H., ROBINSON, B.W., NEWTON, R.S and LAMB, H. Isotopic analysis of low concentrations of sulfate and bicarbonate in glacial meltwaters. Chemical Geology (Isotope Geoscience section) submitted.

[12] RAFTER T.A. Sulfur isotopic variations in nature. Part 2 - A quantitative study of the reduction of barium sulfate by graphite for recovery of sulfide-sulfur for sulfur isotopic measurements. New Zealand J. Sci. and Tech. 38, (1957) 955-968.

[13] ROBINSON B.W. and KUSAKABE M. Quantitative preparation of sulfur dioxide, for $^{34}S/^{32}S$ analyses from sulfides by combustion with cuprous oxide. Anal. Chem.47, (1975) 1179-1181.

[14] ROBINSON B.W. and GRAHAM I.J. The sulfur isotopic composition of mafic - intermediate volcanic rocks, Taupo volcanic zone, New Zealand. In Water- Rock Interaction (eds Kharaka and Maest) Balkema, Rotterdam (1992) 975-978.

[15] MCLARIN, W.R., The groundwaters system and nitrate contamination of the unconfined aquifer, Manakau, Horowhenua. Unpublished MSc thesis, Victoria University, Wellington (1996).

[16] ROBINSON B.W. and BOTTRELL S.H., Discrimination of sulfur sources in pristine and polluted New Zealand river catchments using stable isotopes, Applied Geochem 12 (1997) 305-319.

GROUND-WATER POLLUTION DETERMINED BY
BORON ISOTOPE SYSTEMATICS

A. VENGOSH
Research Department, Hydrological Service,
Jerusalem, Israel

Y. KOLODNY
Institute of Earth Sciences, Hebrew University, Giva't Ram,
Jerusalem, Israel

A.J. SPIVACK
Center for Marine Sciences,
University of North Carolina at Wilmington,
Wilmington, United States of America

Abstract-*Boron isotopic systematics as related to ground-water pollution is reviewed. We report isotopic results of contaminated ground water from the coastal aquifers of the Mediterranean in Israel, Cornia River in north-western Italy, and Salinas Valley, California. In addition, the B isotopic composition of synthetic B compounds used for detergents and fertilizers was investigated. Isotopic analyses were carried out by negative thermal ionization mass spectrometry.*

The investigated ground water revealed different contamination sources; underlying saline water of a marine origin in saline plumes in the Mediterranean coastal aquifer of Israel ($\delta^{11}B=31.7\text{‰}$ to 49.9‰, B/Cl ratio~$1.5x10^{-3}$), mixing of fresh and sea water (25‰ to 38‰, B/Cl~$7x10^{-3}$) in saline water associated with salt-water intrusion to Salinas Valley, California, and a hydrothermal contribution (high B/Cl of ~0.03, $\delta^{11}B=2.4\text{‰}$ to 9.3‰) in ground water from Cornia River, Italy. The $\delta^{11}B$ values of synthetic Na-borate products (-0.4‰ to 7.5‰) overlap with those of natural Na-borate minerals (-0.9‰ to 10.2‰). In contrast, the $\delta^{11}B$ values of synthetic Ca-borate and Na/Ca borate products are significantly lower (-15‰ to -12.1‰) and overlap with those of the natural Ca-borate minerals. We suggest that the original isotopic signature of the natural borate minerals is not modified during the manufacturing process of the synthetic products, and it is controlled by the crystal chemistry of borate minerals.

The B concentrations in pristine ground-waters are generally low (<0.05 mg/l) while contaminant sources (e.g., domestic waste water) are enriched in boron; hence boron isotopes can be used to evaluate the impact of anthropogenic boron on the environment. Moreover, the isotopic composition of contaminated ground-water can reveal the sources of pollution since different sources are characterized by distinguishable isotopic ratios. Sea water ($\delta^{11}B$ =39‰), salt-water intrusion and marine-derived brines (40‰ to 60‰) are sharply different from hydrothermal fluids ($\delta^{11}B=-10\text{‰}$ to 10‰) and anthropogenic sources (sewage effluent: $\delta^{11}B$ =0‰ to 10‰; boron-fertilizer: $\delta^{11}B$ =-15‰ to 7‰). Some differences (up to 15‰) may exist between domestic waste water and boron-fertilizer.

1. INTRODUCTION

Boron is biologically an essential element but is toxic to many plants at high concentrations (> 1ppm). Thus many crops (e.g., orange, lemon, apple) are sensitive to high B levels in irrigation water. High boron levels in drinking water can be also toxic to humans, affecting fertility and pregnancy [1]. The World Health Organization [2] guideline value for boron is 0.3 mg/l and has been considered as the drinking-water standard of the European Community. Nevertheless, in many water resources worldwide, boron concentrations in ground- and surface water exceed this value rendering such water unacceptable according to the European standards. Hence, there is a need for understanding the sources, sinks and mobility of boron in ground-water. Boron can also be used diagnostically in delineating sources of dissolved material and water flow in aquifer systems.

In addition to concentration determinations, boron isotope analyses have been increasingly used in hydrogeological studies during the last decade. This growth has resulted from the recognition of large variations in the natural isotopic composition of boron (at least 90‰), and the development and refinement of mass spectrometric techniques [e.g., 3-7]. The wide range in isotopic composition of the boron sources in water resources, both natural (e.g., sea water, fossil brines, hydrothermal fluids) and anthropogenic (sewage effluents, boron fertilizers, fly ash leachate, landfills effluents), as well as the reactivity of boron with the aquifer matrix make boron a useful natural isotopic tracer for delineating sources of pollution in ground-water systems.

In the present paper, the basic concepts of boron isotopes and analytical techniques are reviewed. The results of the boron isotopic composition of anthropogenic boron and contaminated ground water from different coastal aquifers from Israel, Italy, and California, USA are presented and discussed.

2. BASIC CONCEPTS OF BORON ISOTOPE SYSTEMATICS

Natural boron has two stable isotopes, ^{11}B and ^{10}B which occur in a natural abundance ratio of approximately 4. Variation in the ratio of the two isotopes is expressed in the $\delta^{11}B$ notation, defined as:

$$\delta^{11}B = [\ (^{11}B/^{10}B)_{sample}/(^{11}B/^{10}B)_{NBS \ 951} - 1 \ ] \times 1000.$$

where the SRM-NBS 951 boric acid serves as a standard.

Boron is present in aqueous solutions as $B(OH)_4^-$ ion, undissociated boric acid $B(OH)_3^0$, polyborate ions and borates $[(Na-Ca-Mg)B(OH)_4^+]$. The distribution of these species is controlled by the pH, salinity and specific cation concentrations.

The isotopic fractionation of boron is due to the differences in the interatomic boron/oxygen vibrational energy and symmetry differences between the trigonal boron species (undissociated boric acid $B(OH)_3$) and the tetrahedral anions $(B(OH)_4^-)$. ^{11}B is preferentially partitioned into $B(OH)_3$ (the dominant dissolved boron species at normal pH), while ^{10}B is preferentially incorporated into the $B(OH)_4^-$ which enters the solid phase. The isotopic fractionation factor between the two aqueous boron species at 25°C was estimated as 0.981 [8]. As a result, the large (~90‰) isotopic variation which is recognized in natural reservoirs

18

(see in Fig. 1) makes boron isotopic ratios a potential candidate for tracing the origin of dissolved salts in ground waters.

Previous studies have emphasized the differences between two distinct end-members: (1) marine-derived sources with high $\delta^{11}B$ values (e.g., sea water = 39‰; Dead Sea = 57‰; [9]); and (2) rock-derived sources with relatively low $\delta^{11}B$ values (e.g., Sea of Galilee, $\delta^{11}B$ =24‰, [10]; salt lakes from Qaidam Basin, China, $\delta^{11}B$ = -1‰ to 12‰; [11]).
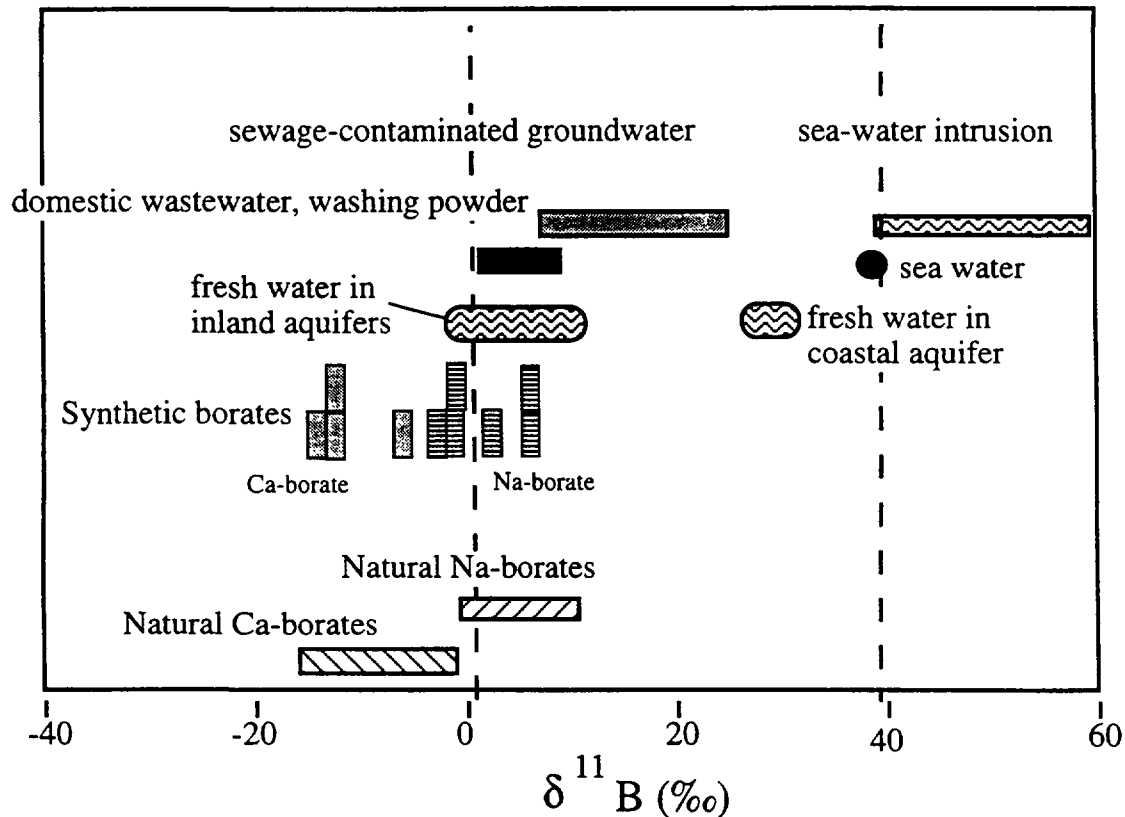
Fig. 1. $\delta^{11}B$ values and range. Note the large difference between sea water and fresh ground water; also ^{11}B depletion in Ca-borate versus Na-borate. Industrial products mimic the isotopic composition of their parent raw materials.

Boron in the atmosphere exists in gaseous and particulate forms. The gaseous boron makes up 97% of total boron in the troposphere. It has been argued [12] that boron in the atmosphere is mainly derived from sea-salt degassing and fumarole gases with a boron residence time of approximately one month. A large isotopic variation is expected in the atmosphere since the isotopic compositions of the source materials are different: the ocean has $\delta^{11}B$ =39‰, volcanic gases boron with $\delta^{11}B$ = 1.5 to 6.5‰ [13], and boron leached from clay particles with $\delta^{11}B$ = -6.6‰ to 15‰ [14, 15]. Indeed such a variability is reflected in a wide range of $\delta^{11}B$ values (0.8 to 35 ‰) reported by Spivack [16] in 4 rainwater samples over the Pacific Ocean. Recently, Eisenhut and Heumann [17] reported a B content of 2.3 mg/l and $\delta^{11}B$ value of 13.1‰ for rainwater from Germany.

The behavior of boron isotopes in the unsaturated zone has been evaluated only partially. Vengosh et al. [18] have shown that adsorption onto clay minerals during the migration of fluids through the vadose zone (calcareous sandstone of the coastal aquifer of

Israel) may modify the original composition of the solution towards higher $\delta^{11}B$ values and lower B/Cl ratios (preferential adsorption of ^{10}B).

The $\delta^{11}B$ values of low-B fresh groundwater (<0.1 mg/l) is determined by a mixture of leached boron derived from the host aquifer rocks (usually with low $\delta^{11}B$) and boron supplied from marine aerosols with a high $\delta^{11}B$. In coastal zones the weight of the marine end-member will be larger, whereas further inland, the low $\delta^{11}B$ fraction becomes more important. Thus, uncontaminated groundwater from the coast of Israel yielded a narrow range of $\delta^{11}B$ of ~30‰ [18], reflecting clearly a marine influence. In contrast, fresh water lakes in the Alps show relatively low $\delta^{11}B$ values (0.9‰ to 6.2‰; [19]) as do ground waters from the Great Artesian Basin in Australia ($\delta^{11}B$ = -16‰ to 2‰; [20]).

3.   ANALYTICAL TECHNIQUES

Boron concentrations in ground water can be determined spectrophotometrically using the reagent Azomethine-H [21].   ICP, atomic emission spectroscopy, ICP-MS [22], and isotope-dilution mass spectrometry were also used for B determination [3,4, 6]. The sensitivity of the two later techniques is significantly higher (a detection limit of ~0.05 mg/l in spectrophotometric technique versus a few ng/l in ICP-MS).

McMullen et al [23] developed a thermal ionization mass spectrometric technique in which $Na_2BO_2^+$ ions were detected (in the mass ratio of 89/88 for $^{11}B/^{10}B$) using a solid-source mass spectrometer. This technique was successfully applied in numerous studies [e.g. 8, 24 ,25]) with a precision of ~2‰. Spivack and Edmond [5] refined this method by substitution of ^{133}Cs for ^{23}Na and producing $Cs_2BO_2^+$ ions which significantly improved the precision to ~0.3‰. Alternatively, the thermal ionization mass spectrometer has been used, in which BO2- negative ions (a mass ratio of 43/42) are measured in a reverse polarity solid-source mass spectrometer, The negative thermal ionization technique is highly sensitive (i.e., a few ng of B sample versus mg B in positive thermal ionization), independent of chemical purity, enables direct loading without B separation amd has a precision of ~2‰ [3,4,6,7,19]. Several attempts have been made to measure the B isotopic ratios by ICP-MS [22], but the poor reproducibility, matrix effects, and low precision (4-7‰), makes this technique only useful for reconnaissance studies.

The separation of B for isotopic analyses has been carried out by using a boron-selective resin, Amberlite IRA-743 [7, 21]. Alternatively, boron can be separated by a standard anionic-exchange resin which reduces possible contributions of impurities [5]. Vengosh et al., [6] have shown that some geological materials (sea water, brines, saline ground water, carbonates) can be loaded directly onto a mass spectrometer filament without chemical separation and analyzed by negative thermal ionization mass spectrometry.

The data presented in this paper were analyzed by negative thermal ionization mass spectrometry. Groundwater samples were separated by B-specific resin, mixed with salts ($MgCl_2$ and $Ba(OH)_2$, or B-free seawater, i.e., seawater from which all the B was removed in a B-specific column) to enhance ionization, loaded onto Re single filaments, and measured by a reverse polarity Finnigan MAT-261 mass spectrometer Germany at the laboratory of Professor Heumann, University of Regensburg, [7,18,19]. Some samples from the coastal aquifer of Israel were measured in a VG-331 mass spectrometer at University of North Carolina at Wilmington, NC. Borate compounds and groundwater samples from California

were measured by a NBS solid-source mass spectrometer at the University of California, Santa Cruz. The mode of filament loading and mass spectrometry procedures were strictly repeated with samples and NBS-SRM standards in order to minimize the variability of mass spectrometer induced isotopic discrimination. A standard deviation of less than 2‰ was determined by NIST SRM-951 and seawater replicates.The mean of the absolute $^{11}B/^{10}B$ ratios of NIST SRM-951 replicates, analyzed along with the samples was 3.9935 ± 0.008 at Regensburg, 4.015 ± 0.005 at Wilmington, and 4.013 ± 0.003 at Santa Cruz.

4.   RESULTS

Contaminated ground water from three different coastal aquifers in Israel, Italy and California have been investigated for their boron isotopic variations. In addition borate compounds that are used for different industrial applications were analyzed for their B isotopic ratios.

Israel:

Salinization of ground water is the main contamination feature of the Mediterranean Coastal Plain aquifer of Israel (Fig. 2). Over-exploitation (up to $450x10^6$ m^3 a year) beyond the natural replenishment ($\sim340x10^6$ m^3) had caused a continual drop in piezometric levels between the 1950's to mid-1980's and formation of deep hydrologic depressions, associated with increases in salinity. Since the middle of the 1980's pumping rates have been reduced and water levels have consequently increased. Nevertheless, salinity continues to increase despite the restoration of the water levels. Saline plumes have developed in the central parts of the aquifer (e.g., Be'er Toviyya; [26]) and in its eastern margins (e.g., Revadim; Fig. 2). The investigated brackish ground water from saline plumes in the inner parts of the aquifer yielded Cl variations of 200 mg/l to 1400 mg/l, B content of 0.1 to 0.7, and $\delta^{11}B$ values in the range of 25‰ to 50‰ (Table 1). The brackish waters are also characterized by high Ca, low Na/Cl (lower than sea water values), marine Br/Cl and SO_4/Cl ratios [19].

Italy:

The quality of ground water in the coastal aquifer of Cornia River (Fig. 3) in north-western Italy has been degraded due to increase in salinity (in some locations >1000 mg/l) and high boron levels. D'Avino and Spandre [27] reported high concentrations of boron (up to 8 mg/l) which exceed irrigation water standards and WHO guidelines. The brackish water are enriched in Ca, Mg, K, and B and depleted in Na relative to sea water, with slightly higher Br/Cl ratios ($2x10^{-3}$ relative to $1.5x10^{-3}$ in sea water). The investigated samples yielded Cl concentrations between 38 to 687 mg/l, boron from 1.3 to 5.35 mg/l, and $\delta^{11}B$ values of -2.4‰ to 9.3‰ (Table 2).

California:

The Salinas Valley, California, is one of the largest coastal agricultural centers in the U.S. It is the headwaters of one of the nation's largest submarine canyons beneath Monterey Bay. This combination presents severe challenges for sustainable agriculture because both anthropogenic effects of cultivation and seawater intrusion through submarine canyon walls have degraded the quality of regional groundwater on which agriculture depends. Extensive water withdrawal associated with the developed agriculture of the north-west of the Salinas Valley (Fig. 3), has caused a significant drop in piezometric levels and intrusion of salt-water into the 180' and 400' aquifer systems. Early signs of salinization were recorded already
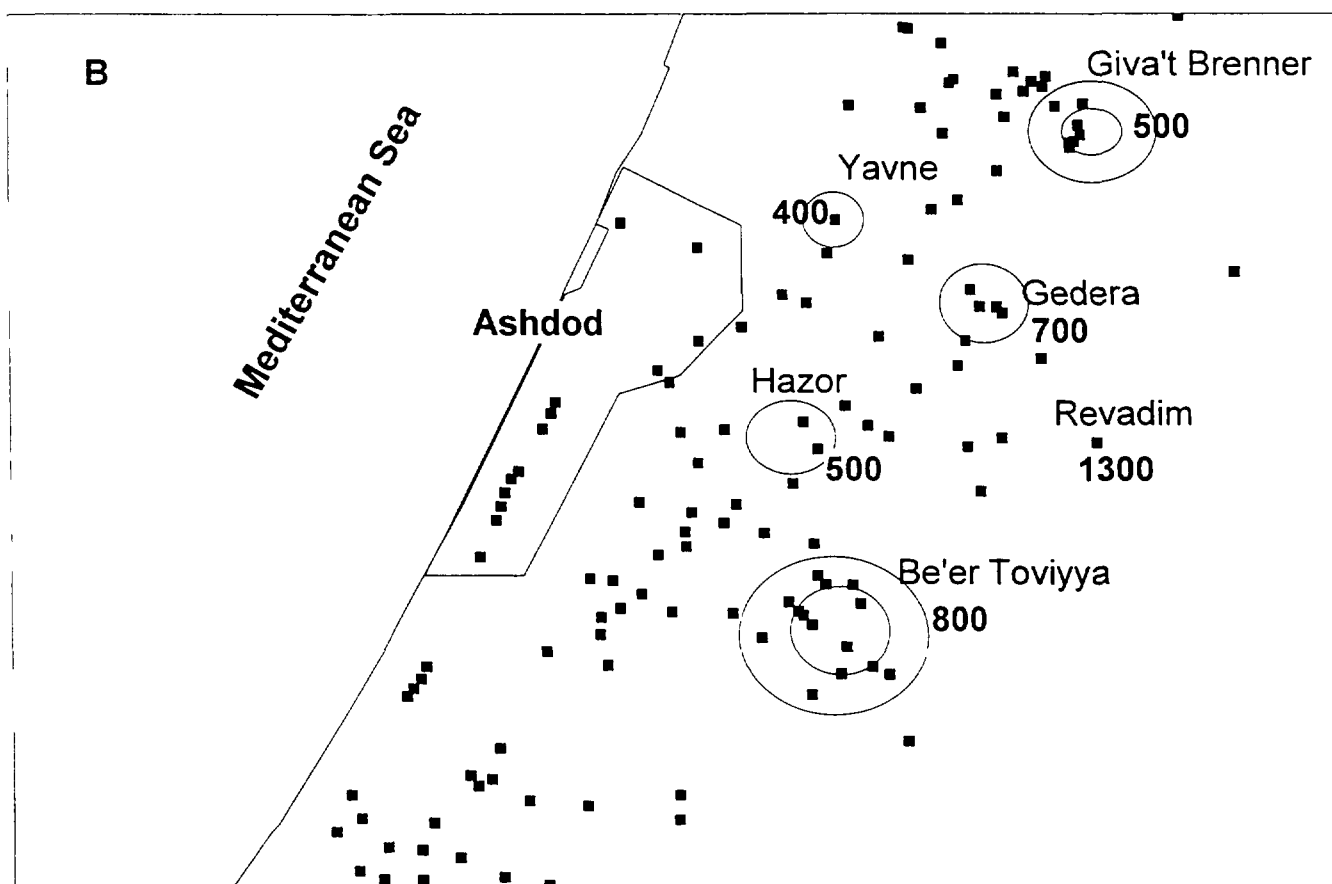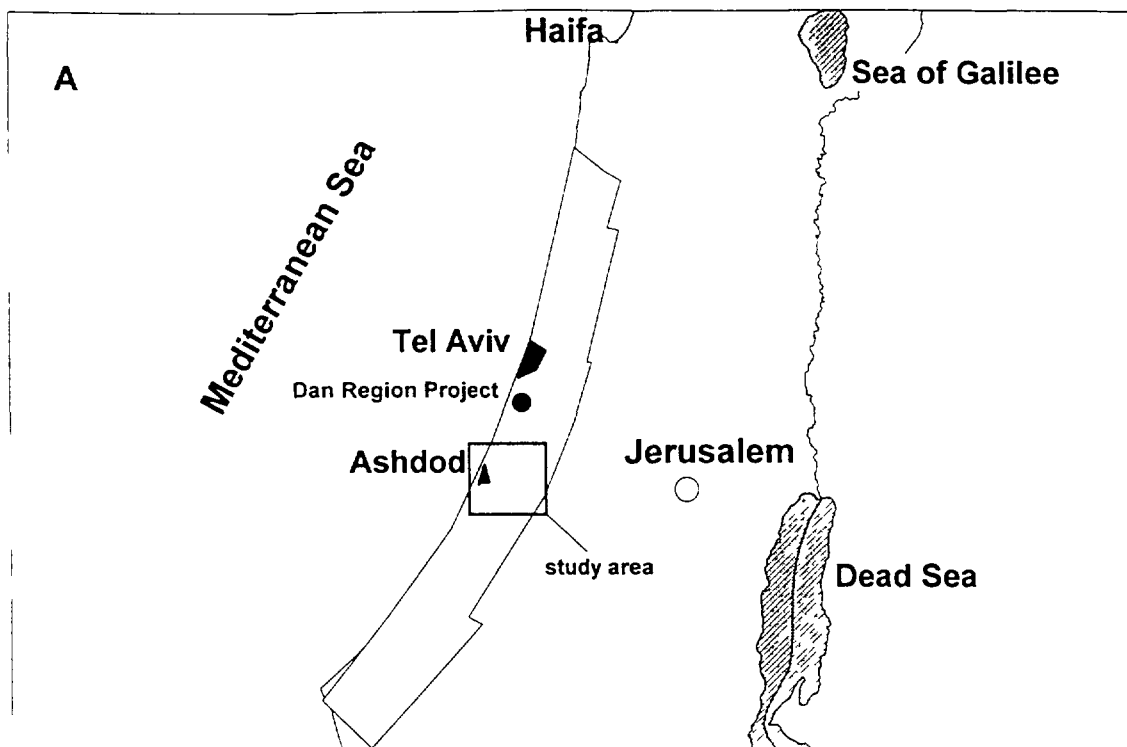
21

Fig. 2. General map of the Mediterranean coastal aquifer of Israel (A) and the study area in its central part (B). The squares in map B are the locations of the wells. The main saline plumes are marked with circles with the highest Cl concentrations (for 1995).

Table 1: Boron isotopic results of brackish ground water from the Coastal aquifer of Israel. $\delta^{11}B$ values are reported in ‰, chloride and boron in mg/l, and B/Cl ratios are molar.

WELL	I.D.	B #	Date	$\delta^{11}B$ (‰)	B	Cl	B/Cl (x10⁻³)	MS *
Be'er Toviyya saline plume								
Kefar Varburg A	12512401	120	12/7/92	45.6	0.26	457	1.88	
Be'er Toviyya 5	12612402	32	13/7/92	46.2	0.18	404	1.48	
Be'er Toviyya 3	12612403	31	13/7/92	47.6	0.26	715	1.17	
Be'er Toviyya 6		202	1/7/93	49.9	0.32	711	1.48	
Be'er Toviyya 7		203	1/7/93	40.3	0.24	544	1.45	
Kefar Varburg D		204	1/7/93	41.4	0.14	257	1.80	
Central saline plumes								
Hazor kibbutz B	13112301	119	20/7/92	32.6	0.20	303	2.13	
Hazor Kibbutz A	13212302	118	19/7/92	31.7	0.16	508	1.03	
Hazor Kibbutz A	13212302	344	1/8/95	35.3	0.29	489	1.94	*
Hazav 1	13312602	117	16/8/92	34.9	0.20	333	2.01	
Ashdod 5	12711701	94	16/7/92	31.9	0.10	410	7.60	
Ashdod 6	12811902	21	16/7/92	33.7	0.33	325	3.33	
Ashdod 2	12911801	20	16/7/92	37.5	0.39	345	3.71	
Ashdod 10	13012001	22	16/7/92	36.6	0.42	333	4.14	
Yavne 13	13712401	91	1/7/92	30.2	0.12	135	2.94	
Yavne 10	13712601	90	1/7/92	34.4	0.20	221	2.94	
Yavne 2	13812401	88	1/7/92	32.9	0.11	405	8.91	
Yavne 3	13812701	89	1/7/92	34.6	0.17	363	1.54	
Yavne 3	13812701	356	1/8/95	43.6	0.16	407	1.29	*
Yavne c	13512203	46	1/7/92	35.6	0.18	221	2.64	
Yavne A	13512301	47	1/7/92	32.9	0.21	227	2.96	
G.Brenner Siman Tov	14013102	6	17/7/92	38.3	0.19	343	1.77	
Giva't Brenner Berkovitz	14213001	11	17/7/92	48.4	0.12	405	0.96	
Giva't Brenner Levinson	14013104	7	17/7/92	28.8	0.19	412	1.52	
G. Brenner Levinson	14013104	353	18/10/95	37.2	0.18	414	1.43	*
Giva't Brenner A	14113103	9	17/7/92	29.6	0.13	328	1.25	
G. Brenner M	14113104	10	17/7/92	24.8	0.14	218	2.05	
Kevuzat Shiler C	14213002	8	17/7/92	48.5	0.10	251	1.35	
Kevuzat Shiler B	14112902	12	17/7/92	44.9	0.13	258	1.67	
Gedera Moa'za	13512901	205	24/5/93	35.1	0.25	463	1.77	
Gedera Moa'za	13512901	208	23/5/93	35.1	0.24	471	1.67	
Gedera Moa'za	13512901	350	31/8/95	39.9	0.20	479	1.37	*
Gedera Gan Mordechai	13512902	207	23/5/93	43.2	0.28	731	1.26	
Gedera Gan Mordechai	13512902	400	6/7/94	34.4	0.32	772	1.36	*
Gan Hadarom A	13412102	207	6/6/93	38.0	0.19	705	0.88	
Gan Hadarom A	13412102	209	6/6/93	30.6	0.18	576	1.02	
Gan Hadarom A	13412102	210	6/6/93	32.1	0.19	640	0.97	
Revadim kibbutz	13113201	295	15/7/94	38.2	0.67	1409	1.56	
Revadim kibbutz	13113201	337	1/8/95	38.5	0.62	1352	1.50	*

MS* VG-336 (Wilmington, North Carolina)

Table 2: Boron isotope results of ground water from Cornia River in north-western Italy, and Salinas Valley, California. $\delta^{11}B$ values are reported in ‰, chloride and boron in mg/l, and B/Cl ratios are molar.

Name	$\delta^{11}B$	Cl	B	B/Cl
Cornia,Italy				
Coltie	-	86	1.3	0.050
C. Olmo	-0.71	687	5.4	0.026
C. Olmo	2.95	402	4.3	0.035
Franciana	0.73	82	4.1	0.164
Salcio	3.14	415	4.1	0.033
Gera	-2.40	4 6	3.4	0.241
Roviccione	9.25	44	3.5	0.261
Casalpiano	-0.57	68	3.0	0.143
C. di Cornia	2.29	38	3.3	0.278
Macchiaita	2.82	40	3.2	0.256
Salinas Valley, California				$(\times 10^{-4})$
Monterey Bay sw	38.4	19000	4.6	7.94
13S/2E -34M2	31.1	726	0.1	5.38
14S/2E-14L2	25.3	650	0.1	5.22
14S/2E-20B1	32.6	1670	0.2	3.99
14S/2E-15L2	24.0	973	0.3	8.26
14S/2E-11C1	38.2	593	0.2	8.07
13S/2E -34N1	26.5	400	0.1	114
14S/2E -03F2	24.7	254	0.3	336

Table 3: Boron isotopic composition of synthetic borate products.

| Material	source	company	$\delta^{11}B$ (‰)
Na-borates			
Na-borate	Turkey	Etibank, Turkey	7.6
Boric acid, tech. grade	Boron, Ca	US Borax	3.8
"Neobor" 2401 granular, 5 mol (penyahydrate)	Boron, Ca	US Borax	6.7
Borax 2101, granular, 10 mol (decahydrate)	Boron, Ca	US Borax	-0.4
Ammonium biborate 4351	Boron, Ca	US Borax	-2.0
Fertibor@	Boron, Ca	US Borax	-0.1
Ca-borates			
Boric acid (derived from Ca-borates)	Turkey	Etibank, Turkey	-13.4
CADYCAL 100 (Ca-borate)	Fort Cady, Ca	Fort Cady Minerals	-12.8
Campion Boronal ($NaCa_5O_9.8H_2O$)	Chilea	Chilean Nitrate Cor.	-13.0
Boron fertilizer	Peru		-4.9
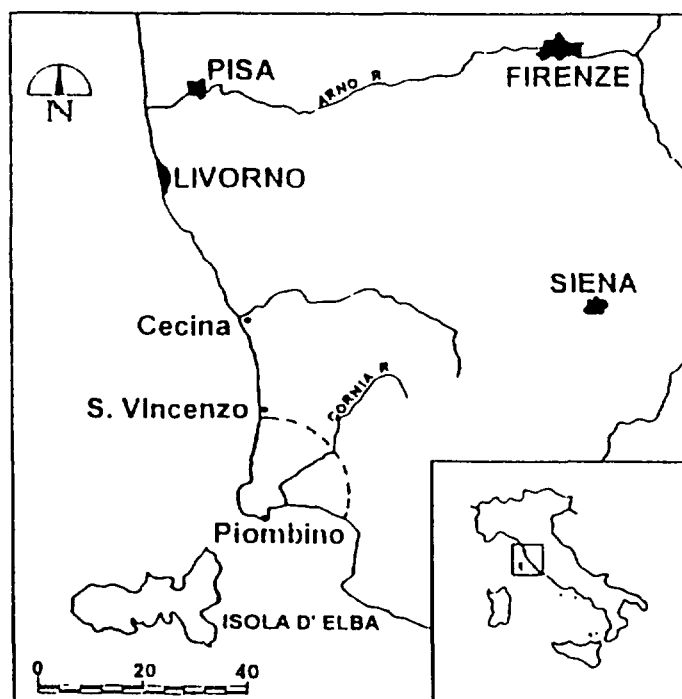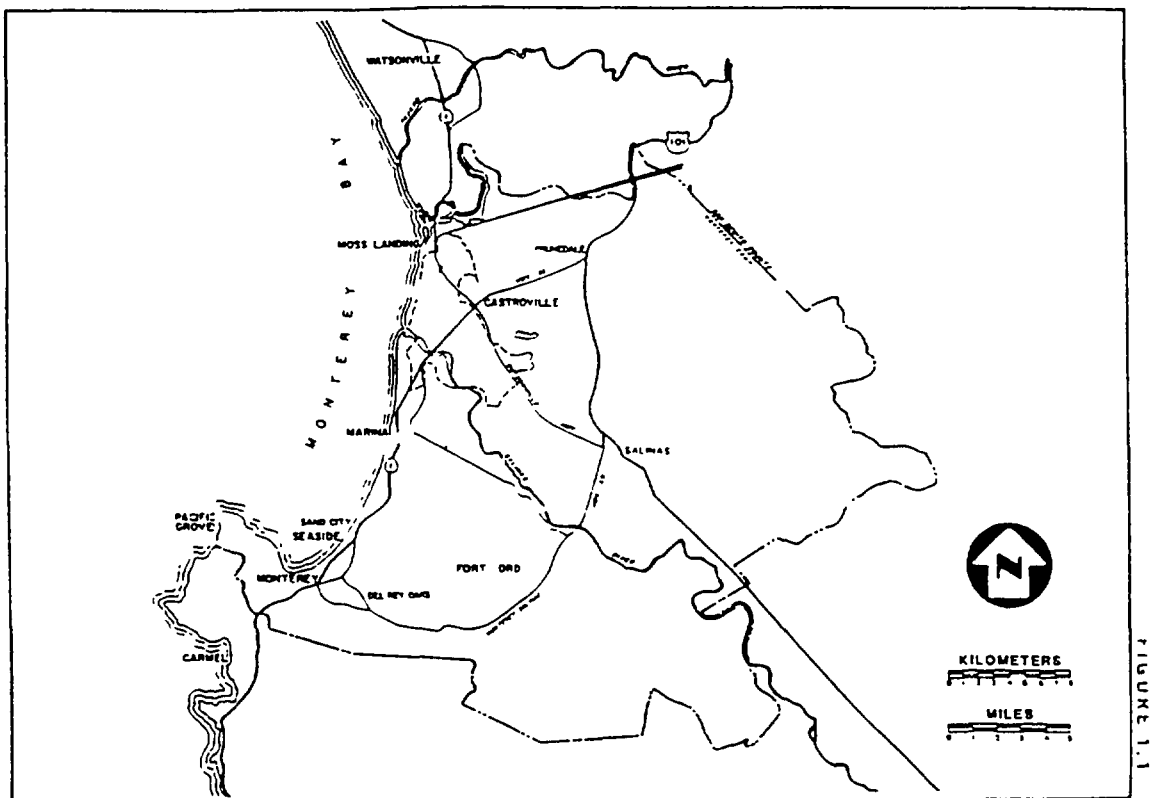
Fig. 3. Location maps of the Salinas Valley coastal area off Monterey Bay, central California, and the coastal aquifer of Cornia River in north-western Italy.

during the 1940's near the coast line of Monterey Bay [28] and the inland encroachment of salt-water has continued [29].

Saline water from the 180' aquifer has been investigated as part as a multi-isotope study of the salinization process of the aquifer. The saline water is characterized by low Na/Cl ratios (lower than sea water values of 0.86) and high Ca concentrations. The investigated samples yielded Cl contents of 250 mg/l to 1670 mg/l, B of 0.1 to 0.3 mg/l, and $\delta^{11}B$ values of 25‰ to 38‰ (Table 2; [29]).

Isotopic analyses of treated domestic waste water from Riverside, California and Santa Anna River in Orange County which receives treated wastewater effluents yielded $\delta^{11}B$ values of 0.25‰ and 1.95‰, respectively.

Synthetic boron products:
Synthetic Na-borate products of US Borate have $\delta^{11}B$ values of -0.4‰ to 7.5‰ (Table 3). The $\delta^{11}B$ values of synthetic Ca-borate and Na/Ca borate products from the U.S.A (CADYCAL100), Turkey (boric acid of EtiBank), and Chile (Champion Boronat) are significantly lower ($\delta^{11}B$=-15‰ to -12.1‰).

5. THE IMPACT OF ANTHROPOGENIC BORON

Boron compounds are widely used in various industrial applications (e.g., glass fiber, ceramics, and fertilizers) but the main industrial applications of boron that apparently affect groundwater systems are washing powders and agricultural applications of boron-fertilizers and boron-pesticides. Sodium perborate ($NaBO_3.H_2O$) is used as a bleaching agent in domestic and industrial cleaning. More than 790,000 tons of sodium perborate were used in Western Europe alone during 1985 [30,31]. Recently, sodium perborate has been introduced into "all-in-one" detergents in North America as an alternative to chlorine bleach and is used as a stain-removing agent in advanced dish washing powders. Since boron, like other inorganic ions, is not removed during waste-water secondary treatment it accumulates in domestic waste-water and consequently in natural aquatic systems [18,32]. Moreover, even during desalinization of domestic waste water using reverse osmosis techniques only 20-30% of boron is removed relative to 99% of chloride [data from 33]. The resistance of B in reverse osmosis can be related to the boron species in which the dominant species at low pH, boric acid, is not removed on the membrane.

Boron compounds are also used as fertilizers and pesticides. In areas of high precipitation and low B in irrigation water, boron fertilizers are added to increase the B content of soil fluids. In the USA the main supply of boron-fertilizers is U.S. Borate Co. which supplies Na-borate products (e.g., Fertibor, Polybor 4601, Borax 2101, Neobor). Since Na-borates are highly soluble and can be leached rapidly through the soil, Ca- and Na/Ca-borates are also used as fertilizers. The relatively lower solubility of the latter result in slow release of boron to the plants. Ca- and Na/Ca borates are produced from natural Ca-borates (Fort Cady, California, USA and Etibank, Turkey) and Na/Ca borates (Chile).

Our data (Table 3) show a clear distinction between the synthetic products of Na-borates ($\delta^{11}B$=-2‰ to 7‰) and those of Ca-borates ($\delta^{11}B$=-15‰ to -12‰). It has also been shown [34,35] that the $\delta^{11}B$ of Na-borate minerals (borax, tincal) are higher than those of Na/Ca (ulexite) and Ca-borates (colemanite, iyoite) of the same geologic origin. The trend is

26

explained by the crystal chemistry of the minerals; minerals with higher BO_3/BO_4 ratios have higher $\delta^{11}B$ values. The boron isotope compositions of the investigated synthetic Na-borate, sodium perborate from California ($\delta^{11}B = 3\pm1‰$; [7,18,19]), and washing powders from Europe (-2.9‰ to 3.1‰; [7, 36] overlap with those of natural Na-borate minerals from California (a total range of -0.9‰ to 10.2‰; Figs 1 and 4). In contrast, the $\delta^{11}B$ values of synthetic Ca-borate and Na/Ca borate products from the USA, Turkey, and Chile, mainly used as fertilizers, have lower $\delta^{11}B$ results (as low as -15‰, Table 3) which mimic those of the natural Ca-borate minerals.

It appears that the boron isotopic composition is not modified during manufacturing of the synthetic products. While sodium perborate is produced solely from Na-borates and is used only in detergents, other boron compounds are used for fertilizers and are manufactured also from Na/Ca and Ca-borates. The borate compounds from Turkey (boric acid of EtiBank, $\delta^{11}B=-13.4‰$) , Chile (Champion Boronat; -15‰) and USA (CADYCAL100; -12.8‰) have a distinguishable lower $\delta^{11}B$ signature which may be used to trace drainage fluids in agricultural areas in which B-fertilizers are being used (Fig. 5). Thus in some cases, boron isotope ratios may delineate different sources of anthropogenic boron (i.e., waste water versus agriculture return flow).
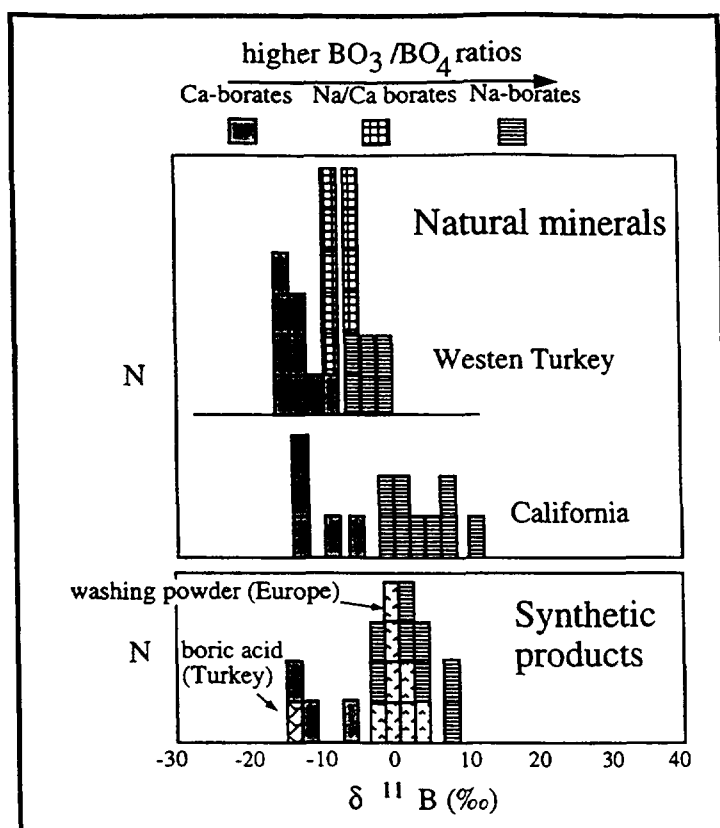

Fig. 4. Isotopic variations of natural and anthropogenic borates. The synthetic products reflect the isotopic composition of their sources: Ca-borates are 'lighter' than Na-borates. Values of natural minerals from [34] and [35].

The nature of anthropogenic boron contamination in groundwaters have been studied in different environmental settings, and is summarized below.

Domestic waste water

Anthropogenic boron in waste water is isotopically distinct from natural boron in groundwater, particularly in coastal aquifers, and thus can be utilized to identify the source of contamination. The $\delta^{11}B$ values of raw and treated sewage effluents from the Dan Region Sewage Reclamation Project in Israel ($\delta^{11}B$=5.3‰ to 12.9‰) overlap with those of natural non-marine Na-borate minerals (-0.9‰ to 10.2‰) but differ significantly from those of regional uncontaminated groundwater (~30‰) and sea water (39‰) [18]. Groundwater contaminated by recharge of treated sewage yields a high B/Cl ratio with a distinctive anthropogenic isotopic signature (7‰ to 25‰). Elemental B and $\delta^{11}B$ variations reflect both mixing of sewage effluents with regional groundwater and boron isotopic fractionation associated with boron removal by adsorption onto clay minerals. The distinctive isotopic signature of anthropogenic boron was recognized, however, in most samples and was significantly different from those of natural sources such as marine-derived saline groundwater (35‰ to 60‰; [18]).

Our results of treated waste water from Riverside and Santa Anna River in Orange County, California also demonstrate that boron isotopes can be used as a sensitive tracer to detect the impact of waste water on fresh water resources. The $\delta^{11}B$ values of Santa Anna River ($\delta^{11}B$=2‰) and treated waste water from Riverside (0.3‰) are similar to Na-borate compounds used in detergents but significantly different from fresh water from coastal areas with higher $\delta^{11}B$ values. In addition, Bassett et al. [37] used the distinctly different isotopic composition of injected treated waste water and irrigation-affected water ($\delta^{11}B$>40‰) to trace the affect of injection into an alluvial aquifer near El Paso, Texas.
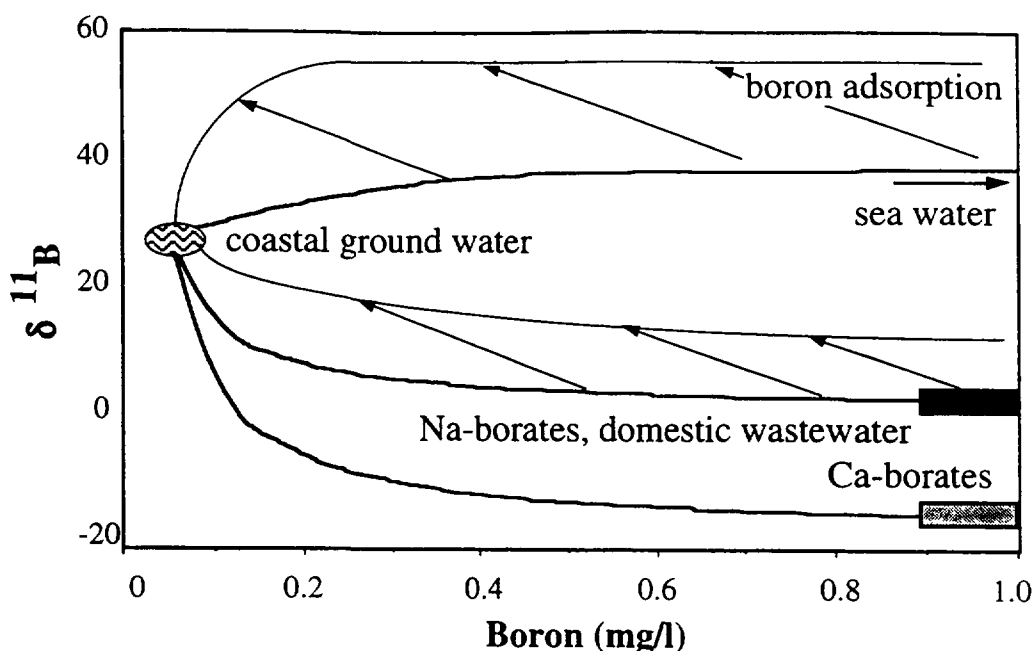

Fig. 5. $\delta^{11}B$-B mixing lines between uncontaminated boron in ground water and possible contaminants: sea water, Na-borates, and ca-borates. Note that: (1) the difference between marine and anthropogenic contamination remains detectable in spite of adsorption modifications; and (2) differences between various anthropogenic sources may be detectable.

Fly ash leachate

Boron is also enriched in coal, resulting in high concentrations of boric acid in fly ash leachate (up to 14 ppm). Davidson and Basset [38] showed that fly ash leachates have a wide range of $\delta^{11}B$ values (-19.2‰ to 15.8‰) which differ from those of local ground-waters.

Landfills

Eisenhut and Heumann [17] demonstrated high B contents (up to 6.7 mg/l) and low $\delta^{11}B$ values (-5.7‰ to 9.6‰) in seepage water from different landfills in south-east Bavaria, Germany. It was suggested that washing powder ($\delta^{11}B$=-2.9‰ to 3.1‰) was one of the main boron source in the landfills although other sources with lower $\delta^{11}B$ were also identified. The distinctive high B and low $\delta^{11}B$ signals of the seepage water was different from those of local groundwater and thus were used to track contaminates flows in the local aquifer [17]. High concentrations of boron are also expected in runoff from feedlots, paper mills, and mining operation that can be used for identifying contaminant sources [38], yet their isotopic signatures have not been constrained.

6. SALT-WATER INTRUSION IN COASTAL AQUIFERS: THE CASE STUDIES OF CALIFORNIA AND ISRAEL

In many coastal aquifers salt-water intrusion frequently occurs due to extensive withdrawals of ground water and reduction of fresh water piesometric levels. Chemical changes in modern sea water composition upon its entry into an aquifer can be caused by mixing with fresh ground water as well as water-rock interactions. In many cases the saline ground water associated with salt-water encroachment in coastal aquifers are enriched in Ca and have low Na/Cl ratios relative to modern ocean water. High salinity near the coast is typical to salt-water intrusion yet other sources with high salinity (e.g., connate brines, agriculture return-flows [39]) can cause salinization, each requiring separate management strategies. We propose the use of boron isotope composition of saline water as an indicator of the origin of salinization. Two specific cases are presented: that of saline ground water from the coastal aquifer of Salinas Valley, California (Table 2) and from the Mediterranean coast of Israel (Fig. 6):

(1) Conservative behavior of boron in which the B concentrations and isotopic ratios reflect mixing between sea water and fresh water with lower $\delta^{11}B$ values. This case was demonstrated in the 180' aquifer of the Salinas Valley with $\delta^{11}B$ values of 25‰ to 38‰ (Table 2) reflecting mixing of regional uncontaminated ground water ($\delta^{11}B$=16‰) with sea water.

(2) Non-conservative behavior of boron in which water-rock interactions, in particular B adsorption resulted in high $\delta^{11}B$ values and lower B/Cl ratios relative to seawater values. This case was demonstrated in saline water from the salt-water intrusion zone of the Mediterranean coastal aquifer of Israel with $\delta^{11}B$ values of 35‰ to 60‰ and B/Cl ratios < 7x10^{-4} [18]. The ^{11}B enrichment and total B depletion of the intruded sea water suggest boron removal, in which ^{10}B was adsorbed preferentially onto clay minerals in the aquifer. The magnitude of ^{11}B enrichment relative to the original sea water is up to 20‰ and is similar to the isotopic shift recorded in other marine brines (e.g., Dead Sea, [9]).

We conclude that salt-water intrusion originated initially from sea water may have a marine or higher $\delta^{11}B$ values and marine or lower B/Cl ratios. This $\delta^{11}B$ signal is different from non-marine brines (e.g., salt-lakes in Qaidam Basin with $\delta^{11}B$ of 0‰ to 10‰; [11]),

hydrothermal fluids, and anthropogenic boron (see above). Thus we suggest that the boron isotopic systematics can be used to monitor early signs of salt-water intrusion into coastal aquifers.

7. INFLUENCE OF HYDROTHERMAL FLUIDS: THE CASE STUDY OF CORNIA RIVER, ITALY

The boron isotope composition of hydrothermal fluids reflects contributions from the sources rocks, typically with a low $\delta^{11}B$ signal and high B/Cl (>>sea water values) ratios, and uptake into secondary phases. In oceanic environments the water-rock interaction with basalt and sediments modified the B isotopic composition of sea water [40-42]. In non-marine settings the geothermal fields are also characterized by low $\delta^{11}B$ values (e.g., Salton Sea, California, $\delta^{11}B$=-2.6‰ to -1.1‰; Yellowstone National Park, $\delta^{11}B$=-9.3‰ to 4.4‰; [43,44]), reflecting the isotopic compositions of the source rocks. The influence of seawater boron with a higher $\delta^{11}B$ in geothermal systems has been traced in central Japan ($\delta^{11}B$=-5.8‰ to 27.1‰; [45]) and Iceland ($\delta^{11}B$=-6.7‰ to 30.7‰; [46]). Experiments at elevated temperatures on seawater-sediment interaction have shown that whereas boron is leached from sediments at T>150°C, it is adsorbed onto the clay mineral at lower temperatures [42]. The clear distinction between the B isotopic composition of rocks and sea water enables us to trace the impact of hydrothermal fluids on fresh water.

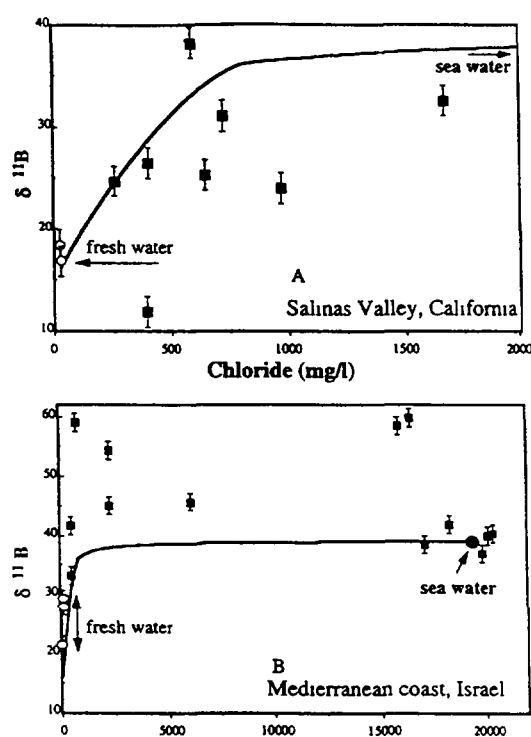Fig. 6. Chloride versus $\delta^{11}B$ values of saline water associated with salt-water intrusion from and Salinas Valley, California (A) and the Mediterranean coast of Israel (B) . The lines represent conservative mixing between sea water and fresh water with lower d11B values.
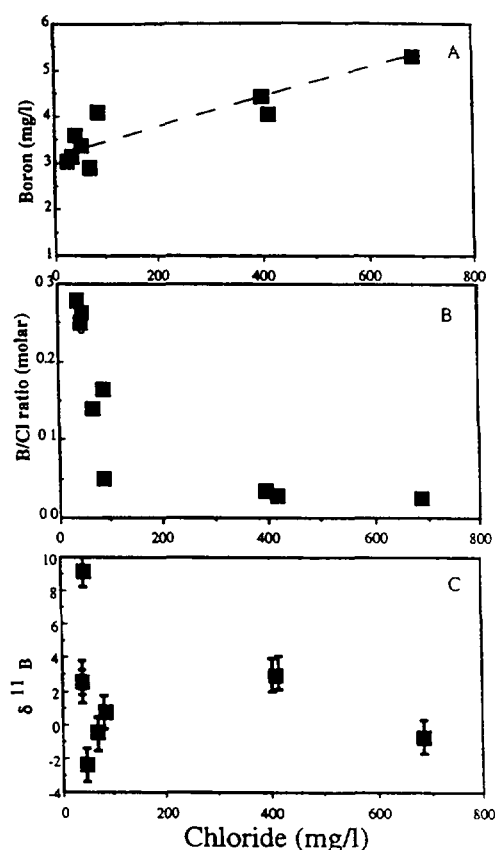
Fig. 7. Chloride concentrations versus boron contents, B/Cl, and $\delta^{11}B$ values of ground water from Cornia River aquifer Italy

The saline water from the coastal aquifer of Cornia River (Fig. 3, [27]) in north-western Italy represent a good example of the application of B-isotopes. The high salinity (>1000 mg/l), and the close vicinity to the sea (Fig.3) would suggest inland encroachment of sea water. Yet the chemical composition (high Ca, low Na/Cl ratios), high B/Cl ratios, and low $\delta^{11}B$ values of -2.4‰ to 9.3‰ rule out this mechanism. The linear correlation between boron with chloride (Fig. 7), suggests a single source for both elements. Thus, we argue that the high salinity and low $\delta^{11}B$ signature (Fig. 7) reflect contamination by underlying hydrothermal fluids that mixed with the local ground water and caused degradation of the quality of ground water in the coastal aquifer of Cornia River .

8.   TRACING THE ORIGIN OF SALINITY IN SALINE PLUMES FROM THE COASTAL AQUIFER OF ISRAEL

The origin of saline plumes in the inner parts of the Mediterranean coastal aquifer (Fig. 2) of Israel is yet unresolved. The potential sources of salinity in this phreatic aquifer are anthropogenic (e.g., imported water from the Sea of Galilee via Israel's National Water Carrier, irrigation or leakage of waste water effluents) or natural sources from underlying saline water. Since each of these sources may have a distinctive isotopic ratio we investigated the chemical and B isotopic ratio of the brackish groundwater from several saline spots in the aquifer.

The boron-chloride relationships in most of the investigated ground water (Fig. 8) suggest that boron, like most of the dissolved ions, behaves conservatively in the aquifer. The B/Cl ratio decreases with salinity, but the saline ground water has a B/Cl ratio of 1.5×10^{-3} that is slightly higher than that of sea water (0.8×10^{-3}). In contrast to fresh ground water (Cl<100 mg/l) with lower $\delta^{11}B$ values (21.2‰ to 32.4‰), the $\delta^{11}B$ values of the investigated brackish water vary from 31.7‰ to 49.9‰ (Fig.8) . Based on the $\delta^{11}B$ variations two types of brackish groundwater are identified: (1) brackish water with high $\delta^{11}B$ values (>40‰), typical of the saline plumes of Be'er Toviyya and Kevuzat Shiler (Fig. 3); and (2) brackish ground water from the other saline plumes in the central aquifer and from the eastern part of the aquifer (Revadim) with a $\delta^{11}B$ range of 30‰ to 40‰ (Table 1). The $\delta^{11}B$ values of the latter group correspond to mixing between a saline source with a marine $\delta^{11}B$ signature and fresh ground water. Similarly, the $\delta^{11}B$ variations of brackish water from Be'er Toviyya saline plume correspond to mixing between a saline source with a high $\delta^{11}B$ signature (> 50‰) and fresh ground water (Fig.8).

The boron isotope compositions of the brackish ground water are significantly different from those of anthropogenic sources, such as sewage effluent ($\delta^{11}B$=0-10‰) or contaminated ground water (10-25‰; [18]) , and thus rule out salinization from leakage or irrigation with sewage effluents. The high $\delta^{11}B$ values are similar, however, to those of saline water associated with salt-water intrusion in the western part of the aquifer [18]. Consequently, the $\delta^{11}B$ values suggest that the brackish ground water is derived from a marine source with a high $\delta^{11}B$ value.

The relatively high B/Cl ratios and $\delta^{11}B$ values of the brackish ground water rule out simple mixing between fresh water (low $\delta^{11}B$ and high B/Cl) and Mediterranean sea water (Cl=22,000 mg/l). The high B content of sea water relative to B in freshwater would dominate the composition (e.g., B/Cl~0.8×10^{-3}) of any mixture. Moreover, mixing of fresh

31

water with saline water that is associated with salt-water intrusion and has higher $\delta^{11}B$ and lower B/Cl ratios [17] would result in even lower B/Cl ratios ($<0.8 \times 10^{-3}$) in order to account for the high $\delta^{11}B$ results. Therefore, we suggest that diagenetic modifications may have modified the entrapped sea water, probably by slight contribution of B from clay minerals in the rocks.

We suggest that most of the saline plumes are derived from a modified-diluted sea water, and that the salinization process is a result of continuous mixing with the saline end-member. The original sea water was modified by adsorption processes (as reflected by high $\delta^{11}B$ values in Be'er Toviyya and Shiler saline plumes), desorption or leaching of B from rocks (as inferred by the relatively high B/Cl ratios), and dilution with fresh water . The boron isotope results are consistent with other geochemical tracers ($\delta^{18}O$, $^{87}Sr/^{86}Sr$, Br/Cl), which also show that the main salinization in the Coastal Plain aquifer is a result of flow of underlying natural, marine-derived saline water [47].

These findings enabled the establishment of a suitable water-quality monitoring program in the Hydrological Service of Israel [48]. In addition, it has been argued that utilization of the brackish water and the underlying saline sources for desalination can reduce the operating cost and energy required, compared to desalination of Mediterranean sea water, and can be an important component in an overall fresh water conservation program in the Israeli Coastal Plain aquifer. The combination of brackish groundwater desalting and groundwater management would result in the production of usable quantities of fresh water and a long-term improvement of the water quality of the aquifer [49].
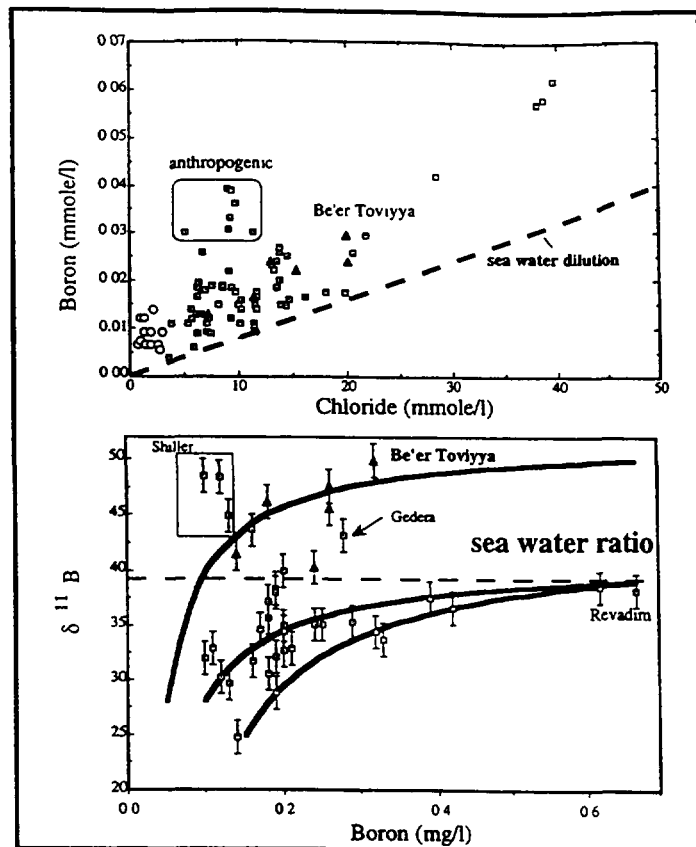

Fig. 8. Brackish water from saline plumes in the coastal aquifer of Israel. Mixing lines represented in B-Cl and $\delta^{11}B$-B spaces. Note the linear mixing of B-Cl relative to hyperbolic mixing of $d^{11}B$-B.

32

9. DISCUSSSION AND CONCLUSIONS

Any strategy aimed at counteracting the harmful effects of the groundwater contamination requires a better understanding of the sources and causes of pollution. The variety of the contamination sources makes this task difficult, however. For example, the increase in the salinity of groundwater in coastal aquifers can be a result of "natural" causes such as sea water intrusion, dissolution of soluble salts in the unsaturated zone, flows of saline water from adjacent or underlying aquifers, or alternatively, anthropogenic contamination such as seepage, irrigation of sewage effluent, and agriculture return flows. Each of these salinization sources may be characterized by a distinguishable elemental and isotopic signature. Hence the use of different geochemical, including isotopic, tracers might provide additional tools for evaluation and identification of the sources of contaminated groundwater.

Boron can be used as a tracer in ground-water because of its high solubility in aqueous solution, natural abundance, and the lack of effects by evaporation, volatilization, and oxidation-reduction reactions [37]. Since boron concentrations in pristine ground-waters are generally low (<0.05 mg/l) and contaminant sources are usually enriched in boron (e.g. sea water, 4.5 mg/l; domestic waste water, 1 mg/l; fly ash leachate, 14 mg/l) the $\delta^{11}B$ of ground-water is highly sensitive to the impact of contamination. The large isotopic variation of the potential sources can be used to trace the origin of the contamination and to reconstruct mixing and flow paths. The main end-members with distinguishable isotopic signals are (Fig. 9):

(1) Salt-water intrusion in coastal aquifers and entrapped marine-origin brines with $\delta^{11}B$ values of $\geq 39‰$ and B/Cl $\leq 8 \times 10^{-4}$;

(2) Non-marine brines entrapped in non-flushed areas in aquifers and aquitrads with $d^{11}B$ values of ~0‰ and B/Cl>8×10^{-4};

(3) Hydrothermal fluids in hydraulic connections to fresh water aquifers with $d^{11}B$ values of ~0‰ and high B/Cl (>>marine ratio).

(4) Contamination by domestic water water and other anthropogenic sources (e.g., fertilizers, pesticides, landfills) in which anthropogenic boron is derived from Na-borates with $d^{11}B$ values of 0‰ to 10‰ and high B/Cl (>marine ratio).

(5) Contamination by fertilizers originated from Ca-borates with low $d^{11}B$ values as - 13‰ and high B/Cl (>marine ratio).

These variations show that marine and Ca-borate sources are well resolved whereas some overlaps may exist between the other contamination sources, hence additional constraints are required to distinguish between these sources. For example, high concentrations of boron have been identified in some surface freshwater (lakes and rivers) in the River Po watershed in Northern Italy [50]. The strong correlation between boron concentration and that of total dissolved phosphorus as well as anionic detergents suggest that the high boron concentrations are related to anthropogenic contamination. On the other hand, the high correlation between boron and chloride (Fig. 7), high Cl contents, and low $\delta^{11}B$ values (-2.4‰ to 9.3‰) in ground-water from the coastal plain of the Cornia River near Pisa, Italy [Table 2; 27], suggest a hydrothermal source .

Mixing of regional ground-water boron with anthropogenic boron is the major factor which determines the distribution of $\delta^{11}B$ in contaminated ground-waters. Typically higher B concentrations in the contaminant end-member result in nonlinear (hyperbolic) boron -

$\delta^{11}B$ mixing curves (e.g., Figs 5 and 6) that enable identification, and in some cases even quantification, of the contaminants in ground water [38]. The $\delta^{11}B$ of ground-water boron can be modified, however, by adsorption onto clay minerals in the aquifer, in particular in clay-rich aquifers and high salinity which enhance B adsorption. The isotopic shift associated with boron retention is a ^{11}B enrichment of about 20‰ and thus contaminated ground-water may have higher $\delta^{11}B$ values relative to the original source.
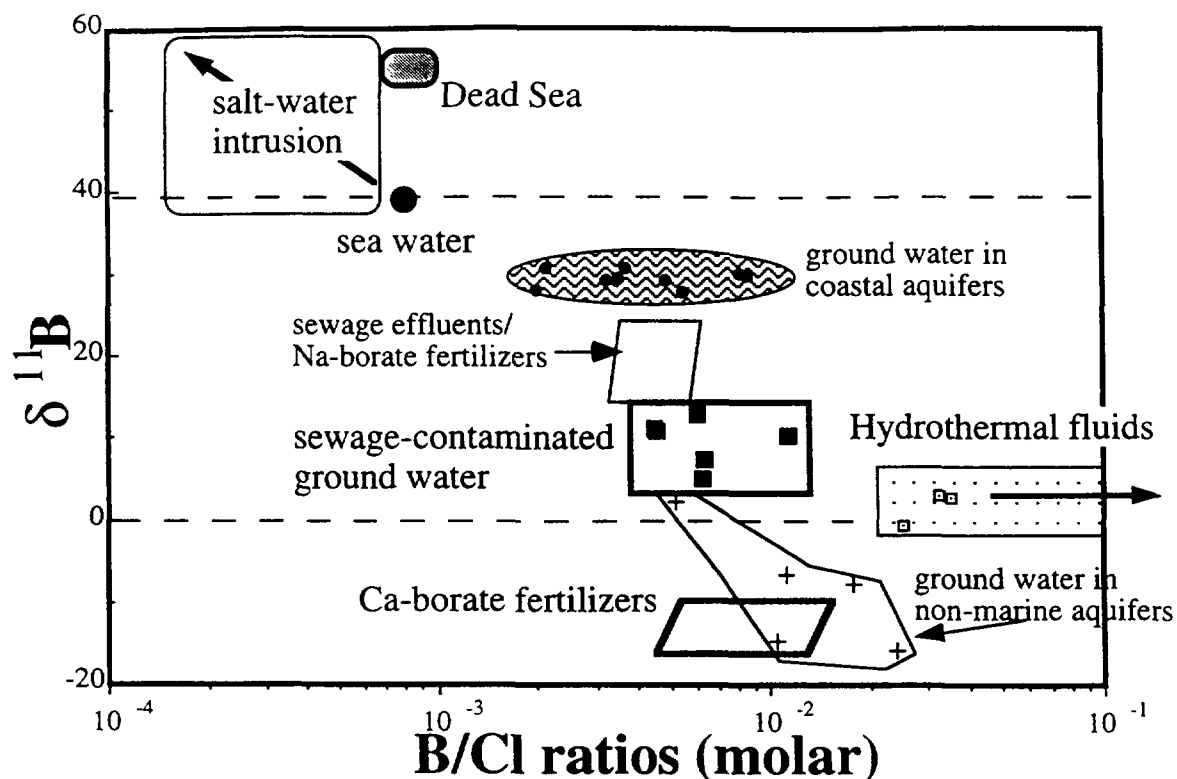
Fig. 9. Variations of B/Cl and $\delta^{11}B$ values of potential contamination sources.

REFERENCES

[1]   Mastromatteo E. and Sullivan F. International Symposium on the Health Effects of Boron and its Compounds. *Environm. Health Perspect. Supplem.*, 102, (1994) 139-141.

[2]   World Health Organization. Guidelines for drinking-water quality. Volume 1, Recommendation, Geneva, (1993) 187 pp.

[3]   Heumann K.G. Isotopic analyses of inorganic and organic substances by mass spectrometry. *Int. J. Mass Spectrom. Ion Phys.*, 45, (1982) 87-110.

[4] Zeininger H. and Heumann K.G. Boron isotope ratio measurements by negative thermal ionization mass spectrometry, Int. J. Mass Spectrom. Ion Phys. 48, (1983) 377 -380.

[5] Spivack A.J. and Edmond J.M. Determination of boron isotope ratios by thermal ionization mass spectrometry of the dicesium metaborate cation. Anal. Chem., 58, (1986) 31-35.

[6] Vengosh A., Chivas A. R. and McCulloch M. T. Direct determination of boron and chlorine isotopes in geological materials by negative thermal-ionization mass spectrometry. Chem. Geol. (Isotope Geosci. Sec.), 79, (1989) 333-343.

[7] Eisenhut, S., Heumann K.G., and Vengosh A. Determination of boron isotopic variations in aquatic systems with negative thermal ionization mass spectrometry as a tracer for anthropogenic influences, Fresenius J. of Analy. Chem. 354, (1996) 903-909.

[8] Kakihana, H., Kotaka, M., and Satoh, S. Fundamental studies on the ion-exchange separation of boron isotopes. Chemical Society of Japan Bulletin, 50, (1977) 158-163.

[9] Vengosh, A.,Starinsky, A., Kolodny, Y. and Chivas, A.R. Boron-isotope geochemistry as a tracer for the evolution of brines and associated hot springs from the Dead Sea, Israel. Geochim. Cosmochim. Acta, 55, (1991) 1689-1695.

[10] Vengosh, A., Starinsky A., Kolodny, Y. and Chivas, A.R. Boron isotope geochemistry of thermal springs from the Northern Rift Valley, Israel. J. Hydrol., 162, (1994) 155-169.

[11] Vengosh, A., Chivas, A. R., Starinsky, A., Kolodny, Y., Zhang Baozhen and Zhang Pengxi, Chemical and boron isotope compositions of non-marine brines from the Qaidam Basin, Qinghai, China. Chem. Geol., 120, (1995) 135-154.

[12] Fogg, T.R. and Duce, R.A. Boron in the troposphere: distribution and fluxes. J. Geophys. Res., 90, (1985) 3781-3796.

[13] Kanzaki, T., Yoshida, M. Nomura, M., Kakihana, H. and Ozawa, T. Boron isotopic composition of fumarolic condensates and sassolites from Satsuma Iwo-Jima, Japan. Geochim. Cosmochim. Acta, 43, (1979) 1859-1863.

[14] Spivack A. J., Palmer M. R. and Edmond J. M. The sedimentary cycle of the boron isotopes. Geochim. Cosmochim. Acta, 51, (1987) 1939-1950.

[15] Ishikawa, T. and Nakamura, E. Boron isotope systematics of marine sediments. Earth Sci. Planert. Let., 117, (1993) 567-580.

[16] Spivack A. J. Boron isotope geochemistry. Ph.D. thesis, Massachusetts Institute of Technology/Woods Hole Oceanographic Institution. (1986) 184 p.

[17] Eisenhut, S.and Heumann K.G. Identification of groundwater contaminations by landfills using precise boron isotope ratio measurements with negative thermal ionization mass spectrometry. Fresenius J. of Analy. Chem. 359, (1997) 375-377.

[18] Vengosh, A., Heumann, K.G., Juraske, S., and Kasher R.. Boron isotope application for tracing sources of contamination in groundwater.Envi. Sci. Tech., 28, (1994) 1968-1974.

[19] Juraske, S. Diploma Thesis, University of Regensburg, Germany (1994).

[20] Vengosh, A., Chivas, A.R., McCulloch, M.T., Starinsky, A. and Kolodny, Y. Boron-isotope geochemistry of Australian salt lakes. Geochim. Cosmochim. Acta. 55, (1991) 2591-2606.

[21] Kiss E. Ion-exchange separation and spectrophotometric determination of boron in geological materials. Anal. Chim. Acta, 121, (1988) 243 - 256.

[22] Gregoire, D.C., Determination of boron isotope ratios in geological materials by inductively coupled plasma mass spectrometry. Anal. Chem. 59, (1987), 2479-2484.

[23] McMullen C.C., Cragg C.B. and Thode H.G. Absolute ratios of B11/B10 in Searles Lake borax. Geochim. Cosmochim. Acta, 23, (1961) 147 - 149.

[24] Schwarcz H. P., Agyei E. K. and McMullen C. C. Boron isotopic fractionation during adsorption from seawater. Earth Planet. Sci. Lett., 6, (1969) 1-5.

[25] Swihart G.H., Moore P.B. and Callis E.L. Boron isotopic composition of marine and non-marine evaporite borates. Geochim. Cosmochim. Acta, 50, (1986) 1297 - 1301.

[26] Vengosh, A. and Ben Zvi, A. Formation of a salt plume in the Coastal Plain Aquifer of Israel: The Be'er Toviyya region. Journal of Hydrology, 160, (1994) 21-52.

[27] D'Avino D. and Spandre R. Presence of boron in groundwater in the coastal plain of the Cornia River, Italy. J. Environm. Hydrol., 3, (1995) 3-10.

[28] Todd, D.K., Sources of saline intrusion in the 400-foot aquifer, Castroville area, California. Monterey County Flood Control and Water Conservation District, Salinas California (1989), 41 pp.

[29] Vengosh, A., Gill J., Reyes A., and Thoresberg K. A multi-isotope investigation of the origin of ground water salinity in Salinas Valley, California. American Geophsical Union, San Francisco, December (1997).

[30] Harben P.W. and Kuzvat M. A Global Geology, Industrial Minerals Information Ltd., United Kingdom (1996) pp.59-73.

[31] Raymond K. and Butterwick L. Perborate. In: de Qude N.T. (Ed.) Detergents. Springer-Verlag, New York, (1992) pp. 288-318.

[32] Waggott A. An investigation of the potential problem of increasing boron concentrations in rivers and water courses. Water Research, 3, (1969) 749-765.

[33] Mills W.R. Orange County water district wastewater reclamation, Talbert Barrier, and recharge project. Annual Report 1996, Orange County water district (1997).

[34] Oi T., Nomura M., Musashi M., Ossaka T., Okamoto M. and Kakihana H. Boron isotope compositions of some boron minerals. Geochim. Cosmochim. Acta, 53, (1989) 3189-3195.

[35] Palmer M.R. and Helvaci C. The boron isotope geochemistry of the Kirka borate deposit, western Turkey. Geochim. Cosmochim. Acta, 59, (1995) 3599-3605.

[36] Heumann K.G., Eisenhut S., Gallus S., Hebeda E.H., Nusko R., Vengosh A., and Walczyk T. Recent developments in thermal ionization mass spectrometric techniques for isotope analysis (A review). Analyst, 120, (1995) 1291-1299.

[37] Basset R.L., Buszka P.M., Davidson G.R., and Damaris Ghong-Diaz. Identification of groundwater solute sources using boron isotope composition, Environ. Sci. & Technol., 29, (1995) 2915-2922.

[38] Davidson G.R. and Bassett R.L. Application of boron isotopes for identifying contaminants such as fly ash leachate in ground-water. Environ. Sci. Technol., 27, (1993) 172-176.

[39] Izbicki J.A. Chloride sources in a California Coastal Aquifer. Ground water in the Pacific Rim Countries, Conference Proceedings, Irrigation Division, American Society of Consulting Engineers, Honolulu, Hi, July 23-35, (1991).

[40] Spivack A.J. and Edmond J.M. Boron isotope exchange between seawater and oceanic crust. Geochim. Cosmochim. Acta, 51, (1987) 1033 - 1042.

[41] Palmer M.R. Boron isotope systematics of hydrothermal fluids and tourmalines: a synthesis. Chem. Geol. (Isotope Geosci. Sect.), 94, (1991) 111-121.

[42] You C.-F., D.A. Butterfield, A.J. Spivack, J.M. Gieskes, T. Gamo, and A.J. Campbell, Boron and halide systematics in submarine hydrothermal systems: Effects of phase separation and sedimentary contributons, Earth and Planet. Sci. Lett. 123, (1994) 227-238, 1994.

[43] Palmer M.R. and Sturchio N.C. The boron isotope systematics of the Yellowstone National Park (Wyoming) hydrothermal system: a reconnaissance. Geochim. Cosmochim. Acta, 54, (1990) 2811-2815.

36

[44] Palmer M.R. and Swihart G.H. Boron Isotope Geochemistry: an overview. In: E.S. Grew and L.M. Anovitz, eds., Boron: Mineralogy, Petrology, and Geochemistry, Mineralogical Society of America, Reviews in Mineralogy, 33, (1996) pp. 709-744.

[45] Musashi M., Nomura M., Okamoto M., Ossaka T., Oi. T., Kakihana H. Regional variation on the boron isotopic composition of hot spring waters from cental Japan. Geochem. J., 22, (1988) 205-214.

[46] Aggarwal J.K., Palmer M.R.Ragnarsdottir K.V. Boron isotope composition of Iceland hydrothermal system. In 7th International Sympo. Water-Rock Interaction WRI-7, Park City, Vol.2, (1992) 893-895.

[47] Vengosh, A., Spivack A. Artzi Y., and Ayalon A. Boron, Strontium and Oxygen isotope tracers for the origin of of brackish ground-water from the Mediterranean coast, Israel. American Geophsical Union, San Francisco, December (1996).

[48] Vengosh, A., Artzi, Y., Zirlin I., Pankratov I., Harpaz H., Rosenthal E., and Ayalon A. Water quality monitoring in the Coastal Plain aquifer of Israel: Givat Brener-Gedera-Yavne area. Hydrological Service of Israel, Report 96/04, (1996) 34 pp (in Hebrew).

[49] Vengosh A. Identification of brackish water in the Coastal Plain aquifer of Israel: sources of salinity and potential for desalinization. Hydrological Service of Israel, Report 95/01, (1995) 55 pp (in Hebrew).

[50] Tartari G. and Camusso M. (1988) Boron content in freshwaters of northern Italy. Water, Air and Soil Pollu., 38, 409-417.

NITRATE POLLUTION OF A KARSTIC GROUNDWATER SYSTEM IN SVATÝ JAN POD SKALOU, CZECH REPUBLIC

F. BUZEK, R. KADLECOVÁ, K. ŽÁK
Czech Geological Survey, Prague, Czech Republic

Abstract - *Due to increasing agricultural activity after the 1960's both shallow and deep water resources in the Czech Republic including karstic systems have been contamined by infiltrating nitrate. Nitrate content of one of the largest spring (19L/s) now varies from 50 to 60 mg/L. To specify the sources of nitrate pollution and collect sufficient data for the prediction of possible future development, flow dynamics, chemical and isotopic composition ($\delta^{18}O$ in water, $\delta^{15}N$ in nitrate) were monitored in the spring and precipitation together with potential sources of pollution (fertilizers, solutes in soil profile). Observed data were modelled by a simple mixing cell model to specify system parameters (volume and mean residence time).*

1. INTRODUCTION

It has been observed that modern agricultural practices involving extensive application of manure and chemical fertilizers have increased nitrate concentrations in shallow and deep groundwater. The monitored spring was used as a source of high quality water for production of bottled water in the past. Production did not continue after the 1960s because of problems with water quality. The nitrate content of the studied spring varies now from 50 to 60 mg /L. To identify the sources of nitrate pollution and evaluate parameters of the karstic system, the stable isotopes ^{18}O and ^{15}N were used together with monitoring of flow dynamics, water chemistry and soil composition. From the space and time variations of stable isotopes as natural tracers of infiltrating precipitation and nitrate, we can specify the pollutant pathways and the size of the groundwater reservoir that may enable prediction of future evolution of water quality of the source.

2. SITE DESCRIPTION

The Bohemian Karst is an extensive karst area formed by Devonian limestone and located in the south-west surroundings of Prague, is known for numerous outflows of karstic water. These springs usually occur near the boundaries between limestone and underlying volcanic (diabases), volcanoclastic (tuffs and tuffaceous rocks) and non-karstic sedimentary rocks (shales). The springs having the largest discharges are, moreover, typically controlled by local or regional faults. The Bohemian Karst represents local elevation with the altitudes in the range from 500 m a.s.l. to about 200 m a.s.l., crosscut by the deep valleys of the Berounka river and the Kaèák stream. The annual precipitation averages 570 mm and the average year temperature varies, depending on the location and altitude, between 7.5 and 9 °C.

The largest of the karstic springs (all branches together above 19 L/s during minimum discharge) discharges in Svatý Jan pod Skalou village, a local pilgrimage place with a large Baroque church and monastery. The spring is characterized by relatively small discharge variability and, during most periods, very stable and relatively high temperature in the range between 11.4 and 11.6 °C, which is higher than the local average annual temperature. The spring infiltration area consists of several quite different parts. A small valley directly above the spring represents its geographical catchment with an area close to 1 km². This forested
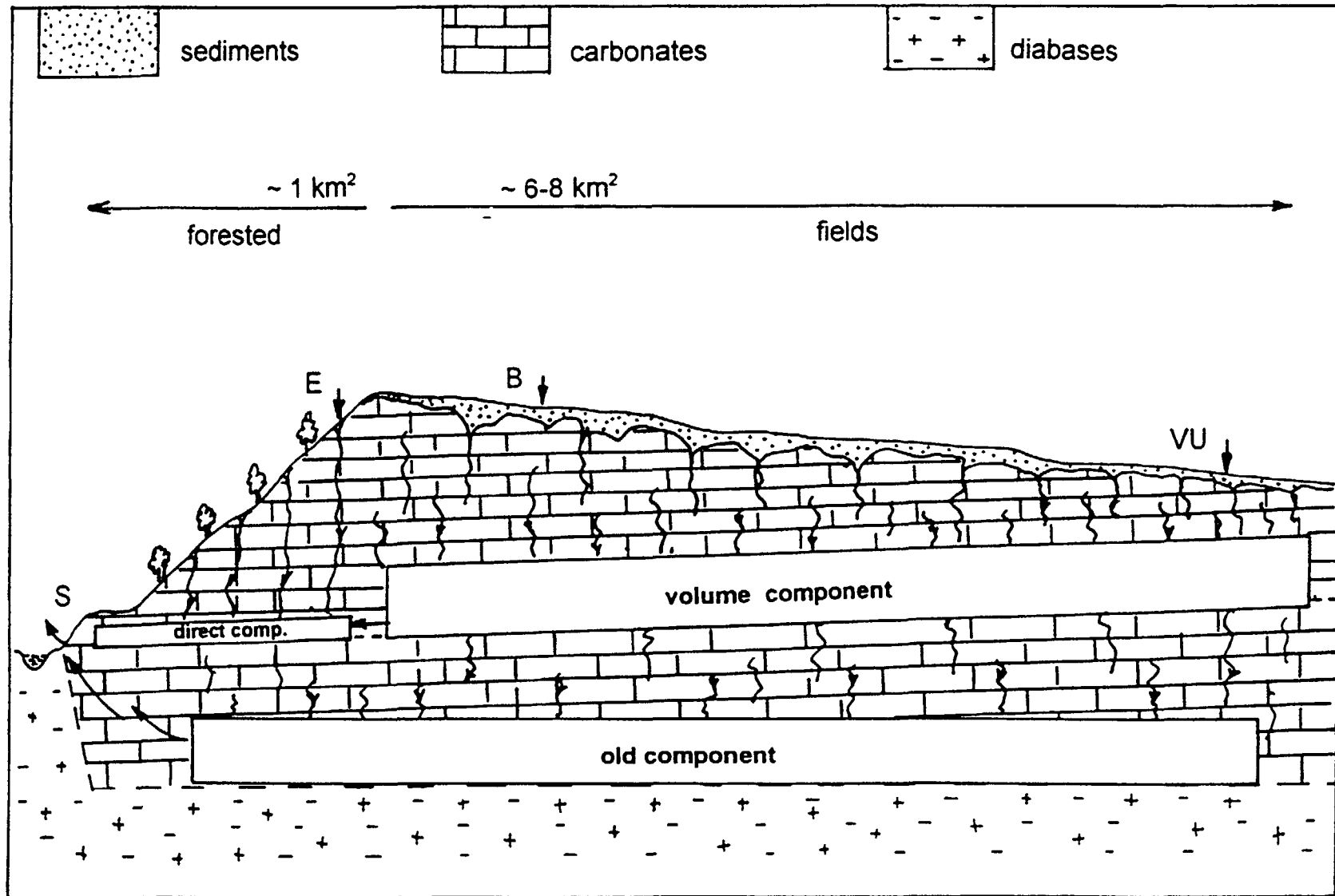
Fig. 1. Schematic cross-section of the karstic groundwater system: S spring, E tracer experiment site, B Bubovice soil profile, VU Vysoký Újezd soil profile.

land (oak-hornbeam assemblage) is characterized by steep slopes and contains several swallow holes which act as periodic ponores (sinking streams in a swallow holes) during large precipitation events. Some abandoned limestone quarries are present in this area, too. The spring discharge which does not decrease below 19 L/s suggests that the real (hydrological) catchment of the spring must be much larger than this small geographical one. The average groundwater unit yield for limestones of the Bohemian Karst is close to 2.8 $L.s^{-1}.km^2$ [1]. Using this value the total spring infiltration area should be in the range between 5 and 7 km^2. The spring infiltration area thus clearly comprises another (dominant) part with slow infiltration and a deep karstic-type reservoir. Analysis of the geological situation shows that the spring infiltration area probably follows the NW flank of a syncline of limestones trending in a NE direction, underlies and overlies by non-karstic rock types (see Fig. 1). At the surface this area is characterized mostly by flat country covered by fields with intensive agricultural activity. This flat elevated surface represents an old peneplain of Cretaceous period. Remnants of Cretaceous marine sandstone occur in the NE part of the study area. The surface of karstic rocks below this peneplain is deeply weathered and, as seen in outcrops in some quarries, very morphologically complex. Depressions in this fossil karst surface were filled with younger Cretaceous and Tertiary sediments. Surface waters from this area are drained now by the Bubovický potok Creek and by the Karlický potok Creek to the SW and SE.

The extent of forests and cultivated fields in the study area is shown on Fig. 1. In the past mostly organic fertilizers (dung, dung-water) were used on the fields. Starting from late 1960s artificial fertilizers started to be overused by local state-controlled Unified Agricultural Cooperatives. In the period from 1968 to 1989 most fields in the area received from 90 to 110 kg N/ha/year. After 1989, as a result of political changes and decreased state support of agriculture, the quantity of fertilizers used decreased dramatically to recent average value 35 kg of N/ha/year (during the last five years liquid fertilizer DAM 390 has been applied at about 100 L/ha „on leaves" during the beginning of vegetational period complemented once per 3 years by 40 t of dung/ha). The significant change in the quantity of applied fertilizers, which occurred after 1989 represents, the unique opportunity to study the changes of nitrate pollution in the deep karstic aquifer.

3. METHODS

Starting on November 1, 1994 regular measurements of temperature, discharge and $\delta^{18}O$ of the spring and precipitation on the possible recharge area have been performed. Precipitation was sampled using PE funnels installed at the recharge area and cumulative (3 or 7 days) samples were collected. The sampling period was twice a week in the first year and once a week in the second year. During large precipitation events the period was shortened to 12 hours to obtain a detailed record of flow dynamics. The $\delta^{18}O$ of water was measured by the standard equilibrium method [2]. The spring water chemistry and $\delta^{15}N$ of nitrate was measured every six or eight weeks. Other water sources, such as springs, streams and wells in the recharge area were monitored bi-monthly for chemistry and $\delta^{15}N$ of nitrate. Only some precipitation samples were monitored for chemistry and $\delta^{15}N$ of nitrate and ammonium to estimate the range of values for infiltrating water. All types of applied fertilizers were analyzed for their $\delta^{15}N$ values. Soil samples for soil extracts were taken from two soil profiles at the sites with different application of fertilizers and different distance from the recharge site (near Bubovice and Vysoký Újezd villages). Samples represent three levels (0-25 cm, 25-70 cm and 70-110 cm or 70-140 cm), corresponding to A, Bv and C horizons. The sampling was done in June 1996, about three months after snow melting and a few small

precipitation events. Samples of soil were placed into PE sampling bags and frozen on site at -80°C using dry ice in cooling boxes for transportation. Upon transportation to the laboratory, the samples were stored in a refrigerator at -16°C. A 500 g sample of soil was extracted with 1L of 1M KCl solution at room temperature by stirring the suspension for about 30 minutes. The extract was filtered through prefilter and fine filter and the filtrate volume was measured. The solution was checked for ammonium and nitrate content, conserved by an addition of thymol and stored in a refrigerator for steam distillation. Solution aliquots were alkalized with MgO and steam distilled (nitrate with the addition of Devarda alloy) into a small excess of diluted sulfuric acid. Ammonium sulphate was dried and stored for $\delta^{15}N$ analyses.

The $\delta^{15}N$ analyses were performed by flash combustion in Fisons 1108 elemental analyzer coupled to Mat 251 isotope ratio mass spectrometer via open-split interface ConFlo I in continuous flow regime. Sample size was from 0.5 to 1mg of N. External reproducibility of $\delta^{15}N$ measurement was 0.15‰, however, overall reproducibility of steam distilled samples was about 0.4 ‰.

4.   RESULTS AND DISCUSSION

4.1.   Flow dynamics

Figure 2 shows the discharge and temperature patterns of the studied spring. The studied hydrological year 1994-95 had high monthly precipitation totals during May and June while the several years before were characterized by precipitation much below long-term average (about 80% of normal). As a result of this, the discharge during autumn 1994 and winter 1994/1995 was extremely low. The discharge of autumn of 1995 was about 25 % higher when compared to 1994.

During the largest precipitation event of the monitored period (from 1. to 2. June, 1995, 59.1 mm of precipitation) local floods occurred in the study area. During this event a new swallow hole appeared in the upper part of the geographical catchment of the Svatý Jan pod Skalou karstic spring (about 1050 m from the spring site) and was immediately used for a simple tracer experiment using NaCl solution as a tracer [3]. This tracer experiment enabled calculation of some parameters of the lowest part of the unknown underground stream system. The discharge of the spring was 24.5 l/s during the experiment. The tracer signal appeared between 19 and 20 hours after injection into the swallow hole, peaked after 26 hours and returned to background level after 37 hours. Supposing no tracer loss in the system the total possible spring discharge (including the branches which were not monitored) was calculated at 36.9 l/s. The volume of water-filled cavities between injection point and discharge (distance 1050 m, altitude difference 127 m) is in the range from 1680 to 2430 m^3.

Based on the hydrograph analysis of the spring, three components of the karst system can be identified [4]. The first one (a short time component) represents the dominant effect of drainage of well conduit parts with a volume close to the traces experiment cavity volume. The second component (a volume component) dominates in the middle parts of the hydrograph's recession and characterizes the emptying of well-connected karstified fractures. Its volume corresponds to 3 10^5 or 4 10^5 m^3. The third component (an old component) represents matrix flow from deeply infiltrated precipitation into deeper parts of the synclinal structure. Its residence time is not known up to now. The tritium concentration for very steady base flow (winter 1994-95) was 23 TU, which is about 12 TU above recent precipitation
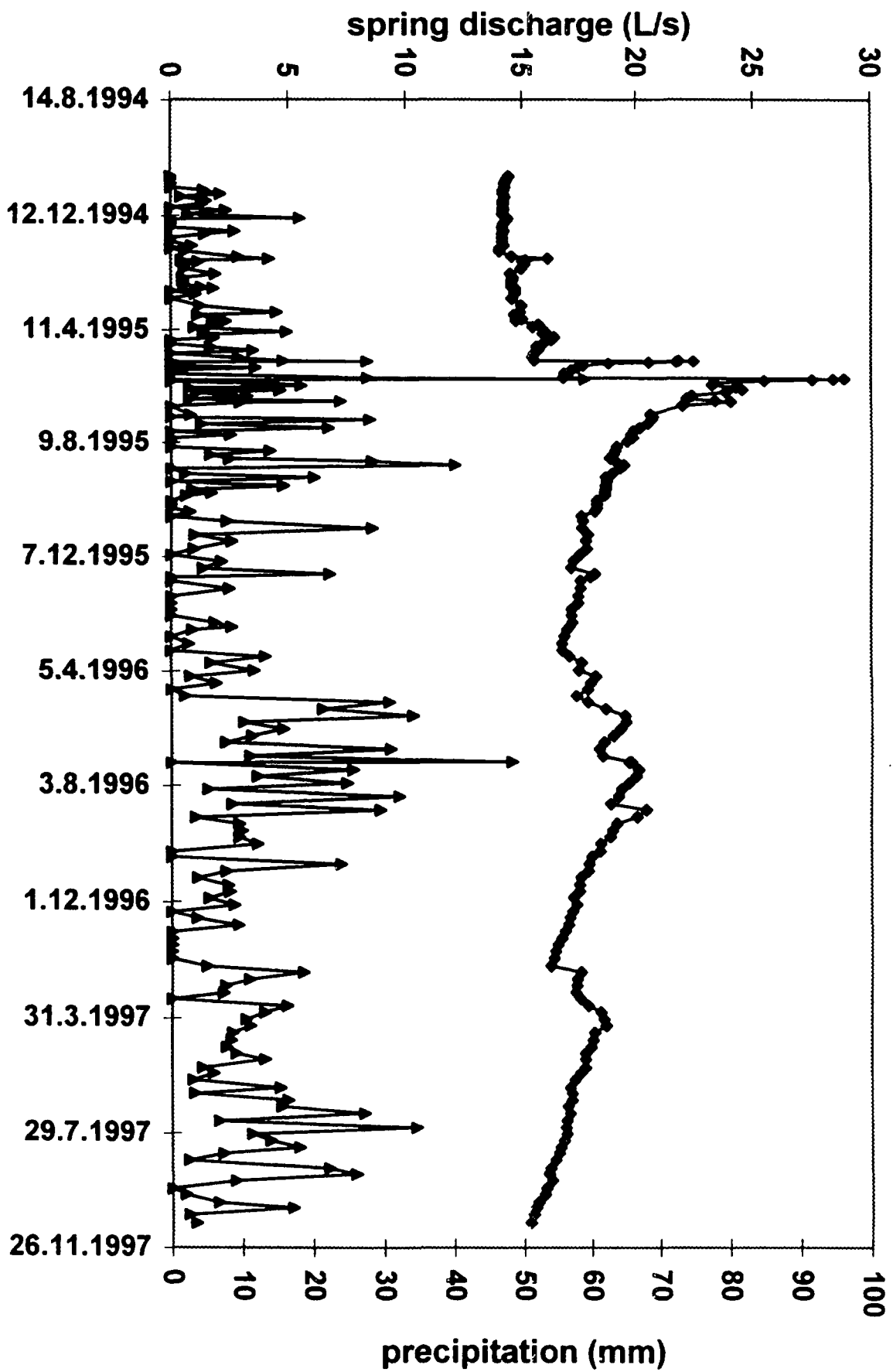
Fig. 2. Spring discharge and precipitation in the recharge area.
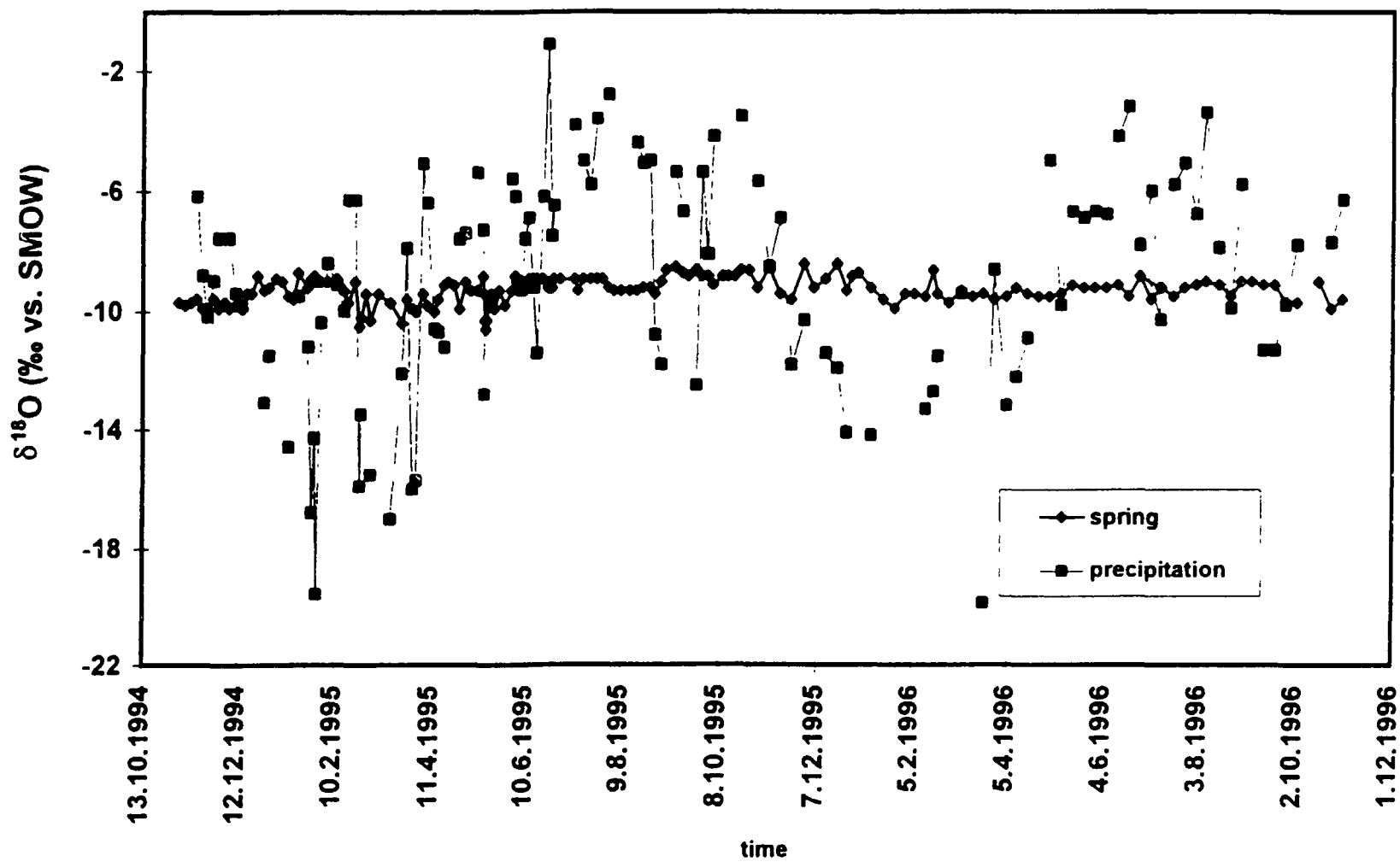
Fig. 3. d^{18}O of discharge and precipitation.

(measured at IAEA laboratories in Vienna). In the past 46 TU was measured in 1986. These data together with recently measured discharge values were used for model age calculation [5].

4.2. $\delta^{18}O$ data

The $\delta^{18}O$ records of spring discharge and precipitation are represented on Fig. 3. Direct contribution of rapidly infiltrated precipitation is low, the variation of discharge $\delta^{18}O$ values corresponds to a dumping effect of the karst volume. The primary (seasonal) variation of $\delta^{18}O$ in precipitation appears in discharge $\delta^{18}O$ values with delay from two to about eight weeks. The complete two year record enables us to evaluate some spring characteristics such as direct component of discharge, infiltration coefficient (necessary for age model calculation) or to estimate an average residence time in the system. The direct or short time component of discharge p was calculated from seasonal weighted values of precipitation and discharge using Eqs.1 and 2:

$$\delta^{18}O_{tot} = p^* \, \delta^{18}O_{prec} + (1-p)^* \, \delta^{18}O_{gw}, \qquad \delta^{18}O_{gw} = \delta^{18}O_{average} \qquad (1)$$

$$\delta = (\delta^{18}O_{tot} - \delta^{18}O_{gw})/(\delta^{18}O_{prec} - \delta^{18}O_{gw}) \qquad (2)$$

Measured values are summarized in Table I, calculated p values are presented in Table II.

The proportion of direct (short time) component of the total discharge of karstic system is low as it corresponds to the relatively low importance of direct inflow on the total karst recharge. The estimation of $\delta^{18}O_{gw}$ for all year period was calculated to be related to the seasonal p values. The value -9.35 ‰ is far from the $\delta^{18}O$ values for base flow conditions (autumn and winter 1994 ~ -9.1‰) and it reflects unusually high precipitation input in spring 1995. In the year 1995 the average discharge is mostly formed by the volume component rather than old groundwater.

The proportion of volume and the old component of the total karst discharge cannot be estimated as easily as the direct precipitation component. We do not know the infiltration in winter and summer period (so we cannot calculate the input $\delta^{18}O$ values of volume reservoir) and a roughly estimated size does not allow to precise estimate of the resulting time shift in $\delta^{18}O$ without modelling of mixing inside the reservoir. The infiltration coefficient a defined as the ratio of summer and winter infiltration $a = a_s/a_w$ can be calculated from the weighted $\delta^{18}O$ of precipitation in winter and summer period (w and s, i and j indices) and $\delta^{18}O_{gw}$ (Eq.3) [6]:

$$a = (S_w P_i d_i - d_{gw} S_w P_i)/(d_{gw} S_s P_j - S_s P_j d_j) \qquad (3)$$

The a value is a relative number i.e. a value 0.5 means twice more infiltration in winter than in summer. With values from Table 1 we can calculate a for 1995 as 0.4 and for 1996 0.3 i.e. $\delta^{18}O_{gw}$ corresponds to ratio of summer and winter precipitation 1:2.5 in 1995 and 1:3.3 in 1996. These values are quite close to the reciprocal ratio of precipitation sums in summer and winter period (see Table I), which means that the infiltrated amounts are roughly the same in winter and summer periods.

Table I: Measured $\delta^{18}O$, precipitation and discharge values and calculated weighted averages

Period	winter 95	summer 95	all 95	winter 96	s ummer 96	all 96
$\delta^{18}O_{prec}$ w.avg.(‰)	-11.34	-7.36	-8.54	-12.25	-7.52	-8.67
$\delta^{18}O_{tot}$ w.avg. (‰)	-9.51	-9.11	-9.27	-9.23	-8.95	-9.08
$SP_i d_i$	-2345	-3593.3	-5938.3	-1785.3	-3298.8	-5084.1
SP_i	206.7	488.3	695	145.7	438.7	584.4
$SQ_i d_i$ *	-1144.2	-1650.6	-2794.8	-1367	-1495.2	-2862.2
SQi *	120.2	181.2	301.4	148	167	315

* Qi are in mm, recalculated from 19l/s average discharge and 7.6 km² of recharge area

Table II: Calculated proportions of precipitation on total discharge

Period	winter 95	summer 95	all 1995	winter 96	summer 95	all 1996
p	0.11	0.08	0.1*	0.05	0.08	0.07*

* all year values calculated with the following estimation of $\delta^{18}O_{gw}$: (1995) -9.35‰ and (1996) -9.11‰

The $\delta^{18}O$ of precipitation plotted against time (Fig. 3), can be approximated by a simple sine function $\delta^{18}O_{prec} = D + A$ sin wt. Supposing that such precipitation infiltrates to „well mixed" groundwater system (an exponential model) with volume V which is discharged with a steady flow rate Q, the average residence time of infiltrated precipitation in groundwater system is T = V/Q. T can be calculated from the attenuation of the sine amplitude A of input to B of output

$$\delta^{18}O_{gw} = D + B \sin(wt+f)$$ (4)

where f is a phase shift, which is usually without any physical meaning because it is from the function definition limited to 3 months maximum. The attenuation is B/A and corresponding residence time T is calculated as [7]:

$$T = 1/2p [(B/A)^{-2} - 1]^{1/2}, \text{ by definition T is in years}$$ (5)

T values calculated from winter and all year periods are summarized in Table III. This varies between 16 (1995) and 21 months (1996). As the direct component of the total discharge has only a minor effect (about 10% in average conditions, up to 20% in the flood events), the residence time estimate represents the karst volume component and deep groundwater component together and can be used for futher estimation of component volumes as related to the total karst volume in model calculations.

Table III. Calculated karstic residence time from attentuation of $\delta^{18}O$

Period	winter95	all 1995	winter96	all 1996
Tx12 (in months)	15.3	16.7	16.4	21.2

4.3. $\delta^{15}N$ of spring nitrates

The nitrate content of the discharge varies with time within a range of about 10% (see Fig. 4). Decrease of nitrate content corresponds with abundant precipitation and can be explained as a dilution effect of direct (or short time) component of total discharge. Direct inflow of precipitation brings low nitrate content from atmospheric nitrate and infiltrated
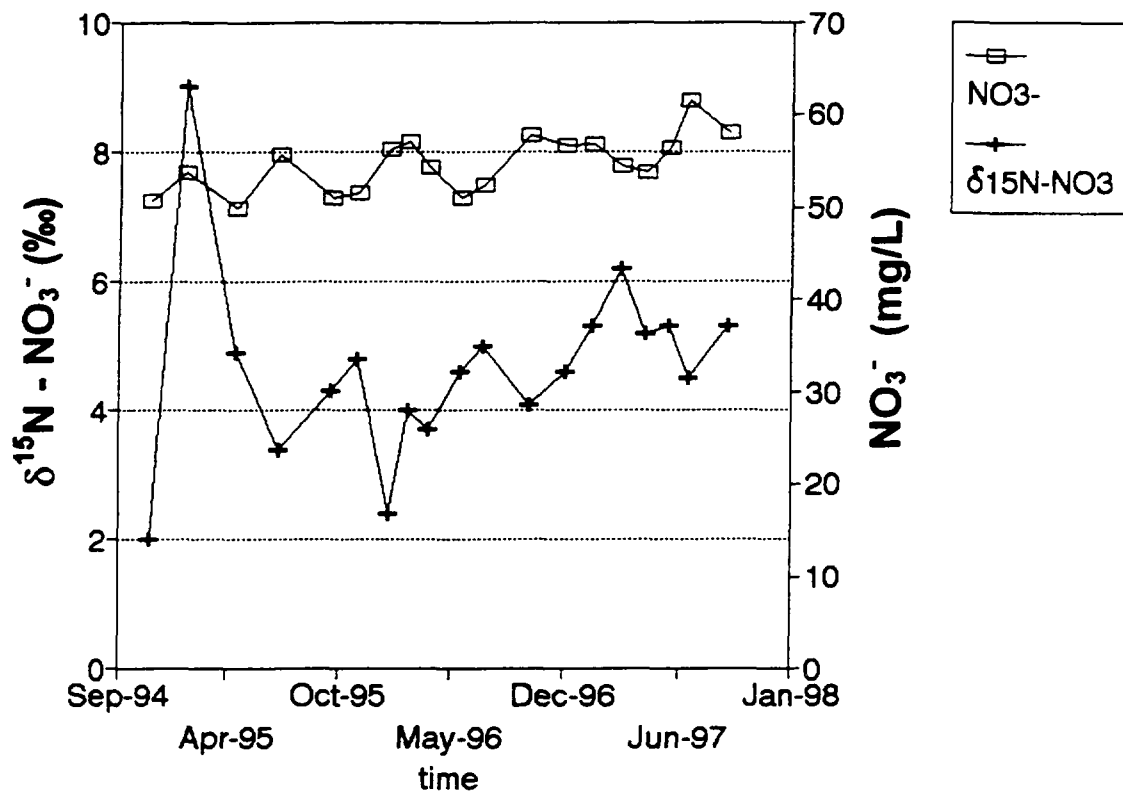
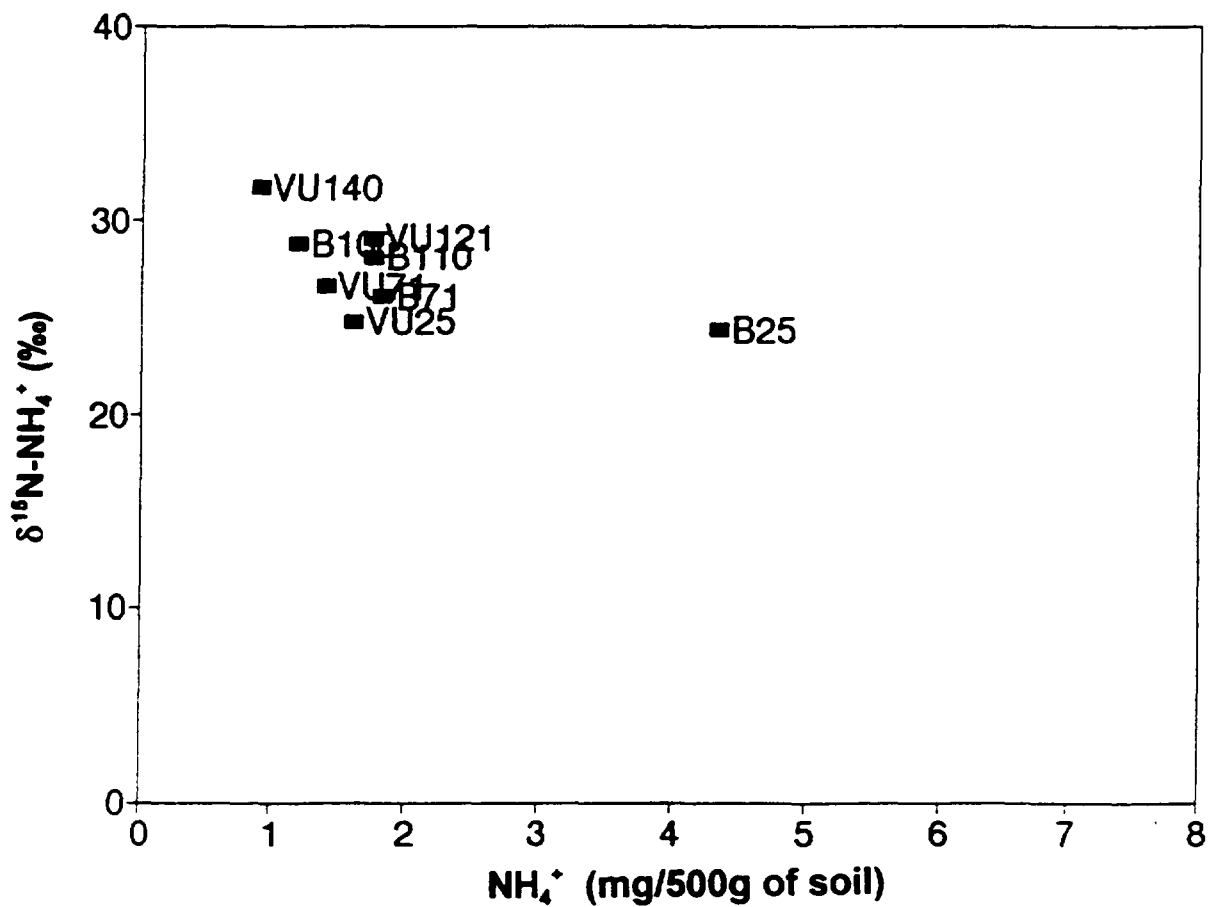Fig. 4. Nitrate content and $\delta^{15}N$ of nitrate in spring discharge.

Fig. 5. $\delta^{15}N$ of exchangeable ammonium in soil extract (B - Bubovice, VU - Vysoký Újezd, numbers correspond to sample depth in cm).

forest soil water which are both in the range of 1-2 mg of nitrate per liter. Most of the nitrate is coming from the karst volume or deep groundwater with nitrate content increasing with time. In contrast to nitrate content, the $\delta^{15}N$ of nitrates varies with time periodically (Fig. 4) from about 5 to 2‰ with one exceptional value around 10‰ in the beginning of study. Two hypotheses have been developed for explanation of $\delta^{15}N$ variation: (i) nitrate from the karst volume and deep groundwater participate with different contributions to overall discharge and both the reservoirs have different $\delta^{15}N$ (karst close to zero and deep groundwater more positive because of denitrification reactions in the aquifer), (ii) nitrate infiltrating to the karstic system has a different $\delta^{15}N$, according with applied fertilizers in the past. The areas of fertilizer application have different distances from the discharge site i.e. infiltrated waters have different travel times in the karstic system and the resulting nitrate mixture varies in $\delta^{15}N$. A deep reservoir with stable nitrate content and $\delta^{15}N$ buffers variation of the karst volume content. Both hypotheses have a weak point in the rather low variation of nitrate content i.e. we have to suppose that sources have similar nitrate content but different $\delta^{15}N$. The very positive $\delta^{15}N$ of discharged nitrate at the beginning of the study has not been completely explained. Probably it resulted from the unusually dry season 1994, with highly nitrified ammonium nitrogen accumulated in the soil and drained with the first heavy storm to the karst volume to be discharged and with delay corresponding to its travel time.

4.4. $\delta^{15}N$ in soil and other sources

To identify infiltrating nitrates soil profiles at two sites were investigated for $\delta^{15}N$ of exchangeable ammonium and nitrate in soil solutes. Profiles are located at about 2 km (site Bubovice=B) and 3.5 km (site Vysoký Újezd=VU) distance from the discharge site. Samples were taken from the Ap horizon (0-25cm), Bv1 and Bv2 horizons (25-71cm, 71-121cm) and C horizon (121-140cm). The $\delta^{15}N$ of ammonium ions is positive, in the range from 25 to 32‰, resulting from extensive fractionation by ammonia loss and following nitrification (see Fig. 5). $\delta^{15}N$ of nitrate produced from these ammonium ions is in the range from 10 to 14‰ (see Fig. 6). Such nitrate is typical for most of the horizons at the Bubovice site. Nitrate of inorganic origin with $\delta^{15}N$ around 0‰ are typical for the Vysoký Újezd site (and 110cm horizon at Bubovice) [8].

Two types of nitrates with different $\delta^{15}N$ were localized in the soils of the probable recharge area of the karst system. One type of nitrate is produced by nitrification of ammonium ions of organic origin and their $\delta^{15}N$ varies around 10‰. Other type of nitrate is the rest of the extensive application of inorganic nitrate fertilizer with $\delta^{15}N$ around 0‰. This nitrate is not changed by any denitrification. According to the agronomic record, we expect that all of the recharge area consists of parts with these two types of nitrate corresponding to fertilizer application in the past. It means that infiltrating precipitation transfer both type of nitrates into the karst volume and the resulting $\delta^{15}N$ of nitrate in discharge varies according to predominance of one of them in the volume component of the karst dicharge.

Infiltrated nitrate was also monitored in small water sources located in or close to the recharge area of the karstic system. Two of them should be mentioned because they represent nitrate infiltrating to shallow groundwater. One is a spring at Sedlec, another a well at Kozolupy (Fig. 6). The $\delta^{15}N$ of spring nitrate varies from 2 to 9 ‰ with more positive values during summer and less positive values in winter. The seasonal effect results both from the source and water mixing. At base flow conditions spring nitrate has $\delta^{15}N$ close to 2‰ which changes to negative or positive values according to inorganic or organic nitrate as they

48
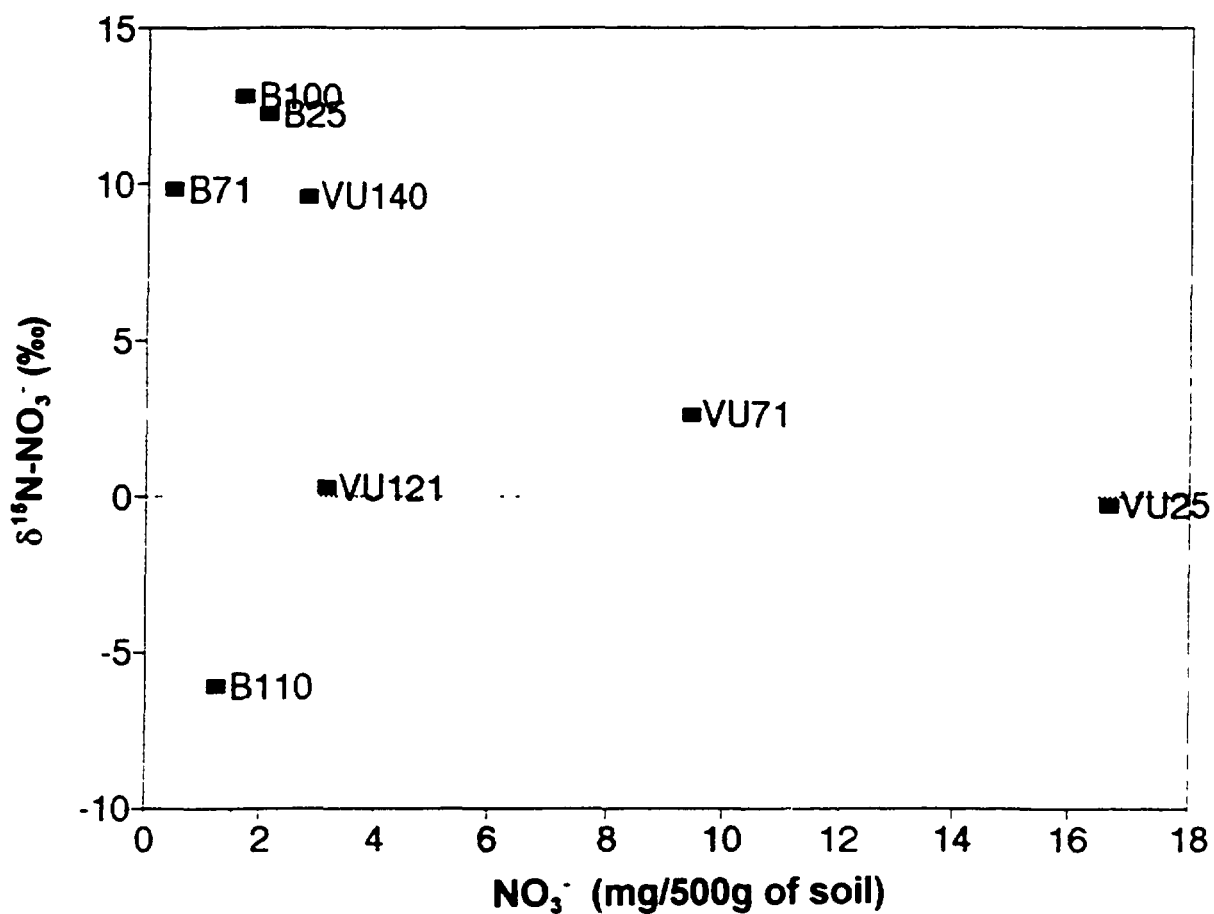
Fig. 6. $\delta^{15}N$ of nitrate in soil extract (B - Bubovice, VU - Vysoký Újezd, numbers correspond to sample depth in cm).
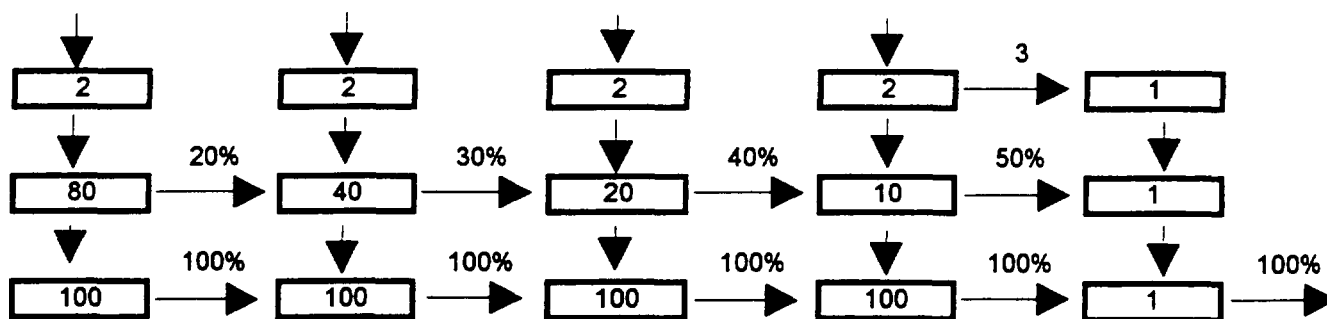
Fig.7. Cell combination used in model calculation. Numbers are volumes of cells (two units correspond to one day average discharge).
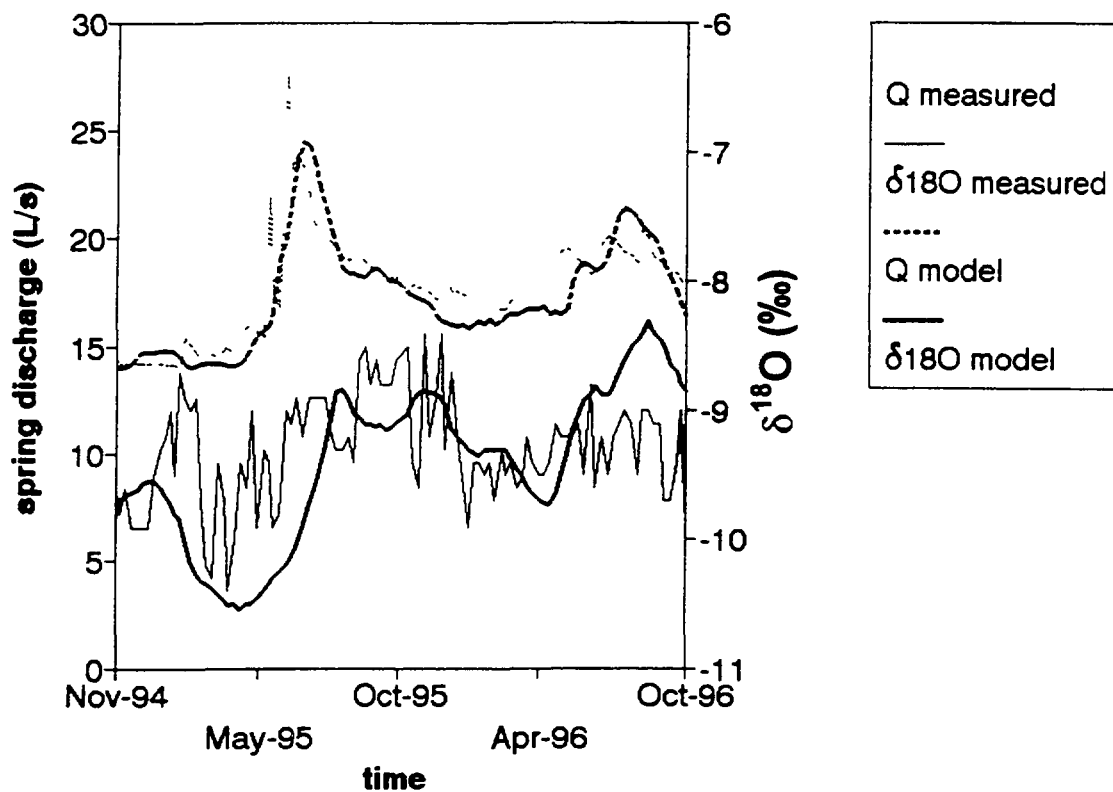
Fig.8. Observed and calculated discharge and $\delta^{18}O$ of the spring.
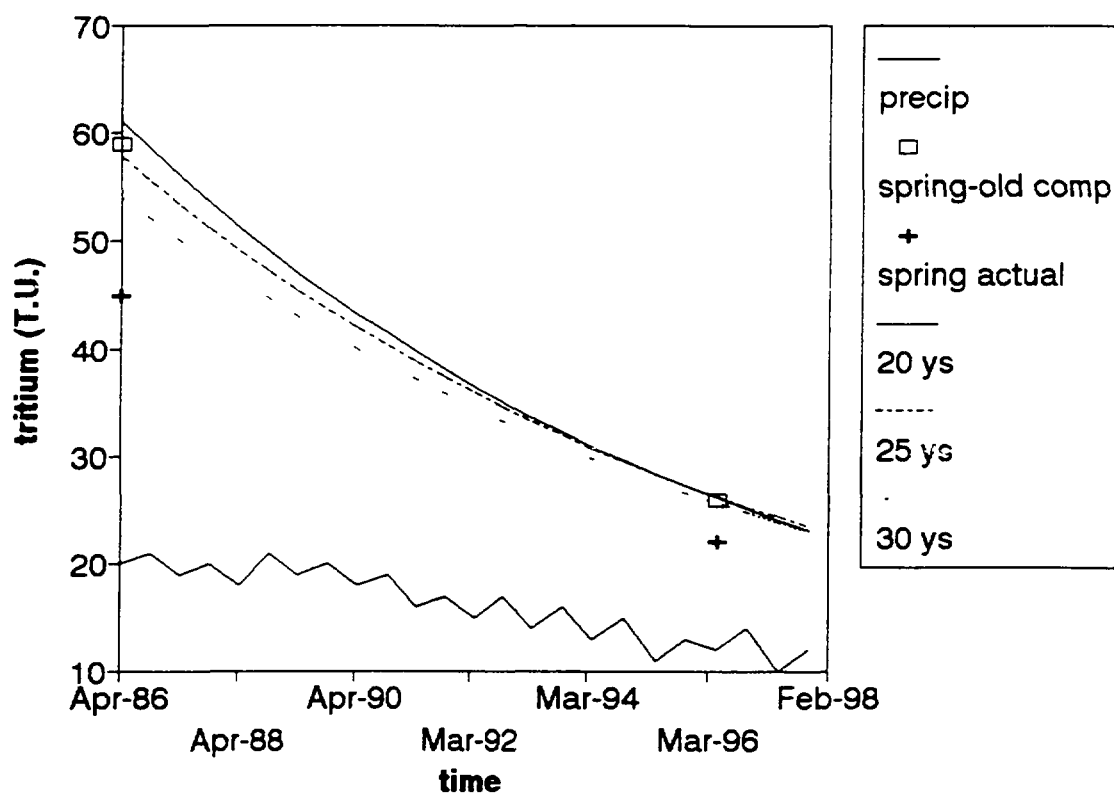
Fig.9. Observed and fitted tritium concentrations for old discharge component
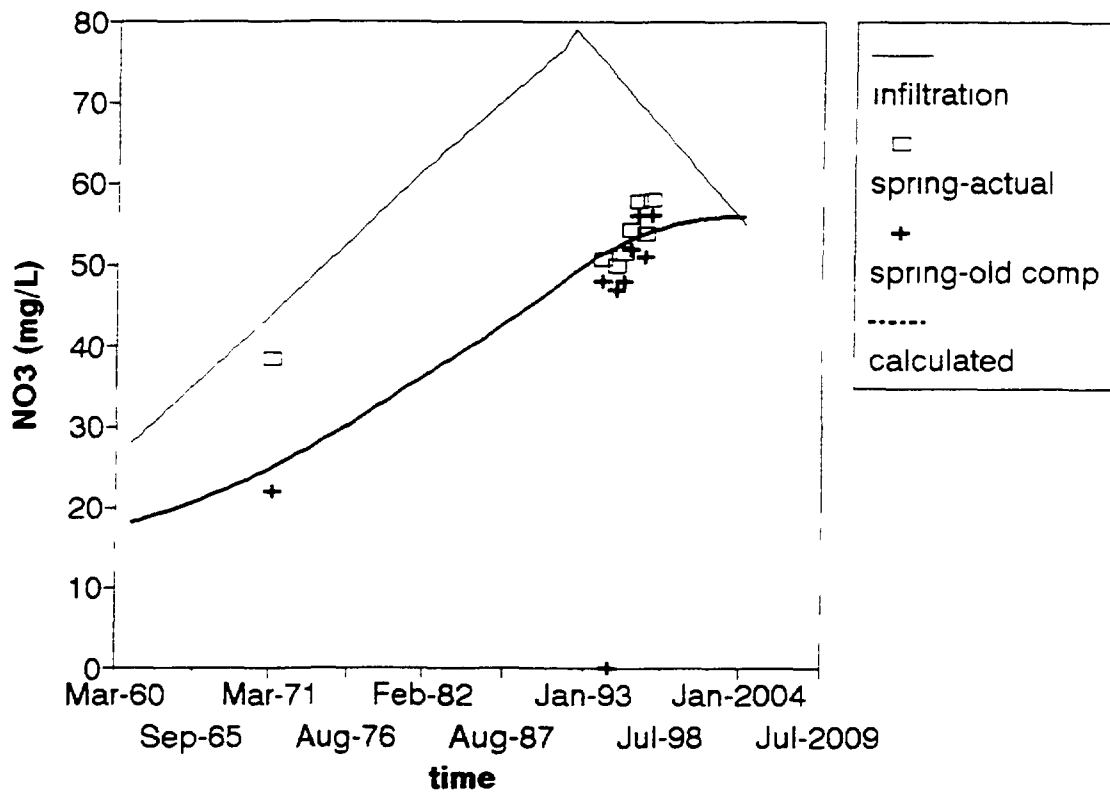
Fig.10. Calculated nitrate content of infiltrated water and old discharge component.
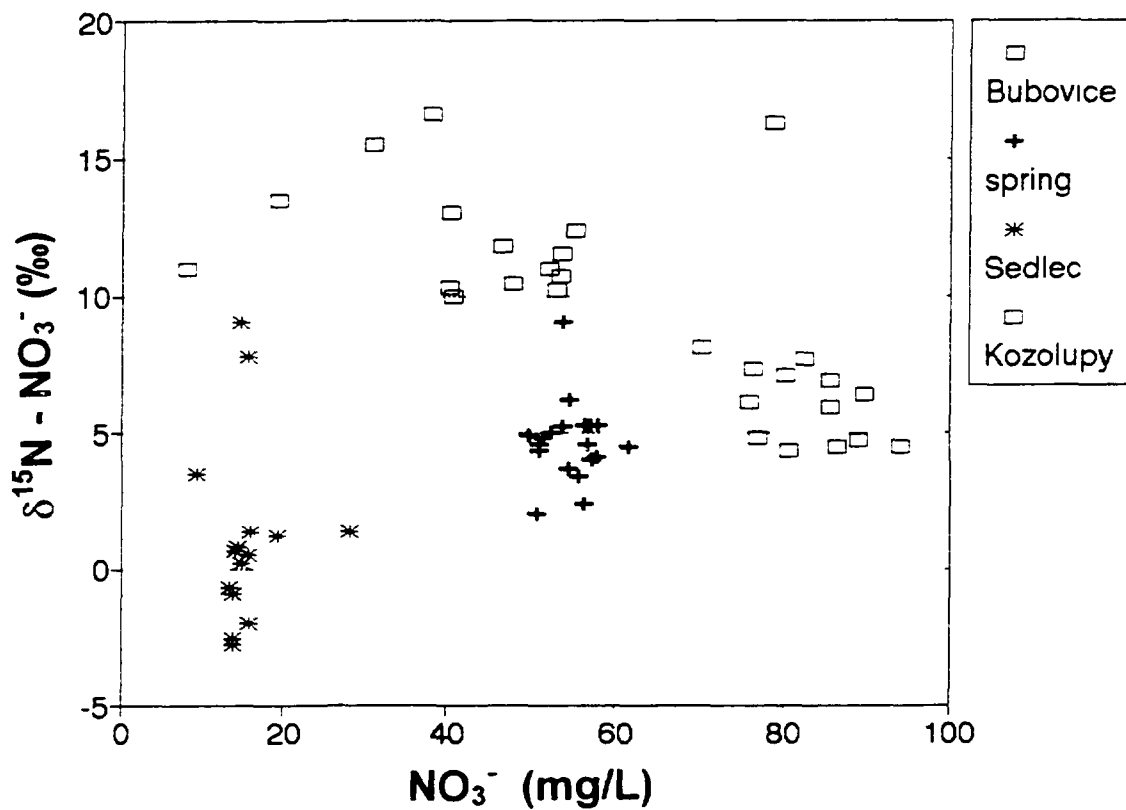
Fig.11. Plot of $\delta^{15}N$ versus nitrate content for all monitored water sources.
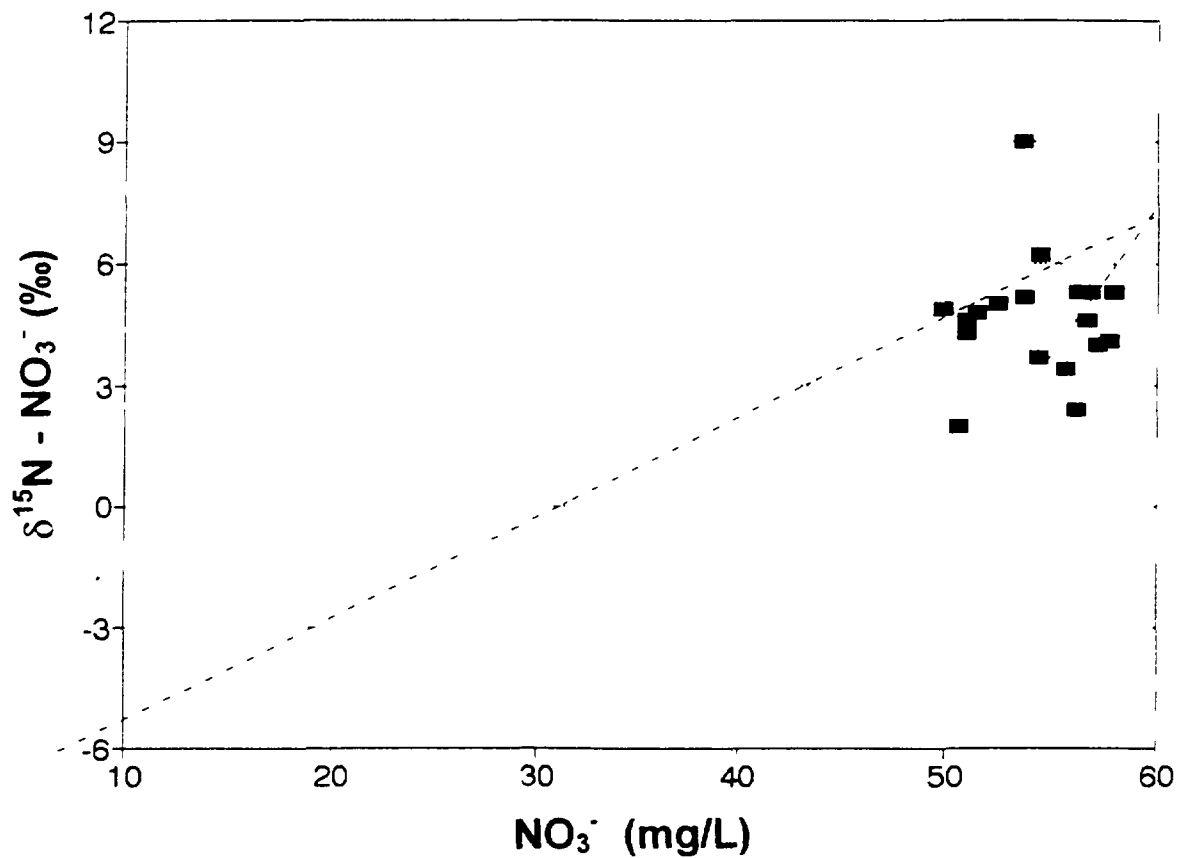
Fig 12 Plot of $\delta^{15}N$ versus nitrate content for the spring.
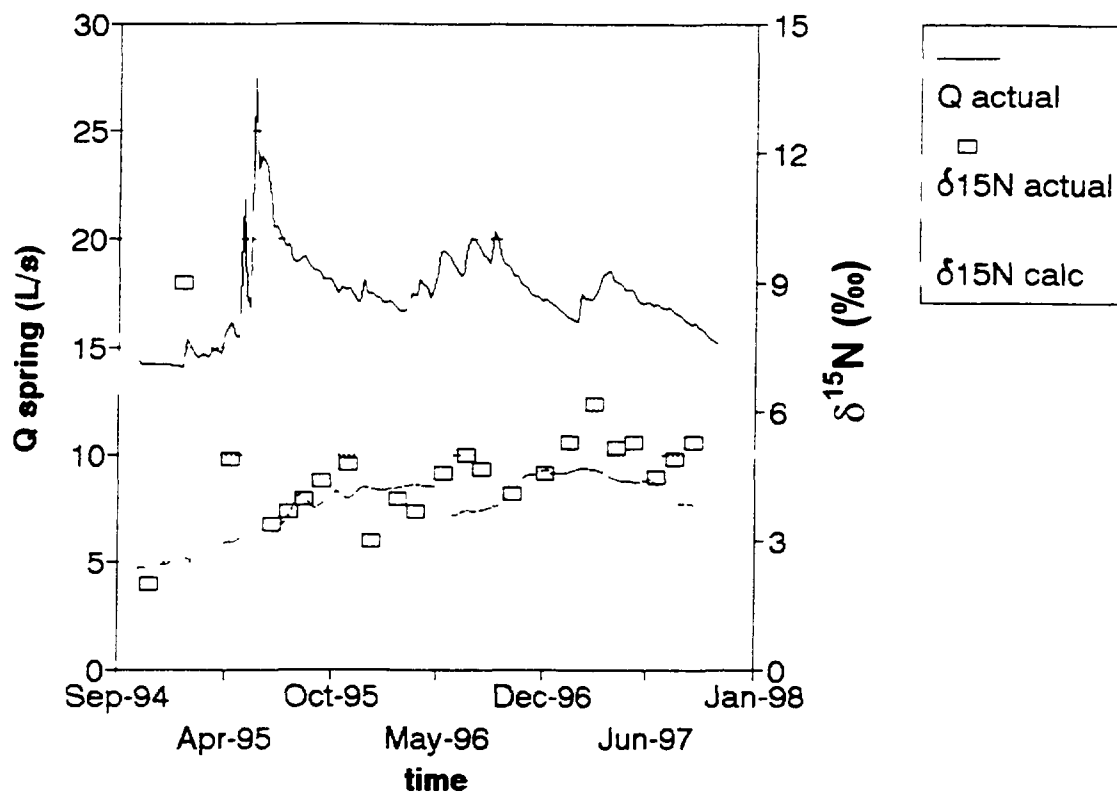
Fig 13 Observed and calculated $\delta^{15}N$ of nitrate in the spring. The same model parameters were used as for $\delta^{18}O$ calculation.

participate in discharge. Average nitrate content is about 15 mg/L with low contamination from agriculture activities (the spring is located outside the fields). The Kozolupy well collects shallow infiltrated water from an agricultural area close to the Bubovice soil profile. Nitrate of organic origin dominates in runoff and the nitrate content is even higher than in the karstic spring.

4.5. System modelling

A compartmental (mixing cell) model [5] was used for discharge and ^{18}O modelling. Cell mixing models proved to be usefull in the modelling of karstic systems [5, 10]. Their advantage is optimalization of both variables, i.e., discharge flow and ^{18}O using a single parameter of cell size (transit time). The program MODEL written by Y.Yurtsever [11] was used. An estimate of cell sizes is based on observed values recalculated for the average discharge of the spring (Fig.7). In the first row, the cell combination represents shallow soil layer keeping recharge water for one day only. The last member contributes as a direct contribution to discharge. In the second row, the horizontal cell combination can be considered as a relatively fast flow through well-connected karstified fractures which partially supply spring discharge and partially infiltrate to the deeper reservoir. In the third row, the horizontal cell combination resembles slow flow from a deeper structure. The total volume of the cells is close to the volume estimated from an attenuation of ^{18}O variation (Eqs. 4 and 5). Calculated values fit the observed variations in discharge and ^{18}O with exception of fast changes within one or two sampling time intervals (Fig.8).

4.6. Turnover time of the deep ground water component

The conceptual model developed for spring discharge and ^{18}O variations cannot be easily used for estimation of turnover time (mean residence time) of the groundwater reservoir. Only a few tritium data from a relatively short period are available and model volume size is too small to give a reasonable estimation of an old component of spring discharge. From the mass balance of discharge, it is estimated that the contribution of old water component is about 60 or 70 % of total discharge. The rest is recent precipitation (direct and fast components). Assuming 60% contribution of an old component, we can estimate its tritium concentration from the measured tritium content of precipitation and discharge. These values together with the value measured ten years ago were used for groundwater age estimation. The input tritium function was calculated from the Vienna record (which is nearly identical with the tritium record measured abou 60 km from the studied area [12]). The same infiltrated amount was assumed during winter and summer periods. The tritium distribution was calculated for groundwater reservoir sizes corresponding to residence time variation of from twenty to thirty years (Fig.9). About twenty two years residence time gives the best fit.

4.7. Nitrate content prediction

A substantial decrease of the applied fertilizers during the most recent years (down to about 35% of dose applied before 1990) enables the prediction of changes in nitrate content of the spring water. With an estimation of groundwater residence time, we can calculate the predicted nitrate content in ground water. For this an input function of infiltrated nitrate was constructed based on both historical and recent data (Fig.10). Using the same type calculation as for tritium we can construct a future development of nitrate content of ground water component. According to this model the nitrate content of the spring will be stabilized in the next six or seven years and will start to decrease in about ten years. As expected, any

remediation of the quality of the groundwater is quite slow even after such a dramatic decrease in applied fertilizers.

4.8.   Modelling of ^{15}N in spring

The conceptual model of system flow may be further used for calculation of δ^{15}N in discharge. Inputs are not so well defined as in the case of ^{18}O in precipitation (more heterogenic) and the time interval is longer. To be sure about the δ^{15}N range of possible infiltrating inputs into the karstic system, we compared the nitrate content and δ^{15}N of the spring and all other water sources in the area (Fig.11). From the plot of δ^{15}N versus concentration we can identify possible sources (if measured) contributing to spring discharge. Theoretically the δ^{15}N of the spring should be combined from water monitored at Sedlec and Kozolupy. A dilution effect of direct atmospheric input can be estimated from measured precipitation samples, in which δ^{15}N varies in the range from -2 to -10‰ and nitrate content from 5 to 10 mg/L, or from the extrapolation of δ^{15}N versus concentration plot of the spring (Fig.12). From the latter, two types of „mixing" lines were identified with end members (marginal points) corresponding to: -6‰ and 8 mg/L for an average atmospheric input, 2‰ and 52 mg/L for ground water component, and 7‰ and 60 mg/L for recently infiltrating water. It is difficult to reconstruct their time variation. It seems to be a crucial problem in the case of modelling of δ^{15}N in the spring discharge. Using Sedlec and Kozolupy data together with an average atmospheric input as the actual input functions for the model we obtain δ^{15}N variation which is in the range of observed values but the calculated period is nearly twice as long as the actual period (Fig.13).

5.   DISCUSSION

The parameters of the conceptual model of flow and ^{18}O in discharge were derived under simplified assumptions (constant volume of the system, limited number of inputs and mixing cells) and may serve as a starting point for further study. The actual system obviously changed its volume during the study as can be seen from different values of base flow at the beginning and after the first and second years of observation. Including volume changes into the model is not possible and can be substituted by modification of input function only, which would mean an a posteriori change of actual data. Calculated discharge and its δ^{18}O are assumed to be continually mixed before output from the system. Actual discharge is mixed in large horizontal channels close to the output and discharged water is inhomogenic in composition and flow dynamics. Moreover, the unsaturated zone is formed by large fissures in the vertical direction which are discontinous in flow according to infiltration. Following an abundant precipitation event fissures are filled with fast infiltration because of shallow soil zone and develop a hydrostatic pressure against groundwater flow to supress it. This is obvious from the δ^{18}O record of discharge which varies within the measured interval from the actual value to some „bias" value which is nearly constant. The process is repeated regularly after sufficiently high precipitation. In the model this was approximated by a „threshhold" value, but the flow is not pulsing as an actual discharge would.

An estimate of ground water turnover time is an important parameter for any type of calculation of future nitrate content in the spring. The calculated value is very probably an overestimation because of existence of stagnant zones which contribute to tritium concentration by diffusion but do not contribute to mobile water. Nitrate calculation will not be affected if nitrate is distributed similarly to tritium.

54

The conceptual model used which was acceptable for flow and $\delta^{18}O$ modelling fails in the case of $\delta^{15}N$ of dissolved nitrate. It may result from unknown inhomogenities either of isotopic composition of the infiltrated nitrate, or from different mobility of water and dissolved component. Any adsorption effects can be excluded in the case of nitrate, as well as additional reactions changing the isotope composition (denitrification) which is highly unlikely in the aerated unsaturated zone. Different mobility of dissolved nitrate and water can occur by delay of dissolved tracer in a microporous structure when mobile water is transported through fractures or karstic channels, or during partial saturation of the soil zone. The surface of karstic rocks below the soil layer is deeply weathered and very complex morphologically. Some sites are covered by a rather shallow soil layer, some sites develop deep pockets with high storage capacity for dissolved tracers which are mobilized only with infiltrating water. Abundant precipitation events which saturated even deep pockets transport substantially more nitrate than small events. Considering a short period of $\delta^{15}N$ variation in discharge water, such „flush" of nitrate inputs in the karstic system seem to be more probable than delayed diffusive transport.

6.   SUMMARY

Data from flow dynamics, ^{18}O and tritium were sufficient for estimation of volume of the karstic system and residence times of three contributions (direct infiltration, fast and old component) of spring discharge. Estimated turnover time of the old component (about twenty two years) could be used for calculation of spring nitrate content in future. Sources of nitrate pollution were identified from $\delta^{15}N$ in soil solutes at sites with different agronomic records (sequential use of organic and inorganic fertilizers). Spring discharge nitrate is formed from an atmospheric source (an average nitrate content of 8mg/L and $\delta^{15}N$ -6‰) and two groundwater components with nitrate content from 50 to 60 mg/L and $\delta^{15}N$ values from 2 to 7‰. Atmospheric nitrate has a diluting effect only in the range of 10% maximum. The contribution of groundwater components varies in time more frequently than can be described by the model developed for flow dynamics and ^{18}O. It may result from different mechanism of water and nitrate transport within the unsaturated zone.

ACKNOWLEDGEMENTS

REFERENCES

[1] Skoøepa J. , Vèíslová B., Permeability of rocks and chemical composition of groundwaters of Silurian and Devonian of the Barrandian area, J.Geological Sci., Hydrogeology and Engineering Geology, Vol.12 (1975), 49-65 (in Czech).

[2] Buzek F. A rapid procedure for preparing oxygen-18 determination in water samples. Isotopenpraxis, 19 (1984), 70-72.

[3] Žák K., Kadlecová R., Kadlec J.,Kolèava M., The response of karstic springs in the Svatý Jan pod Skalou (Bohemian Karst, Czech Republic) to large precipitation events during May-June 1995 and a new periodic ponor in the valley of Propadlé vody , Èeský kras Vol.22 (1996), 41-47 (in Czech).

[4] Shevenell L. Analysis of well hydrographs in a karst aquifer: estimates of specifi yields and continuum transmissivities. J.Hydrol.174 (1996), 331-355.

[5] Yurtsever Y. and L.Araguas Araguas, Environmental isotope applications in hydrology: an overview of the IAEA's activities, experiences, and prospects. In: Peters N.E. et al. (Eds.) Tracers in Hydrology. IAHS Publ.215 (1983).

[6] Grabczak J., Maloszewski P., Rozanski K., Zuber A., „ Estimation of the Tritium Input Function with the Aid of Stable Isotopes", Catena 11 (1984), 105-114.

[7] Siegenthaler U., Sauerstoff-18, Deuterium und Tritium im Wasserkreislauf - Beitrage zu Messtechnik. Modellrechnung und Anwendungen, Ph.D.Thesis, University of Berne, Berne (1971)

[8] Hübner H. ,Isotope effects of nitrogen in the soil and biosphere. In: Fritz P. and Fontes J.C. (Eds.) Handbook of Environmental Isotope Geochemistry, Vol.2b. The Terrestrial Environment, pp. 361-425.Elsevier, Amsterdam (1986).

[9] Buzek F., Hanzlik J., Hruby M. and Tryzna P. Evaluation of the runoff components on the slope of an open-cast mine by means of environmental isotopes ^{18}O and T. J. Hydrol.127 (1991), 23-36.

[10] Maloszewski P. and Zuber A. Lumped parameter models for interpretation of environmental tracer data. in: Manual on mathematical models in isotope hydrology. IAEA-TECDOC-910 (1996), pp.9-59.

[11] Yurtsever Y. Models for tracer data analysis, in: Guidebook on Nuclear Techniques in Hydrology, Tech.Rep.Ser.91. (1983), IAEA Vienna.

NITRATE POLLUTION OF GROUNDWATER AROUND
A SEWAGE STABILIZATION POND, KERALA INDIA

XA9848327

K. VASU. A. SHAHUL HAMEED, K.T. VELAYUDHAN,
S. JACOB, M. MATHEW
Nuclear Hydrology Division,
Centre for Water Resources Development and Management,
Kerala, India

Abstract- *An investigation was carried out to determine the influence of the sewage stabilisation pond of the Calicut Medical College on the quality of water in the open dug wells which are situated in and around the stabilisation pond. The study revealed that domestic wells are becoming increasingly polluted with nitrate inspite of heavy rainfall in the region. The level of nitrate in the observation wells was found to be vary widely during different seasons: from 1.1 to 49.8, 0.7 to 19.5 and from 2.1 to 38.3 mg/l during pre-monsoon, monsoon and post-monsoon periods, respectively. One well had nitrate exceeding the maximum permissible limit specified for drinking water by Bureau of Indian Standards. The problem is more pronounced in summer when the level of nitrate is observed to be on the higher side.*

1. INTRODUCTION

Groundwater, which is generally thought to be well protected from what is happening at the surface of the earth is becoming increasingly contaminated by many pollutants. Water carries the pollutants when put to use for domestic, agricultural and industrial purposes. Urban areas with a high degree of industrial and domestic activity, together with agricultural operations in their immediate surroundings, have industrial effluents, domestic sewage and agricultural wastes discharged into streams or disposed on the land, thus encouraging the migration of pollutants to the underlying groundwater during recharge. Nitrate appears to be one of the major pollutants reaching groundwater from all the above mentioned activities. It is of major concern particularly for the health of infants [1,2].

In India, it is estimated that 20 to 50% of the wells in areas of high population density produce water with nitrate above 50 mg/l, thus causing health hazards [3,4]. As nitrate is soluble in water, its movement is fast in soil. Even soil rich in clay, nitrate is not greatly attenuated compared to water since the similarity of electrical charge between the clay fraction of the soil and the nitrate prevents its adsorption on to the clay surfaces.

Groundwater is the major source of drinking water in Kerala. The region has a population density of 750 persons per square kilometre and has about 250 open dug wells per square kilometre. Urban sewage, industrial effluents and agricultural residues are the major sources of pollutants of groundwater in the region. An investigation was carried out to determine the influence of the sewage stabilisation pond of a medical college and hospitals on the quality of groundwater sources.

2. DESCRIPTION OF THE STUDY AREA

2.1 General location

The study area falls within the Calicut Medical College Campus where the sewage stabilisation pond is situated. The site lies between 75° 49' and 75° 53' East longitude and, between 11° 16' and 11° 18' North latitude (Fig 1). It is a high rainfall region with humid tropical climate. The annual precipitation is around 3500 mm and the temperature varies from 22 to 33° C. More than 75% of the annual rainfall falls during the south-west monsoon months of June to August and about 15% during the north-east monsoon months of September to November. The rest of the precipitation occurs as summer or pre-monsoon showers during the months of December to May.
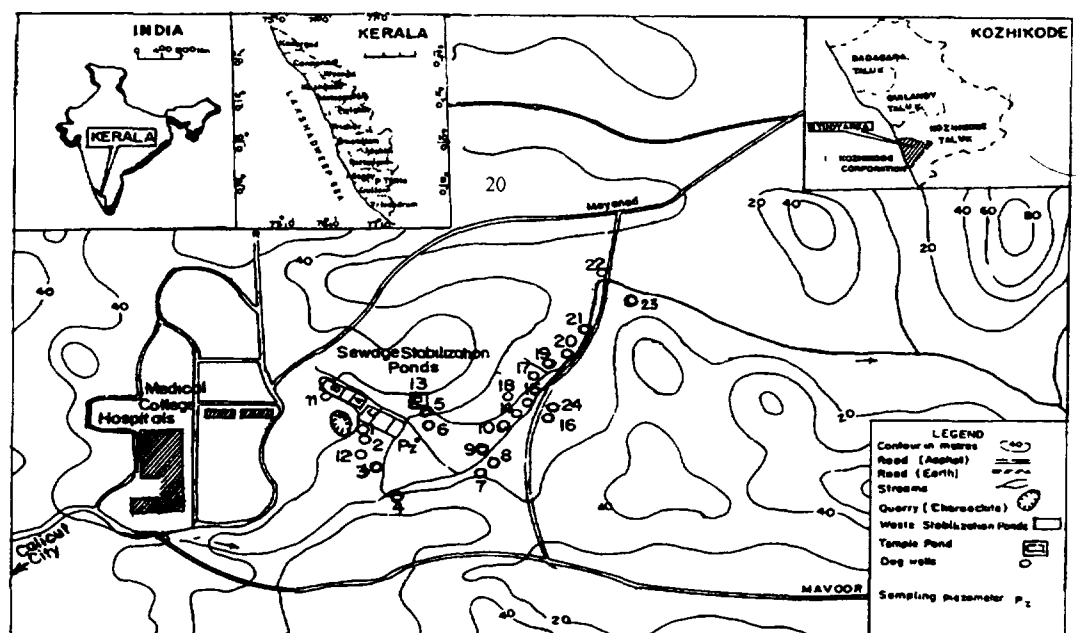
Fig. 1 Study area showing the source of pollutants and observation wells

The area is a part of high grade granulitic terrain of Precambrian age. It is covered with lateritic soil and crystalline bedrock which is exposed at a few places. The bedrock in the area is gneissic charnockites and exhibits medium grained granulitic texture. Observations made on the exposed bedrock show two sets of vertical and one set of oblique joints trending N 85° E and N 15° W, respectively. The mineral foliation in the rock trends NW-SE and has a dip of 80° E. The crystalline rocks are intensely deformed during more than one phase of orogeny. The overburden in the area is laterite formed by the weathering of crystalline basement rocks. The laterites are of residual and fairly mature type. The overburden thickness above the basement rocks varies from place to place owing to the irregular topography. On an average, it is about 9 m as observed from the existing open dug wells.

The study area forms part of the midlands region of Kerala with elevation between 7 and 75 m above MSL. The terrain is undulating in nature with gently sloping residual hills separated by valley fills. The sewage stabilisation pond is situated on the slope of a hillock and at the side of a seasonal stream course.

3. METHODOLOGY

Twenty four water samples comprising of 23 open dug wells and one from the pond in the area of investigation were collected to study the groundwater quality. Two samples were drawn from the sewage stabilisation pond to assess and quantify the different pollutants. Soil samples were drawn from the study site at different depths up to 1 m to determine their physical and physico-chemical properties. A suction type multilevel point sampler was installed 25 m away from the sewage stabilisation pond. For this, a borehole was drilled at the site to a depth of 10 m. A casing pipe made of PVC, having an outer diameter of 110 mm and holes of 4 mm made at regular intervals of 1 m was lowered. In order to draw water samples at different depths, nylon tubes of 4 mm OD were directly connected to the main pipe at the openings. The space between the soil and the outer surface of the casing pipe was filled with sand and the openings in the pipes were covered with nylon filter material to prevent the entry of sand and other solid soil particles into the nylon sampling tubes (Fig 2). Water samples were drawn at 1 m depth interval from the multilevel point sampler.

The effluents and water samples drawn from the observation wells during pre-monsoon, monsoon and post-monsoon periods and those collected at different depths from the multilevel point sampler were analysed for their chemistry. The analyses of their physico-chemical properties were according to methods reported in literature [6,7].

4. RESULTS AND DISCUSSION

4.1 Soils of the area

The area is underlain by the laterite formation which is separated from the basement rocks by a lithomarge zone (clay zone above the bedrock). The soils are red laterite type containing a high amount of gravels. Its clay content increases with depth. The soils in the upper valley portions are well-drained and are reddish brown in colour. In the middle and lower slopes, the water table is shallow, with poor drainage and the soils dry out less frequently. This is reflected in increasing degree of hydration of iron. These soils have brownish yellow colour. The lithomarge clay in the valley portion where the piezometers are located has an average thickness of four metres which is much higher than the clay horizons in the slopes.

The soil chemistry indicates that the soil at the site of the investigation is fairly rich in plant nutrients such as nitrogen, phosphorus and potassium. The influence of the sewage stabilisation pond on the nutrient level of soil cannot be ruled out. Elements like nitrogen, phosphorus and potassium are high compared to local soils.

4.2 Sewage stabilisation pond as a potential source of nitrate pollution

Different forms of nitrogen arise from the sewage stabilisation ponds. Ammoniacal, nitrate and nitrite are the most important forms of nitrogen expected. Due to high microbiological and biochemical reactions normally expected in a sewage stabilisation pond, many other intermediate organic forms of nitrogen such as amines and amides may also be present in appreciable quantities. However, these forms of nitrogen have little mobility in the soil unless they are biochemically and microbiologically converted into simpler oxidised inorganic forms of nitrogen. Stabilisation of the sewage ensures the conversion of organically bound nitrogen into the mobile form.

Fig. 2 Suction type multilevel point sampler for sampling groundwater from different depths.

Fig 3: Groundwater table contours and flow direction in the area of investigation

TABLE I. Physico-chemical properties of a) a representative soil of the region and b) soils surrounding the stabilisation pond.

a) a representative soil of the region

Sl No	Depth (cm)	pH	Organic carbon %	N %	P(P$_2$O$_5$) %	K(K$_2$O) %	Sand %	Silt %	Clay %
1	0-30	6 5	0 52	0 05	0 05	0 16	43 54	19 61	31 68

b) soils surrounding the stabilisation pond

Sl No	Depth (cm)	pH	EC	Organic Carbon %	N %	P (P$_2$O$_5$)%	K (K$_2$0) %	Sand %	Silt %	Clay %
1	0-30	4 5	90.22	1 00	0 10	0 18	0 16	49 8	22 8	27 2
2	30-60	4 5	67.88	0 83	0 09	0 16	0 17	44 8	22 0	30 6
3	60-90	4 5	60 12	0 63	0 06	0 14	0 16	36 0	25 0	36 6
4	90-120	4 4	81 51	0 61	0 07	0 14	0 16	37 3	23 4	37 2

Table II. Chemistry of effluent in the sewage stabilisation pond

Period	pH	EC	Cl	SO$_4$	NO$_3$	PO$_4$	F	Ca	Mg	Fe
Pre monsoon 1995	6.6	550	55.7	10 2	204	5 4	0.7	13.8	6 7	0.5
Monsoon 1995	7 8	671	45.0	20.0	168	6 4	0 6	11.2	6 6	0.4

All parameters except pH and EC are expressed in mg/1
pH in pH units and EC in µScm ^{1}

The sewage stabilisation pond receives as much as 50,000 litres/day of effluents from the medical college and the attached hospitals. The effluent comprises mostly of wastes of organic nature, human excreta, washings, residues of drugs and pharmaceuticals. The chemistry of the effluents indicates that except for nitrate, all other species like chloride and sulphate are present at very low concentrations. The nitrogen level found in the sewage stabilisation pond is of the order of 204 and 168 mg/1 during the summer and monsoon periods, respectively. The nitrogen level is comparatively less during the rainy days.

4.3 Groundwater condition in the area and nitrate pollution in the observation wells

The groundwater in the area occurs under unconfined conditions. Most of the dug wells extend to the lithomarge zone. Some of the wells sited on the upper hill slopes have encountered hard rock. The depth of wells ranges from 5.5 to 10 m on upper hill slopes and between 1.3 and 3.5 m in valley bottoms. There is a high intra and inter seasonal fluctuation of water table in the upper slopes of hills, but in the valley bottoms, the fluctuation is considerably less. The depth to water level is between 1.8 and 8.7 m on the hill slopes and, between 0.05 and 2 m in the lower valley areas. The maximum water level rise in the aquifers is observed during the high rainfall months of July and August, whereas the lowest water levels are observed in the late summer months of April and May.

Figure 3 shows the general groundwater flow pattern in the study area. The groundwater flow is from the west, north and south hill slopes with respect to the stabilisation pond It discharges into the central valley then drains to the north eastern direction which is the principal direction of groundwater flow in the area. The northwest part of the area has a major source of groundwater The waste stabilisation pond is situated on the upper valley slope in the west where groundwater flow is towards south-west and south-east directions, finally draining towards north-east. The rock exposure near the stabilisation pond dips in southeast direction which may be the reason why the flow lines in the sewage stabilisation pond area deflect in the same direction near the rock exposure

The spacing between the groundwater table contours in the lower area near the piezometer sites is wide which indicates that the hydraulic conductivity of the aquifer in the valley bottom is low This observation is consistent with the fact that the thickness of lithomarge clays which have a low hydraulic conductivity is more in the valley bottoms than in the hill slopes The

twenty three open dug wells selected for the study of pollution from nitrate showed that there are 7 to 12 wells with nitrate of appreciable quantity during different seasons of observation. One of the wells (No.3) has nitrate concentration of 50mg/l during summer, which is exceeding the maximum permissible limit of 45 mg/l prescribed for drinking water [5]. In most of the wells, nitrate level appeared to be above 10 mg/l during pre- and post- monsoon seasons, showing that they are susceptible to nitrate pollution. However, during the monsoon period, all the observation wells have nitrate less than 20 mg/l (Table III). The temple pond (No.13)is not used for drinking.

4.4 Extent of nitrate pollution in the area of investigation

The extent of pollution is shown in Fig.4. Out of all the observation wells, 48% have nitrate less than 10 mg/l during the pre monsoon period. This increased to 70% during the monsoon period but decreased to 61% during the post-monsoon period. A nitrate range of 10-25 mg/l was observed in about 39, 30 and 26% of the observation wells during pre-monsoon, monsoon and post-monsoon seasons, respectively. 13% of the wells have nitrate above 25mg/l during the pre- and post- monsoon seasons. These wells have nitrate exceeding 50% of the maximum permissible limit specified for drinking water by the Bureau of Indian Standards.

TABLE III. GENERAL QUALITY OF WATER IN THE OBSERVATION WELLS DURING DIFFERENT SEASONS (1994-95)

Well No.	Pre-monsoon					Monsoon					Post-monsoon				
	pH	EC	Cl	SO$_4$	NO$_3$	pH	EC	Cl	SO$_4$	NO$_3$	pH	EC	Cl	SO$_4$	NO$_3$
1.	6.2	80	13.0	1.0	5.5	7.7	128	17.0	2.0	14.2	6.6	59	12.0	3.0	5.1
2.	6.6	105	18.5	ND	11.0	7.8	150	19.0	1.0	14.2	7.0	85	20.0	1.3	10.6
3.	5.0	140	24.5	ND	49.8	5.4	120	17.0	ND	17.7	6.2	90	18.0	0.5	38.3
4.	5.4	85	20.5	ND	21.0	5.6	104	18.0	1.0	4.4	6.7	67	18.0	6.0	13.7
5.	5.7	110	20.5	0.8	27.3	5.8	150	24.0	2.0	8.8	5.7	95	23.0	3.0	28.6
6.	6.0	175	36.5	3.3	25.8	5.9	204	29.0	5.0	16.8	6.6	130	30.0	6.5	9.0
7.	5.4	60	29.5	ND	17.1	6.8	92	16.0	0.5	9.7	6.6	55	16.0	0.8	18.8
8.	5.6	74	17.0	0.5	17.7	7.0	104	18.0	1.0	14.2	7.0	65	17.0	1.8	13.5
9.	6.7	230	34.0	1.0	8.4	7.4	244	29.0	4.0	8.8	7.3	235	20.0	9.0	4.9
10.	6.7	250	34.5	2.5	24.4	7.7	281	29.0	6.0	6.6	7.2	160	27.0	6.6	8.1
11.	6.0	93	21.5	ND	12.2	6.2	113	19.0	0.5	19.5	6.2	95	20.0	0.8	25.8
12.	5.9	90	22.5	ND	11.1	7.3	88	17.0	1.0	12.4	6.4	71	19.0	1.0	23.0
13*.	6.2	265	38.0	4.3	24.4	6.3	235	32.0	3.5	13.7	5.4	166	28.0	6.5	48.7
14.	6.7	135	22.5	2.5	6.6	7.0	214	25.0	10.0	4.9	7.6	113	16.0	4.1	4.5
15.	7.0	335	44.5	2.5	15.1	7.8	85	39.0	9.5	2.7	7.3	265	40.0	12.5	6.4
16.	5.7	55	14.5	ND	10.1	7.0	271	15.0	ND	5.8	7.1	63	18.0	1.3	7.3
17.	5.9	45	10.5	1.0	1.6	6.4	79	12.0	2.0	2.5	6.6	65	14.0	1.8	4.4
18.	6.0	45	11.5	1.0	4.7	6.6	79	13.0	2.0	3.3	7.1	48	13.0	3.3	4.0
19.	6.4	50	14.0	1.3	1.1	6.1	88	13.0	2.5	2.3	7.2	60	14.0	2.5	2.1
20.	5.9	60	12.0	0.5	6.4	7.2	85	14.0	1.5	6.6	6.9	80	16.0	2.3	13.6
21.	7.3	235	11.0	3.0	3.9	7.8	162	8.0	6.0	0.7	7.6	140	11.0	5.0	5.0
22.	6.3	100	14.0	4.5	2.4.	7.0	128	14.0	7.5	2.3	6.6	95	13.0	4.3	3.5
23.	6.5	115	16.5	1.0	1.1	6.4	73	19.0	2.5	1.4	7.2	73	15.0	2.3	ND
24.	6.2	40	14.0	ND	8.3	7.1	79	17.0	ND	4.9	6.8	48	18.0	1.0	5.0

All parameters except pH and EC are expressed in mg/1   ND : Non detectable
pH in pH units and EC in µScm^{-1}.   * : Temple pond
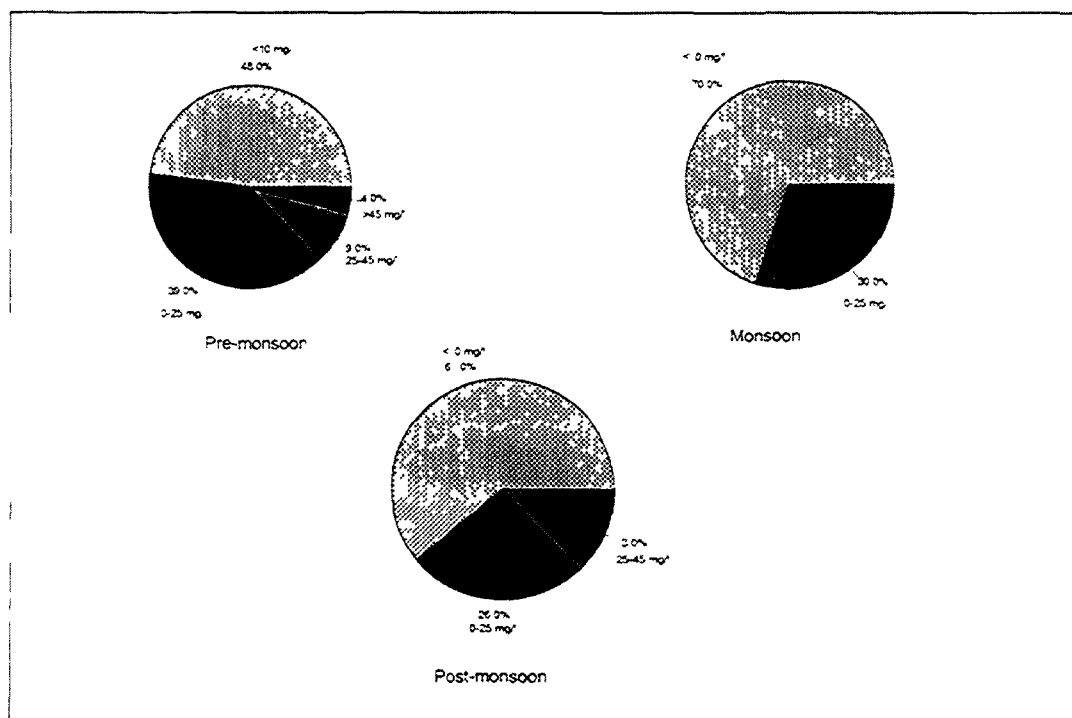
Fig. 4 Percentage distribution of wells and the extent of nitrate pollution

The variations observed in nitrate during pre-monsoon, monsoon and post-monsoon period are presented in Fig.5 in comparison with the maximum permissible limit of nitrate in drinking water. It is observed that most of the observation wells have considerably low nitrate during the monsoon months probably due to dilution.

4.5 Movement of nitrate in the soil

Though nitrogen compounds present in the sewage in the organically bound form do not directly pose any threat to groundwater, the stabilisation through enzyme catalysed biochemical transformation of these compounds into more water soluble inorganic forms like nitrite, nitrate and other similar oxidised forms of nitrogen can result in their fast movement downwards. Once the nitrogen is transformed to nitrate, the mobility of nitrogen is enhanced by its solubility in water, thus it moves easily with the medium. However, the influence of the soil organic matter, in fact, retards its downward movement by adsorption at the protonated sites of the organic matrix. Hence, in terms of quantity, nitrate level is always observed to be more in the surface or the immediate subsurface layers of the soil. In the deeper aquifer, it is virtually low. This is what is observed in the samples collected from the multilevel point sampler at different depths (Fig 6). Nitrate is observed to be high in the surface layers. However, in the areas where the soils are clayey and devoid of organic matter and humus, more and more nitrate can be expected in the

63

groundwater. Compared to nitrate, other ions like chloride and sulphate do not show any significant decrease with depth. They almost remain at the same level.
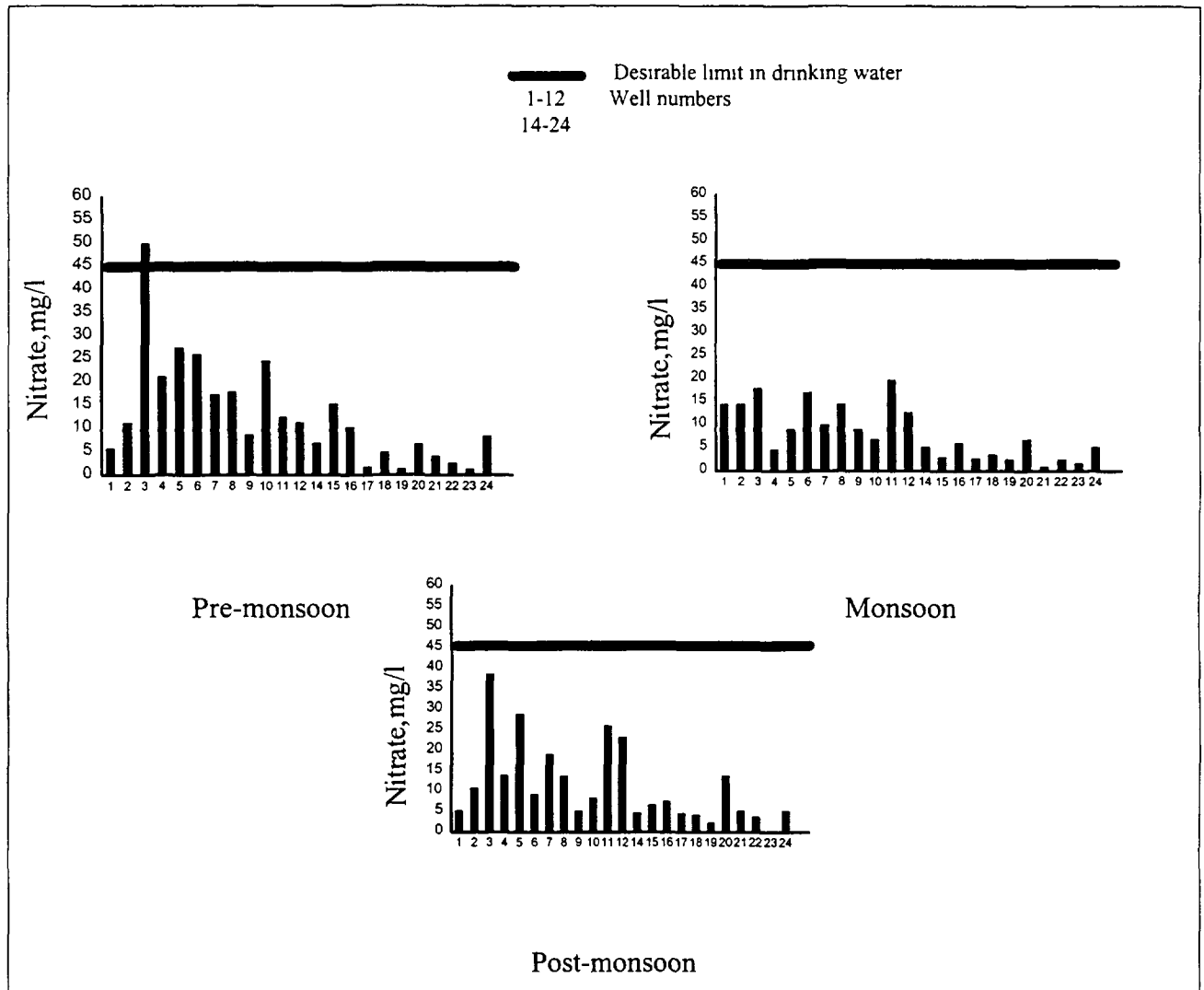
Fig. 5: Nitrate levels in the observation wells as compared to the maximum permissible limit in drinking water

5. CONCLUSIONS

The investigation carried out indicated that the sewage stabilisation pond can be a potential threat to groundwater quality. The level of nitrate in the observation wells varies widely during different seasons. Some of the wells in the immediate surrounding of the stabilisation pond are polluted with nitrate inspite of heavy rainfall in the region. A few more domestic wells in the area are likely to be polluted particularly during the dry months. The problem is more pronounced in summer when the level of nitrate is observed to be on the higher side.

64
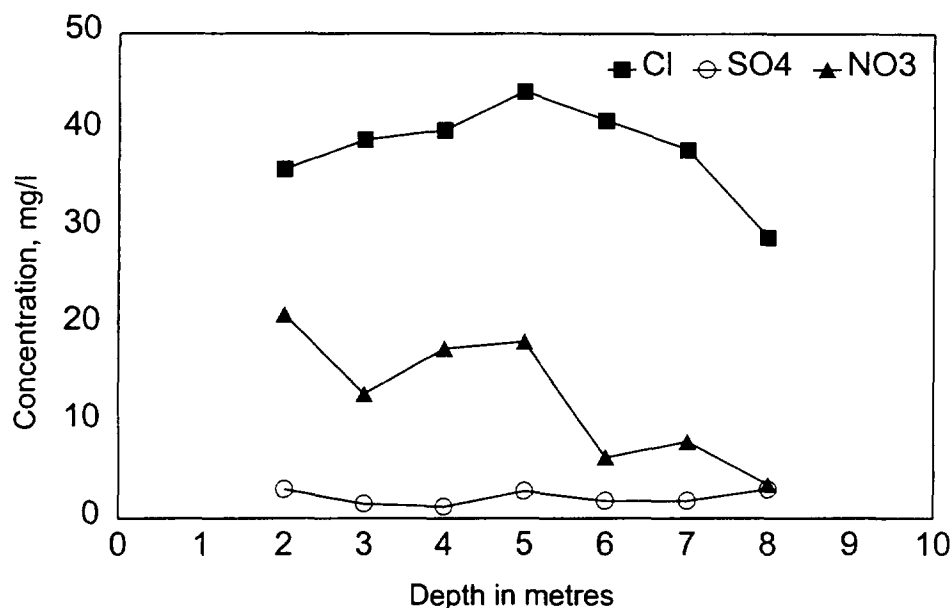
Fig.6: Distribution with depth of nitrate, chloride and sulphate in the site of investigation.

REFERENCES

[1]   Ozha , D.D. and Jain P.C., Imbalance of some chemical constituents in the ground waters of arid environment of Rajasthan   J. I.W.W.A. XXV (II)   (1993) 31.

[2]   Joshi, V.A., Namoti, M.V. and   Vaidya, M.V.,   Incidence of nitrate in Kurnool District   J. I.W.W.A. XXI (4) (1989) 351.

[3]   Comly , H. H.,   Cynosis in infants caused by nitrates in well water   J.Amer. Med. Assoc. 129 (1945) 112 .

[4]   Pande, S. P., Hassan, M.Z. and Saxena, K.L., Nitrates and nitrites in the environment J.I.W.W.A. XVIII (3) (1986).

[5]   Indian Standard. Drinking water-specification (First Revision), IS 10500: 1991 Bureau of Indian Standards, New Delhi-110 002.

[6]   Jackson, M. L.," Soil chemical analysis", Prentice Hall of India (Pvt) Ltd, New Delhi (1950).

[7]   Standard methods for the examination of the water and waste waters, 19th edition, APHA, AWWA, WEF, Washington DC (1995).

ORIGIN, PROCESS AND MIGRATION OF NITRATE COMPOUNDS IN THE AQUIFERS OF DAKAR REGION, SENEGAL

XA9848328

A.A. TANDIA, C.B. GAYE, A. FAYE
Département de Géologie,
Université Cheikh Anta Diop,
Dakar, Senegal

Abstract - *Dakar is a peninsula inhabited by a population of about 2 million people in 1996. With population growth, water demand has increased, inducing seawater intrusion in some dug wells and piezometers of the peninsula. The NO_3 content in the groundwater is above the WHO allowable concentration of 50 mg/l. In the unconfined part of the aquifer, all the samples from wells are contaminated by high NO_3 contents which rose from 100 mg/l in 1987 to more than 250 mg/l in 1996. Only a limited area is affected by NO_3 pollution in the confined layer. The significant correlation between Cl and NO_3 in the unsaturated zone indicates an anthropogenic pollution, a fact which indicates the increasing risk of pollution of potable water resources. Studies in the unsaturated zone and familiarity with the sanitation practices in the area indicate that the horizontal and vertical flux are linked mainly to the defective septic tanks and direct organic waste elimination into the soil by more than 40% of the inhabitants. The correlation between tritium values and nitrate shows that the source of nitrate is recent.*

1. INTRODUCTION

Dakar, the capital city of Senegal with estimated population of 2 million people in 1996, is one of the urban centres in west Africa. In the past, 80% of the water supply was drawn essentially from local aquifers at a rate of 3,000 cubic meters per day. Demographic expansion (Table 1) has led to an increase in water demand. This situation induces sea water intrusion in several parts of the local coastal aquifers.

In order to avoid continuing contamination by sea water intrusion, it was recommended to reduce or stop abstraction in some wells and tap the water supply from Thiaroye area, east of the peninsula. In this area, the inhabitants (Table 1) are faced with the lack of facilities for water supply and sanitation. A combination of poor sanitation practices and drought in recent years have induced a severe groundwater pollution by nitrate [1, 2]. To investigate this, around one hundred analyses comprising the major inorganic constituents, faecal coliforms and isotopes (^{18}O, ^2H, ^3H, ^{14}C, ^{13}C) were carried out on yearly water samples taken from piezometers, hand-pumped wells and dug wells in different area of the peninsula from 1987 to 1997 (Fig.1). The results are intended to help water suppliers evolve short and long term solutions for the management of groundwater.
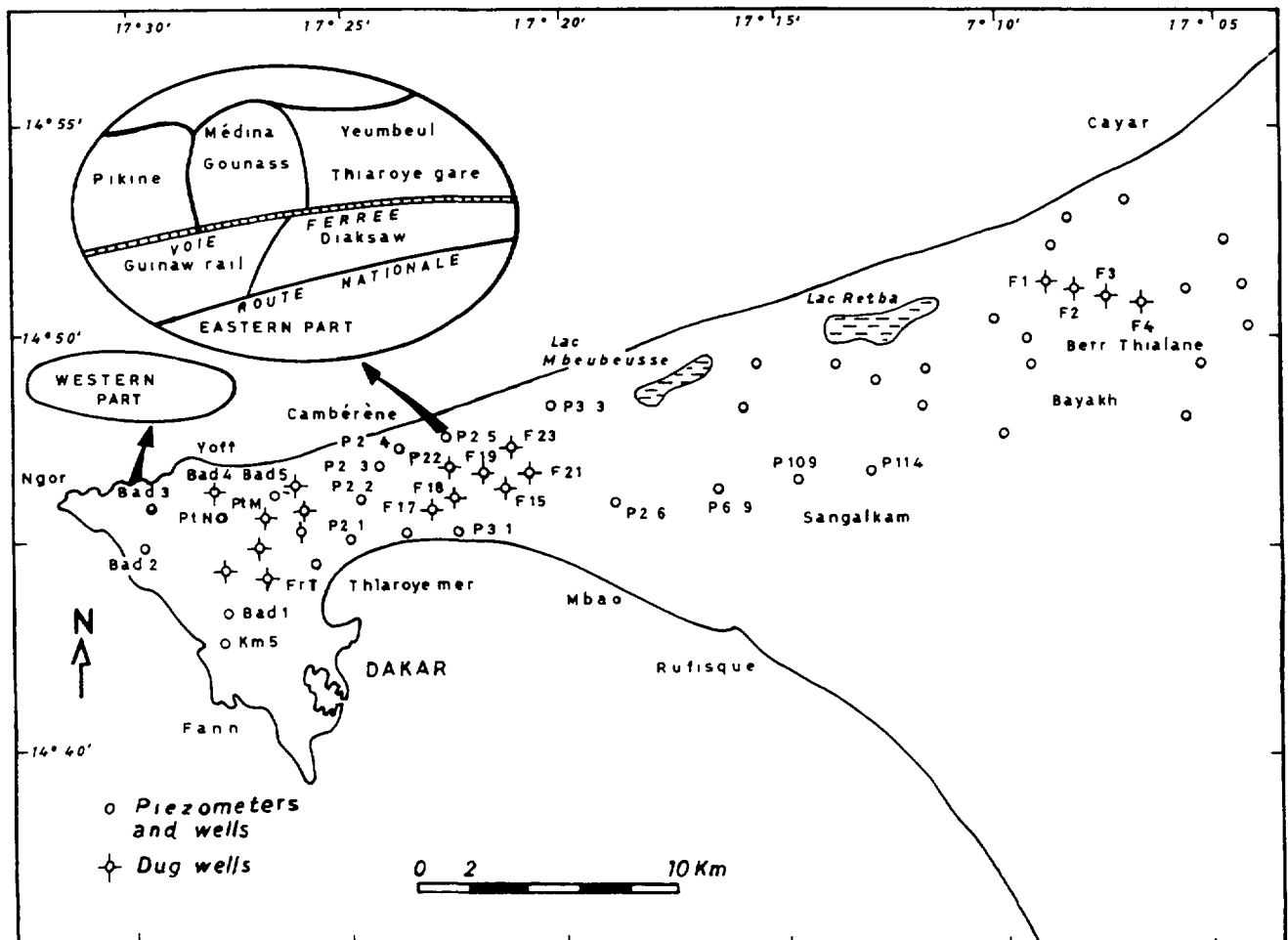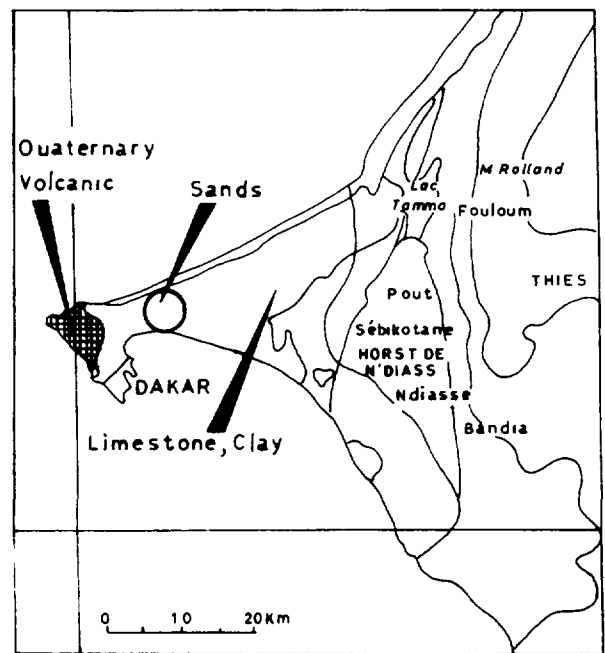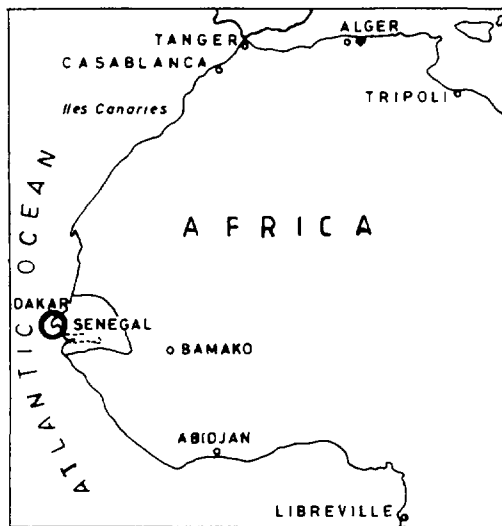
FIG 1. Location of the study area and wells in Dakar region

Table 1: Increasing of population in the eastern part of the peninsula (Thiaroye) [3].

DATES	POPULATION
1955	8,300
1959	23,000
1960	28,800
1964	55,500
1966	76,000
1967	82,000
1969	132,200
1970	132,500
1973	200,000
1976	280,000
1980	420,000
1983	500,000
1990	700,000

2. METHODS OF INVESTIGATION

The samples were collected after the wells were pumped for 1 to 2 hours. They were analysed for NO_3^-, Cl^-, SO_4^{2-} were done by using the high performance liquid chromatography method (HPLC - Dionex QIC analyser), Ca^{2+}, Mg^{2+}, Na^+ by spectrometry method (JASCO, model 7800, UV/VIS) and HCO_3^-, CO_3^{2-} by volumetric method. The chemical analyses were done at the Department of Geology of Dakar University while the isotope analysis of the water sample was done in the IAEA Hydrology Section in Vienna. The samples for Coliform bacteria were stored under cooled conditions and analysed at the Ecole Supérieure Polytechnique (ESP) laboratory in Dakar University.

3. HYDROGEOLOGICAL CONDITIONS

The peninsula has two aquifers systems [4], a semi-confined infrabasaltic aquifer in the western part and the unconfined Thiaroye aquifer in the eastern part (Fig. 2). The infrabasaltic aquifer is composed of pure sand capped by volcanic lavas while the Thiaroye aquifer varies from coarse to clayey sand. The thickness of the aquifer varies from 50 to 80 meters from west to east. Previous studies, using isotopes [2] showed that the recharge by rainwater occurs mainly in the eastern parts between July to October (Fig. 3). Some recharge could also occur through infiltration in the basalt. Transmissivities range from 10^{-2} to $9 * 10^{-3}$ m²/s in the western part and from $1.6 * 10^{-3}$ to $6.75 * 10^{-3}$ m²/s in the eastern part [5]. Although eighty percent of the drinking water supply for Dakar comes from groundwater (Fig. 4) as a consequence of drying of wells, the production from the eastern part has gradually decreased.
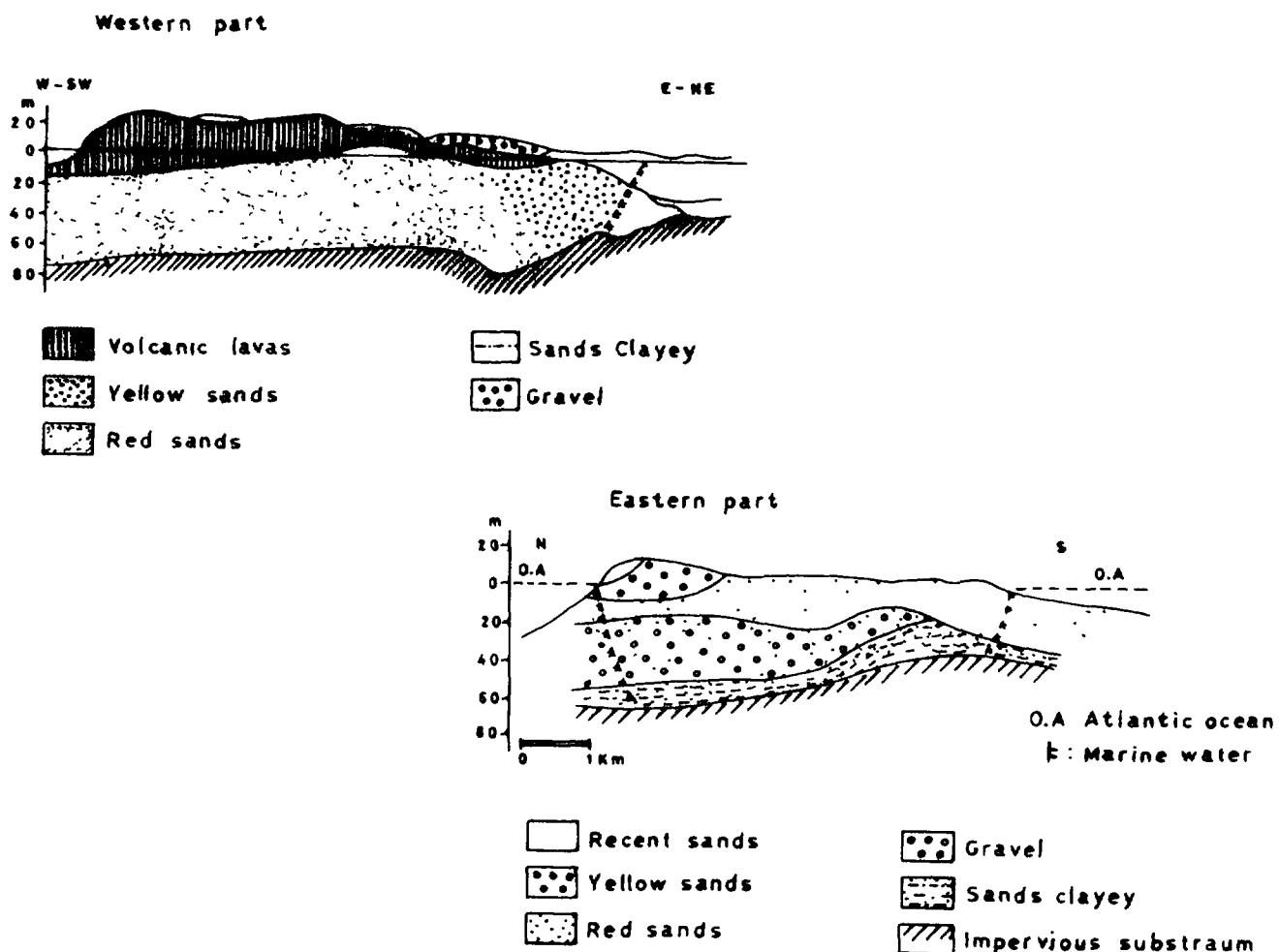
FIG. 2: Geology of the Dakar area aquifer system

4. RESULTS AND DISCUSSIONS

The major chemical constituent of groundwater in Dakar area (Tables 2 and 3) indicates that the water is of the Na-Cl type (Fig.5) of the sodic-chloride type. Electrical conductivities range from 500 to 2700mS/cm and the pH from 4.5 to 7.0. The quality of the water in wells in the eastern and western parts is generally acceptable with the exception of widespread nitrogen and bacteriological contamination. However, water from the city distribution network is of excellent quality and conforms with the international drinking water standards.

Table II: Some major chemical constituents of the groundwater in the eastern part of Dakar area
(July 1996 - mg/l)

Code of well sampled	Ca	Mg	Na	K	Cl	NO3	SO4	HCO3	Fecal coliforms (/100ml)
1	90.3	31.1	146.2	87.6	224.9	307.9	129.5	0	0
2	121.6	38.5	154.5	78.5	222.7	265.4	137.0	176.9	0
3	136.3	39.4	141.4	82.9	237.1	320.9	178.6	48.8	0
4	103.1	41.1	118.2	38.0	200.8	264.4	65.2	201.3	7200
5	80.0	40.9	174.8	135.9	297.4	45.5	8.7	578.5	39800
6	101.7	44.5	117.4	42.7	167.5	233.0	94.2	183.0	100
7	109.2	59.4	143.5	24.3	193.4	260.8	56.2	176.9	n.m
8	70.9	30.3	108.6	21.1	179.9	283.9	29.2	48.8	n.m
9	58.6	22.3	116.8	36.5	182.3	231.9	29.8	48.8	n.m
10	98.7	19.0	131.2	39.8	167.4	209.8	175.8	183.0	n.m
11	93.6	39.9	122.4	33.1	186.7	229.7	39.7	0	n.m
12	30.2	14.1	54.6	5.8	163.5	220.3	56.0	170.8	1800
13	71.1	21.6	108.1	17.0	170.7	102.4	144.4	183.0	6300
14	54.6	17.3	85.2	8.5	92.3	109.9	22.7	183.0	200
15	35.6	18.6	99.9	14.0	115.0	186.8	18.3	61.0	0
16	38.2	19.5	95.3	8.9	147.0	249.7	15.7	91.5	0
17	79.4	31.4	125.4	36.8	220.6	359.6	66.0	183.0	3300
18	99.5	58.8	137.5	29.6	224.9	188.3	252.1	117.8	0
19	199.8	57.2	151.3	80.0	221.2	367.5	205.2	152.5	700
20	169.8	81.1	162.4	88.5	258.1	74.1	262.4	610.0	50100
21	157.7	61.6	153.3	45.8	216.9	178.3	326.0	176.9	400
22	42.0	19.3	104.8	19.1	115.7	221.7	25.7	48.8	n.m
23	38.0	18.2	78.2	21.3	89.5	161.7	22.5	54.9	n.m
24	41.0	18.4	48.6	14.9	66.8	132.2	13.4	48.8	00
25	49.2	28.3	89.3	14.3	102.7	215.4	13.6	122.0	200
26	78.2	20.4	93.2	24.9	143.9	261.3	19.9	54.9	n.m
27	71.8	24.5	106.2	29.7	163.7	182.5	33.9	176.9	n.m
28	48.7	18.4	85.6	22.9	113.8	191.2	23.7	140.3	n.m
29	45.6	16.7	89.1	16.3	111.4	184.4	23.2	122.0	11700
30	61.9	21.2	96.0	20.3	123.1	140.0	58.1	146.4	n.m
31	34.7	18.2	30.4	8.5	45.4	89.9	13.7	57.9	n.m
32	60.4	18.1	97.2	19.2	157.9	284.3	25.6	0	n.m
33	100.6	35.8	114.6	38.7	173.9	250.0	81.7	152.5	5700
34	55.0	35.4	66.7	19.2	100.8	42.9	116.2	140.3	500
35	80.9	27.8	92.5	35.4	138.1	257.0	37.9	152.5	n.m
36	47.8	22.2	69.0	13.7	95.7	128.3	30.3	161.6	n.m
37	50.1	25.9	95.1	13.4	124.6	124.3	74.1	148.0	200
38	79.1	23.6	123.6	37.7	170.5	209.9	83.0	146.4	n.m
39	70.1	28.4	115.6	27.7	166.4	168.2	63.7	130.2	n.m
40	35.1	13.7	66.1	9.7	101.6	133.0	15.8	30.5	n.m
41	51.6	24.2	98.7	12.5	153.1	146.2	52.1	152.5	0
42	58.4	15.2	83.5	12.2	112.1	118.4	94.0	152.5	0
43	51.6	20.9	103.1	37.4	158.9	127.4	88.4	170.8	n.m
44	33.2	13.0	70.3	8.7	71.8	101.0	15.5	128.1	n.m
45	32.5	15.8	67.9	11.2	99.8	120.9	19.1	0	n.m
46	28.5	13.2	65.4	8.2	78.5	111.8	20.4	128.1	n.m
47	11.1	14.9	90.6	11.1	130.5	153.2	28.7	140.3	n.m

n.m = not measured
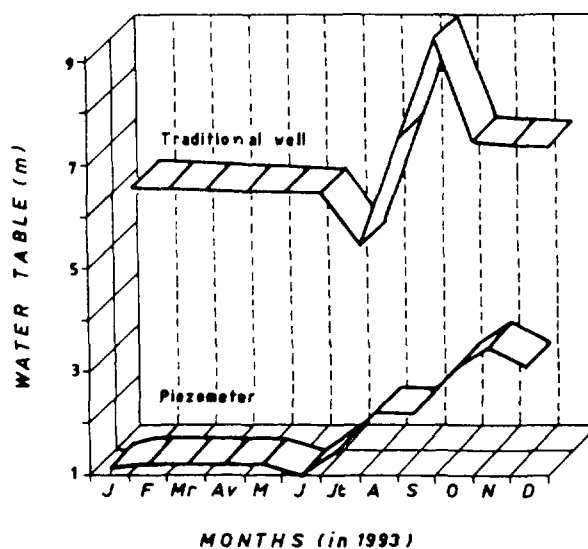
FIG 3. Relationship between water table of groundwater and the rainy season Recharge occurs from June or July to October
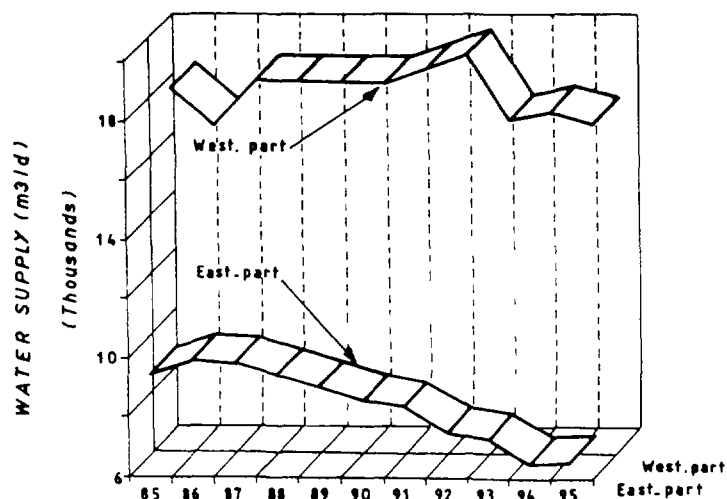
FIG 4 Production of drinking water supply from the dug wells (in western part and eastern part, from 1985 to 1995

Table III: Some major chemical constituents of the groundwater in the western part of Dakar area
(May 1995 - mg/l)

Code of well sampled	Mg	Ca	Na	K	NO3	SO4	Cl	HCO3
Bad1	7.2	48.0	85.0	11.0	13.4	17.2	204.7	19.6
Bad2*	46.1	140.0	97.0	9.0	31.0	46.9	261.6	315.7
Bad2	36.4	220.0	284.0	30.0	71.8	95.3	484.8	502.7
Bad3*	21.8	80.0	431.0	13.0	71.4	150.9	807.9	282.0
Bad3	47.3	228.0	580.0	28.0	103.7	242.9	1049.7	349.5
Bad4*	12.1	100.0	66.0	6.0	69.5	23.0	139.8	233.0
Bad4	18.2	90.0	58.0	6.0	96.1	22.8	113.3	197.4
Bad5	12.1	40.0	57.0	9.0	8.7	11.8	107.0	116.5
Bad6	2.4	20.0	32.0	4.0	16.7	15.4	38.5	45.9
Point N	41.5	65.6	130.0	6.0	129.6	59.3	303.1	30.6
Point M	19.4	20.0	43.0	3.0	18.5	14.1	66.7	91.9
Front T.	39.6	34.8	52.0	3.0	107.6	19.6	123.1	85.8
Camp pénal	14.5	48.0	49.0	3.0	15.3	13.8	92.7	159.4

* double piezometer

72
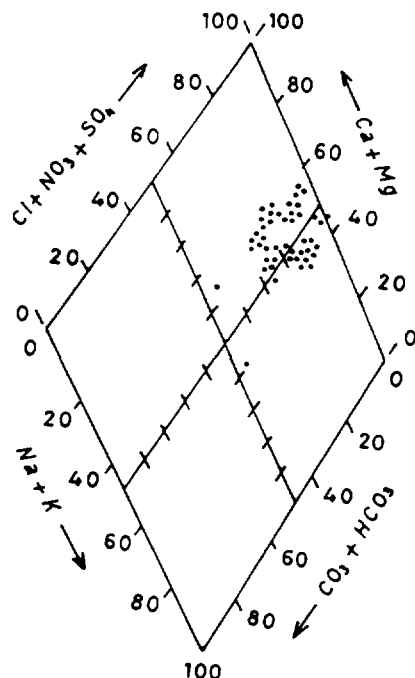
FIG. 5:   Piper diagram of the groundwater

The mean nitrate content in the groundwater in the western part of the peninsula is about 50 mg/l while it is much higher at 400 mg/l in the eastern part (Thiaroye area) and 20 mg/l beyond Thiaroye area. In all well samples, nitrate concentration in the groundwater is higher in the eastern part than in the western part. The nitrate values are above the OMS limits of 45 mg/l (Fig.6 and Fig.7) and increases each year: from 100 mg/l in 1987 to 200 mg/l in 1990 (Table IV).

ST : Santieubeu,. MY : Médina Yeumbeul, Nd : Ndiobene, YS2 : Yeumbeul 52
DSI: Darou Salam I.
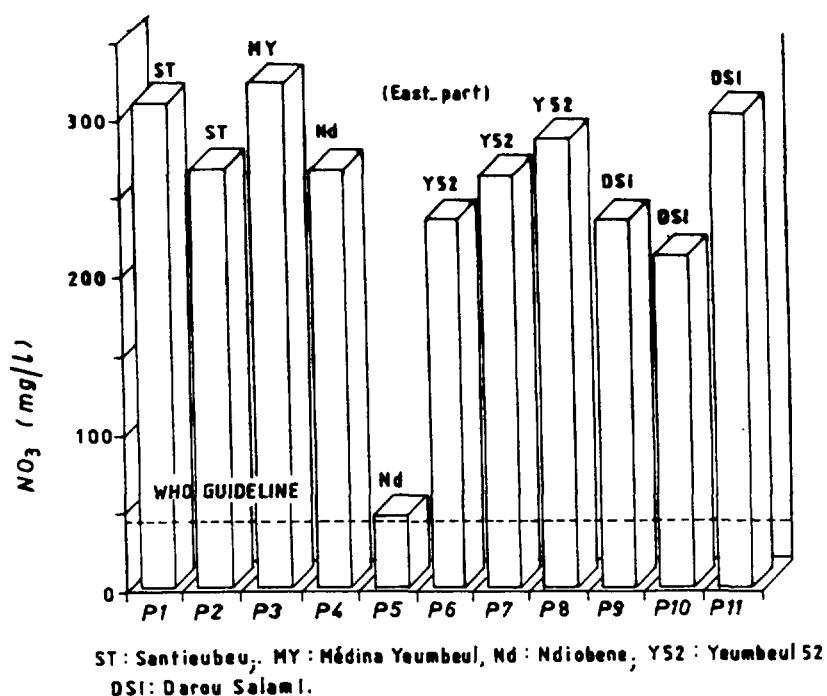
FIG. 6: Nitrate content in traditional wells

73
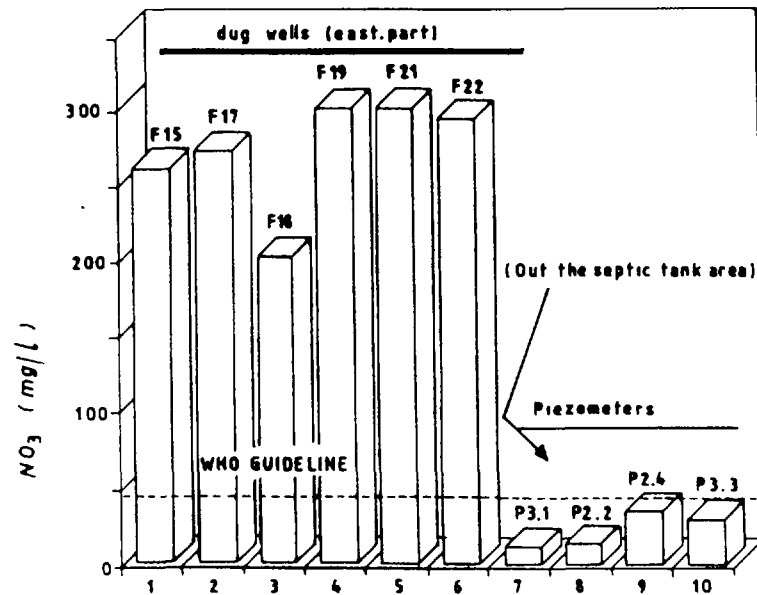
FIG. 7: Nitrate content in dug wells and piezometers

Table IV: Nitrate concentration in dug wells , in mg/l.

Dug wells	Nov 87	Jan 88	Mar 88	May 88	Jul 88	Sep 88	Nov 88	Jan 89	Mar 89
F19	100	130	140	160	170	180	205	220	33
F18	120	132	141	148	168	170	173	270	71
F17	-	121	195	205	220	223	235	250	10

The nitrate content in rainfall which is around 1 ppm [6] is extremely low when compared to those in groundwater. The relation NO_3^- vs Cl^- of groundwater indicates a significant correlation corresponding to an anthropogenic pollution. The relation NO_3^- vs distance between wells and latrines (Fig. 8) confirm this interpretation. It shows elsewhere that nitrate concentration increases in the wells which are located near the latrines and for the same distance wells/latrines, nitrate concentrations are higher when the latrine is older
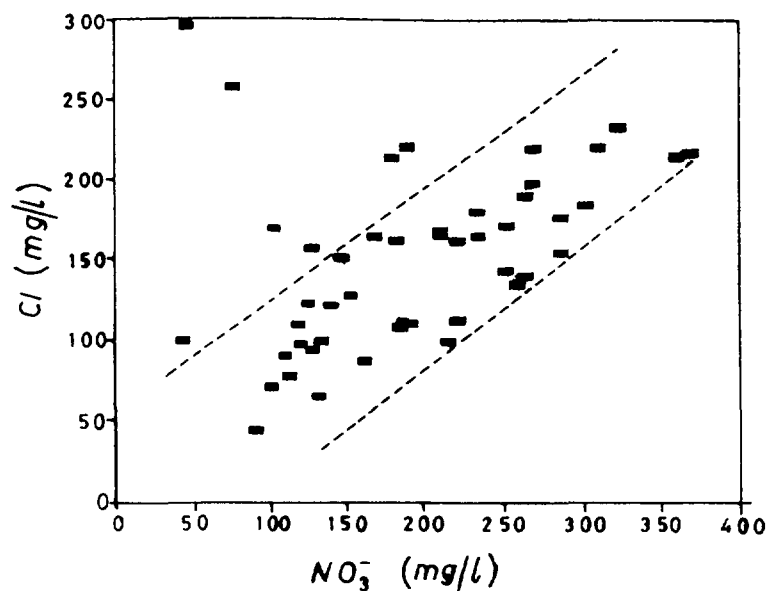
FIG. 8: NO_3^- vs Cl^- of groundwater

74
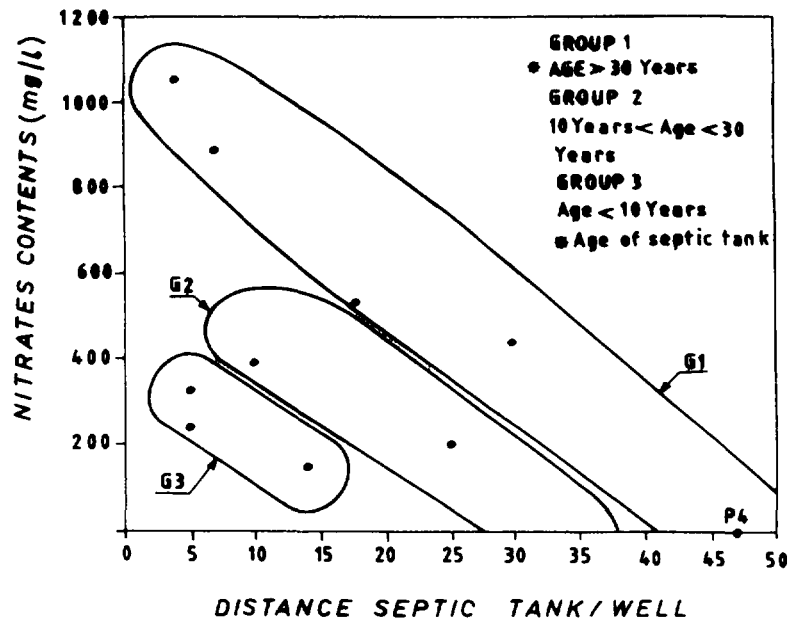
FIG. 9 : NO_3^- vs distance between wells and septic tank
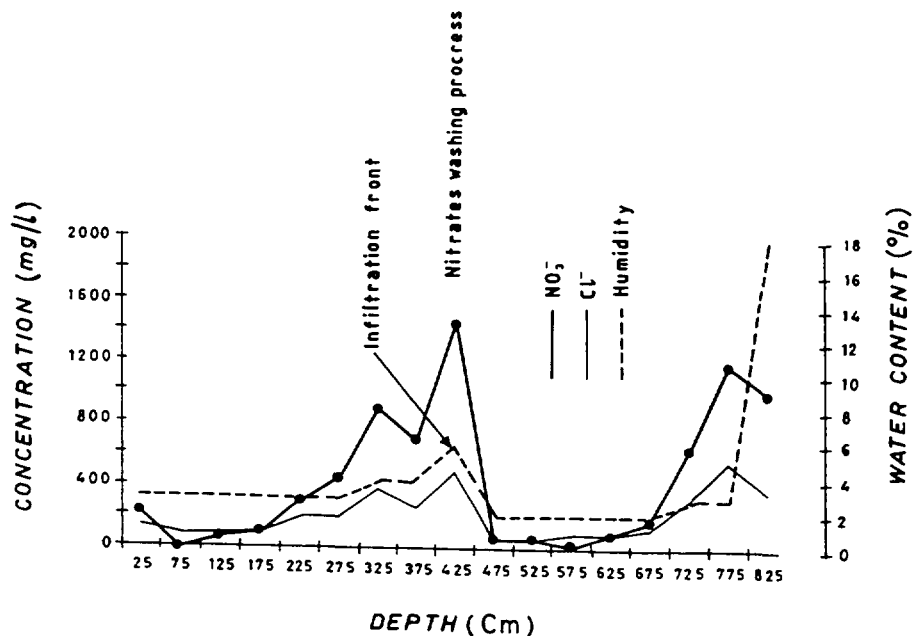
FIG. 10 shows a vertical movement of rain water in the unsaturated zone.

The high nitrate content at 4.5 m (Fig. 10) represents the influence of human activity. In the same way, there is another peak at 8 m which corresponds to the previous rainy season. The soil water shows in the same period the front of infiltration towards the groundwater. The mean value of nitrate content in the unsaturated zone is around 800 ppm. It indicates the function of Thiaroye soil in the basin to absorb nitrates. This high level of nitrate is mainly due to 3 causes (Fig.11): domestic waste, waste waters and excrement.
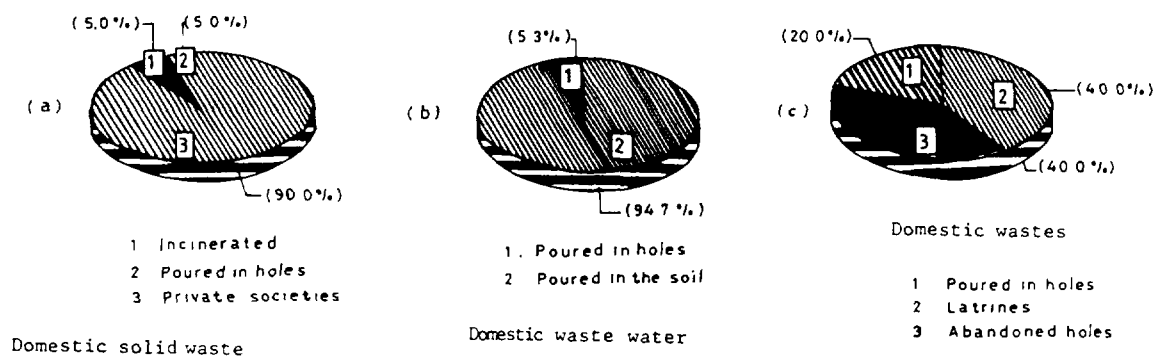
FIG.11: Sanitation practice in Thiaroye basin

Table V: Some isotopes in groundwater of Dakar area, May 1995

Code of station sampled	Deuterium delta per mill	Oxygen -18 delta per mill	Tritium UT	C-13 per mill PDB	C-14 (%)
Western part					
Bad1	-35	-5.1	0.53		
Bad2*	-24	-4.6	0.80		
Bad2	-29	-3.9	5.06		
Bad3*	-35	-5.5	4.15		
Bad3	-38	-5.4	1.62		
Bad4*	-37	-5.3	7.98		
Bad4	-37	-5.6	6.79		
Bad5	-37	-5.9	1.15		
Bad6	-34	-5.3	3.60		
Point N	-35	-5.6	2.77		
Point M	-36	-5.5	0.48		
Front T.	-38	-5.4	1.77		
Camp pénal	-37	-5.9	0.93	-16.33	95.2
Autoroute	-36	-	-		
P2.2	-37	-5.7	2.55		
Eastern part					
P2.4	-40	-5.5	3.94		
P3.1	-36	-6.4	0.60		
P3.2	-40	-5.8	-		
P2.6	-36	-5.8	-		
P2.2	-38	-5.3	2.55		
P2.4	-36	-5.4	3.94		
P3.3	-35	-5.6	0.78		
F15	-40	-4.9	5.94		
F17	-35	-5.4	4.87		
F18	-36	-5.6	6.57		
F19	-34	-5.3	4.92		
F21	-31	-5.1	4.35		
F22	-37	-5.3	4.74		

* = double piezometer

76

According to Table V, the δ^2H content of -35.6 per mille and the $\delta^{18}O$ concentration of +5.2 per mille in groundwater are the typical isotopic signature characteristic of phreatic water in the Sahelian area where the evaporation is high [7].

The relationship between ^{18}O and ^2H (Fig.12) indicates the following linear regression equation:

$$\delta\,^2H = 4.2\,\delta\,^{18}O - 12$$

The distribution of the values around the World Meteoric Water [8] confirms that the recharge of the Dakar aquifer comes from monsoon rains. It indicates the flow of the groundwater from the eastern part to western part of the peninsula. This phenomenon contributes to generalise the nitrate pollution along the flowpath from eastern part to western part where the nitrate content is around 50 mg/l. Figure 13 shows that the nitrate content and deuterium in rainfall which are around 1 mg/l and -54%o [3], respectively are extremely low when compared to those from evaporated groundwater and which has probably undergone microbiological reactions (Group 2) [1]. It is very likely, therefore, that dug wells located west of the peninsula (Bad 2 with 71.8 mg/l, Bad 3 with 103 mg/l, Point N with 129.6 mg/l and Front T. with 107.6 mg/l) where the nitrate content is only around 10 mg/l (Group 1), are contaminated by groundwater flowing from eastern part.
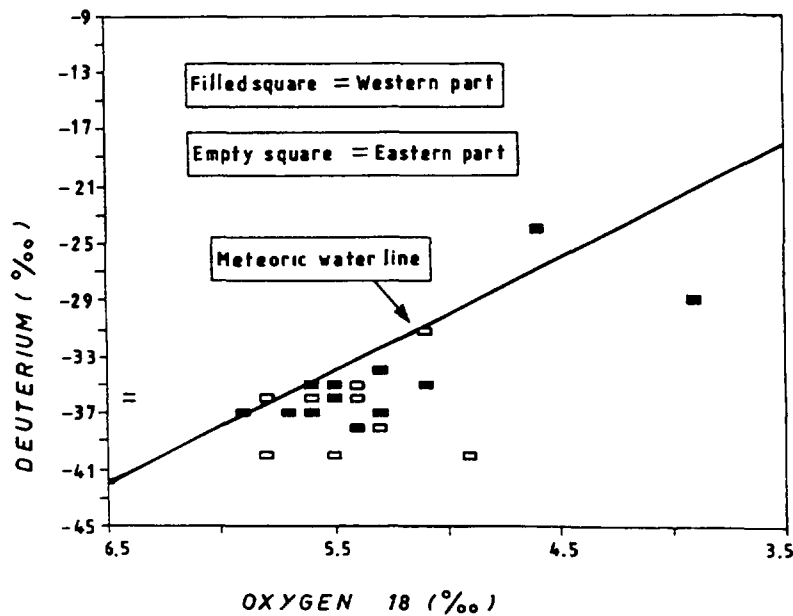
FIG. 12: Deuterium versus ^{18}O for Dakar area groundwater.

High concentrations of nitrate have also been identified in some evaporated points of the unconfined aquifer (Fig.14) suggesting an evaporation effect on nitrate content. In fact, the recharge of the aquifer occurs after rainfall has evaporated, a phenomenon that is

Western part

GROUP 1

120

NITRATES (mg/l)

80

40

GROUP 2

Evaporation. Pollution and microbiological effect

Evaporation + microbiological effect

Rain water

10

12
5
7

6 4 3

2

11 9
8 1

1 = Bad 1
2 = Bad 2 h
3 = Bad 2 b
4 = Bad 3 h
5 = Bad 3 b
6 = Bad 4 h
7 = Bad 4 b
8 = Bad 5 h
9 = Bad 6 h
10 = Pt.N
11 = Pt.M
12 = Fr.T

h = Shallow
b = Deep

0

-60   -40   -20   0

DEUTERIUM (‰)

Eastern part

GROUP 1

300

NITRATES (mg/l)

200

100

In inhabited area

Out inhabited area

GROUP 2

Evaporation. Pollution and microbiological effect

Evaporation + micro - biological effect

Rain water

1 = P3 1
2 = FJ5
3 = F 17
4 = F 18
5 = F 19
6 = F 21
7 = F 22
8 = P 22
9 = P 2.4
10 = P3.3

7 3 5 6
2

4

9 10
8 1

0

55   45   35   25

DEUTERIUM (‰)

FIG. 13: Deuterium versus nitrate in groundwater. The microbiological effect reflect all processes which produced NO_3 from organic matter by bacteriological action. The contamination for Group 1 is induced by groundwater flowing from the east while wells in Group 2 are unaffected by pollutants.

78

generally observed in arid and semi-arid region when the groundwater is shallow. Likewise, high nitrate concentrations (>45mg/l) must be recent because previous studies in 1972 [5] have shown low level of nitrate (<45 mg/l) indicating an increase in time. The relation of NO_3^- vs ^3H shows a significant correlation with high values of tritium which characterises the actual rainfall (Fig.14). The presence of high activities of ^{14}C (80%) is in good agreement with this recent recharge of groundwater.

Values   chararacterizing
The actual rainfollgiven
by piston flow model:

$UT = UT_x . e^{-\lambda(x-i)}$

UT = Tritium content
x = Year of sampling
i = Year origin
$\lambda = Ln\ 2/T$; T= 12, 43 Year

● Eastern part
O Western part
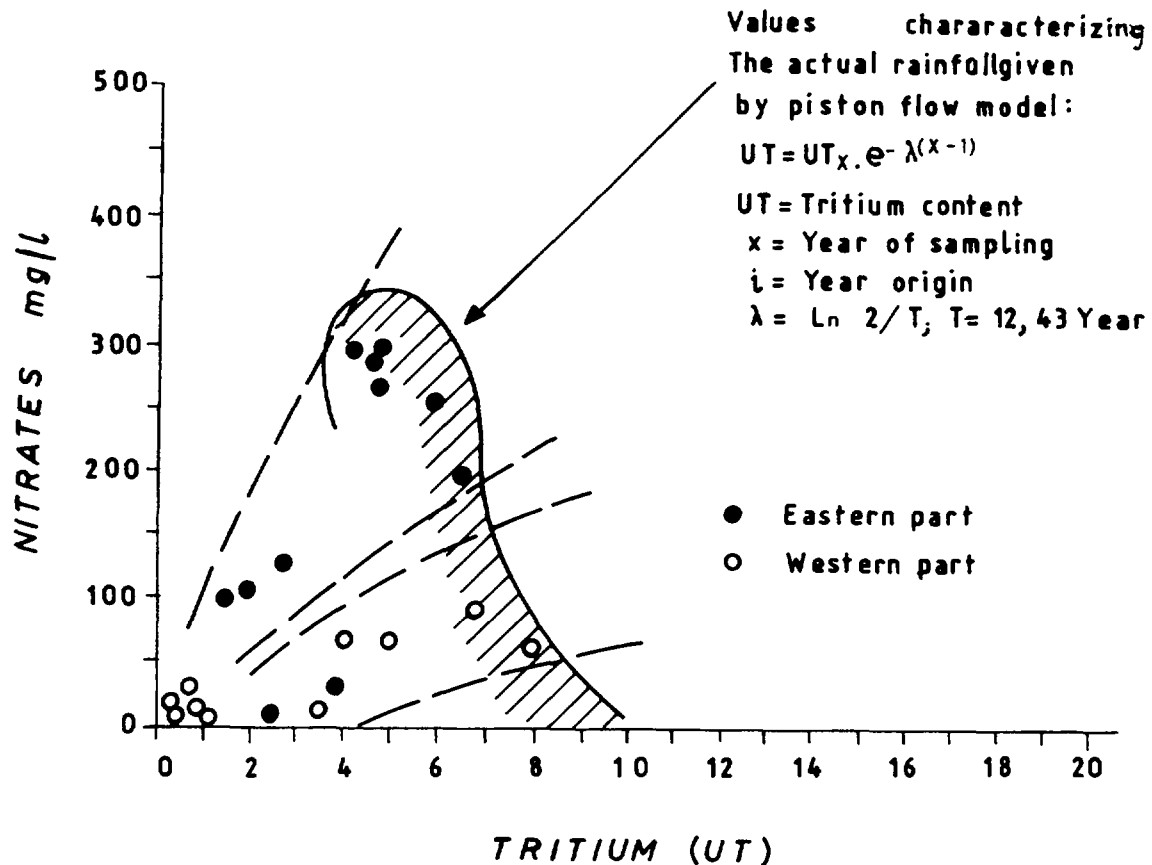
TRITIUM (UT)

Figure 14: Nitrate concentrations versus tritium. Groundwater affected by recent pollution showing the trititum content in rainfall.

5.   CONCLUSION

The groundwater of Dakar region is contaminated by nitrates and faecal coliforms from anthropogenic sources. The mechanisms of contamination are mainly the soil washing and nitrate injection from latrines. The results obtained during this study show that the proper construction of dug and hand-pumped wells as well as a safe distance between septic tanks and wells are necessary. Its also necessary to implement an

education programme or modify the well modernisation process (sealing of the opening with concrete and installation of a water hand or foot pump).

Stable isotopes, tritium and carbon 14 are used to obtain a better understanding of nitrate contamination of groundwater; tritium in groundwater indicates that nitrate concentration is recent. This has been confirmed by the presence of high activities of ^{14}C (80%), in good agreement with recent recharge of groundwater. The distribution of the values of ^{18}O and ^{2}H around the World Meteoric Water Line [3] indicate that the recharge of the Dakar aquifer system originates from the monsoon rainfall after it has been exposed to evaporation process. The cluster of points relating ^{18}O and ^{2}H indicates the flow of groundwater from the east to the western part of the peninsula. This situation contributes to nitrate pollution along the flowpath from the east to west where nitrate pollution in groundwater is more serious.

REFERENCES

[1]   COLLIN, J.J. et SALEM, G. (1989): Pollution des eaux souterraines par les nitrates dans les banlieues non assainies des pays en développement. Cas de Pikine (Sénégal). Note technique BRGM SGN/3E, 89/27; 11p.

[2]   GAYE, C.B. (1980): Etude hydrogéologique, hydrochimique et isotopique de la nappe aquifère infrabasaltique de la presqu'île du Cap-Vert (Sénégal). Thèse 3°cycle, Univ.Dakar.

[3]   VERNIERES, M. (1971): Etapes et modalités de la croissance de Dagoudane Pikine, banlieue de Dakar, ORSTOM, Dakar, Senegal.

[4]   MARTIN, A. (1970): Les nappes de la presqu'île du Cap-Vert. Leur utilisation pour l'alimentation en eau de Dakar. Pub.BRGM 1970; 50p.

[5]   OMS (1972): Approvisionnement en eau et assainissement de Dakar et ses environs. Rapport Projet 1972; SEN 3201 tome I; 104p + annexes.

[6]   TRAVI, Y., GAC, J.Y., FONTES, J.C., FRITZ, B.(1987): Reconnaissance chimique et isotopique des eaux de pluie au Sénégal. Géodynamique 1987. 2: 43-53

[7]   FAYE, A., TANDIA, A.A., TRAVI, Y., PRIOL, J.Le et FONTES, J.C. (1993): Apport des isotopes de l'environnment à la connaissance des quifères de Casamance (extrême sud du Sénégal).

[8]   CRAIG, H. (1963): Isotopic variations in meteoric waters, Science 133.1702. Washington.

[9]   COMLY, H (1945): Cyanosis in infants caused by nitrates in well water. JAMA, 129; 112-116.

THE INFLUENCE OF BROWN COAL EXPLOITATION IN POLAND ON THE GROUNDWATER POLLUTION AS DETERMINED BY ISOTOPIC ANALYSES OF SULPHATE

S. HAŁAS, A.TREMBACZOWSKI,
Mass Spectrometry Laboratory, Lublin

W. SOŁTYK
OBRTG, Warsaw

Poland

Abstract - *This research deals with pollution impact on natural water resources in the industrial area of Bełchatów, central Poland, where a large brown coal deposit is exploited and the coal is burned in an electric power plant. To trace the sources of groundwater pollutants the stable isotope analysis of oxygen and sulphur in sulphates was applied. The mass-spectrometric analysis was performed on SO_4^{2-} samples from numerous wells and piezometres in the excavation area. By repetitive sampling performed in November 1994, May 1995 and December 1996 significant changes of SO_4^{2-} concentration and sulphur and oxygen isotopic ratios in several sites were recorded. The interpretation of isotope ratios allowed us to recognize three groups of sulphates: (1) from the leaching of Permian salt dome, (2) produced by the leaching of soluble sulphates from an ash pool and (3) produced by oxidation of natural sulphides in water-bearing rocks.*

1. INTRODUCTION

Sulphates belong to common pollutants in groundwaters. By means of a standard chemical method one can only indicate the presence of sulphates and study the variations of their content. Chemical methods say little about the origin of sulphates. The sources of sulphates can be elucidated by means of $\delta^{34}S$ and $\delta^{18}O$ measurements. The isotopic compositions, combined with SO_4^{2-} concentration can indicate sources and processes in groundwater systems.

Sulphates of different origin in waters comprise: (1) *Dissolved evaporites*. They are easy to identify because of their $\delta^{34}S$ values >10‰ and $\delta^{18}O$ values >12‰ [1]. The waters that dissolve the sulphates are characterized by considerable sulphate concentrations, usually about a few hundred mg/L up to 2 g/L. (2) *Sulphates formed by sulphide oxidation* have similar sulphur isotope composition with respect to oxidized sulphides [2], [3], [4]. Usually $\delta^{34}S$ values of those sulphates are negative. Also $\delta^{18}O$ values are negative, because most of their oxygen is derived from water oxygen [5], [6], [7], [8]. The concentration of those sulphates in water does not need to be high. (3) *Atmospheric sulphates* are mainly formed during the combustion of fuels. Usually their $\delta^{34}S$ values range from 2‰ to 8‰, while $\delta^{18}O$ values >12‰, which results from oxidation in air [9], [10], [11], [12], [13]. Atmospheric sulphates may also be derived from sea water sulphates in coastal areas [14]. The concentration of these sulphates is rather low, typically between 1 and 30mg/L. (4) The *sulphates from oxidized organic matters* have a similar $\delta^{34}S$ values to that of sulphur in plants [15], [11], [4]. These values are often similar to atmospheric sulphates while $\delta^{18}O$ values <10‰ makes them distinct from atmospheric sulphates [13]. Their concentration varies seasonally from several tens to several mg/L. (5) *The sulphates which come from the leaching*
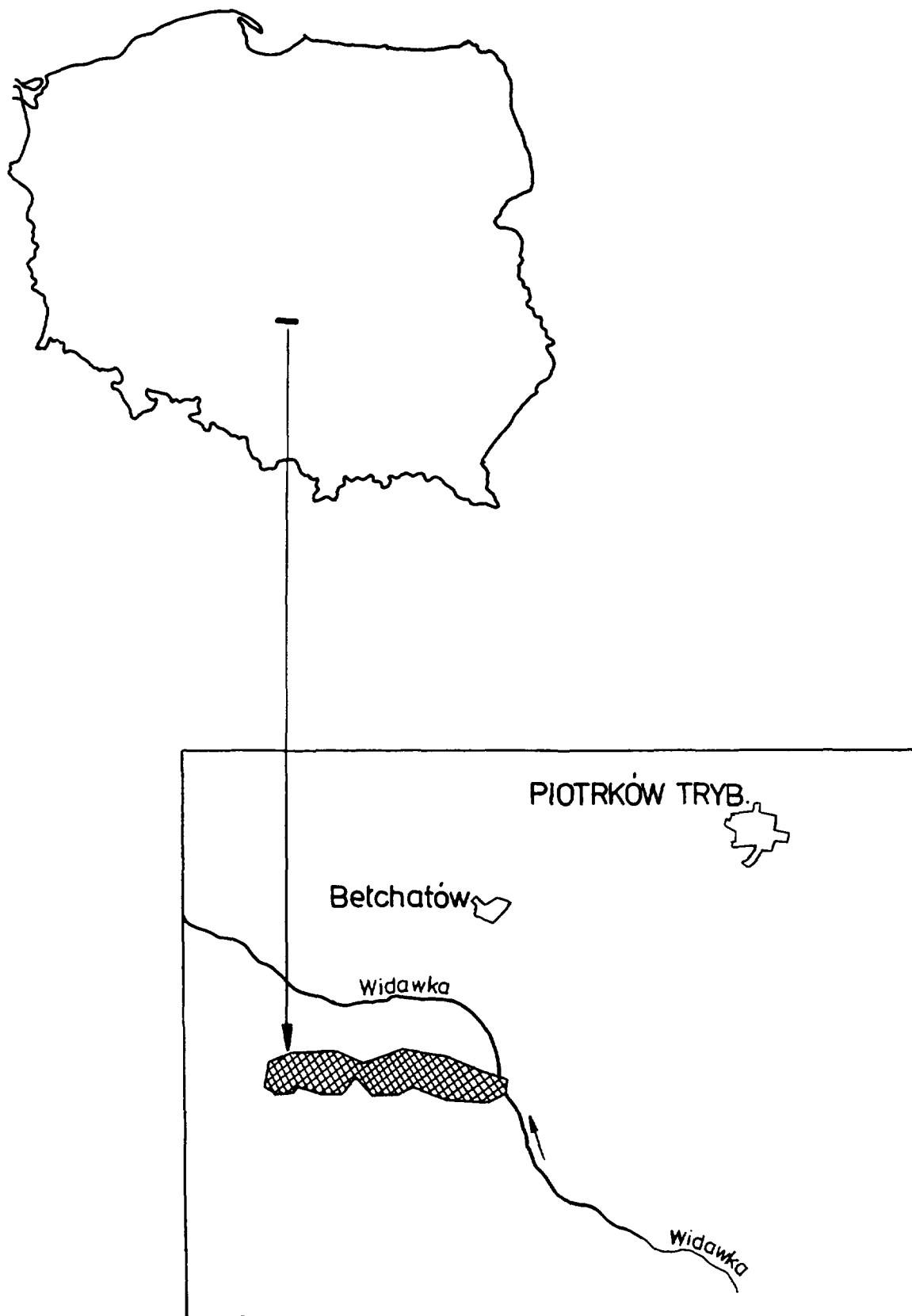
FIG.1. The location of the study area.

of artificial fertilizers may occur locally. Their $\delta^{34}S$ values usually exceed 10‰ and $\delta^{18}O$ values >16‰, as a consequence of their production procedures.

The original isotopic compositions of sulphates can be altered by some processes, such as bacterial reduction of sulphates. This process diminishes the sulphate concentration and significantly enriches the remaining sulphate in heavy isotopes. The isotope enrichment can be enormous for sulphur and somewhat smaller for oxygen. Inasmuch as both elements are enriched in heavy isotopes simultaneously their isotopic compositions are correlated [16]. During the formation of sulphates by oxidation of reduced forms of sulphur (S^0, S^{2-}) oxygen is mainly incorporated from water [5], [6], [2], [4], [17], [7], [8] and enriches the formed sulphates in the lighter isotope of oxygen. The isotopic composition of sulphur changes little during the oxidation and thus sulphates formed possess sulphur whose isotopic composition is similar to the primary components [15], [11], [4]. The dissolution of sulphates does not change their isotopic compositions. When different sulphates are mixed, the final isotopic composition of the mixture becomes the weighted mean.

Ashes produced by power stations are the curse of our times. They contain a lot of harmful ingredients which seep into groundwaters and contaminate them. The ashes contain sulphur compounds from combusted coal, which are oxidized to sulphates and get into waters. Sulphates do not belong to the most dangerous compounds, however they may be easily monitored and their presence enables us to observe the infiltration of polluting substances into waters. The $\delta^{34}S$ and $\delta^{18}O$ measurements have been used for studying the infiltration of ash-borne pollutants into groundwaters in the Czech Republic [18], [19].

In central Poland, near the Bełchatów town there is a big brown coal mine and an electric power station (see Fig. 1 for location of this area). The industrial region of Bełchatów provides a good opportunity for testing stable isotope techniques in tracing sources of pollution. The research was initiated in 1983, only for a narrow practical aspect - a warning against the infiltration of the brines into outpumped water. The first results were published [20]. This more extensive work presents the patterns of sulphates from groundwaters in Bełchatów area, whose origin was identified using the isotopic compositions.

2. DESCRIPTION OF THE STUDY AREA

The large resources of brown coal lie in a tectonic trough 40 km long and from 1.5 km to 2 km wide (see Fig. 2). The deposit lies under a 140 m thick cap-rock (Quaternary and Tertiary). The cap-rocks consist of sands and clays. The average thickness of the coal deposit is about 55 m. The coal deposits are underlain by Jurassic and Cretaceous rocks [21], [22].

Weakly mineralized groundwaters occur to a depth of 700 m. Their chemical composition is variable. Shallow groundwaters appear at depth of ca. 10 m under the surface in the Quaternary sands and clays. These waters are more variable in their chemical composition than deeper waters. Their mineralization varies from 120 mg/L to 3,000 mg/L, predominantly about 500 mg/L. Deeper waters with mineralization about 300 mg/L are characterized by smaller chemical variability. All of the water horizons have good hydraulic contact and they are practically connected. The filtration factors are different, from 2 m/d in the Tertiary rocks to 20 m/d in the Quaternary. Impermeable layers are present too [22].
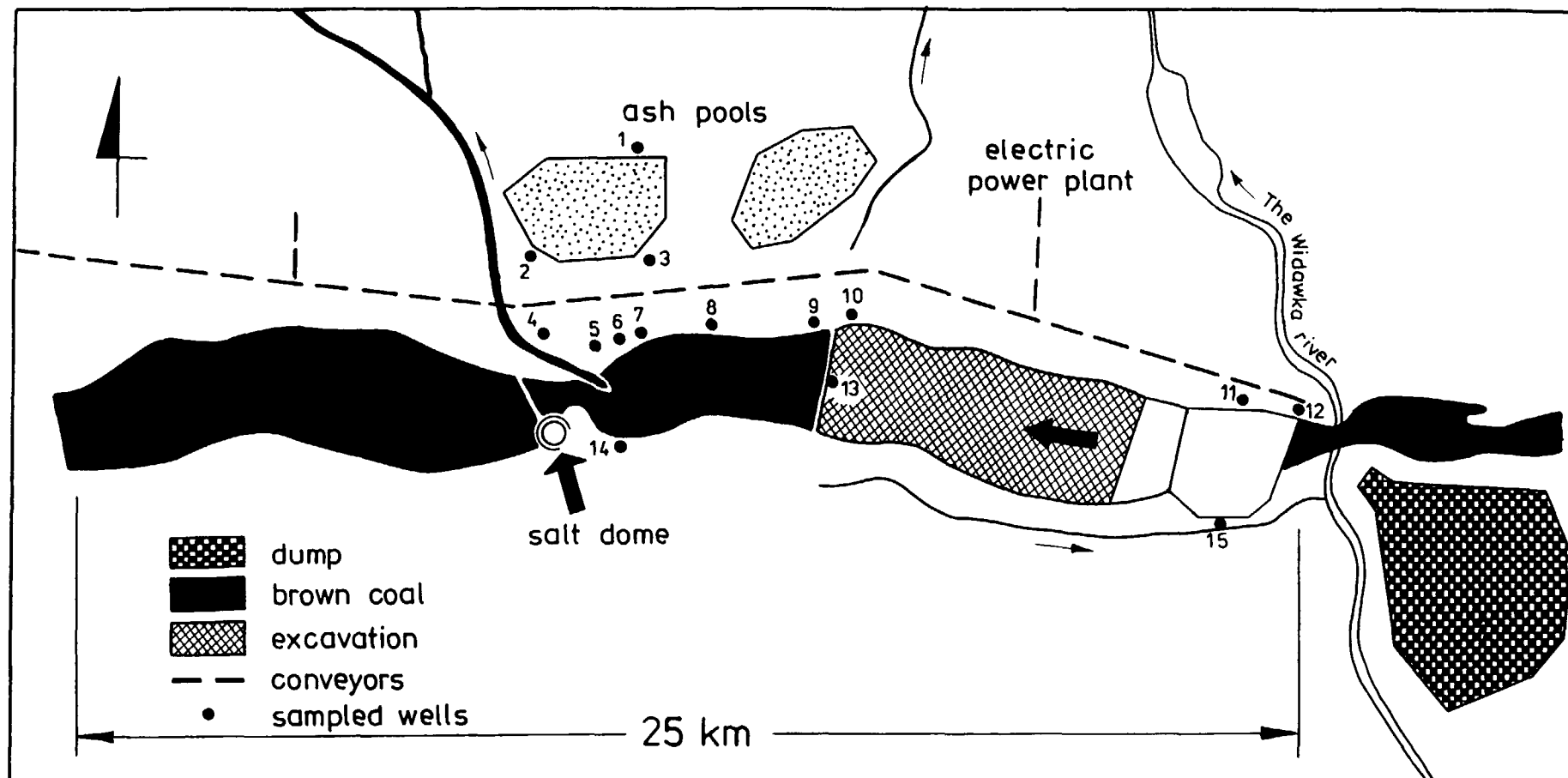
FIG.2. The study area. The numbers of the wells are: **No. 1** is P-4, **No. 2** is P-35, **No. 3** is 66/30, **No. 4** is 139 N, **No. 5** is 136 N, **No. 6** is 125 N, **No. 7** is 131 N, **No. 8** is 115 N, **No. 9** is 109 N, **No. 10** is 106 N, **No. 11** is 27 N-2, **No. 12** is 5 N bis, **No. 13** is 108H, **No. 14** is 101S, **No. 15 is** 18 S bis.

The drainage system of the wells around the Bełchatów mine forms a parallel barrier which protects the excavation against flooding. Some of these wells are 200 m deep or even deeper, up to 400 m. The total rate of water pumping exceeds 500 m³/min. The depression radius is estimated to be 20 km and the depression area is about 1,600 km².

The exploitation of brown coal resources causes major disturbances in the natural environment. Intense dewatering of the exposure area causes extended depression and disappearance of surface waters. The circulation of groundwaters becomes disturbed. Waters do not flow down a natural slope, but from the surrounding to the depression centre (i.e. to the excavation). The changes of the waterflow cause further complications. Many chemical species can now appear in the water, their concentration has increased over the period of exploitation.

The changes in the groundwater system have been detected by means of 200 piezometres and 2,000 wells in the depression area. The reduction of the water table exceeds 10 m. The groundwaters are intensively mixed while pumped up to the depth of 350 m. Deeper groundwaters which lie under this depth are not disturbed, so the admixture of deeper, more mineralized groundwater may be excluded. The lateral infiltration does not introduce water of different chemical composition. The outpumped water is weakly mineralized and is utilized to supply the tap-water pipe system.
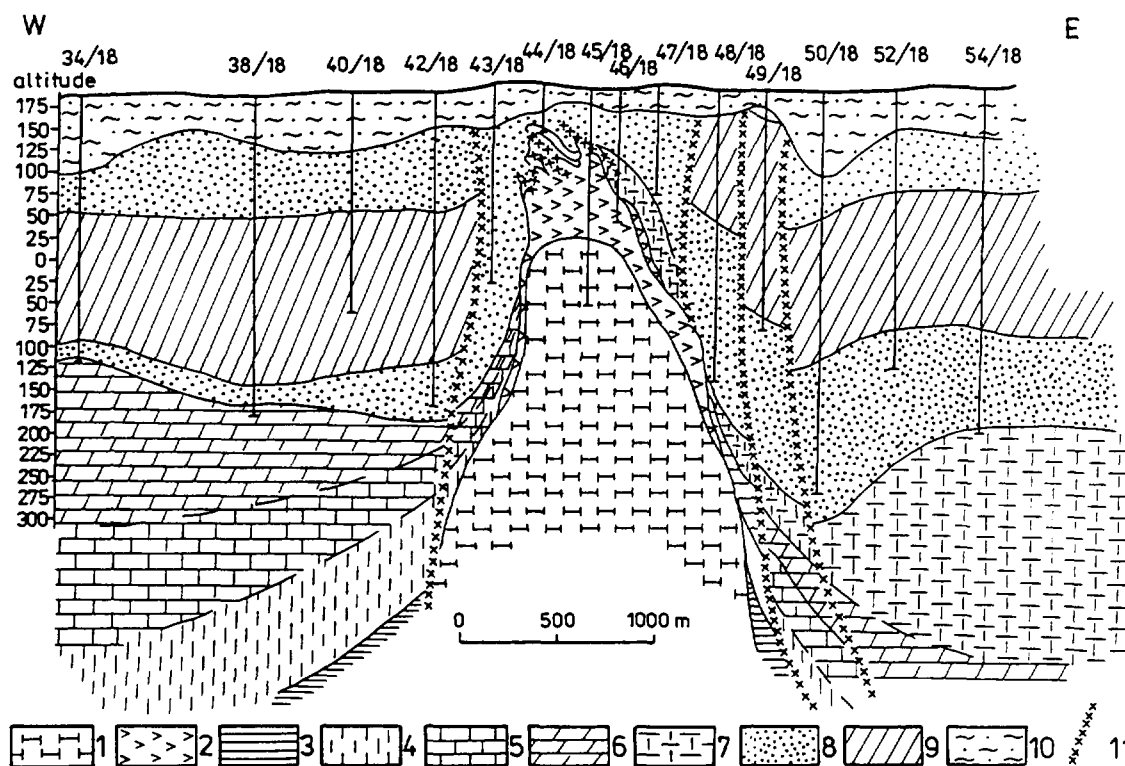
FIG.3. Geological section through the Dębina salt dome (after Baraniecka, 1980).
1-Permian salt, 2-dome cap rock, 3-Lower Jurassic, 4-Middle Jurassic;Upper Jurassic: 5-Oxfordian, 6-Kimmeridglan; Upper Cretaceous: 7-Maestrichtian; Tertiary: 8-sub- and supra coal series of sands and silts, 9-coal series; 10-Quaternary, 11-fault lines.

The presence of a salt dome in the middle part of the deposit (Fig. 3) causes another disturbance. The lowering of the water table near the salt dome may cause the infiltration of the brine into the outpumped water, which can destroy the pumps and strongly increase the mineralization of the water. Therefore, careful monitoring of the water is necessary in the wells in the vicinity of the salt dome.

The combustion of coal in the electric power station pollutes the environment with gases, dusts and ashes. The ashes are washed out from the site of the conflagration and conveyed by water by means of the pipeline system into the sedimentation pools. The ash has been stored there since 1983. The excess of water seeps down and the pollutant infiltrates into groundwaters. Thus, the chemical composition of the groundwater and of the pumped water is changed and monitoring is necessary. At present, the wet ashes are transported by the conveyor without water and stored in the excavation. This method was applied to reduce the groundwater pollution.

Since 1983 the groundwaters have been studied by both chemical and isotope methods for early warning against increase of salinity. If the sulphate concentration increases, it will be necessary to know the origin of sulphates and to determine whether they come from the ashpool or from the salt dome. The latter would be a warning signal. We applied $\delta^{18}O$ and $\delta^{34}S$ analyses of dissolved sulphates in order to identify their origin. It was necessary to monitor the groundwater and also measure $\delta^{34}S$ values to detect the presence of the dissolved sulphate of the Permian gypsum which covers the salt dome. The isotopic composition of the Permian evaporites is well known [1]. $\delta^{34}S = 11‰$ and $\delta^{18}O = 11‰$. The presence of SO_4^{2-} ion with such an isotope composition would be the result of the leaching of the salt dome cover. Hence, it would be an early signal that brines may be infiltrating into groundwaters. The determination of the rate of sulphate penetration into groundwaters, especially from the ashpools, is another application of the $\delta^{18}O$ and $\delta^{34}S$ analyses of sulphates.

3.   ANALYTICAL PROCEDURES

The samples of water were poured into very clean plastic vessels of about 3 L volume. The samples were collected from the studied area and transported to the laboratory by car. Then the water samples were filtered and the sulphate ion was precipitated as $BaSO_4$ by $BaCl_2$ solution acidified with HCl. In this way an influence of any microbiological activity in the collected sulphate samples was excluded. Then the pure $BaSO_4$ was weighed, so that the SO_4^{2-} concentration could be found, and subsequently prepared in separate vacuum lines to CO_2 or SO_2 .For $\delta^{18}O$ analysis the $BaSO_4$ was reduced with graphite at 1,000 °C by the Rafter-Mizutani method   to CO which subsequently was converted to CO_2 in a glow discharge [23]. For $\delta^{34}S$ analyses the $BaSO_4$ was decomposed to SO_2, with $NaPO_3$ at 850°C, by the Hałas and Wołącewicz method [24].

The measurements of $\delta^{34}S$ and $\delta^{18}O$ values were performed with the dual inlet system and the triple collector mass spectrometer [25], [26]. The isotope data of $\delta^{18}O$ are expressed versus VSMOW standard while $\delta^{34}S$ is expressed versus CDT (see [27]. Every sample had been prepared twice and also measured at least twice, in order to obtain better precision of the average delta values than 0.08 ‰ (in terms of standard deviation of the average delta), from both $\delta^{34}S$ and $\delta^{18}O$ measurements.

4. RESULTS AND DISCUSSION

We have studied the sulphates coming from waters sampled in the following areas: (i) the salt dome area, (ii) the wells surrounding the ash-pool and (iii) the wells near the dry ash storage. The samples were collected three times: in November 1994, in May 1995 and in December 1996. In May 1995 we collected only 16 samples of groundwaters. Most of them came from the same groundwaters which were sampled in November. In December 1996 samples of groundwaters were taken only from the wells lying on the edge of the excavation. Table 1 presents the results of measurements for groundwaters dewatering the salt dome area. Samples Nos. 1 - 11 are the sulphates from the wells, while Nos. 12 - 20 are from piezometers.

Table 2 presents the results for other groundwaters: samples Nos. 21 - 28 represent the sulphates from the wells surrounding the ashpool, Nos. 29 - 43 the sulphates from the wells dewatering the storage of dry ashes in the excavation from the South and the North, Nos. 44 - 54 the sulphates from the wells lying between the ashpool and the excavation. The difference
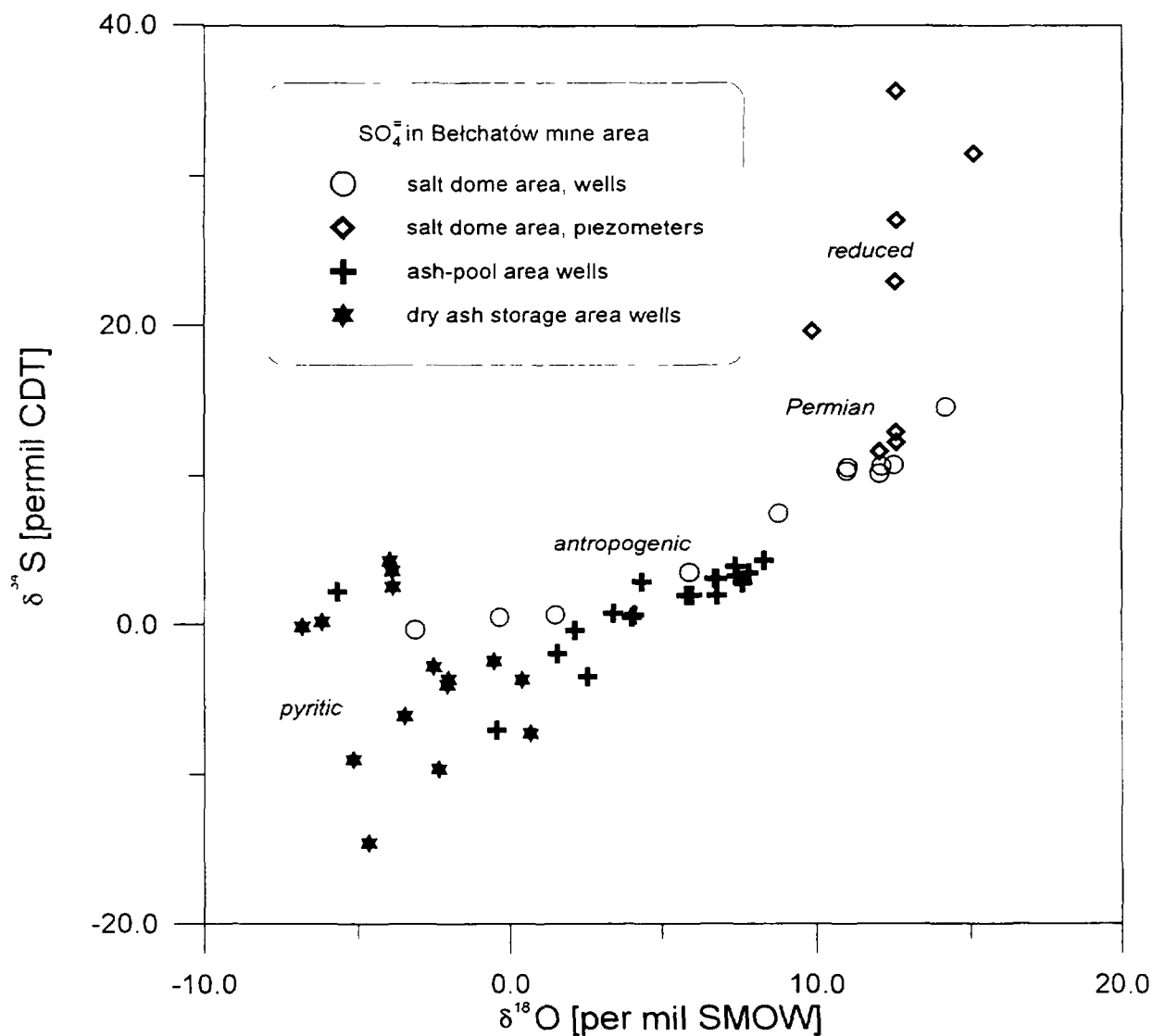
FIG.4. $\delta^{34}S$ and $\delta^{18}O$ of sulphates from different groundwaters of the Bełchatów mine.

Table 1. The isotopic and chemical data of selected groundwaters from the Belchatów brown coal mine in the salt dome area.

sample No.	well No.	depth [m]	SO_4^{2-} [mg/L]	$\delta^{34}S_{CDT}$ [‰]	$\delta^{18}O_{VSMOW}$ [‰]
wells					
1	5 SD	242.0	42.3	+0.46	-0.35
2	6 SD	241.0	73.6	-0.38	-3.13
3	11 SD	191.0	283.2	+10.71	+12.48
4	12 SD	200.0	214.2	+10.61	+12.08
5	22 SD	240.3	20.1	+0.65	+1.52
6	27 SD	178.7	3.3	+7.48	+8.77
7	30 SD	239.8	199.3	+10.13	+12.01
8	24 SD[b]	242.6	18.0	+3.47	+5.86
9	26 SD[b]	262.5	9.0	+14.55	+14.16
10	30 SD[b]	239.8	240.0	+10.55	+11.00
11	10 SD[b]	156.9	65.8	+10.30	+10.97
piezometers					
12	PD-8	287	4.3	+35.58	+12.54
13	PD-5C	255	2.5	+27.00	+12.59
14	PD-6C	252	1.1	n.a.	
15	19 SDp	272	91.2	+22.90	+12.52
16	PD-7	175	3.8	+19.60	+9.85
17	PD-27	208	1011.4	+11.59	+12.01
18	PD-9 B	60	1001.3	+12.87	+12.55
19	PD-39	141	1471.1	+12.20	+12.57
20	PD-41	182	9.5	+31.44	+15.08

[b]sampled in May 1995

in their isotopic composition is significant, which helps to identify their origin. These results are plotted in Fig. 4, where the distinction is made according to the location of the wells. It is seen, however, that points in Fig. 4 are also grouped according to the origin of the sulphates (see comments below).

The salt dome area. A higher concentration of sulphate, more than 200 mg/L, may be observed in the groundwaters in some of the wells (samples Nos. 3, 4, 7, 10 and 11 in Tab. 1. These sulphates have $\delta^{34}S$ values ≈ 10‰ and $\delta^{18}O$ values ≈12‰, typical values for the Permian evaporate [1]. Sample No. 10 (taken in May) comes from the same well as sample No. 7 (sampled in November). The well represented by sample No. 11 sampled in May is located between wells Nos. 3 and 4 measured in November.

Sample No. 9 has sulphur and oxygen enriched in heavy isotopes, and this may be caused by reducing bacteria because the concentration of the sulphate is low (9 mg/L). However, this sulphate may be of different origin.

Table 2. The isotopic and chemical data of selected groundwaters from the Bełchatów brown coal mine in locations specified.

sample No.	well No.	depth [m]	SO_4^{2-} [mg/L]	$\delta^{34}S_{CDT}$ [‰]	$\delta^{18}O_{VSMOW}$ [‰]
the ashpool					
21	from the ashpool	surface	183.4	+1.94	+5.93
22	P-4	15	125.0	+3.21	+7.39
23	P-35	32	195.8	+1.95	+6.74
24	66/30	24	89.3	+3.86	+7.33
25	from the[b] ashpool	surface	190.0	+0.65	+4.10
26	P-4[b]	15	150.0	+4.28	+8.28
27	P-35[b]	32	108.0	+2.76	+7.56
28	66/30[b]	24	258.0	+0.46	+4.02
the wells lying on the edge of the excavation					
29	41 N[c]	176.0	52.0	-2.44	-0.54
30	33 N[c]	175.0	145.0	-7.22	+0.68
31	29 N-1[c]	179.0	147.0	-2.80	-2.53
32	27 N-2	179.0	161.9	-6.11	-3.47
33	5 N-bis	311.0	60.8	-9.03	-5.15
34	1 A-1[c]	330.0	7	-3.65	+0.40
35	2 E-2[c]	307.0	54.0	-4.02	-2.08
36	14 E-bis[b]	209.7	109.0	-14.62	-4.64
37	14 S-1[c]	242.0	552.0	+3.56	-3.88
38	18 S-bis	244.0	309.6	-0.18	-6.80
39	18 S-bis[b]	244.0	258.0	+0.17	-6.16
40	18 S-bis[c]	244.0	462.0	+2.50	-3.86
41	22 S-bis[c]	238.0	113.0	+4.24	-3.96
42	89 N[c]	230.0	61.0	-9.66	-2.37
43	93 N[c]	225.7	47.0	-3.65	-2.05
the wells lying on the edge of the ashpool					
44	106 N[b]	167.0	110.0	-1.92	+1.58
45	109 N[b]	243.0	92.0	+2.82	+4 34
46	115 N	240.0	31.3	-0.39	+2.16
47	125 N	244.5	67.8	+3.04	+6.73
48	63 A-1[b]	202.0	70.0	+3.08	+6.67
49	131 N	230.0	15.5	+0.74	+3.42
50	81 A[b]	233.0	4.0	+3.42	+7.78
51	136 N	243.0	3.2	+1.92	+5 78
52	139 N[b]	244.0	8.0	-3.46	+2.58
53	108 H[b]	120.5	600.0	+2.16	-5 69
54	101 S	246 0	9.6	-7.04	-0.45

[b]sampled in May 1995
[c]sampled in December 1996

In other wells the sulphates have nothing in common with gypsum (samples Nos. 1, 2, 5. These sulphates may come from oxidized pyrites or from soil. Sample 6 may be a mixture of sulphates of evaporitic and other origin. This well is located between the wells which are represented by samples 5 and 7. The investigation of the isotopic composition of sulphates in the wells of this area is very useful. Also sample No. 8 has nothing in common with gypsum, as well as samples No. 1 or No. 5.

The piezometers turned out to be worse indicators for isotope analyses than the wells. The values $\delta^{34}S$ and $\delta^{18}O$ of sulphates Nos. 17, 18 and 19 suggest evaporitic origin (the $\delta^{34}S$ about 12‰ and $\delta^{18}O \approx 12$‰), but other results of $\delta^{34}S$ and $\delta^{18}O$ are typical for the reducing process which enriches sulphates in heavy isotopes (sulphur is usually more enriched than oxygen) and decreases the concentration of sulphates. It is hard to say what the primary isotopic composition of these sulphates was, hence their origin remains unknown. During the reduction, the concentration of the sulphate decreases and the δ values increase. Such high values $\delta^{34}S$ up to 35‰ and $\delta^{18}O$ up to 15‰ were observed together with a very low concentration of the sulphate, from 9 to 1 mg/L (see sample No. 20). Probably these groundwaters do not flow fast enough and the stagnancy of the water permits the bacterial reduction of sulphates. Only in the waters in which the concentration of sulphates is high, the values of $\delta^{34}S$ and $\delta^{18}O$ may be unchanged. So, the values of samples Nos. 17, 18, 19 which represent the waters with a high concentration of sulphates (more than 1 g/L) are similar to the evaporitic sulphate. These waters come from the piezometers situated under the top of the salt dome.

Wells surrounding the ashpool. The brown coal used in the power station contains about 0.5% sulphate and 0.78% sulphide, which are oxidized during combustion [28]. The concentration of sulphates has increased since the beginning of the storage (since 1983) in the wells surrounding the ashpool. These wells are represented by samples Nos. 21 - 28 in Table 2. The sulphate ion concentration in these waters is high, about 100 - 250 mg/L. Samples No. 21 and 25 come directly from the pool. Samples Nos. 22, 26, 23, 27, and 24, 28, which come from the wells surrounding the ashpool, have similar isotopic composition. The $\delta^{34}S$ values range from 0 to 4‰ and $\delta^{18}O$ values from 4 to 8‰, respectively and they are similar in November and in May. These patterns are typical for anthropogenic sulphates and the isotopic composition of these sulphates confirms their origin; there is no doubt that these sulphates come from the ashes.

Samples Nos. 45, 47, 48, 49, 50, 51, which come from the wells located between the ashpool and the excavation, have similar isotopic composition. Also these sulphates come from the ash.

Sample No. 54 comes from the well which is bored on the other side of the excavation and has nothing in common with the ashpool. Indeed, $\delta^{34}S$ and $\delta^{18}O$ are typical for oxidized sulphides. Also, sulphate of sample No 46 comes from the well which is not influenced by the ashpool (see Fig. 2).

The isotopic composition of samples Nos. 44 and 52 is rather typical for oxidized sulphides, like in sample No. 54 or No. 46. Water in these wells is not influenced by the ashpool.

Wells near the dry ash storage. Presently, ashes are conveyed without water and stored in the excavation. An increase of the sulphate concentration in the groundwaters which are outpumped from this region has been noticed by Sołtyk [29]. These groundwaters are represented by samples Nos. 29 - 43. Their sulphates have the most negative values of $\delta^{34}S$ up to -14.6 and $\delta^{18}O$ -6.8‰, which excludes the possibility that these sulphates might be coming from the ash. The δ values are typical for the sulphide oxidation processes. The negative values of $\delta^{18}O$ suggest that more than 70% of the oxygen [7], [8] comes from the water with δ ^{18}O = -10.5‰, typical value for shallow groundwater in Poland [13].The oxidized material may come from sulphides in coal or from the Cretaceous rocks.

Sample No. 53 from the centre of the excavation is very interesting. This groundwater has a very high concentration of sulphate (600 mg/L) but $\delta^{34}S$ and $\delta^{18}O$ value suggests that this sulphate is formed by sulphide oxidation rather in water than during combustion in air, so it probably has nothing in common with ashes.

5. CONCLUSION

The use of $\delta^{34}S$ and $\delta^{18}O$ allows us to distinguish between sulphates coming from the leaching of a Permian salt-dome, those coming from oxidized sulphides in the groundwater and those of anthropogenic origin (leached from the ashes). It is clear from the data obtained so far that the oxygen and sulphur isotope ratios of the dissolved sulphates are informative of their origin.

The samples of groundwaters from the wells are more representative for the investigation of the isotopic compositions of sulphates than from the piezometers.

ACKNOWLEDGEMENTS

REFERENCES

[1] CLAYPOOL G. E., HOLSER W. T., KAPLAN I.R., SAKAI H., ZAK I. The age curves of sulfur and oxygen isotopes in marine sulfate and their mutual interpretation, Chem. Geol. **28**, (1980) 199-261.

[2] KROUSE H. R., VAN EVERDINGEN R. O. Interpretation of oxygen isotope data for sulphate in subsurface waters. Int. Assoc. Geochemistry and Cosmochemistry 5th. Int. Symp. Water-Rock Interaction, Reykjavik, Iceland, August 8 - 17, (1986) 663-666.

[3] FRITZ P., BASHARMAL G. M., DRIMMIE R. J., IBSEN J., QUERESHI R. M. Oxygen isotope exchange between sulphate and water during bacterial reduction of sulphate, Elsevier Science, Chem. Geol. **79**, (1989) 99-105.

[4] KROUSE H. R., GOULD W. D., McCREADY R. G. L., RAJAN S. O incorporation into sulphate during the bacterial oxidation of sulphide minerals and the potential for oxygen isotope exchange between O_2, H_2O and oxidized sulphur intermediates, Earth and Planetary Science Letters, **107**, (1991) 90-94.

[5] LLOYD R. M. Oxygen -18 composition of oceanic sulphate Science **156**, (1967) 1228-1231.

[6] LLOYD R. M. Oxygen isotope behaviour in sulfate water system, J.Geophys. Res. **73**, (1968) 6099-6110.

[7] TORAN L. Sulfate contamination in groundwater from a carbonate-hosted mine, Journal of Contaminant Hydrology 2, (1987) 1-29.

[8] TORAN L., HARRIS R. F. Interpretation of sulfur and oxygen isotopes in biological and abiological sulfide oxidation. Geochim. et Cosmochim. Acta **53**, (1989) 2341-2348.

[9] CORTECCI G, LONGINELLI A. Isotopic composition of sulfate in rain water, Pisa, Italy. Earth Planet Sci. Lett **8**, (1970) 36-40.

[10] KROUSE H. R. Sulphur isotopes in our environment, Handbook of Environmental Isotope Geochemistry vol. I, The Terrestrial Environment A., Fritz P., Fontes J. Ch., Elsevier, (1980) 35-471.

[11] KROUSE H. R. Sulfur isotope studies of the pedosphere and biosphere, in Ecological Studies, vol. **68**, Stable Isotopes in Ecological Research edited by Rundel P. W., Ehleringer J. R. and Nagy K. A., (1989) 422-444.

[12] KROUSE H. R., GRINIENKO V. A. (Editors) Stable isotopes natural and anthropogenic sulphur in the environment, Scope 43. John Wiley & Sons, Chichester, New York, Brisbane, Toronto, Singapore. (1991)

[13] TREMBACZOWSKI A. Sulphur and oxygen isotopes behaviour in sulphates of atmospheric groundwater system, observation and model. Nordic Hydrology, **22**, (1991) 49-66.

[14] MIZUTANI Y., RAFTER T. A. Oxygen isotopic composition of sulphates. Part 5. Isotopic composition of sulphate in rain water grace field New Zealand. *N. Z. J. Sci.* **12**, (1969) 69 - 74.

[15] KROUSE H. R., TABATABAI M. A. Stable Sulfur Isotopes, American Soc. of Agronomy-Crop Science Society of America-Soil Science Society of America Sulfur in Agriculture, Agronomy Monograph no. **27**, (1986) 169-205.

[16] MIZUTANI Y., RAFTER T. A. Isotopic behaviour sulphate oxygen in the bacterial reduction of sulphate. Geochem. J. **6**, (1973) 183-191.

[17] HOLT B. D., KUMAR R. Oxygen isotope fractionation for understanding the sulphur cycle, in 1991 SCOPE, John Wiley & Sons Ltd, (1991) 27-41.

[18] SMEJKAL V. Oxygen isotopic composition of sulphates from some mineral waters and mine waters in western Bohemia. Isotope Hydrology 1978, IAEA Vienna (1979) 83-98.

[19] SMEJKAL V. Isotopic recognition of sulphate contamination source of groundwaters and surface waters in the proximity of energetic industry ash storages, (in Czech), Vodni hospodarstvi, **3**, (1990) 114-118.

[20] HAŁAS S., SOŁTYK W., TREMBACZOWSKI A. [18]O and [34]S in sulfates of groundwaters in brown coal deposit. Influence of salt dome and surface pollution on the groundwaters. Extended Synopsis IAEA Vienna, (1987) 205- 207.

[21] BARANIECKA M. D., CIEŚLIŃSKI S., CIUK E., DABROWSKI A., DABROWSKA Z., PIWOCKI M., WERNER Z. Geological structure of the Bełchatów region, (in Polish), Przegl¹d Geologiczny **28**, (1980) 381-391.

[22] TUREK. S. Hydrogeochemical conditions in area affected by drainage of brown coal deposits in the Bełchatów region (in Polish). Przegl¹d Geologiczny 28, (1980) 397-401.

[23] MIZUTANI Y. An improvement in the carbon - reduction method for the oxygen isotopic analysis of sulphates. Geochem. J. **5**, (1971) 69-77.

[24] HAŁAS S., WOŁACEWICZ W. Direct extraction of sulfur dioxide from sulfates for isotopic analysis. Anal. Chem. **53**, (1981) 685-689.

[25] HAŁAS S. An automatic inlet system with pneumatic changeover valves for isotope ratio mass spectrometer, J. Phys. E.: Sci. Instrum. **18**, (1979) 417-420.

[26] DURAKIEWICZ T., HAŁAS S. Triple collector system for isotope ratio mass spectrometer. I.F. UMCS Report, (1994) 131-132.

[27] IAEA-TECDOC-825 Reference and intercomparison materials for stable isotopes of light elements, IAEA Vienna (1995).

[28] PIWOCKI M. The ways of protection of natural environment on the mine areas, (in Polish). Wyd. SGGW-AR, Warszawa (1990) 170-190.

[29] SOŁTYK W. Water chemistry of Bełchatów area (archival data, unpublished) (1994).

FLUORIDE CONTAMINATION IN THE LAKES REGION OF THE ETHIOPIAN RIFT:
Origin, mechanism and evolution

Y. TRAVI, T. CHERNET[*]
Laboratoire Hydrogéologie, Université d'Avignon
Avignon. France

Abstract - *The closed lake basins occupying the Main Ethiopian Rift are characterised by unique hydrogeological conditions which have resulted in very high contents of fluoride associated with highly concentrated sodium bicarbonate waters. The origin, mechanism and evolution of fluoride contents have been examined successively by studying, (i) the reservoirs which provide this element in solution, (ii) the hydrochemical context, and (iii) the hydrological evolution which modifies the concentrations. Groundwaters of the ignimbrites present low values compared to those of the lacustrine sediments which can provide contents 5 to 10 times greater. The non equilibrium initial stage between the alkalinity and the calcium, derived from weathering of volcanic rocks, is responsible for the specific chemical evolution and the very high fluoride values. Furthermore, in the thermal waters, the high temperatures (especially those up to 100°C) and the presence of large amounts of CO_2 coming from depth increase significantly the fluoride contents. Finally, the fluoride concentrations can change depending on the interrelation of ancient or present surface waters and groundwaters (mixing) and on the hydrological balance (concentration and dilution processes)*

1. INTRODUCTION

The harmful biological effect of the fluoride ion gives this element an important place in the quality of drinking water. Its presence in small quantities prevents tooth decay; however when it is in excess quantity it provokes dental or bone fluorosis. The upper limit for potability is around 1 mg/l. Observations carried out in North and West Africa indicate that this problem is often widespread. It is the case, for example, in Senegal, Niger, Morocco, Algeria and Tunisia. In these countries, harmful concentrations are associated with phosphatic and some igneous rocks. Maximum contents of fluoride are around 10 mg/l and they are controlled by the hydrodynamics of the aquifer and by the fluorite saturation . In some cases, in these non acidic waters, the ion pair MgF^+ is also concerned (Travi,1993).

In Ethiopia, previous studies have shown that extensive areas, with high F- values in natural waters are very frequent, and they are almost exclusively in the Main Ethiopian Rift (MER) (Chernet and Travi, 1993). Furthermore in all the hydrological systems (groundwaters. thermal waters, surface waters) the higher values are localised in the Lakes Region (up to 300 mg/l).

The objective of this paper is to summarise the results of three years' fieldwork, (Chernet, 1998) including previous data, trying to determine the specific conditions of high fluoride removal in the Lakes Region which is located 130-280 km south of Addis Ababa. Considering its very low concentration in rainfall, the fluoride ion originates in the reservoir;

---

* Present address: P.O. Box 40950 Addis Ababa, Ethiopia.

then it is controlled by hydrochemistry and it changes with hydrological evolution, particularly by mixing between surface waters and groundwaters and according to the hydrological balance (dilution - concentration process)(Chernet and Travi, 1995). These three points will be examined successively after a brief presentation of the hydrogeological setting.

2.   HYDROGEOLOGICAL SETTING

The Ethiopian Rift is a part of the East African Rift system and the Lakes Region of closed basins lies in this rift, 150-300 km south of Addis Ababa between latitudes 6° 50' N and 8° 19' N and longitudes 38° 7'E and 39° 24'E. The average width of the rift valley in the region is 70 - 80 km and it runs in a general north - south direction with a total area of about 16000 km^2. In general, the altitude is about 2500 m at the plateau and about 1600 m at the rift floor. The rainfall distribution in the year is typical of the type in the rift valley to the north of the Lakes Region and adjacent to the escarpments with one peak in July-August and another smaller peak in March-May. The average annual rainfall in the region ranges between 600 and 1100 mm, while the potential evapotranspiration ranges between 1000 mm and 2500 mm.

Groundwater lies in volcanic rock aquifers essentially located on the plateau, and lacustrine sediment aquifers in the bottom of the rift. The volcanic rocks are largely ignimbrites (60% of the area), but also alkaline basalts and trachybasalts, recent basalts and acidic complexes (rhyolites, tuffs, pumice and obsidian). They have moderate to high permeability with borehole yields of 0-6 l/s. Lacustrine sediments, the second extensive unit (16% of the area) consist of alternating fine and coarse beds and they are predominantly fine to medium grain. They show low to moderate potential of 1-5 l/s.

The region is a large closed basin of rift valley lakes which are hydrologically interconnected. Each lake has a different level of being closed and of being replenished-discharged-evaporated (Fig.1) which largely accounts for the level of its salinity. Surface and groundwater flows concentrate towards the Shalla Lake, filling up a large caldera in the rift floor, at the lowest elevation. The Lake Region is known to be characterised by geothermal features especially in the areas east and north of Awasa, east and south of Shalla, and north of Langano. Several thermal springs and fumaroles are noted in these localities.

3.   ROLE OF THE RESERVOIR

The role of the reservoir has been firstly examined by comparing fluoride contents and the geological nature of the reservoir. On the escarpment sides of the rift, fluoride contents reach no more than 3 mg/l with a gradient downward; most of the cold springs found in the highlands have a fluoride content less than 0.6 mg/l compared to 2.6 mg/l in the lowlands (Buko spring near the Children's Village). Some thermal waters can reach 7 mg/l.

In the groundwater of the lacustrine sediments the amount of fluoride is 5 to 10 times greater than that of the ignimbrites and they generally present a larger range of values. Thus, there is evidence of thermal contribution and hydrological influence due to the proximity of the lakes. As a consequence, in order to determine the specific role of the lacustrine sediments three series of leaching experiments have been carried out.

In order to estimate the fluoride content in the solution when it reaches equilibrium with the sediment, samples have been submerged in distilled water in polyethylene bottles.

96
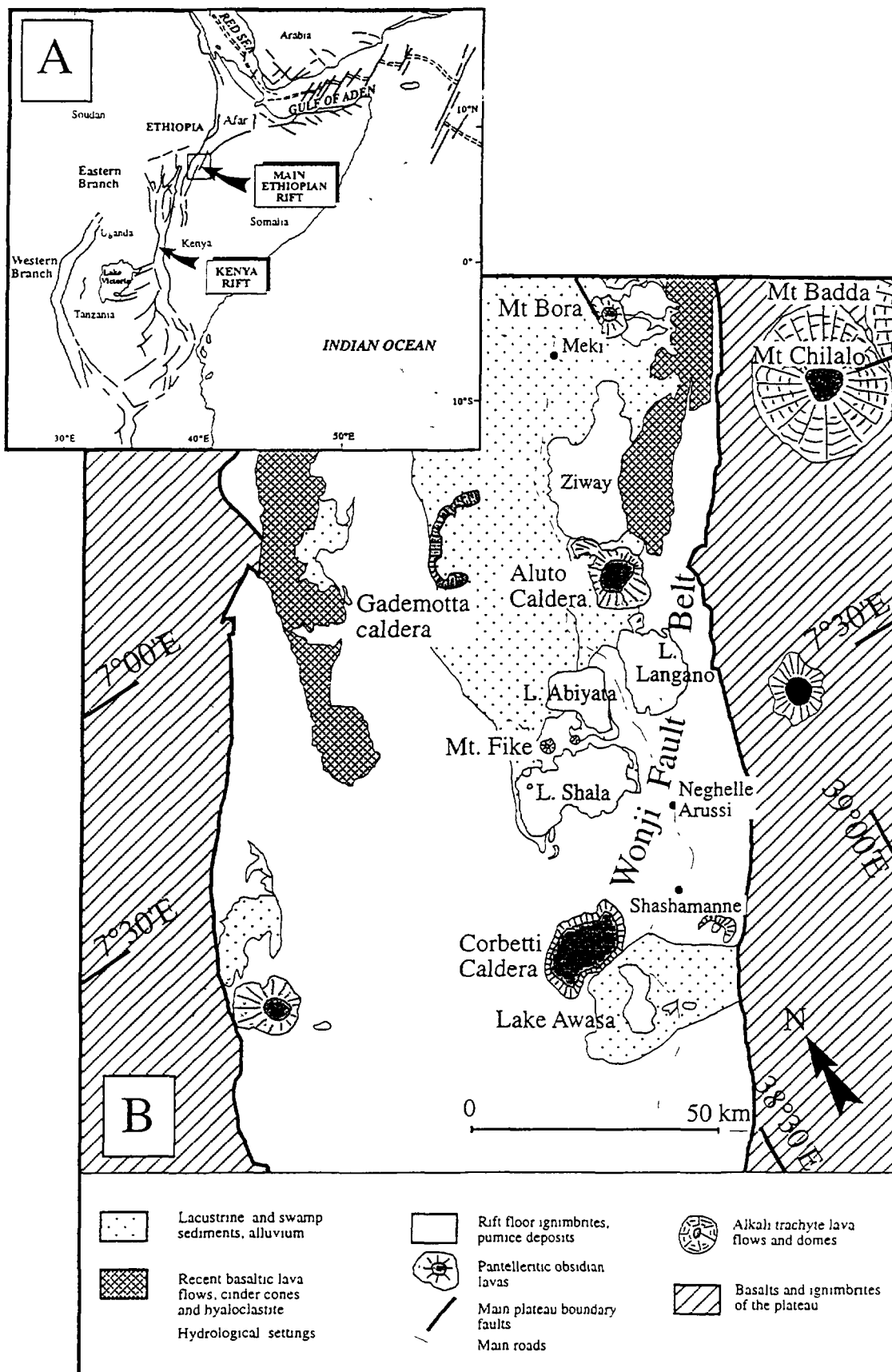
Fig. 1. Location map.

Two kinds of evolution have been reported (Fig 2). The samples which stabilize rapidly for contents of less than 10 mg/l and the others which stabilise for values near 20 mg/l or attain very high values. The results obtained can be related to the geographic position, vertical or lateral, with respect to the lakes.

The influence of CO_2 on the dissolution and equilibrium of $CaCO_3$ and CaF_2 has been studied by comparing the results of the same samples when the bottles are closed or open.
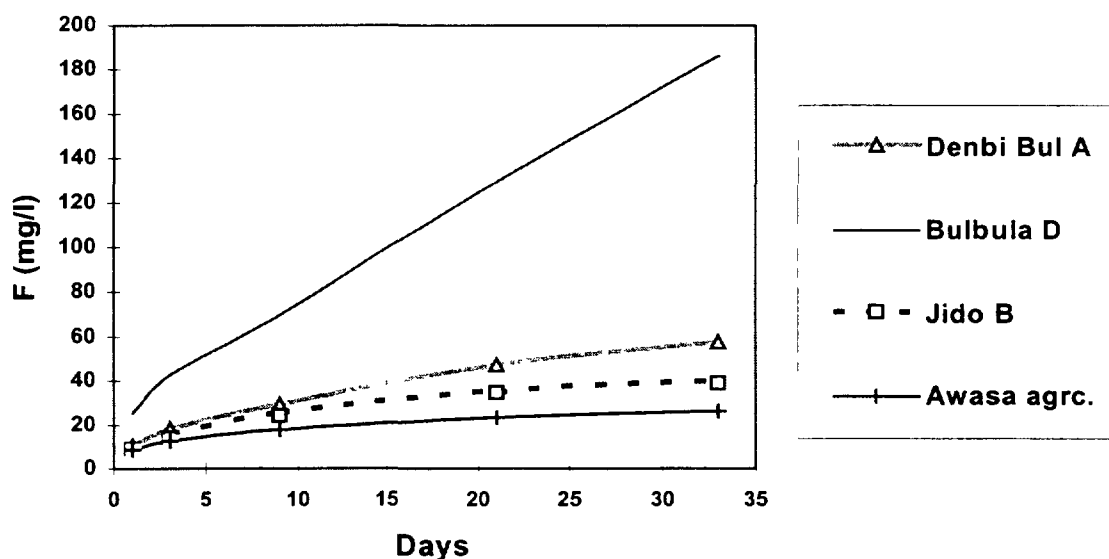
Fig 2. Results of leaching experiments

These experiments have shown the following results:
- rapid dissolution of the fluoride is generally observed in all samples showing probably the presence of free F⁻ adsorbed to clays;
- for some samples the level of stabilisation is not reached or not reached quickly, which indicates that the control of CaF_2 is noted in certain cases and not in others.
- in some cases, the presence of CO_2 can strongly increase the fluoride content;
- the geographic distribution of these sediments mineralised in fluoride in the zone around the lakes, if examined with a good knowledge of the chemical evolution of the surface waters of the rift, indicate that the fluoride can be used as a paleohydrologic tracer.

4. HYDROCHEMICAL CONTROL ON FLUORIDE

All hydrochemical data of the present and past studies have been plotted on a Piper diagram (Fig. 3). The waters of the region evolve from a calcium bicarbonate type on the highlands to sodium bicarbonate type towards the lakes, and finally to a mixture of bicarbonate, sulphate and chloride type around the lakes, related to thermal features.

All the data have been treated in the computer software AQUA (Valles et al., 1996) in terms of geostatistics, statistics and chemical equilibrium. Concentration diagrams show that sodium, alkalinity and fluoride are relatively conservative and can be used as tracers. The successive precipitation of calcite, magnesium silicate, amorphous silica and sometimes fluoride seems to be suggested.

The waters of the area are generally saturated with calcite. When equilibrium is attained, the ratio of the activity of Ca^{2+} and CO_3^{2-} evolves in the branch $CO_3^- > Ca$, confirming the law of the alkalinity residual. The equilibrium with fluorite is often attained for medium or very concentrated waters (Fig 4).The solutions evolve in the branch $F^- > Ca^{2+}$ which conforms to the generalised law of the alkalinity residual applied to the precipitation of calcite and fluorite (Ribolzi et al., 1996). The decrease in the activity of calcium slows the evolution towards equilibrium with fluorite.

For the most concentrated waters (in lakes) the equilibrium of the sodium fluoride shows moderate under saturation. Therefore, it is possible that at the time of the process of a localised drying up of the sediments this mineral can form and store the fluoride in a form which is rapidly soluble.
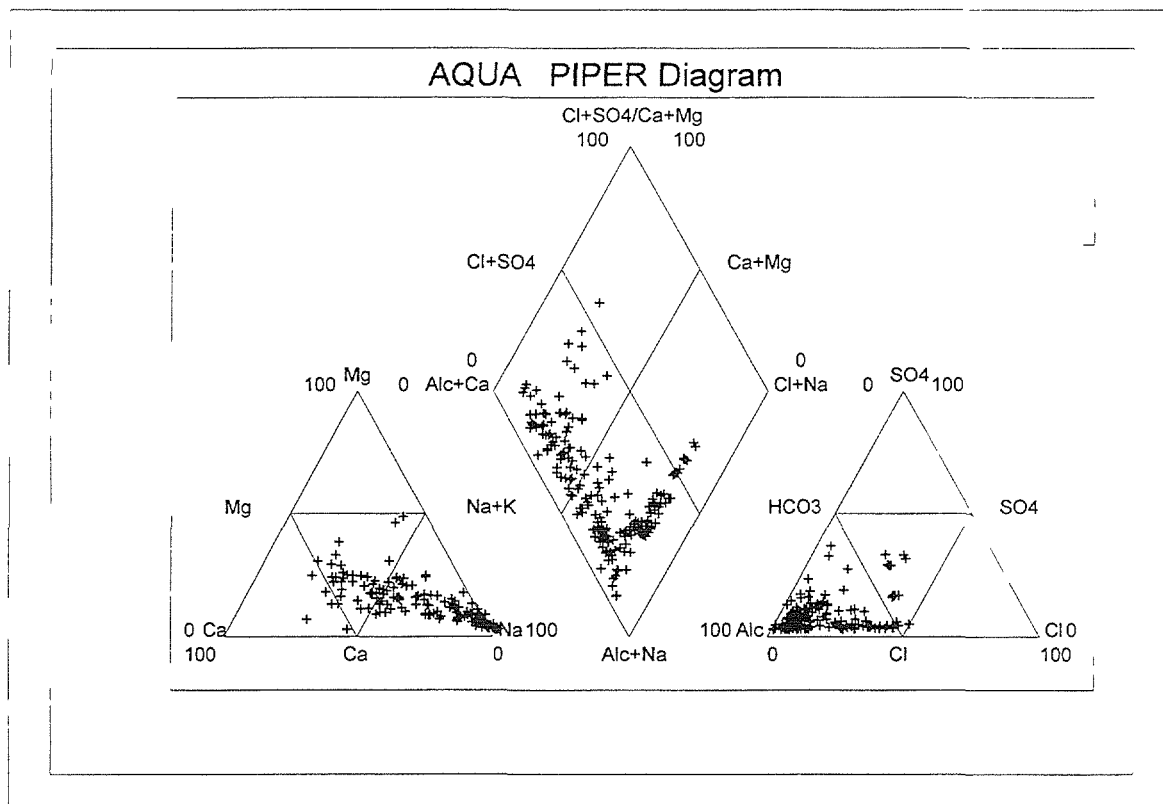
Fig 3. Piper diagram - Chemical characteristics of the natural waters of the area

The influence of the different origins of the waters, superficial groundwater or thermal waters, were able to be observed. Primarily, the acquisition of high fluoride contents and the alkaline-sodic characteristics depend on the non equilibrium initial stage between the alkalinity and the calcium as a result of weathering and dissolution of the volcanic rocks. When the waters concentrate, the precipitation of calcite leads to a decrease in the chemical activity of calcium, which leads to a strong solubility of fluoride; in surface waters the small amount of calcium which remains in solution does not allow direct control of the calcium on the concentration of fluoride. So, by the effect of climate (evaporation), this element concentrates without being significantly affected by the precipitation of fluorite. The fluoride content of thermal waters increases with the temperature up to 100°C. This is related to the fact that the solubility of calcium carbonate decreases without increasing the temperature and at the same time the solubility of fluorite is increasing (Chernet et al., 1997).

AQUA EQUILIBRIUM SOLUTION-FLUORITE

$log(Ca++)$

$2*log(F-)$
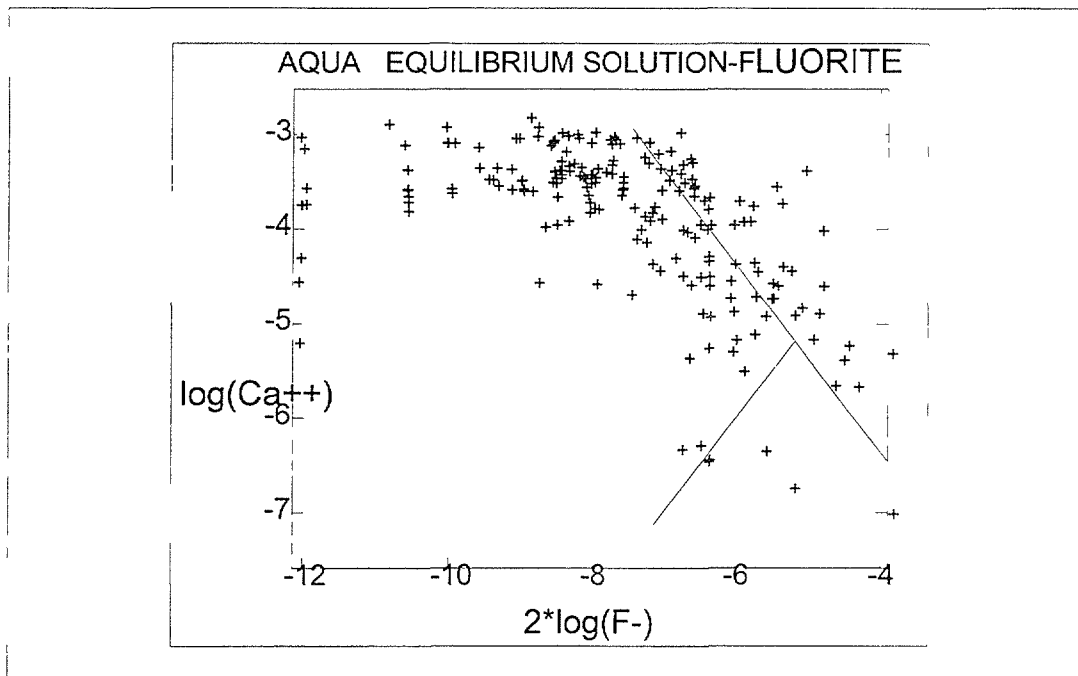
Fig 4 . Equilibrium solution diagram of fluorite concerning the natural waters of the area

5.   HYDROLOGICAL EVOLUTION

Hydrometeorologic data from several stations were processed to understand the hydrologic characteristics of the area and to calculate the water balances of the lakes.

Isotope investigations of ^{18}O, ^{2}H, ^{13}C, and ^{14}C were carried out on the rain waters, surface waters, and groundwaters. The input signals were made precise (Fig 5), using the data from Addis Ababa (IAEA network). The rain signals were taken based on 5 stations in the region and Addis Ababa during the main rainy months of June - September of the years 1993-95, and with the surface waters coming from the highlands.

The non-evaporated samples generally lie on a line with deuterium excess of about 15 per mil. The samples coming from the rift show the same distribution as for Addis Ababa, with the same clear difference between the main rainy season and the other seasons which are dry. The global weighted mean is -2.9 $\delta^{18}O$. The weighted mean for the rainy season over the region is 0.30 $\delta^{18}O$.

Waters of rivers coming from the sides of the rift are homogenous (between -1.5 and -2.4‰) and they represent the average values of the rains. Thus the stable isotopes appear to be very useful tracer to study the present and ancient hydrological processes and particularly evaporated surface waters and groundwater interrelations in the low parts of the rift. Some negative values indicate the presence of an altitude effect on the waters of the highlands. Some of these waters can reach directly via the groundwater to the plain (for example north east of the Ziway lake).

100
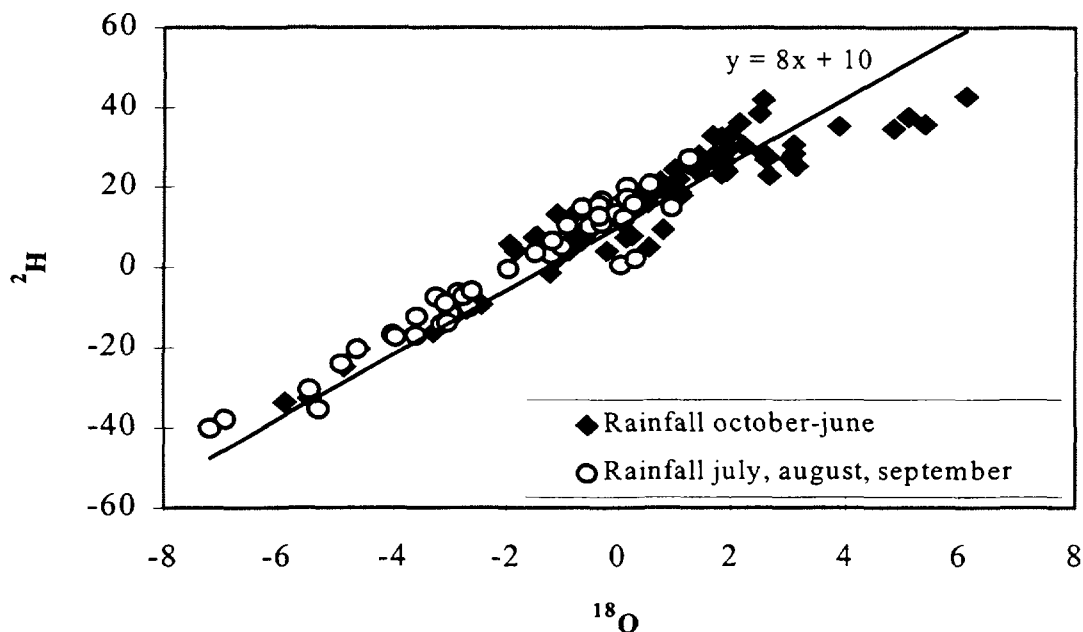
Fig 5 . Relation between ^{18}O and ^{2}H of the rainfall in Addis Ababa and the Lakes Region 94, 95), data for Addis Ababa taken from IAEA, Environmental Isotope Data (61-89)
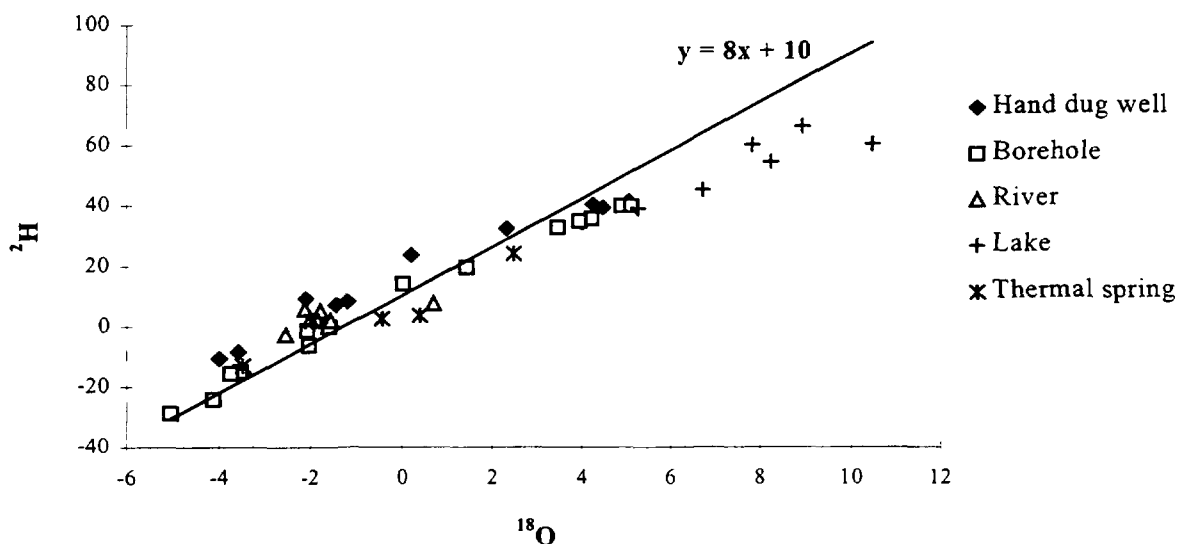
Fig. 6. Relation between 18-O and 2-H in the surface waters and ground waters.

The natural waters of the region can be characterised in a ^{2}H-^{18}O graph (Fig 6). Two categories can be identified: the waters near the input signal and the waters more or less evaporated. The groundwaters show three types of values: the waters near the input signal, waters which have been evaporated, and some samples which are more depleted. Being localised near the west side, they probably characterise local fossil groundwaters. The evaporated waters are located around the lakes, in particular between Ziway and Abiyata (Fig 7), showing clearly the presence of the exchange of water between the lakes and groundwaters (recharge and discharge).

101
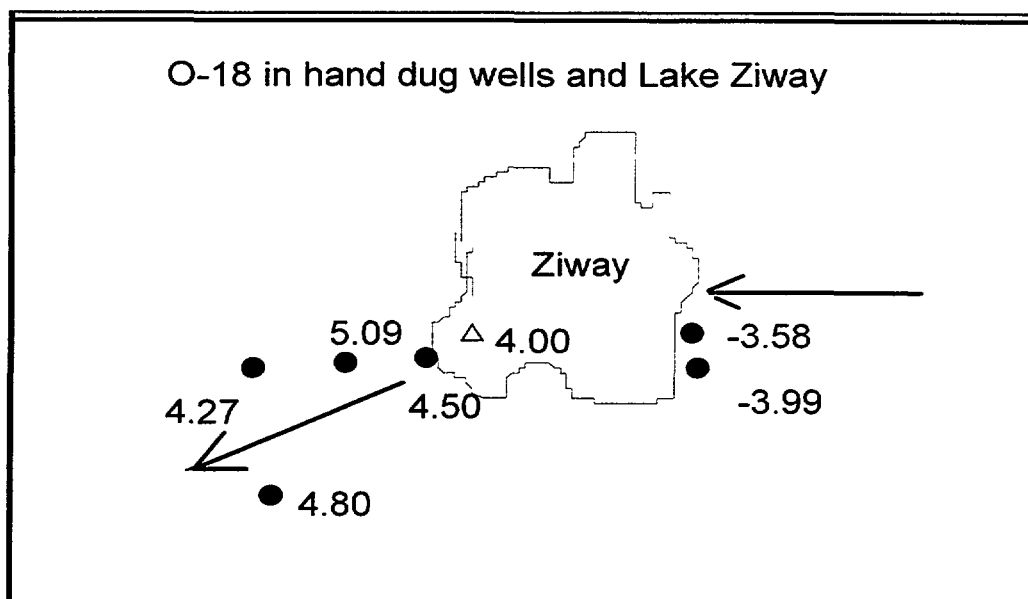
Fig 7. Utilisation of ^{18}O in the estimation of the direction of movement of the ground waters around Lake Ziway

Tritium contents were determined on water in 5 boreholes located in the central part of the plain; very low values are observed (0.8 to 1.7 TU), showing the absence of present day groundwaters, which is in agreement with the low piezometric fluctuations and the large depth of the groundwater.

Table 1 : ^{14}C, ^{13}C, et ^{18}O data for borehole waters

Borehole Site	A% DE 14-C	Estimated Age (years)	$\partial^{13}C$
Arsi Negelle	89.4 ± 1.1	895 ± 95	-11.95
Abiyata usine	62.2 ± 0.5	3810 ± 70	-2.54
Ziway B Mola	90.0 ± 1.2	840 ± 110	-1.21
Langano B Mola	40.8 ± 0.6		-3.60
Meki	86.9 ± 0.5	1130 ± 50	-10.30
Bulbula	77.7 ± 0.7	2030	-3.53
Source Shalla	33.5 ± 1.4		-2.45

Some ^{14}C and ^{13}C were measured on total dissolved inorganic carbon (Table 1). Arsi Negelle, Koshe and Meki boreholes, located at the limit of the plain, outside the influence of lake water show isotopic composition between -8‰ and -11,95‰. Taking into account the isotopic fractionation between CO_2 and bicarbonate ion, this corresponds to a CO_2 of C_4 type as it has been measured in soil gases of the region (-14 to -15‰) (Travi et al., 1997). Enriched values (Table 1) represent mixing with evaporated lake waters and in two cases the additional influence of deep CO_2 (Shalla springs and Bekele Mola borehole). In these two last zones, near active faults, ^{13}C values around -1‰ have been measured in soil CO_2 .

The lakes being in equilibrium with the atmosphere, and in the absence of carbonate in the aquifers, the measurements between Ziway lake and Abiyata lake do not necessitate age corrections and the ages of these groundwaters fall between 800 and 3000 years. The high contents of fluoride are found in the same zone and are therefore largely dependent on present and ancient infiltration of lake waters.
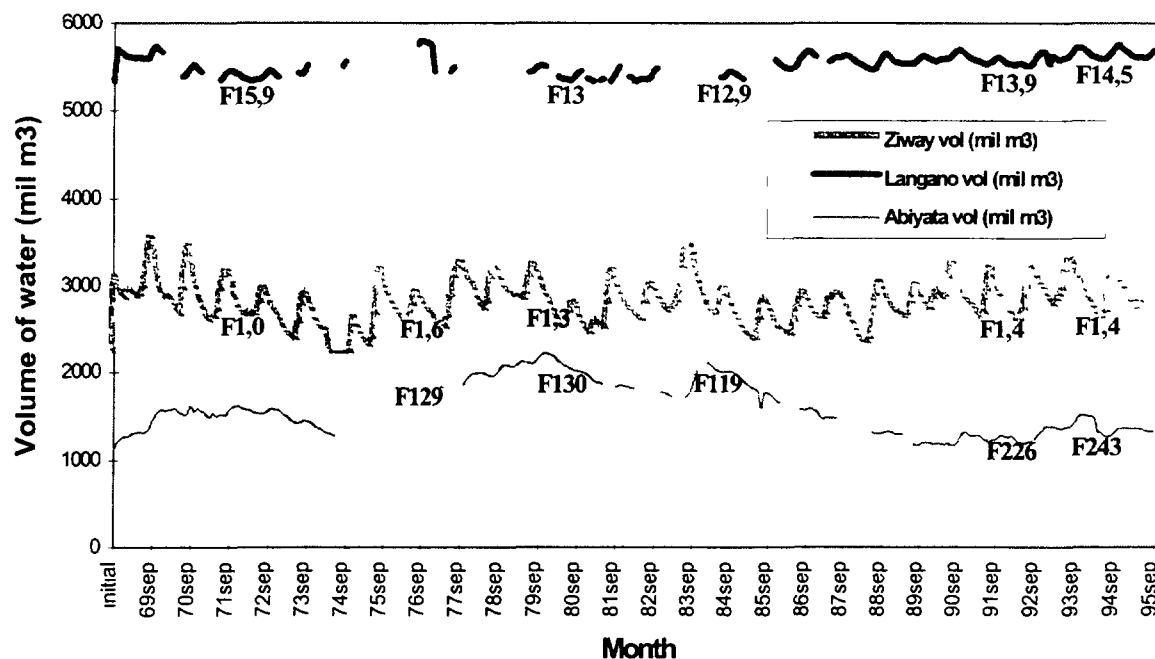
Fig 8 . Variation in volume of water of the lakes during the years 1969-1995 (F129 = Fluoride in mg/l)

A study of the variation in the volume of the lakes in the last 30 years has been carried out (Fig 8). It shows a considerable change in volume of water of Lake Abiyata which became recently closed. This has also resulted in a change in the content of fluoride. In open lakes, low or medium values are observed ; they are directly related to the hydrological balance of the lake (input output, reserve and evaporation volume). The simulated evolution of the chemical characteristics during the process of concentration of waters by evaporation (AQUA model) shows a good agreement with measured data, except in the thermal influence zone. As a result of the specific evolution of alkaline waters (discussed in section 4), the fluoride ion evolves like a conservative tracer with the evaporation and dilution process. Thus, it can be estimated using the hydrological balance.

6.   CONCLUSIONS

In the Lakes Region, the origin and the evolution of fluoride content depends on, (i) the nature of the reservoir, essentially ignimbrites and lacustrine sediments, (ii) the hydrochemical processes ; fluorite equilibrium maintains low or medium values in groundwaters or open lakes. In thermal waters, temperature and deep CO_2 allow high values despite a fluorite control. In surface waters evaporation allows very high values, (iii)

hydrological features which can change the content by mixing surface and groundwaters and modifying the volume of the lakes.

The main factors implied in the concentration of fluoride can be summarised as in the following table:

Table 2 Factors affecting the concentration of fluoride

ORIGIN
• **Volcanic rocks** ————————→ **Low levels** (0 - 3 mg/l) • **Lacustrine sediments** ————→ **Low or high levels** (5 - 30 mg/l)
HYDROCHEMICAL CONTROL **(fluorite equilibrium control, alkalinity residual of calcite-fluorite)** **Groundwater and open lakes** ———→ **Medium values**
TWO PROCESSES FOR HIGH FLUORIDE CONTENT • **Temperature & CO$_2$** ————→ **With fluorite control, thermal springs** • **Evaporation** ————————→ **Without fluorite control, closed lakes**
HYDROLOGICAL EVOLUTION • **Mixing of water, lake and groundwater** • **Hydrological balance**

The leaching experiments indicate that in lacustrine sediments the fluoride content could be used as a paleo-tracer. Furthermore, in relatively concentrated water, the fluoride ion is found to be conservative and it can be used for hydrological tracing.

BIBLIOGRAPHY

Chernet, T. - 1998 - Etude des mécanismes de minéralisation en fluorure et éléments associés de la région du rift éthiopien. Thèse de Doctorat, Université d'Avignon, 210 p.

Chernet, T., and Travi, Y., 1993. Preliminary observations concerning the genesis of high fluoride contents in the Ethiopian rift. Geoscientific Research in Northern Africa. Thonweihe & Schandelmeier (eds), Balkema, Rotterdam, pp 651-655.

Chernet, T. and Travi, Y. - 1995 - Evolution de la contamination fluorurée dans la zone des lacs du rift éthiopien. Approches chimique et isotopique. Isotopes in water ressources management. Proceedings of an IAEA symposium, pp. 457-460.

Chernet, T., Travi, Y. and Gibert, E. - 1997 - The occurrence and hydrogeochemistry of fluoride in natural waters in the Ethiopian rift. International symposium on flood basaltes, rifting and palaeoclimates in the Ethiopian rift and Afar depression, Addis Ababa, February 3 to 14th, 1997, p. 36.

Ribolzi ,O., Valles, V. and ., Bariac, T. - 1996 - Comparison of hydrograph deconvolution using residual alkalinity, chloride and oxygen 18 as hydrochemical tracers. Water Res. Res., 32, 4, pp 1051-1059

Travi, Y., 1993. Hydrogéologie et hydrochimie des aquifères du Sénégal. Hydrogéochimie du fluor dans les eaux souterraines. *Mém. Sci. Géol.* Strasbourg, 155p.

Travi, Y., Gibert E., Chernet T. 1997. Reconstitutions paléohydrologiques dans la zone des lacs du rift éthiopien en liaison avec les teneurs isotopiques de la matière organique. *Isotope techniques in the study of past and current environmental changes in the hydrosphere and the atmosphere*, Proceedings of an IAEA symposium, Vienne, avril 1997..

Valles, V. Ribolzi, O.,de Cockborne, A.M., Cornieles,M. - 1996 - Présentation de AQUA, logiciel de géochimie appliqué aux problèmes environnementaux. GRESSAP, 10 Septembre 1996, ORSTOM, Montpellier.

APPLICATION OF ISOTOPE TECHNIQUES TO GROUNDWATER POLLUTION RESEARCH FOR XIANGSHAN URANIUM ORE FIELD, CHINA

LIU FULIN, LIU PEILUN
Beijing Research Institute of Uranium Geology,
Beijing, China

ZHU CHUANDE, WU XIAOWEI, ZENG YINSHENG
East China Bureau of Geology,
Jiangxi Province, China.

Abstract - *The investigation of groundwater pollution due to uranium deposits focused on the most important uranium metallogenic area--Zhoujiashan district of Xiangshan uranium orefield, China. Groundwater collected from five completed exploration boreholes in the area is regarded as the pollution source and is traced and analysed by using isotope as well as radio-hydrochemical techniques. In addition, the pollution situation of a small uranium ore pile for heap-leaching and a big uranium ore open pit are monitored by the same techniques. It has been experimentally proven that the uranium concentration and the uranium isotope ratio $^{234}U/ ^{238}U$ in natural waters are two sensitive indicators of radioactive pollution in natural waters. It was concluded that under present conditions, exploration of uranium deposits may not cause serious groundwater pollution of radioactive elements (U,Ra,Rn and Th), however, it is difficult to avoid the serious surface water pollution coming from the exploitation of uranium ore by a big open pit.*

1. INTRODUCTION

Radioactive pollution is a special kind of pollution which may be originated from various natural and artificial nuclides. Radioactive elements such as uranium, radium and radon are widely distributed in nature. As the diffusion rate of radium in water is extremely low and it is easy to be adsorbed by various solid materials (such as soil and different colloidal materials), radium does not migrate in most cases, very far from its source.

Radon is an inert gas which exists in atomic form. It can not enter the structure of minerals or chemical compounds nor be transported in natural water. Moreover, the half life of radon isotope ^{222}Rn is only 3.825d, so in natural conditions, it is not able to migrate far from its production place. The radioactive element thorium is not distributed as commonly as uranium and its concentration in natural water is quite low (about 0.5~1.0 µg/l). As viewed from geochemistry, most of thorium compounds are stable, weak in volatility and difficult to be dissolved in water. Especially since thorium in aqueous solution does not take part in redox reaction, it is impossible for it to cause obvious radioactive pollution to surface water drainage [1].

The radioactive element uranium is a kind of valence-changeable element. In an oxidizing medium or by the action of acidic or intensely alkaline groundwater, it can be changed from U^{4+} to U^{6+} uranyl cation (UO^{2+}) and dissolved in water. In a reducing medium, however, it is transformed from U^{6+} into U^{4+} and precipitated. Most of uranium minerals in nature, therefore, are difficult to dissolve in natural water (pH=7). Thus, uranium

concentration in natural water is one of the most important recognizable indicator of radioactive pollution [2].

Fig.1 Relationship between uranium isotope ratio and uranium concentration in groundwater

A -Water halo of hydrothermal type of uranium deposit; B-Water halo of impregnated uranium molybdenum deposit, C-Water halo of uranium-phosphorus deposit in metamorphic rock, D-False anomaly halo: 1) Water halo in granite; 2) water halo in Tertiary sandstone [3].

As the increment of radioactive element concentration in natural water may result from different factors, both true and false anomalous halos in water are consequently generated. The determination of the isotope contents or the activity ratio of the radioactive elements is one of the most effective methods to recognize the genesis of radioactive anomalies in water and to discriminate the false anomalies from the true ones. Experiments show that the activity ratio of $^{234}U/^{238}U$ in water gradually decreases with increase of uranium concentration as the water coming from non-mineralized rocks enters into uranium orebodies. When ^{234}U and ^{238}U in water are in equilibrium state, the activity ratio $^{234}U/^{238}U$ becomes 1 [3,4]. Curves A and B of Fig. 1 show the behavior of water haloes of hydrothermal and impregnated uranium molybdenum deposits, respectively. With the increase of U-concentration in water, the activity ratio $^{234}U/^{238}U$ gradually decreases in the case of hydrothermal U-deposits and rapidly increases in the second case (Fig. 1B). Curve C represents the analytical results of the activity ratio $^{234}U/^{238}U$ in the dispersion halos in water of a uranium-phosphorus deposit in metamorphic rock. This figure shows that the variation of activity ratio $^{234}U/^{238}U$ is bigger and resembles the superimposition of curves A and B. Curve D shows false uranium anomalies in water of two districts, in which the activity ratios $^{234}U/^{238}U$ are all situated at the background level. In short, when the uranium concentration in water reaches the anomalous value and its activity ratio $^{234}U/^{238}U$ is simultaneously near 1, it indicates the occurrence of the hydrothermal uranium mineralization process. When the activity ratio $^{234}U/^{238}U$ in water of sedimentary and metamorphic rock area is 5-10 times higher than the background, it means that impregnated uranium deposits exist.

108

It has also been discovered that the activity ratio $^{226}Ra/^{228}Ra$ in water of non-mineralized igneous rocks and sedimentary rocks is generally less than 0.5. However, the ratio in water of uranium ore is equal to 2 or greater. The activity ratio $^{230}Th/^{232}Th$ in water of non-mineralized rocks is, in general, less than 5, but that in water associated with uranium ore may increase up to several hundred accompanied by an increment of ^{230}Th concentration in water (Fig.2,3) [3].
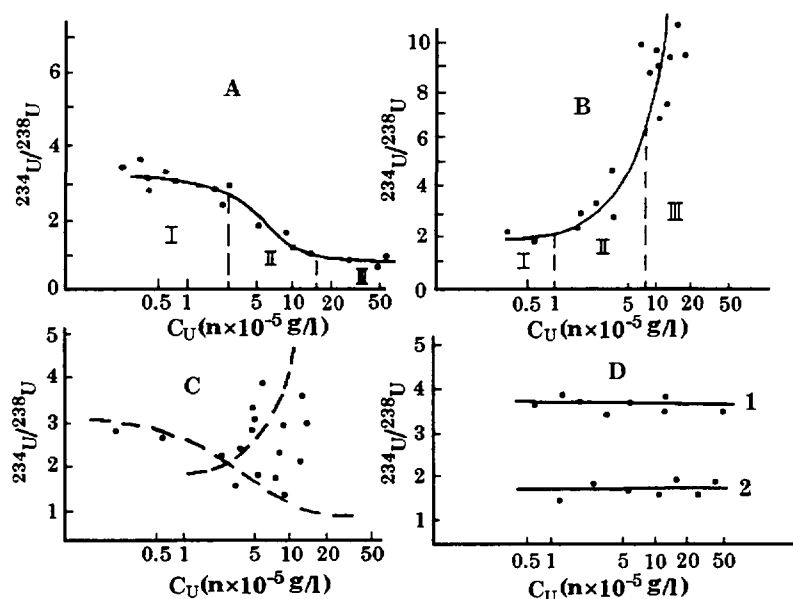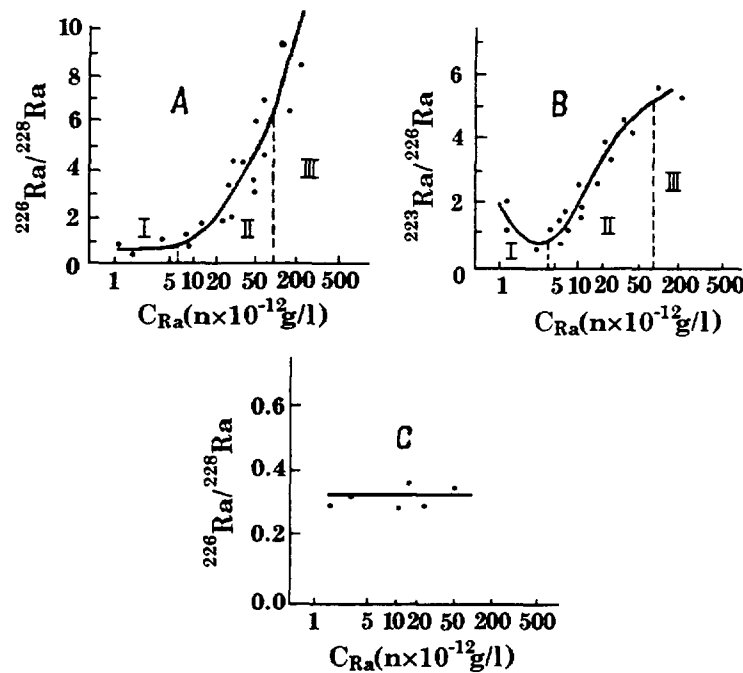

Fig.2 Relationship between radium isotope ratio and radium concentration in groundwater.
A.B-Water halo of uranium deposit; C-Water halo of false anomaly in granite. [3]

In summary, the recognition criteria for a radioactive anomaly in groundwater is as follows: $^{234}U/^{238}U \cong 1$, $^{226}Ra/^{228}Ra >$ or $=2$ and $^{230}Th/^{232}Th > 20$.

These parameters can also be used as the basic data for the study of radioactive pollution of groundwater (Table 1).

Table 1. Obvious anomaly and obvious normal value of radioactive isotopic ratio
in anomalous water [3]

Isotope ratio	Igneous rock		Sedimentary and metamorphic rock	
	Obvious anomaly	Obvious normal value	Obvious anomaly	Obvious normal value
$^{234}U/^{238}U$	$\cong 1.0$	> or =3	> or =5	-
$^{226}Ra/^{228}Ra$	> or =2	< or =0.5	> or =2	< or =0.5
$^{230}Th/^{232}Th$	>20	<1	>20	<1
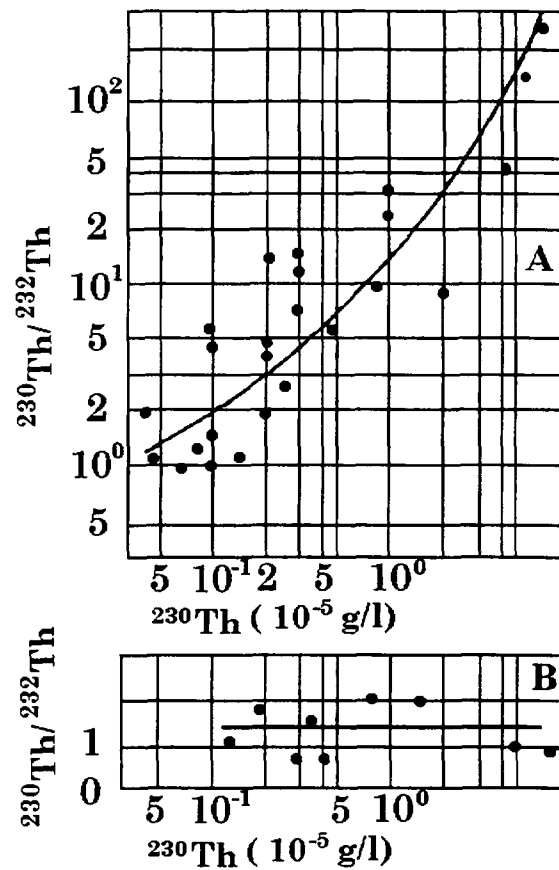
Fig.3 Relationship between activity ratio $^{230}Th/^{232}Th$ and ^{230}Th concentration in natural water

A--Water halo of uranium deposit; B--Water in granite. [3]

2.   PRESENT INVESTIGATIONS

2.1.   Description of the study area

The Xiangshan uranium orefield is one of the largest U-orefield in China, containing many uranium deposits in the Mesozoic acidic volcanics. It is situated in a volcanic basin (the Xiangshan basin) which is located in the southwestern part of the Ganhang tectonic belt in Jiangxi province, China (Fig. 4).

The Xiangshan uranium orefield has been developed for more than 30 years and much geological and hydrogeological research work has been carried out. Results of the above work are used as the foundation for the investigation of groundwater pollution in this area [5-10].

The basement of the Xiangshan basin consists of Sinian biotite-quartz schist, phyllite and coal-bearing formation. The cover is composed of Upper Jurassic volcanics which are divided into the lower part--the Daguding Formation and the upper part--the Ehuling Formation. The former one mainly consists of sandstone, siltstone, welded tuff and rhyodacite. The latter is made of sandy conglomerate, siltstone, welded tuff and thickly-bedded porphyroclastic lava. The whole volcanic series dips at about 20° to 30° towards the

centre of the Xiangshan basin. Collapse structures are well developed including ring fractures, downcast flexure and interlayered fissures.
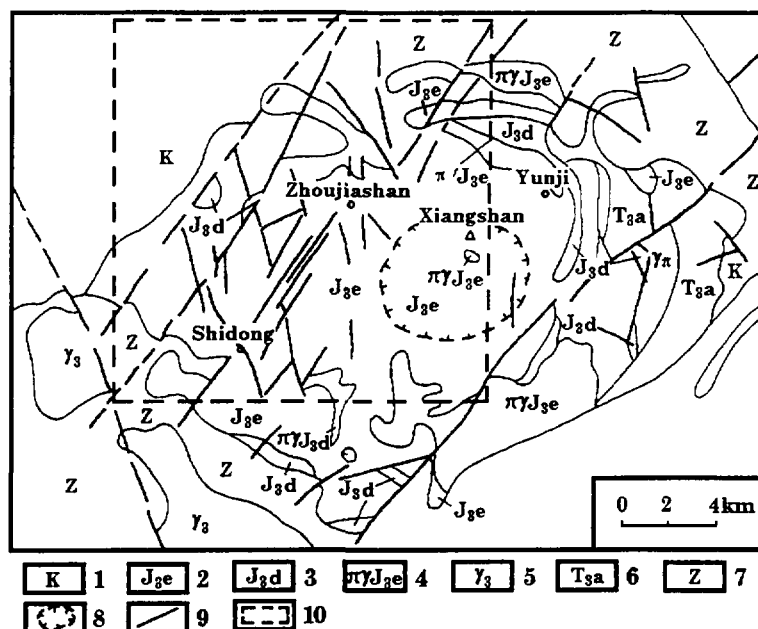
Fig.4. Schematic geological map of Xiangshan uranium orefield

1.Red sandy conglomerate, Cretaceous. 2.Ehuling Formation, Upper Jurassic. 3.Daguding Formation, Upper Jurassic. 4.Sub-porphyritic granite, Ehuling Formation, Upper Jurassic. 5.Granite. 6.Sandy conglomerate and sandstone, Upper Triassic. 7.Sinian metamorphics. 8.Volcanic ring collapse structure 9.Fracture structure. 10 Boundary line of the investigated area.

Two main types of uranium mineralization have been recognized in the Xiangshan uranium orefield: One is the sodium metasomasis type with a mineralization age of 115.2 ± 0.5Ma, developed in the eastern and the northern part of the Xiangshan uranium orefield. Another is the fluorite-hydromica type with a mineralization age of 97.6 ± 7.6Ma, developed in its western part. The above two mineralization ages were calculated from U-Pb isochron of pitchblendes [6]. The detailed research indicates that the main ions in the ore-forming solution of sodium metasomasis uranium deposits are Na^{+} and Ca^{2+}, HCO_{3}^{-} and minor Cl, originally alkaline which later on evolved to an acidic solution. The ore-forming solution of fluorite-hydromica uranium deposits are dominantly Na^{+}, Ca^{2+}, HCO_{3}^{-} with minor F^{-}, SO_{4}^{2-}, and Cl^{-}. The ore-forming solution was originally acidic to weakly acidic which evolved into alkaline during metallogenic process.

The investigated area is located in the western part of the Xiangshan uranium orefield with an area of about 260 km^2. The area has a subtropical, humid rainy climate. The mean annual temperature of this area is about 18 °C, the highest in summer at 39.6 °C and the lowest in winter at -9.2 °C. The annual rainfall in the area is from 1500mm to 2200mm while the annual evaporation capacity is from 1200mm to 1600mm. The area belongs to a middle-low mountain area with moderate erosion, denudation and faulting. The area exhibits a higher relief in the southeast and a lower one in the northwest with significant elevation difference, steep mountains and deeply-dissected valleys leading to conditions which encourage surface runoff. The main surface drainage system in this area includes a series of brooklets, such as: Shidong-brooklet, Shutong-brooklet and Zhoujiashan-brooklet which flow over the Gongxi river (Fig. 5).

One of the main discharge patterns of the groundwater is the overflow of spring water including the overflow of water from the completed exploration boreholes. In the investigated area, the overflow water merges into the Gongxi river via corresponding brooklets. Thus, groundwater pollution, especially radioactive pollution which results from the overflow water of the completed exploration boreholes in the district with rich uranium deposits can be traced in brooklets and rivers. Rainwater passing through the uranium ore pile or the uranium ore open pit may transport radioactive pollutants into brooks, then to the main river.

2.2. Field sampling

In order to investigate groundwater pollution that results from the exploration of uranium deposits and to compare that with the surface water pollution, 15 water samples were collected. Among them, there are 5 borehole water samples (1, 4, 7, 9, 10), 8 brooklet water samples (2, 3, 5, 8, 11, 12, 13, 14) and 2 river water samples (6, 15). The surface water samples 14, 15 were taken from the north of a quite big uranium ore open pit. The brooklet water sample 12 is situated near a small uranium ore pile for heap-leaching. Each sample was measured for radioactivity, hydrochemistry and stable isotopes. Temperature of water samples and air were measured in the field while the geological and hydrogeological characteristics were described.
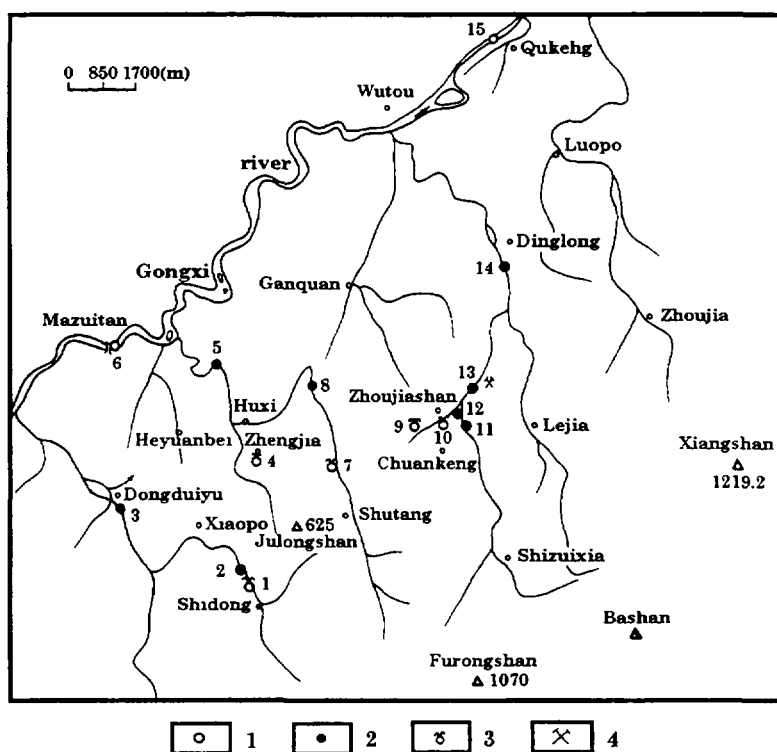

Fig. 5 Location of sampling points

1. River site. 2. Brooklet site. 3.Completed exploration borehole site. 4.Uranium ore open pit site.

2.3. Laboratory analysis

The 15 water samples were measured for $K^+ + Na^+$, Ca^{2+}, Mg^{2+}, HCO_3^-, SO_4^{2-}, Cl^-; U, Th, Ra, Rn; M(or TDS), δ^2H, $\delta^{18}O$ and pH as well as the ratios of the radioactive isotopes $^{234}U/^{238}U$, $^{230}Th/^{232}Th$. As the half life of radon isotope ^{222}Rn is only 3.825d, radon concentrations were measured by the emanation ionization method in the same day of the field sampling.

P_{350} extractive chromatography was used to determine the radioactive isotopic ratios $^{234}U/^{238}U$ and $^{230}Th/^{232}Th$ of natural water samples. Five liters of water sample are taken, then acidified using concentrated nitric acid (HNO_3). Ferric chloride ($FeCl_3$) and ammonium chloride (NH_4Cl) used as carriers are added, then ammonia (NH_4OH) is added to adjust the pH to a value of 8-9, for the coprecipitation of ferric hydroxide with uranium and thorium hydroxide. The precipitate is dissolved by using concentrated nitric acid, then a mixed solution containing 15% HNO_3 and 15% $Al(NO_3)_2 \cdot 9H_2O$ is prepared for chromatography. After the mixed solution is passed through the P_{350} teflon support column, uranium and thorium are purified, then thorium is mixed with the hydrochloric acid (HCl) and the uranium with the sodium fluoride (NaF). The mixture is thereafter separately electro-deposited on different stainless steel disks. After the disks are rinsed and dried, they are measured with α-spectrometry. The net counts in the energy region of the isotopes of U and Th in the same spectrum are compared, then the ratios of $^{234}U/^{238}U$ and $^{230}Th/^{232}Th$ of natural water samples are obtained [11, 12].

Hydrogen isotope samples were prepared using the metal uranium method. The hydrogen gas was collected in special tubes and measured in a Finnigan-MAT251 gas isotope mass-spectrometer. The precision of the method is about ±1‰. The CO_2-H_2O equilibrium method is used to measure the ratio of oxygen isotope. The precision of the method is about ±0.2‰.

3. RESULT AND DISCUSSION

In March 1997, 15 water samples in the investigated area were collected for studying the radioactive pollution caused by the exploration and the exploitation of uranium deposits. Tables 2, 3, 4 show the hydrochemical results, the concentrations of U, Th, Ra and Rn, the activity ratios ($^{234}U/^{238}U$ and $^{230}Th/^{232}Th$) and the stable isotopic contents (δ^2H and $\delta^{18}O$). According to these results, some main points can be obtained as follows.

Table 2. shows that the concentrations of the cations $K^+ + Na^+$, Ca^{2+} (especially $K^+ + Na^+$) and the anion HCO_3^- of five borehole water samples (1, 4, 7, 9, 10) are obviously higher than those of other surface water samples. This fact indicates that the five borehole water samples (1, 4, 7, 9, 10) are in close space relationship with the ores of fluorite-hydromica uranium deposits. As the brooklet water sample 12 is near a small uranium ore pile for heap leaching, the concentrations of the cations Ca^{2+}, Mg^{2+} and the anion SO_4^{2-} are obviously higher than those of other surface water samples, while the concentrations of cations $K^+ + Na^+$ and anions HCO_3^- and Cl^- are all close to zero with pH equal to 5.2, the lowest in the 15 water samples collected in the investigated area. Apparently, the the small uranium ore pile for heap leaching was affected by sulphuric acid. Although the brooklet water sample 13 is not far from the brooklet water 12, as it is shown in Fig. 5, its concentrations of cations $K^+ + Na^+$, Ca^{2+}, Mg^{2+} and anions HCO_3^-, SO_4^{2-}, Cl^- show no

113

obvious difference with those of other surface water samples. This fact indicates that the brooklet water sample 13 has not been affected by the uranium ore pile.

Table 3 shows that the concentrations of radioactive elements radium and thorium of the 15 water samples collected in the investigated area (except the brooklet water sample 12) show no obvious regular variation. This phenomenon might be closely related to the radioactive hydrochemical features of radioactive elements radium and thorium as mentioned above. The concentrations of radioactive elements uranium and radon of five borehole water samples (1, 4, 7, 9, 10) and the brooklet water sample 12 are all obviously higher than those of other surface water samples, which reveals that the above anomalous concentrations rapidly disappear as soon as the waters coming from above five boreholes (1, 4, 7, 9, 10) and the brooklet water 12 flow into a brook or a river. In other words, no obvious radioactive pollution caused by them would occur in this area. As the locations of borehole water samples (1, 4) are slightly far from the uranium rich Zhoujiashan mineralization district than those of borehole water samples (7, 9, 10), as it is shown in Fig. 5, it is reasonable that the concentrations of radioactive elements uranium and radon (especially uranium) of borehole water samples (1, 4) are less than those of borehole water samples (7, 9, 10). The variation of uranium concentrations of brooklet water samples (13, 14) is quite significant, while their Ra, Th and Rn concentrations show no obvious change, which once more indicates that the concentration of uranium in water is one of the most important indicator for evaluating the radioactive pollution.

Table 4. shows that the activity ratios $^{234}U/^{238}U$ (1.07, 0.98, 1.14) of borehole water samples (7, 9, 10), respectively are closer to 1 than those of borehole water samples (1,4) which have ratios of (1.83, 1.54) respectively. This reveals that the borehole water samples (7,9,10) are closer to the equilibrium state of ^{234}U and ^{238}U in water than the borehole water samples (1.4). This phenomenon is also coincident with the fact that the locations of borehole water samples (7, 9, 10) are closer to the uranium rich Zhoujiashan mineralization district than those of borehole water samples (1,4). The activity ratios $^{234}U/^{238}U$ of brooklet water samples (12, 13, 14) are 0.99, 1.08, 0.98 respectively. This fact indicates that the brooklet water sample 12 and 14 are closer to the equilibrium state of ^{234}U and ^{238}U in water than the brooklet water sample 13, because the former is closer to a small uranium ore pile for heap leaching than the latter. The uranium concentration of sample 14 is 130×10^{-7}(g/l) which is much higher than the background value, indicating that it is difficult to avoid serious surface water pollution coming from the rainwater passing through a big uranium ore open pit. There is no a regular distribution of thorium activity ratio $^{230}Th/^{232}Th$ of the 15 water samples. This fact shows that the activity ratio $^{230}Th/^{232}Th$ in water can only be used as a supplemental recognition parameter for evaluating the radioactive pollution.

4.   CONCLUSIONS

It has been theoretically and practically proven that the uranium concentration in natural waters is one of the most important indicators for evaluating the radioactive pollution as compared with other parameters, such as concentrations of radium, radon and thorium. In addition, the activity ratio of $^{234}U/^{238}U$ in water is a sensitive indicator for evaluating the natural water pollution. Activity ratios $^{226}Ra/^{228}Ra$ and $^{230}Th/^{232}Th$ in water can only be used as the supplementary indicators.

As most of surface waters are near neutral, the exploration of uranium deposits may cause no obvious groundwater pollution by radioactive elements (U, Ra, Rn and Th). However, it is difficult to avoid the serious surface water pollution coming from the exploitation of uranium ore by a quite big open pit.

Table 2. Results of hydrochemical simplification analysis of 15 water samples in the investigated area

Sample number	Ca^{++} (mg/l)	Mg^{2+} (mg/l)	$K^{+}+Na^{+}$ (mg/l)	Cl^{-} (mg/l)	SO^{2-}_{4} (mg/l)	HCO^{-}_{3} (mg/l)	M (TDS) (mg/l)	pH (Value)	Temperature(°C) Water	Air
1	24.05	8.27	22.75	4.25	8.64	118.81	186.77	6.5	16	23.5
2	4.81	1.22	12.80	7.10	1.92	37.34	65.19	7.2	17	22
3	3.61	1.95	12.00	7.10	6.72	29.24	60.62	7.3	19	13
4	4.00	1.21	74.75	7.10	5.76	177.57	270.39	7.4	19	22
5	2.40	1.46	10.75	4.96	6.72	23.70	49.99	6.2	17.5	14
6	3.61	1.70	13.75	9.93	3.84	31.12	63.95	5.5	15	20
7	0.80	0.73	84.00	5.67	2.88	153.72	247.80	7.2	15	26
8	1.60	1.44	12.00	7.45	3.84	23.79	50.12	6.4	15.5	13
9	36.07	3.13	27.00	5.67	10.56	168.74	251.17	7.0	12.5	18
10	28.09	7.68	27.25	4.96	6.72	173.96	248.66	7.2	12.5	24.5
11	1.60	1.44	11.75	5.67	8.64	20.14	49.24	5.4	13	12
12	96.99	13.13	0	0	34.56	0	144.68	5.2	12	11
13	1.60	1.44	9.25	4.96	4.80	20.14	42.19	6.0	13	12
14	1.20	1.68	10.00	5.67	3.84	21.96	44.35	6.0	19	15
15	2.80	2.40	21.00	24.11	6.72	21.96	78.99	5.8	20	16

Table 3. Radioactive element concentration of 15 water samples in the investigated area

Sample number	type of water sample	U $(\times 10^{-7})$ (g/l)	Th $(\times 10^{-7})$ (g/l)	Ra $(\times 10^{-7})$ (g/l)	Rn (Bq/l)
1	Borehole water	10.40	0.011	0.28	175.49
2	Brooklet water	6.50	0.204	0.10	2.42
3	Brooklet water	1.56	2.979	0.34	3.06
4	Borehole water	0.52	0.010	0.11	446.78
5	Brooklet water	0.26	2.750	1.00	3.19
6	River water	0.26	4.721	0.29	3.68
7	Borehole water	14.30	11.460	1.29	330.33
8	Brooklet water	0.52	0.071	9.25	3.58
9	Borehole water	14.30	47.020	0.95	320.14
10	Borehole water	59.80	5.270	2.44	803.45
11	Brooklet water	2.60	0.198	0.15	13.59
12	Brooklet water	7800.00	71.270	170.00	512.99
13	Brooklet water	0.26	4.580	1.07	4.63
14	Brooklet water	130.00	7.998	2.34	2.88
15	River water	130.00	4.354	0.29	2.26

Table 4. Radioactive isotope ratio and stable isotope composition
of 15 water samples in the investigated area

Sample number	Type of water sample	Radioactive isotope ratio		Stable isotope composition(‰)	
		$^{234}U/^{238}U$	$^{230}Th/^{232}Th$	$\delta^2H(-V-SMOW)$	$\delta^{18}O(-V-SMOW)$
1	Borehole Water	1.83	549.4	-37.0	-7.02
2	Brooklet Water	1 16	85 9	-30.4	-6.38
3	Brooklet Water	1 45	6 05	-29.2	-6.33
4	Borehole Water	1.54	1547.9	-40.4	-7.08
5	Brooklet Water	1.03	7.45	-32.6	-6.90
6	River Water	1.33	0.65	-36.0	-6 07
7	Borehole Water	1.07	0.33	-48.7	-8.66
8	Brooklet Water	0.28	262.4	-41.2	-7.25
9	Borehole Water	0.98	7.17	-40.7	-7.42
10	Borehole Water	1.14	5 71	-37 2	-7.19
11	Brooklet Water	0.72	119.0	-46.3	-7 09
12	Brooklet Water	0.99	38.6	-40.4	-6.47
13	Brooklet Water	1.08	9.97	-47.6	-7.31
14	Brooklet Water	0.98	7.70	-50.7	-6.80
15	River Water	0.90	0.69	-37.6	-5.88

ACKNOWLEDGEMENTS

REFERENCES

[1]   Yang Jie, Hydrogeology Foundation of Uranium Minerals, Atomic Energy Press, Beijing (1988)

[2]   Yang Zhongyao, Environment Hydrogeology, Atomic Energy Press, Beijing (1990).

[3]   Gao Wanlin, Radioactive Hydrogeochemical Prospecting, Atomic Energy Press, Beijing (1980)

[4]   Lin Ruifen, Wei Keqin, Wang Zhixiang, A Study of $^{234}U/^{238}U$ Ratio in Ground waters of Taiyuan Area, Shanxi Province, Geochimica, 3 (1986) 193-201

[5]   Li Xueli, Shi Weijun, Sun Zhanxue, Genetic Model of Uranium Metallogensis in Discharge Area (Depressurization Area) of Fossil Hydrothermal system, Galaxy of Research Achievements of Uranium Geology of China, Editorial Department of URANIUM GEOLOGY, Beijing (1996) 103-111

[6]   Chen Fanrong, Shen Weizhou, Wang Dezi, Liu Changshi, Isotopic Geochemistry of Uranium Ore-Field No 1220 and the Implication to Ore Genesis, Geotectonia et Metallogenia, 14 1 (1990) 69-77

[7]   Li Xueli, Study on the Relationship Between Jiangxi Hot-Spring Genesis and Uranium Mineralization, Journal of East China Geological Institute, 15 3 (1992) 201-220.

[8]   Li Xueli, Sun Zhanxue, Zhou Wenbin, Hydrogeochemical Characteristics of Ore-Forming Fossil Hydrothermal System in Xiangshan, Journal of East China Geological Institute, 15 3 (1992) 234-242

[9]   Zhou Wenbin, Li Xueli, Shi Weijun, Mantle Heat Flow in Xiangshan Area, Journal of East China Geological Institute, 15 3 (1992) 249-254

[10]   Shi Weijun, Zhou Wenbin, Yuan Xiaoqin, The Basic Principle and Criteria for Ore Prospecting of Uranium Neutralizing-Reduction Mineralization, Journal of East China Geological Insitute, 15   3 (1992) 255-262

[11]   Fan Meiying, A Method Using Di-(1-Methylheptyl) Methyphosphate Chromatographic Separation for Measuring the Activity Ratios of $^{234}U/^{238}U$ and $^{230}Th/^{232}Th$ by Alpha-Spectrometry, Journal of Nuclear and Radiochemistry, 12 1 (1990) 59-64

[12]   Gu Dingxiang, Wang Ling, Chen Mingxiu, Sequential Determination of Isotopes of U, Th, Ra. Pb and Their Activity Ratios in Environmetal Water Samples, Galaxy of Research Achievements of Uranium Geology of China, Editorial Department of URANIUM GEOLOGY, Beijing (1996) 377-383

116

ISOTOPIC AND CHEMICAL CHARACTERISTICS OF GROUNDWATER IN BEIJING CITY

WEI KEQIN, LIN RUIFEN
Guangzhou Institute of Geochemistry,
Chinese Academy of Sciences,
Guangzhou, China

Abstract - *The characteristics of the alluvial-diluvial aquifer of the Beijing area were studied by means of environmental isotopes, especially tritium, which may be considered as a useful natural tracer to demonstrate the pollutant behavior in groundwater aquifer. The results of tritium monitoring indicate that the natural regime of the groundwater system of the Quaternary aquifer has been destroyed due to intensive exploitation. Two subsystems could be divided based on tritium data. Subsystem A with active circulation was formed in the course of exploitation. Subsystem B is of slow circulation. The $\delta^2 H$ and $\delta^{18} O$ values of the groundwater are higher in the western suburb than that in eastern suburb. The sketch maps of $\delta^2 H$ and $\delta^{18} O$ isolines reflect a mixing between ground waters from the baserock and from the local vertical recharge. The trace elements Sr, Ru and Rh have a very special distribution in groundwater system with very high concentrations in the north-eastern part of the old Beijing city. The results of $^{87}Sr / ^{86}Sr$ measurement show that Sr in groundwater of the Quaternary aquifer is from the groundwater of the basement rock. High concentrations of Sr in groundwater of the Quaternary aquifer are not related to any special pollution source.*

1. INTRODUCTION

The water supply of Beijing city comes from both groundwater and surface water. Groundwater is intensively exploited from the Quaternary aquifer of the alluvial plain due to a rapid increase of population and development of industry. Continued lowering of the water level and deterioration of the groundwater quality are grave consequences of this exploitation.

The knowledge of infiltration and dispersion characteristics of the shallow aquifers is important for investigating the processes involved in pollutant movement, its attenuation and degradation in groundwater system. We attempt to study these characteristics of the alluvial-diluvial fan aquifer of the Beijing city by use of environmental isotopes, especially tritium, which may be considered as a useful natural tracer to demonstrate the pollutant behavior in groundwater aquifer.

Tritium in groundwater of the Beijing city was monitored in the 1970's by the authors. According to IAEA-Research Contract No. 8199 the tritium content of groundwater was measured in 1995 and 1997. Preliminary field investigations were performed in May 1995 and water samples were collected in June 1995 and May 1997. These samples were analyzed for their tritium content, major chemical ions, minor chemical constituents and trace elements. Sr isotopic ratio, $\delta^{18}O$ and $\delta^2 H$ analyses were measured for some water samples. All the data obtained and the interpretations are summarized and presented in this paper.

2. HYDROGEOLOGY OF THE INVESTIGATED AREA

2.1 Geography and Geomorphology

Beijing city is located around 40°north latitude, 116° east longitude. There are rolling hills in the west and the north. The mountains in the west are usually called Western(Xishan) Mountains. The mountainous areas close to the plain have an elevation of about 500-100 meters. To the southeast a broad alluvial plain, lower than 100 meters (mainly 50-30 meters) above sea level, is extended right to the Bohai sea. At the foot of the Xishan Mountains there are diluvial plains. The topography is higher in the northwest and lower in the southeast with a slope of about 3 ‰ in the northwest and 1 ‰ in the southeast[1].

2.2 Climatic Characteristics

Beijing City is located at medium latitudes, where the activities of the Asian monsoon are obvious and the climate is of typical continental temperate zone. The spring is arid and windy; the summer is hot and rainy; the autumn is fresh and sunny; and the winter is cold and dry. The mean air temperature is 12°C. The mean annual precipitation is about 630 mm, mainly (76%) concentrated in June to August. Precipitation in spring is usually less than 60 mm, and it is around 10 mm in winter. The monsoon climate in China is characterized by great changes both in temperature and rainfall from year to year. For instance, precipitation in 1959 was 1406 mm in Beijing, while in 1891 it was only 169 mm[1].

2.3 Hydrogeological Conditions

Beijing City is located on the alluvial-diluvial plain of the Yongdinghe River. Therefore, a zonal distribution is observed. From the west to the east, as well as from the north to the south, grain size of the sediments becomes finer, one layer aquifer turns to be an aquifer of several layers, a phreatic aquifer is replaced by a confined aquifer, the permeability

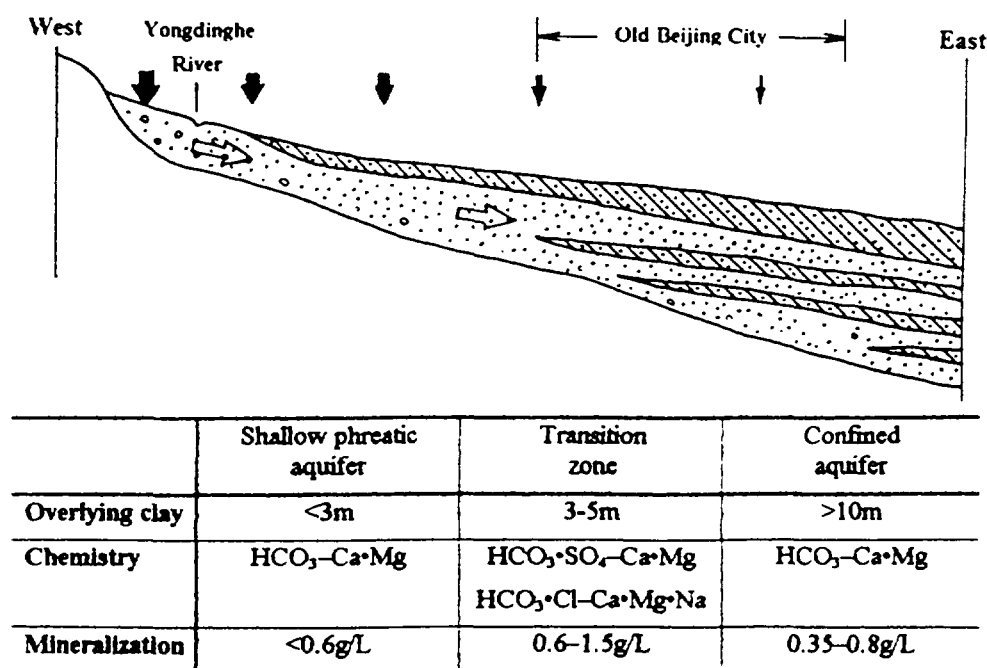|	Shallow phreatic aquifer	Transition zone	Confined aquifer
Overlying clay	<3m	3-5m	>10m
Chemistry	HCO₃–Ca•Mg	HCO₃•SO₄–Ca•Mg HCO₃•Cl–Ca•Mg•Na	HCO₃–Ca•Mg
Mineralization	<0.6g/L	0.6-1.5g/L	0.35-0.8g/L

Fig.1   Hydrogeological conditions of Beijing City and its suburbs

118

and aquifer yield decrease (Fig.1). The Quaternary aquifer in Beijing City is recharged by both lateral flow from the mountainous area and vertical flow in the alluvial plain. Beijing City is supplied by both groundwater and surface water. The exploitation of the groundwater is concentrated mainly from the Quaternary aquifer in the alluvial plain. Groundwater there has been exploited intensively due to rapid development of industry and increase of population. It leads to grave consequences of continued descent of the water table by 0.5-1.0 m / year[1]. A conical depression of the water table around the center of the city has been formed and the exploitation conditions have worsened.

3. MAJOR CHEMICAL CONSTITUENTS

13 water samples were collected in June, 1995. No.1-16 were from drill holes and No.17 was from the Yongdinghe River. No.20-23 were collected from drill holes in May, 1997. The highest mineralization, 1.2g/L, is observed in the sample from drill hole No.8, the chemical type is $HCO_3 \cdot SO_4 \cdot Cl$ —$Ca \cdot Mg \cdot Na$, which is typical for the groundwater of the transition zone. The lowest mineralization, 0.3g/L, is measured from the water sample No.13, its chemical type is HCO_3—$Ca \cdot Mg$, which is characteristic of the groundwater of the shallow phreatic zone. The content of major ions for these samples is listed in Tab.I.

The Yongdinghe alluvial-diluvial fan has a zonal distribution from the west to the east, as well as from the north to the south, as it has been described in the previous section.

Based on the zonal distribution of the groundwater system, it is expected that the lower content of the major ions in   groundwater   should be near the recharge area, while the

Table I   Major Chemical Constituents of the groundwater (mg/L)

| No	K^+	Na^+	Ca^{+2}	Mg^{+2}	HCO_3^-	CO_3^{-2}	Cl^-	SO_4^{-2}	Note
1	2.62	38.0	119	36.1	337	6.72	80.6	122	
3	3.14	40.5	108	38.9	424	6.72	45.5	99.9	
4	4.18	65.3	160	57.4	513	8.06	109	139	
6	2.27	25.4	79.4	35.5	312	6.72	45.5	79.2	
7	2.37	38.3	91.4	38.1	335	6.72	77.8	78.8	
8	6.42	86.7	185	54.2	506	<TL*	130	217	TL-Test limit
9	2.37	28.2	51.3	24.1	284	<TL	21.7	35.0	
12	2.65	45.2	99.8	47.7	366	<TL	130	64.6	
13	2.57	8.25	41.7	17.2	171	<TL	21.0	35.0	
15	3.51	48.3	115	51.6	321	6.72	104	98.7	
16	4.10	76.0	150	51.5	362	<TL	163	155	
17	4.64	55.6	40.1	28.4	238	8.06	49.0	98.4	River Water
18	5.58	64.4	124	43.9	407	6.72	84.1	123	
20	11.7	79.8	173	65.3	519	<TL	112	192	
21	4.32	72.5	170	69.9	519	<TL	125	163	
22	4.21	75.2	167	66.2	522	<TL	111	141	
23	3.20	69.1	142	72.0	387	<TL	134	158	
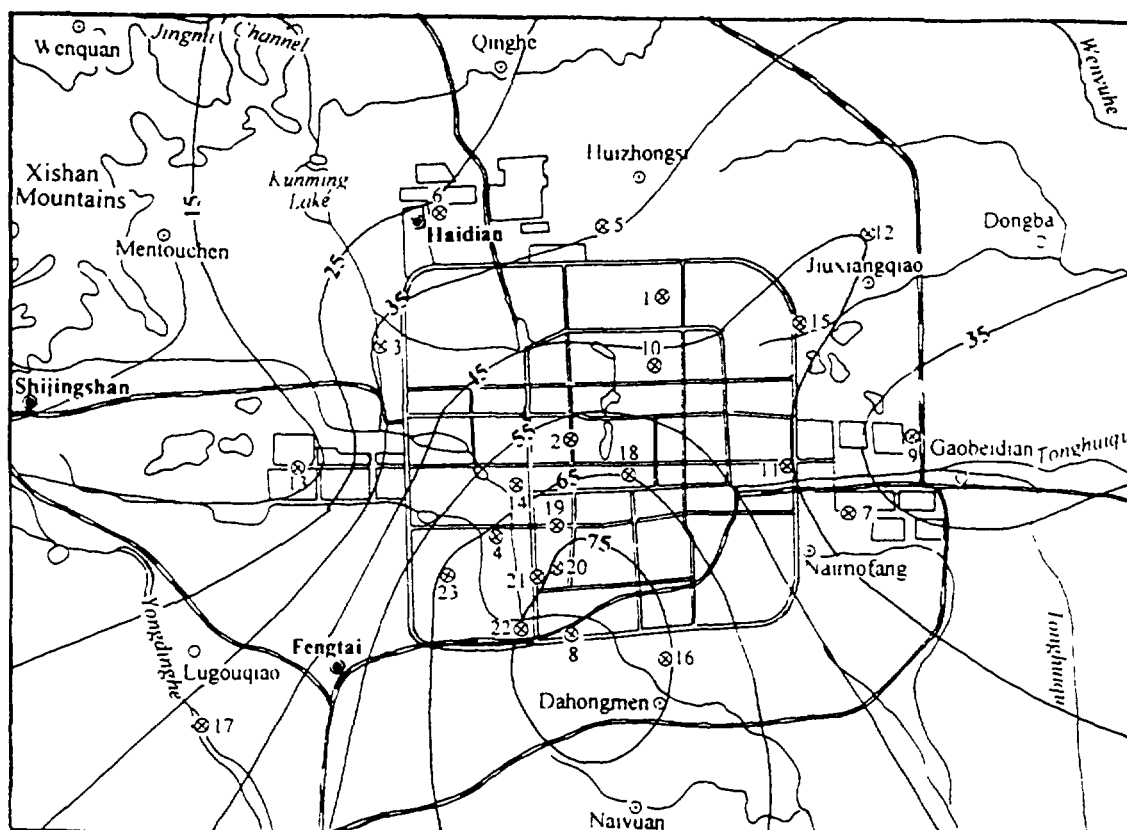
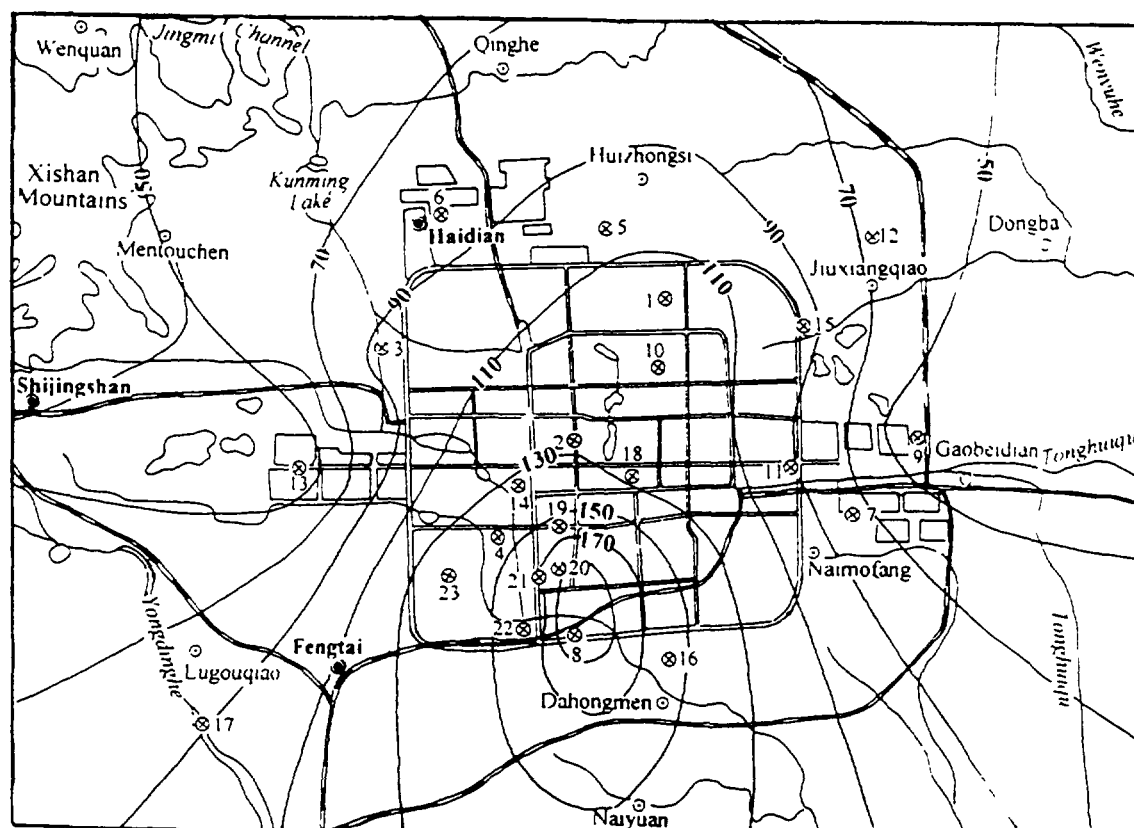Fig. 2   Na$^+$ isolines (mg/L) in groundwater.

Fig. 3   SO$_4^{-2}$ isolines (mg/L) in groundwater

higher content is on the downstream side. Fig.2 is a sketch map of the Beijing area. The old Beijing city is in the center. The distance from the west to the east on this sketch map is approximately 35 km. The isolines of the Na^+ content in groundwater are marked on this sketch map. Fig.2 shows, that the Na^+ content increases gradually from the west to the east. It is obviously because the western suburb is close to the recharge area. But the highest content of Na^+ is observed not in eastern suburb, but in southern suburb. Fig.3 shows the isoline of the SO_4^{-2} ion in groundwater. Overall, all the major ions in groundwater have approximately this kind of distribution pattern.

4. MINOR CHEMICAL CONSTITUENTS

Water samples were analyzed for minor chemical constituents using the ICP-MS method. The results of these analyses are used to: a/ to assess the quality of the water; b/ to ascertain the groundwater systematic together with the isotopic data. The contents of some minor elements in groundwater of Beijing city are given in Table II.

Table II   Minor chemical constituents in groundwater (µg/L)

No	Cr	Mn	Fe	Cu	Zn	As	Se	Pb	Note
1	22.3	<0.16	89.6	4.26	1.47	4.61	1.63	3.73	
3	2.59	0.25	62.1	2.39	<1.40	3.22	2.66	0.82	
4	1.30	<0.16	149	3.57	<1.40	3.28	3.67	0.39	
6	1.51	<0.16	60.7	2.59	<1.40	1.71	<1.38	0.45	
7	7.86	<0.16	73.0	2.67	<1.40	3.12	<1.38	0.78	
8	1.61	<0.16	94.1	3.37	2.00	3.80	3.72	1.38	
9	6.22	0.17	41.6	1.39	<1.40	18.3	<1.38	0.23	
12	5.02	<0.16	60.5	1.91	<1.40	3.31	<1.38	0.76	
13	3.31	0.49	66.4	3.55	1.46	5.34	<1.38	1.74	
15	5.32	0.16	93.7	2.68	<1.40	6.54	2.09	0.91	
16	13.0	0.21	125	2.15	<1.40	7.03	1.76	0.36	
17	6.48	<0.16	64.0	4.39	<1.40	5.60	<1.38	1.96	River Water
18	11.4	<0.16	89.5	1.62	<1.40	1.34	2.06	0.50	
20	44.6	2.40	170	6.18	17.4	2.45	6.71	8.03	
21	23.3	2.02	50	1.96	2.85	1.21	5.94	6.44	
22	21.9	1.91	80	2.74	46.6	1.37	3.99	12.4	
23	18.7	1.09	60	2.78	3.94	1.91	-	0.33	

As it can be seen from Fig. 4 that the ground water has very low content of minor constituents. The exception is Fe, Cr and Se for the drill hole No.20., the content of which is close to the recommended limit for drinking water in China[2]. The content of Cd, which is not marked in Fig.4   is lower or close to the test limit for the ICP-MS method (0.014µg/L) on all the water samples.
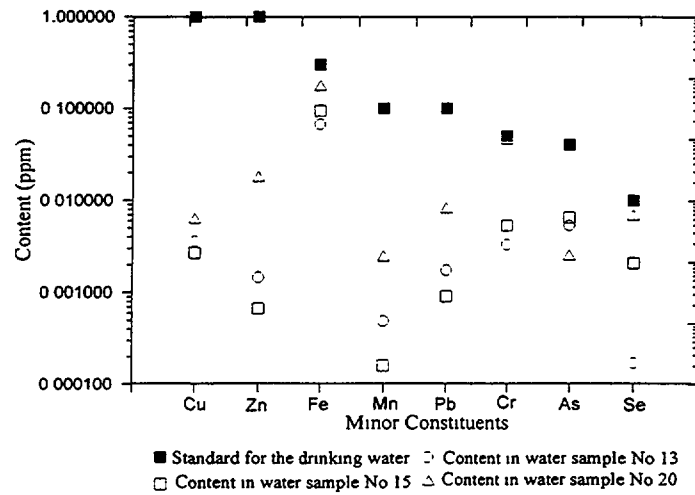
Fig.4   Minor chemical constituents of the groundwater.

Almost all the minor chemical constituents in ground water have similar geographical distribution as for the major chemical ions. High concentration is observed near the drill hole No.20 in the southern suburb. The only exception is As. It seems that the content of As in ground water is low in the western suburb, and increases gradually from the west to the east along the natural ground water flow (see Fig. 5). Obviously, As in ground water has a different origin from other minor chemical constituents.
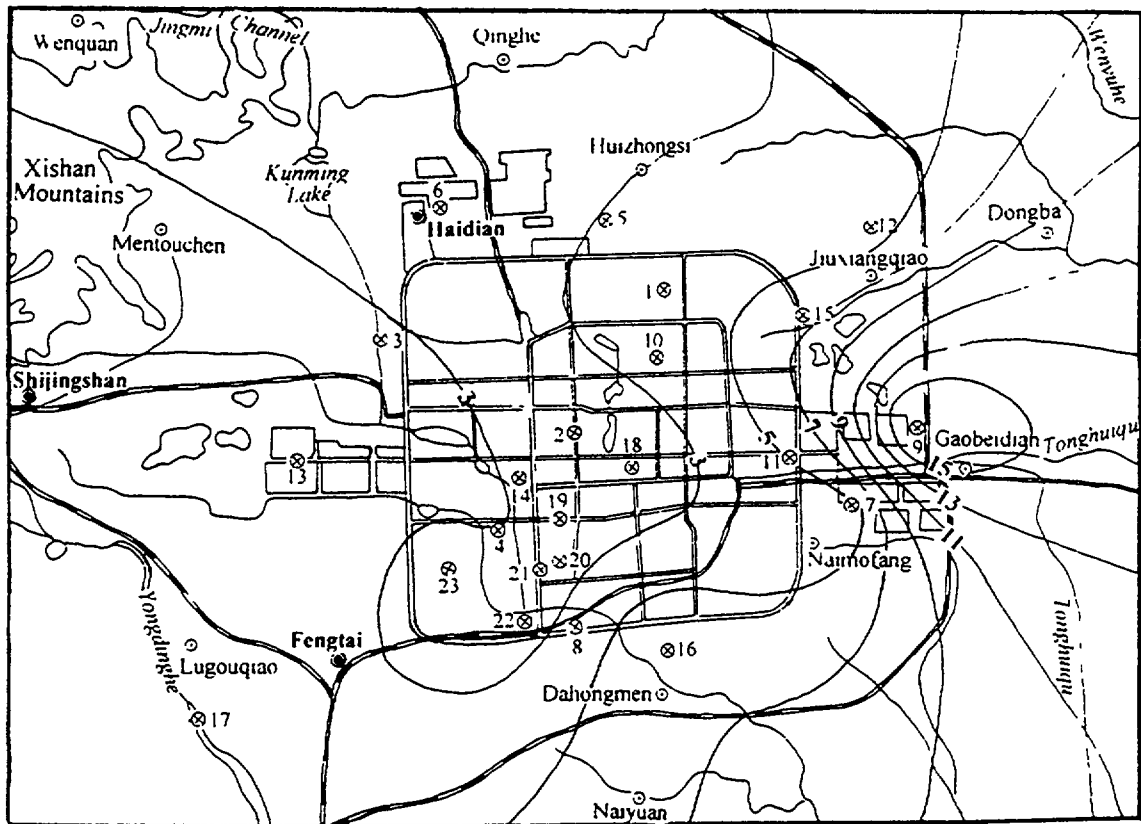
Fig.5   Distribution of As (μg/L) in groundwater.

5. STABLE ISOTOPE COMPOSITION

δ^2H and $\delta^{18}O$ of some groundwater samples of Beijing area were measured. Fig. 6 shows that the content of ^2H in groundwater of the western suburb is higher than that in the eastern suburb. The difference between the δ values of groundwater samples may result from mixing of some recharge components. It infers that the Quaternary aquifer is recharged not only by the vertical infiltration of local rainwater, but also by the lateral flow from the mountainous area. The δ values of the ground water recharged from the Western Mountains should be lower than that of local rainwater, as it is expected from the so-called «altitude effect». If mixing is in Quaternary aquifer between lateral flow of relative low δ values with vertical recharge of higher δ values, geographical distribution of δ values should be opposite as it has been shown in Fig. 6. Gradually decreasing of the δ values from the west to the east infers a mixing between the groundwater from baserock and the groundwater of local recharge.
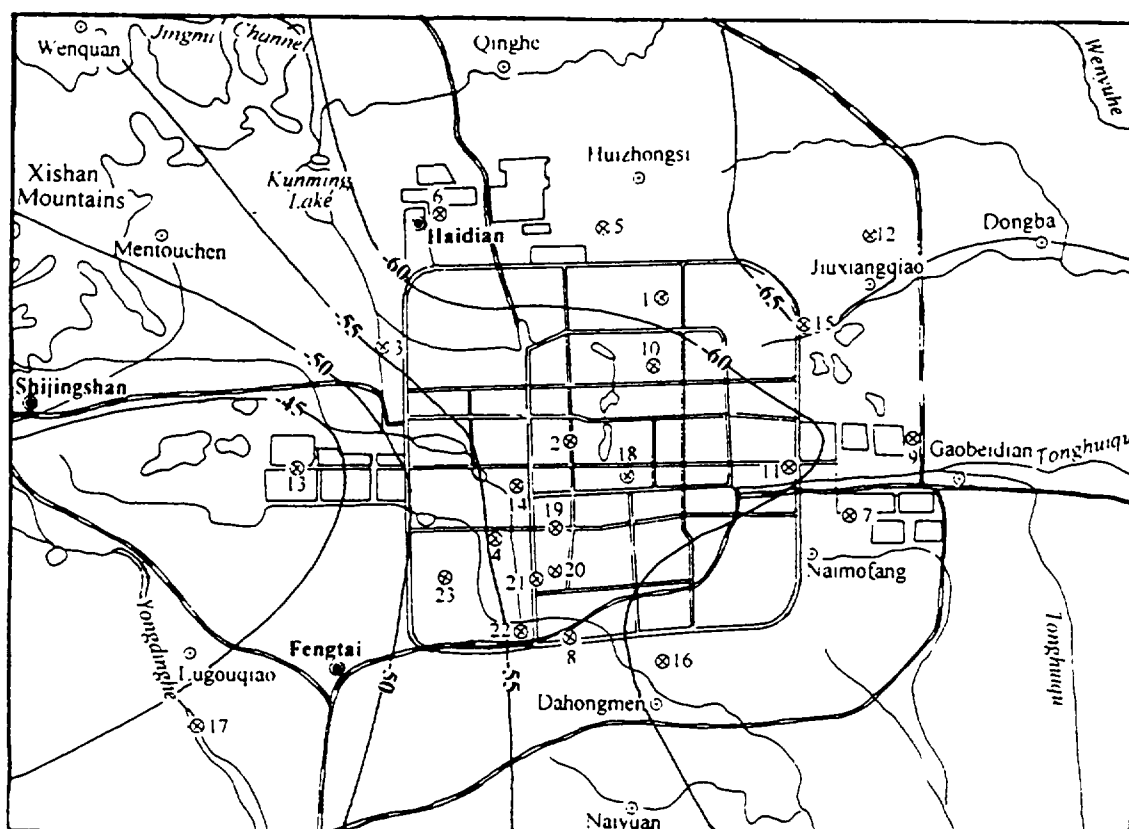
Fig. 6   Sketch map of the δ^2H isolines.

The isotope composition of the rainwater in Beijing area (Meteorological Station, N39°48', E116°28', 31.5 m above see level) was monitored in 1979 and 1980[3]. The weighted values of δ^2H and $\delta^{18}O$ for 1979 were -40.6‰ and -7.87‰, and for 1980 were -61.7‰ and -9.31‰, respectively. Beijing is located in the Asian Monsoon area, and the climate is characterized by great changes in temperature and rainfall from year to year. The annual precipitation in 1979 in Beijing area was 718.4 mm, while it was 380.7 mm in 1980. Obviously, the mean values of isotope composition of the rainwater in Beijing area could not be obtained from short-term monitoring data[4].   This is why we can not discuss this mixing process quantitatively by use of stable isotope data.

The stable isotope distribution in groundwater may not be strongly influenced by the exploitation. Therefore, the δ^2H isolines in Fig.6 may reflect the main natural groundwater flow. It has been noted in previous section that the content of As in groundwater increases gradually from the west to the east along the natural ground water flow. Distribution of As in groundwater is perhaps also related to the mixing process of two recharging sources.

6. TRITIUM CONTENT

All the tritium data obtained are listed in Table III.

Table III		Tritium content of the groundwater (TU)			
No	1975-05	1980-05	1995-06	1997-05	Note
1	36	33.4	42.4		
2	155	128			
3	173	137	37.1		
4	215	127	115	47.9*	collected in 1996-10
5	<TL	12.2			
6		36.0	20.1		
7		5.6	12.2		
8	197	142	58.1	51.1*	collected in 1997-01
9		9.4	3.5		
10		107			
11		34.4			
12		14.3	19.5		
13	144	89.1	35.6	21.3*	collected in 1996-12
14		158			
15		16.0	16.1		
16		37.5	49.8	39.2*	collected in 1997-02
17	100		25.3		River Water
18			34.6	27.8*	collected in 1996-12
20				33.9	
21				45.7	
22				53.6	
23				25.2	

It should be noticed, that some drill holes, from which the water samples were collected in 1975 or 1980, were out of use in 1990's. So changes in tritium content of groundwater in this case have to be followed from other drill holes.

Tritium-free groundwater was found in 1975 in drill hole No.5 in the northern suburb. It means that 23 years after the beginning of the atmospheric nuclear bomb tests water sample from drill hole No.5 was pre-bomb water.   The highest tritium content in 1975 (215TU at the drill hole No.4) was in the groundwater of the southwestern suburb. In 1980 the highest tritium content of 158TU was observed at drill hole No.14, located not far from the drill hole

124

No.4 (see Fig.7). Water sample from drill hole No.8, located in the southern suburb, had also rather high tritium content (142TU). While all the water samples of low tritium content were distributed in the eastern suburb. Water sample from drill hole No.5 (tritium-free in 1975) had tritium content 12.2TU in 1980. This is a clear message of presence of artificial bomb-test tritium. Take into account that the last pre-bomb precipitation occurred in 1951, and the distance from the west to the east in the sketch map is approximately 35 km, the flow rate of the groundwater in the northern part of the city could be evaluated as far less than 1 km/year.
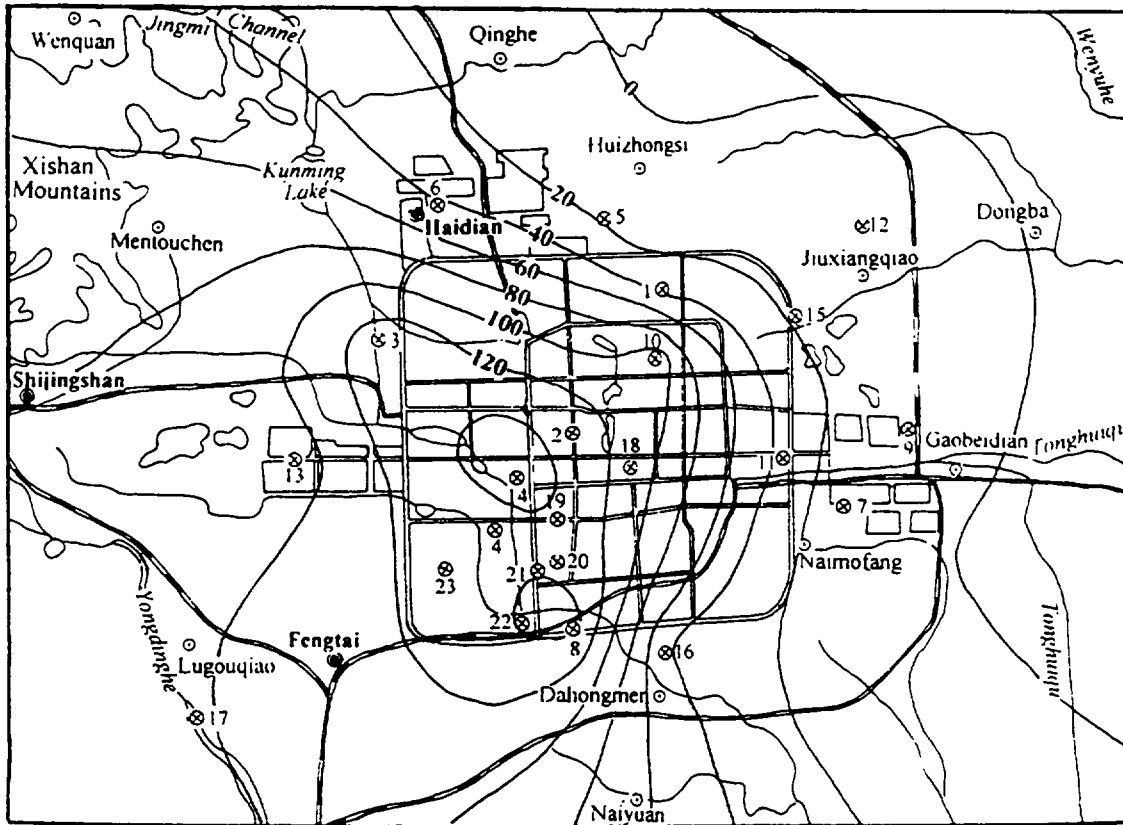
Fig.7　Sketch map of tritium isolines (TU) in 1980.

It is generally admitted that the piston flow model does not apply to groundwater flow[5]. Since different tritium contents of groundwater have been found in different parts of the area, the pure mixing model is also not the case for the groundwater system of Beijing area. However, the highest tritium content in groundwater may correspond to the recharge of 1963, or to some extent may be related to the recharge of 1963. In this case it could be expected that the highest tritium content spot in the sketch map will move gradually eastwards from upstream to downstream. This kind of transient behavior of the bomb-produced tritium may be used to demonstrate the pollutant behavior in groundwater aquifer.

From comparing the sketch maps of the tritium isolines in 1980 (Fig.7) and 1995, it was surprised that the distribution pattern in 1995 was almost the same as that in 1980. Actually, the tritium concentration peaks in the sketch maps of tritium isolines appear in the same place and have not moved eastwards since 1975 till 1995, but the high tritium values

have decreased. Tritium in groundwater has the same distribution pattern as those of the major chemical ions. It implies that the high tritium concentrations around the peak area is not caused by the recharge of 1963. It may be related to the intensive exploitation of groundwater in the center of Beijing city and a deep cone of depression of groundwater table formed in the southern suburb. Intensive pumping of the groundwater has changed the natural regime of the groundwater system, and a large scale of cone of depression could be considered as a terminal of the groundwater system.

Of course, the tritium peaks in the same place on the sketch maps of the tritium isolines in the last 20 years might also be caused by the waste disposal from several definite sources. A special investigation was organized in 1996 to check the waste disposal related to artificial tritium in the southern suburb. It was suggested that there are no pollution sources of artificial tritium around the area of tritium peaks.
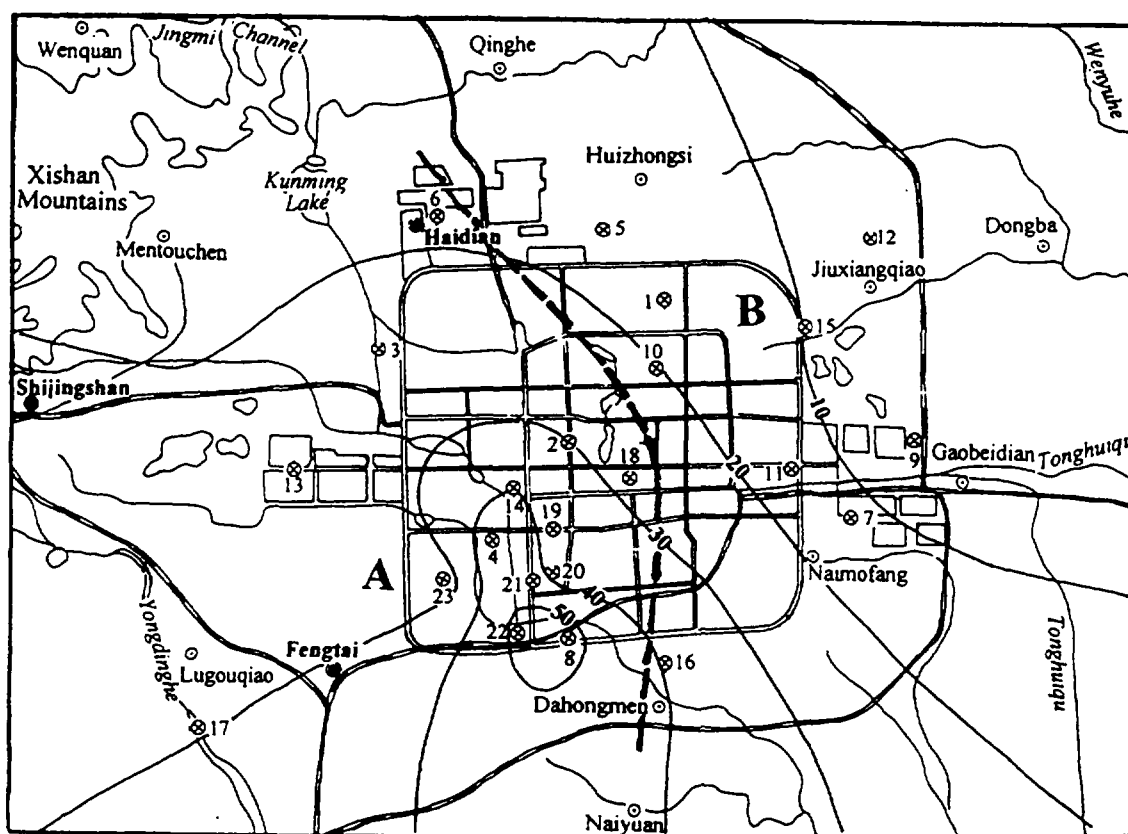
Fig.8   Sketch map of tritium isolines (TU) in 1997.

To make sure if there is really a zone with high tritium content in groundwater, or if it is just a very limited spot, four additional groundwater samples (No.20, 21, 22, 23) were collected in May 1997 near the tritium peak (drill holes No.4 and No.8). Together with other tritium data a sketch map of tritium isolines for 1997 was obtained (Fig. 8), which shows the same tritium distribution as in 1995. Therefore, it is confirmed that the tritium peak has remained at the same place since 1975.

Fig.9 illustrates the tritium concentrations of the groundwater in different parts of Beijing city in the period of 1975-1997.

126
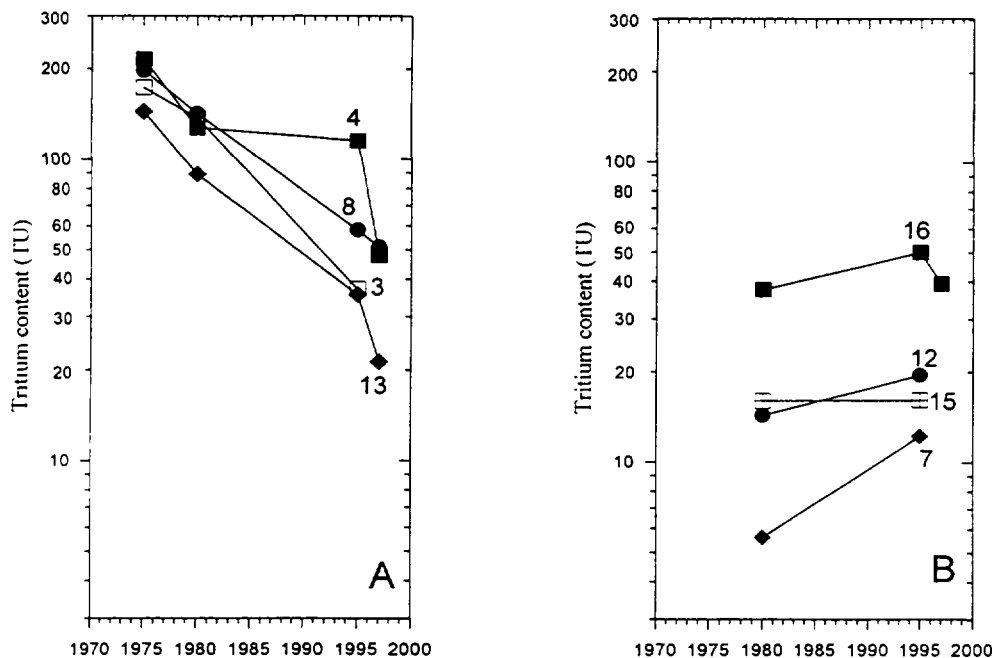
Fig. 9 Tritium concentrations of groundwater in the period of 1975-1997.

Artificial tritium was produced mainly in the period of 1952-1964 by the atmospheric thermal nuclear bomb tests. After 1964 the tritium levels of precipitation were still high in comparison with those of the pre-bomb period. It is illustrated in Fig.9 how the groundwater system responded afterwards to the great input of tritium. Figure A shows an exponential decrease in tritium concentrations in drill holes No. 4,8,3,13. All these drill holes are in the western and southwestern part of the investigated area. At the same time tritium concentrations of the groundwater from drill holes No.12,15,7 increased gradually at least up to 1997, drill hole No.16 up to 1995, as it has been shown in figure B. Based on this difference in response to the input of tritium, the dotted line in Fig. 8 divides the grounwater system into two subsystems;

A: subsystem with active circulation. The tritium concentrations decreased exponentially from 1975. It implies that the impact of the maximum input of bomb-produced tritium in 1963 is decreasing in this subsystem, but the artificial tritium has not been removed totally. The turn-over time of the groundwater in this subsystem should be less than 12 years.

B: subsystem with slow circulation. The tritium concentrations of water samples from some drill holes in this subsystem were lower than test level (4TU) in 1975. Since 1975 the concentrations were increased gradually at least up to 1995. It means that the turn-over time of the groundwater in this subsystem should be more than 32 years. For drill hole No.16, if the tendency of decrease of the concentration since 1995 could be confirmed by further investigation, the turn-over time can be estimated as 32 years.

Subsystem A was formed during the course of exploitation. Actually, the groundwater system, which was illustrated in Fig.1, should have a zonal distribution from low mineralization to high mineralization, from a relatively simple chemical type to a more or less complicated one. But as it can be seen from the explanation to Fig.1, the groundwater with

127

high mineralization and complicated chemical type was not in the downstream area, but in the transition zone. This is not a normal distribution. Consequently, the natural regime of the groundwater system in Beijing area has been destroyed. The area of high content of major chemical elements and high tritium content may be considered as the artificial terminal of the groundwater system. Subsystem A must be a highway from the recharge to the discharge under intensive exploitation. A part of the groundwater in subsystem B flows downwards to the east. The other part turns back to the cone of depression also due to exploitation. Therefore, in the case of serious pollution in the recharge area, only a small portion of the pollutants could be removed by the natural groundwater flow eastwards. Most of the pollutants could only be pumped out from the groundwater system during exploitation.

7.   TRACE ELEMENTS

Results of the ICP-MS analyses for some trace elements are listed in Table IV.

Table IV   Some trace elements in groundwater of Beijing city (μg/L)

No	Li	Ge	Y	Ru	Rh	Ba	U	Sr	$^{87}Sr/^{86}Sr$	Note
1	5.97	<0.029	0.0369	0.17	0.055	144	5.64	1665	0.70950±3	
3	8.93	<0.029	0.0074	0.051	0.018	107	5.43	498	0.71053±3	
4	7.94	<0.029	0.0067	0.071	0.024	103	7.27	671		
6	3.14	<0.029	0.0098	0.096	0.032	81.2	4.00	979		
7	5.22	<0.029	0.0120	0.098	0.035	113	4.17	975		
8	10.5	<0.029	0.0096	0.062	0.021	55.7	7.52	584		
9	4.68	0.062	0.0106	0.059	0.021	49.7	2.36	661	0.70940±4	
12	6.92	0.037	0.0111	0.099	0.034	107	3.90	1026		
13	1.68	<0.029	0.0100	0.012	0.005	68.5	0.67	154	0.71055±8	
15	5.48	<0.029	0.0244	0.23	0.079	131	3.75	2371	0.70925±8	
16	10.1	<0.029	0.0095	0.080	0.026	72.3	5.59	826		
17	10.0	<0.029	0.0062	0.035	0.013	70.3	3.77	348	0.71021±20	River water
18	8.38	<0.029	0.0105	0.10	0.035	87.3	6.80	983	0.70989±2	
20	3.06	<0.029	0.094	<0.005	0.025	131	5.15	882	0.71047±4	
21	2.82	<0.029	0.092	<0.005	0.027	165	6.16	948		
22	2.55	<0.029	0.162	<0.005	0.026	160	5.77	924		
23	1.04	0.040	0.014	<0.005	0.025	161	4.72	888		
24	4.62	<0.029	0.043	0.009	0.081	85.7	1.69	2827	0.70928±2	Mineral water

Some trace elements, such as Li, Y, Ba and U, have a similar distribution pattern to that for Na and SO_4. The content of Ge was generally very low, but a relative high content of Ge was observed in the eastern suburb, so the distribution pattern of Ge is the δ^2H type.

The content of trace element Sr in the groundwater is rather high (see Table IV) and its distribution is a very special Sr pattern (Fig.10). The highest concentration was observed in the drill hole No.15, while the lowest was in the western suburb, at the drill hole No.13. The

same distribution pattern was found for the elements Ru and Rh (Fig.11). This kind of distribution pattern may not be related to intensive exploitation.

In order to ascertain the origin of the Sr in groundwater of the Quaternary aquifer, the $^{87}Sr/^{86}Sr$ ratio was measured on VG-354 mass-spectrometer for 7 groundwater samples, 1 river water sample and 1 bottled mineral water from a deep drill hole in metamorphic rock. The Sr isotope ratios are listed in Table IV and given in Fig. 10 under the number of the drill hole. The Sr content and $^{87}Sr/^{86}Sr$ ratio of the bottled mineral water from metamorphic rock is 2.83 mg/L and 0.70928, respectively. The water sample from drill hole No.15 has a Sr content of 2.37 mg/L (highest Sr concentration in Quaternary aquifer) and $^{87}Sr/^{86}Sr$ ratio of 0.70925. Based on the values of $^{87}Sr/^{86}Sr$ ratio it seems that the Sr of these two water samples has the same origin. It implies that the high concentrations of Sr in the eastern suburb is not related to a special pollution source.

As can be seen from Fig. 10, the values of the $^{87}Sr/^{86}Sr$ ratio decrease gradually from the west to the east. This probably results from a mixing of two components. The Yongdinghe River water (No.17) shows lower Sr content. Its $^{87}Sr/^{86}Sr$ ratio is 0.71021, which is close to that of the Yangtze River (0.7109) in China and of the Mississippi River (0.7102) in North America[6]. It may represent one mixing component of shallow groundwater. The bottled mineral water represents the deep groundwater component from baserock, which has lower $^{87}Sr/^{86}Sr$ ratio but higher Sr concentration. Such a Sr isotope study may serve as an additional tool to identify the origin of the ground waters and the origin of Sr itself in groundwater systems.
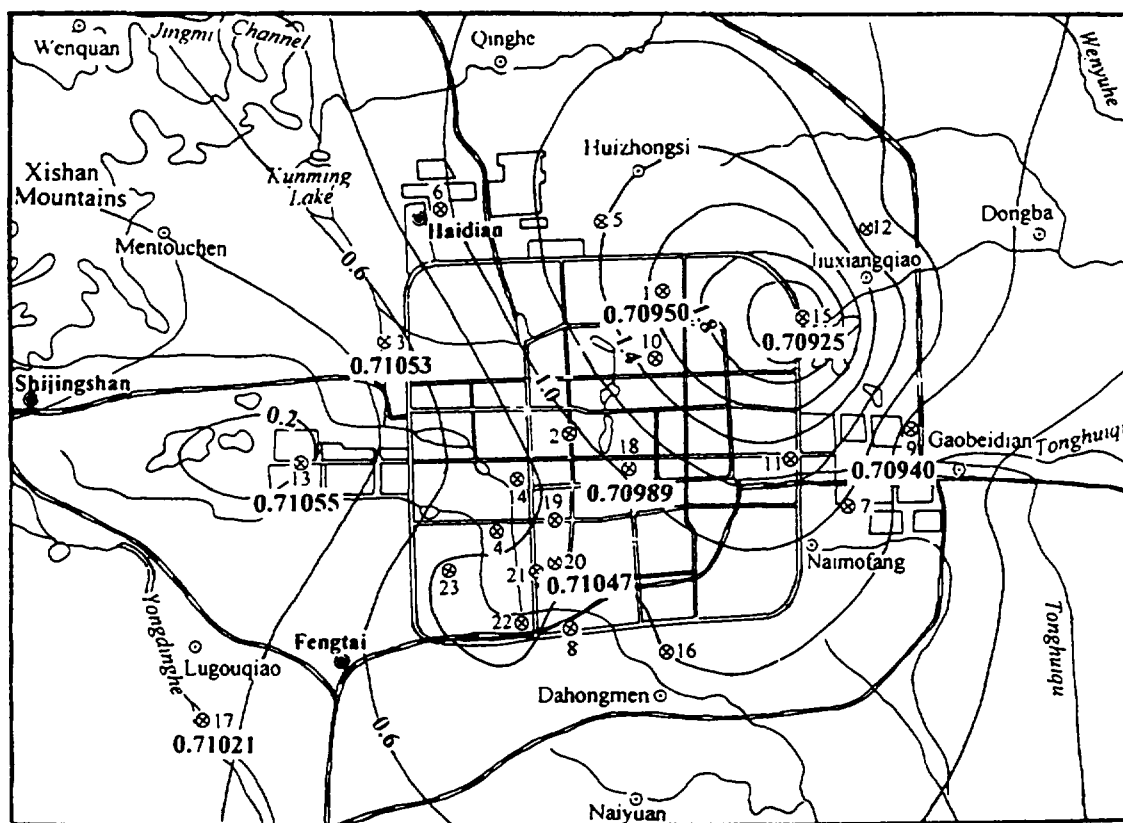

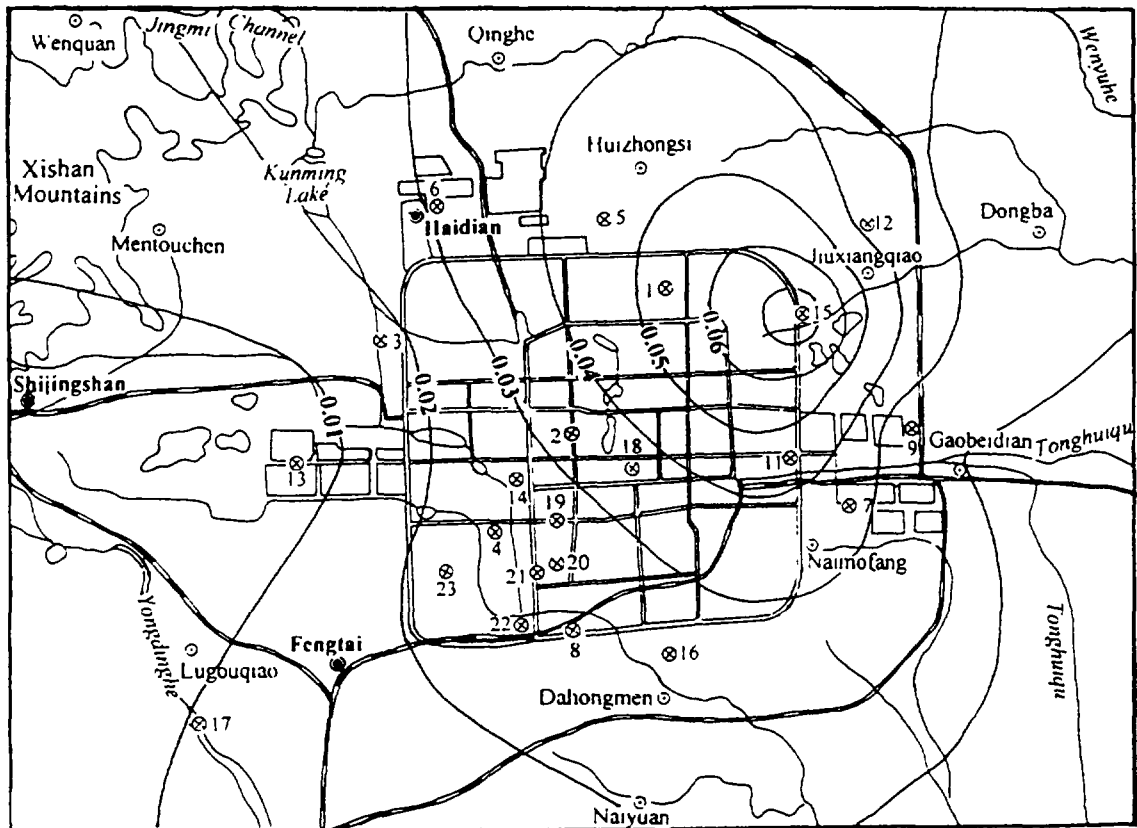Fig.10   Sr isolines (mg/L) and $^{87}Sr/^{86}Sr$ ratios of groundwater.

Fig.11   Rh distribution (μg/L) in groundwater.

8.   CONCLUSIONS

1. The results of tritium monitoring indicate that the natural regime of the groundwater system of the Quaternary aquifer in the Beijing area has been destroyed due to intensive exploitation.   This message was confirmed by the investigation of stable isotopes, major and minor chemical constituents and trace elements. Two subsystems could be divided based on tritium data. Subsystem A with active circulation was formed in the course of exploitation. It must be a highway from the recharge to the discharge under intensive exploitation. The tritium concentrations in this subsystem were decreasing exponentially since 1975. It implies that the impact of the maximum input of bomb-produced tritium in 1963 was diminishing, but the artificial tritium has not been removed totally. The turn-over time of the groundwater in this subsystem should be less than 12 years.   Subsystem B is of slow circulation. The concentrations were increasing gradually at least up to 1995. It means that the turn-over time of the groundwater in this subsystem should be more than 32 years.   It infers, that in the case of serious pollution only a small portion of the pollutants could be removed by the natural groundwater flow eastwards. Most of the pollutants in groundwater system could only be pumped out from the groundwater system during exploitation.

2. The δ^2H and $\delta^{18}O$ values of the groundwater are higher in western suburb than that in eastern suburb.   The sketch maps of δ^2H and $\delta^{18}O$ isolines reflect a mixing between ground waters from the baserock and that of local recharge.

130

Characteristics of groundwater of local recharge:

      a. High values of δ^2H and $\delta^{18}O$,   -45‰, -7.0‰ respectively;
      b. Low content of Arsenic,   1-2 μg/L;
      c. Low content of Sr,   0.4 mg/L;
      d. High value of $^{87}Sr/^{86}Sr$ ratio,   .0.71055.

Characteristics of groundwater from the baserock:

      a. Low values of δ^2H and $\delta^{18}O$,   -65‰, -9.4‰; respectively;
      b. High content of Arsenic,   18 μg/L;
      c. High content of Sr,   2.8 mg/L;
      d. Low value of $^{87}Sr/^{86}Sr$ ratio,   .0.70928.

3. The trace elements Sr, Ru and Rh have a very special distribution in groundwater system with very high concentrations in the north-eastern part of the old Beijing city. The results of ^{87}Sr / ^{86}Sr measurement show that Sr in groundwater of the Quaternary aquifer is from the basement rock groundwater. High concentrations of Sr in groundwater of the Quaternary aquifer are not related to any special pollution source.

ACKNOWLEDGEMENTS

REFERENCES

[1] Editorial Committee "Report on the Environment Quality of Beijing City", Environment Quality of Beijing City in 1993. June, 1994 (1994).

[2] Hygienic standard of drinking water TJ-20-76 (1976).

[3] Wei Keqin, Lin Ruifen, Wang Zhixiang, Deuterium, oxygen-18 and tritium content in precipitation in the Beijing area. SCIENTIA SINICA (B series) 8 (1982) 754-757.

[4] Wei Keqin and Lin Ruifen, The influence of the monsoon climate on the isotopic composition of precipitation in China. GEOCHIMICA, 23 1 (1994) 33-41.

[5] Fontes, J.Ch., "Dating of groundwater", Guidebook on Nuclear Techniques in Hydrology, International Atomic Energy Agency, Vienna (1983) 285-317.

[6] Palmer, M.R. and Edmond, J.M., The strontium isotope budget of the modern ocean. Earth and Planetary Science Letters, .92 (1989) 11-26.

ORIGIN OF BANK FILTERED GROUNDWATER RESOURCES COVERING THE DRINKING WATER DEMAND OF BUDAPEST, HUNGARY

I. FÓRIZS
Laboratory for Geochemical Research of the Hungarian Academy of Sciences

J. DEÁK
Water Resources Research Centre Plc.

Budapest, Hungary

Abstract - *The ratio of Danube water/infiltrated precipitation has been determined using stable oxygen isotope data on four parts of the protection area of the bank filtered water works supplying drinking water for Budapest, Hungary. These ratios comparing to those calculated by hydraulic modeling rarely match each other. The Danube water transit time calculated for few wells by isotopic data are usually shorter than those determined by hydraulic modeling. The relation between the $\delta^{18}O$ values and the nitrate, chloride and sulfate pollutants shows that the source of the pollutants is on the island area (sewage water, agricultural activity and salt used for de-icing asphalt roads).*

1. INTRODUCTION

The drinking water demand of more than two million inhabitants of Budapest is mainly covered by bank filtered water of the River Danube. In 1990 the average drinking water consumption of Budapest was 976,000 m^3/d [1], and it was 780,566 m^3/d in 1995 [2]. The bank filtered wells are located on the both sides of the Danube north and south of Budapest, in Budapest, and on the bank shores of the Szentendre Island and Csepel Island (Fig. 1).

The ratio of the Danube water and the infiltrated precipitation in the supplied water is a very important question related to the drinking water quality. The infiltrated precipitation is potentially polluted by agricultural activity and communal waste water of unsewered settlements. The mixing of these two types of waters has been investigated by stable oxygen isotope ratio.

The $\delta^{18}O$ values of the water samples have been measured, evaluated and compared with the chemical composition of the water. The hydraulic modeling of the water flow system in the uppermost aquifer on the Szentendre Island has been made in a frame of an independent programme at the Technical University of Budapest [3]. The ratio of Danube water/infiltrated precipitation, and Danube water transit time have been determined for some wells by hydraulic model and the stable oxygen isotope data as well. Data obtained by the two methods have been compared.

In the first year (1995) of our project we studied the most northern and middle part of the Szentendre Island and the area of the Dunakeszi Water Works on the left bank of the Danube (Fig. 1, 2, 3 and 6) determining the origin of the shallowest groundwater and the pollutants. In the second year (1996) we studied the Csepel Island area (Fig. 1 and 10) for the same purpose.
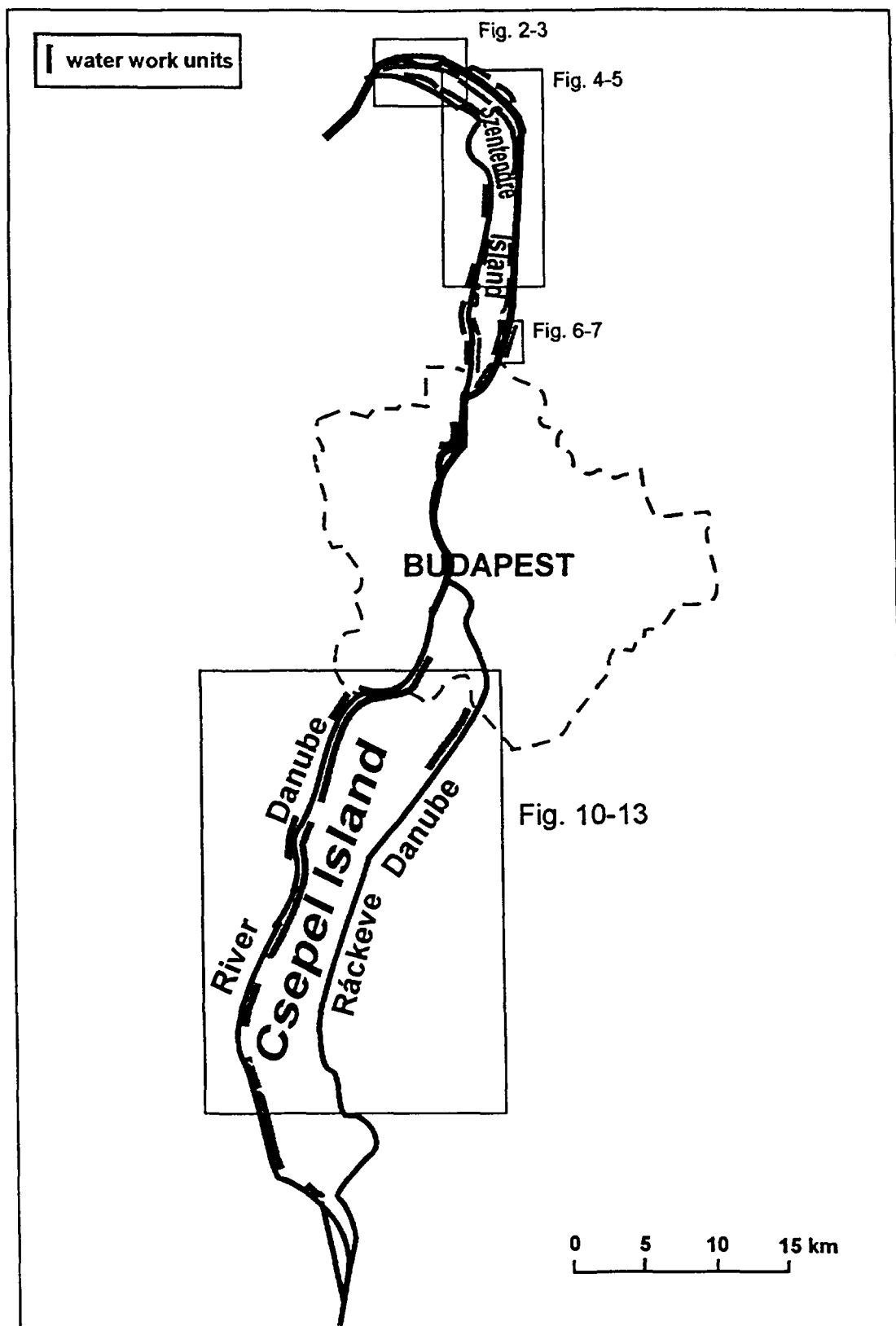
Fig. 1. Sketch map showing the bank filtered water work units supplying Budapest.
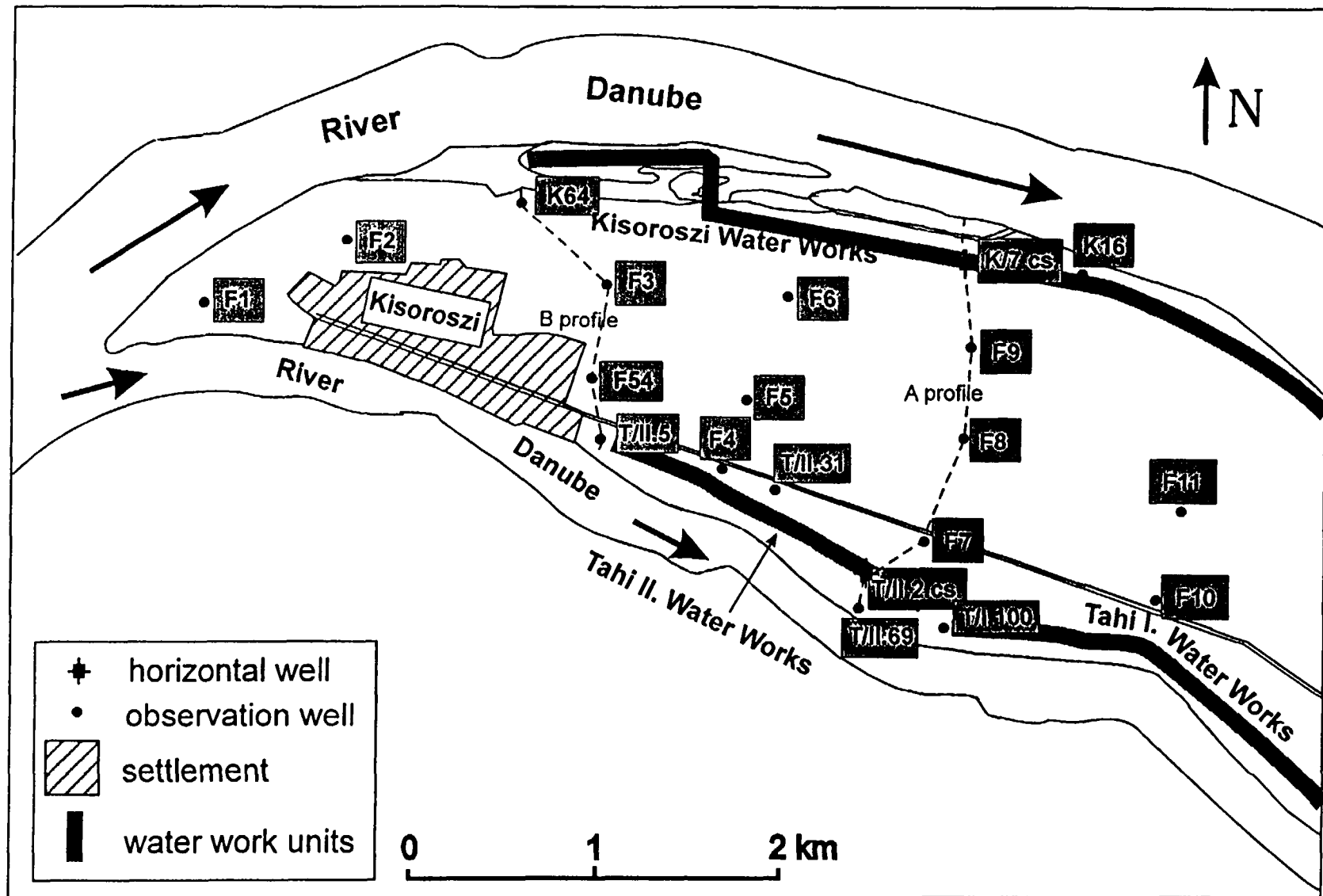
Fig. 2. Sketch map of the northern part of the Szentendre Island showing the names and locations of the wells sampled.

$\delta^{18}O$
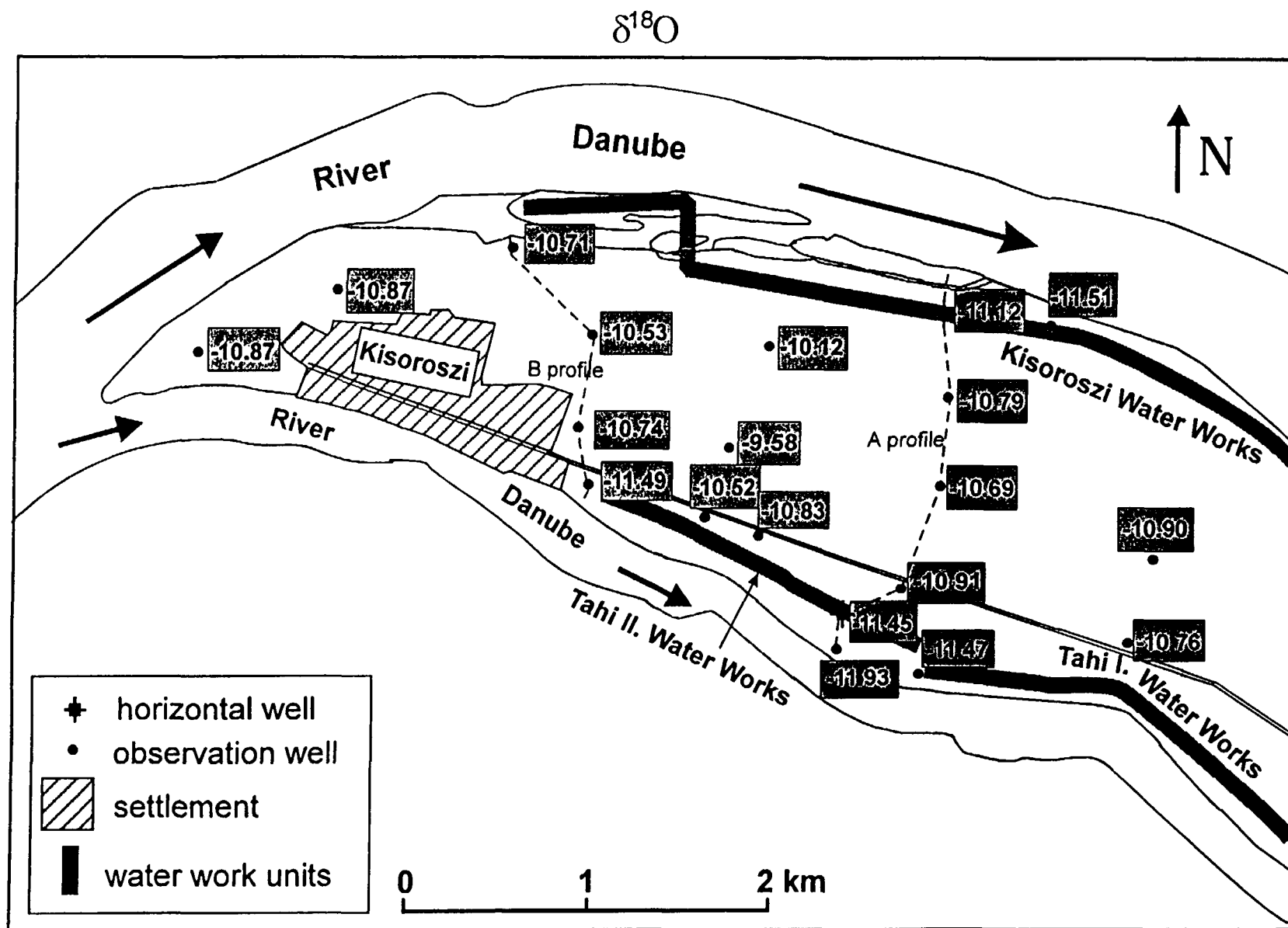
Fig. 3a. The stable oxygen isotope compositions of the wells sampled on the northern part of the Szentendre Island.

NO$_3$
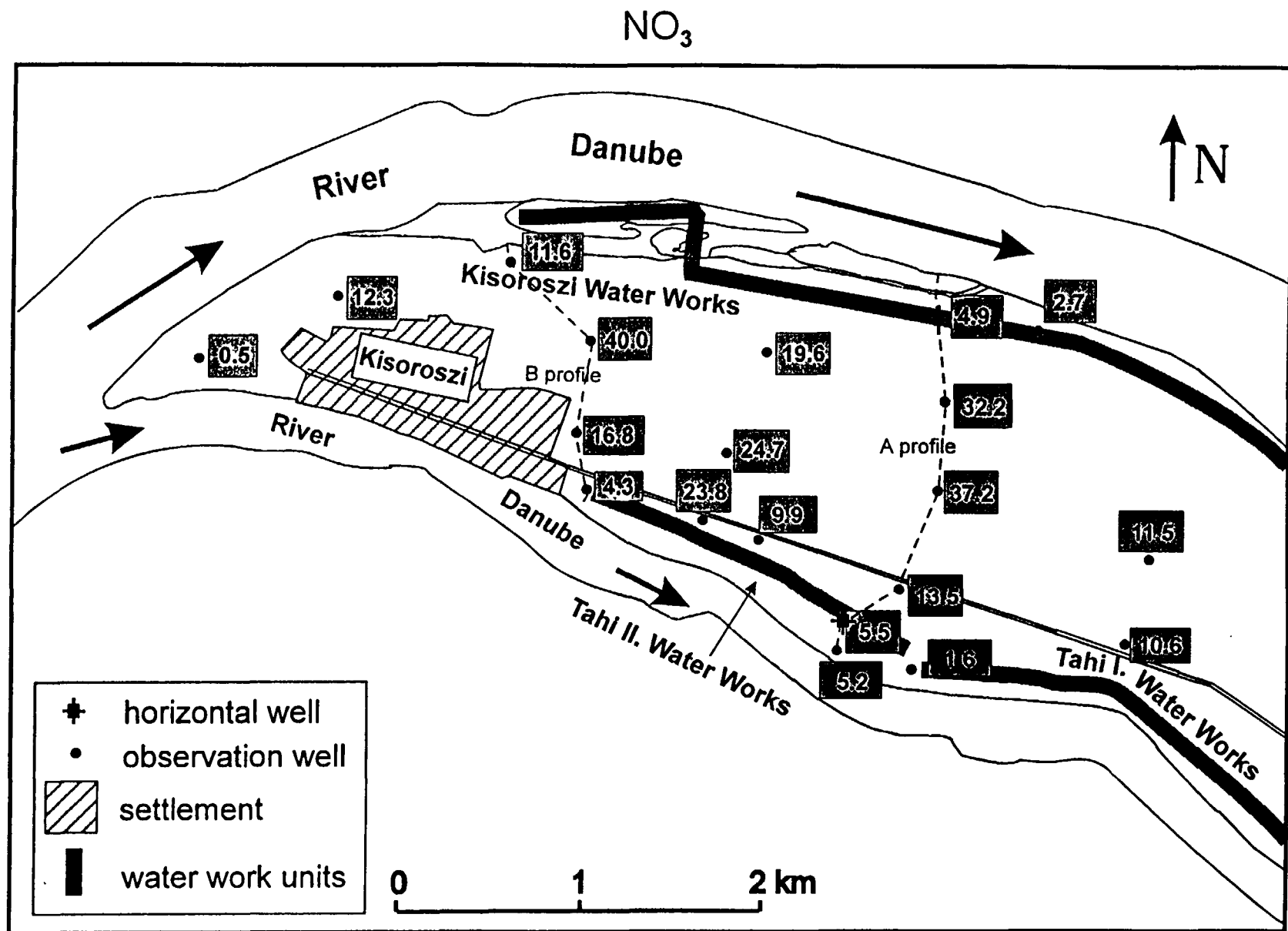
Fig. 3b. The nitrate content of the wells sampled in the northern part of the Szentendre Island.

Cl
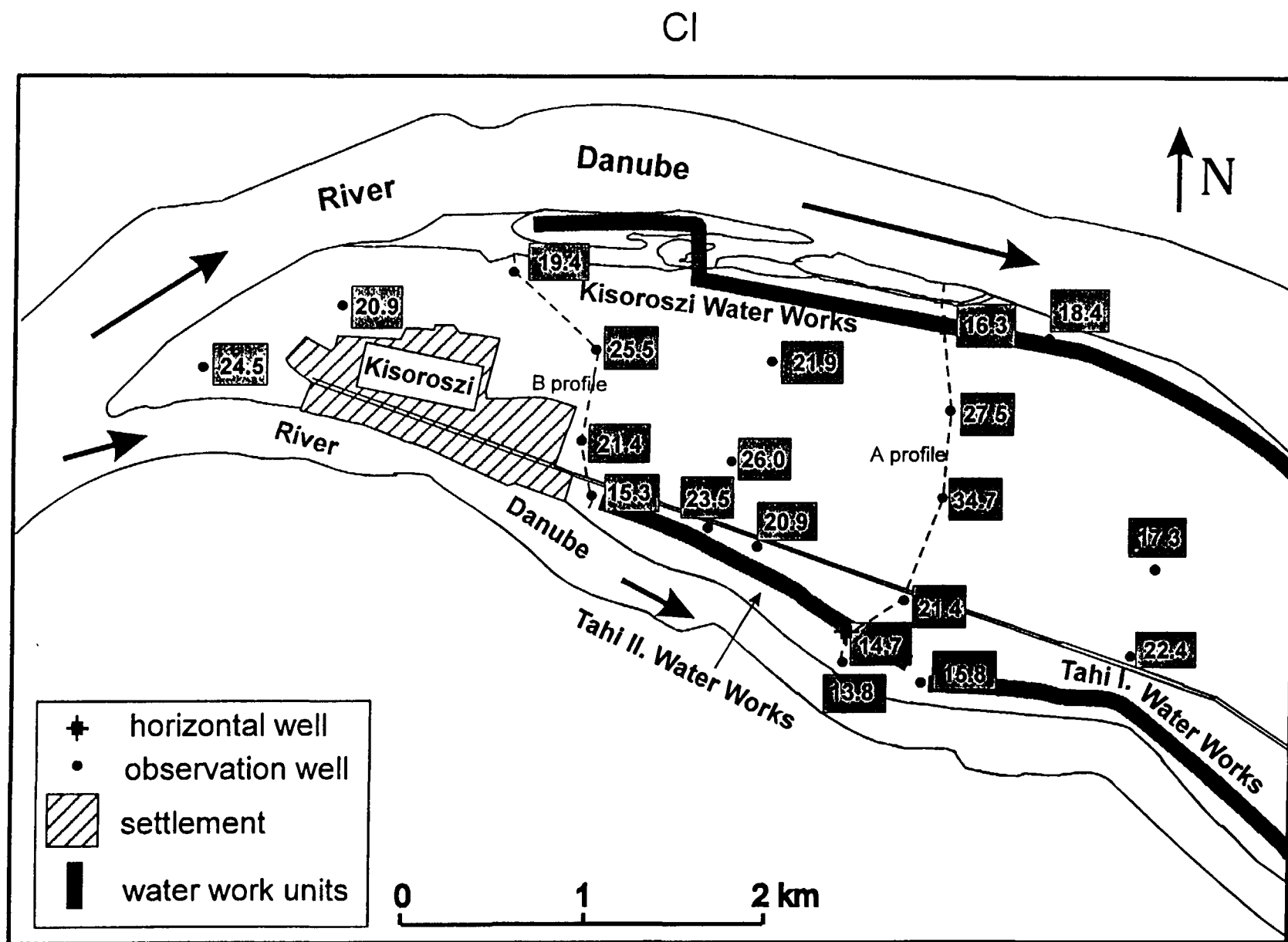
Fig. 3c. The Cl content of the wells sampled in the northern part of the Szentendre Island.
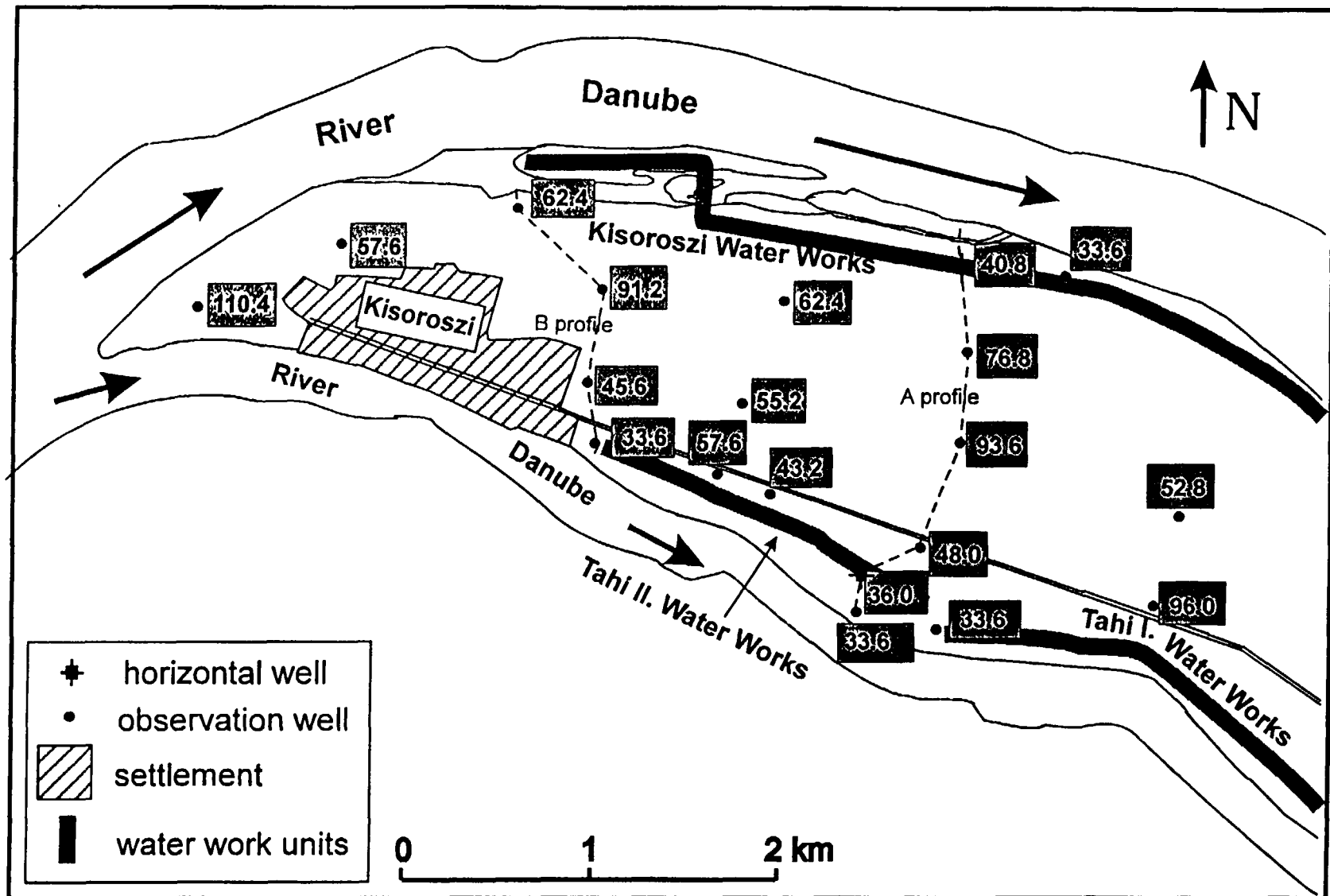
Fig. 3d. The sulphate content of the wells sampled in the northern part of the Szentendre Island.
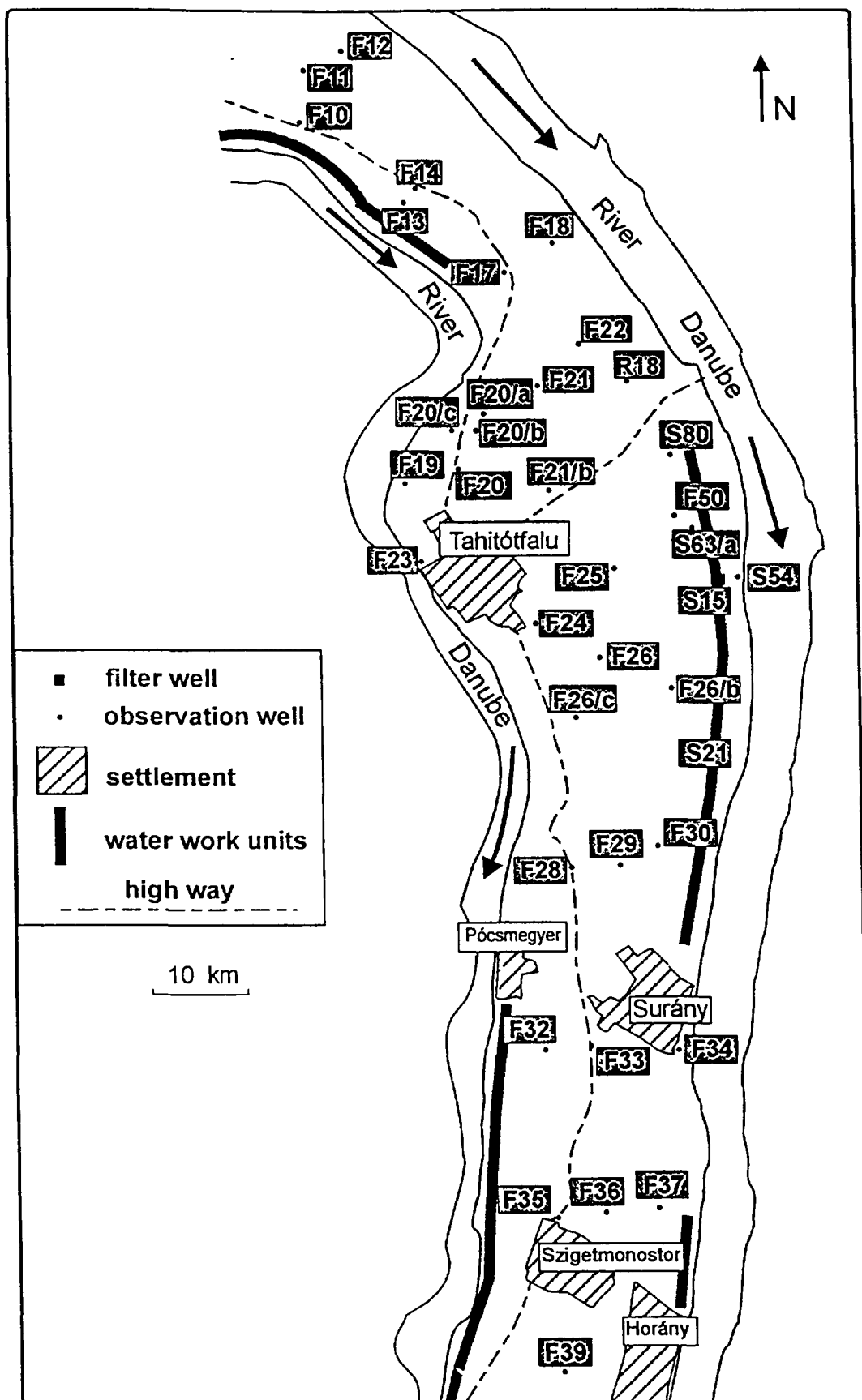
Fig. 4. Sketch map of the middle part of the Szentendre Island with the names and locations of wells sampled.

$\delta^{18}O$
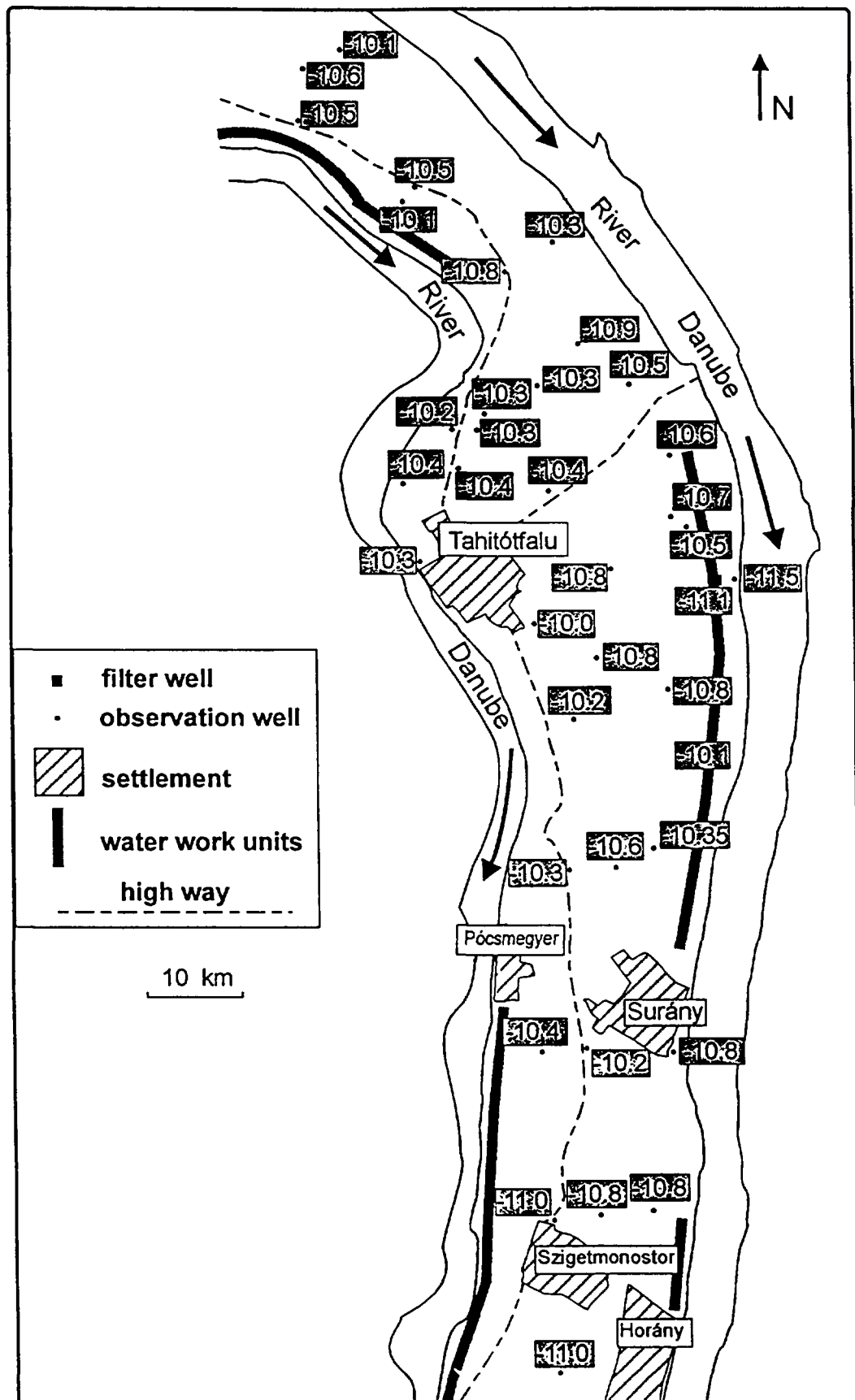
Fig. 5a. The stable oxygen isotope composition of the wells sampled in the middle part of the Szentendre Island.
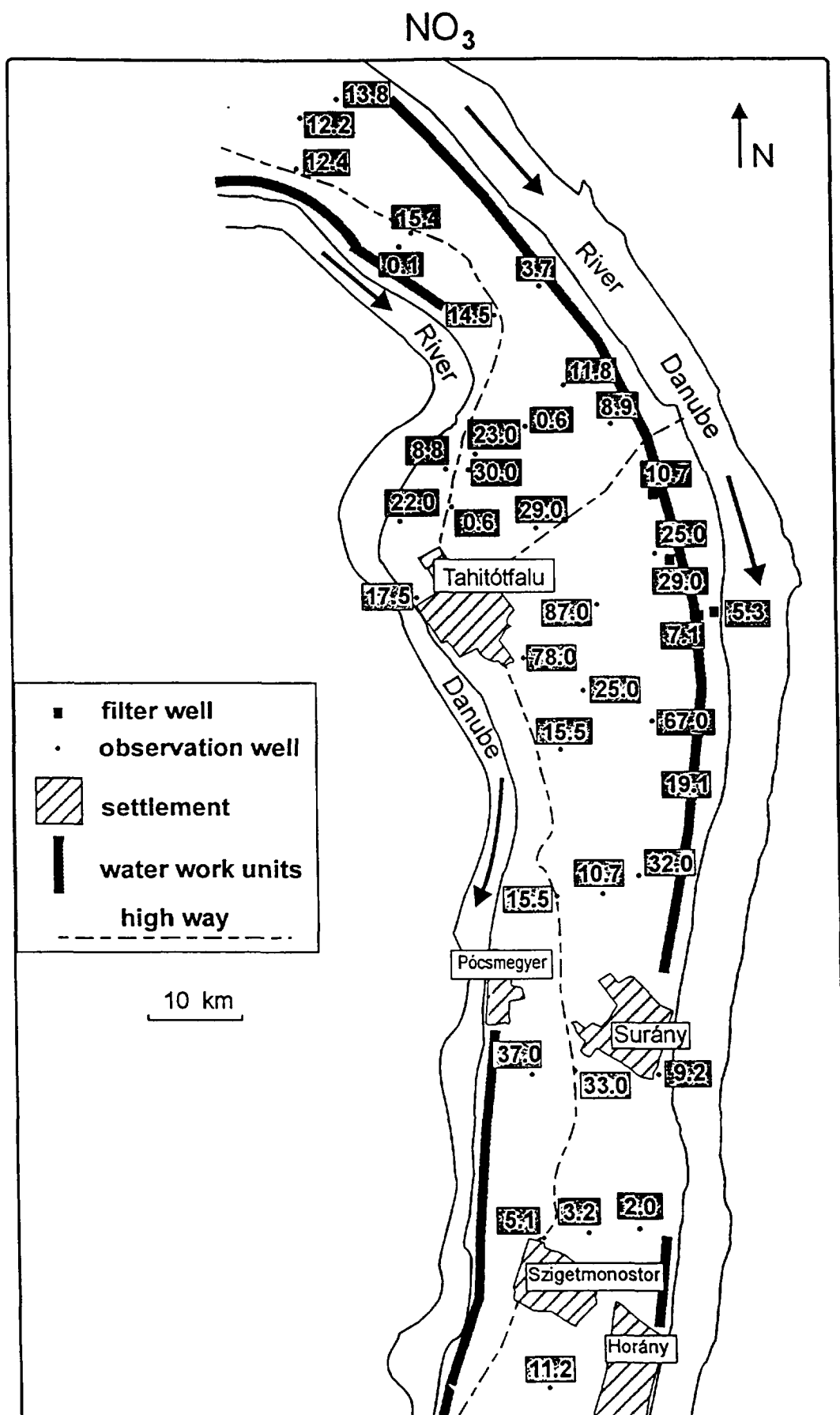
Fig. 5b. Nitrate content of the wells sampled in the middle part of the Szentendre Island.
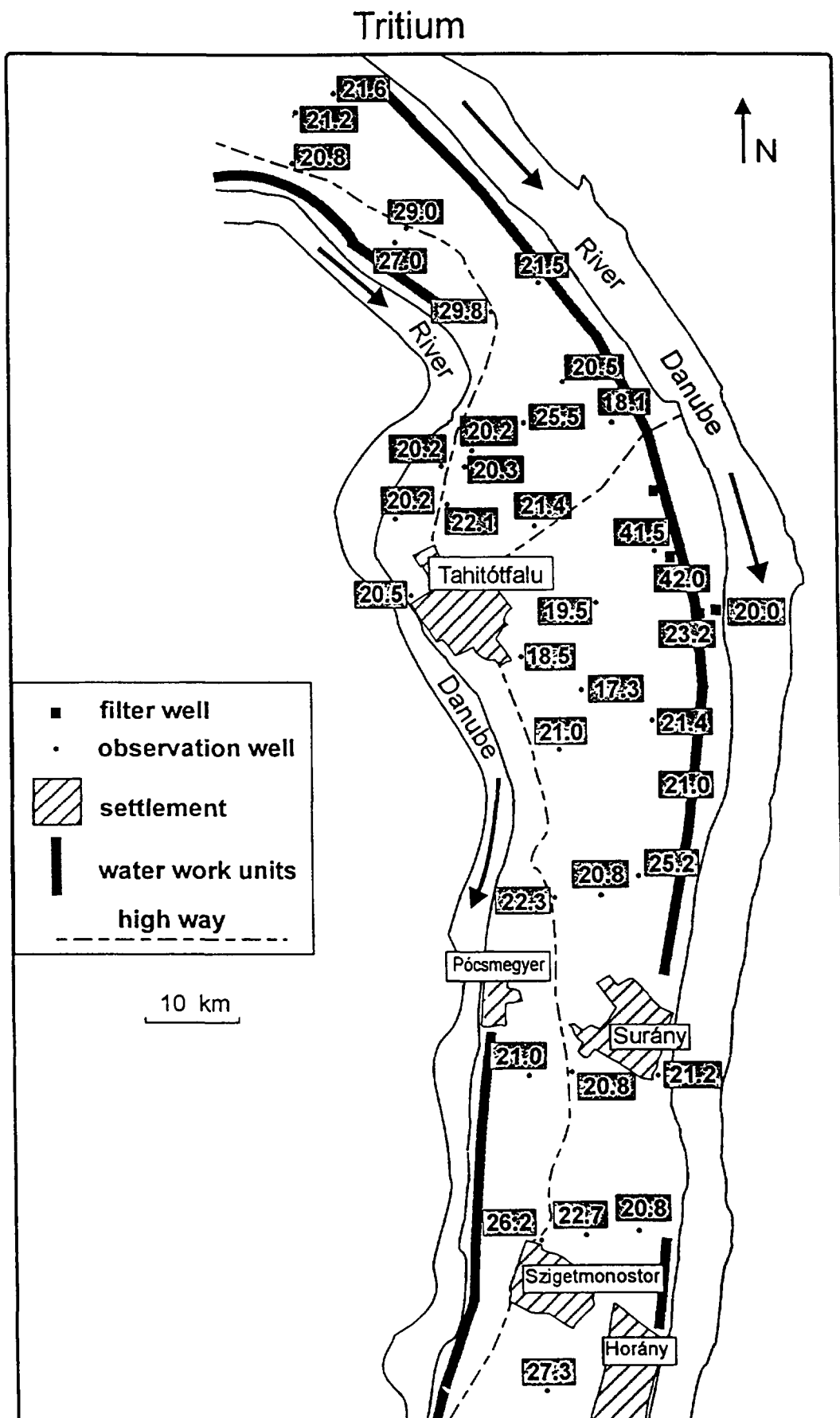
Tritium

Fig. 5c. Tritium content of wells sampled in the middle part
of the Szentendre Island.
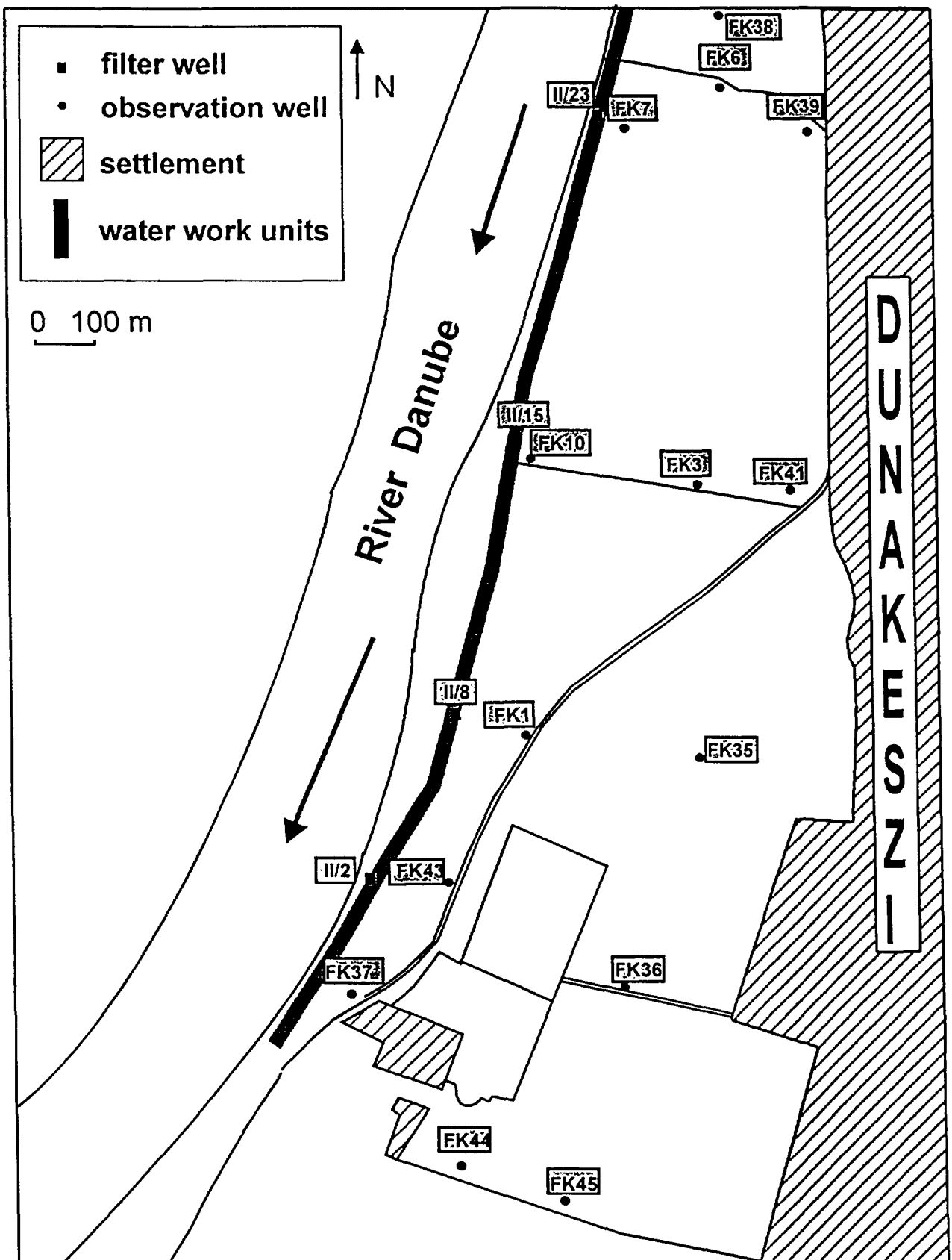
Fig. 6. Sketch map of the area of the Dunakeszi Water Works showing the name and location of the sampled wells.
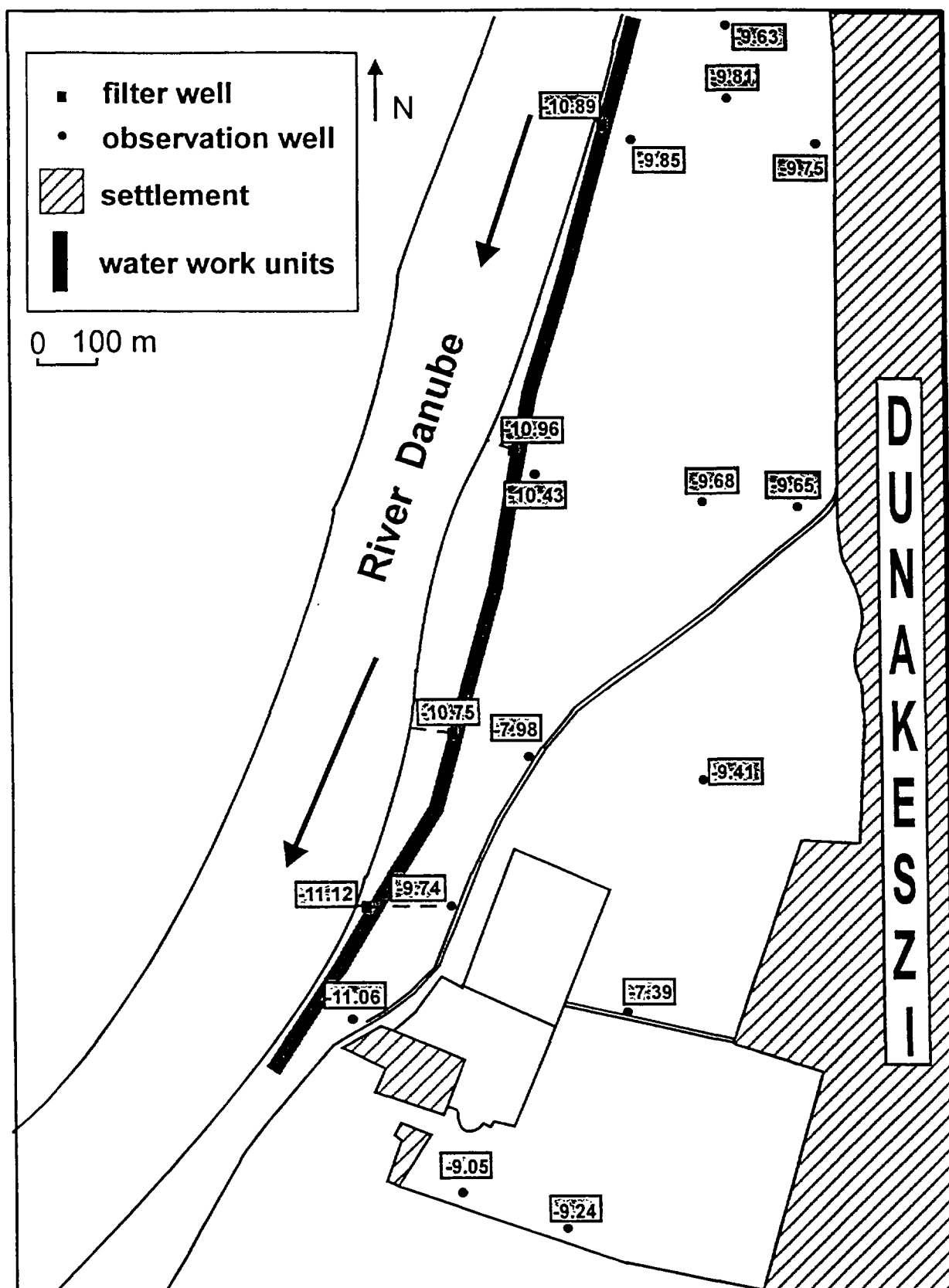
Fig. 7. The stable oxygen isotope composition of the sampled wells of the Dunakeszi Water Works.
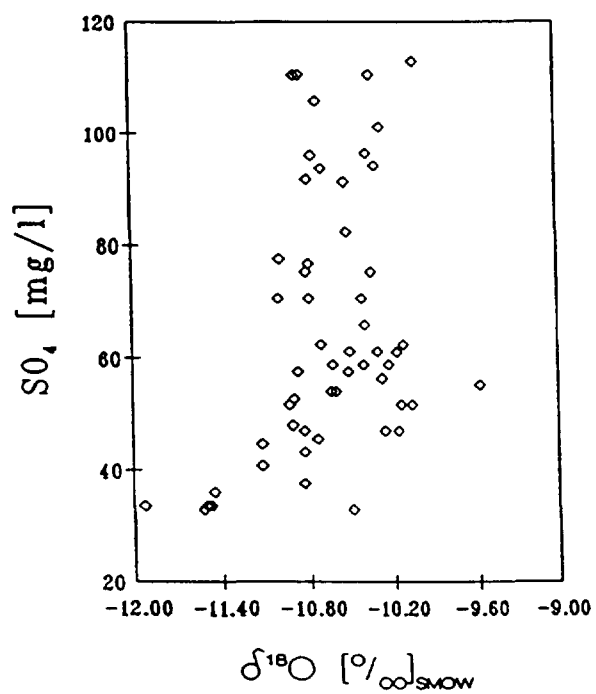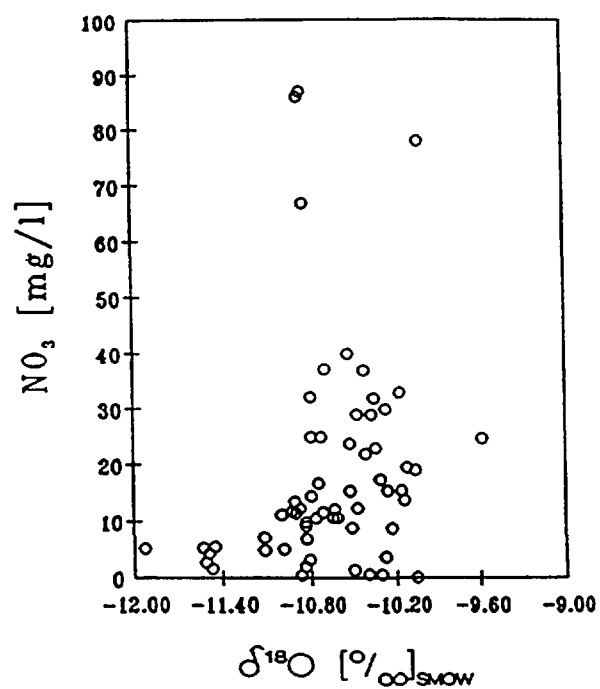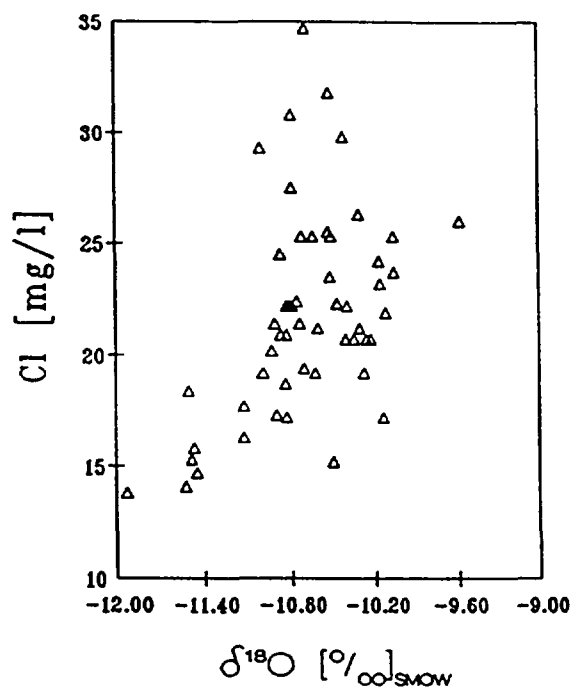
Fig. 8. Chloride, nitrate and sulphate vs. stable oxygen isotope composition of water samples collected on the Szentendre Island.

146
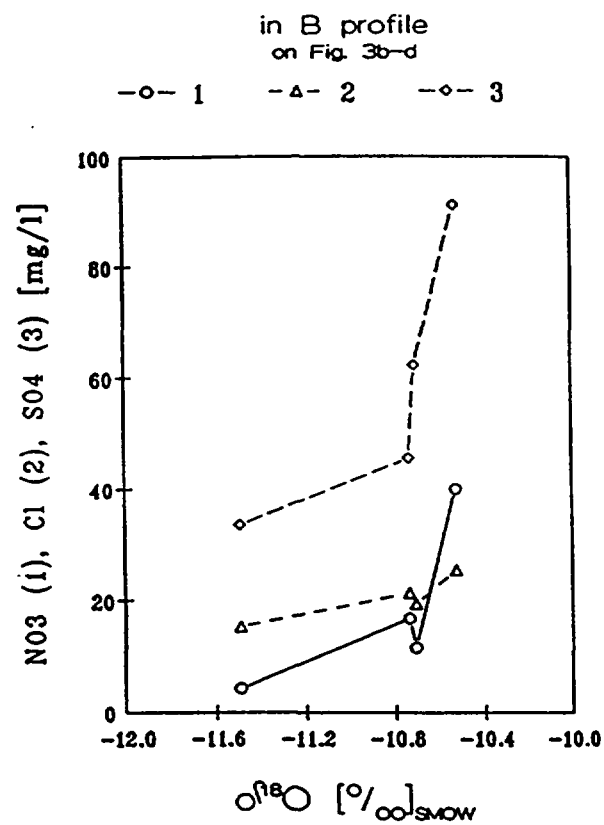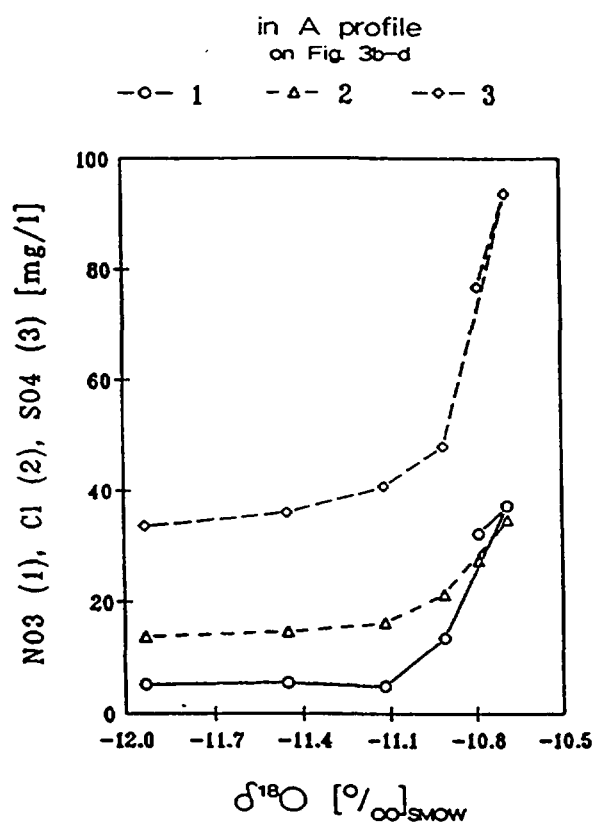
Fig. 9. NO_3, Cl, SO_4 vs. $\delta^{18}O$ in profiles A and B indicated on Fig. 2.
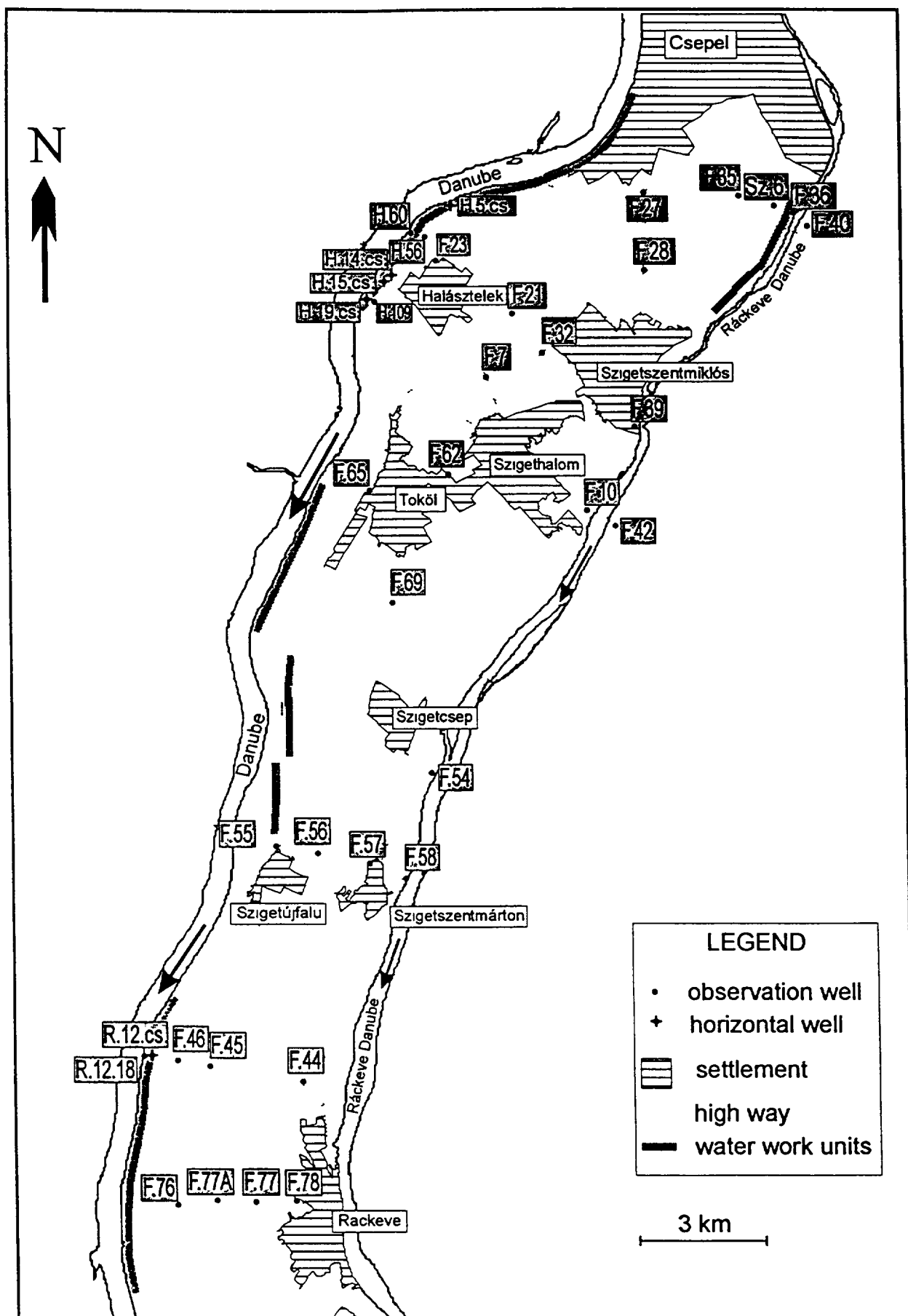
Fig. 10 Sketch map of the Csepel Island showing the locations of the wells
studied

2. TECHNIQUES APPLIED

2.1. Isotope analysis

Stable oxygen isotope measurements have been made on Finnigan MAT delta S mass spectrometer. The results are expressed in the conventional delta (δ) notation in per mille (‰) relative to the VSMOW (Vienna Standard Mean Ocean Water) international standard in the following way.

$$\delta^{18}O = \frac{R_{sample} - R_{standard}}{R_{standard}} * 1000 \quad [\text{‰}],$$

where R_{sample} and $R_{standard}$ indicates the $^{18}O/^{16}O$ ratios of the sample and standard respectively.

Samples were prepared according to the conventional CO_2-H_2O equilibration method first described in [7].

Tritium measurements were made in the TriCarb Lab of the Water Resources Research Centre, Budapest, Hungary (analyst Miklós Süveges) by the conventional scintillation method.

2.2. Chemical analyses

The NH_4, NO_3, NO_2, Cl and SO_4 content of the water samples were measured by the methods described in the Hungarian National Norm for drinking water quality determination. All the data have been got from the Water Works of Capital Corp. (Fővárosi Vízművek Rt., Budapest, contact person Ádám Kontúr).

2.3. Calculation of Danube water component

The basis for determining the origin of the drinking water supplied from bank filtered wells is the fact that the $\delta^{18}O$ value of Danube water is significantly different from the locally infiltrated precipitation [8]. The $\delta^{18}O$ value of the Danube water varies seasonally between -10 and -12 ‰. Its annual mean value for the period of 1991-96 is -11.24‰ at Vienna [4], -11.0‰ at Bratislava [5], and -11.0‰ at Medve (half way between Budapest and Bratislava) [6]. As there is no considerable inflow into the Danube between Budapest and Bratislava, we can use the value of -11.0‰ as the average $\delta^{18}O$ value of River Danube near Budapest. The multi-annual *mean* of infiltrating precipitation in Hungary is -9.5‰ [9].

Using this difference we can calculate the mixing ratio of Danube water/infiltrated precipitation by $\delta^{18}O$ data measured in production wells according to the following equation:

$$\delta^{18}O_{well} = x*\delta^{18}O_{Danube} + (1-x)* \delta^{18}O_{infiltrated\ precipitation}$$

From this the ratio of Danube water in percent is:

$$x_{Danube} = \frac{\delta^{18}O_{well} - \delta^{18}O_{infiltrated\ precipitation}}{\delta^{18}O_{Danube} - \delta^{18}O_{infiltrated\ precipitation}} * 100\ (\%).$$

149

3. RESULTS AND INTERPRETATIONS

3.1. Northern and middle part of the Szentendre Island

3.1.1. Stable oxygen isotope data

Stable oxygen isotope measurements have been made on 80 samples from the above mentioned two areas. The name and locality of the wells sampled are indicated on Figs. 2 and 4. Results of stable oxygen isotope measurements are summarized in Tables I and II. Two profiles (indicated on Figures 2-3a-d) more-or-less perpendicular to the flow line of the River Danube have been studied.

All the wells are located on the river island. The two production wells (Table I) are very close to the river bank. Their $\delta^{18}O$ can be used for transit time calculations (see later), because the Danube water component in these production wells are almost 100% according to the hydraulic modeling [3].

The $\delta^{18}O$ values of the observation wells on the northern part of the Szentendre Island range between -9.6 and -10.9‰. These values are more negative than that of the local infiltration, so the shallowest groundwater of the island is a mixture of Danube water and the local infiltration. Going from the river bank to the center of the island, the Danube water component is less and less.

The $\delta^{18}O$ values of the observation wells on the middle part of the Szentendre Island vary between -10.1‰ and -11.0‰ (Table II, Fig. 5a). All of these data are more negative than that of the mean annual precipitation indicating that the shallowest groundwater has a considerable Danube water component. While in the northern part of the Szentendre Island the most positive values can be found in the midline of the island, in the middle part of the island no such a distribution can be found. Two observation wells (F10 & F11, Tables I, II, and Figs. 2, 3a, 4, 5a) have been sampled twice, first in June ($\delta^{18}O$ = -10.76, -10.90‰), second time in September (-10.47, -10.63). Second time the $\delta^{18}O$ values were more positive by 0.28‰ in both wells.

3.1.2. Tritium

The tritium content of the water samples collected in the middle part of the Szentendre Island has been determined in the Water Resources Research Center (VITUKI). Results can be found in Table II, and are plotted on Fig. 5c. The tritium content of the water samples varies in a rather narrow range of 17-30 TU (tritium unit), with two exceptions (S-63/a and F-50) where the tritium content is around 42 TU. These two wells are close to each other and may indicate a) a rather old water (the average T content of the precipitation at Nick (Hungary) in 1994 was 11.8 TU, in 1995 was 16.0 TU, and that of the Danube in 1994 was 24.9 TU [10]; higher sulfate and chloride contents support this idea) or b) a very young Danube water component (in August 1995 the mean T content of the Danube was 92 TU [10]).

3.1.3 Water chemistry

Table III and IV show the concentrations of some components, which are important contaminants. The areal distribution can be seen at the Figs. 3b-d and 5a-b. It is very interesting to

Table I Stable oxygen isotope composition of the water samples collected on the area indicated on Fig. 2 (sampling in May-June 1995).

Name of well	$\delta^{18}O$ [‰]$_{SMOW}$	name of well	$\delta^{18}O$ [‰]$_{SMOW}$
Production wells		*Observation wells (continued)*	
T/II.2. cs.	-11.45	F-1	-10.87
K/7. cs.	-11.12	F-2	-10.87
		F-3	-10.53
		F-4	-10.52
		F-5	-9.58
Observation wells		F-6	-10.12
		F-7	-10.91
T/I.100	-11.47	F-8	-10.69
T/II.31	-10.83	F-9	-10.79
T/II.69	-11.93	F-10	-10.76
T/II.5	-11.49	F-11	-10.90
K-16	-11.51	F-54	-10.74
K-64	-10.71	F-68	-10.85

Table II Stable oxygen isotope composition and tritium content of the water samples collected on the middle part of the Szentendre Island (Figs. 4, 5a, 5c, samples were collected in August-September, 1995)

Name of well	$\delta^{18}O$ [‰]$_{SMOW}$	tritium [TU]	name of well	$\delta^{18}O$ [‰]$_{SMOW}$	tritium [TU]
Production well			*Observation wells (continued)*		
S-15	-11.12	23.2	F-21	-10.31	25.5
Observation wells			F-21/b	-10.37	21.4
S-21	-10.06	21.0	F-22	-10.93	20.5
S-54	-11.53	20.0	F-23	-10.31	20.5
S-63/a	-10.47	42.0	F-24	-10.02	18.5
S-80	-10.64		F-25	-10.84	19.5
R-12	-10.50	16.8	F-26	-10.79	17.3
R-16	-10.83	23.4	F-26/a	-10.86	19.5
R-18	-10.51	18.1	F-26/b	-10.83	21.4
F-10	-10.47	20.8	F-26/c	-10.16	21.0
F-11	-10.63	21.2	F-28	-10.26	22.3
F-12	-10.14	21.6	F-29	-10.61	20.8
F-13	-10.06	27.0	F-30	-10.35	25.2
F-14	-10.52	29.0	F-32	-10.42	21.0
F-17	-10.79	29.8	F-33	-10.17	20.8
F-18	-10.28	21.5	F-34	-10.83	21.2
F-19	-10.41	20.2	F-35	-10.99	26.2
F-20	-10.40	22.1	F-36	-10.81	22.7
F-20/a	-10.34	20.2	F-37	-10.84	20.8
F-20/b	-10.27	20.3	F-39	-11.00	27.3
F-20/c	-10.23	20.2	F-50	-10.72	41.5

Table III Some chemical components of the water samples collected on the middle part of the Szentendre Island (Figs 4, 5a-b)

Name of well	NH$_4$ [mg/l]		NO$_3$ [mg/l]		NO$_2$ [mg/l]		Cl [mg/l]		SO$_4$ [mg/l]	
	1	2	1	2	1	2	1	2	1	2
Production well										
S-15	0 02	0 01	7 3	7 1	0 00	0 00	19 9	17 7	40 8	44 7
Observation wells										
S-21	0 00	0 01	13 9	19 1	0 00	0 01	23 5	25 3	50 4	51 7
S-54	0 02	0 40	6 3	5 3	0 02	0 03	16 3	14 1	38 4	32 9
S-63/a	-	0 00	-	29 0	-	0 01	-	36 5	-	124 7
S-80	0 00	0 00	14 2	10 7	0 00	0 01	24 5	25 3	52 8	54 1
R-12	0 00	0 02	1 6	1 4	0 00	0 01	17 3	15 2	48 0	32 9
R-16	0 00	0 02	6 6	6 9	0 00	0 00	20 9	17 2	48 0	37 6
R-18	0 14	0 03	5 3	8 9	0 00	0 00	23 5	25 3	67 2	61 2
F-10	0 01	0 01	10 6	12 4	0 00	0 00	22 4	22 2	96 0	91 7
F-11	0 03	0 00	11 5	12 2	0 00	0 01	17 3	19 2	52 8	58 8
F-12	0 01	0 01	12 8	13 8	0 01	0 00	15 8	17 2	55 2	51 7
F-13	1 45	1 77	0 1	0 1	0 01	0 03	20 9	23 7	124 8	159 9
F-14	0 01	0 00	17 4	15 4	0 00	0 00	31 1	31 8	88 8	82 3
F-17	0 00	0 13	11 3	14 5	0 00	0 00	22 4	22 2	72 0	70 6
F-18	0 01	0 03	7 1	3 7	0 01	0 00	18 4	19 2	48 0	56 4
F-19	0 03	0 01	20 6	22 0	0 00	0 00	22 9	20 7	60 0	58 8
F-20	0 01	0 00	8 9	0 6	0 00	0 00	19 4	22 2	67 2	65 9
F-20/a	1 24	34 10	25 2	23 0	0 00	0 02	53 0	49 9	124 8	110 5
F-20/b	3 70	11 80	22 9	30 0	0 00	0 00	38 8	48 5	96 0	101 1
F-20/c	0 00	0 00	6 6	8 8	0 00	0 01	18 9	20 7	52 8	58 8
F-21	0 00	0 00	16 8	0 6	0 00	0 00	23 5	21 2	108 0	94 1
F-21/b	0 00	0 03	35 2	29 0	0 00	0 00	39 8	37 4	96 0	96 4
F-22	0 01	0 03	10 6	11 8	0 01	0 00	18 9	20 2	55 2	51 7
F-23	0 01	0 00	11 2	17 5	0 00	0 02	26 0	26 3	48 0	61 2
F-24	0 00	0 06	74 1	78 0	0 00	0 01	49 9	48 5	120 0	112 9
F-25	0 00	0 00	76 8	87 0	0 01	0 01	44 9	55 6	96 0	110 5
F-26	0 00	0 05	23 7	25 0	0 00	0 00	33 7	30 8	96 0	91 7
F-26/a	0 01	0 05	70 5	86 0	0 01	0 01	60 2	58 6	129 0	129 4
F-26/b	0 00	0 05	66 4	67 0	0 00	0 01	56 1	51 0	139 0	134 1
F-26/c	0 00	0 05	13 7	15 5	0 00	0 00	18 9	23 2	31 1	47 0
F-28	0 01	0 01	11 7	15 5	0 00	0 00	17 9	20 7	48 0	47 0
F-29	0 00	0 01	17 2	10 7	0 01	0 00	21 9	21 2	48 0	54 1
F-30	0 00	0 01	27 1	32 0	0 02	0 02	20 9	20 7	79 2	75 3
F-32	0 02	0 01	22 2	37 0	0 00	0 00	25 5	29 8	72 0	70 6
F-33	0 01	0 01	34 4	33 0	0 00	0 00	20 9	24 2	67 2	61 1
F-34	0 01	0 01	10 7	9 2	0 00	0 01	20 4	22 2	48 0	47 0
F-35	0 02	0 03	2 8	5 1	0 00	0 00	18 4	19 2	76 8	77 6
F-36	0 02	0 03	1 2	3 2	0 00	0 00	22 9	22 2	79 2	75 3
F-37	2 61	0 01	0 5	2 0	0 04	0 01	18 4	18 7	40 8	37 6
F-39	0 01	0 00	11 3	11 2	0 09	0 01	21 1	29 3	57 6	70 6
F-50	0 00	0 00	19 1	25 0	0 00	0 01	25 5	25 3	96 0	105 8

1 first sampling May-June, 1995
2 second sampling August-September, 1995

compare the $\delta^{18}O$ values with the chloride, nitrate and sulfate content of the water samples collected on the Szentendre Island (Fig. 8). A slight trend can be observed. The more positive the $\delta^{18}O$ value the higher is the Cl, NO_3 and SO_4 content. The more positive $\delta^{18}O$ value means higher component from the infiltrating precipitation, and lower component from the River Danube. The relation between the $\delta^{18}O$ value and the chemical components is more striking along the A and B profiles on the northern part of the Szentendre Island (Fig. 3b-d, and Fig. 9). This trend is a clear indication that the source of the Cl, NO_3 and SO_4 pollutants is on the island and not the   Danube water.

3.2   Dunakeszi Water Works

This water works was established on the left bank of the River Danube and the area differs from the others, because it situates not on a river island. The $\delta^{18}O$ values of all the filter wells are the to or more positive than the average $\delta^{18}O$ value of the Danube (Table V, Fig. 6-7) indicating that the infiltrated precipitation component is considerable.

The $\delta^{18}O$ values of the observation wells range between -9.1 and -11.1‰ (Table V, Fig. 6-7). The most negative ones are the closest spatially to the Danube. About 500-800 meters off the river, the Danube does not affect the stable oxygen isotope composition of the shallowest groundwater.

Table IV Some chemical components of the water samples collected in the northern part of the Szentendre Island (Fig. 2, 3b-d)

Name of	NH$_4$		NO$_3$		NO$_2$		Cl		SO$_4$	
well	[mg/l]		[mg/l]		[mg/l]		[mg/l]		[mg/l]	
	1	2	1	2	1	2	1	2	1	2
Northern part of the Szentendre Island										
Operating wells										
T/II.2.cs	0.00	0.01	5.5	6.6	0.00	0.00	14.7	15.1	36.0	35.3
K.7.cs.	0.00	0.01	4.9	5.0	0.00	0.00	16.3	14.1	40.8	32.9
Observation wells										
T/I.100	0.00	0.01	1.6	2.8	0.00	0.00	15.8	14.7	33.6	42.3
T/II.31	0.01	0.03	9.9	13.9	0.00	0.01	20.9	20.7	43.2	44.7
T/II.69	0.00	0.01	5.2	6.2	0.00	0.00	13.8	10.7	33.6	37.6
T/II.5	0.00	0.01	4.3	6.7	0.00	0.00	15.3	12.6	33.6	38.0
K-16	0.03	0.01	2.7	4.3	0.02	0.01	18.4	15.2	33.6	35.3
K-64	0.02	0.14	11.6	16.5	0.02	0.02	19.4	23.2	62.4	70.6
F-1	0.31	0.27	0.5	0.3	0.00	0.00	24.5	27.8	110.4	117.6
F-2	0.00	0.00	12.3	12.9	0.00	0.00	20.9	19.7	57.6	56.4
F-3	0.00	0.01	40.0	41.0	0.00	0.19	25.5	29.8	91.2	72.9
F-4	0.01	0.03	23.8	19.3	0.00	0.01	23.5	26.3	57.6	49.5
F-5	0.01	0.03	24.7	25.0	0.00	0.01	26.0	25.8	55.2	70.5
F-6	0.00	0.03	19.6	23.0	0.00	0.01	21.9	21.7	62.4	75.3
F-7	0.00	0.00	13.5	20.0	0.00	0.00	21.4	20.9	48.0	54.1
F-8	0.00	0.00	37.2	36.0	0.00	0.03	34.7	19.1	93.6	91.6
F-9	0.02	0.08	32.2	29.0	0.01	0.03	27.5	28.3	76.8	61.1
F-54	0.00	0.02	16.8	21.0	0.00	0.00	21.4	23.2	45.6	47.0

1: first sampling May-June, 1995
2: second sampling August-September, 1995

Table V Stable oxygen isotope composition of the water samples collected on the area of the Dunakeszi Water Works (Fig. 6) and of Danube water.

Name of well	$\delta^{18}O$ [‰]$_{SMOW}$	name of well	$\delta^{18}O$ [‰]$_{SMOW}$
Production wells		*Observation wells (cont'd)*	
II/2	-11.12	FK-10	-10.43
II/8	-10.75	FK-35	-9.41
II/15	-10.96	FK-36	(-7.39)
II/23	-10.89	FK-37	-11.06
Danube	-11.52	FK-38	-9.63
(28.06.95)		FK-39	-9.75
Observation wells		FK-41	-9.65
FK-1	(-7.98)	FK-43	-9.74
FK-3	-9.68	FK-44	-9.05
FK-6	-9.81	FK-45	-9.24
FK-7	-9.85		

3.3 Origin of groundwater and its relation to pollutants on the Csepel Island

3.3.1 Stable oxygen isotope and chemical data

The stable oxygen isotope composition and the concentration of some chemical components of water samples studied are in the Table VI.

The stable oxygen isotope data are plotted on Fig. 11. The $\delta^{18}O$ values of the water of the production wells are around -11.0‰ (Table VI, Fig. 11), which is identical with that of the average $\delta^{18}O$ value of the Danube. So we can draw a conclusion that the water supplied by the production wells are 100% or very close to 100% of Danube water. The $\delta^{18}O$ values of the observation wells varies in a rather wide range from -7.89‰ to -11.85‰ (Table VI, Fig. 11).

Usually in the inner part of the island the $\delta^{18}O$ value is identical or very close to that of the infiltrated multiannual precipitation (-9.3‰) (see Tököl, north and west of Szigetszentmiklós and southwest of Szigetújfalu on Fig. 11).

There are two observation wells on the left bank side of the Ráckeve Danube (the smaller branch), these are F40 and F42 (Fig. 10). The corresponding $\delta^{18}O$ values are -9.31‰ and -8.90‰ (Fig. 11), which are identical with the $\delta^{18}O$ value of the infiltrating precipitation. At the same time the $\delta^{18}O$ values of the observation wells on the right bank side (F36, F39, F10, F54, F58, Fig. 10 and 11) are more negative (from -10.43‰ down to -10.87‰) showing the effect of the Ráckeve Danube. Although we do not have $\delta^{18}O$ data for the Ráckeve Danube, we can suppose that it is the same as that of the Danube (or a little bit more positive). Keeping in mind that the water level in the Ráckeve Danube is higher by about 1-3 meters than the water level in the Danube, it is reasonable to suppose that the shallowest groundwater flows from east-northeast to west-southwest. This supposition is supported by the $\delta^{18}O$ values as well. The groundwater on the left bank side is not affected, while that on the right bank side of the Ráckeve Danube is affected by the river water. The water of the Ráckeve Danube infiltrates into the gravel material, then mixes with the infiltrated precipitation and flows to the direction of southwest-west. Also we can suppose that the shallowest groundwater on the left bank side of the Ráckeve Danube flows under the river and mixes with the infiltrating

Table VI   Stable oxygen isotope and chemical composition of
water samples collected on the Csepel Island (Fig 10)

Production wells

Name	Date	$\delta^{18}O$	NH_4	NO_3	Cl
H 5	12 09 96	-11 00	0	5	23
H 14 cs	13 09 96	-11 01	0	8	20
H 15 cs	13 09 96	-10 93	0	10	24
H 19 cs	13 09 96	-11 01	0	8	22
R 12	30 08 96	-11 14	0	3	23

Observation wells

F 7	06 09 96	-10 35	0	24	64
F 10	27 08 96	-10 32	0	24	90
F 21	16 09 96	-9 43	0	640	283
F 23	12 09 96	-11 85	0	1	176
F 27	16 09 96	-9 03	0	135	139
F 28	13 09 96	-9 61	0	22	211
F 32	10 09 96	-9 10	1	180	314
F 35	09 09 96	-7 89	0	210	121
F 36	09 09 96	-10 87	1	2	21
F 39	27 08 96	-10 60	2	105	87
F 40	27 08 96	-9 31	0	310	73
F 42	27 08 96	-8 90	0	210	137
F 44	06 09 96	-10 26	0	8	49
F 45	05 09 96	-9 22	0	18	40
F 46	30 08 96	-9 39	0	18	33
F 54	06 09 96	-10 72	10	1	32
F 55	30 08 96	-9 85	0	4	38
F 56	30 08 96	-10 76	0	39	53
F 57	06 09 96	-10 81	0	28	43
F 58	06 09 96	-10 59	7	1	34
F 62	04 09 96	-9 37	0	32	36
F 65	03 09 96	-8 48	0	60	60
F 69	03 09 96	-9 34	0	115	36
F 76	29 08 96	-9 49	0	1	28
F 77	05 09 96	-9 96	1	2	147
F 77A	05 09 96	-9 80	1	1	103
F 78	05 09 96	-10 74	1	350	179
H 56	11 09 96	-10 86	0	1	32
H 60	13 09 96	-10 91	0	1	19
H 109	11 09 96	-10 44	0	2	38
SZ 6	09 09 96	-10 27	0	220	111
R 12 18	30 08 96	-11 15	0	1	22

$\delta^{18}O$
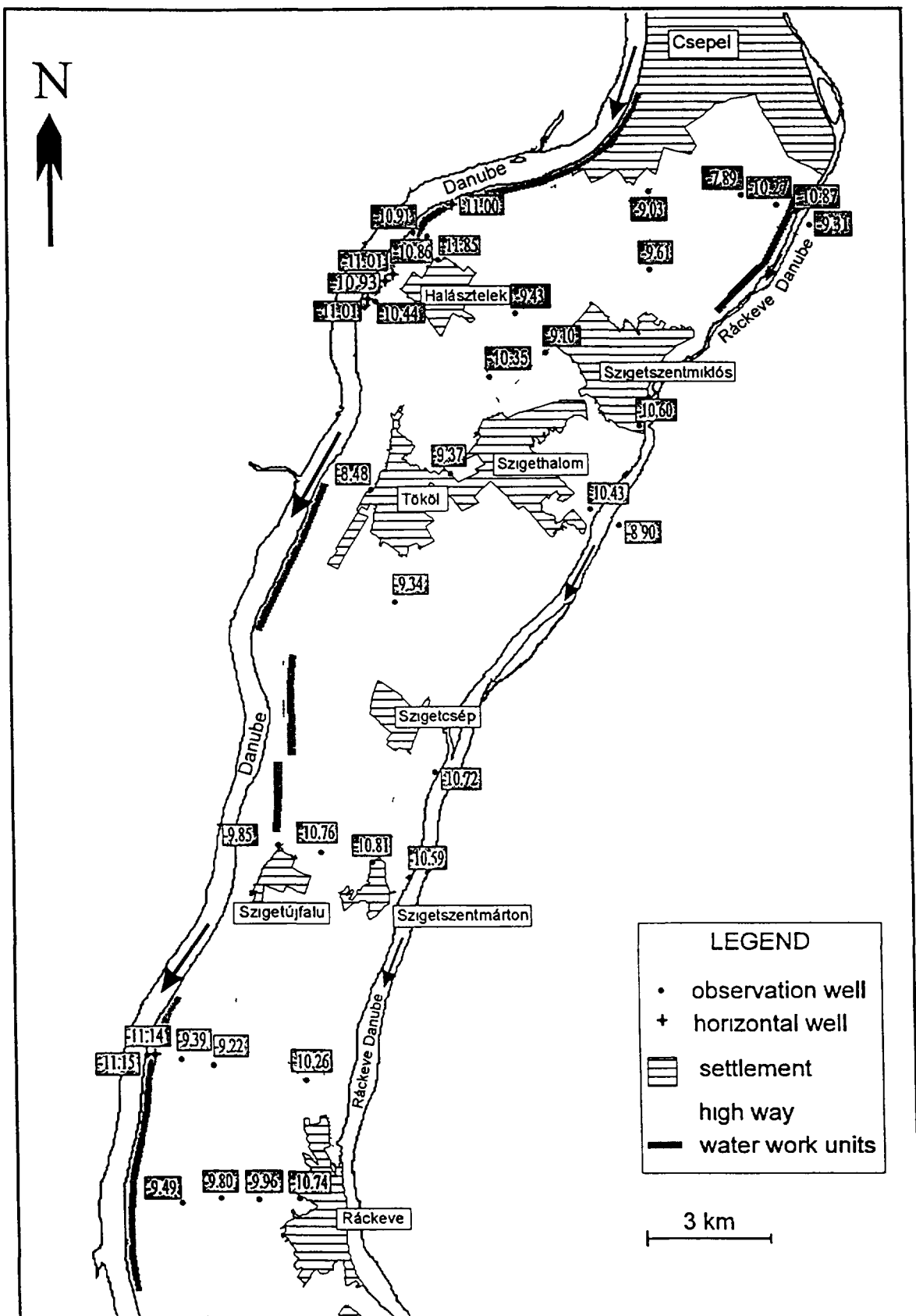

Fig. 11 The stable oxygen isotope composition of the wells sampled on the
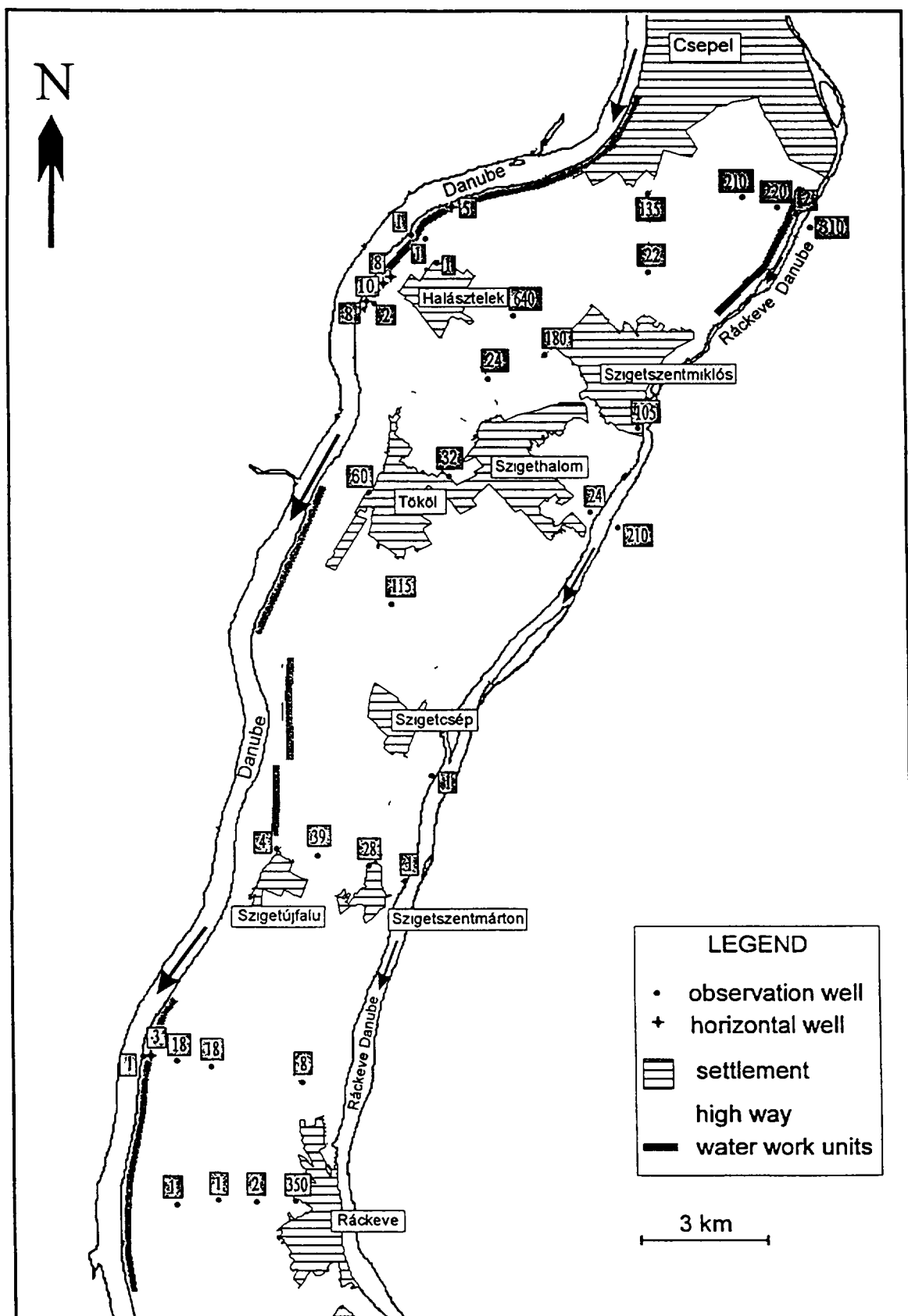Csepel Island.

156

NO_3

Fig. 12 The nitrate content of the wells sampled on the Csepel Island
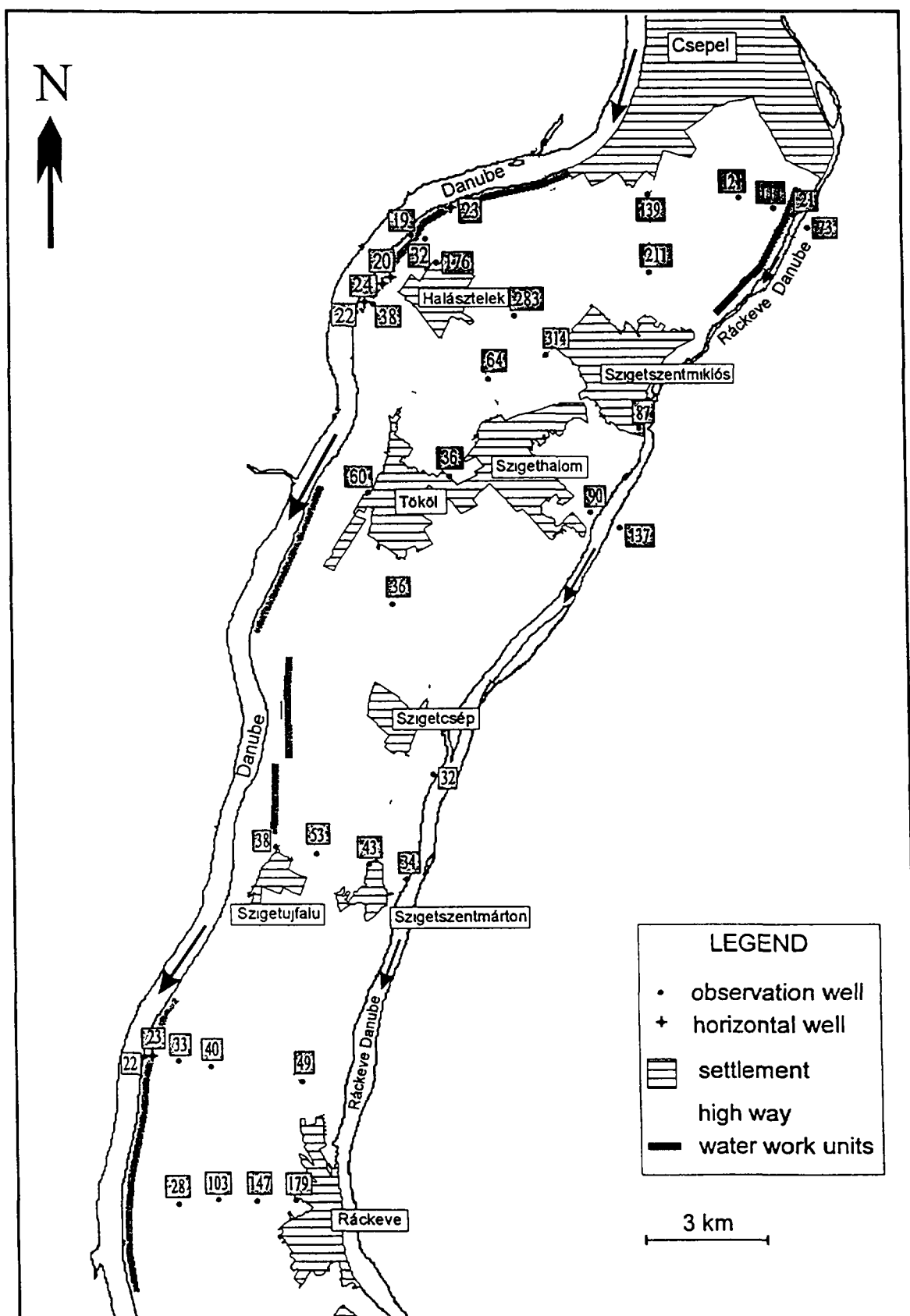
Cl

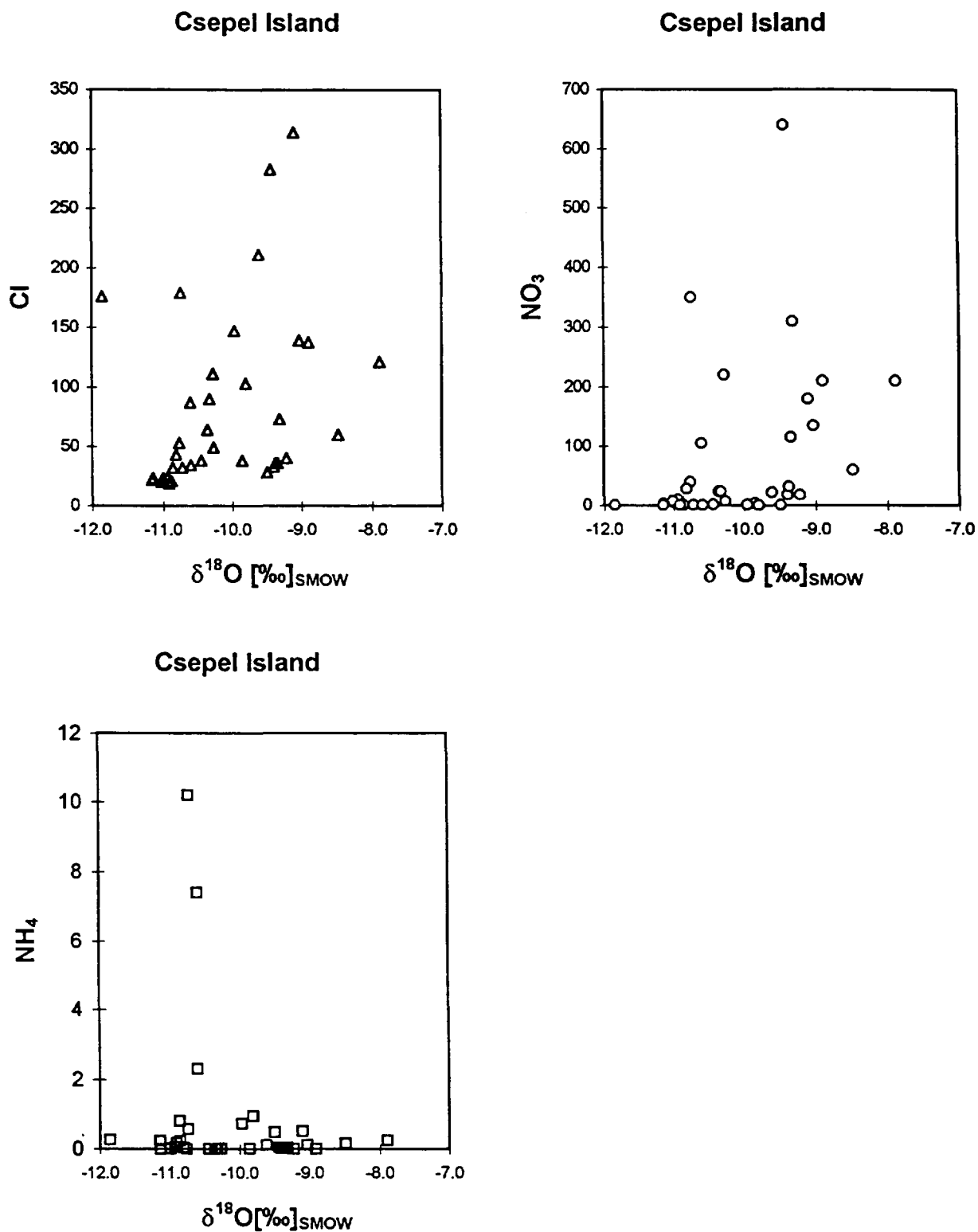Fig. 13 The chloride content of the wells sampled on the Csepel Island

Fig. 14 Chloride, nitrate and ammonium content vs. stable oxygen isotope composition of water samples collected on the Csepel Island.

Ráckeve Danube water. The water table levels [3] support these suppositions, because the water level on the left bank side of the Ráckeve Danube nearby and between the two studied observation wells (F40, F42; Fig. 10) is higher than on the right bank side. This flowing system discharges into the Danube.

The Danube (big branch) has only a little effect on the shallowest groundwater of the Csepel Island, especially where there are chains of production wells (Fig. 11). The production wells exploit a lot of water and this way serve as a barrier and only a little amount of Danube water gets behind the production wells. This can happen in two cases: 1. highest Danube water level or 2. when a group of production wells are out of work because of maintenance. So the $\delta^{18}O$ value of the observation wells "behind" the production wells are rather close to that of the infiltrating precipitation or between the average Danube water and the infiltrated precipitation (F46= -9.39; H109= -10.44; H56= -10.86‰).

3.3.2. Pollutants: nitrate, chloride and ammonium

The distributions of the above pollutants are rather irregular (see Fig. 12 and 13). The main source of nitrate in many cases is the communal sewage water, see e.g. Ráckeve, Tököl, Szigetszentmiklós and Csepel settlements. The agricultural activity is also a source of nitrate. The main source of chloride pollution is the salt used in winter time for de-icing the asphalt roads.

Comparing the data of these pollutants with $\delta^{18}O$ values (Fig. 14) we can observe a slight correlation. We can find higher nitrate and chloride concentrations when the $\delta^{18}O$ value is greater than -11.0‰ (with one exception, F23), it means when the water has component of infiltrated precipitation.

Between the ammonium content and $\delta^{18}O$ value there is no correlation (Fig. 14). Usually higher concentration of ammonium can be found where the chemical condition is rather reducing.

4. COMPARING THE HYDRAULIC AND ISOTOPIC MODELS ON THE SZENTENDRE ISLAND

4.1. Transit time calculated by hydraulic modeling and stable oxygen isotope data

The two dimensional hydraulic modeling of the flowing system in the shallowest aquifer of the Szentendre Island has been made by Gy. Molnár at the Technical University of Budapest, Hungary [3]. For the hydraulic modeling the following data were used: Danube water level, water level in the observation wells, bottom and upper surface morphology of the aquifer, hydraulic conductivity, exploitation rate, rate of precipitation and infiltration. These data were collected during the years of 1992, 1993 and 1995. Using the software of this hydraulic modeling the ratio of Danube water/infiltrated precipitation and the transit time of Danube water from the river to the wells have been calculated for some wells (see Table VIII and IX).

In the case of some production and observation wells, where the Danube water ratio was close to 100% (according to the hydraulic modeling), the transit time of Danube water was calculated (Table VIII) using stable oxygen isotope data measured in the wells and the $\delta^{18}O$ values of the Danube water at Bratislava, Slovakia (Fig. 15). The calculation was made

in a very simple way: taking the $\delta^{18}O$ value of the well, the same value was looked for back-way on the $\delta^{18}O$ curve of the Danube (Fig. 15) considering the 2-3 days needed for the Danube water to get from Bratislava to the Szentendre Island. Dispersion has not been taken into account. These transit times are in the range from half to 3 months (Table VIII). The uncertainty is ± 5 days.

Comparing the transit times calculated by stable oxygen isotope data to the transit times determined by hydraulic modeling (Table VIII) we can conclude that in 4 out of 7 cases (T.II.5; T.II.69; T.II.2. cs.; S-15.cs.) the latter ones are two-three times longer, in 2 out of 7 cases (T.I.100; K.7.cs.) the former ones are longer, and 1 out of 7 cases the two data are almost the same (S.54). Explanations for this discrepancy can be 1) imperfect input parameters used for hydraulic modeling 2) isotopic data were determined only once for the wells, while the hydraulic modeling was based on data collected during three years 3) the water level of the Danube at the time of sampling was unusually high (Table VII). This high water level could resulted in a faster water flow, and so shorter transit time.

Table VII Danube water levels at three points along the Szentendre Island

	Nagymaros	Vác	Budapest
Mean water level in June 1995 (cm)	357	399	508
Mean water level of June averages from 1986-1995 (cm)	206	224	339
Mean water level of year averages from 1986-1995 (cm)	136	148	259

For a more characteristic and more reliable isotopic modeling a time series data collecting would be necessary.

Table VIII. The stable oxygen isotope composition, tritium data and calculated Danube water ratio and transit time for some wells on the Szentendre Island

Well number	Isotopic comp.		Ratio of Danube water [%]		Transit time from the Danube		Tritium	Date of sampling
	$\delta^{18}O$ [‰]$_{SMOW}$		Hydraulic model	Isotopic model	Hydraulic model	Isotopic model	[TU]	
T.II.5	-11.49		91	~~138~~	84 days	~ 40 days		08.06.95
T.II.69	-11.93		100	~~169~~	37 days	~ 15 days		07.06.95
T.II.2. cs.	-11.45		98	~~135~~	130 days	~ 40 days		12.06.95
T.I.100	-11.47		99	~~137~~	25 days	~ 40 days		06.06.95
K.7. cs.	-11.12		96	~~113~~	29 days	≥ 60 days		12.06.95
S-15.cs.	-11.12			~~113~~	34 days	~ 15 days	23.2	31.08.95
S-54	-11.53		99	~~141~~	23 days	~ 20 days	20.0	31.08.95
K-64	-10.71		61	84	16 years			
S-63/a	-10.47		12	67	64 years		42.0	
S-80	-10.64		100	79	31 years			
F-25	-10.84			93	38 years		19.5	

161

Danube at Bratislava
(data from Michalko, Bratislava)
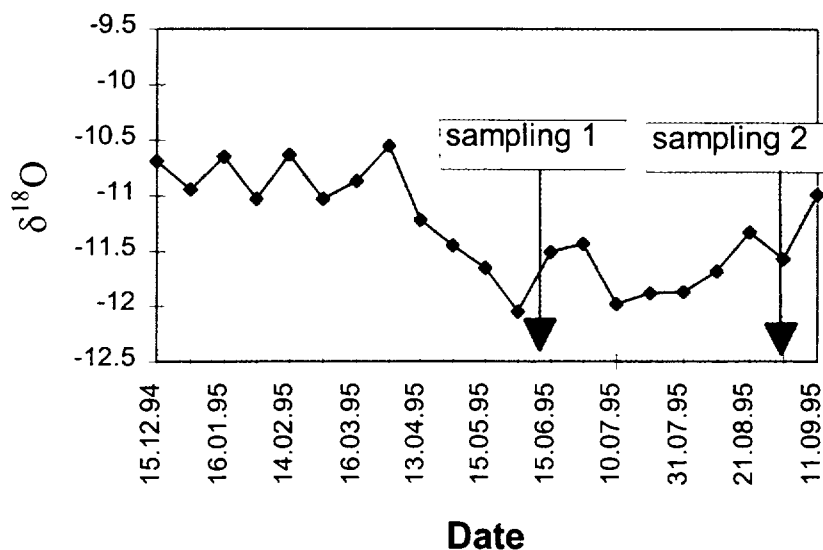
Fig. 15 Stable oxygen isotope composition of the River Danube at Bratislava, Slovakia in the year 1995. Data from [5].

Table IX Stable oxygen isotope composition and the calculated ratio of Danube water components in % for the wells in the inner part of the Szentendre Island.

Well number	Isotopic composition	Ratio of Danube water %	
	$\delta^{18}O$ [‰]$_{SMOW}$	hydraulic model	isotopic model
F-1	-10.87	99	91
F-2	-10.87	84	91
F-5	-9.58	31	5
F-6	-10.12	27	41
F-9	-10.79	8	86
F-10 Jun.6.	-10.76	88	84
F-11 Jun.6.	-10.90	62	93
R-16	-10.83	91	89
S-63/a	-10.47	12	67
F-10 Sept.7.	-10.47	88	65
F-11 Sept.12.	-10.63	62	75
F-12	-10.14	35	43
F-20	-10.40	87	60
F-20/a	-10.34	90	56
F-20/b	-10.27	88	51
F-21	-10.31	86	54
F-21/b	-10.37	62	58
F-24	-10.02	76	35
F-25	-10.84	39	89
F-26	-10.79	46	86
F-26/a	-10.86	42	91
F-29	-10.61	51	74
F-36	-10.81	74	87
F-37	-10.84	89	89

162

4.2. Ratio of Danube water calculated by hydraulic modeling and stable oxygen isotope data

In the inner part of the Szentendre Island, where the transit time of the Danube water calculated by the hydraulic model fell into the range of decades (e.g. K-64; S-63/a; S-80; F-25 in Table VIII) the ratio of Danube water/infiltrated precipitation have been calculated by both models (Table IX). Data are plotted on Fig. 16. Hence the transit times in these cases are more than ten years, the supposition has been made that the water in these observation wells are well mixed and their $\delta^{18}O$ values are an average values characteristic for the ratio of mixing. Comparing the ratios calculated by the two different models we can see (Fig. 16) that the two calculated ratios are rarely the same. There is a high discrepancy in many cases.

Two wells (F-10 and F-11) were sampled two times (in June and September 1995). The $\delta^{18}O$ values of the first sampling was -10.76‰ and -10.90‰, while of the second sampling they were -10.47‰ and -10.63‰ respectively (Table IX). The differences are significant. As a consequence the calculated Danube water ratios differ considerably as well. So our supposition regarding the well mixed water in the inner part of the Szentendre Island was false. The ratio of Danube water/infiltrated precipitation changes frequently even in those observation wells where the transit time is some decades.
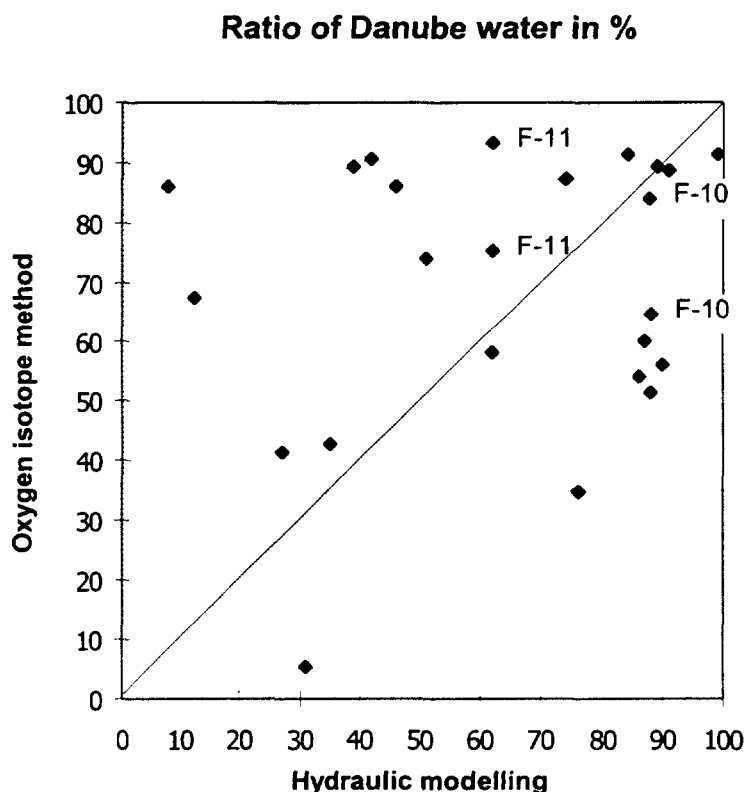
Ratio of Danube water in %

Fig. 16 Ratio of Danube water in % calculated by hydraulic and isotopic methods are plotted.

5. SUMMARY

On the Szentendre Island the groundwater in the observation wells contains a considerable amount of Danube water. The Danube "flows" under the island.

In the case of the Dunakeszi Water Works, left bank of the River Danube and not island area, the Danube component of the supplied drinking water is less than 100%. The shallow groundwater behind the production wells is affected by the Danube in a lane of 500-800 m off-shore. The Danube water component decreases gradually.

Comparing the $\delta^{18}O$ values with the Cl, NO_3 and SO_4 content of the water samples collected on the Szentendre Island, we can see a trend: the more positive the $\delta^{18}O$ value the higher is the Cl, NO_3 and SO_4 content. This is a strong indication that the source of the Cl, NO_3 and SO_4 pollutants is on the island and not the Danube water.

Csepel Island area: from the stable oxygen isotope data we can conclude that the Ráckeve Danube affected the right bank side groundwater only, but not the left bank side groundwater. This fact indicates that the groundwater in the shallowest aquifer flows from east-northeast to south-southwest. Most probably the Danube discharges this flowing system.

Comparing the nitrate and chloride contents with the $\delta^{18}O$ values, we can conclude that the water has higher amount of these pollutants where it has an infiltrated precipitation component.

The transit time of Danube water calculated by hydraulic modeling is longer in average than those calculated by the stable oxygen isotope data. For more reliable calculation based on isotopic data a time series sampling of both the Danube and the wells would be necessary (if possible along a flow path).

The ratio of Danube water/infiltrated precipitation calculated by hydraulic modeling based on data collected during three years (average ratio) rarely matches this ratio calculated by stable oxygen isotope composition measured ones in the wells. The reason is that the ratio of these two kinds of water changes frequently even in those wells where the transit time of the Danube water is some decades.

ACKNOWLEDGEMENTS

REFERENCES

[1] ÖLLŐS, G., WISNOVSZKY, I., BAKONYI, P., BUZINKAY, P., LIEBE, P., RADVÁNYI, R., RÁTH, I., SALI, E., SZOLNOKI, CS., Integrated Water Resources Management in Urban and Surrounding Areas (Case study). Budapest Technical University, "Római Kiadói és Nyomdaipari" Publishing Co., Budapest (1993).

[2]   Fõvárosi Vízmûvek Részvénytársaság (Water Works of Capital Corp., a brochure in Hungarian, 1996).

[3]   MOLNAR, GY., Determining the hydrologic protection area of the water works on the Szentendre Island by means of hydraulic modelling. Report. Archive of the Fõvárosi Vízmûvek Rt. (Water Works of Capital Corp.), Budapest (in Hungarian, 1996).

[4]   RANK, D., Bundesforschung- und Prüfzentrum Arsenal, Vienna, personal communication.

[5]   MICHALKO, J., Data from the Archive of the Geological Survey of the Slovak Republic, Bratislava (1996), personal communication.

[6]   DEÁK, J. Water Resources Research Centre, Budapest, personal communication.

[7]   EPSTEIN, S., MAYEDA, T., Variation of ^{18}O content of waters from natural sources. Geochimica Cosmochimica Acta 4 (1953) 89-103.

[8]   DEÁK, J., DESEÕ, É., BÖHLKE, J.K., RÉVÉSZ, K., "Isotope hydrology studies in the Szigetköz region, Northwest Hungary", Isotopes in Water Resources Management (Symp. Proc. Vienna, 1995), Vol. 1, IAEA Vienna (1996) 419-432.

[9]   FÓRIZS, I., Origin of groundwaters and determination of recent shallow groundwater component by stable isotope measurements. Ph.D. thesis, Kossuth University, Debrecen (in Hungarian with English abstract, 1995).

[10] SÜVEGES, M., Water Resources Research Centre, Budapest, personal communication.

APPLICATION OF ISOTOPE TECHNIQUES TO INVESTIGATE GROUNDWATER POLLUTION IN INDIA

K. SHIVANNA, S.V. NAVADA, K.M. KULKARNI, U.K. SINHA, S. SHARMA
Isotope Division, Bhabha Atomic Research Centre,
Mumbai, India

Abstract -*Environmental isotopes (^2H, ^{18}O, ^{34}S, ^3H, and ^{14}C) techniques have been used along with hydrogeology and hydrochemistry to investigate:(a). the source of salinity and origin of sulphate in groundwaters of coastal Orissa, Orissa State, India and (b) to study the source of salinity in deep saline groundwaters of charnockite terrain at Kokkilimedu, South of Chennai, India. In the first case, as a part of a large drinking water supply project, thousands of hand pumps were installed from 1985. Many of them became quickly unacceptable for potable supply due to salinity, increased iron and sulphate contents of the groundwater. In this alluvial, multiaquifer system, fresh, brackish and saline groundwaters occur in a rather complicated fashion. The conditions change from phreatic to confined flowing type with increasing depth. The results of the isotope geochemical investigation indicate that the shallow groundwater(depth;<50m) is fresh and modern. Groundwater salinity in intermediate aquifer (50 - 100m) is due to the Flandrian transgression during Holocene period. Fresh and modern deep groundwater forms a well developed aquifer which receives recharge through weathered basement rock. The saline groundwater found below the fresh deep aquifer have marine water entrapped during late Pleistocene. The source of high sulphate in the groundwater is of marine origin.*

In the second case, under the host rock characterization programme, the charnockite rock formation at Kokkilimedu, Kalpakkam was evaluated to assess its suitability as host medium for location of a geological repository for high level radioactive waste. Four deep boreholes were drilled in this area, the depth varying from 200 to 618 m. In these boreholes, large variations in groundwater salinity were observed over a distance of only a few hundred meters and no regional pattern could be identified. The results of the isotope investiation show that there are two different sources of salinity in this area. Among the four, in borehole BH-1, the salinity could be attributed to infiltrated sea water together with the contribution of solute from the pseudotachylites observed along the fractures and shear zones in the host rock. In the other three bore holes (BH-2, BH-3 & BH-4), the solutes which are responsible for salinity of these waters are mostly from sheared and fractured charnockite rock Further, tritium results show that these well are getting local recharge.

1. THE SOURCE OF SALINITY AND ORIGIN OF SULPHATE IN COASTAL AQUIFERS OF ORISSA

1.1 Background

As part of a large drinking water project, thousands of hand pumps were installed from 1985 onwards in the coastal areas of Orissa State. Many of them became quickly unacceptable for potable supply due to the salinity of the groundwater (Chloride content: 6 - 7400 mg/L) as well as increased iron (Fe^+ :0.0 - 19 mg/L) and sulphate content (SO_4^{-2}: 2.0 - 1400 mg/L).

Generally groundwater salinity originates from one or more of the following mechanisms: (a) intrusion of old or modern marine water, (b) mixing of meteoric water with connate water or fluid inclusions, (c) concentration of dissolved salts by evaporation near the

soil surface during slow diffuse recharge, (d) dissolution of aquifer material and (e) anthropogenic sources. Each of these mechanisms will have a distinct effect on some of the geochemical and isotopic relationships of the groundwater. If the mixing of meteoric water with recent or connate marine water is the primary cause of salinity, then variations in the salinity of the aquifer are expected as a result of variations in the degree of mixing. The $\delta^{18}O$ against either deuterium or chloride values of groundwater should then be positively correlated and plot on the mixing line between the compositions of sea water and fresh water [6]. If salinity is primarily due to the concentration of dissolved salts by evaporation, then the $\delta^{18}O$ - δ^2H relationship will have a low slope reflecting kinetic fractionation. In addition, a plot of chloride against either isotope will be positively correlated, as increased evaporation would result in isotopic enrichment as well as increased chloride concentration. If salinity is due to the leaching of evaporitic salts by rapid percolation through preferential pathways, then the groundwater should retain a δ^2H - $\delta^{18}O$ relationship similar to that of regional rainfall. As the leaching processes do not affect the isotopic composition of water, there would be no correlation between chloride and isotopic composition. Apart from ^2H and ^{18}O, the ratios of stable isotopes of sulphur ($^{34}S/^{32}S$) suggest the source of dissolved sulphur species and provide information about the reactions and geochemical processes affecting them. Hence, the Delang - Puri Sector in coastal Orissa was chosen for isotope hydrological investigation to identify the source of salinity, origin of sulphate and hydrodynamic conditions of saline groundwaters.
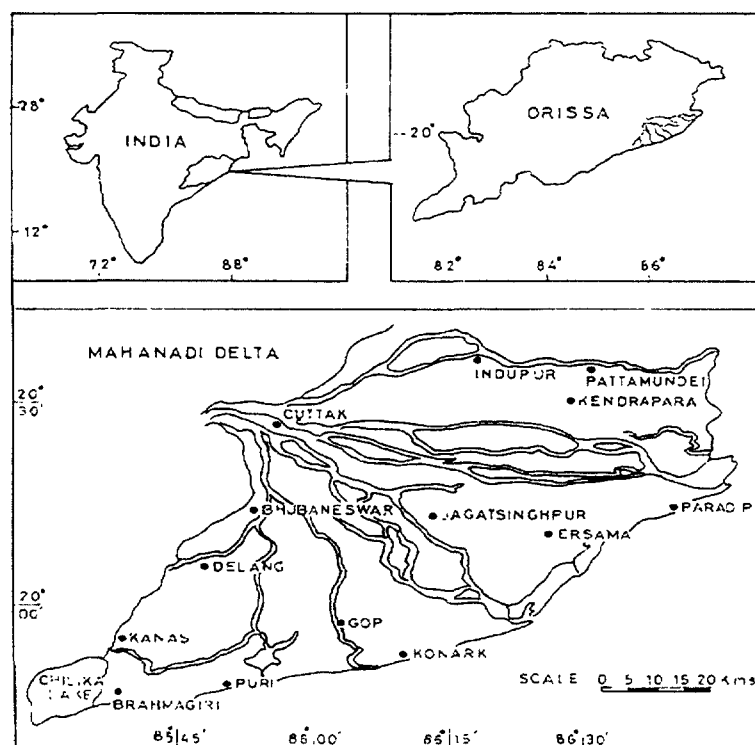
FIG. 1: Location map of Mahanadi delta

1.2 Hydrogeology of the area

The Delang - Puri sector in coastal Orissa forms the southwestern part of the Mahanadi delta which is an arcuate type of delta with an aerial extent of about 9000 km^2. It lies between 19° 40'N to 20° 35' N and 85° 40' E to 86° 45'E. The annual average rain fall in this area is about 1800 mm. The delta was formed during the last few thousands of years by continuous supply of sediment load from a huge catchment which has been deposited into a subsiding

168

faulted basin, partly fluvial and partly marine, under varying energy conditions (Fig.1). On the landward side, to the West and Northwest of Delang, the area is an undulating upland with isolated hills and lateritic peneplains. The hills are mostly the resistant remnants of charnockite , kondalite and granitic gneisses, belonging to the Archean complex. The deltaic land is represented by vast plains of fluvial, lacustrine and marine origin intersected by less prominent rivers.

The Delta is covered by thick alluvium underlain by Archean rocks. The thickness of the alluvium varies from 20 m at Jagadalpur to more than 600 m at Puri (Fig.2). the dark grey sediment horizons were deposited in a near shore shallow marine basin. The unfossiliferous yellow brown sediment horizon is sandwiched between two dark grey sediment horizons indicating a change in environmental conditions during evolution of the delta.
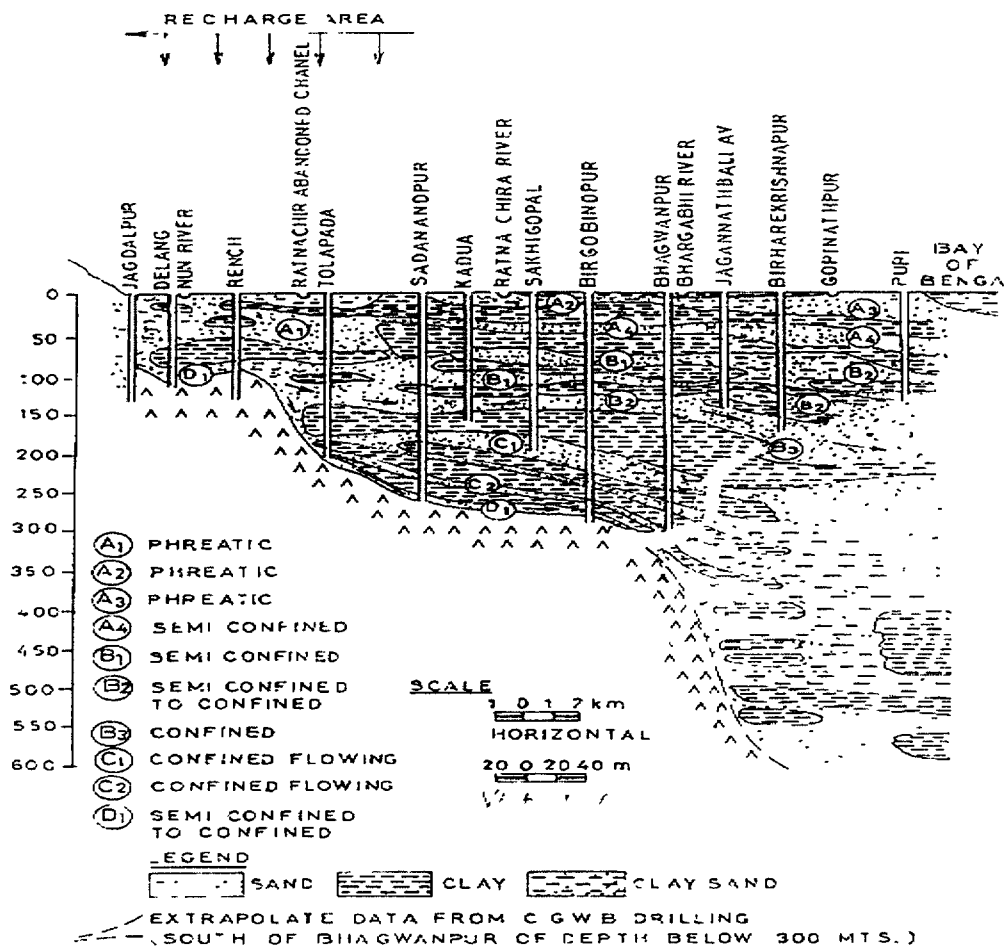
FIG. 2: Hydrogeological section along Delang - Puri sector

A number of piezometers which were drilled by the Danish International Development Agency (DANIDA) for hydrogeological investigation revealed the presence of a multiaquifer system down to a depth of about 300 m. These aquifers have been divided as shallow (Depth: <50 m), intermediate (Depth: 50 -100 m) and deep (Depth >100 m) aquifers. Fresh, brackish and saline groundwaters occur in a rather complicated fashion. Both lateral and depth wise variation in salinity is noticed. The shallow aquifer occurs under phreatic conditions and deeper aquifers change from leaky confined to artesian flowing type with increasing depth. The large number of exploration boreholes carried out by DANIDA [1] suggest that the depth to the water table (fresh water) varies from 2 to 17 m below ground level. The thickness of this phreatic aquifer ranges from 5 to 40 m. The deep fresh water aquifer is found extensively

169

along the Delang - Puri sector, and occurs at water aquifer is found extensively along the Delang - Puri sector, and occurs at depths between 102 m and 165 m. The total thickness of this aquifer ranges from 25 to 80 m and generally the thickness increases towards the South. The fresh water aquifer is sandwiched between saline water aquifers. The general trend of groundwater flow is towards the southeast and the gradient is steeper towards the inland side (Delang area 2.2 m/km) compared with the coastal area (0.6 m/km near Puri). The steeper gradient, deeper water levels and diverging flow lines in the Delang area close to Kumundal hills indicate the recharge area. The converging flow lines and shallow water table in the southern part indicate the discharge area (Fig.3). The peizometric surface contour map (Fig. 4) shows the movement of groundwater to the south. A groundwater mound is observed in the Eastern part sloping towards the south. The groundwater mound may possibly be due to upward leakage from the artesian aquifer. The hydraulic gradient of the peizometric surface varies from 0.2 to 0.3 m/km.
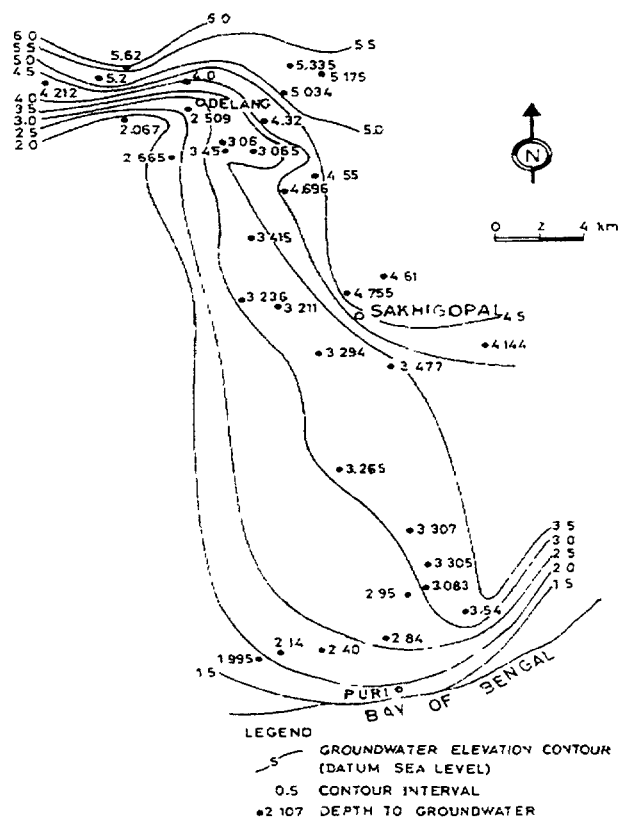
FIG. 3: Water table contour map
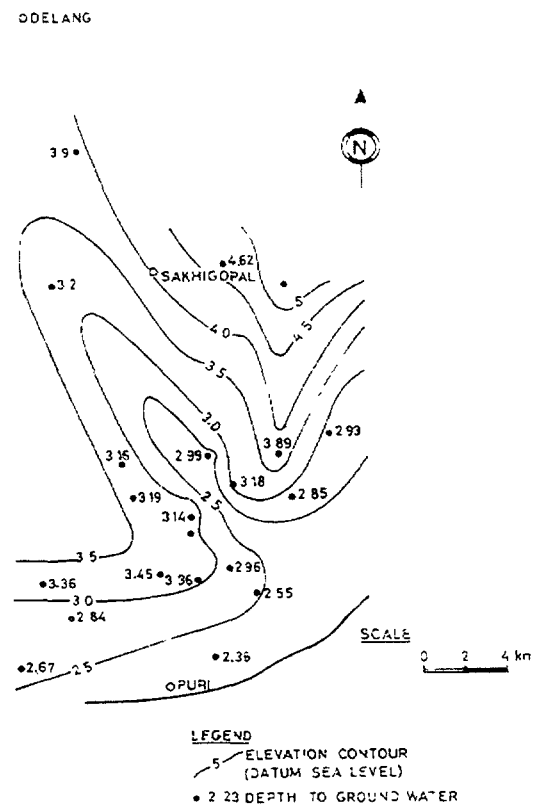
FIG. 4: Peizometric contour map

1.3   Hydrochemistry

In the Delang - Puri Sector, groundwater quality varies from fresh water to saline with electrical conductance (EC) ranging from 250 µS/cm to 29700 µS/cm. In the Delang area, mostly shallow groundwaters are fresh, with average EC of 1200µS/cm and average chloride content of 150 mg/L. Fresh waters are of Ca-Mg-HCO₃ type. The hydrochemical facies in this area in general changes from $HCO_3 \rightarrow HCO_3+Cl \rightarrow Cl +HCO_3 \rightarrow Cl$. This deviates from the general depthwise hydrochemical sequence given by Schoeller [7]. The presence of H₂S in

170

saline groundwaters has been observed. This possibly explains the absence of SO_4 +HCO_3, SO_4 + Cl facies. The brackish waters are of $NaHCO_3$ type, indicating base exchange where as saline waters are of NaCl type. A few groundwater samples were analysed for bromide, strontium and iodide and the results are presented in Table 2. Most of the saline groundwaters show enrichment of Sr, Br and I, indicating long residence times as well as the influence of sea water (Fig. 6, 7 and 8).
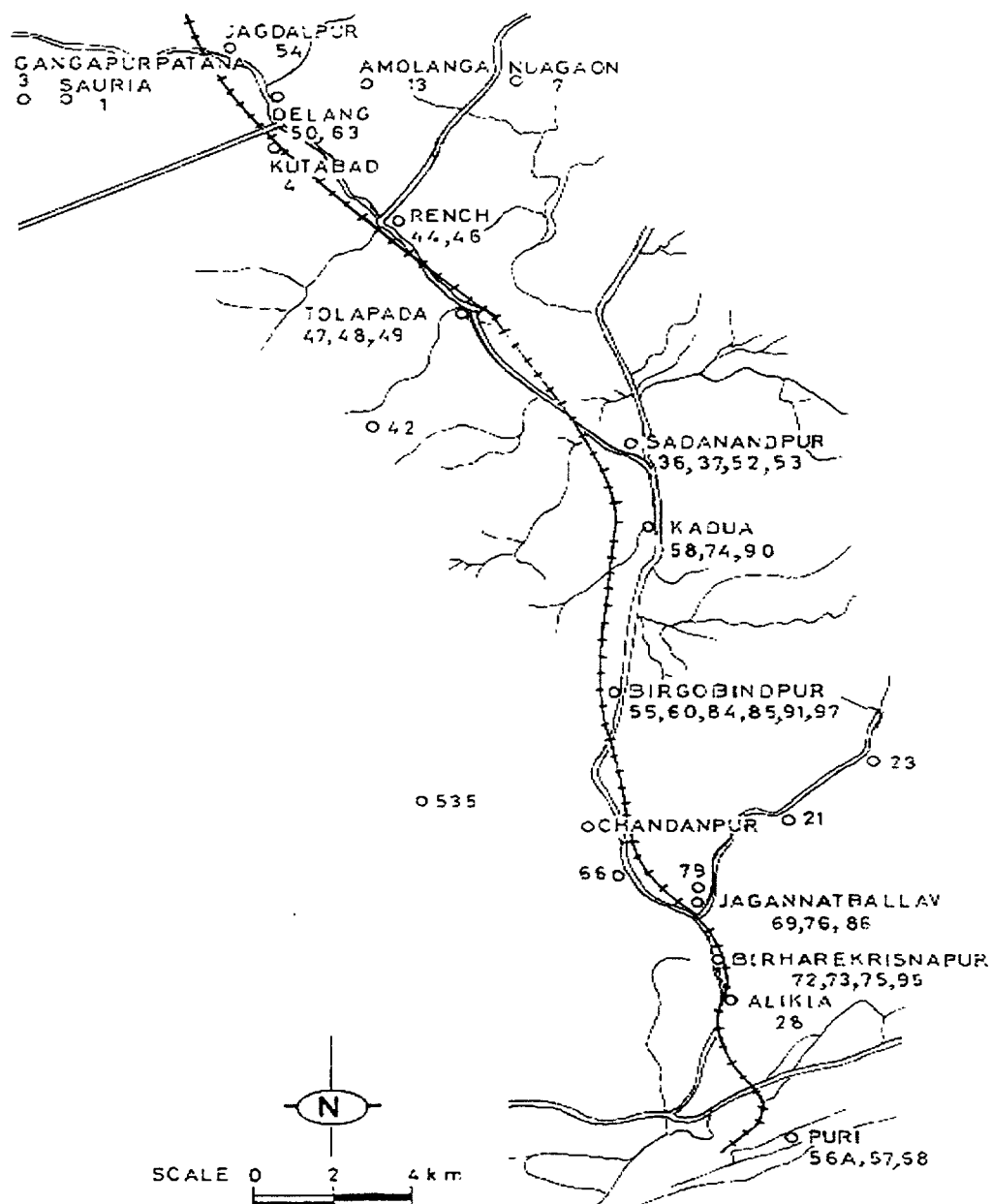
FIG. 5: Location of samples in Delang - Puri sector
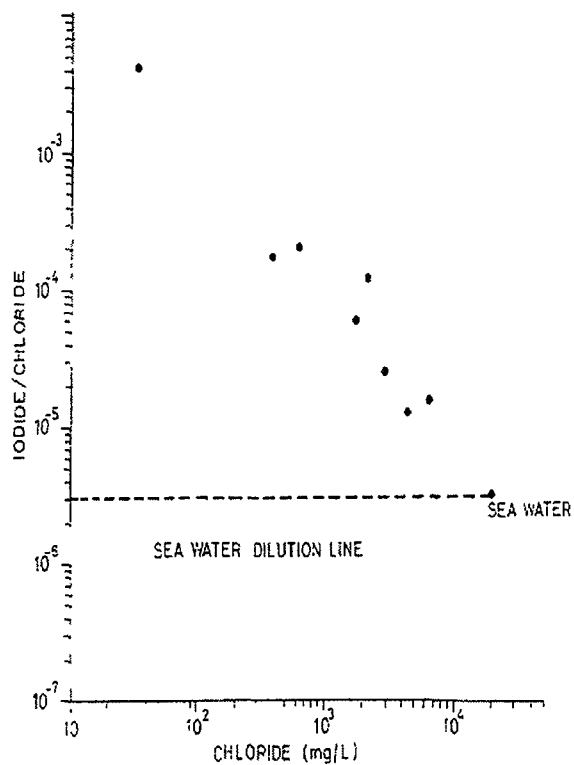
FIG. 6: Iodide/Chloride Vs Chloride plot
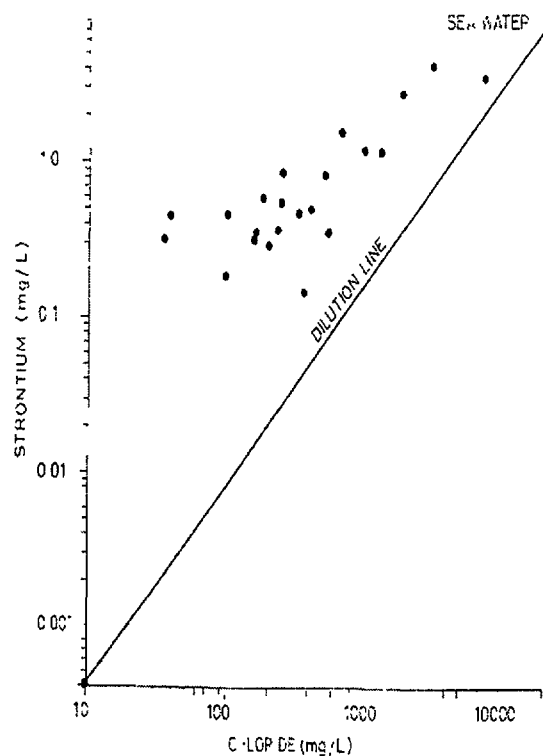
FIG. 7: Strontium Vs Chloride
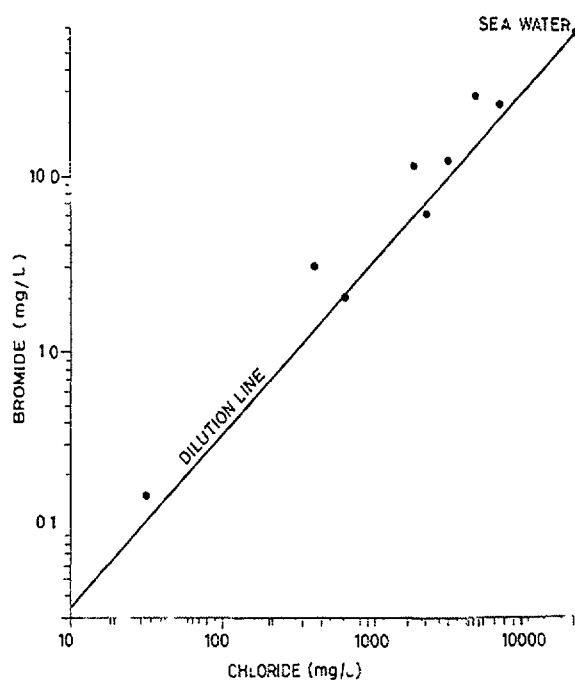
FIG. 8: Bromide Vs Chloride plot
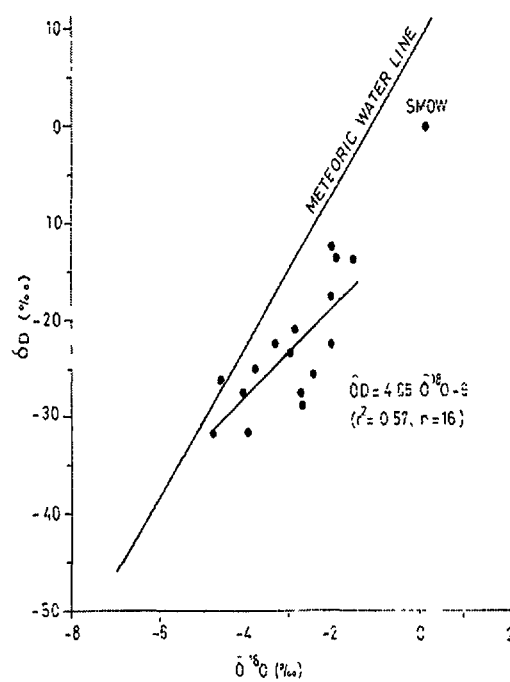
FIG. 9: δ^2H Vs δ^{18}O plot of surface water

172
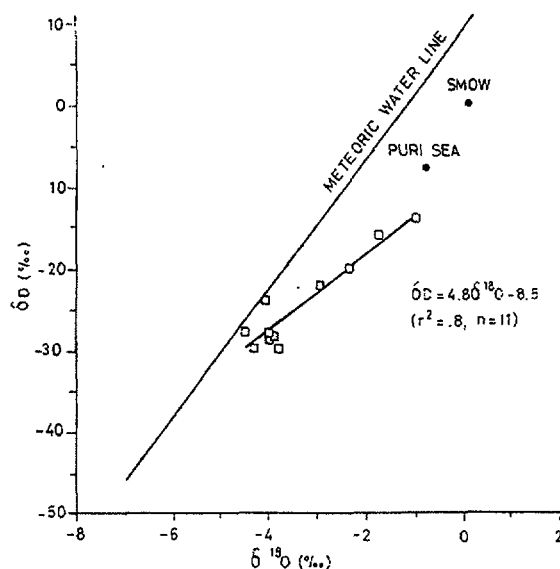
FIG. 10: δ^2H Vs $\delta^{18}O$ plot of shallow zone(<50m)
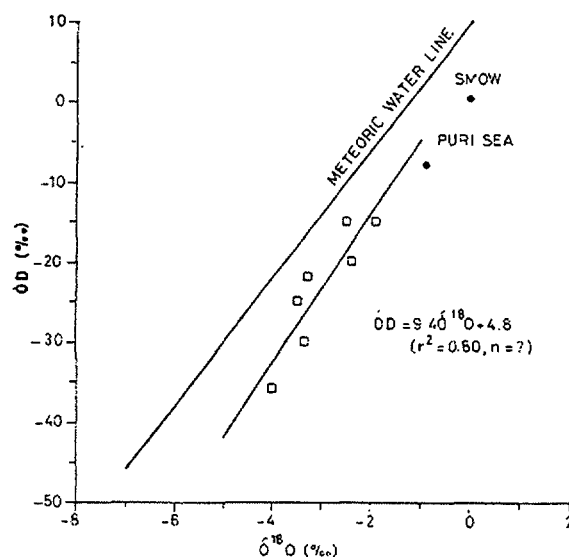
FIG: 11 δ^2H Vs $\delta^{18}O$ plot of intermediate zone(50 - 100m)

1.4 Isotope studies

From the Delang - Puri Sector, more than one hundred water samples from different depths as well as surface water bodies were collected for ^2H ^{18}O, ^{34}S, ^3H and ^{14}C measurement. Sample locations are shown in Fig.5. Selected samples were measured for ^2H and ^{18}O using a 602E mass spectrometer supplied by VG ISOGAS, UK. For saline groundwaters, carbon -14 sampling was carried out using the gas evolution method. This method is used because of low total dissolved inorganic carbon, high salinity and presence of H_2S in the samples. In the case of fresh water, the precipitation method was used and ^{14}C content was measured using LKB liquid scintillation counter (model 1215 Rock Beta-II).Radiocarbon ages were corrected using 67 pMC (highest radiocarbon content of deep groundwater with high ^3H content sampled in the recharge area) as initial activity for those samples where ^{13}C of carbonate could not be measured. For a few samples where ^{13}C could be measured the ^{14}C ages were corrected using the Pearson's model [4]. For tritium, samples collected from the field were distilled initially and 500 g of water is electrically reduced to about 12g and counted using LKB scintillation counter (model 1215) For ^{34}S, barium sulphate was precipitated at site and ^{34}S of aqueous sulphate were analysed at Atomic Minerals Division, Hyderabad. Isotope as well as selected chemical results are given in Table 1, 2, 3 and 4.

Table I. Isotope data of surface waters of coastal Orissa

Source	δ^2H (‰)	$\delta^{18}O$ (‰)	^3H (TU)
Puri Beach	-12 3	-2 1	4 1
Puri Sea	-08 0	-0 9	5 0
Chilka Lake	-19 0	-2 1	3 9
Mangala River	-13 6	-1 59	7 1
Dhakupada Pond	-31 5	-4 8	6 1
Birpratappur Pond	-24 9	-3 83	6 5
Precipitation	-26 0	-4 6	7 0
Ratnachira River	-31 4	-4 0	-NA-
Nun River	-21 0	-2 9	-NA-
Daya River	-22 3	-3 4	-NA-
Chandanpur River	-23 2	-3 0	-NA-
Birhara Pond	-25 4	-2 47	-NA-
Bhargavi River	-27 5	-2 75	-NA-

NA - not analysed

Table II. Isotope and chemical data of groundwaters of coastal Orissa

Well No	Location	Depth m	EC μS/cm	δ^2H ‰	$\delta^{18}O$ ‰	^3H TU	Br mg/L	I μg/L	Cl mg/L
PT-1	Sauria	40	540	-30	-4 3	0 6			60
PT-3	Gangpurpatna	16	780	-16 0	-1 8	1 0	-	-	78
PT-4	Kothabada	26	590	-22 0	-3 0	2 5	-	-	55
PT-7	Naugaon	26	380	-28 5	-3 9	0 8	-	-	32
PT-13	Amolanga	28	750	-	-3 6	0 9	-	-	46
PT-21	Chalis Batia	148	1530	-24	-2 7	0 5	-	-	241
PT-23	Tarasramhanspur	127	1380	-18 3	-2 5	0 5	-	-	188
PT-28	Alikia	18	1050	-28 0	-4 0	0 8	-	-	145
PT-36	Sadanandpur	109	7250	-27 0	-4 2	1 4	6 1	239	2067
PT-37	Sadanandapur	128	2530	-14 2	-1 5	1 9	2 0	124	610
PT-42	Dasbidyadharpur	-	580	-31 0	-4 3	0 0	-	-	57
PT-44	Rench	64	6230	-20 0	-2 4	2 4	11 5	98	1702
PT-46	Rench	126	660	-22 0	-2 7	8 0	0 9	-	89
PT-47	Tolapada	25	530	-30 0	-3 8	1 7	0 15	133	32
PT-48	Tolapada	53	560	-29 0	-4 0	-	-	-	35
PT-49	Tolapada	190	3580	-19 0	-2 4	-	4 8	-	900
PT-50	Delang	108	920	-	-	0 2	-	-	92
PT-52	Sadanandapur	31	11100	-20 0	-2 4	1 1	30 7	-	3474
PT-53	Sadanandpur	128	2430	-15 0	-2 3	0 6	-	-	613
PT-54	Jagadalpur	118	880	-29.0	-4 4	0 8	-	-	124
PT-55	Birgovindpur	136	1940	-21 0	-2.8	3 0	3 0	66	379
PT-56	Puri	33	120	-24 0	-4 1	2 0	-	-	18
PT-57	Puri	118	12200	-18 0	-2 9	1 4	28 0	53	4254
PT-58	Kadua	125	1580	-15 0	-2 2	2 0	-	-	259
PT-60	Birgovindpur	76	19970	-15 0	-1 9	1 1	25 0	96	6168
PT-63	Delang	106	1540	-15 0	-2 5	1 7	-	-	347
PT-66	Birbalbhadrapur	109	1280	-15 0	-2 5	1 7	-	-	216
PT-67	Chandanpur	161	260	-13 0	-1 3	8 2	0 3	-	21
PT-68	Puri	91	8200	-22 0	-3 3	1 6	12 0	70	2836
PT-69	Jaganathballav	124	890	-18 0	-2 8	1 3		-	89
PT-72	Birharekrishnapur	16	1670	-13 9	-1 0	3 9	-	-	227
PT-73	Birharekrishnapur	140	940	-21 7	-2 5	3 7	-	-	160
PT-74	Kadua	125	1440	-17 0	-1 9	4 0	-	-	230
PT-75	Birharekrishnapur	173	1660	-20 0	-2 0	4 2	-	-	312
PT-76	Jagannathballav	173	890	-16 0	-2 2	4 9	-	-	92
PT-78	Erabang	94	1660	-36 0	-4 0	6 3	-	-	351
PT-79	Balia Neelkantha	130	1050	-15 0	-2 5	4 9	-	-	167
PT-84	Birgovindpur	193	5570	-15 0	-1 6	0 5	10 1	-	1659
PT-85	Birgovindpur	243	21120	-14 0	-2 0	0 6	34 9	-	7374
PT-86	Jagannathballav	124	830	-20 0	-1 6	-	-	-	78
PT 87	Erabang	56	1810	30 0	-3 4	2 0	-	-	411
PT-90	Kadua	125	3890	-09 0	-1 0	1 4	-	-	1042
PT-91	Birgovindpur	135	1820	-16 0	-1 8	0 0	1 7	-	440
PT-95	Birharekrishnapur	174	-	-17 0	-2 3	-	-	-	-
PT-97	Birgovindpur	250	29700	-10 0	-1 5	-	103	-	-

Table III. Carbon -14 ages of groundwaters of coastal Orissa

Well No	Location	EC (μS/cm)	Depth (m)	^{14}C age (years)
PT-1	Sauria	540	40	450*
PT-3	Gangpurpatna	780	16	modern
PT-37	Sadanandpur	2530	128	17100*
PT-46	Rench	660	126	modern
PT-47	Tolapada	530	21	650*
PT-48	Tolapada	560	53	900*
PT-49	Tolapada	3580	187	33300*
PT-52	Sadanandpur	11100	artesian	24200•
PT-57	PURI	12200	115	12550
PT-84	Birgovindpur	5570	184	19200•
PT-85	Birgovindpur	21120	240	23450•
PT-97	Birgovindpur	29700	250	23100
PT-X	Ramchandrapur	16200	60	7350•
PT-Y	Rench	2230	31	700•

Note • - Ages corrected using 67 pMC as initial activity * - Ages corrected using δ^{13}C values

Table IV. Sulphur -34 results of coastal Orissa

well no	Location	Depth (m)	EC (μs/cm)	SO$_4$ (mg/l)	δ^2H (‰)	δ^{18}O (‰)	δ^{34}S (‰)	^{3}H (TU)	^{14}C age (years)
PT-36	Sadanandpur	106	7250	360	-27	-4 2	22 8	1 4	17100
PT-26	Rench	65	6230	269	-20	-2 4	8 4	2 4	-
PT-74	Kadua	125	1440	192	-17	-1 9	16 4	4	-
PT-57	Puri	118	12200	326	-18	-2 9	20 8	1 4	12550
PT-60	Biragobindpur	76	19970	730	-15	-1 9	24	1 1	-
PT-85	Biragobindpur	243	21120	259	-14	-2	43 8	0 6	24450
PT-95	Birharekrisnapur	175		19	-17	-2 3	11 5		-
	Puri sea			2208	-08	-0 9	21	5 0	
	Chilka lake			864	-19	-2 1	20 1	3 9	

1.5 Results and Discussion

A few surface water samples were analysed for ^{2}H, ^{18}O and ^{3}H content . The δ^2H and δ^{18}O values vary from -32 ‰ to -12‰ and -5‰ to -1.5‰ respectively. Precipitation samples collected during field work have δ^2H and δ^{18}O values of ~-28 ‰ and -4 ‰ respectively. ^{3}H content in precipitation and other surface waters varies from 4 TU to 7 TU. These samples show the effect of evaporation on the δ^2H - δ^{18}O plot (Fig.9).

175
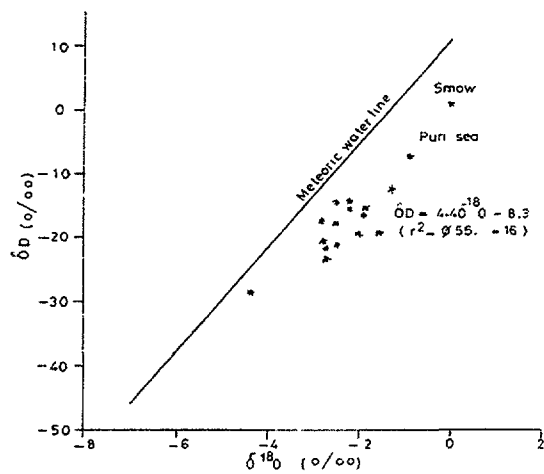
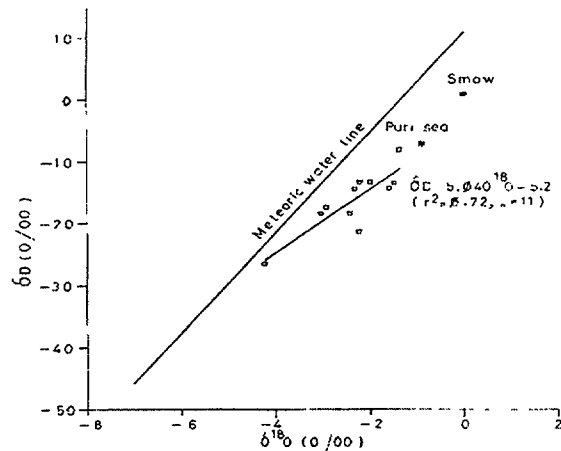FIG. 12: δ^2H Vs $\delta^{18}O$ plot of deep zone fresh groundwater (>100m)

FIG. 13: δ^2H Vs $\delta^{18}O$ plot of deep zone saline groundwater (>100m)

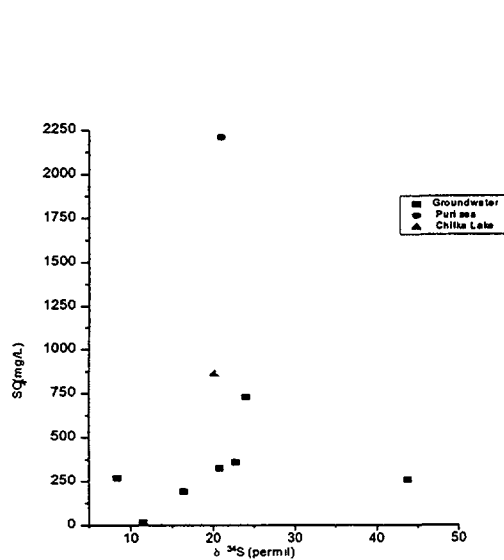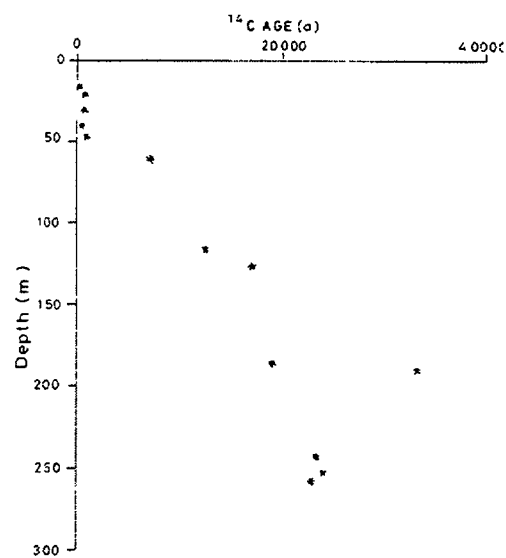
FIG. 14: Sulphate Vs Sulphur-34 plot

FIG. 15: ^{14}C age Vs Depth plot of groundwaters

176

For shallow groundwaters, $\delta^2 H$ and $\delta^{18}O$ values are in the range of -30 ‰ to -15 ‰ and -4 ‰ to -1.0 ‰. These samples fall on an evaporation line on the ^2H - ^{18}O plot similar to that of surface waters (Fig.10). This indicates that the shallow aquifers of Delang area receive recharge through outcrops of basement rocks exposed on the northwestern parts of Delang area (Fig.2). In the southern plain, the recharge could be infiltration of surface waters.

In the intermediate zone groundwater samples fall parallel to global meteoric line in $\delta^2 H$ and $\delta^{18}O$ plot.(Fig.11) The level of tritium in this aquifer is negligible, indicating absence of modern recharge. The EC of the samples varies from 1500μS/cm (Delang) to 20,000μS/cm (Birgobindpur) and most of the samples are saline (Fig.2-B1). Some of the samples collected from Rench, Birgobindpur, and Puri show Cl/Br ratios of 148, 247 and 236 respectively. A saline sample collected from Birgobindpur is enriched in $\delta^{34}S$ (+24 ‰) compared to the sea water value of +20‰ and at Rench $\delta^{34}S$ value is +8.4 ‰. The sample which is collected from Pratapramchandrapur shows ^{14}C age of about 7600 years BP. The saline groundwaters of this zone could be a mixture of fresh water and sea water entrapped during sea transgression in the Holocene.

The deeper aquifer (Fig.2-B2) fresh groundwaters isotopic composition is similar to surface water (Fig.12). Fresh groundwaters collected from the deep aquifer show high tritium (3-8 TU) and depleted $\delta^{34}S$ values (Kadua: +16.4‰ and Birharikrishnapur:+11.5‰) compared with the sea water value. This aquifer could be receiving recharge from the western side and mostly through fractures and joints of the basement rocks. The deepest fresh water aquifer (Fig.2-D1) near the basement show very high ^{14}C age (29,000 years BP)

The saline groundwaters of deep aquifer fall along a line in $\delta^2 H$ -$\delta^{18}O$ plot with $\delta^2 H$ = 5.4 $\delta^{18}O$ - 5.2 (r^2 - 0.72, n = 11, (Fig.13). Most of the deep aquifer saline samples show enriched $\delta^{34}S$ values (+20.8‰ to +43.8‰) compared with sea water value and radiocarbon ages are in the range of 12,000 years BP to 24,000 years BP with negligible tritium (Fig.14 &15). The EC values range from 2400 to 30,000 μS/cm. These old saline waters could have been entrapped during a marine transgression in the late Pleistocene.

1.6   Discussion

During the late Quaternary, a major glacial episode started at about 25000 years BP and produced a major eustatic decrease with minimum ocean level of about -90 m to -120 m at 18000 years BP [3]. Then climatic set back produced melting of ice caps and rise in sea levels, which was practically terminated at 7000 years BP. The end of the Pleistocene was marked by world wide warming. During this post glacial period, the Flandrian transgression occurred which affected most parts of globe, up to 6000 years BP, where after, recession took place to the present conditions [2].

The hydrogeological and isotope studies indicate the two episodes of sea level fluctuation took place in the Delang - Puri sector up to Tolapada. The first one corresponds to the Pleistocene interglacial stage and the other during Flandrian in the Holocene. The saline groundwaters of the deep aquifer in the Delang- Puri Sector could have been entrapped during eustatic rise in the late Pleistocene interglacial episode and shallow saline groundwaters during the Flandrian transgression.

It can be observed that most of the saline samples fall on a sea water - fresh water dilution line in the Bromide - chloride plot. This indirectly indicates that the source of the salinity of the groundwater is sea water. In strontium - chloride as well as iodide - chloride plots, most of the saline groundwater samples fall above the mixing line indicating enrichment of strontium and iodide. These saline waters could possibly have acquired these chemical species from sediment and this indirectly indicates the long residence of groundwater in the aquifer. Most of the saline groundwaters have been considerably enriched in $\delta^{34}S$ (+20.8 ‰ to +43.8 ‰) with respect to the sea water value (Fig.14). Occurrence of H_2S and - Ve Eh (-35 mv) show reducing conditions. This large enrichment could be due to continued bacterial reduction of marine sulphate to sulphide over a period of time. This is further confirmed by very low SO_4/Cl ratio of 0.035 compared to sea water value of 0.13. Fresh groundwater samples from Rench, Kadue and Birharekrishnapur show $\delta34S(SO4)$ values from +8 to +16‰ below the marine sulphate value. They receive recharge from basement rocks and flood plains in the western part. Hence they have some component of non marine sulphates

1.7   Conclusion

The isotope geochemical studies of saline groundwaters of coastal Orissa indicate that:

- Shallow fresh groundwaters are modern and they are recharged through flood plains and outcrops of basement rocks.
- Saline groundwaters of the intermediate zone are mostly due to the Flandrian transgression during Holocene.
- Deep fresh groundwaters receive recharge through basement rocks.
- The deep fresh water occurring in weathered basement rock is a potential source for exploitation.
- Deep saline groundwaters are connate marine waters which were entrapped during late Pleistocene interglacial stage.
- The source of sulphate in saline groundwater is due to marine sulphates which has undergone bacterial reduction.

2.   STUDIES ON DEEP SALINE GROUNDWATERS OF CHARNOCKITE TERRAIN AT KOKKILIMEDU

2.1   Background

Kokkilimedu is located 80 km south of Chennai City. It lies between longitude 80° 3` to 80° 12`E and latitude 12° 27` to 12° 38`N. The topography is an Easterly gentle sloping terrain between the Eastern Ghats and the Bay of Bengal. The mean annual rainfall is about 1237 mm. Under the host rock characterisation programme for safe disposal of radioactive waste, four deep bore holes were drilled in this area (Fig.16). One bore hole (BH-1) was drilled to 600 m depth and the other three (BH-2, BH-3 and BH-4) were drilled to 618 m, 566 m and 200 m respectively.

In BH-1, it was observed that the groundwater salinity increases with depth. Below a depth of 350 m, the chloride concentration is more than twice that of sea water (chloride concentration-41,200 mg/L). In BH-2, the salinity increases with depth but it is less than sea water. The maximum chloride concentrations encountered in this bore hole is 9800 mg/L at 500 m depth. The BH-3 and BH-4 show low salinity at the deeper level compared to shallow depth. The maximum salinity observed in these bore hole is 880 mg/L and 2500 mg/L at 75m

and 200m depth respectively. Therefore isotope geochemical investigations were carried out in this host rock characterisation programme to understand the salinisation mechanism and the hydrodynamic conditions of deep groundwaters.
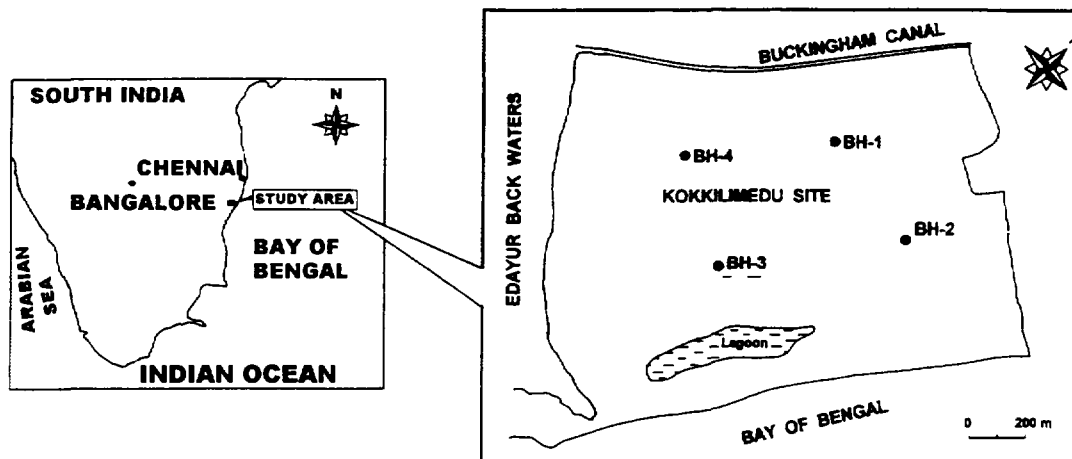
Fig 1 Sample location map (Kokkilimedu)

2.2 Hydrogeology

The investigated area is covered by 15 to 20 m thick alluvium, underlain by hard and compact charnockite rock. The alluvium forms the top aquifer, bearing meteoric water. The charnockite rock consists of quartz, feldspar, biotite and pyroxene. These minerals are resistant to weathering. Hence the rate of reaction and the transfer of solutes into the groundwater is slow. Borehole cores of the study area indicate the presence of pseudotachylites along the fractures and joints indicate tectonic upliftment associated with retrograde metamorphism. Pseudotachylites are mostly greenish dark materials, predominantly clay, altered feldspar, quartz, chlorite, biotite, etc.. [5]. Fracture fillings varying in thickness from 3.0 mm to 0.5 m. As these rocks are dense and compact, groundwater is restricted to joints and fractures which form a limited confined aquifer. Groundwater flow follows the topography and flows towards the southeast. Groundwater levels vary between 7.0 to 9.0 m above mean sea level.

Water samples were collected from boreholes (from different depths using a depth sampler), rain water and a few surface waters such as the Buckingham canal and the Bay of Bengal. These samples were analysed for major ion chemistry and a few samples were analysed for ^2H, ^{18}O and ^3H. The results are given in Table V. The regional meteoric relationship between ^2H and ^{18}O was established from the regression of rain fall data collected at Chennai by the Institute for Water Studies in 1995.

2.3 Major ion trend and water - rock interaction

Water samples collected from BH-1 show low pH (5.8 to 7.3) whereas the pH of BH-2, BH-3 and BH-4 groundwaters are in the range of 7.4 to 8.8. The entire boreholes were sampled with a vertical interval of 50 m and the variability of chemical composition with depth was observed. Both increase and decrease in the concentration of chloride and other species occurred with depth in all four boreholes. This is indicative that the water in the borehole is stratified.

The groundwaters of the Kokkilimedu area have interacted to a considerable extent with the weathered charnockite rock. This can be seen from the variations of the dissolved species Na^+, K^+, Mg^{+2} and Ca^{+2} with chloride content in Figs. 17 and 18.

In BH-1, plots of chloride against Na^+, K^+, Mg^{+2} and Ca^{+2} (Fig.2) indicate linear relationships with a lesser slope than the sea water - fresh water mixing line. A linear relationship generally indicates the mixing of saline and fresh groundwater. Ion exchange processes is possibly responsible for the depletion of significant amounts of Na^+ and K^+ as well as the enrichment of Ca^{+2} and Mg^{+2}.

In BH-2, Cl⁻ against Na^+, K^+, Ca^{+2} and Mg^{+2} plots show bimodal slopes (Fig.18). It occurs over a depth range of 150-300 m. The change in the slope is important because it occurs where the hydraulic conductivity is rapidly increasing or decreasing. The two different clusters of samples with different slope observed in chloride against cation plots suggest a transition of water from the weathering zone at shallow depth to permeable rocks, where the salts are leached to obtain the final salinity. Similar situation was also observed at 75-150 m in BH-3.

2.4   Isotope Results

The isotope and chemical data are interpreted and the δ^2H - $\delta^{18}O$ and $\delta^{18}O$-Cl⁻ relationships are shown in Fig-4 & 5. Samples collected from different depths in BH-1 have enriched δ^2H and $\delta^{18}O$ content (δ^2H: -6 to -4‰ and $\delta^{18}O$: -1.8 to -0.6‰) compared with samples of BH-2 and BH-3. They fall away from the meteoric line in one cluster indicating evaporation effect or influence of sea/Buckingham canal water. On $\delta^{18}O$ - Cl⁻ plot, the shallow zone sample in BH-1 show some mixing trend with sea water/Buckingham canal water. The deep zone samples in BH-1 show similar $\delta^{18}O$ compared to the shallow zone sample, indicating that further, salinization could be due to leaching processes.

Samples of BH-2 and BH-3 are more depleted than BH-1 samples in stable isotopic content and their δ^2H and $\delta^{18}O$ values are in the range of -32.8 to -26.3‰ and -6.6 to -4.4‰. These samples fall close to the regional meteoric line. In this case no relationship can be observed between isotopic content and increasing salinity in the $\delta^{18}O$ - Cl⁻ plot (Fig.20). The poor correlation between $\delta^{18}O$ - Cl⁻ indicates that the salinity in this case is mostly due to dissolution of aquifer matrix, and fracture fillings. Further, the high tritium content was observed in surface water such as pond water (145 - 479 TU), Buckingham canal (62 TU), Bay of Bengal water (23 TU) as well as in shallow groundwater (62 - 119 TU). This high tritium content is mainly due to effluent from nuclear power plant which is located just 0.5 km West of this site. The groundwaters of BH-1, BH-2, BH-3 and BH-4 also show high tritium content (15 to 155 TU). This could be due to the mixing of surface water with groundwater.

2.5   Conclusion

The isotope geochemical investigations suggest that the observed high salinity in BH-1 can be attributed to infiltrated sea water/Buckingham canal, together with the contribution of pseudotachlight observed along the fractures and shear zones in charnockite rock. In the case of BH-2 and BH-3, mixing of sea water does not contribute to saline conditions as the isotopic and chemical relationships do not correlate with sea water. Their salinity is mostly from solute acquired from sheared and fractured host rock.

180
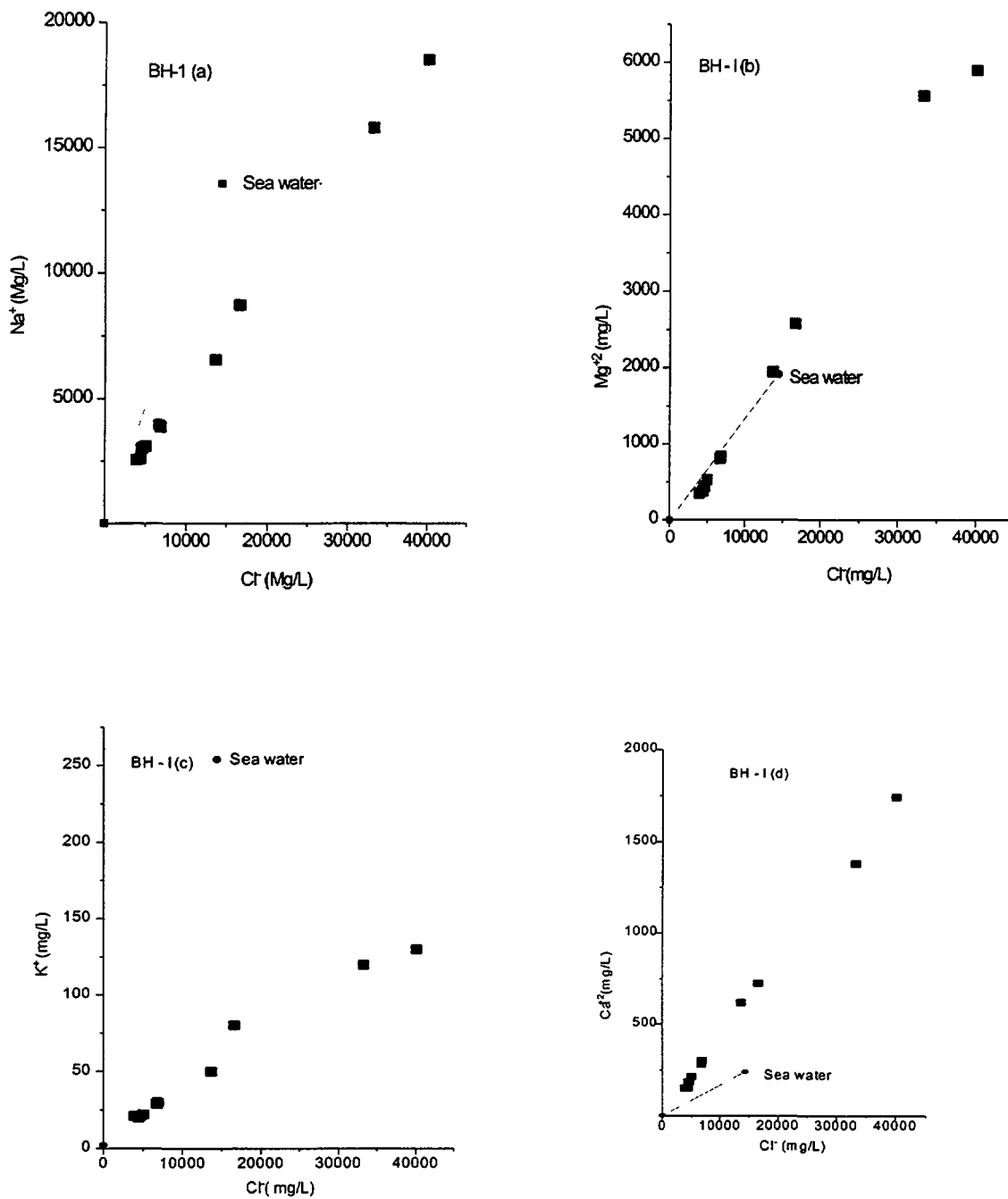
FIG. 17(a-d): Variation of the dissolved species Na^+, K^+, Mg^{+2} & Ca^{+2} with Cl^- content in BH-I
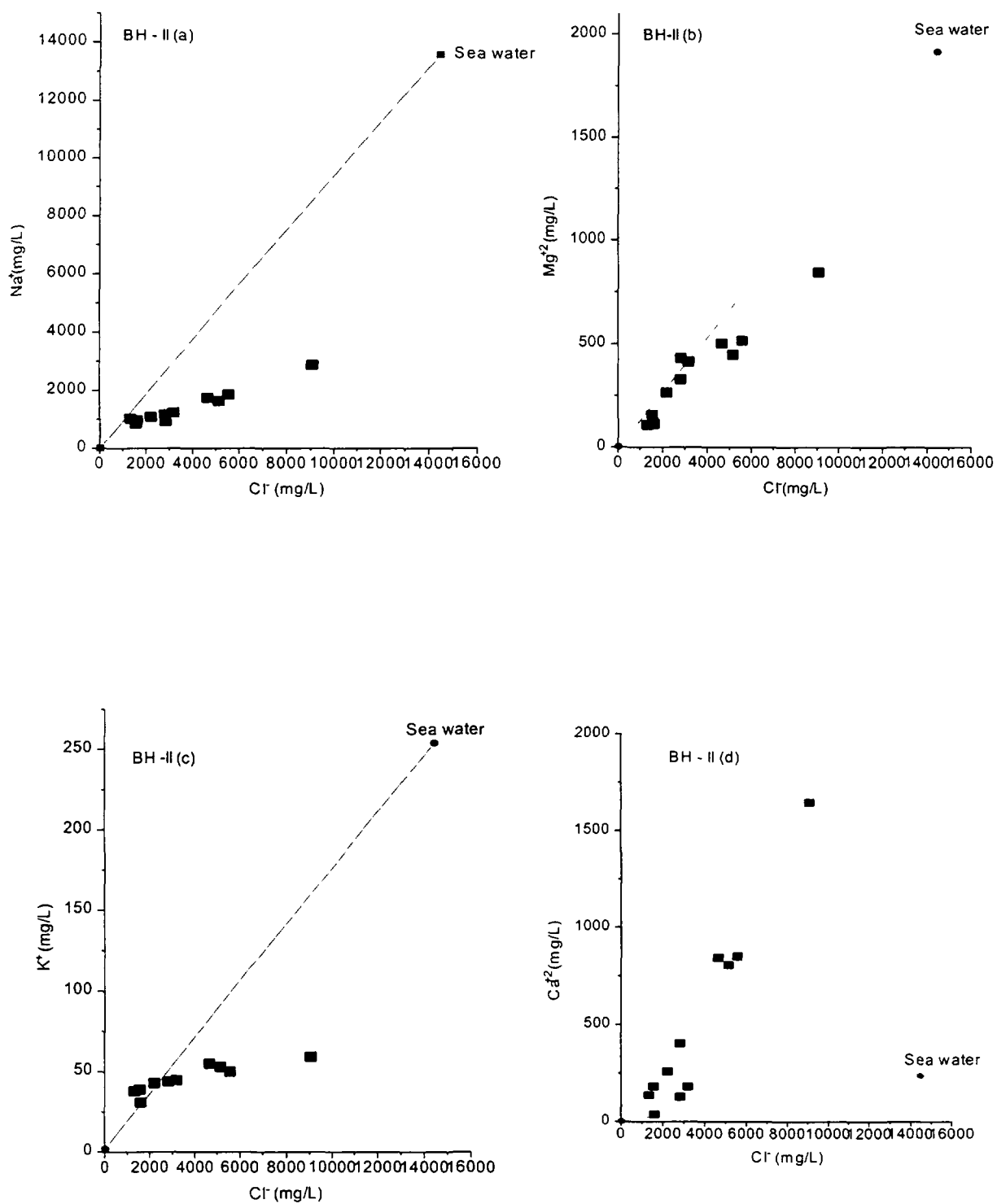
FIG. 18(a-d): Variation of the dissolved
species Na^+, K^+, Mg^{+2} & Ca^{+2} with Cl^- in BH-II

182

FIG. 19: δ^2H - δ^{18}O plot
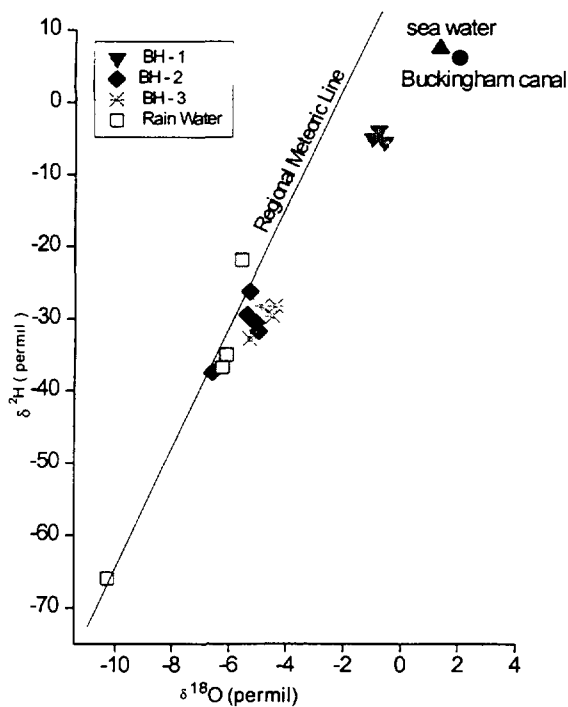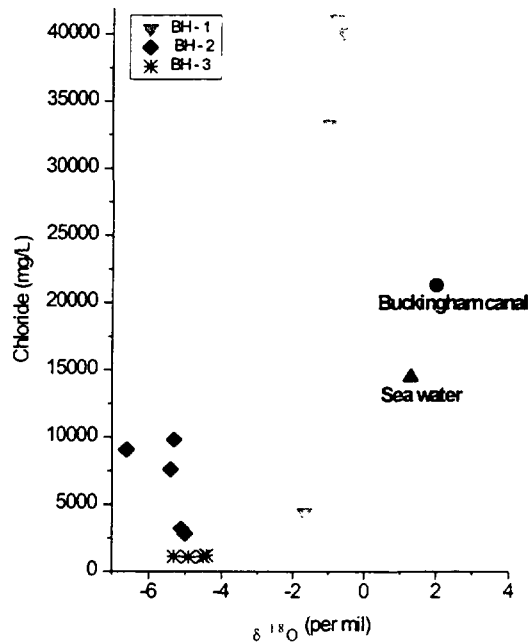
FIG.20:δ^{18}O - Cl⁻ plot

Table V. Isotope results of groundwaters of Kokkilimedu

Sample idetification & at what depth sample collected (m)	Chloride (mg/L)	Sulphate (mg/lL	δ^2H (‰)	δ^{18}O (‰)
Rain water			- 36.8	- 6.26
Rain water			-21.9	-5.57
Rain water			-35.0	-6.1
Rain water			-66.0	-10.3
Sea water	14455	2500	+07.5	+01.3
Buckingham canal	21315	3000	+06.2	+02.0
BH-1 (400)	41160	3500	-3.9	-0.8
BH-1 (450)	33320	3200	-5.0	-1.0
BH-1 (500)	40180	2800	-5.5	-0.6
BH-2 (20)	2816	0038	-31.8	-5.0
BH-2 (40)	3185	0045	-30.6	-5.1
BH-2 (400)	7595	0450	-29.9	-5.4
BH-2 (450)	9065	0650	-37.5	-6.6
BH-2 (500)	9800	0800	-26.3	-5.3
BH-3 (20)	1176	-	- 28.3	- 4.4
BH-3. (40)	1,127	1,450	- 32.8	- 5.3
BH-3 (350)	1,070	1,350	- 28.3	- 4.9
BH-3 (400)	1,078	1,480	- 29.7	- 4.5

183

REFERENCES

[1] DANIDA, Orissa drinking water project - Hydrological investigations Danish International Development Report, 8 vols. 1993.

[2] Holmes, A; Principles of physical geology, Nelson. London, 1975.

[3] Morner, N.A; The position of ocean level during the interstadial at about 30000 BP - A discussion from the climatic glaciologic point of view, Can.J.Earth SCI., 8, 132 - 143, 1971.

[4] Pearson, F.J.Jr., White, DE., Carbon -14 ages and flow rates of water in Carrizo sand, Atascosa County, Texas, Water Resour. Res.,3, 251 - 261, 1967.

[5] V Arumugum, Site characterization for location of radioactive waste repository: A case study, Ph.D. thesis, IIT, Bombay, 1994.

[6] B.R.Payne, The status of isotope hydrology today, J. Hydrol., 100: 207-237, 1988.

[7] Schoeller, H., Arid zone hydrology- recent develop. UNESCO, Rev. Reicardi. 12, 1959.

THE APPLICATION OF STABLE CARBON ISOTOPE RATIOS AS WATER QUALITY INDICATORS IN COASTAL AREAS OF KARACHI, PAKISTAN

R.M. QURESHI, A. MASHIATULLAH, T. JAVED,
M.A. TASNEEM, M.I. SAJJAD
Environment Research Group, PINSTECH, Islamabad

M. SALEEM, S.H. KHAN, S.H.N. RIZVI
National Institute of Oceanography, Karachi

S.A. SIDDIQUI, R. QARI
Centre of Excellence in Marine Biology,
University of Karachi, Karachi

Pakistan

Abstract - Stable carbon isotope ratios $(\delta^{13}C)$ of total dissolved inorganic carbon (TDIC), total inorganic and organic carbon in bottom sediments, as well as sea plants in polluted water sources, non-polluted Karachi Sea water and pollution recipients are used to elaborate pollution scenario of shallow marine environment off Karachi coast. These results are supplemented with stable isotope composition of nitrogen $(\delta^{15}N)$ in seaweeds and mangroves, toxic/trace metal concentration in sea-bottom sediments, total Coliform bacterial population, electrical conductivity, temperature and turbidity. Isotopic data shows that the mangrove ecosystem and the tidal fluctuations play a key role in controlling contamination inventories in shallow sea water off Karachi coast, specifically the Manora Channel. The Karachi harbour zone is found to be the most heavily polluted marine site in Manora channel during high as well as low tide regimes. Significant concentrations of toxic metals such as Pb, Ni, Cr, Zn, V, U are observed in off-shore sediments of Karachi coast. The results show that sewage and industrial wastes are the main sources of heavy metal pollution in Karachi Harbour, Manora Channel exit zone and the southeast coast. However, as compared to other coastal areas, the Karachi coast is moderately polluted. Studies suggest incorporation of quick remedial measures to combat pollution in shallow marine environments off Karachi Coast.

1. SIGNIFICANCE OF OVERALL PROBLEM

Seawater of the coastal regions near large industrial and population centers normally receives large quantities of sewage and industrial waste water which pollutes the living and recreational environments of coastal waters. Karachi is located on the northern boundary of the Arabian Sea. It is the largest city in Pakistan with coast line extending up to about 30 km. It is estimated that nearly 300 million gallons per day of domestic and industrial waste water is generated. This waste water is drained into Karachi sea mainly via Layari River, Malir River/Ghizri Creek and Korangi Creek (Fig. 1).

Manora Channel is a navigational channel and it connects the Karachi Port with the Arabian Sea in the south (Fig. 2). It spreads over an area of 7.17 km and includes the Karachi Harbour and the Keamari Fish Harbour. About 3.4 million cubic meter water enters and leaves the channel during a tidal cycle. The channel entrance is narrow and easily silted. The
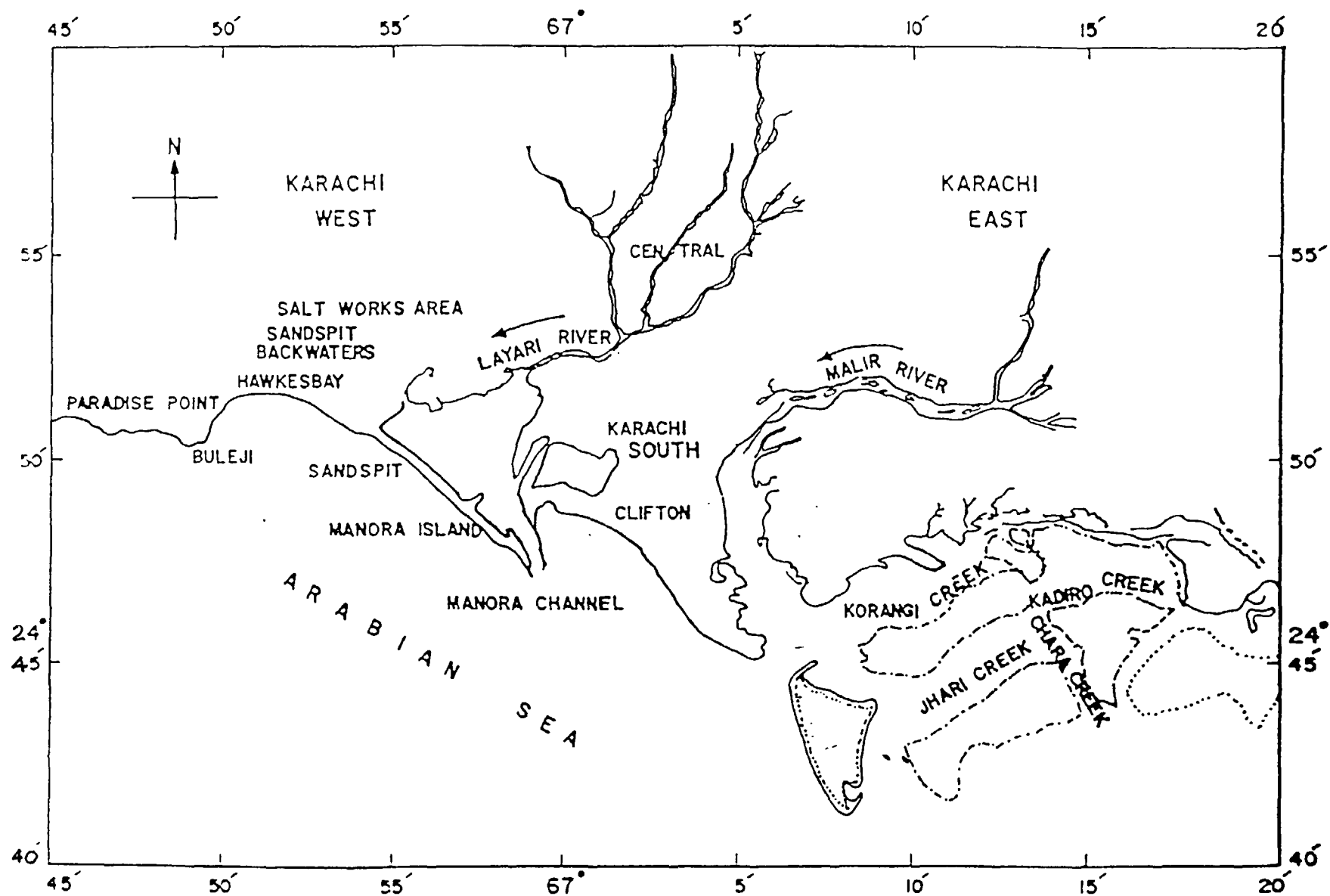
Fig. 1   Coastal map of Karachi (Pakistan) indicating polluted rivers drainage course in Manora
Channel and Ghizri/Korangi Creek.
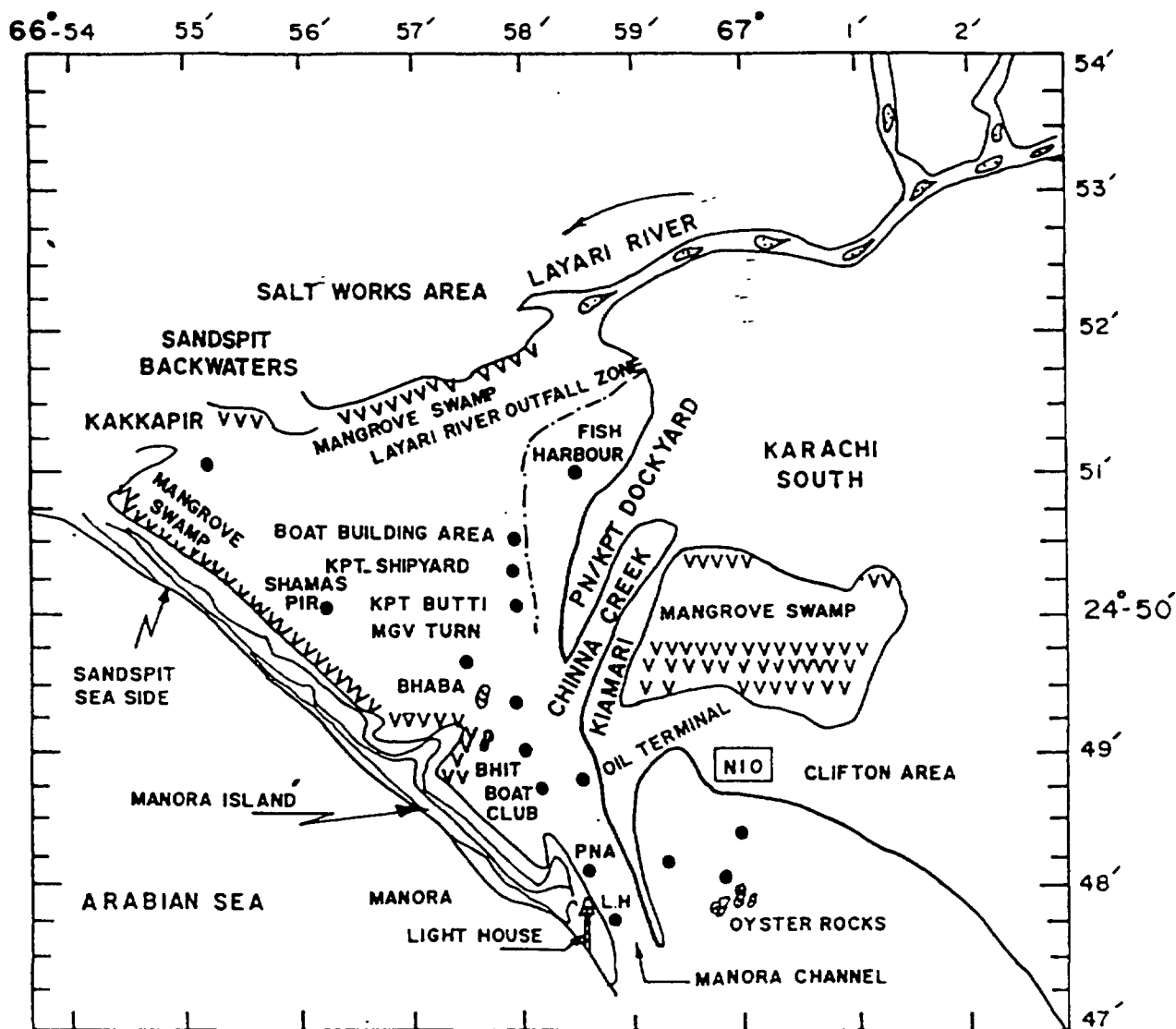
Fig 2   Details of sampling points in Manora Channel & Karachi harbour

addition of sediments in the Karachi harbour area is mainly brought by the Layari River and the status of sediment input load is so bad that the channel has to be dredged year round. About 45600 cubic meters of silt is removed from the channel annually, therefore, its depth is maintained by regular dredging throughout the year. River Layari flows through urban centers, where it is loaded with sewage/effluents of domestic origin from the north-western areas of Karachi and of industrial origin from the Sind Industrial Trading Estate (S.I.T.E.). Ultimately, the Layari River discharges large quantities of untreated and semi-treated domestic wastes on the north-western end of the Manora Channel. The Layari River outfall waters thus contain significant inorganic pollution in terms of sulfates, nitrates, carbonates, calcium, allum, magnesium, arsenic, and heavy metals and   organic pollution   mainly pesticides, herbicides, PCB's, cyanides, PAHC's, and plasticizers, cresols, floating plastics particles etc. The suspended matter is said to reach the coast at an average rate of 30 tones/day. Karachi Harbour/Manora Channel receives a variety of chemicals   such as calcium carbonate (115.74 metric tonnes/day), total dissolved solids (317 metric tonnes per day) and iron oxides (5.14 metric tonnes per day). The quantity of domestic wastes produced per household in Karachi varies from 100 to 280 liters per day.   The abiological and biological

187

dissolution of organic matter in bottom sediments of Manora channel also add to the deterioration of water in the channel. It is an overcrowded port and an estimated 3900 ships leave and enter the port annually. About 19.1 million tonnes cargo is handled including the oil. The Manora Channel also has a Naval Port and a Fish Harbour. Cargo ships, fish trawlers and mechanized boats of national and international origin pump-out dirty bilge and sludge into sea water. Cleaning of oil tankers at harbour is responsible for the discharge of the washings along with all contaminants which ultimately enter the sea. Fish market and fish processing plants at the fish harbour also discharge their solid wastes and effluents directly into the Manora channel. Upchannel environment also receives untreated domestic wastes from five villages located at Manora Island, Bhaba Island, Bhit Island, Shams Pir and Kakka Pir.

Manora Channel area is now considered to be the most heavily polluted marine site in Pakistan. Some sporadic and small scale pollution surveys involving classical hydro-geochemical and/or biological techniques have been made in the past to estimate the pollution status along the coast of Karachi [1, 2, 3, 4]. The fish habitat and the mangroves in the Manora Channel/Karachi harbour and backwater areas are now under considerable stress. It has been documented that the discharge of sewage and industrial pollutants in the Karachi harbour/Manora Channel has not only caused depletion of the Oyster beds in and around Karachi harbour area but the shrimps and fishes which were abundant in the Manora Channel, Manora Seaside and Hoxbay area have migrated to the deeper waters [5, 6]. Nevertheless, inspite of very high pollution levels in the Karachi Harbour area, it is still being used for bathing by tourists and the local population. The southeast coast of Karachi is mainly polluted by drainage of Malir River/Ghizri Creek and Korangi Creek domestic sewage and industrial waste effluents.

2. PRESENT INVESTIGATIONS

2.1 Objectives

The main objective of this paper is to document for the first time conjunctive use of environmental stable carbon isotope techniques and classical non-nuclear analytical techniques for evaluation of the shallow marine pollution trends off Karachi coast with special reference to the Manora Channel / Karachi Harbour area. Studies include determination of stable carbon isotope ratios ($\delta^{13}C$) of (i) total dissolved inorganic carbon (TDIC), (ii) total inorganic and organic carbon in bottom sediments, (iii) sea plants (mangroves & seaweeds); stable isotope composition of total Kjeldahl nitrogen ($\delta^{15}N$) in seaweeds and mangroves, toxic/trace metal concentration in sea-bottom sediments, total Coliform bacterial population, electrical conductivity, and turbidity in polluted water sources (Layari River downstream and outfall zone), non-polluted Karachi Sea water and pollution recipients (Manora Channel, Karachi Harbour and its backwaters).

2.2 Sampling and Analysis

Field sampling was performed at various interval of time during the period from April 1995 to September, 1997. This period was selected to cover the possible spectrum of changes in pollution transport pattern due to seasonal variable winds of the monsoon system. During the winter (October- February), the northwest monsoon winds are relatively weaker, resulting in diminishing upwellings along the western margins of the Arabian Sea [6]. During the

188

northwest monsoons (October-February), the seawater from the nearshore and offshore Indus Delta enters the coastal waters of Karachi from the southeast and moves along the coast towards the northwest or westwards and then to the western coast of Karachi [7]. The first sampling was performed in May 1995, the second sampling from 11-18 January 1996, the third sampling from 4-6 December 1996 and the fourth sampling from 24-27 September 1996.

Mangroves, seaweeds, sediments, and high tide and low tide water samples were collected from *polluted water sources* and *pollution receiving bodies* namely: (i) Manora Channel, (ii) South-East Coast of Karachi (Clifton-Ibrahim Haideri Coastline), (iii) Oyster-Rock Zone /Manora Channel Exit (iv) North-West Coast of Karachi (Manora seaside-Paradise Point Coastline), and (v) non-polluted region of Karachi-sea. In order to elaborate on pollution levels of Karachi harbour area, water samples were collected during the last hour of low tide regime along 5 profiles perpendicular to the KPT-Shipyard and Naval Dockyard starting from the open highlands facing Layari mangrove forests to the Bhaba Island. In the Manora Channel mains, water samples were also collected at three intervals between peak high tide to peak low tide period. The polluted rivers were approached by road during the low tide period whereas sampling in the Manora Channel/Karachi Harbour was performed using conventional mechanized tourist Boat. Sediment samples were collected with the help of a conventional Peterson Grab and contained in high quality polyethylene bags. Pre-treated mangrove leaf and seaweed samples were obtained from Centre of Excellence in Marine Biology (CEMB), University of Karachi, Karachi. Water samples have been collected within 10 m depth contour.

The location of sampling points was determined with the help of a Garmin GPS-100 Personal Navigator™ (M/S Garmin, 11206 Thompson Avenue, Lenexa, KS 66219). In-situ measurements of turbidity, electrical conductivity (E.C.), temperature were performed on all water samples. The time for the occurrence of a low or high tide was deduced from the standard TIDE TABLE GUIDE-1995 as published by the Pakistan Navy. Turbidity was measured with a battery operated portable turbidimeter (Model 6035, JENWAY). Electrical conductivity and temperature were measured with a portable conductivity meter (Model HI 8633, M/S HANNA Instruments). Water samples for stable carbon isotope analysis were collected in leak-tight doubled stoppered plastic bottles and spiked with 0.1M $HgCl_2$ solution to eliminate bacterial activity for preservation of TDIC.

All samples were stored in the laboratory under cooled conditions prior to analysis. Total Coliform bacteria (E.Coli/100 ml water sample) were determined within 24 hours of sample collection using a dual incubator (PAQUALAB Model 50, ELE International, U.K.). Water samples for stable carbon isotope analysis were filtered firstly through Whatman-42 filter papers and then through 0.45 micron nitrocellulose filters. Sample preparation for stable carbon, and nitrogen isotope analysis of TDIC, inorganic fraction in the sediments, and organic fraction in seaweed & mangrove samples was performed according to standard procedures [8, 9]. Stable isotope analyses were performed using Mass Spectrometers and expressed as delta (δ) per mil (‰) values relative to international standards namely: PDB (Pee-Dee Belemnite) for ^{13}C analysis, Air-N_2 for ^{15}N analysis (reproducibility better than 0.1 ‰ PDB for δ ^{13}C and 0.2 ‰ Air-N_2 for δ^{15}N measurements). Selective toxic/trace element analyses (except uranium analysis) of dried/pulverized sediments (80 mesh size) are performed with ICP-OES (Model 3580, Applied Research Laboratories, Switzerland) using standards namely SL-1, SL-3 and Soil-5 as well as with Flame Atomic Absorption Spectrophotometer (Perkin Elmer Model 3300, only for Cu, Cr, Ni, Pb, Zn) and Graphite

Furnace Atomic Absorption Spectrophotometer (Model HGA-600, only for Cd analysis). The concentration of uranium in sediments was measured with a 26-000 Jerrel Ash Fluorometer.

3.   RESULTS AND DISCUSSION

3.1   Water pollution profiles

3.1.1   Input functions of pollution sources: Electrical conductivities of polluted river outfall zones are much less than the non-polluted Karachi sea waters. Converse is true for Coliform bacterial population and turbidity. E.Coli, E.C., turbidity and temperature of the Layari River downstream water prior to outfall in Karachi harbour/Manora Channel are respectively in the range of: >300 coliform counts per 100 ml, 2.1-2.96 mS/cm, 6.15-37.6 NTU and 20.5 - 28.7 °C. Similarly, for the Layari River outfall area towards Karachi Harbour, E.Coli, E.C., turbidity and temperature were: >300 coliform counts, 21.5 - 52.7 mS/cm, 4.2 - 68.3 NTU and 20.2 - 27.8 °C respectively. E.Coli, E.C., turbidity and temperature of the Malir River downstream water prior to outfall in Gizri/Korangi Creek are respectively in the range of: >300 coliform counts per 100 ml, 3.8 - 6.2 mS/cm, 7.8 - 26.6 NTU and 19.9 - 27.8 °C. Similarly, for the Malir River outfall area viz. Gizri/Korangi Creeks, E.Coli, E.C., turbidity and temperature were: >300 coliform counts, 3.2 - 44.9 mS/cm, 8.4 - 38.6 NTU and 20.8 - 27.6 °C respectively. For the Karachi Sea, E.Coli, E.C., turbidity and temperature were: ~175 Ecoli/100 ml , 52.9 - 55.6 mS/cm, 1.06 - 6.7 NTU, 20.1 - 21.2 °C respectively. pH was measured only during the first sampling phase whereas, coliform population was measured for the first two sampling phases. Layari River has pH value lower than the Malir River/Gizri Creek. The Layari River outfall has pH values in the range of: 8.14 - 8.36. Carbon isotope composition of the TDIC in polluted river water is also quite distinctive. The Layari River has a $\delta^{13}C$ values in the range of -6.9 to -2.6 ‰ PDB. The Malir River has a $\delta^{13}C$ values in the range of - 9.6 to -4.2 ‰ PDB. Malir River outfall zone (Ghizri/Korangi Area) has $\delta^{13}C$ values in the range of -8.9 to -2.3 ‰ PDB. The Karachi sea blue waters have a $\delta^{13}C$ value in the range of -0.79 to +0.6 ‰ PDB (Table-I). However, it is interesting to note that although, electrical conductivity of polluted Layari River outfall increases significantly due to large scale mixing of sea water, the Layari river outfall zone has quite depleted $\delta^{13}C$ values (ranging from: -4.3 to -10.2 ‰ PDB) as compared to the polluted Layari river waters and the Karachi sea blue waters. In fact, its average $\delta^{13}C_{TDIC}$ composition is comparable with that for Layari River downstream. This is attributed to the impact of mangrove swamps in the Layari River outfall zone. As soon as, the high tide gushing waters enter the mangrove swampy areas, they dissolve isotopically depleted CO_2 which is biogenically produced in mangrove swamps during high/low tide regimes (duration: ~ 6 hours each). This may be clarified by the neap tide $\delta^{13}C$ values in the Layari River outfall zone, which are relatively enriched in ^{13}C as compared to the spring tide regime values. These average $\delta^{13}C_{TDIC}$ values of the Layari River outfall zone are, therefore, taken as inorganic carbon isotope input functions of Layari River outfall for evaluation of mixing characteristics of polluted Layari River mouth waters in Manora Channel.

3.1.2   Carbon isotopic evaluation of pollution: The conventional physio-chemical and biological measurements not only lack in high precision but these also do not reflect on the type of pollution source. On the other hand, stable carbon isotope analysis of TDIC have not only high precision of measurement (better than 0.1 ‰ PDB) but the inputs due to various pollution sources and the types can be realized by their characteristic $\delta^{13}C$ range. These data are discussed in the following section.

190

3.1.2.1 Manora channel pollution profile: The Manora Channel consists of stations from Keamari Fish harbour in West Wharf Area to Manora Lighthouse exit near Naval Radar post. The pollution profile of this area is discussed in the following section in terms of two sub-profiles.

Karachi Harbour Sub-Profile: The Karachi Harbour sub-profile (zone between Layari River Mouth & Naval Dockyard/Bhaba-Bhit Island) is the main recipient of pollution load brought by Layari River, its tributaries and the mangrove swamps. Total coliform counts are more than 300 per 100 ml in almost all the samples taken from the main harbour area during the lowest and the highest tidal conditions. These high levels of coliform render the harbour waters unfit for bathing activities. No uniform distribution of E.Coli was observed during the lowest tide conditions in the harbour area. Electrical conductivity is in the range of 44 - 50 mS/cm during the highest tidal conditions and 32 - 52 mS/cm during lowest tidal conditions. A decrease in E.C. at lowest tidal conditions is attributed to large scale mixing of Layari River outfall water with the Karachi sea water in the harbour area. Turbidity levels during calm sea regimes (January-December) are normally lower than the values for the rough sea period (August-September). In general, turbidity levels during high tide regimes are lower than the values measured for low tide periods due to dilution caused by inputs of relatively less turbid sea water. No specific differences in temperature were observed during the lowest to highest tidal conditions. It is apparent that the relatively more enriched $^{13}C_{TDIC}$ values in the Karachi Harbour channel at high tide conditions are replaced by quite depleted $\delta^{13}C_{TDIC}$ values at low tide condition, thereby, indicating a fair proportion of the pollution inventory from Layari River outfall area into the Karachi Harbour/Manora Channel during low tide regime. The physiochemical and bacteriological analysis have given a rough evaluation of the aerial extent of the polluted zone in the Karachi harbour area in response to mixing of Layari River water with the Karachi Sea water under high and low tide conditions. Further studies were carried out to identify the boundary of high and low pollution zones in the Karachi Harbour area during last hour of the low tidal regime (Table-II). For this purpose five pollution profiles were tracked across the Karachi harbour channel starting from the Karachi Port Trust building down to the Bhaba Island. Table-III presents the findings of this exercise. It is evident that the more polluted zone is characterized by fairly negative $\delta^{13}C_{TDIC}$ values. Slight increase in the $\delta^{13}C_{TDIC}$ values at the extreme of Layari Outfall Channel close to the KPT Shipyard boundary are attributed to the overspill and addition of relatively clean sea waters retreating from the Keamari Fish Harbour Channel at low tide condition. This influx of sea water in the Layari River Channel of Karachi Harbour zone may also be verified by a corresponding increase in the E.C. values for these samples.

Manora Channel Mains sub-profile: The Manora Channel Mains sub-profile (zone between Boat Club & Manora Lighthouse), electrical conductivity values range between 44.1 - 46.9 mS/cm during low tide conditions and 50.1 - 52.8 mS/cm during high tide conditions. Turbidity levels range between 7.9 - 19.4 NTU during low tide conditions and 2.1 - 14.3 NTU during high tide conditions. Similarly, coliform bacterial population ranges between 179 to 258 & >300 for high and low tide regimes respectively. No uniform distribution of E.Coli was observed during the lowest tide conditions in the harbour area and the Manora Channel Mains. Occasionally, the physiochemical and carbon isotope data of samples collected in the vicinity of Bhaba/Bhit Islands and Pakistan Naval Academy (PNA) are off-set due to influx of sewage from these residential zones. In order to further elaborate on the findings, samples were collected at three intervals during the low tide regime at various locations along the Manora Channel Mains. The first sample was collected as the high tide
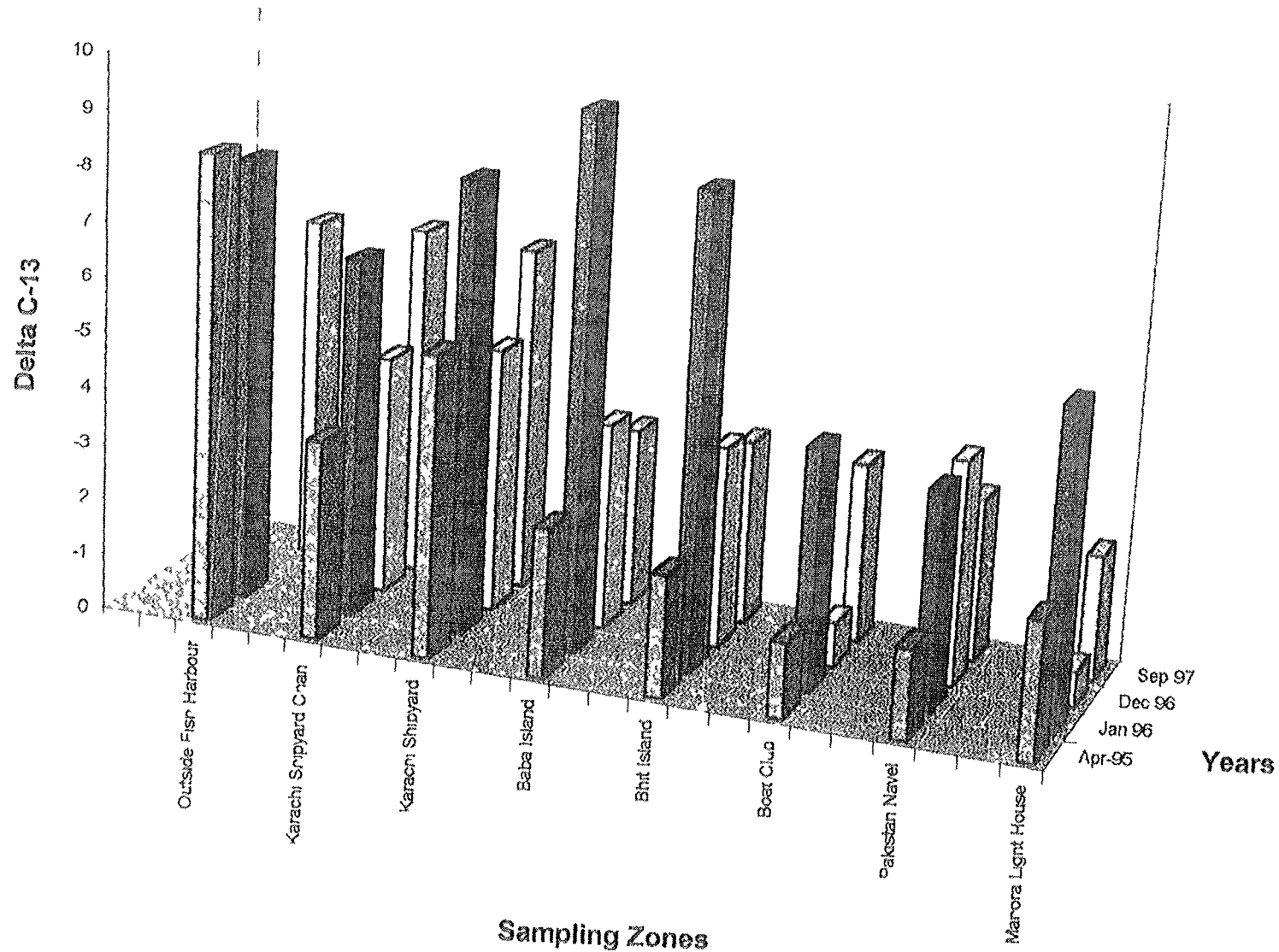
Fig. 3: Evolution of $^{13}C_{TDIC}$ in Karachi Harbour/ Manora Channel (1995-1997)

started lowering. The second sample was taken at the middle of low tide regime. The third sample was taken at the lowest of tide level. Results are presented in Table-IV. It is evident that pollution inventories at each measuring stations increase with the decrease in tide level. Further the severity of pollution decreases as we move out of the channel towards open sea.

Fig. 3 shows a overall scenario of evolution of $\delta^{13}C_{TDIC}$ values for the Karachi Harbour/Manora Channel for the four sampling phases under low tidal conditions.

3.1.2.2 Oyster Rocks-Manora Channel Exit Profile: Oyster Rocks are located in open sea close to entrance of Manora Channel facing Clifton beach. The *Oyster Rocks profile* includes stations namely: KPT Oil Jetty, Oyster Rocks and the shore-line facing National Institute of Oceanography (NIO) & Marina-Heights. Here electrical conductivity values range between 48.0 - 49.2 mS/cm during low tide conditions and 59.7 - 51.7 mS/cm during high tide conditions. Turbidity levels range between 4.8 - 7.9 NTU during low tide conditions and 2.0 - 3.9 NTU during high tide conditions. Total Coliform counts range between 0-35 counts per 100 ml and $\delta^{13}C_{TDIC}$ values range between -1.8 to -2.7 ‰ PDB during low tidal conditions. Although, this area is much flushed by open sea waters, slightly high proportions of pollution between NIO-Oyster Rocks & Marina-Heights are attributed to impact of waste discharge from local sewage drains near KPT Oil Terminal close to the end of Clifton Beach.

3.1.2.3 South-East Coast Pollution Profile: The South-East Coast of Karachi faces open sea and extends from Clifton beach near KPT Oil Terminal to Ibrahim Haideri Fish Harbour in Korangi Industrial area. Here, electrical conductivity values range between 42.9 - 46.5 mS/cm during low tide conditions (only up to Gizri Creek area) and 47.1 - 51.7 mS/cm during high tide conditions. Turbidity levels range between 3.6 - 11.7 NTU (only up to Gizri Creek area) during low tide conditions and 1.7 - 7.52 NTU during high tide conditions. Significantly high values of Coliform counts: ~100 to >300 are observed all along the coast. The $\delta^{13}C_{TDIC}$ data may be discussed in two sub-profiles. The *Clifton sub-profile* includes stations from Marina Plaza (White Pyramid Building) to start of Gizri Creek area. This area is quite flushed by sea tides.). Slightly high pollution levels near Naval Jetty are attributed to impact of waste discharge from local sewerage drains. During extreme low tide conditions, the $\delta^{13}C_{TDIC}$ of Clifton Casino is -4.39 ‰ and in Gizri Creek zone -8.1 ‰ PDB indicating significant pollution level. The *Korangi sub-profile* includes stations from start of Korangi area to Ibrahim Haideri Fish Harbour. Here, $\delta^{13}C_{TDIC}$ values are in the range of -1.05 to -6.79 ‰ PDB. Due to occurrence of a storm, it was not possible to collect low tide water samples in this area. However, samples collected at the shore-line during low tide regime indicate increasing pollution levels for various locations along this sub-profile. Tables-V present results of time evolution of pollution mixing trends at these locations. It appears that pollution levels increase during a shift from highest to lowest tide regime, thereby indicating influx of pollution from on-shore pollution sources.

3.1.2.4 North-West Coast Pollution Profile: The North-West Coast of Karachi faces open sea and extends from Manora Light-House (sea side) to Paradise/Sunehry Point area. Here electrical conductivity values range between 48.2 - 52.9 mS/cm during low tide conditions and 48.6 - 52.9 mS/cm during high tide conditions. Turbidity levels range between 1.5 - 2.7 NTU during low tide conditions and 0.9 - 1.5 NTU during high tide conditions. Significantly high Coliform counts are also observed. Here, $\delta^{13}C_{TDIC}$ values are in the range of +2.4 to -

Table-I Physiochemical and stable carbon isotope input functions of polluted rivers and pollution recipients along the coast of Karachi- Pakistan (1995-1997)

Sampling Zone		Temp. (Deg. C)	E.C. mS/cm	pH	Turbidity NTU	Total Coliform	$\delta^{13}C$ (‰ PDB)
Layari River Downstream (pre outfall in harbour)	Range	20 5-28 7	2 1-2 96	7 07	6 15-37 6	>300	-6 89 to -2 55
	Average (n=4)	24 2	2 56	7 07	20 5	>300	-5 22
Malir River (pre outfall)	Range	19 9-27 8	3 8-6 2	7 7	7 8-26 6	>300	-9 5 to -4 20
	Average (n=4)	24 05	4 84	7 7	16 58	>300	-7 40
Layari River Outfall (Karachi Harbour)	Range	20 2-27 8	21 5-52 7	8 14-36	4 2-68 3	>300	-10 22 to -4 3
	Average (n=13)	47 87	40 65	8 25	27 39	>300	-7 39
Ghizri Creek	Range	20 8-27 6	3 2-44 9	-	8 4-38 6	>300	-8 9 to -2 31
	Average (n=3)	24 275	23 36	-	22 83	>300	-5 72
arachi Sea	Range	20 1-21 2	52 9-55 6	-	1 06-6 7	~ 175	-0 79 to -0 60
	Average (n=4)	20 65	54 27	-	3 19	-	0 0625

* N D = Not measured

Table-II Physiochemical, bacteriological and stable carbon isotope analysis of water samples taken across apparent pollution mixing boundary in Karachi Harbour/ Manora Channel at lowest tide condition (Date 2-5-1995)

Profile Description	Latitude/ Longitude	E.C. (mS/cm)	Turbidity (NTU)	Total Coliform	$\delta^{13}C$ ‰ PDB
Bhaba Island					
Outside mixing boundary	N 24-49-35 E 66-57-55	52 4	5 6	NIL	-5 23
Inside mixing boundary within Layari channel	N 24-49-34 E 66-57-52	50 3	7 4	>300	-8 03
Naval Dockyard					
Outside mixing boundary	N 24-49-51 E 66-57-50	51 4	5 6	12	-10 49
Inside mixing boundary within Layari channel	N 24-49-53 E 66-57-51	49 6	10 5	>300	-9 45
Karachi Shipyard					
Outside mixing boundary	N 24-50-06 E 66-57-54	51 6	4 98	50	-18 14
Inside mixing boundary within Layari channel	N 24-50-07 E 66-57-54	50 8	9 8	>300	-11 08

194

Table-III δ^{13}C pollution profile tracking across Karachi harbour channel (April 1995)

Profile Description	Sampling time	Latitude	Longitude	E.C. (mS/cm)	Turbidity (NTU)	Total Coliform	δ^{13}C (‰ PDB)
PROFILE-1(A): Location: In between Boat building Area and Karachi Shipyard. Date: 30-4-1995							
Prior to apparent mixing boundary	1530 hrs	N 24-50-23	E 66-57-47	45 4	5 41	>300	-4 01
Prior to apparent mixing boundary	1540 hrs	N 24-50-20	E 66-57-52	53 4	5 25	36	-4 2
Just before mixing boundary	1550 hrs	N 24-50-19	E 66-58-00	49 5	16 2	>300	-6 72
At apparent mixing boundary	1600 hrs	N 24-50-18	E 66-58-04	43 4	29 8	>300	-9 58
Middle of Layari outfall channel	1610 hrs	N 24-50-15	E 66-58-05	46 5	11 8	>300	-9 47
Extreme of Layari outfall channel	1620 hrs	N 24-50-21	E 66-58-03	50 4	8 2	>300	-6 73
PROFILE-1: Location: Opposite Karachi Shipyard , Date: 26-4-1995							
Prior to apparent mixing boundary	1400 hrs	-----------	-----------	53 0	7 9	176	-4 42
Prior to apparent mixing boundary	1410 hrs	-----------	-----------	52 8	5 08	216	-5 64
At apparent mixing boundary	1415 hrs	-----------	-----------	53 8	6 02	> 300	-9 72
Middle of Layari outfall channel	1420 hrs	-----------	-----------	39 4	25 5	> 300	-10 22
Extreme of Layari outfall channel	1425 hrs	-----------	-----------	45 6	27 7	> 300	-8 6
PROFILE-2 Location: Karachi Shipyard close to Butti, Date: 30-4-1995							
Prior to apparent mixing boundary	1630 hrs	N 24-50-08	E 66-57-42	49 6	8 2	20	-4 42
Prior to apparent boundary	1635 hrs	N 24-50-03	E 66-57-51	51 7	8 4	24	-4 9
Just before mixing boundary	1642 hrs	N 24-50-01	E 66-57-57	47 4	18 5	NIL	-9 71
At apparent mixing boundary	1652 hrs	N 24-49-59	E 66-58-01	49 5	23 5	20	-10 62
Middle of Layari outfall channel	1711 hrs	N 24-50-01	E 66-58-04	51 6	9 5	>300	-9 59
Extreme of Layari outfall channel	1700 hrs	N 24-50-00	E 66-58-04	50 4	13 6	>300	-9 61
PROFILE-3 Location: In between Bhaba Island Mangroves and Shipyard/Navel Dockyard Boundary, Date: 30-4-1995							
Prior to apparent mixing	1515 hrs	N 24-49-49	E 66-57-29	46 1	9 4	36	-3 68
Prior to apparent boundary	1525 hrs	N 24-49-52	E 66-57-36	46 5	8 7	NIL	-5 23
Just before mixing boundary	1540 hrs	N 24-49-50	E 66-57-42	47 6	13 5	NIL	-3 22
At apparent mixing boundary	1550 hrs	N 24-49-51	E 66-57-46	49 9	20 4	>300	-6 83
Middle of Layari outfall channel	1600 hrs	N 24-49-54	E 66-57-59	50 4	19 4	20	-5 04
Extreme of Layari outfall channel	1630 hrs	N 24-49-53	E 66-58-06	48 4	13 6	54	-8 04
PROFILE-4 Location: In between Bhaba Island Jetty and end limit of Navel Dockyard Store, Date: 30-4-1995							
Prior to apparent mixing boundary	1630 hrs	N 24-49-32	E 66-57-48	49 4	13 2	>300	3 95
Prior to apparent boundary	1640 hrs	N 24-49-32	E 66-57-53	50 6	0 8	>300	-4 7
At apparent mixing boundary	1650 hrs	N 24-49-32	E 66-57-57	50 4	11 4	>300	-7 77
Middle of Layari outfall channel	1705 hrs	N 24-49-33	E 66-58-00	49 7	13 4	>300	-8 43
Extreme of Layari outfall channel	1715 hrs	N 24-49-33	E 66-58-05	51 4	11 2	>300	-7 43

Table-IV Physiochemical, bacteriological and stable carbon isotope analysis of lowest to highest tide water samples in Manora Channel mains (Date: 2-5-1995)

Tide Level	Collection time	E.C. (mS/cm)	Turbidity (NTU)	Total Coliform	δ ^{13}C ‰ PDB
Bhit Island Jetty	N 24-49-00 E 66-58-03				
Highest	1230 hrs	51 2	6 97	21	-4 03
Median	1530 hrs	50 9	7 2	42	-4 57
Lowest	1830 hrs	51 1	7 0	14	-7 48
Boat Club	N 24-49-34 E 66-58-08				
Highest	1230 hrs	52 1	6 73	15	-4 73
Median	1530 hrs	51 6	6 97	>300	-4 96
Lowest	1830 hrs	52	6 81	48	-5 63
Pakistan Naval Academy (PNA)	N 24-48-03 E 66-58-24				
Highest	1230 hrs	51 6	7 84	NIL	-4 78
Median	1530 hrs	51 2	7 92	7	-5 6
Lowest	1830 hrs	50 4	7 98	>300	-6 91
Manora Lighthouse	N 24-47-49 E 66-59-05				
Highest	1230 hrs	52 8	6 8	16	-3 44
Median	1530 hrs	51 9	7 2	42	-3 69
Lowest	1830 hrs	52 1	6 4	15	-4 53
Oyster Rocks Facing NIO	N 24-53-34 E 66-59-56				
Highest	1230 hrs	52 3	5 7	NIL	-3 5
Median	1530 hrs	51 1	5 89	46	-3 74
Lowest	1830 hrs	51 0	6 96	6 96	-3 74

Table-V Low tide δ ^{13}C evolution profile tracking along south east coast of Karachi (Sep. 1997)

Time	Korangi-Phatti zone	Ibrahim Haideri (Fish Harbour)	Ghizri Creek Zone	Ghizri Mouth Zone	Clifton Casino Zone	Clifton NIO Zone
0900	-2 71	-2 29	-4 71	-1 52	-2 96	-0 91
1030	-2 75	-2 52	-5 36	-2 /87	-3 72	-0 61
1200	-2 66	-2 51	-4 06	-2 87	N D*	-0 92
1400	-2 58	-1 83	-3 08	-2 56	-2 16	-1 34
1530	-3 52	1 67	-3 56	-2 84	-2 51	-0 30
1700	-2 07	-2 03	-2 53	-2 85	-3 95	-0 60

Table-VI Low tide δ ^{13}C evolution profile tracking along north west coast of Karachi (Sep. 1997)

Time	Manora Seaside Zone	Sandpit Seaside Zone	Buleji Seaside Zone	Power House Seaside Zone	Sunehry Point Zone
1000	-0 61	-0 86	-0 96	-0 70	-0 15
1200	-0 63	-1 77	-1 09	0 53	-1 59
1330	-1 63	-3 14	-0 66	-0 15	0 60
1500	-0 38	-0 41	-1 58	-1 11	-1 58
1630	-3 71	-0 63	-0 60	-1 33	-1 27
1800	N D *	-0 99	-0 76	-2 43	-0 85

N D * Not measured due to loss of sample

196

Table-VII $\delta\,^{13}$C and $\delta\,^{15}$N Composition of mangrove leaves and seaweeds in Manora Channel and along the Karachi coast.

Sample No.	Plant Type	Species Name	$\delta\,^{13}$C (‰ PDB)	$\delta\,^{15}$N % Air N_2
Manora Channel				
68	Sea Weeds	Ulva Spp (green)	-15 04	18 68
69	Sea Weeds	Ulva Spp (green)	-15 49	14 59
69 USP	Sea Weeds	Ulva Spp (green)	-14 31	9 73
70	Sea Weeds	Ulva Spp (green)	-15.55	9 13
71	Sea Weeds	Ulva Spp (green)	-17.29	7 84
72	Sea Weeds	Ulva Spp (green)	-13.39	N D
73	Sea Weeds	Ulva Spp (green)	-13.35	13.37
74	Sea Weeds	Ulva Spp (green)	-15.49	13 95
61	Mangrove	Avecinia marina	-27.85	12.28
62	Mangrove	Avecinia marina	-27 71	12.26
63	Mangrove	Avecinia marina	-26.95	10.47
64	Mangrove	Avecinia marina	-26.93	11.35
65	Mangrove	Avecinia marina	-26.72	6.18
66	Mangrove	Avecinia marina	-27.27	13 15
67	Mangrove	Avecinia marina	-27.51	8.32
Along Coast of Karachi				
Buleji				
26	Sea Weeds	Caulerpa manorensis (green)	-15.8	10.33
27	Sea Weeds	gracilara corticata (red)	-18.73	12.08
28	Sea Weeds	Staechospermum margimum (brown)	-14.01	10.76
29	Sea Weeds	Sargasaum tennirium (brown)	-17.11	9 79
30	Sea Weeds	Sargasaum lancedotum (brown)	-17.37	11 12
31	Sea Weeds	Spathoglossum varible (brown)	-14.47	10 08
32	Sea Weeds	Scinaia indica (red)	-18 6	10.95
33	Sea Weeds	halymenia porphyroid (red)	-31.12	7.78
34	Sea Weeds	Sargassum wightii (brown)	-13.73	11.16
35	Sea Weeds	Bangia atrupupurea (red)	-17.92	10.6
36	Sea Weeds	Coelarhrum muelleri (red)	-21.63	10.29
37	Sea Weeds	Halymedatuna (green)	-9.92	10 64
38	Sea Weeds	Laurencia piatifidaar (red)	-17.82	10 75
39	Sea Weeds	Sarcodia dichotoma (red)	-19.24	11.67
40	Sea Weeds	Gelidium usmangani (red)	-15.05	8 66
41	Sea Weeds	Chaetomorpha antinnen (red)	-15.49	10.26
42	Sea Weeds	Agardhilla robusta (red)	-21.06	10.2
43	Sea Weeds	Bryopsis pinnata (green)	-13.7	11 76
44	Sea Weeds	Sarconema furcellatum (red)	-19.53	10 35
45	Sea Weeds	Utotea indica (green)	-11.57	13 73
46	Sea Weeds	Caulerpa taxifolia (green)	-14.71	11 34
47	Sea Weeds	Petalonia fascia (brown)	-13.2	8 9
48	Sea Weeds	Enteromorpha compressa (brown)	-17.82	10 11
49	Sea Weeds	Deronema abbottiae (red)	-17.28	12 03

(Table-VII continued)

50	Sea Weeds	Gracilaria follifera (red)	-13.06	11.45
77	Sea Weeds	Ulva spp. (green)	-14.93	15.54
Pacha				
1	Sea Weeds	Codiuum elongatum (green)	-13.58	15.54
2	Sea Weeds	Valoniopsis pachyneum (green)	-13.29	17.76
3	Sea Weeds	Caulepa scalpelliformis (green)	-16.05	14.01
4	Sea Weeds	Ulva fasciata (green)	-4.91	14.03
5	Sea Weeds	Cystoseira spp. (red)	-12.95	12.62
6	Sea Weeds	Jania adherence (red)	-9.49	12.08
7	Sea Weeds	botryocladia leptopoda (red)	-25	13.87
8	Sea Weeds	Codium latum (green)	-13.4	11.87
9	Sea Weeds	Colpomenia sinuosa (green)	-8.8	10.75
10	Sea Weeds	Sargassum sqarrosum (brown)	-15.11	12.22
11	Sea Weeds	Lyengaria stellata (brown)	-8.94	12.99
12	Sea Weeds	Caulerpa peltata (green)	-21.14	10.16
13	Sea Weeds	Galaxura (red)	-11.35	11.79
14	Sea Weeds	Padina tetrastromatica (red)	-16.55	14.52
15	Sea Weeds	Gracelaria pygrnea (red)	-12.88	9.9
16	Sea Weeds	Padina pavonia (brown)	-10.02	9.09
17	Sea Weeds	Asparagopsis sandfordiana (red)	-19.44	13.35
18	Sea Weeds	Hypnea musciforrmis (red)	-14.69	12.57
19	Sea Weeds	Leurencia obtusa (red)	-17.41	11.57
20	Sea Weeds	Caulerpa racemosa (green)	-17.07	13.09
21	Sea Weeds	Dictyota dichoma (brown)	-15.76	12.6
Paradise Point				
22	Sea Weeds	Sargassum biveanum (brown)	-15.78	11.37
23	Sea Weeds	Champia compressa (red)	-14.68	10.94
24	Sea Weeds	Scinaia hattei (red)	-18.66	10.78
25	Sea Weeds	Hypea valentiae (red)	-15.07	10.97
78	Sea Weeds	Ulva Spp (green)	-14.87	11.39
79	Sea Weeds	Ulva Spp (green)	-14.67	9.32
Hawkes Bay				
75	Sea Weeds	Ulva Spp (green)	-14.54	10.25
76	Sea Weeds	Ulva Spp (green)	-14.08	9.75
Korangi Creek				
51	Mangrove	Avecinia marina	-28.2	9.51
52	Mangrove	Avecinia marina	-28.3	10.56
53	Mangrove	Avecinia marina	-27.57	11.4
54	Mangrove	Avecinia marina	-27.94	11.31
55	Mangrove	Avecinia marina	-27.37	7.16
54	Mangrove	Avecinia marina	-27.66	11.64
57	Mangrove	Avecinia marina	-27.88	10.79
58	Mangrove	Avecinia marina	-26.88	6.52
59	Mangrove	Avecinia marina	-27 97	7.91
60	Mangrove	Avecinia marina	-28.03	10.4

Table-VIII δ ^{13}C comparison of inorganic & organic fraction of bottom sediments and water (TDIC) Karachi harbour / Manora Channel

Sample Location	Latitude/ Longitude	δ ^{13}C (Inorg.) Sediment 95/96	δ ^{3}C (org.) Sediment 95/96	δ ^{13}C TDIC Low tide 95/96
Polluted Input Sources				
Layari River Downstream (Pre-Harbour outfall Zone)	N 24-52-27 E 67-52-01	-1.57 (-1.54)	-25.91	-9 57 (-6 89)
Malır River Downstream	N 24-49-27 E 67-05-31	N.D.	-12.77	N.D.
Layari River Outfall Area (Karachi Harbour & Manora Channel Backwaters)				
Layari River Outfall (Opposite Karachi Fish Harbour)	N 24-51-01 E 67-58-25	-2.77	-26.55	-3.41
Layari River Outfall (Shamspır Village Channel Side)	N 24-50-34 E 66-55-39	-1.25	-26.57	-8.00
Layari River Outfall (Kakkapır Village Backwaters)	N 24-50-05 E 66-55-35	-1.20	-26.40	-8.01
Layari River Outfall (Shamspır Village Backwaters)	N 24-49-50 E 66-57-27	-0.91	N.D.	N.D.
Karachi Harbour Mains				
KPT-Shipyard (Buttı), Karachı Harbour /Close to Layari Outfall	N 24-49-59 E 66-58-02	-0.59	-15.46	-7 43 (-8.16)
Boat Buildıng Area, Karachı Harbour (KPT Shıpyard Channel)	N 24-50-15 E 67-07-15	-1.91	N.D.	-8.39 (-6.46)
Kaemari Fish harbour (KPT Shıpyard Channel)	N 24-50-59 E 67-58-39	-4.52	-19.14	-8.01
Kaemari Boat Basın (Karachı Harbour Coast Guard Jetty)	N 24-48-58 E 66-38-30	-1.60	N.D	N D.
Mangrove Forest Turn Btw. Bhıt Island & Shamaspır (Khı. Harbour)	N 24-51-08 E 66-55-05	-1.87 (-1.82)	-18.01	-3.40
Manora Channel Mains				
Bhıt Island (Manora Channel)	N 24-49-10 E 66-58-00	-1.22 -0.56	-10.58	-3.53 -8.48
Bhaba Island (Manora Channel)	N 24-49-27 E 66-57-52	0.08 -0.24	-18.67	-5.34 -9.59
Kaemari oıl Termınal (Dredged Sample, Manora Channel)		-1.57	N.D.	N.D.
Boat Club (Manora Channel)	N 24-49-27 E 66-57-52	-1.18 -1.86	N.D.	-2.62 -4.27
Pakıstan Naval Academy (Manora Channel)	N 24-48-07 E 66-58-26	-0.68 -0.34	N.D.	-2.15 -3.85
Manora Lıghthouse (Manora Channel)	N 24-47-33 E 66-38-54	0.64 -0.68	N D.	-1.34 -5.61

199

Sample Location	Latitude/ Longitude	$\delta^{13}C$ (Inorg.) Sediment 95/96	$\delta^{3}C$ (org.) Sediment 95/96	$\delta^{13}C$ TDIC Low tide 95/96
Polluted Input Sources				
Layari River Downstream (Pre-Harbour outfall Zone)	N 24-52-27 E 67-52-01	-1.57 (-1.54)	-25.91	-9.57 (-6.89)
Malir River Downstream	N 24-49-27 E 67-05-31	N.D.*	-12.77	N.D.
Manora Channel Exit	N 24-47-33 E 66-38-54	0.64 -0.68	N.D.	-1.34 -5.61
North-West Coast				
PNS Himaliya (Karachi Sea, North-West Coast)	N 24-48-30 E 66-56-29	-1.61	N.D	-0.87
Sandspitt (Karachi Sea, North-West Coast)	N 24-49-15 E 66-55-23	-1.13	N.D.	-0.22
Kakkapir (Karachi Sea, North-West Coast)	N 24-49-55 E 66-53-55	-0.26	N.D.	-0 272
Buleji (Karachi Sea, North-West Coast)	N 24-49-04 E 66-50-41	-0.75	N.D.	-0 77
Power House South (Karachi Sea, North-West Coast)	N 24-50-13 E 67-47-56	-0.31	N.D.	-0 601
South-East Coast				
Oyster Rocks (Karachi Sea, South-East Coast, Clifton)	N 24-48-18 E 66-59-50	-1.21 -1.82	N.D.	-1.18
BTW NIO & Manora Lighthouse (Clifton Coast)	N 24-48-20 E 66-59-33	N.D.	N.D.	-2.67
BTW Oil Jetty & Oyster Rock (Clifton Coast)	N 24-48-12 E 66-59-22	-1.46	N.D.	1.89
Marina Heights-III, Clifton (Clifton Coast)	N 24-48-00 E 67-00-27	-1.39	N.D.	-1.926
Bhutto Casino, Central Clifton (Clifton Coast)	N 24-47-37 E 67-01-39	-2.16	N.D	-0.517
BTW Marina Club & Jetty (Defense Area Coast)	N 24-46-23 E 67-03-01	-1 92	N.D.	-0.376
Gizri Coast Area	N 24-45-16 E 67-03-35	-1.2 -1.4	-7.86	-0.44 (-2.75)
Ibrahim Haideri Jungle	N 24-46-01 E 67-07-15	-1.2	-13.9	-6.06 (-0.563)
Ibrahim Haideri Fish Harbour	N 24-47-03 E 67-08-39	-2.43	-12.84	-6.97 (-1.08)
Korangi Fish Harbour		-1 31	N.D.	-1 96
Korangi- Phitti Junction		-1.05	N.D.	-0.31

N D.   Not measured

200

Table-IX Toxic/trace metal concentration in bottom sediments of Karachi Harbour/ Manora Channel

Sediment Sample Location	Latitude / Longitude	Collection Date/ Depth	Mn %	Cr (ppm)	Cu (ppm)	Ni (ppm)	Pb (ppm)	Sr (ppm)	U (ppm)	V (ppm)	Zn (ppm)
Layari River Outfall Area											
Layari River Outfall (Karachi Harbour)	N 24°-51'-01" E 66°-58'-25"	29-4-95 (1.5 m)	0.03	293.00	N.D.	48.78	49.46	192.00	0 883	69.80	537.60
Layari River Outfall (Shamspir Village Channel side)	N 24°-50'-34" S 66°-55'-39"	20.-4-95 (1.2 m)	0.04	106.00	N.D.	32.40	22.41	297.00	0.975	64.80	111.40
Layari River Outfall (Kakapir Village Channel side)	N 24°-50'-05" S 66°-55'-35"	29-4-95 (1.2 m)	0.04	89.00	N.D.	36.99	21.88	339.90	0.658	60.00	85.00
Karachi Harbour Area											
KPT Shipyard (Butti) Karachi Harbour/ Close to Layari Outfall	N 24°-49'-59" S 66°-58'-02"	26-4-95 (2.5)	0.03	92.12	N.D.	1.53	18.93	449.05	1.041	45.64	83.94
Boat Building Area Karachi Harbour/ Close to Layari Outfall	N 24°-50'-21" S 66°-58'-03"	26-4-95 (3 m)	0.04	319.84	N.D.	56.46	33.84	307.77	1.660	88.26	666.28
Keamari Fish Harbour	N 24°-50'-59" S 66°-58'-39"	26-4-95 (3 m)	0.03	102.00	ND.	25.56	29.36	313.90	0.791	39.00	581.00
Manora Channel Mains											
Bhit Island	N 24°-49'-00" S 66°-58'-03"	26-4-95 (3.5)	0.05	70.00	N.D.	30.60	21.68	348.50	0.433	55.60	96.20
Bhaba Island	N 24°-49'-27" S 66°-57'-53"	26-4-95 (3.5 m)	0.04	80.00	N.D.	27.54	20.56	393.40	0.550	48.80	95.60
Keamari Oil Terminal	N 24°-48'-08" S 66°-59'-13"	26-4-95 (6 m)	0.06	82.00	N.D.	39.06	23.71	262.20	0.408	67.80	524.00
Light House (Manora Channel Inner Exit)	N 24°-47'-33" S 66°-58'-54"	26-4-95 (6.9 m)	0.03	14.00	N.D.	7.04	9.00	581.30	0.383	15.80	15.60

N.D.   Not measured

Table-X   Toxic/trace metal concentration in bottom sediments along the coast of Karachi.

Sediment Sample Location	Latitude / Longitude	Collection Date/ Depth	Mn %	Cd (ppm)	Cr (ppm)	Cu (ppm)	Ni (ppm)	Pb (ppm)	Sr (ppm)	U (ppm)	V (ppm)	Zn (ppm)
Karachi Sea South East Coast												
Btw. Oil Jetty/ Oyster Rocks (Clifton Coast)	N 24°-48'-12" S 66°-59'-22"	29-4--95 (3.5 m)	0.09	N.D.	85.00	N.D.	58.86	27.03	193.10	0.241	118.20	161.00
Bhutto Casino) (Clifton Coast)	N 24°-47'-32" S 67°-01'-39"	29-4--95 (4.5 m)	N.D.	0.21	33.01	16.09	46.06	22.4	N.D.	N.D.	N.D.	73.2
Naval Jetty (Clifton Coast)	N 24°-47'-04" S 67°-03'-01"	29-4--95 (7.5 m)	N.D.	0.14	25.79	13.41	43.37	19.12	N.D.	N.D.	N.D.	51.9
Btw Marina Club & Naval Jetty (Defence Coast)	N 24°-46'-23" S 67°-03'-01"	29-4--95 (6.4 m)	N.D.	0.11	26.54	13.49	46.46	10.61	N.D.	N.D.	N.D.	59.5
Ghizri Coast	N 24°-45'-23" S 67°-03'-39"	17-1-96 (7.4 m)	0.04	0.09	12.00 / 12.5	6.75	18.80 / 27.5	16.94 / 21.15	217.80	0.283	41.80	41.40 / 36.5
Manora Channel Exit												
Btw. NIO & Manora Lighthouse (Clifton Coast)	N 24°-48'-20" S 66°-59'-33"	29-4--95 (3.5 m)	0.05	N.D.	70.00	N.D.	43.65	22.92	216.00	0.191	97.60	119.60
Btw. Oil Jetty/ Oyster Rocks (Clifton Coast)	N 24°-48'-12" S 66°-59'-22"	29-4--95 (3.5 m)	0.09	N.D.	85.00	N.D.	58.86	27.03	193.10	0.241	118.20	161.00
Light House Manora Exit	N 24°-47'-53" S 66°-59'-04"	29-4--95 (3.5 m)	N.D.	0.18	19.23	18.56	38.46	21.15	N.D.	N.D.	N.D.	48.68
Karachi Sea North West Coast												
PNS Himaliya	N 24°-48'-30" S 66°-56'-29"	16-1-96 (8.3 m)	N.D.	0.08	23.69	15.63	37.91	21.5	N.D	N.D.	N.D.	49.25
Sandspit (Karachi Coast, North West Coast)	N 24°-49'-15" S 66°-55'-23"	16-1-96 (7.3 m)	0.04 / N.D.	N.D. / 0.11	33.00 / 15.0	N D. / 8.25	23.94 / 35.0	15.42 / 15	325.00 / N.D.	0.408 / N.D.	49.60 / N..D.	49.80 / 32.0
Buleji (Karachi Coast, North West Coast)	N 24°-49'-04" S 66°-50'-41"	16-1-96 (8.3 m)	0.06 / N.D	N.D. / 0.15	80.00 / 25.5	N.D. / 20.04	38.13 / 37.6	25.10 / 17.91	375.30 / N.D.	0.358 / N.D	88.50 / N.D.	80.40 / 45.8
Kakka pir (Karachi Coast, North West Coast)	N 24°-49'-55" S 66°-53'-55"	16-1-96 (9.6 m)	N.D.	0.10	18.18	8.78	36.66	17.71	N.D.	N.D.	N.D.	29.05
Power House (Karachi Coast, North West Coast)	N 24°-50'-12" S 66°-47'-56"	16-1-96 (5.8 m)	0 13	N.D.	20.00	N.D.	12.48	25.10	--	0.95	36.80	80.40

N D.   Not measured

0.81 ‰ during high tide condition and -0.61 to -0.82 ‰ during low tide conditions. There is also some suggestion of Layari River pollution input in Paradise Point area due to a circular movement of polluted breakwaters off Manora Channel. These results indicate that North-West coast of Karachi is much less polluted as compared to South-East Coast. This is due to the fact that North-West coast is not highly populated and industrialized. Also, pollution load of small villages on North-West coast is mostly drained to backwaters of Manora Channel except for a small strip near Paradise point. Tables-VI present results of time evolution of pollution mixing trends at various locations along the northwest coast during mid low to mid high tide regime. It appears that pollution levels at Manora seaside station, Sandspit seaside station and power house station start increasing after a shift from lowest tide to highest tide regime, thereby indicating influx of pollution from breakwater zone off Manora Channel exit. Occasional high shifts in the Buleji Seaside station are attributed to sudden input of waste from Buleji Village.

3.2   Sea plants pollution profile

3.2.1   Mangrove pollution: Table-VII presents the stable carbon isotope composition of mangroves (Avecinia Marina) leafs and seaweed samples (mainly species of Ulva). The $\delta^{13}C$ values of mangroves in the backwaters of Manora Channel range between -26.7 to -27.9 ‰ PDB and are quite in agreement with $\delta^{13}C$ values quoted in literature for the tropical mangroves in Malaysia [10]. However, Mangroves in the polluted Korangi Creek industrial area (facing open sea) are more depleted in ^{13}C (range: -26.9 to -28.3 ‰ PDB) as compared to Backwaters of Sandspit area. This depletion is attributed to high inputs of industrial waste related organic chemicals in Korangi Creek area. These $\delta^{13}C$ values will serve as reference to identify future inputs of pollution in mangrove growth areas along the coast of Karachi. $\delta^{15}N$ values of mangroves in the Manora Channel range between +6.2 ‰ to +13.2 ‰ air N_2 and are quite comparable with values for the Korangi Industrial area Creek Mangroves (+6.5 ‰ air N_2 to +11.6 ‰ air N_2.). These values suggests biological fixation of Nitrogen from manure/wastes deposited by Layari river and its tributaries in Manora Channel Backwaters as the $\delta^{15}N$ values of NH_4^+ & NO_3^- in manure/domestic waste range between +14 to + 17.3 ‰ air N_2 and +11 to +38.4 ‰ air N_2 [9].

3.2.2   Seaweed pollution: In Manora Channel, $\delta^{13}C$ values of seaweeds (mainly species of Ulva) lie in the range from -13.35 ‰ PDB to -17.29 ‰ PDB. A trend towards more negative $\delta^{13}C$ values indicates impact of pollution in their respective growth areas. In case of northwest coast, $\delta^{13}C$ values of seaweed (mainly species of *Ulva*) lie in the range from -4.9 ‰ PDB to -31.1 ‰ PDB (Table-VII). Large variations in $\delta^{13}C$ of seaweeds in Buleji and Pacha areas suggest incorporation of carbon from the domestic/industrial sources. Like mangroves, $\delta^{15}N$ values of seaweeds pertaining to Manora Channel & the inshore off northeast coast range between +7.84 ‰ to +18.68 ‰ air N_2 and suggest biological fixation of Nitrogen from manure/wastes deposited by Layari river and its tributaries in Manora Channel Backwaters and sewage drains in Buleji and Pacha areas along the northwest coast.

3.3   Sea bottom sediment pollution

3.3.1   Carbon Isotope Composition: Sediments pertaining to Manora Channel are fine sands with appreciable amounts of clayey fraction and micaceous minerals. The organic carbon in the sediments ranges around 0.45 %. The higher carbon contents are found in sediments of Karachi Harbour and Layari River outfall zone. Table-VIII shows a comparison of $\delta^{13}C$

values of sea bottom sediments and water samples in the study area. Clearly the inorganic $\delta^{13}C$ values of sediments are typical of marine shells and carbonate minerals. However, it is evident that relatively more depleted $\delta^{13}C$ values ranging between -1.25 to -4.52 ‰ PDB for inorganic carbon and -15.9 to -26.6 ‰ PDB for organic carbon are found in the Layari River outfall and the Karachi Harbour zone. The Manora Channel Mains has relatively enriched $\delta^{13}C$ values ranging between -0.34 to -1.86 ‰ PDB for inorganic carbon to -10.58 to -18.67 ‰ PDB. In this zone, more negative values of inorganic carbon are found in the zone between Bhit Island and Boat Club. Although more data related to organic carbon of sediments is yet awaited, it is clear that the entire harbour bottom sediments are polluted with organic waste derived from mangrove forests and the Layari River outfall zone.

Sediments pertaining to the northwest coast are more silty and contain fine to coarse sand with about 20 % calcium carbonate content. In contrast, sediments pertaining to Manora Channel exit and the south-east coast are fine sands with appreciable amounts of micaceous minerals, clayey fraction and comparatively low calcium carbonate content of about 10 %. The organic carbon in the sediments range between 0.24 % to 0.45 %. The higher carbon contents are found in in-shore sediments of southeast coast and the Manora channel exit. Table-V-III shows a comparison of inorganic and organic $\delta^{13}C$ values of sea bottom sediments and water samples in the study area. $\delta^{13}C$ values of Layari River downstream are in the range of -1.5 ‰ PDB for inorganic carbon and -25.9 ‰ PDB for the organic carbon. Along the coast, inorganic $\delta^{13}C$ values ranging between -0.3 to -2.43 ‰ PDB are typical of marine shells and carbonate minerals. Relatively more depleted inorganic $\delta^{13}C$ values ranging between (-1.05 to -2.43 ‰ PDB) are found in the sediments of southeast coast as compared to the northwest coast (-0.26 to -1.61 ‰ PDB). In the southeast, coastal sediments closer to the local waste drains are more depleted (-2.16 ‰ PDB near Bhutto Casino zone, -2.43 ‰ PDB near Ibrahim Haideri Fish Harbour). This is also reflected in the significantly depleted $\delta^{13}C$ values around -13 ‰ PDB. The input sources mainly, the Manora Channel exit has relatively enriched inorganic $\delta^{13}C$ values ranging between -0.34 to -1.86 ‰ PDB. Along the northwest coast, the Manora Island zone is characterized by relatively more depleted values of inorganic $\delta^{13}C$ values around -1 ‰ PDB. The remaining coast has inorganic ^{13}C values mostly below 0.3 ‰ PDB. This also shows that this part of Karachi sea is relatively least polluted.

3.3.2. Trace element analysis of sediments: Table-IX presents the minor & trace element concentrations in shallow sea bottom sediments in Manora Channel. It may be noted that significantly high average concentrations of Cr (89-319 ppm), Ni (1.5-56 ppm), Pb (9-49ppm), V (15-69 ppm) and Zn (15 - 581 ppm) are found in the Layari River outfall and Karachi Harbour zone. Similar concentrations of Cr (29-336 ppm), Ni (29-51 ppm), Pb (16-56 ppm) and Zn (71-170 ppm) have been found by the National Institute of Oceanography (NIO)-Karachi, in four samples of the Karachi Harbour area [3]. Karachi harbour is found to be the most polluted zone whereas, the Manora Channel Mains is relatively less polluted zone. These values are quite in agreement with the results obtained from $\delta^{13}C_{TDIC}$ composition. The presence of high concentration of these toxic metals in Harbour sediments is attributed to input of industrial waste effluents related to leather tanning industries, electroplating industries, battery material, waste from Karachi shipyard & Naval dockyard into the Karachi harbour area. For a small scale study in the Korangi-Phitti Creek, IAEA-Marine Environment Laboratory (Monaco) has reported concentrations of: Cr in the range of 2-19 ppm, Ni in the range of 3-7 ppm, Pb in the range of 3-13 ppm and V in the range of 4-13 ppm [1]. Concentrations of uranium (U) in Karachi sea sediments are not high. However, contents of U

in sediments pertaining to Layari River mouth area and Karachi Harbour area are higher as compared to sediments collected from Manora Channel entrance and areas facing open sea. Similar concentrations of Cr, Ni, Pb, V and Zn have been reported in the literature for Oman Harbour, Kuwait Harbour, Bahrain Harbour and Bombay Harbour [11].

Table-X presents trace element concentrations in selective shallow sea bottom sediments of Karachi Sea Southeast coast, Manora Channel exit and the northwest coast. It may be noted that significantly high average concentrations of Cr (12-85 ppm), Ni (18-58 ppm), Cu (6-16 ppm), Pb (10.6-27 ppm), Cd (0.09-0.21 ppm), U (0.241-0.283 ppm), Sr (193-217 ppm), V(42-118 ppm) and Zn (41.-161 ppm) are found in the Manora Channel Exit zone. Similar concentrations of Cr (20-26 ppm), Ni (35-42 ppm), Pb (19-21 ppm), Cu (11-17 ppm), Cd (0.14-0.215 ppm) and Zn (ppm) have been reported by the National Institute of Oceanography (NIO)-Karachi, in coastal sediments off Karachi [3, 11, M. Saleem, National Institute of Oceanography, unpublished data, personal communication]. The sediments pertaining to the southeast coast off Karachi have relatively high concentrations of these toxic elements except (Sr, U) as compared to the northwest coast. For a small scale study in the Korangi-Phitti Creek, IAEA-Marine Environment Laboratory (Monaco) has reported concentrations of: Cr in the range of 2-19 ppm, Ni in the range of 3-7 ppm, Pb in the range of 3-13 ppm and V in the range of 4-13 ppm [1]. Concentrations of uranium (U) in Karachi sea sediments are not high. However, contents of U in sediments pertaining to Layari River mouth area and Karachi Harbour area are higher as compared to sediments collected from Manora Channel entrance and areas facing open sea. The high concentrations of toxicity in sediments of southeast coast of Karachi are due to several factors. Firstly, Korangi-Phitti creek on southeast coast mostly receives domestic sewage, agrochemical wastes, industrial waste waters etc. Secondly, sediments along this coast have high contents of clayey matter which have in-turn high absorption or trapping capacity for metals. Thirdly, this distribution is due to impact of monsoons. During the winter (October - February), the northwest monsoon winds are relatively weaker, resulting in diminishing upwellings. The seawater from the nearshore and off-shore Indus Delta enters the coastal waters of Karachi from the southeast and moves along the coast towards the northwest or westwards and then to the western coast of Karachi. Thus, it moves in the southwest direction to the offshore area. During this type of a circulation pattern in the open sea, small clockwise gyres are developed along the beach. During the southwest monsoon (May - September), the dominant direction of seawater flow in the coastal waters of Karachi remains clockwise, i.e. the major flux of seawater from the offshore area enters the coastal waters of Karachi at the western part of the coast from the southwest direction. During this type of a circulation pattern in the open sea, small anti-clockwise gyres are developed along the beach. Due to weak speed of water in the winter monsoon and the south-west direction water movement in the summer monsoon, the contaminated water plume is not effectively spread in the direction of northwest coast. Thus metal rich water accumulates in the sediments of southeast coast and the Manora channel exit zone.

4.   CONCLUSIONS AND RECOMMENDATIONS

The present results clearly indicate that the inshore shallow sea waters off Karachi coast are being continuously polluted by input of unplanned and untreated disposal of industrial and domestic waste water into the Karachi sea via Layari River outfall. The physiochemical and bacteriological analysis have given a rough evaluation of the aerial extent of the polluted zone in the Karachi harbour area and the Manora Channel Mains in response to

mixing of Layari River water with the Arabian Sea water under high and low tide conditions. The mangrove ecosystem seems to play an important role in controlling the level of contamination in the Layari River outfall zone and the Karachi Harbour area in response to high tidal fluctuations. Nevertheless, the severity of pollution inventory decreases as we move out of Bhaba/Bhit islands towards the Manora Channel exit (open sea zone). This pollution is also reflected in the stable isotope composition of carbon (^{13}C) in TDIC pool, organic carbon in bottom sediments, mangrove leaves and seaweeds grown in the Layari River outfall area and the Manora Channel backwaters area. Some general conclusions and recommendations drawn from this study are as following:

(1) Environmental stable isotope techniques may be used as dynamic pollution indicators of coastal marine environments.

(2) Tidal fluctuations and monsoons play a key role in controlling the distribution of contamination inventories in shallow sea water off Karachi coast.

(3) Manora channel is the most polluted zone along the coast of Karachi, both during high and low tidal conditions.

(4) The southeast coast of Karachi is significantly polluted during low tide conditions since it receives polluted waters from Manora channel exit as well as from Malir river (Ghizri creek) and Korangi creek.

(5) The northwest coast of Karachi is least affected by polluted waters of Manora channel.

(6) Stable carbon and nitrogen isotope composition of sea plant leafs and sediments also reflect pollution inventories from industrial and domestic sources.

(7) The concentrations of toxic metals such as Pb, Ni, Cr, Zn, V are quite significant in sediments of Karachi harbour area Manora channel exit & Oyster rock zone due to input of industrial wastes/effluents into the harbour area via Layari river and transport of contaminated sediments from the southeast coast due to impact of monsoons.

(8) The continuous pollution inventories along the coast of Karachi will have adverse effects in terms of (i) increase in toxicity levels of marine food chain; (ii) considerable stress on fish habitat and mangroves; (iii) corrosion of cargo ships and navel vessels; and (iv) significant ill effects on the health of bathing tourists and inhabitants of Bhaba & Bhit islands, naval dockyard and Manora channel.

Immediate remedial actions are required to combat pollution inventories in the Manora channel-Karachi harbour area & other contaminated zones along the coast of Karachi. It is recommended that:

(1) All industrial units in Karachi must treat waste effluents prior to discharge into Layari river, Malir river, Gizri creek, Korangi creek or large volume local waste drains.

(2) Waste treatment plants should be installed downstream of Layari river and Malir river to eliminate pollution in the Karachi harbour and inshore waters off southeast coast of Karachi.

(3) More studies are required to track record of pollution inventories, areal distribution of pollutants and their impact on the marine food web and mangrove forests etc.

ACKNOWLEDGEMENTS

REFERENCES

[1]   MARINE POLLUTION BASELINE SURVEY IN THE KORANGI - PHITTI CREEK, PAKISTAN. Final Report of the IUCN Contract NO. OD/CDC/201/IAEA - Pakistan Baseline Survey, Project 9128. Prepared by the IAEA-Marine Environmental Studies Laboratory, International Laboratory of Marine Radioactivity, IAEA Oceanographic Museum, MC 98000, Monaco (November, 1987).

[2]   ALI, I; S. Jilani. Study of contamination in the coastal waters of Karachi. In: THE ARABIAN SEA, Living Marine Resources and the Environment (eds. M. F. Thompson, N. M. Tirmizi), Vanguard Books (Pvt) Ltd., 45 The Mall, Lahore, Pakistan (1995) 653-658.

[3]   KHAN, S. H., M. SALEEM., A preliminary study of pollution in Karachi harbour. In: Marine Science of the Arabian Sea. (eds. M. F. Thompson, N. M. Tirmizi), American Institute of Biological Sciences, Washington D. C. (1988) 539-547..

[4]   AHMED, M. An assessment of the magnitude of coastal pollution in Pakistan through a study of its fauna and fisheries. Thalassia Juglosl, 13, pp: 395-412 (1977).

[5]   QURAISHEE, G.S. Influence of the Indus River on the marine environment. In: International Conference on the Management of the Environment. pp: 111-112. Pakistan Academy of Sciences, Islamabad.

[6]   KHAN, A.A., Monsoon changes and paleoproductivity in Northwestern Arabian Sea sediments. In: THE ARABIAN SEA, Living Marine Resources and the Environment (eds. M. F. Thompson, N. M. Tirmizi), Vanguard Books (Pvt) Ltd., 45 The Mall, Lahore, Pakistan (1995) 587 - 598.

[7]   RIZVI, S.H.N.; T.M.A. KHAN; S.M. ALI; J. BAQUER. Circulation patterns in the Karachi coastal waters in relation to the outfalls. In: THE ARABIAN SEA, Living Marine Resources and the Environment (eds. M. F. Thompson, N. M. Tirmizi), Vanguard Books (Pvt) Ltd., 45 The Mall, Lahore, Pakistan (1995) 641-652.

[8]   GUIDEBOOK ON NUCLEAR TECHNIQUES IN HYDROLOGY, Technical Report Series No. 91 (1983 Edition), International Atomic Energy Agency (IAEA), Vienna, Austria (1983).

[9]   FRITZ, P., J. C. FONTES (Eds.), Handbook of Environmental Isotope Geochemistry, Vol. I, Vol. II, Elsevier, New York (1980).

[10]   RODELLI, M. R., J. N. GEARING, P.J. GEARING, N. MARSHALL, A. SASEKUMAR, Stable isotope ratios as a tracer of mangrove carbon in Malaysian ecosystems", Oecologia (Berlin), 61 (1984) pp:326-333.

[11]   SALEEM, M., G. N. QAZI, Distribution of trace metals in the sea-water and surficial sediment of the Karachi harbour. In: THE ARABIAN SEA, Living Marine Resources and the Environment (eds. M. F. Thompson, N. M. Tirmizi), Vanguard Books (Pvt) Ltd., 45 The Mall, Lahore, Pakistan (1995) 659 - 666.

USE OF STABLE ISOTOPES IN THE INVESTIGATION OF THE EFFECTS OF WASTEWATER REUSE ON GROUNDWATER IN MEXICO

P. J. CHILTON, M.E. STUART, W.G. DARLING
Hydrogeology Group, British Geological Survey,
Wallingford, United Kingdom

Abstract - *Agricultural irrigation with wastewater is widely practised in Mexico, often in areas where the underlying aquifers are used for potable water supply. Studies in two areas of the country have examined the fate and behaviour of contaminants from untreated wastewater. The use of $\delta^{18}O$ and δ^2H isotopes was integrated with hydrogeological techniques such as core drilling, geophysics, major ion and trace element analysis of water samples, soil sampling and simple modelling. In both study areas, the isotope data helped to confirm the hydrochemical results. Conventional plots of δ^2H and $\delta^{18}O$ provide indications of altitude differences and evaporation processes in looking at sources of recharge. Plotting $\delta^{18}O$ against chloride provides a convenient way of distinguishing groundwater types. In León, isotopic data confirmed that recharge to the deep volcanic-rock aquifer underlying the area of wastewater irrigation came partly from the surrounding mountains where this formation outcrops. In the Mezquital Valley, recharge to groundwaters beneath the valley floor originates from infiltration of wastewater. Comparison with data from 25 years ago indicated that isotopic compositions at some locations have become significantly less depleted in $\delta^{18}O$, suggesting that the contribution from irrigation water had increased. The study has demonstrated the importance of establishing good conceptual models at an early stage of such investigations, particularly where multiple and changing sources of groundwater recharge are anticipated.*

1. INTRODUCTION

Water is a scarce resource in semi-arid regions, such as north and central Mexico. The very rapid urban growth of recent decades has produced increasing demands for potable water, and the need for greater food production is readily apparent. As a result of this growth and industrialisation, surface water resources are either fully utilised or now of poor quality. The improved coverage in large cities of water-borne sewerage systems produces enormous volumes of wastewater for disposal, and increasing recognition is being given to the value of wastewater as an important resource. The use of wastewater for irrigation is well established and strategies for improved management are likely to be required. The principal benefit of water reuse is the conservation of natural water resources, with more water being available to grow crops. Properly planned reuse of wastewater can alleviate surface water pollution and take advantage of the nutrients for crop growth.

Stable isotope studies have comprised an integral component of two major, multidisciplinary projects. The present paper is focused on the isotope component, drawing on the wider hydrochemical studies as required for clarity and when appropriate for the interpretation of results. In low-temperature hydrogeological environments, the main use of oxygen and hydrogen stable isotopes is to provide information on the physical processes which groundwaters have been subjected to. The two main processes which could be operating in these cases are those caused by altitude differences and by evaporation. The first

of these is indicated by an increase in heavy isotope depletion in rainfall from greater altitudes. In practice, this means that $\delta^{18}O$ and δ^2H values become more negative when recharge occurs at higher altitudes.Typical altitude-related depletions are of the order of 0.25‰ $\delta^{18}O$ and 2‰ δ^2H per 100 m. However much the altitude of origin may change, the isotopic content of recharge should fall on the local $^{18}O/^2H$ meteoric slope. With evaporation, however, isotopic ratios are enriched along gradients with generally a lower slope of around 5 for open water and as low as 2 for soil water evaporation. Most groundwaters showing signs of evaporation are the result of comparatively rapid infiltration of previously-ponded surface water, and tend to fall on slopes with gradients of 4-5. The stable isotopes of water are, therefore, well suited to assist investigations in which the hydrogeology is complex and in which it is anticipated that there may be several sources and mechanisms of recharge. They can provide additional insight into these mechanisms, particularly when used in conjunction with conventional inorganic hydrochemical results, as in the present studies.

The overall objective of the investigation was to determine the effects of wastewater reuse for irrigation on the underlying groundwater, under conditions typical of semi-arid regions. The possible impacts from increased recharge, and in terms of deterioration in groundwater quality, were examined in two areas of Mexico. The specific objectives were to:

- determine the influence of wastewater irrigation on groundwater recharge, flow and discharge regimes,

- identify controls on groundwater quality and the effectiveness of infiltration through the soil in attenuating pollutants originating in the wastewater,

- establish whether the groundwater systems were in equilibrium with respect to quality, and

- define requirements for protecting groundwater quality.

The work was carried out under the technical cooperation programmes of the UK Department for International Development and the European Commission. Therefore, developing methodologies for such studies which could be taken up by partners from the National Water Commission of Mexico was also an important objective.

2.   WASTEWATER REUSE AND GROUNDWATER

Reuse of wastewater can have major impacts on groundwater. In some situations, the substantial volumes of additional recharge may completely alter the local hydrogeology. Perched aquifers and new groundwater flow regimes and discharge points may be created. Impacts may be simultaneously positive in terms of water resource conservation and negative as some degradation of groundwater quality can be expected. Municipal wastewater generally contains high concentrations of dissolved inorganic and organic constituents. The content of nitrogen, phosphorus and potassium, as well as many micronutrients is likely to be high enough to supply crop requirements, and excess nutrients in the water infiltrating beneath the fields can produce unacceptable groundwater pollution with either ammonium or nitrate. Other inorganic constituents such as sodium, chloride and sulphate may be present at concentrations which could pose a threat to groundwater quality. Domestic wastewater can contain some trace heavy metals, but these may reach much higher concentrations where there

210

is a substantial component of industrial effluent in municipal wastewater. In this case, organic compounds such as the chlorinated solvents may also be present in the wastewater. The contaminants which are probably of most immediate concern are pathogenic micro and macro organisms. Those which are most persistent in the subsurface environment and have a low minimal effective dose will pose the greatest risk to potable water supplies.

Thus, improper disposal of untreated wastewater directly into aquifers which are also used for water supply could cause serious health risks. On the other hand, properly controlled and managed disposal of untreated or partially-treated wastewater at the ground surface for irrigation can provide significant additional resources of acceptable quality water. However, adequate knowledge of the hydrogeology, infiltration processes and movement and natural attenuation of pollutants is required for effective design and management of such systems. The two projects were designed to obtain such knowledge, and the way in which the isotope studies contributed is described in the following sections of the paper. Full descriptions of the main studies are given in BGS et al. (1996, 1998) and Chilton et al. (1998).

3. LEON

3.1 Physical and Hydrogeological Setting

The city of León, in Guanajuato State, is situated in a wide upland valley at an altitude of 1800 m, about 500 km north of Mexico City. It has one of the fastest growing populations in Mexico, currently about 1.2 million, which is highly dependent on groundwater resources for public water supply. The climate is semi-arid, with an average annual rainfall of about 600 mm, so there is also a heavy dependence on irrigation for agricultural crops. As is commonly the case for intermontane basins such as this, the highly variable geology produces complex hydrogeological conditions. The basin is underlain by a sequence of acid volcanic, lacustrine and alluvial deposits. Within this sequence, ignimbritic tuffs form a complex regional aquifer, which also outcrops on the valley flanks. Groundwater is drawn from this complex aquifer system within and downstream of the city, including areas which have been subjected to wastewater reuse for agricultural irrigation for up to 40 years (Figure 1). Groundwater is also heavily exploited for agricultural irrigation and for industrial activities. As a consequence of the heavy abstractions, falling groundwater levels have been observed for some years in the area to the south of the city. In the area of heaviest abstraction, levels are falling by 1-3 m/a, and the total decline may be of the order of 90 m between 1959 and 1995 (Chilton et al., 1998). In contrast, in the area of wastewater irrigation, groundwater levels are within 5-10 m of the ground surface and are relatively stable, indicating the influence of the additional infiltration from the irrigated fields.

A conceptual model of the evolution of groundwater conditions in the valley is suggested in Figure 2, in which a) represents the initial conditions with a relatively shallow regional water table and natural recharge on the valley floor and from the mountains. As the population increased, groundwater usage for potable supply and irrigation grew, and the wastewater collected from the city began to be used for irrigation. Sketch b) represents conditions around 15-20 years ago. More recently, the increased abstraction for public supply and irrigation has produced the drawdowns referred to above and the cone of depression shown in c). Beneath the area of wastewater irrigation, downward hydraulic gradients could be induced close to the deep pumping boreholes, and this would encourage deeper penetration of poorer quality water.
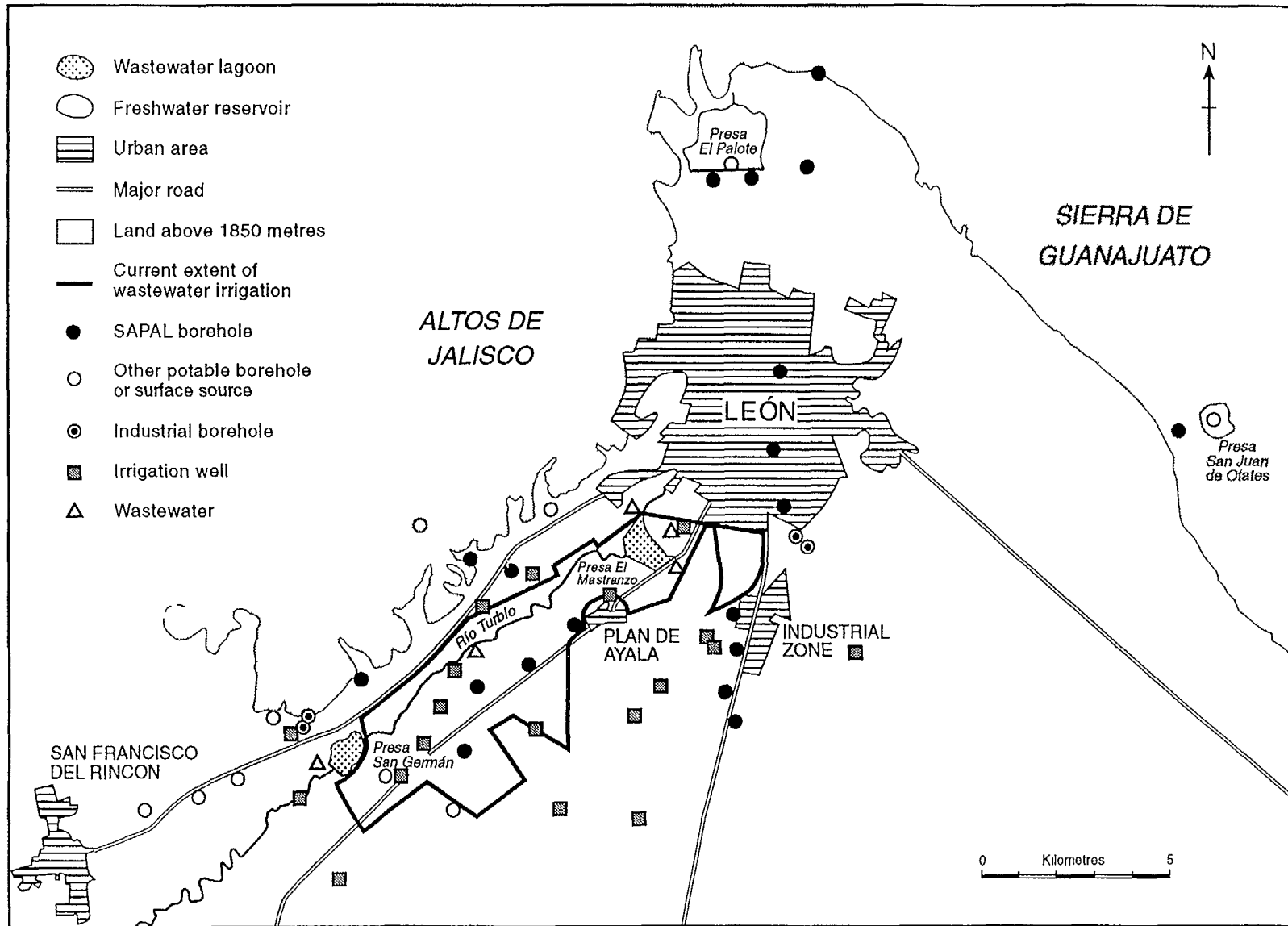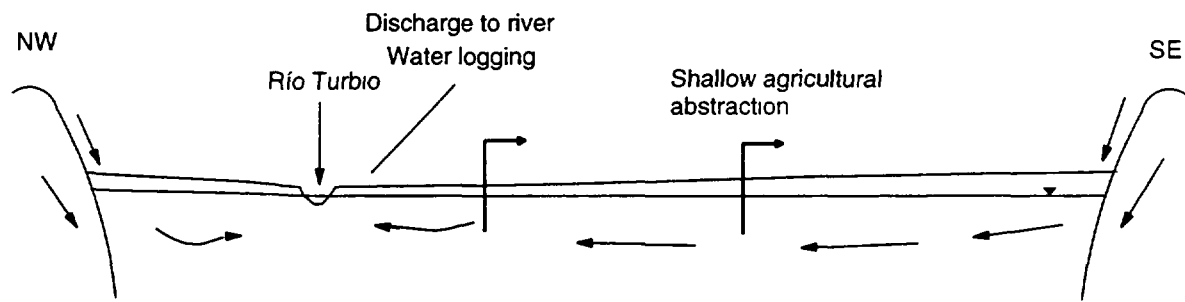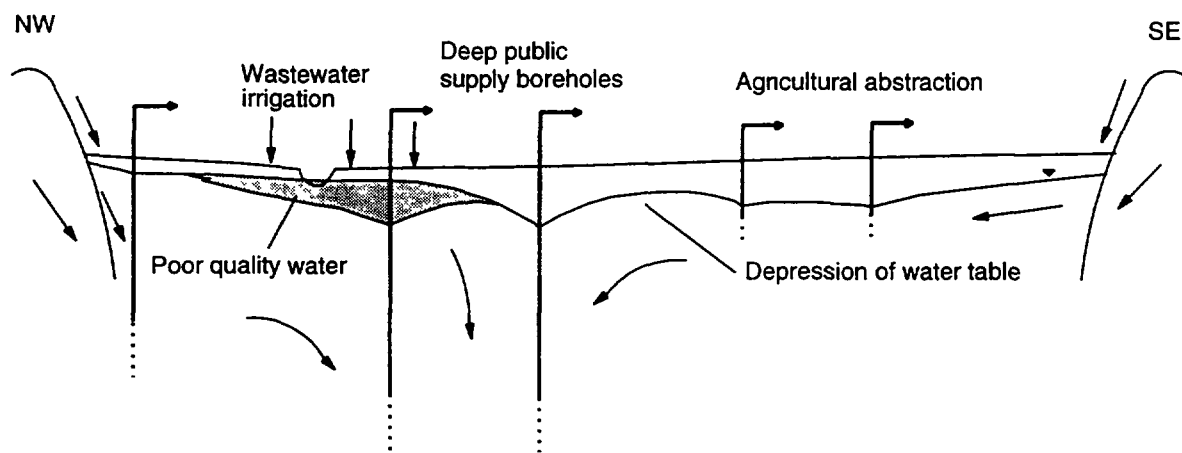
Legend:

- Wastewater lagoon
- Freshwater reservoir
- Urban area
- Major road
- Land above 1850 metres
- Current extent of wastewater irrigation
- SAPAL borehole
- Other potable borehole or surface source
- Industrial borehole
- Irrigation well
- Wastewater

SIERRA DE GUANAJUATO

ALTOS DE JALISCO

Presa El Palote

LEÓN

Presa San Juan de Otates

Presa El Mastranzo

Río Turbio

PLAN DE AYALA

INDUSTRIAL ZONE

SAN FRANCISCO DEL RINCON

Presa San Germán

0 Kilometres 5

FIG. 1: Groundwater and wastewater sampling sites in the León valley.

a) Original conditions

b) Development of shallow aquifer and regional falling water levels
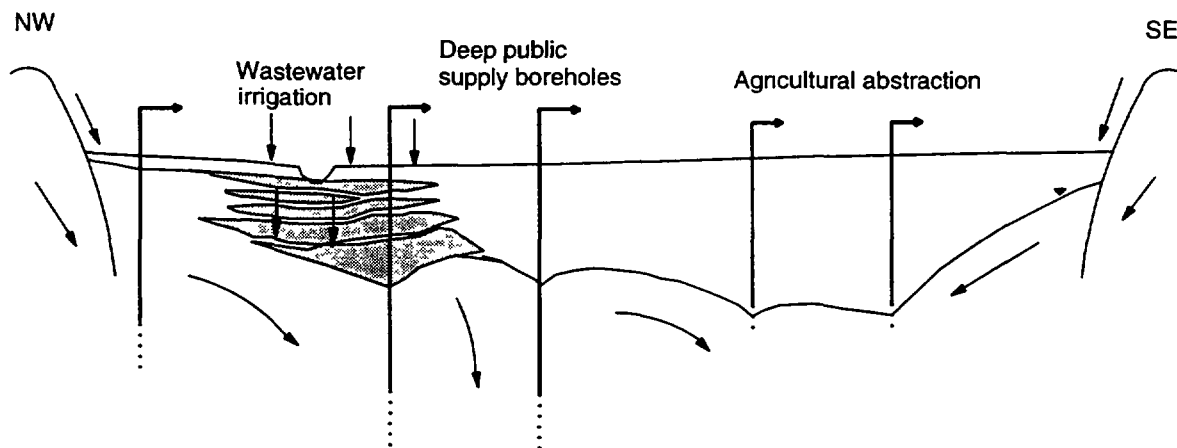
c) Present situation

FIG. 2. Conceptual evolution of the groundwater system in the León valley.

León generates wastewater which is likely to be highly polluting due to effluent derived from the leather processing and shoe manufacturing industry, which is one of the most prominent in Latin America. Several of the leather manufacturing processes carried out at the more than 500 individual premises give rise to highly polluting effluents. Sodium chloride, used to preserve hides before tanning, and hexavalent chromium used in curing are of particular concern. These effluents are combined with domestic wastewater via sewers which feed into a series of open canals carrying the wastewater directly into the irrigation area. About 85% of the city's population is provided with mains sewerage, and some 2600 to 2900 l/s of wastewater is used to irrigate about 3000 ha of land to the south-west of the city along the Rio Turbio (Fig.1).

3.2   Sampling

Groundwater quality in the study area was determined by means of a programme of regular sampling to provide representative geographical coverage of the city and surrounding rural areas and zone of wastewater irrigation, and of the deep and shallow parts of the aquifer sequence. Sampling included supply boreholes of SAPAL - the municipal water undertaking, private boreholes and wells and the lagoons and canals of the wastewater distribution system (Fig.1).   Samples were collected two or three times each year during the project for major ions, minor ions, trace elements and faecal coliforms. In all, some 45 water samples were collected in 1993 and 1994 for stable isotope analyses, which were carried out at the laboratories of the British Geological Survey.

3.3   Results and Discussion

The regular sampling indicated that regional groundwater quality in the sequence of volcanic and lacustrine aquifers is good, consistent with its meteoric origins. Overall background levels of mineralisation are low, and this allows groundwater affected by infiltrating wastewater to be readily distinguished from unpolluted waters (Chilton et al., 1998) by the elevated concentrations of most major ions, including calcium, sodium, bicarbonate, chloride, sulphate and nitrate and by low dissolved oxygen. Comparison of groundwater chloride concentrations in the vicinity of the Rio Turbio in 1984 and 1994 (Chilton et al., 1998) indicates the rapid growth of the area of shallow groundwater affected as the wastewater irrigation has extended south-westwards along the course of the river (Fig.1).

Plotting δ^2H against $\delta^{18}O$ in the conventional way (Fig. 3) demonstrates that the greatest isotopic depletion, which is normally associated with recharge originating at the highest altitude, is found in groundwater samples from the south and south-east of the study area, beyond the area of wastewater irrigation. These are the open squares towards the left side of Figure 3. This supports the conceptual model that the ignimbritic aquifer deep beneath the valley floor is recharged predominantly by infiltrating rainfall where this formation is exposed in the surrounding mountains (Figs. 1 and 2). Samples from closer to the high ground on the northern edge of the Turbio Valley (Fig. 1) appear to be recharged more locally. Waters which are unaffected by post-precipitational modification can be regarded as those which are more depleted than about -10‰ $\delta^{18}O$ and -70‰ δ^2H. On this basis, all of those waters which are affected by such modification lie within the area of wastewater irrigation, or are associated with surface water.
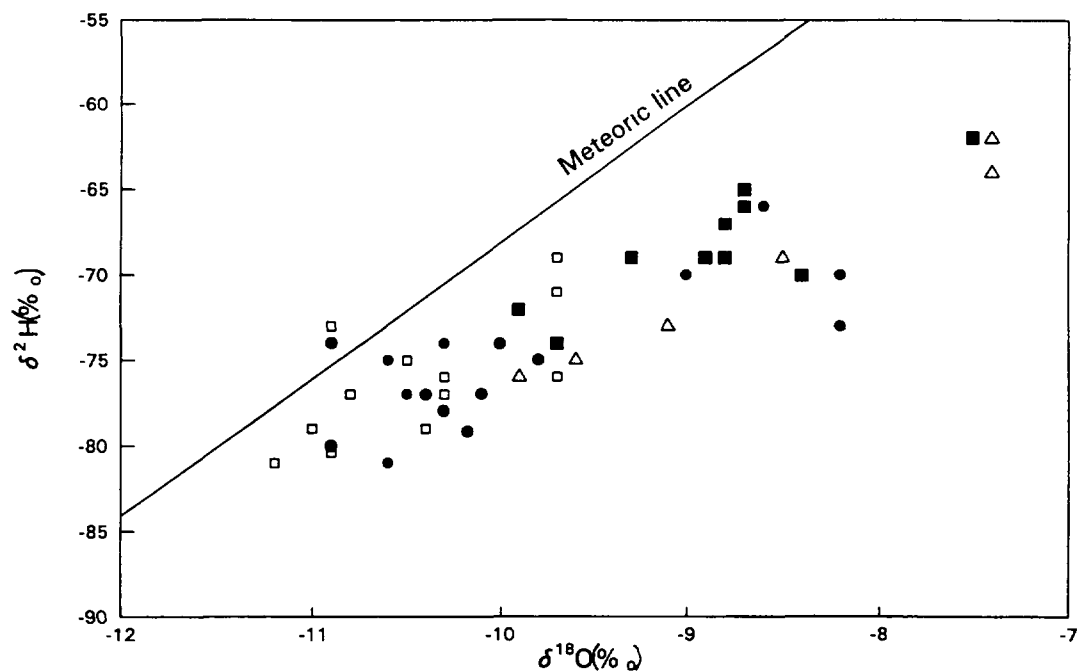
214

● Potable supply wells   ■ Irrigation wells in wastewater area

△ Wastewater   □ Irrigation wells outside wastewater area

FIG. 3. Conventional plot of δ^2H against δ^{18}O for León samples.
See Figure 4 for legend.
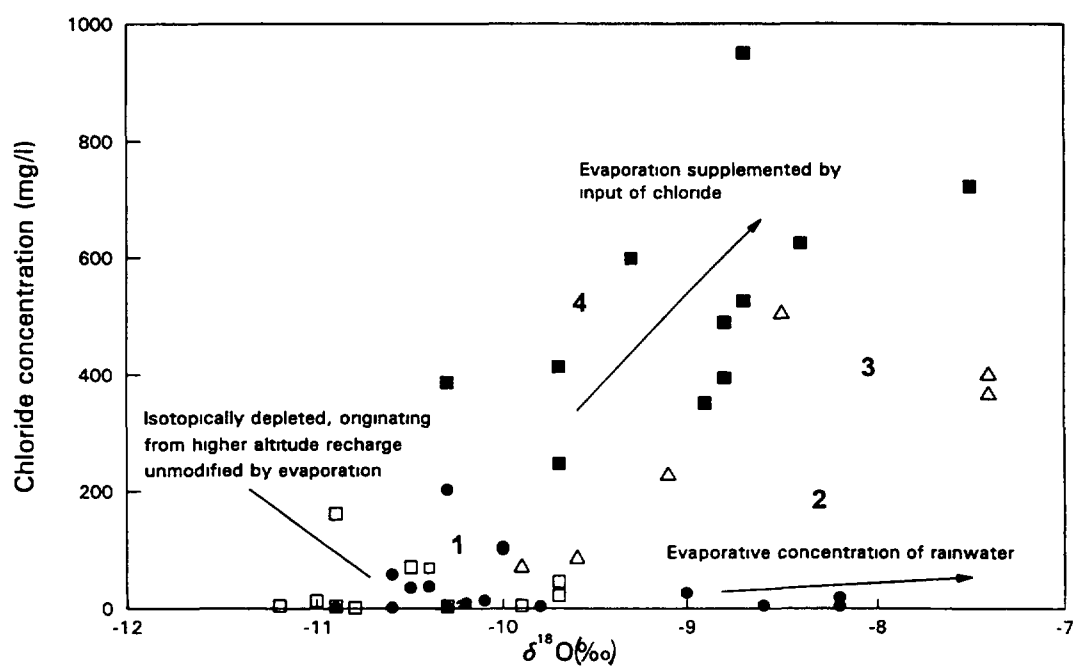
● Potable supply wells   ■ Irrigation wells in wastewater area

△ Wastewater   □ Irrigation wells outside wastewater area

FIG. 4. Chloride concentrations against δ^{18}O for León samples.

Plotting chloride concentration against $\delta^{18}O$ allows the sampled waters to be resolved into the four main types numbered on Figure 4:

1) waters apparently unmodified by evaporation, more depleted than -10‰ $\delta^{18}O$ and almost always having less than 100 mg/l chloride;

2) waters to the north of the city (Fig. 1) from wells of the SAPAL city wellfield, which are apparently related to simple evaporative concentration of rainfall which alters the $\delta^{18}O$ and to a lesser extent the δ^2H more noticeably than the chloride concentration;

3) wastewaters in which evaporative concentration of $\delta^{18}O$ and chloride has been supplemented by further input of chloride from anthropogenic sources;

4) a similar but rather more widely-scattered set of groundwaters which appear isotopically not to be more evaporated than the wastewaters, but have generally higher chloride concentrations.

Most of the samples forming the last of these types are from within the area of wastewater irrigation (solid squares on Fig. 4) and their chemical and isotopic compositions imply significant impact of wastewater infiltration on the underlying groundwater and penetration of poor quality water to the intake horizons of the irrigation wells and boreholes. The public supply boreholes within and close to the area of wastewater irrigation remain in the first group listed above, even including borehole Turbio 2 with its elevated chloride concentration (Stuart and Milne, 1997).

Four samples were collected for ^{13}C analysis. Although there are few data, the following points can be made. From the two groundwater samples collected outside the area irrigated with wastewater, the background $\delta^{13}C$-DIC values are similar at -9.16 and -9.34‰. This is thought to represent a simple case of reaction between soil CO_2 at around -16‰ (as the freshwater-irrigated plants such as maize are C_4 types, which produce CO_2 which is significantly "heavier" than that from most other plants) and carbonate minerals in the range -3 to 0‰, without further exchange reactions having taken place. In the area of wastewater irrigation, plant CO_2 may be supplemented by CO_2 from the oxidation of waste organic matter. If there were some organic matter with the more usual $\delta^{13}C$ signature of around -26‰, it would explain the somewhat more negative $\delta^{13}C$-DIC value of -10.71‰ of the groundwater sample from the outer, more south-westerly part of the irrigated area (Fig. 1). The heavier value of -7.26‰ from the centre of the area of wastewater irrigation is either a sign of long residence time (leading to exchange with carbonate minerals) or, more likely, dissolution of sodium carbonate crusts which would have a "heavy" value owing to exchange with the atmosphere. The sodium concentration of this sample is indeed significantly higher than that of the other samples. More data would be required for a more confident interpretation.

4. THE MEZQUITAL VALLEY

4.1 Physical and Hydrogeological Setting

The Mezquital Valley contains one of the largest and oldest schemes for agricultural irrigation using urban wastewater in the world, having commenced in 1896 and grown
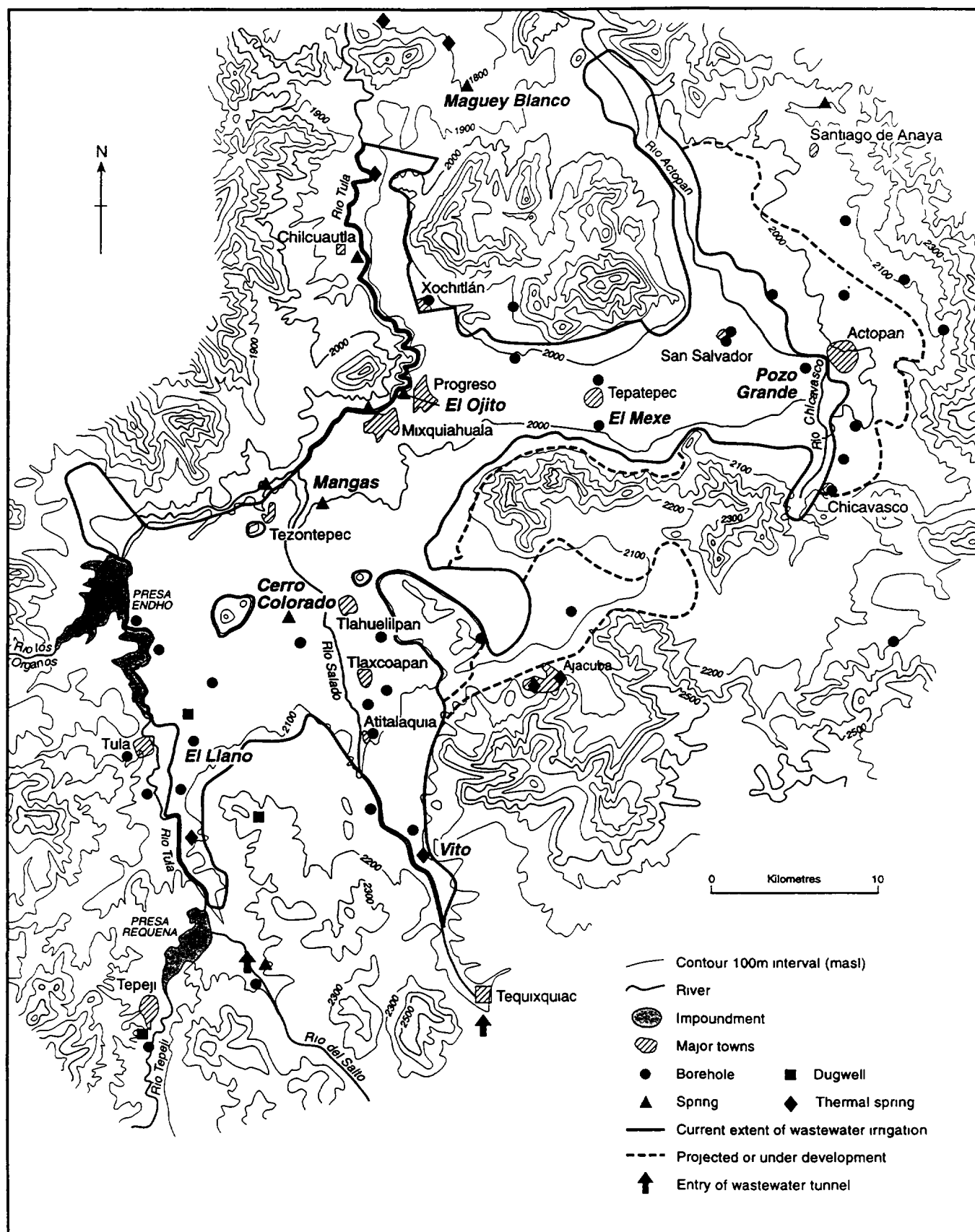
216

FIG. 5. Sampling sites in the Mezquital Valley.

217

steadily since with the expansion of the city and greater availability of wastewater. The valley is situated in the south western part of Hidalgo State, about 50 km north of Mexico City, from which it currently receives about 70% of the sewage effluent from an estimated population of over 20 million. Presently about 40,000 l/s of wastewater are used to cultivate some 45,000 ha of previously semi-arid land (Fig. 5). This effluent constitutes the main source of water sustaining all development in the Mezquital Valley, which has very limited natural water resources.

Canals and tunnels convey the wastewater through the interfluve from Mexico City. A complex system of reservoirs, principal canals and laterals has been developed to control and distribute the water to the irrigated land. The reservoirs collect some freshwater from surrounding hills and mountains. Distribution losses from the wastewater canal system and infiltration from the irrigated land have resulted in increased groundwater recharge, creating a new aquifer system in an area of previously limited groundwater resources. This provides the potable water-supply for the estimated 500,000 people living in the area. Groundwater levels have risen and new groundwater discharge zones and springs have appeared. There are also now localised problems of soil water logging and salinisation in some of the groundwater discharge zones. Extensive lining of canals was carried out in the 1980s and 1990s.

Like León, the climate is semi-arid, with an annual rainfall of about 450 mm on the valley floor, rising to 600 mm over the surrounding hills. The general geological setting is similar to that of León, with the result that the hydrogeology of the valley is complex, consisting of a series of multilayered aquifers with the general directions of groundwater flow from south to north in the west of the valley (Fig. 5), associated with the Rivers Tula and Salado and to the east in the eastern part of the valley towards the River Actopan. Thermal springs are present at the southern edge of the valley at Actopan and Vito and beyond the northern limits of the valley (Fig. 5). Further details of the hydrogeology are given in BGS et al. (1998).

Because the wastewater system is so long-established, no data exist for the natural conditions. The conceptual hydrogeological model (Fig. 6) suggests that the natural groundwater system would have been maintained by limited groundwater recharge either by infiltration of storm runoff at the valley margins or by subsurface inflow, supplemented by limited direct infiltration from occasional storms on the valley floor. Local base levels and controls on groundwater discharge would have been provided by the incised valley of the River Tula (Fig. 6a) and the Actopan, and groundwater levels would have been relatively deep (>50 m) over much of the valley. The prolonged irrigation with wastewater has completely modified the groundwater recharge and flow regime, in effect creating a new shallow aquifer system (Fig. 6b). Infiltration from the distribution system and the irrigated land came to dominate the recharge on the valley floor. Although the early stages of this process cannot be confirmed by observations, it is clear that rising groundwater levels and new spring discharges have resulted. As this new groundwater system became established, more new discharge points were created and groundwater levels in some discharge areas have reached the ground surface, causing local waterlogging and salinisation (Fig. 6c).

As early as 1962, there was concern about degradation of groundwater quality and chemical analysis of shallow groundwater in the Mezquital valley showed contamination by wastewater. A study carried out on behalf of the IAEA by Payne (1976) concluded that the Cerro Colorado spring, the most significant source for public water supply in the valley, now contained a significant proportion of irrigation water. Further work in the 1980s (Del Arenal,
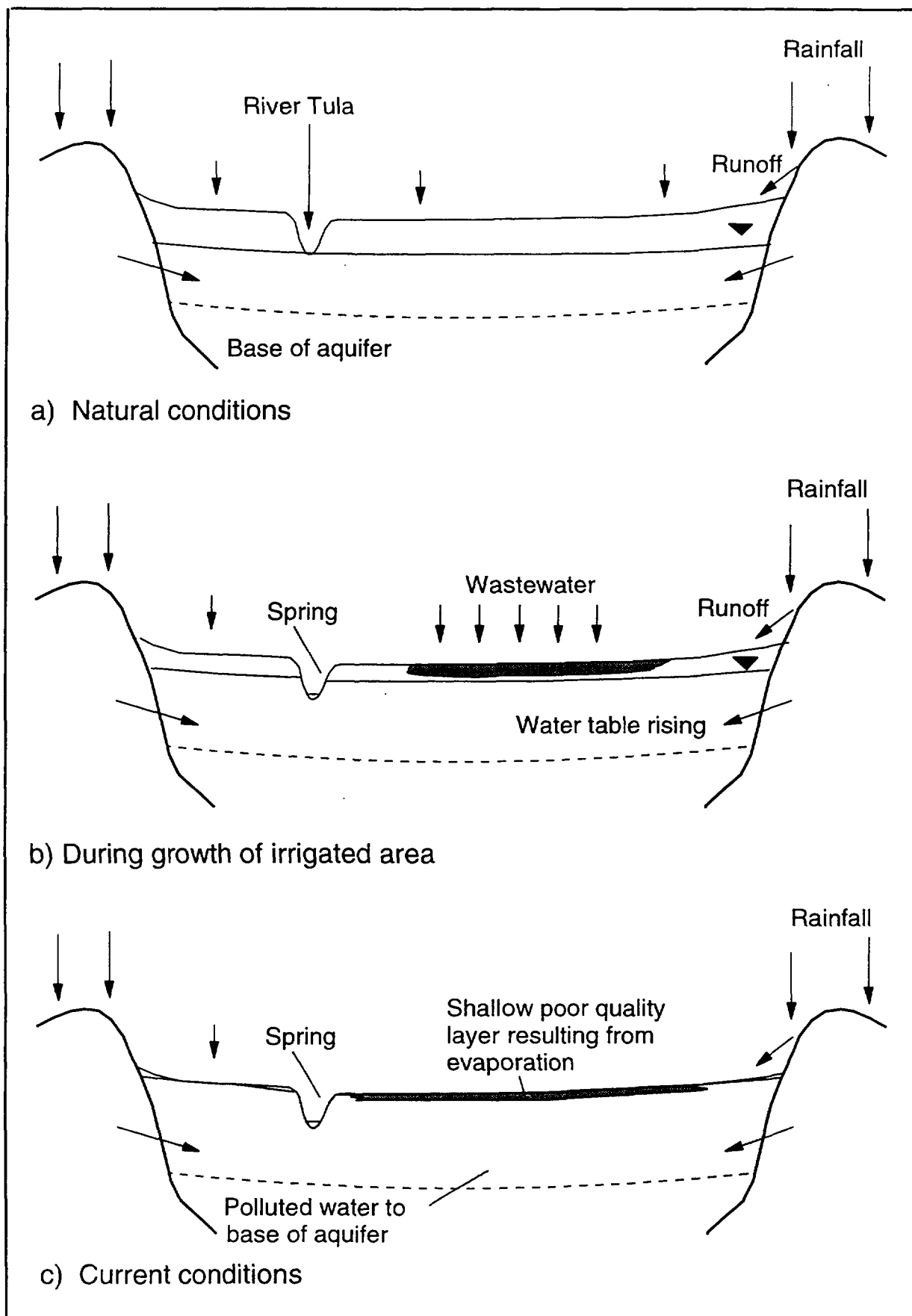
218

Rainfall

River Tula

Runoff

Base of aquifer

a) Natural conditions

Rainfall

Wastewater

Spring

Runoff

Water table rising

b) During growth of irrigated area

Rainfall

Shallow poor quality
layer resulting from
evaporation

Spring

Polluted water to
base of aquifer

c) Current conditions

FIG. 6. Conceptual model of the evolution the groundwater system in the
Mezquital Valley.
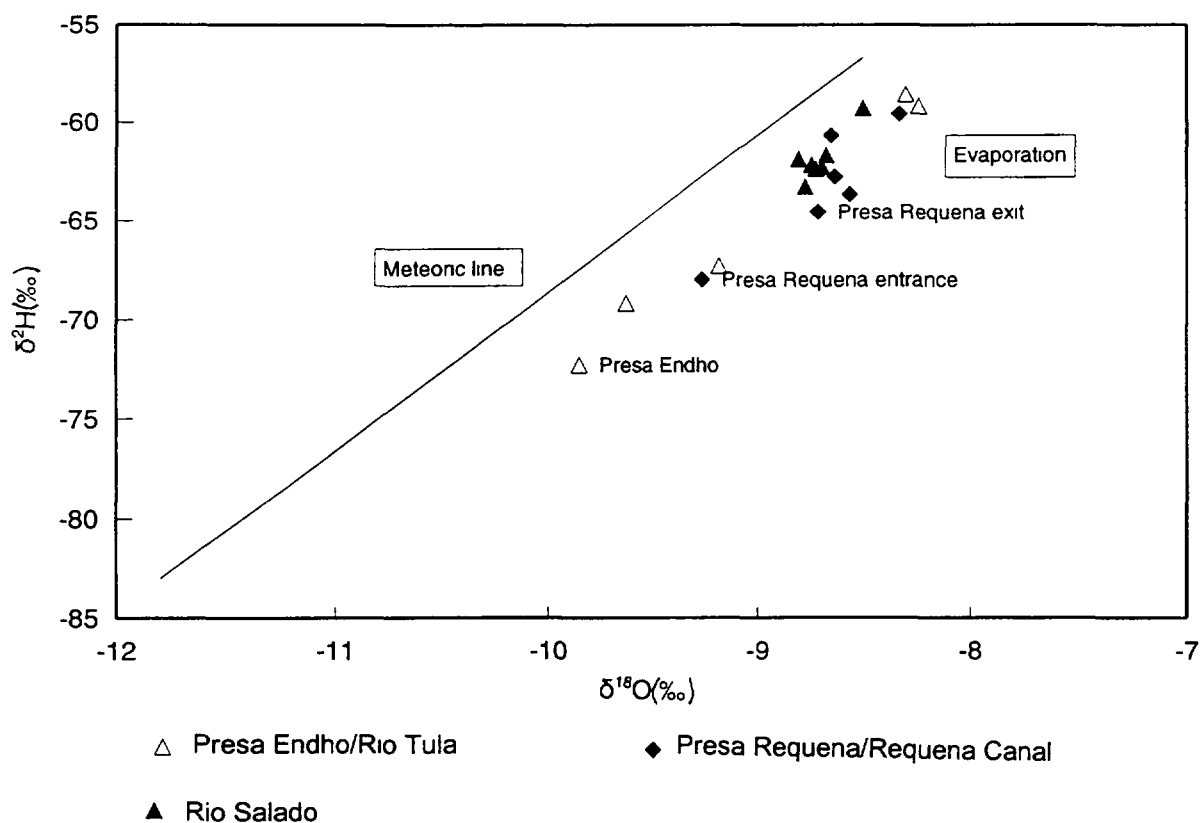
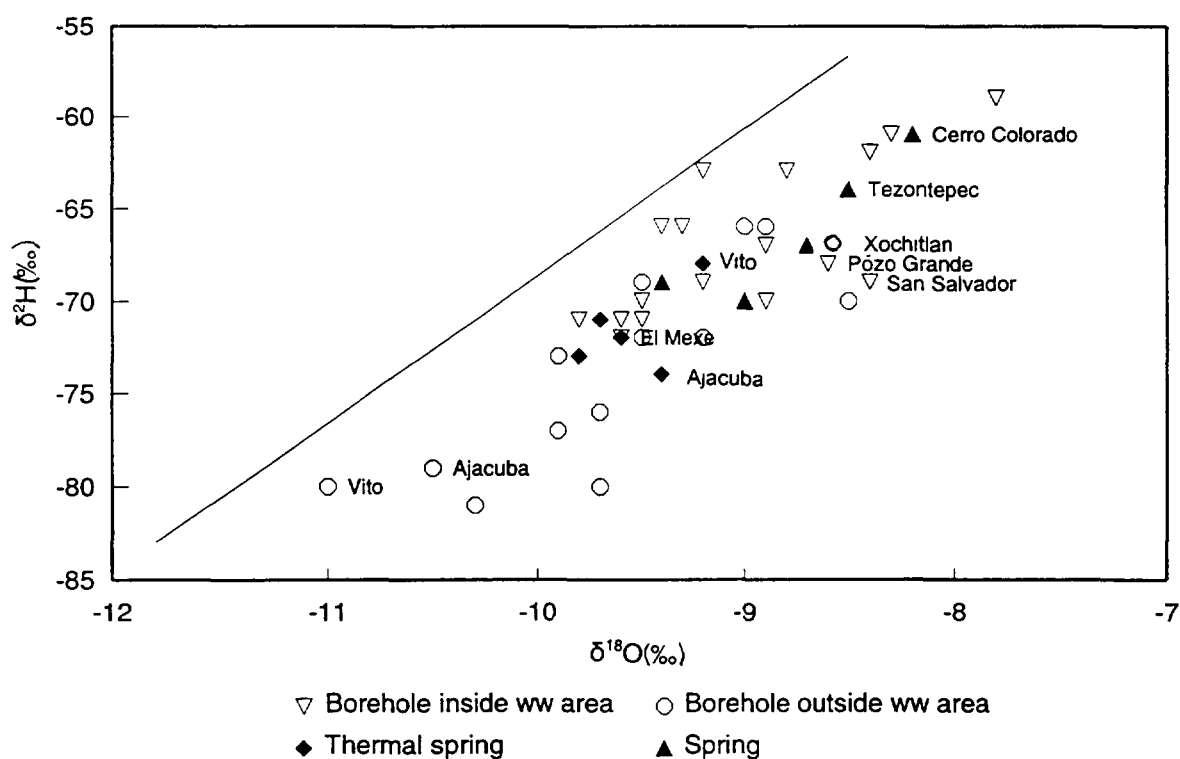FIG. 7. δ^2H against $\delta^{18}O$ for Mezquital wastewaters (after Payne, 1976).

FIG. 8. Conventional plot of δ^2H against $\delta^{18}O$ for samples collected from the Mezquital Valley in the present study.

1985) and early 1990s confirmed the influence of wastewater infiltration on groundwater quality, but the present study provided the first comprehensive picture of quality throughout the valley.

4.2 Sampling

As for León, groundwater quality was determined in the present study by means of a programme of regular sampling. Again sampling points were selected to provide good geographical coverage (Fig. 5), links to existing data from previous studies and an indication of quality at different depths. Forty three samples were analysed for stable isotopes.

4.3 Results and Discussion

Payne (1976) analysed a number of samples from various points in the wastewater system in 1971-1972, before completion of the Emisor Central wastewater tunnel from Mexico City. Plotting these data on a δ-diagram with distinguishing symbols for wastewaters originating from three parts of the system (Fig. 7), showed that the dataset has a fairly linear form with slope parallel to the regional meteoric line (Cortes et al., 1997). At that time, the Presa Endho (Fig. 5) contained relatively fresh water. Water from the exit was the most isotopically depleted in this dataset (Fig. 7), reflecting its origin as rainfall on the surrounding mountainous catchment. Successive samples from downstream along the Rio Tula (the open triangles on Fig. 7) are indicative of increasing evaporation. As this is unlikely to have occurred during its short transit in the river bed, it supports the suggestion in the conceptual model (Fig. 6) that the Rio Tula must be receiving groundwater discharge and drainage from the irrigated fields. Water in the main canal from the Presa Requena (the solid diamonds on Fig. 7) and the Rio Salado (the solid triangles) were isotopically indistinguishable at that time. The Presa Requena (Fig. 5) received water from the Rio del Salto as well as fresh water, and the Rio Salado (Fig. 5) was the main wastewater input to the valley. Evaporation from the Presa Requena is suggested by the lower slope between the entrance and exit samples (Fig. 7).

Examination of the stable isotope data from the present study (Fig. 8) in the context of the map of the study area (Fig. 5) indicates that, at the perimeter of the wastewater irrigation area, groundwaters are rarely more enriched than -9‰ $\delta^{18}O$ and -65‰ δ^2H. The exceptions, for example Xochitlán (Fig. 8), are waters abstracted from the large limestone massif which outcrops between the Tula and Actopan River valleys on the northern edge of the Mezquital Valley (Fig. 5). Piezometric data from the study (BGS et al., 1998) suggest there may be deep groundwater throughflow from the area of wastewater irrigation towards Maguey Blanco (Fig. 5), where the quality of the springs are clearly influenced by wastewater. These can therefore be regarded as the limiting values for groundwater recharged outside the valley areas. Payne (1976) assumed that the most depleted waters which he found (at El Mexe and Tepatepec, Fig. 5) originated from local precipitation. The present study shows that the groundwater system may have changed and that the most depleted water (Fig. 8) is found at sites in the east of the Actopan valley and at Ajacuba and Vito, along the southern margins of the valley (Fig. 5). The altitude range suggested by isotope values for these samples is of the order of 600 m, apart from Vito, which has an extremely depleted isotopic composition (Fig. 8), suggesting a source of recharge at high altitude, the possible cause of which is not clear.

Plotted on the conventional δ-diagram (Fig. 8), the dataset has a fairly linear form, well within the bounds of typical rainfall variation, though somewhat displaced from the
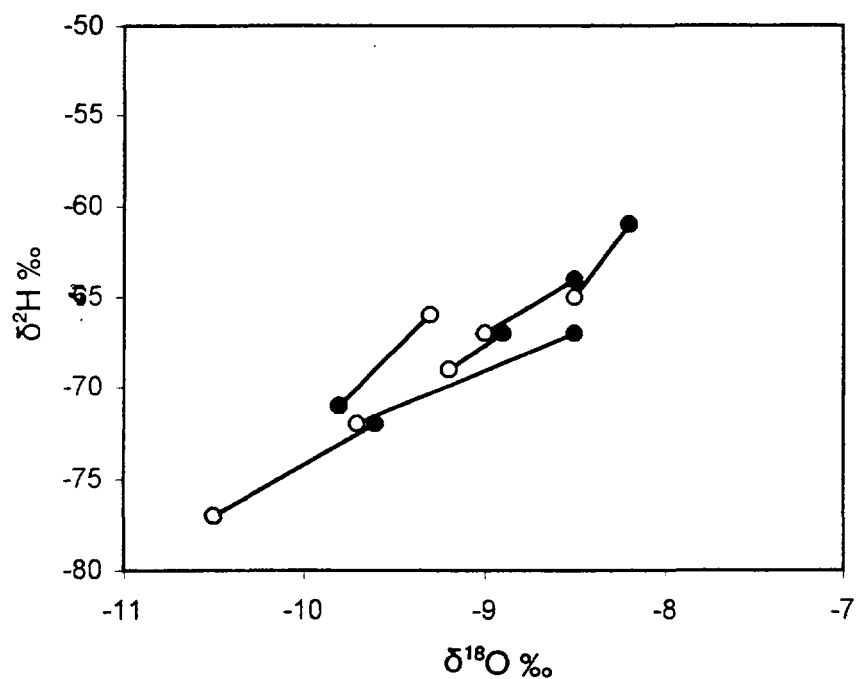
FIG. 9. Changes in δ^2H and $\delta^{18}O$ between 1971 (light circles) and 1994 (dark circles).

∇ Borehole inside ww area   ○ Borehole outside ww area   ◆ Thermal spring
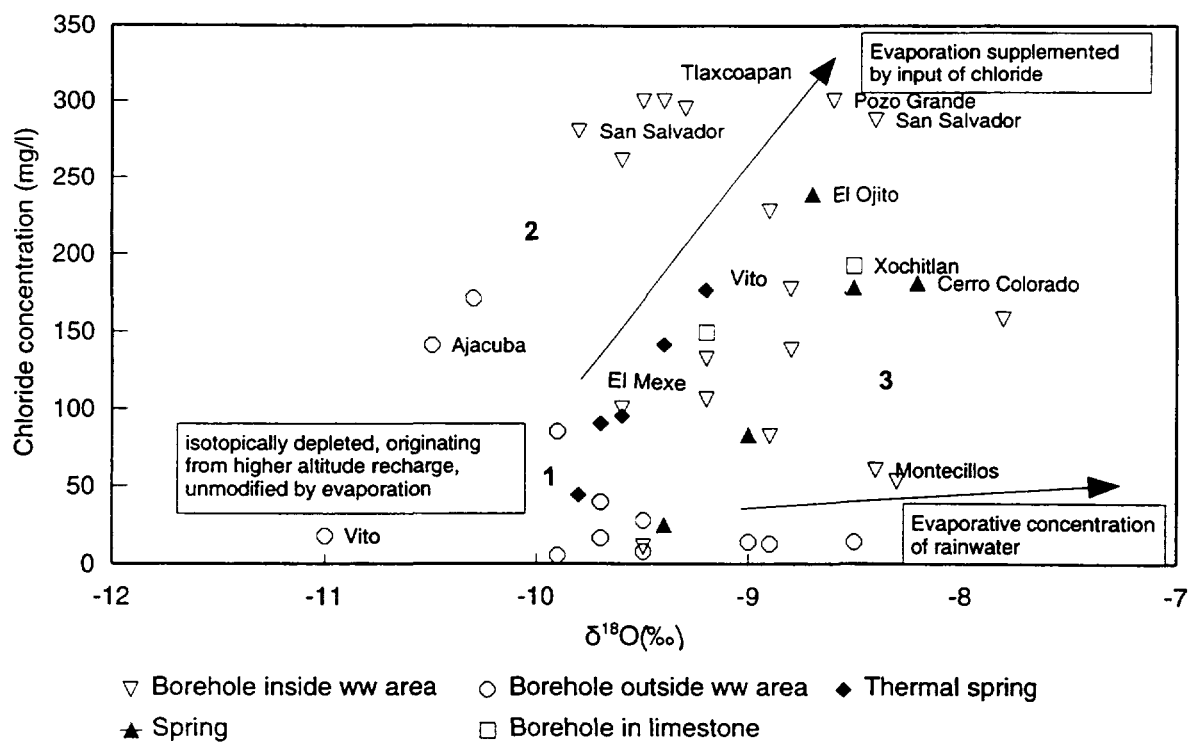
▲ Spring   □ Borehole in limestone

FIG. 10. Chloride concentrations against $\delta^{18}O$ for Mezquital Valley samples

regional meteoric line. There is no marked break of slope at the limits for external recharge proposed above (-9‰ $\delta^{18}O$ and -65‰ δ^2H), which suggests that evaporative processes may not have had a particularly important effect on the local groundwaters. Indications are that in the Tula Valley some groundwaters are the result of local, unmodified recharge, whereas in the Actopan Valley most recharge appears to originate externally. Most of the dugwell and ambient spring groundwaters appear to be local in origin with some probably affected by minor evaporation (eg Cerro Colorado, Fig. 8).

In 1971-72 the depleted stable isotope content of Pozo Grande (Fig. 5) suggested local recharge of non-evaporated water but this has now changed. Generally the sites analysed at that time and again during the present study have become significantly less depleted in $\delta^{18}O$, suggesting a greater contribution from irrigation water (Fig. 9).

The thermal springs would be expected to be supplied by high-altitude recharge sufficient to drive deep circulation. The high sulphate concentration found in some of these springs, due presumably to dissolution of gypsum, is also seen in groundwater from a borehole at El Llano (Fig. 5). This borehole is situated near a canal which carries of wastewater originally abstracted from the area of these thermal spring sources. The respective isotopic values support the sulphate data in suggesting that water from the canal, somewhat evaporated, may have contaminated the well water.

Plotting chloride against $\delta^{18}O$ allows the waters to be resolved into three main types, which are numbered on Figure 10:

1)   waters apparently unmodified by evaporation, more depleted than -9‰ $\delta^{18}O$ and having less than 50 mg/l chloride. These come mainly from beyond the southern perimeter of the area of wastewater irrigation.

2)   waters apparently little modified by evaporation, more depleted than -9‰ $\delta^{18}O$ and having more than 50 mg/l chloride. These come from boreholes close to the perimeter of the irrigated land, from areas currently under development, such as Ajacuba, and the Tlaxcoapan area, which has a long history of irrigation with relatively saline water from the Rio Salado.

3)   waters modified by evaporation and having more than 50 mg/l chloride. These include the majority of the samples from the lower-lying parts of the area and include Pozo Grande, Cerro Colorado, the major discharges to the Tula and sources in the northern limestone, and are more likely to reflect the impact of irrigation with wastewater.

Payne (1976) also measured tritium activity in groundwater samples in 1971-1972. Cerro Colorado (Fig. 5) had the highest content measured during the survey (36 TU), showing that even a few years after first appearance of the spring the content of modern water was relatively high. Other groundwater discharges in this area (Mangas and Tezontepec, Fig. 5) were also high in tritium. In the San Salvador area (Fig. 5), tritium contents were moderate and indicative of relatively recent water (10-20 TU). Together with stable isotope content and chemical analyses, this was strongly indicative of irrigation water.

The group of thermal springs to the north of Maguey Blanco (Fig. 5) showed consistently low tritium content (1-2 TU) and the water was estimated to be more than 40

years old. No tritium was present at El Mexe or Tepatepec (Fig. 5). These boreholes are reputed to be 400 m deep but there is no information on screen depth. The author concluded that the water was more than 50 years old.

5. CONCLUSIONS

A combination of hydrogeological techniques have been used to study the impact of wastewater reuse on groundwater in two areas of Mexico. In both areas, conceptual models of the local hydrogeological system were developed at an early stage of the studies, illustrating the multiple sources and complex processes of groundwater recharge. As these various sources are of very different quality and have changed in importance with time, understanding and quantifying them was a key objective of the studies.

At León, the deep ignimbritic aquifer of the valley floor continues to receive recharge from its outcrop on the valley flanks, whereas the upper part of the aquifer sequence beneath and close to the area of wastewater irrigation has been strongly affected by infiltrating wastewater. Plotting chloride concentration against $\delta^{18}O$ allowed the origins of waters to be resolved, and confirmed the findings of conventional hydrochemical analyses in supporting the conceptual model proposed. The geophysical survey, drilling programme and groundwater sampling confirmed the deep penetration of poor quality water, and the most persistent and mobile contaminant originating from the wastewater was chloride.

The stable isotope data for Mezquital confirm that, for groundwaters beneath the valley floor, most of the current recharge originates by infiltration of wastewater. The more isotopically-depleted samples are located towards the edges or outside the valley, and reflect recharge from local rainfall. The initial conceptual hydrogeological model has been largely supported by the subsequent data. Again, plotting $\delta^{18}O$ against chloride provides a convenient way of distinguishing water types. Comparison with data from a previous study some 25 years ago indicated that isotopic compositions at some sites had become significantly less depleted in $\delta^{18}O$, suggesting that the contribution from irrigation water had increased.

The study has demonstrated the importance of establishing conceptual models at an early stage of such investigations, particularly where multiple and changing sources of groundwater recharge are anticipated. Conceptual models should be used to guide the investigations, including deciding on methods to be used, and sampling regimes to be set up. In such studies, isotopic interpretations should be undertaken within the conceptual hydrogeological framework established, and in conjunction with conventional hydrochemical data. Taken together, hydrochemical and isotopic data can confirm the proposed hydrogeological framework, as was largely the case in the present study, or suggest ways in which it should be modified.

ACKNOWLEDGEMENTS

REFERENCES

BGS/CNA/SAPAL/UACH 1996 Effects of wastewater reuse on urban groundwater resources of León, Mexico. *British Geological Survey Technical Report* WD/95/64, 101pp.

BGS/CNA/LSHTM 1998 The impact of wastewater reuse on groundwater in the Mezquital Valley, Hidalgo State, Mexico. *British Geological Survey Technical Report WD/98/.*

Chilton P J, Stuart M E, Escolero O, Marks R J, Gonzalez A and Milne C J. 1998 Groundwater recharge and pollutant transport beneath wastewater irrigation: the case of León, Mexico. *In*: Robins N S (Ed) *Groundwater Pollution, Aquifer Recharge and Vulnerability*. Geological Society of London, Special Publication **130**, 153-168.

Cortes A, Durazo J and Farvolden R N. 1997 Studies of isotopic hydrology of the basin of Mexico and vicinity: annotated bibliography and interpretation. *J. Hydrology*, **198**, 346-376.

Del Arenal R 1985 Estudio hidrogeoquimico de la porcion Centro-Oriental del valle del Mezquital, Hidalgo. *Inst. De Geologia, UNAM, Revista*, **6** (1), 86-97.

Payne B R 1976 The interaction of irrigaton water with groundwater and the River Tula in the Mezquital Valley. IAEA-SARH unpublished report.

Stuart M E and Milne C J 1997 Groundwater quality implications of wastewater irrigation in León, Mexico. *In: Chilton et al (Eds) Groundwater in the Urban Environment: Problems, Processes and Management*. Balkema, Rotterdam, 193-198.

225

THE IMPORTANCE OF TRACER TECHNOLOGY IN COMBINED BOREHOLE INVESTIGATIONS

H. ZOJER
Institute of Hydrogeology and Geothermics, Joanneum Research, Graz, Austria

Abstract - *In an experimental field for a waste disposal site, investigations have been carried out applying methods from geology, hydrology, hydrogeology, hydrochemistry, environmental isotope hydrology and tracer technology. All data obtained result to a dynamic drainage model of groundwater. The combined interpretation of borehole data guarantees a high-grade knowledge of groundwater exfiltrating to the surface drainage, which enables proper control measures of the disposal site and an effective groundwater protection.*

1. HYDROGEOLOGICAL BACKGROUND

A proper interpretation of borehole data requires combined investigations that include tracer methods. Conventional data are limited and only available from the geological description of strata, as well as pumping tests, while in some selected cases, only data derived from geophysical logging. In an experimental field, investigated for a potential waste disposal site in Upper Austria, a reasonable number of boreholes have been drilled (Fig. 1). The geological structure is defined by Neogene layers, mostly consisting of extensive sand and clay sequences. In almost all geological units, fissures and joints having widths up to some centimeters appear locally. The main tectonic fractures are directed at WNW-ESE, accompanied by secondary joints indicating tension processes along that fault zones. Therefore, the main pre-conditions for the permeability are controlled by a net of joints and fissures while porosity of the media is of secondary importance for the flow of groundwater.

There is no doubt that permeability, as a main aquifer parameter, gives evidence for the understanding of solute transport phenomena. Investigations of permeability showed values in the magnitude of 10^{-11} and 10^{-3} m/s. The wide scattering of data is due to: a) the intercalation of porous and fissured parts of the aquifer; and b) the different evaluation methods like pumping, flow meter, packer and tracer tests as well as on geophysical borehole logging and soil mechanic indications.

Regular measurements of groundwater level and spring discharge were performed and provide indications on the flow pattern of groundwater (Fig.1), but they must be considered insufficient for the determination of the local catchment. Small seasonal fluctuations of groundwater level have been observed near spring outlets representing the discharge zone and at boreholes with a considerable thickness of the unsaturated zone, thus damping vertical flow processes. However, these effects have not been generally recognized but only as indicators of preferential flow conditions in the recharge area of the aquifer.

2. AQUIFER DYNAMICS

The water cycle implies the concept, that water, infiltrated to the underground, is re-emerging to the surface after a certain turnover time and in an unknown distance from the recharge location. Groundwater circulation is adjusted to the natural drainage [1]. It was therefore essential to determine whether groundwater and the associated dissolved solids of the investigated aquifer are discharging to the local streams (Fig. 1) or farther downstream to the same surface drainage or maybe to a larger stream within the drainage network. For such a conceptual model, the unsaturated zone is of minor importance.

Between infiltration and exfiltration of groundwater there exists a dynamic equilibrium. It is determined by hydraulic as well as by solute parameters resulting to the fact, that in the recharge zone, a dominant downward movement of water molecules and solutes

Figure 1. Location map of boreholes and groundwater contours.

occurs, while in the exfiltration zone the water movement is directed upwards [1]. This is the most important consequence for choosing waste disposals sites, since the knowledge of the hydrogeological conditions for groundwater exfiltration finally allows the control of contaminants and furthermore the setting of measures for the rehabilitation of possible disposal damages.

3. TURNOVER TIME OF GROUNDWATER

The age distribution of groundwater is defined in this case by the tritium content. The investigated area is located between Unterseliger and Pisdorfer Bach (Fig. 1). A rough overview of the data show a large scattering between almost zero and 70 TU. Figure 2 offers an insight to the relation between tritium concentration and groundwater level.
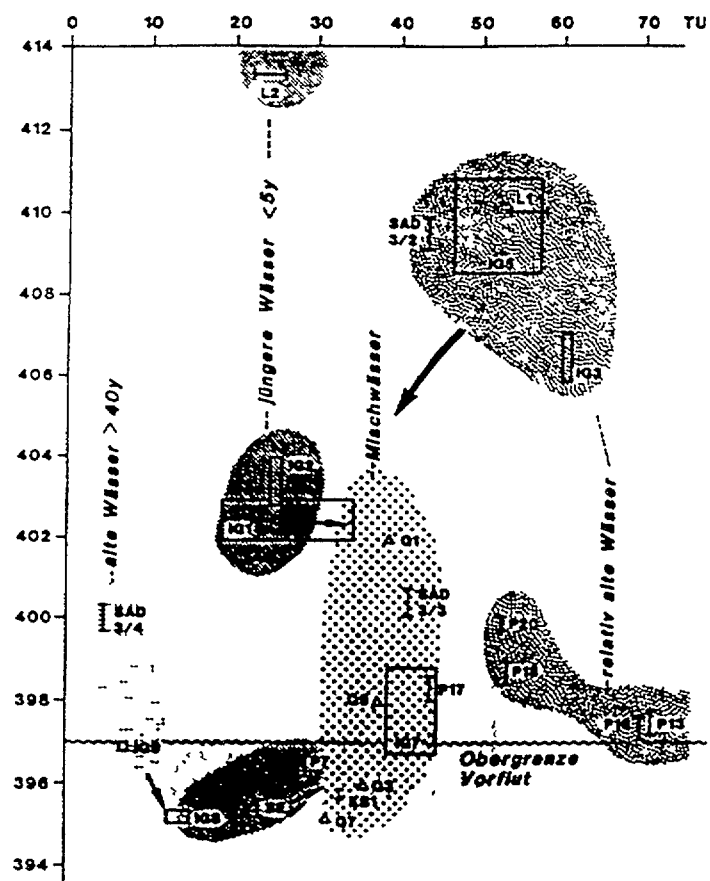
228

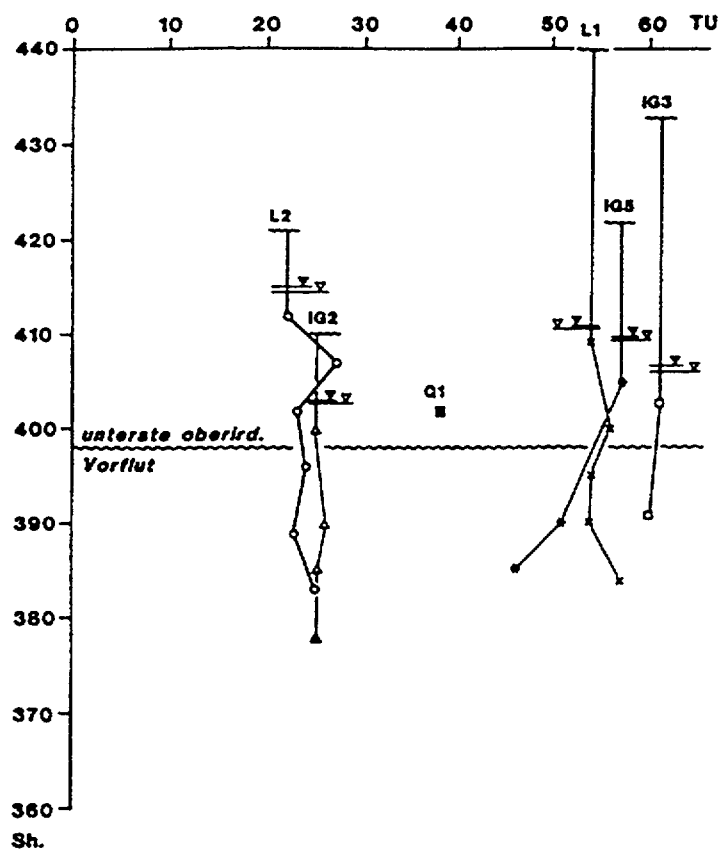FIG. 2: Relation of groundwater level and tritium content

FIG 3 Tritium profiles in boreholes of upper Unterselig Valley

229

Considering the fact that the tritium content of precipitation and infiltration water varies at present between 15 and 20 TU, the oldest groundwater, not exceeding 5 to 10 TU, can be easily distinguished having a turnover time of more than 40 years. Such groundwater is exfiltrating along a fractured zone parallel to the Pisdorf Valley to the surface drainage, represented by the boreholes SAD 3/4 and IG 9. In the latter, the sodium content is slightly increased, which points to a deep circulation of groundwater

The youngest groundwater is exposed in boreholes L 2, IG 2, IG 1, P 3 and P 7. In the most cases the groundwater is locally recharged through a very thin zone overlying the groundwater. The groundwater in the southern part (near Pisdorf Valley) is composed by groundwater of different origins and ages, grouped into two as a young/shallow and a deep circulating components.

4.   VERTICAL MOVEMENT OF GROUNDWATER

In order to gain optimal results for a dynamic infiltration-exfiltration model a programme of combined borehole investigations has been conducted as follows:

- geophysical borehole logging
- flowmeter measurements
- tracing the whole water column to obtain preferential flow paths
- measurement of filter velocity by one point dilution method
- point-injection of tracers to obtain information on the vertical water movement (downwards or upwards)
- vertical profiles of selected parameters, especially of natural tritium

In the upper part of Unterselig Valley the boreholes L 1, L 2, IG 5, IG 3 and IG 2 have been drilled for distinct measurements. Borehole profiles of tritium are shown in Figure 3. The tritium content of groundwater from the drillings L 2 and IG 2 is varying between 20 and 25 TU and does not considerably change by depth, which obviously indicates to the presence of a young groundwater, infiltrated at the flanks and not circulating very deep. A tracer injected in borehole IG 2 at a depth of 21 m was transported upwards, thus recording clear exfiltration conditions to the surface drainage (Unterseliger Bach). Tritium profiles at L 1 and IG 3 show likewise no changes of the concentration by depth but with a considerable high content of 50 to 60 TU, which corresponds to a mean transit time of 20 to 30 years. Both boreholes are located in the recharge groundwater zone indicated by a slightly downwards movement of groundwater derived from point injections of tracer. The same is supposed for borehole IG 5. However, due to the tritium profile a structuring of groundwater turnover time is remarkable - the upper part of groundwater seems to be older than the lower one. It is evident, that the vertical movement of water in the unsaturated zone is slowed down because of less permeability. On the other hand the borehole is touching in the deeper part of the aquifer a fractured net system which causes a fast groundwater exchange. These processes are confirmed by flow meter measurements.

The boreholes IG 1, P 2, IG 7, P 7 and L 3 are located in the lower part of Unterselig Valley. With regard to the tritium profile (Fig. 4) the groundwater of IG 7 is identified as well mixed in the whole aquifer (^{3}H about 40 TU). In contrast, boreholes IG 1 and P 2 show the same mixed groundwater, but overlain by groundwater of young age, caused by a quick infiltration through a thin unsaturated zone. The very well mixed groundwater at borehole IG 7 shows a downwards movement indicated by a tracer injection about 5 m below groundwater level. That seems to be a very surprising result since the borehole is situated only some 100 m near to the local drainage. It is evident, that groundwater from this area is not exfiltrating along the shortest course to the local surface drainage as indicated by the groundwater contour map (Fig. 1) rather it is discharging much more downstream into the same drainage stream after the junction of Unterseliger and Pistorfer Bach. In borehole L 3 tracer experiments have not been performed, but the tritium profile in Figure 3 proves a young water portion in the
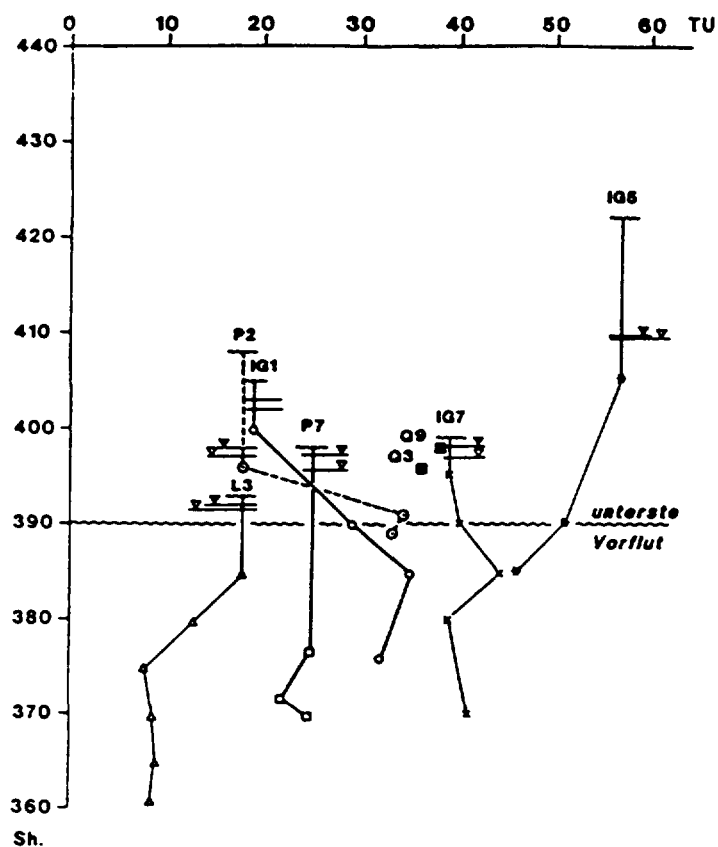
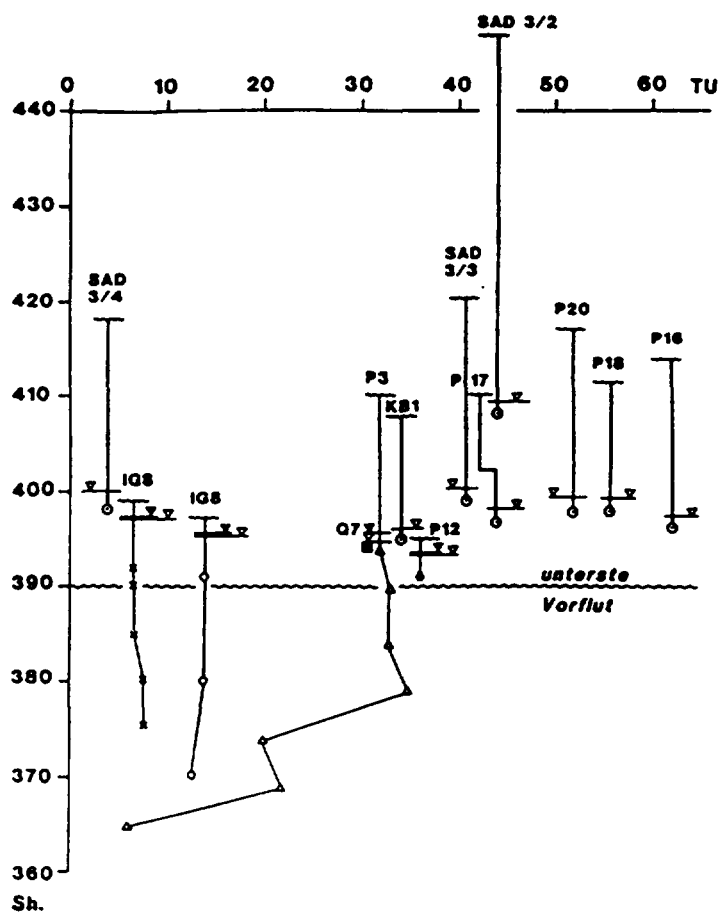FIG. 4: Tritium profiles in boreholes of lower Unterselig Valley

FIG. 5: Tritium profiles in boreholes of Pisdorf Valley

231

upper section of the aquifer, which is very locally recharged. But deeper than 15 m below groundwater level, a rather old water with a tritium content less than 10 TU has been determined. No upwards movement of groundwater in this borehole can therefore be assumed.

Figure 5 reflects the horizontal and vertical distribution of tritium in the recharge area of Pisdorfer Bach. The immediate function of the local drainage is clearly pronounced, expressed by an upwards water movement in boreholes IG 9, IG 8 and P 3 from tracing experiments. The tritium profile of P 3 indicates furthermore mixing processes of different water portions along the whole borehole.

5.   UNDERGROUND DRAINAGE MODEL

The most important results of the investigation are the determination of recharge and discharge zones within the fissured and porous aquifer. They are essential for the hydrogeological assessment of a waste disposal:

a. The groundwater in the proposed disposal area is overlain by a considerable infiltration zone with different permeability, which provides a rather high storage capacity.

b. In the North, groundwater is flowing fast towards Unterseliger Bach, more downstream of the creek the groundwater is mixed from more components of different recharge and age.

c. The steep slope in the South, towards Pisdorfer Bach, is tectonically influenced. Old groundwater indicates a deep reaching circulation. Mixed groundwater from ascending portions and from shallow origin have also been found.

d. The most Eastern boreholes (IG 7, L 3), referring to their location and groundwater pattern, give the impression that they are in exfiltration zone of the nearby local drainage. This is decidedly not the case, based on tritium profiles and tracer tests in boreholes.

e. The exfiltration of groundwater occur farther downstream of the valley field which acts as a "natural barrier" to the neighbouring regions.

6.   DISPOSAL SITE ASSESSMENT

Each scientific discipline is developing its own assessment criteria. This is true particularly for hydrogeology considering the term "barrier", which is not solely remaining to the geological view. This term should be extended to "natural barrier" in order to include all interdisciplinary aspects originating from geology, hydrogeology, chemistry and biology. For the field of hydrogeology the knowledge of drainage conditions are of prime importance on which groundwater flow dynamics are adjusted.

With reference to the conventional definition of the term "geological barrier" it is admittedly difficult to come to an overall agreement, since in the investigation area it will not be possible to reach a "geological barrier" in a technically attainable depth. Furthermore it must be noticed that the disposal site is located above a fractured aquifer with a reasonable permeability. Nevertheless a positive hydrogeological assessment can be expressed because the drainage conditions are known and effective with respect to hydraulics and solute transport in groundwater.

For the case of a contaminant intrusion to groundwater, the flow paths can be followed. It is therefore essential to establish proper measures for the control of the disposal site and the

232

protection of groundwater quality. For that reason the development of multi-control systems depending on a very well defined infiltration-exfiltration relationship is necessary.

7. CONCLUSIONS

In order to gain optimal results for a dynamic infiltration-exfiltration model a programme of combined borehole investigations has been realized:

- geophysical borehole logging
- tracing of the whole water column to obtain preferential flow paths
- flowmeter measurements
- measurement of filter velocity by one point dilution method
- point infection of tracers to get information on the vertical water movement (downwards or upwards)
- vertical profiles of selected parameters, especially of natural tritium

All obtained data result to a dynamic drainage model of the aquifer. The dilution tests together with flowmeter measurements show very clearly the preferential flow especially in fissures and fractures indicated by the geological-tectonic structure. Most reasonable results can be derived from the point injection tracer tests and the tritium profiles. Starting from the recent input concentration of some 10 to 20 TU there exists a wide variety of the tritium content in the groundwater by areal distribution and by depth, located between 0 and 70 TU. A grouping of the different groundwater components enables an excellent insight to the dynamics of the groundwater system. In some of the boreholes a rather high and stagnant tritium content by depth (50 - 60 TU) is associated with a slightly downwards movement of groundwater in the borehole, which indicates the infiltration area of groundwater. It is overlain by an unsaturated zone with a reasonable thickness. Other boreholes are characterized by a groundwater stratification of different age, in some cases even old water overlies younger components. According to results of tracer tests and flowmeter measurements, such phenomena are affected by preferential flow conditions along fractures in the deeper part of the aquifer.

The combined interpretation of borehole data guarantees a high-grade knowledge of exfiltration conditions of groundwater to the surface drainage, which enables effective control measures of the disposal site and groundwater protection.

REFERENCE

[1]Chapman, D. (Ed.) 1992. Water quality assessments. 585 pp. London: Chapman & Hall.

APPLICATION OF RADIOISOTOPE TECHNIQUES TO CONTROL FLOW PROCESS DURING ARTIFICIAL COASTAL AQUIFER RECHARGE

F. ARDAU, G. BARBIERI, G. BARROCU, E. PIRASTRU
Department of Territorial Engineering, University of Cagliari,
Cagliari, Italy

Abstract - *Radioisotope techniques was applied for studying the flow and transport processes in a coastal confined aquifer during an artificial recharge experiment to check the feasibility of controlling salt water intrusion by a hydrodynamic barrier. As no other water source is available, artificial recharge is done using treated wastewaters. Flow and effective velocity, hydraulic conductivity, transmissivity, diffusivity and effective porosity have been determined by means of I-131 radioisotope in single- and multi-well tests.*

1. INTRODUCTION

The definition of the hydraulic characteristics of aquifers is essential when planning remedial actions, that may include zoning of vulnerable areas, regulating groundwater management and artificial recharge. Radioisotope techniques was applied to study the flow and transport processes in an artificial recharge experiment designed to control saltwater intrusion. Field measurements of piezometric levels, hydrogeochemical analysis and pumping tests have been performed within the context of the European Community-funded Avicenne Project on development of water resource management tools for problems of seawater intrusion and contamination of fresh water resources in coastal aquifers [1].

The experimental site is located in the zone of Capoterra, south west Sardinia, Italy (Fig.1), near the south-west coast of the Bay of Cagliari, in the delta plain of the Rio Santa Lucia, 2.5 Km inland between the S. Gilla lagoon and the salt-works.

The geological formations are, from top to bottom, alluvial deposits, fluvial and lacustrine sediments, recent and ancient terraced alluvial of the Quaternary, fractured granites and metamorphic schists of the Palaeozoic.

2. HYDROGEOLOGICAL OUTLINE

The hydrogeology of the Capoterra floodplain is particularly complex, due both to natural factors, such as the geology of the area, the nearby sea and the presence of lagoons and the salt-works, and to anthropogenic factors, owing to the development of irrigated agriculture, and above all industrial expansion.

Phreatic groundwater occurs in the recent alluvium underlain by a clay layer, beneath which lies another multilayer aquifer, semi- or locally confined. Groundwater occurs in sand and gravel layers with interbedded clay lenses of recent alluvial deposits. Both the phreatic and the confined aquifers are recharged laterally from the west through the major fractures of the granite bedrock, consisting of paleozoic granites and schists. The water table has dropped to below mean sea level in some areas where groundwater is over-exploited to meet the growing demands of agricultural and industrial activities.
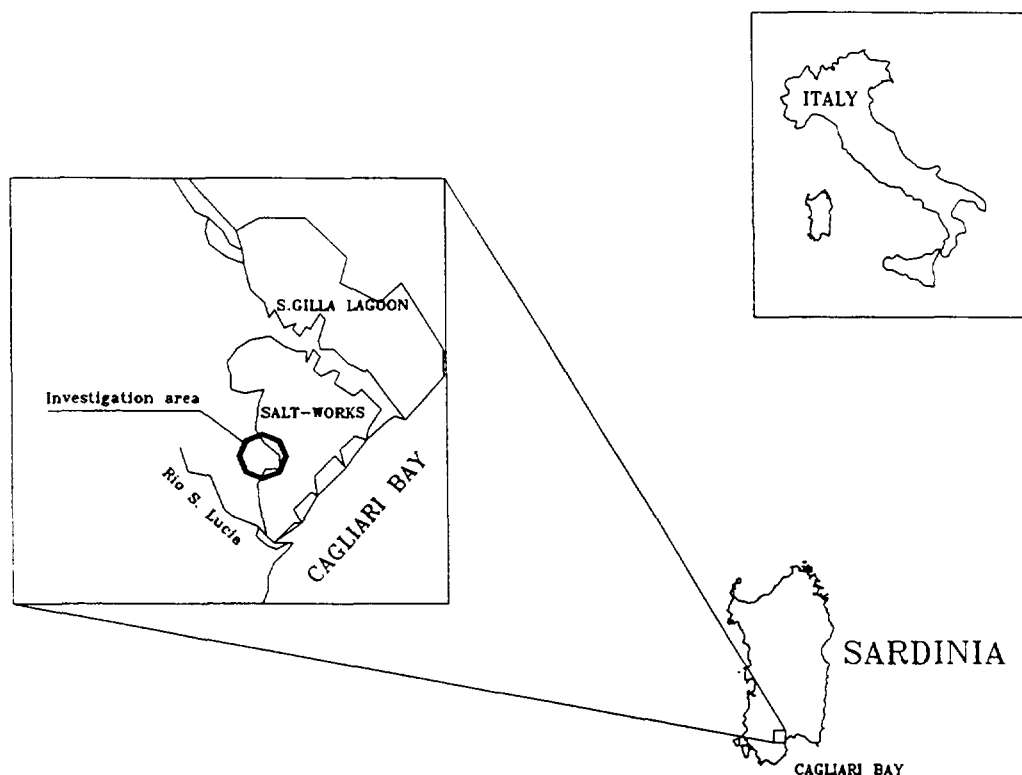
Fig. 1 - Location of the experimental recharge site

A control and monitoring network of the coastal aquifer system has been set up and hydrogeological and hydrogeochemical measurements are taken periodically at selected observation wells. The complete set of data forms a database which is constantly updated and used for graphically processing water levels and hydrochemical characteristics. The observation well network got under way in 1992 and today comprises some 145 wells, 79 shallow excavated wells and 66 deep drilled wells selected from among the 497 wells identified in an area of nearly 30 Km^2.

The hydrogeochemical observations in the monitoring network have indicated widespread seawater intrusion in both the phreatic and confined aquifers. This phenomenon may be attributed to the uncontrolled groundwater abstraction from the wells in the zone and to the direct infiltration underground of brackish waters coming from the salt-works and the lagoon.

Artificial recharge experiments have been carried out and are currently in progress in the surface phreatic aquifer using a drainage trench, and in the underlying confined aquifer by means of wells.

236

3. APPLICATION OF RADIOISOTOPE TECHNIQUES

Isotope tracers can be particularly useful when studying coastal aquifers where hydrochemical data may be contradictory and the hydrogeological and conceptual models are rather complicated. In fact, in some cases salinity may be attributed not only to saltwater intrusion but also to connate salt water or salt content in the solid phase. Coloured and salt tracers are not recommended when investigating coastal areas, especially if the aquifer is hosted in montmorillonitic clay. Coloured tracers have to be used in high concentrations and may be absorbed and measurements with salt tracers are not significant in interface zones where salinity varies widely from place to place.

Tracer techniques consist of injecting tracers into a well, and monitoring in situ, in one or more measurement wells, how its concentration varies in time with the natural groundwater flow. The single-well and the multi-well method proposed by Drost and Klotz [2, 6] have been adopted to study the coastal aquifers of the Capoterra area.

The single-well method consists of injecting a small amount of lightly blended radioactive tracer from a special bottle in a well where one or more probes are fixed at a pre-established depth to survey γ radiations. As the water flows through the well, the tracer becomes more and more diluted and thus groundwater filtration velocity, flow direction, aquifer horizontal and vertical permeability, transmissivity are measured.

In particular, we can determine the filtration velocity V_f by means of the following equation:

$$V_f = \frac{\pi * r}{2 * \alpha} \frac{1}{\Delta t} \ln \frac{C_0}{C_t}$$

where:
r = well radius;
α = correction factor, function of the characteristics of the well;
C_0 = tracer concentration at time t_0;
C_t = tracer concentration at time t;
$\Delta t = t - t_0$.

Where one or more wells are available downstream from the input well, the multi-well method may be adopted. If possible for a more meaningful measurement one well should be located along the flow line and two others slightly displaced from it. The upstream well is used for tracer injection while the downstream wells are used for measuring variations in tracer concentration with time.

Groundwater effective velocity, specific yield and storativity, as well as longitudinal and transversal dispersion coefficients may be determined with this method. In particular the effective velocity V_{eff} can be calculated using the formula:

$$V_{eff} = \frac{L}{\Delta t}$$

where:
L = distance between injection well and measuring well;
Δt = time between tracer injection and concentration peak in measuring well.

The instruments for detecting radioisotope tracers are very sensitive, so that they can be used even with tracers in very low concentrations and measurements are made in situ without perturbing flow. The measuring instrument used here consists of a NaI probe (Tl) connected to a Silena SNIP computer, capable of storing and analysing the γ-ray spectrum measured.

Both methods have been utilised in the confined aquifer in the Capoterra experimental site to study flow during an artificial recharge test to control sea water intrusion. Tracer techniques are expected to provide reliable information on the development of the hydrodynamic barriers created by pumping treated water into the interface zones of the two aquifers.

4. TRACER EXPERIMENTS

The study area extends for some 5000 m^2 over the Capoterra floodplain (Fig. 2), 2.5 Km inland from the coast in front of the wastewater treatment plant of the Consortium for Cagliari Industrial Development Area (CASIC), which supplies the water for the artificial recharge tests.

Boreholes drilled in the area concerned together with hydrogeological observations indicated the presence in the Quaternary alluvial of two aquifers, a deep confined aquifer overlain by a phreatic one near the surface. These aquifers are separated by a clay horizon with average thickness of around 4 m (Fig. 3).
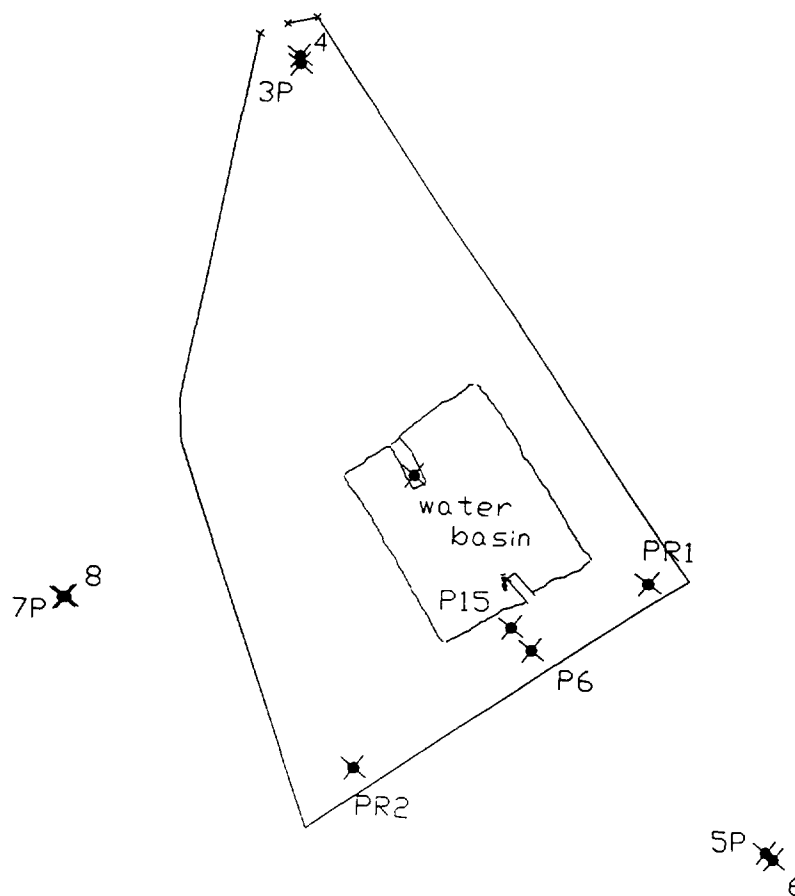

FIG. 2 - Well network in the experimental recharge site

The tests have been done on the confined aquifer, about 5 m in thickness, which is hosted in sands with gravel and clay between 15.50 and 20.50 m below ground level, using in particular wells P15 and P6 for artificial recharge and tracer tests.

Earlier hydrogeological studies [1, 3] conducted in the site allowed to determine hydraulic gradient (i) and storativity coefficient (S), by Theis and Jacob methods, of the confined aquifer, as follows:

$i = 5.1 * 10^{-3}$

$S = 5.24 * 10^{-4}$

The tracer experiments were carried out in natural flow conditions as well as during artificial aquifer recharge.

Initially, Technecium-99 was used as tracer since it is readily available and can be used in relatively high concentrations. However, the fact that this tracer has a half life of just 6.01 hours means that it would decay below the detection limit characteristic of the measuring instrument used before it will arrive to well P6. For this reason it was decided to try Iodine-131 which was not so easy to get hold of and more expensive. However, the half-life of 8.05 days ensured greater probability of success, even in the presence of particularly low filtration rates [4].

4.1 Tests in natural flow conditions

The test was performed using both the single-well and multi-well methods. 1 mCi (37 Mbq) of I-131 was injected into well P15 and the variation in tracer concentration was measured before into the well P15 and then in well P6, 3 m downstream from the former.

In the injection well P15 (r = 0.075 m, α = 3) the concentration was found to change from an initial value C_0 = 4.956 Mcps to C_t = 0.625 Mcps in a time Δt equal to 2^h 10'. The concentration peak in the measuring well P6, situated 3 m downstream from the injection well P15, was observed at Δt = 18^h 27' 42" = 0.769 d after tracer injection into the latter. Based on these experimental data, the filtration velocity and effective velocity have been determined in natural flow conditions:

$$V_f = \frac{\pi*0.075}{2*3*7800} \ln \frac{4956.000}{625.993} = 1.042*10^{-5} \text{ m/s} = 0.9 \text{ m/d}$$

$$V_{eff} = \frac{3}{0.769} = 3.9 \text{ m/d}$$

It has been possible thus to calculate hydraulic conductivity K, transmissivity T, specific discharge Q, diffusivity D and specific yield n_e of the confined aquifer (Table I).

Table I - Hydraulic characteristics of the confined aquifer

V_f (m/d)	V_{eff} (m/d)	K (cm/s)	T (m^2/s)	Q $(m^3/d/m)$	D (m^2/s)	n_e
0.9	3.9	$2.04 * 10^{-1}$	$1.02 * 10^{-2}$	4.5	19.5	0.23

Department of Territorial Engineering	
SCALE 1 50	DATE 18/11/97
DRILL GAUGE 150 mm	

elevation (m) | thickness (m) | depth (m) | stratigraphy | description | well logging (/) | scale 1 50 | rqd (/)

topsoil

fine sand

coarse sand with pebbles
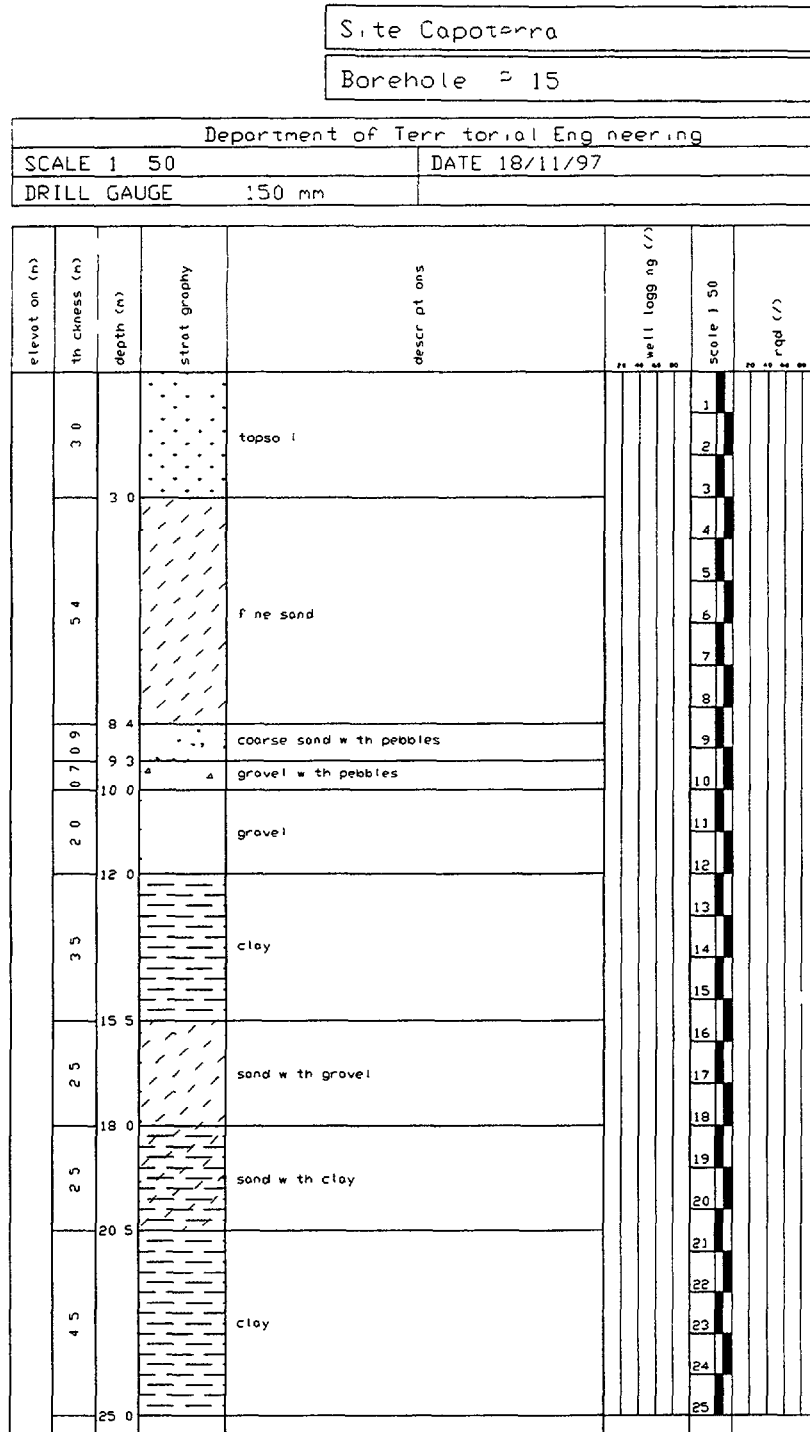
gravel with pebbles

gravel

clay

sand with gravel

sand with clay

clay

Fig. 3 - Lithostratigraphy of borehole P15

4.2 Tests in artificial recharge conditions

The test was carried out during the artificial recharge operation, injecting the tracer into well P15 and measuring the time it took to arrive in well P6 as well as the variation in tracer concentration. For aquifer recharge, a constant flow rate Q_r of 3.3 l/sec was introduced into the recharge well. This resulted in an almost immediate rise in the water level of 1.31 m in well P15 and 0.99 m in well P6.

I-131 was used as tracer at an amount of 1 mCi (37 Mbq) introduced in a special bottle [5]. The operation started at 12.30H while the probe was placed in well P6 downstream. After 15 minutes, radioactivity values increased from the natural value of 41.500 counts per 100 seconds, to 123.900, then to 146.100, 167.300, etc. The tracer detection curve, obtained by subtracting the natural value, is plotted in Fig. 4. A peak (231.300 cps) was observed at 33'40" = 2020" after tracer injection. Effective velocity of the water during artificial recharge was:

$$V_{eff} = 3.00 / 2020 = 1.15 * 10^3 \ m/s = 28.3 \ m/d$$
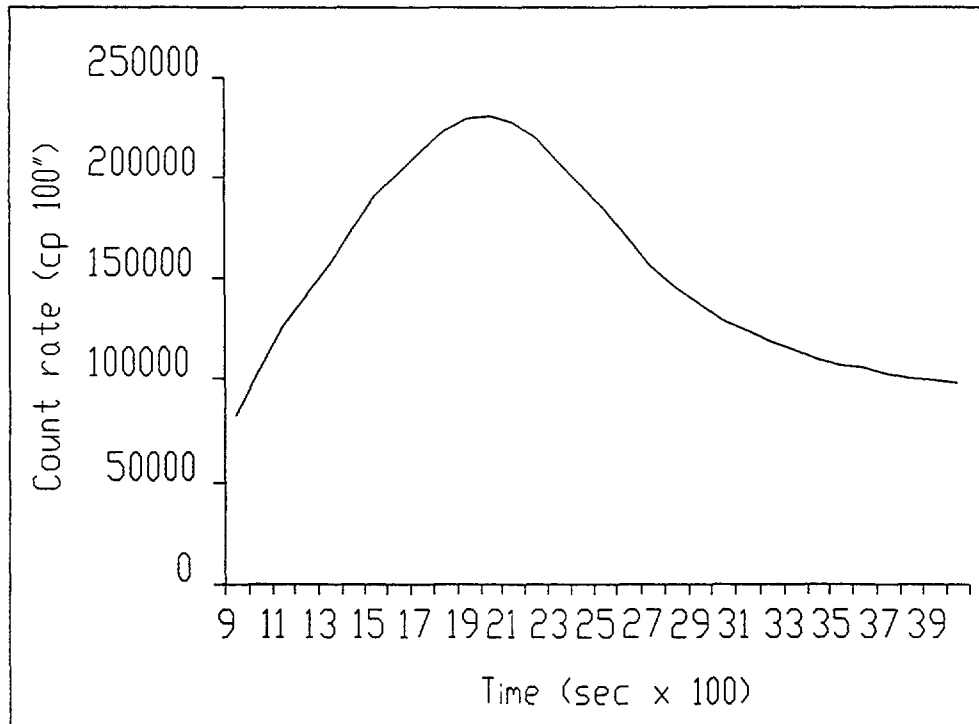
Fig. 4 - Tracer detection curve during artificial recharge

5. CONCLUSIONS

The experiments has demonstrated the optimal characteristics of using I-131. Despite the small doses used in groundwater tracing, the relatively long half-life of this tracer means that it maintains a sufficient detectability level for long times, which also makes it suitable for multi-well techniques.

Single- and multi-well tests have been carried out in the experimental site at Capoterra in natural flow conditions enabling all the hydraulic characteristics of the confined aquifer to be determined: discharge and effective velocity, hydraulic conductivity, transmissivity, diffusivity and effective porosity.

A multi-well test was also carried out during artificial recharge of the confined aquifer introducing a constant flow rate of around 3 l/sec, which resulted in a rise in hydraulic head of 1.31 m in the injection well. This test has shown the practically immediate response of the aquifer in terms of pressure and a significant increase in effective velocity from 0.9 to 128.3 m/d.

These preliminary tests have demonstrated the efficiency of radiometric tracers both for defining the hydrogeological characteristics as well as for studying flow processes and for controlling the evolution of the up-building cone during artificial recharge of the aquifers.

241

REFERENCES

[1] Barrocu G., Fidelibus M.D., Sciabica M.G., Uras G. (1993) - Hydrogeological and hydrogeochemical study of saltwater intrusion in the Capoterra coastal aquifer system (Sardinia). *Proc. 13th Salt-Water Intrusion Meeting*, Cagliari, Italy, 103-111.

[2] Drost W. (1989) - Single-well and multi-well nuclear tracer techniques - *International Hydrological Programme*, Unesco, Paris, pp. 1-96.

[3] Barrocu G., Sciabica M.G., Uras G., Cortis A., Vernier E. (1997) - Saltwater intrusion and artificial recharge modelling in the coastal aquifer system of Capoterra (Southern Sardinia). *Proc. International Conference on Water Problems in the Mediterranean Countries*, Near East University Civil Engineering Department Nicosia, North Cyprus (in press).

[4] Ardau F., Barbieri G., Pirastru E. (1996) - Applicazioni di tecniche radioisotopiche in idrogeologia. *V Convegno Nazionale dei Giovani Ricercatori di Geologia Applicata*, Cagliari, Italy (submitted).

[5] Tazioli G.S. (1973) – *Metodologie e tecniche radioisotopiche in idrogeologia* – Geologia Applicata e Idrogeologia, Bari, vol.III, parte II, pp. 209-229.

[6] Drost W., Klotz D. (1983) - Aquifer characteristics - *Guidebook on Nuclear Techniques in Hydrology*, N° 91, IAEA, Vienna, pp. 223-256.

CONTAMINANT TRANSPORT IN AQUIFERS: IMPROVING THE DETERMINATION OF MODEL PARAMETERS

C.V.S. SABINO, R.M. MOREIRA, Z.L. LULA, Y. CHAUSSON
Nuclear Technology Development Center,
National Nuclear Energy Commission

W.F. MAGALHÃES
Department of Chemistry,
Federal University of Minas Gerais

M.N. VIANNA
Department of Nuclear Engineering,
Federal University of Minas Gerais

Belo Horizonte, Brazil

Abstract - *Parameters conditioning the migration behavior of cesium and mercury are measured with their tracers ^{137}Cs and ^{203}Hg in the laboratory, using both batch and column experiments. Batch tests were used to define the sorption isotherm characteristics. Also investigated were the influences of some test parameters, in particular those due to the volume of water to mass of soil ratio (V/m). A provisional relationship between V/m and the distribution coefficient, K_d , has been advanced, and a procedure to estimate K_d's valid for environmental values of the ratio V/m has been suggested. Column tests provided the parameters for a transport model. A major problem to be dealt with in such tests is the collimation of the radioactivity probe. Besides mechanically optimizing the collimator, a deconvolution procedure has been suggested and tested, with statistical criteria, to filter off both noise and spurious tracer signals. Correction procedures for the integrating effect introduced by sampling at the exit of columns have also been developed. These techniques may be helpful in increasing the accuracy required in the measurement of parameters conditioning contaminant migration in soils, thus allowing more reliable predictions based on mathematical model applications.*

1. INTRODUCTION

Migration behaviors of fission products and of actinides in the geosphere and specifically in aquifers are a major concern in the design and safety assessment of nuclear waste repositories. This study deals with only one main fission product: ^{137}Cs. It has been prompted by the construction of the first larger scale radwaste repository in Brazil, designed to receive part of the source and contaminated debris generated by an accident with a therapeutic irradiation unit, which occurred in 1987 in the town of Goiânia, about a hundred kilometers west of the capital Brasília. Tests were also carried using ^{203}Hg as tracer. The reason for this is the great interest in environmental contamination by mercury, which is intensively used in gold extraction activities spread over a large extent of the country.

Having reached the soil contaminants such as these can be transported to and through the aquifer layer by the mechanisms of advection, dispersion, transfers between liquid and solid phases, besides chemical reactions. Tracer techniques are commonly used to study these mechanisms, especially the first three. Migration experiments are frequently run in the laboratory by means of batch and column tests. Although exact field conditions are hardly

reproducible in such measurements the main features of the transport processes can be retained, once due care and interpretative judgment are employed.

A lot of effort has been expanded both in the development and refinement of experimental methods, and a vast amount of data has been generated which have been effectively used for engineering purposes. The literature is fertile in this field; references 1, 3, 4, and 5 being some few representative samples.

Applying these techniques to the two problems at hand, some shortcomings were found to influence the results obtained. These are related in part with physical factors, such as the relative amount of solid and liquid used in the test or the isotherm chosen to represent between phases. But experimental features have a great share, and much depends on the way sampling and counting are performed.

It was then decided to investigate both experimental and data treatment procedures susceptible of improving this methodology. An often disregarded feature in the literature is the quantification of the degree of improvement reached through a refinement either in experiment or in data processing. Therefore it has been endeavored to support whenever possible any claims on betterment in results with statistical tests.

Data on the migration of cesium and other fission products in Brazilian soils will be mainly of use in the design and safety assessment of radwaste repository facilities. Mercury migration data is expected to help, among other things, in preparing regulatory impact statements and in planning remedial actions in contaminated areas.

2.   MATERIAL AND METHODS

In batch tests the soil and liquid phases are shaken in a closed vessel and thus brought in intimate and accelerated contact, and once equilibrium is attained they are separately analyzed for the contaminant distribution. These tests are thus restricted to the investigation of the sorption step. In column experiments the contaminate liquid percolates a soil layer and hence they are able to more fully account for all the associated migration mechanisms, including those of a hydrodynamic nature. Radioactive tracers considerably ease the task of contaminant transport observation and measurement.

2.1.   Methodological shortcomings

The partition of the solute between the liquid and solid phases at equilibrium is expressed by the K_d coefficient. It is directly calculated from batch tests results. However considerable care is required when applying experimental data. Partition is influenced by the solvent composition, the solute concentration and the sorbent to solvent ratio. This means that K_d is not a constant, its experimental values being strictly valid only for the conditions obtained in the measurement procedure.

Conditions in batch tests deviate a lot from those existing in nature, much more so than in column tests. Notwithstanding, batch tests are by far simpler and faster, and even though hampered by diverse shortcomings they afford a practical means to speedily obtain data urgently demanded in the initial stages of repository design, if not for other reasons at least for screening decisions, the possibility for later refinements always remaining open.

244

One of the largest deviations of batch test conditions from the environment has to do with the volume of solvent to mass of solids ratio (V/m). In the conditions of groundwater flow this ratio is quite low; it cannot be reproduced in batch tests otherwise one would deal with a pasty mixture and the mixing procedure would not work.

Coefficient K_d can be indirectly obtained in column tests by backcalculating it from the retardation factor, i.e. the ratio between the contaminant and liquid phase transit times, using Equation (2) in Section 2.3. The retardation factor R_f of the sorbed contaminant can be determined both by comparison of the tracer and solvent velocities (these being obtained from the flowrate, accounting for the porosity of the bed) or by measuring their residence times in the column. The latter method can be accomplished by tagging both the dissolved contaminant and the liquid phase with distinguishable tracers. Tritiated water is the natural choice for aqueous solvent. But the displacement of tritium inside the column cannot be detected by an external radiation probe (the simpler and accurate "thru-the-wall" sampling mode) and thus has to be materially sampled and counted in a liquid scintillator (the tricky "mixing cup" sampling mode). This introduces a distortion since the sampling procedure will span over some time interval, however short, required to secure an activity consistent with a reliable measurement.

The major experimental difficulty which has been met with in the column runs was related with the collimation of the radioactive tracer signal. Fine collimation is mandatory for accurate resolution of spatial tracer distribution inside the column. An alternative often used is to extrude the solid from the column (freezing being used to secure its integrity), slicing it, and counting the differential layers. Besides the difficulty of getting desirably thin slices, the major drawback has to do with the definitive interruption of the test; i.e.: this technique amounts to a single scan in the whole run.

Our choice has been a mobile probe sliding along the external wall of the column, driven by a fine tuned motor and continuous screw assembly. The challenge posited to this scanning mode is to assure a collimation good enough to suppress signals from planes other than the one just in front of the collimator slit. This has been tried by narrowing down the slit as much as feasible on a cost-to-benefit basis. Even thus this did not eliminate signals coming from neighboring layers.

2.2. Soil samples and tracers

Soil samples collected at the repository site in Goiânia and at the premises of our Institute in Belo Horizonte had their physical properties, such as bulk and mass density, and porosity duly measured. Their mineralogical constitution and chemical composition were asserted by x-ray diffractometry and x-ray fluorescence, respectively. All test samples were previously dried and sieved to minus 100 mesh.

Cesium was traced by ^{137}Cs, obtained from aliquots of an original 0.8 mCi carrier-free $^{137}CsCl$ solution. Mercury was traced by ^{203}Hg, obtained at the TRIGA MARK1 reactor in our Institute, by irradiation of $HgCl_2$ (P.A.) dissolved in distilled water and aqua regia. After 4 h of irradiation at a neutron flux of 1×10^{11} $n.cm^{-2}.s^{-1}$ a specific activity of 70 KBq/g (1.9 µCi/g) Hg^{2+} has been obtained.

2.3. Batch and column tests methodology

The pH in the batch tests was kept at 5.5 and the solution volume was 60 ml; V/m being varied by the amount of sediment added. Aliquots of 3 KBq (80 nCi) were used; they were added to soil samples placed in plastic vials, varying from 0,011g to 5 g in weight, and the liquid volume completed with demineralized water. The samples were shaken for 30 min at 25°C and filtered in a special setup, from which the filter holder could be disassembled and transferred to the counting system, warranting a constant geometry. Both soil and supernatant were counted. The liquid was placed inside standard polyethylene vials; ^{137}Cs was counted in a NaI(Tl) well detector, and [203]Hg in a Ge-Li detector. Their pulses were fed to a multichannel analyzer interfaced with a PC, one of whose tasks was to analyze the gamma spectrum using the Maestro II - ORTEC software. Counting geometry is not the same for liquid and solid samples, which requires a correlation procedure.

Column runs with cesium are unbearably time consuming, unless very short layers of solids are used, due to the intensively sorptive characteristics of the Cs^+ ion. Despite this drawback it has been decided to use a larger column to better explore the radiotracer transit features, besides minimizing distortions introduced by the sample collection procedures. Homogeneity in packing and in flow distribution over the cross-section is critical for the reliability of the results. The design and packing methodologies developed at the GSF-Neuherberg, and reported by Klotz [1] have been adopted. Several packing procedures were tested: adding soil together with water, packing under shaking, adding water first and displacing it with the soil, etc. The one which proved to be the best consisted in packing the soil in successive narrow layers 5 cm thick in the column previously filled with water.

The Plexiglas column was 1 m long and 5.4 cm in internal diameter. A Plexiglas diffuser at the column entrance homogeneously distributes the feed flow. Water was fed at a constant rate from a Mariotte vessel placed 4 m above the column. Tracer was introduced via a septum near the flow control valve just before the column entrance. The instantaneously injected activities were 370 Bq (10 μCi) ^{137}Cs and 480 Bq (13 μCi) [3]H.

A 3" x 3" NaI(Tl) detector was placed inside a lead shielding 3 cm thick, which could be driven alongside the external wall by a motor coupled to reduction bevel gears. Scanning could thus be performed either continuously or at preset positions. Counts were integrated for 400 s, and duplicate records taken at 5 cm intervals. A scheme of the column setup is shown in Figure 1.

The distribution coefficient and retardation factor were calculated from their defining equations:

$$K_D = \frac{V}{m} \frac{C_s}{C_l} \tag{1}$$

$$R_f = \frac{v_{fluid}}{v_{contaminant}} = 1 + \frac{\rho_b K_D}{\eta} \tag{2}$$

in the batch and column tests, respectively. In Equation (1), C_s and C_l are the sorbate concentrations in the solid and liquid phases, at equilibrium. In Equation (2), v stands for the velocity, ρ_b for the bulk density of the soil and η for its porosity.

246

mariotte vessel

counting system

Valve

diffuser at
entrance

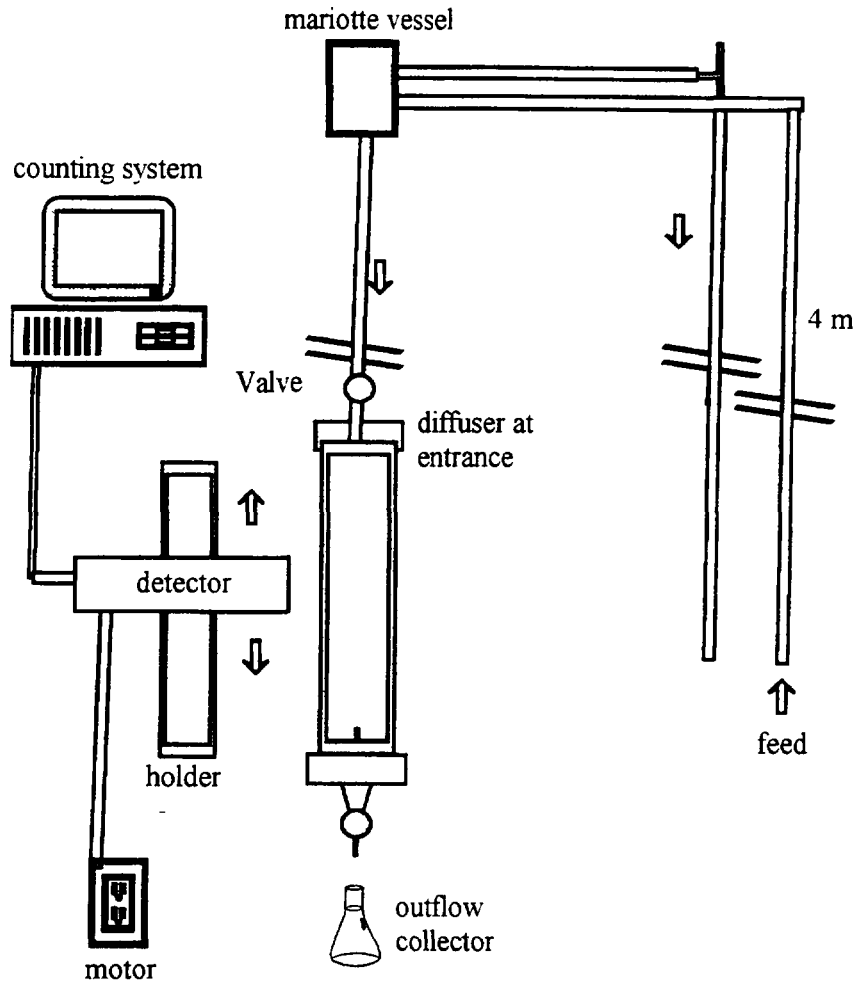4 m

detector

holder

motor

outflow
collector

feed

Figure 1 - Scheme of the column experimental setup

3. STUDIES WITH BATCH TESTS

3.1. Improving parameter fitting to sorption isotherms

Isotherms describe sorption behavior by relating the concentration of the sorbate at the solid phase to the concentration present at the liquid phase: $S = f(C)$. Sorption is quantified by the distribution (or partition) coefficient :

$$K_d = S/C \qquad (3)$$

where S is the sorbate to sorbent mass ratio (g/g) and C the solute concentration (g/cm^3) in the liquid phase. Thus Equation (3) can be regarded as the linear adsorption isotherm $S = K_d C$, which in turn reflects the asymptotic behavior of the Langmuir isotherm :

$$S = \frac{b S_m C}{1 - b C} \qquad (4)$$

247

for low concentration values. In Equation (4) S_m is the sorption capacity and b is a constant. This model has a theoretical foundation, but assumes homogeneity of the adsorption sites. In this sense the Freundlich isotherm :

$$S = KC^n$$

(5)

may be more realistic, since it can be derived by assuming an exponential distribution of the heat of adsorption at different sites. K and n in Equation (5) are constants. However this enthalpy is applicable only if $S << S_m$, so that saturation effects are avoided. Sposito's derivation of the adsorption isotherm, stemming from the earlier work of Sips, accounted for a limited sorption capacity, thus broadening the applicability of the Freundlich isotherm [2]. The Sips-Sposito (S-S) isotherm can be written in the form:

$$\frac{S_m \, S}{S_m + S} = K \, C^n$$

(6)

In order to evalute the sorption capacity S_m at the equilibrium conditions of the test the Dubinin-Radushkevitch (D-R) isotherm, derived on basis of the potential theory of adsorption, can be employed:

$$S = S_m \exp\left\{-k\left[RT \ln\left(1 + \frac{1}{C}\right)\right]^2\right\}$$

(7)

where R is the gas constant, T is the absolute temperature and k is the isotherm constant. The D-R isotherm has the advantage over the previous isotherms, of not assuming a monomolecular adsorption layer. Although derived from different basic assumptions, S_m can be determined from the D-R isotherm whenever there are empirical evidences as to the appropriateness of the different isotherms to a particular system, leaving only two parameters to be fitted in the S-S isotherm. Thus, the accuracy of K and n, obtained from a least-squares fit to Equation (6), can be improved.

The fit of the data obtained in this work is shown in Figure 2. The parameters determined with the D-R isotherm are $Sm = (0.635 \pm 0.008)$ μCi/g and $k = (0.044. \pm 0.008)$. Using these values, the parameters involved in the S-S isotherm, Equation (6), were calculated, the results being $K_S = (0.920 \pm 0.005)$ and $n = (0.42 \pm 0.07)$.

The time dependency of cesium adsorption was also tested. Starting with 10^{-10} M carrier-free ^{137}Cs solutions, soil-water contact tests from up to ca. 6 days revealed that in the first 60 seconds liquid phase activity plunged from 80 nCi to 4 pCi. The data in Figure

3 how the subsequent evolution; the absorption of the solute is immediate. It may be inferred that sorption kinetics will not play any significant role in the migration of cesium in the prototype. After being adsorbed cesium sticks quite firmly to the soil: as Figure 4 shows, at the above cesium concentration only when the soil mass is too small has desorption been observed.
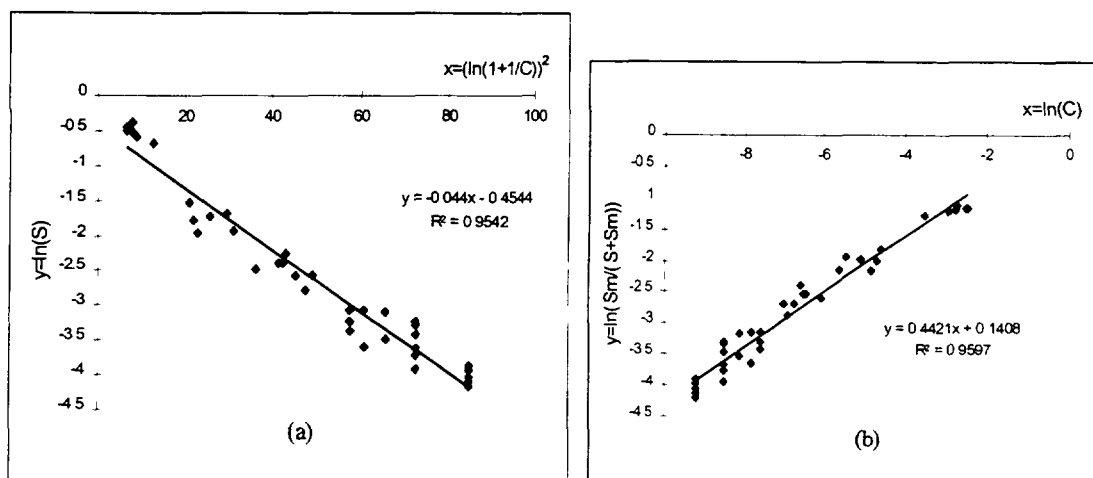
248

Figure 2 - Fit of ^{137}Cs adsorption in Goiânia soil (a) Dubinin-Radushkevitch isotherm; (b) Sips-Sposito isotherm.
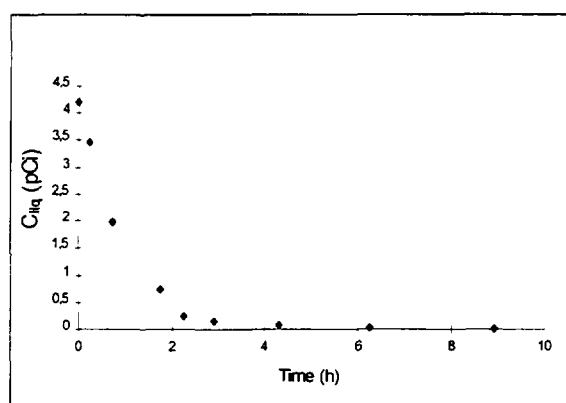

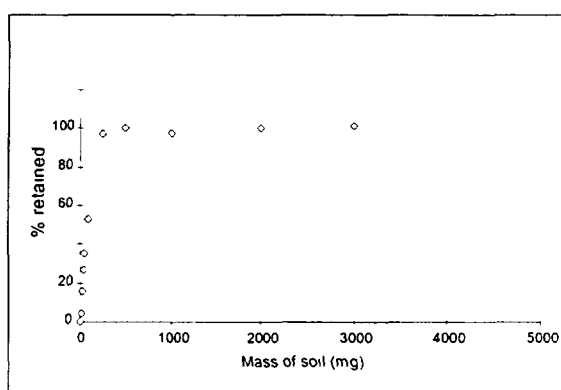Figure 3 - Time dependence of ^{137}Cs adsorption to the Goiânia soil.

Figure 4 - ^{137}Cs desorption behavior in the Goiânia soil

3.2. Accounting for the influence of the mass volume to mass ratio on K_d

As mentioned, a relationship was observed between K_d and V/m in both ^{137}Cs and ^{203}Hg sorption in batch tests. Such tests have to be carried at a much higher V/m ratio than that usually met in groundwater flow (in the case of the Goiânia soil $V/m < 0.0028$ dm^{3}g), otherwise the pasty material would be impossible either to stir or filter. It was thus found desirable to carefully investigate the phenomenon.

A vast amount of literature has been dedicated to this behavior. It has been summarized, among many others, in references [3] and [4]. In general there is a great deal of controversy on the subject of the influence of solids concentration on K_d. Some authors have tried to define a general trend between V/m and K_d but even this could not be firmly established [5].A sample of the results we have obtained with the soils previously mentioned is shown in Figures 5 and 6.
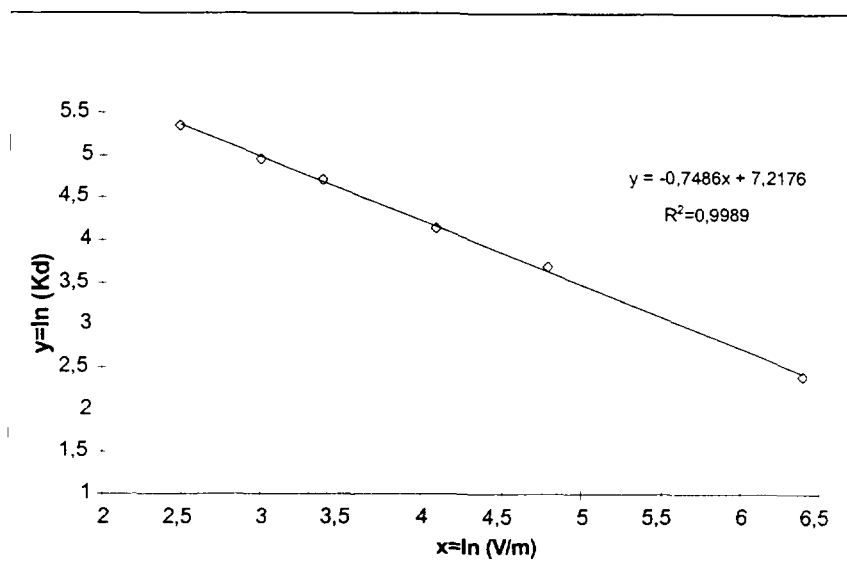
249

Figure 5 – Variation of K_d with the V/m ratio for ^{203}Hg
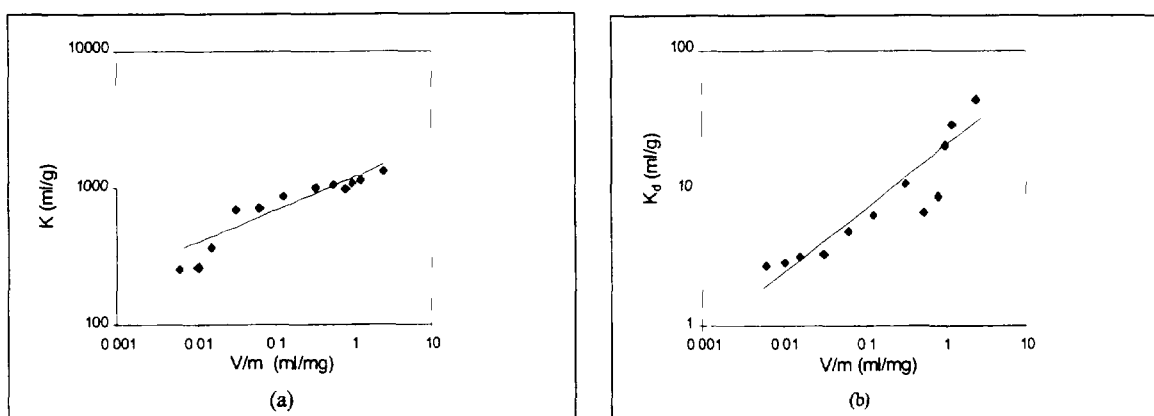in the Goiânia Soil

Figure 6 – Variation of K_d with the V/m ratio in the Belo Horizonte soil.
^{137}Cs, (b) ^{203}Hg

It can be seen that opposite trends have been obtained with the Goiânia and Belo Horizonte soils. As for the later, a single regression does not succeeded in fitting the whole range of encompassed V/m values. At the lower limit of experimental V/m's there is a clear tendency to stabilization of K_d with increasing soil masses. In all tests with ^{137}Cs it has been observed that this tendency was fully established at 0.01 dm^3/g, whereas with ^{203}Hg it was reached earlier at 0.03 dm^3/g. Thus, a regression including only data within this lower range could be extrapolated to the very small V/m ratios characteristic of underground water flow, with a better chance of obtaining more meaningful estimates of K_d.

3.3. The isotherms and the mass to volume to mass ratio

Some consideration was given to the how and the why of the interference of V/m on the sorption parameter. From the material balance applied to the batch test:

$$m\,S + V\,C = M\,S_0 + V\,C_0 \qquad (8)$$

250

where S_o and C_o are the initial solute concentration in the solid and liquid phases, respectively, using the definition: $K_d = S/C$, and since $S_o \cong 0$ and $C_o >> C$, one gets :

$$K_d \cong \frac{V}{m}\left(\frac{C_0}{C}-1\right) \cong \frac{V}{m}\left(\frac{C_0}{C}\right) \qquad (9)$$

If the ratio C_o/C were constant for each experiment (starting from the same C_0) , this simplified derivation would point to a linear relationship between K_d and V/m. But actual data show otherwise. The explanation is that changes in the V/m ratio influence the final solute concentration C, i.e.: $C = f(V/m)$.

Now, this functionality can be obtained from any adequate isotherm. For instance, from the Freundlich isotherm and from Equation (9):

$$K_d = \frac{S}{C} = KC^{n-1} = \frac{V}{m}\left(\frac{C_0}{C}\right) \quad \Rightarrow \quad C = \left(\frac{V}{m}\right)^{\frac{1}{n}}\left(\frac{C_0}{K}\right)^{\frac{1}{n}} \qquad (10)$$

and inserting this back in the expression for K_d :

$$K_d = C_0^{\frac{n-1}{n}} K^{\frac{1}{n}} \left(\frac{V}{m}\right)^{\frac{n-1}{n}} \qquad (11)$$

where $0 < N < 1$. Thus, a plot of $log(K_d)$ vs. V/m should yield a straight line. This test has been carried with independent data from the experiments in which V/m was varied and C_0 kept constant and from those with constant V/m and variable C_0. Fitting both sets to Equation (11), the following has been obtained :

$$K_d = 1400\left(\frac{V}{m}\right)^{-0.75} \quad \left(r^2 = 0.9990\right) \qquad K_d = 0.74\, C_0^{-0.89} \quad \left(r^2 = 0.9918\right) \qquad (12)$$

and the corresponding values of N were (0.57 ± 0.02) and (0.53 ± 0.03), respectively. The excellent agreement between these two completely independent set of experimental results supports the theoretical development above and qualifies the Freundlich isotherm as a trustworthy model for the representation of adsorption processes.

3.4. Sorption behavior of individual soil components

The peculiar sorption characteristics of each individual mineral component will combine in a manner dependent on its quantity, but also on other possibly interacting factors, to yield the final sorption behavior of a given soil. Even though it would be rather difficult to predict the composite behavior from those of the various components, an effort is being undertaken to correlate their contributions. At the present time the sorptive behavior of the main components has been investigated.

X-ray diffractometry analysis has identified ten main components in the Goiânia soil: kaolinite, gibbsite, goethite, haematite, ilmenite, magnetite, muscovite, quartz, rutile, and zircon. Pure samples of these minerals have so far been subjected to batch tests. Figure 7 shows the results obtained with kaolinite and quartz. With the sole exception of quartz, all the other mineral components exhibited the same trend in K_d as kaolinite .
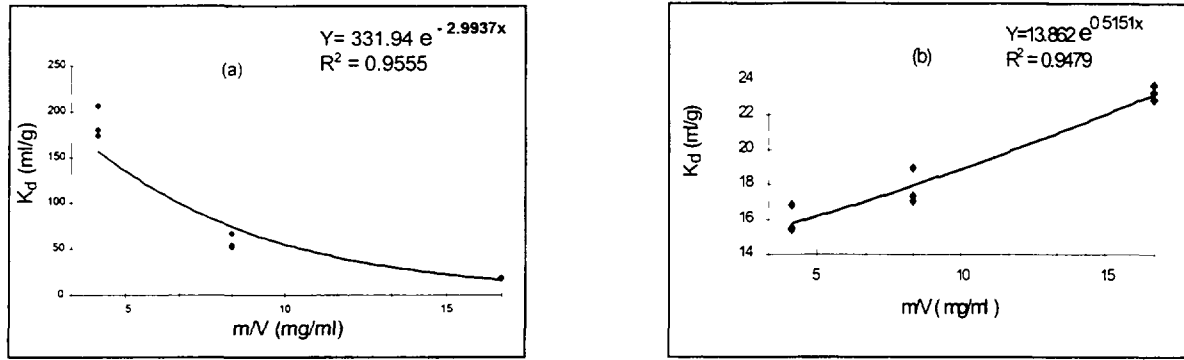
Figure 7 - K_d dependence on m/V ratio for individual soil components
(a) kaolinite; (b) quartz

4. STUDIES WITH COLUMN TESTS

4.1. Transport model

As described in Section 2.3 the column diameter is large enough and the flow uniformly distributed over its cross-section; it was then assumed that the 1-D advection-dispersion model would be adequate:

$$\frac{\partial C}{\partial t} = D\frac{\partial^2 C}{\partial x^2} - v\frac{\partial C}{\partial x}$$ (13)

in which D and v are actually the reduced axial dispersion coefficient D_x / R_f and fluid velocity v_x / R_f. Following an instantaneous impulse injection of a quantity M of tracer over the cross section area S, i.e.: $C(x,0) = (M/\eta S)\delta(x)$, and accounting for a linear increase in the background count rate, count distribution along the column is shaped by the solution:

$$C_{(x)} = A + Bx + \frac{M}{\eta S\sqrt{4\pi Dt}}\exp\left[-\frac{(x-vt)^2}{4Dt}\right]$$ (14)

The main aim of model fitting is the determination of the dispersion coefficient D_x and the contaminant velocity $v = v_x / R_f$. Thus the factor R_f can be determined either from a fit to this (or any other realistic) model or independently, by running traced water through the column and comparing the transit times of ^{137}Cs and, say, ^{3}H. In this last case, a lesser number of parameters is left to fit in Equation (14) which, again, increases the reliability of the values thus determined. Besides, this double tracer method allows the independent backcalculation of K_d using Equation (2).

4.2. Tracing the water flow

Tritiated water is the ideal tracer for the water flow, since it does not undergo adsorption in surfaces within the soil pores. But then, a direct record of its elution with a probe at the exit (thru-the wall mode) is not possible since tritium is a low energy beta emitter. Therefore, it must be sampled (mixing cup mode) for counting.

252

Now, each discrete sampling spans over a finite time period which cannot be made smaller than a threshold value related to the sensitivity of liquid scintillators. Physically, each discrete sampling performs an integration in the time axis whose effect must be taken into account when fitting the data to the tracer transport model.

There is an alternative way in which this can be easily implemented. Instead of differentiating the ^3H response thus measured it is easier, and more reliable, to numerically integrate the residence time distribution model over the time interval corresponding to each discrete sampling. Assuming the 1-D advection-dispersion model, and indicating the sampling time span by Δt, then Equation (14) gives at the exit of a column of length L:

$$C_{L,t} = A + BL + \frac{M}{\eta\, S\sqrt{4\pi D}} \int_{t-\Delta t/2}^{t+\Delta t/2} \frac{1}{\sqrt{\tau}} \exp\left[-\frac{(L-v\tau)^2}{4D\tau} \right] d\tau \qquad (15)$$

The above integration can numerically be implemented by gaussian quadrature. Then a new variable is defined:

$$z = \frac{2\,t-(t_1+t_2)}{t_2-t_1} \qquad (16)$$

where $t_1 = t - \Delta t/2$ and $t_2 = t + \Delta t/2$. Thence the integration is accomplished by the numerical approximation:

$$\int_{t_1}^{t_2} f(t)\,dt \cong \frac{(t_2-t_1)}{2} \sum_{i=0}^{n} w_i\, f\left(\frac{z_i\,(t_2-t_1)+t_2+t_1}{2} \right) \qquad (17)$$

where z_i, the roots of a Legendre polynomial, and the weight factors w_i associated with them are shown in Table I for the fifteen point formula used in this work.

Table I - Values of the roots and weight factors used in the numerical integration

z_i	w_i
0, 00000 00000 00000	0, 20257 82419 25561
± 0, 20119 40939 97435	0, 19843 14853 27111
± 0, 39415 13470 77563	0, 19616 10001 15562
± 0, 57097 21726 08539	0, 16626 92058 16994
± 0, 72441 77313 60172	0, 13957 06779 26154
± 0, 84820 65834 10427	0, 10715 92204 67172
± 0, 93727 33924 00706	0, 07036 60474 88108
± 0, 98799 25180 20485	0, 03075 32419 96117

The parameter values thus determined are shown in Table II, whereas Table III presents the matrix of their correlation coefficients.

Table II - Parameter values

Parameter	Value determined by fit
M^*	(8,3 ± 0,3) 10^7 counts*s
D	(0,86 ± 0,08) $cm^2\,s^{-1}$
v	(0,18 ± 0,01) $cm\,s^{-1}$
A	(2600 ± 400) counts
B	(1,0 ± 0.2) counts s^{-1}

$(M^* = M / S\eta\sqrt{4\pi D})$

253

Table III - Parameter correlation coefficient matrix

	M*	D	v	A
D	0,594			
v	-0,032	-0,122		
A	0,677	0,673	0,046	
B	0,598	0,552	0,128	0,975

Table III confirms a low correlation between the intervening parameters, except for those of the baseline (A and B). This independence strengthens the confidence both in the determined values and in the physical assumptions implied in the model. This claim is further strengthened by the indication of an excellent correspondence between data and mode, as evinced by both the slope and the linear correlation coefficient R^2 of the line in Figure 8.

4.3. Optimizing collimation

In the first column setup tested (Setup I) the slit was 0.5 cm long and 0.3 cm wide. A ^{137}Cs point source of 3 x 10^3 Bq (80 nCi) activity was placed at the external wall of the column, midway its length, and the collimated probe was slid along its vertical course; the measured distribution displayed a rather poor resolution. Collimation was thereafter improved by gradually thickening the shield up to 6 cm, and narrowing the slit down to 0.005 cm wide by 2 cm long (Setup II). The improvement is shown in Figure 9. It can be seen that even after the shielding reached the thickness of a lead brick and the slit was as thin as a credit card, the ensuing peak was still somewhat smeared.
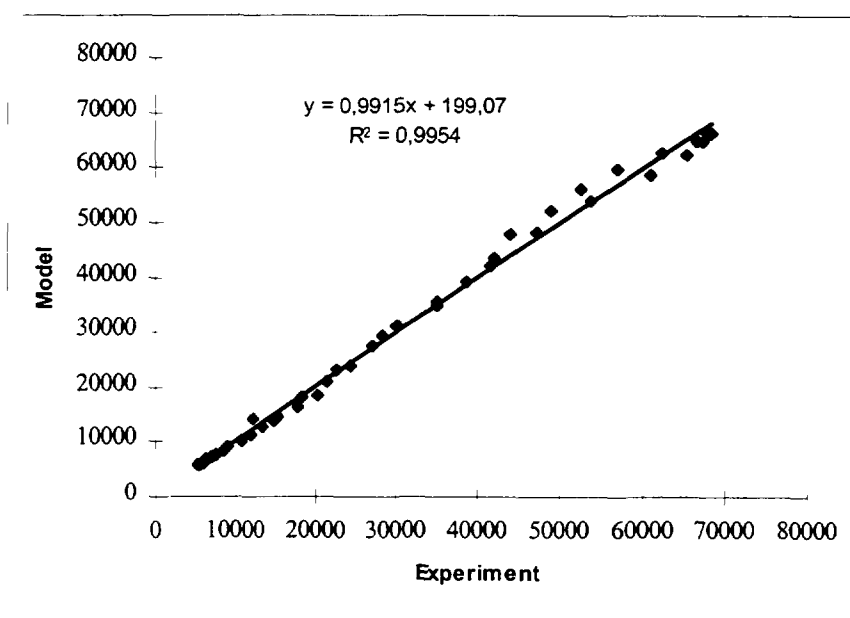
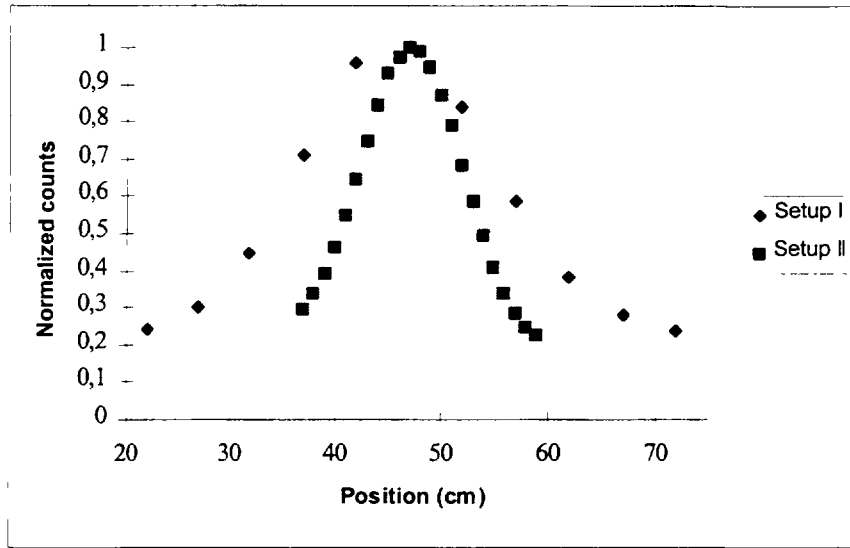Figure 8 - Correlation between experiment and model – water phase transport

Figure 9 - Measured count rate distributions due to the point source, with different collimation effectiveness

Cost-benefit considerations dissuaded further mechanical betterment. Nonetheless a statistical measure of the enhancement was needed, inasmuch as filtering techniques were to be used later on. This has been done as follows: the point source response should fit a gaussian superimposed upon a straight baseline, much in the same way as Equation (14):

$$C_x = A + Bx + \frac{M'}{s\sqrt{2\pi}}\exp\left[-\frac{(x-p)^2}{s^2}\right] \tag{18}$$

where p is the position of the source and the standard deviation s can be conveniently related to the full width of the peak at half maximum ($FWHM$) by: $s = (FWHM)/2\sqrt{2\ln 2}$. This can be used as a figure of merit for collimation efficiency. As throughout this paper, fitting the experimental count distribution $c(x)$ to the model $C_{(x)}$ is accomplished by minimization of the chi-square weighted by the inverse of the variance of the data:

$$\chi^2 = \sum_{i=1}^{N}\left\{\frac{1}{\sigma_i^2}\left[c_i(x)-C_{(x)}\right]^2\right\} \tag{19}$$

The count rate being assumed Poisson distributed, to each count is attributed: $\sigma_i = \sqrt{c_i}$.

The results obtained with the optimization effort are shown in Tables IV and V. The global correlation for a given parameter is defined as the correlation between it and the linear combination of those others parameters with which it is more closely correlated.

Table IV - Results from shielding optimization

Parameter	Setup I	Setup II
A (counts)	(2400 ±300)	(2700 ± 300)
B (counts/cm)	(32 ± 8)	(18 ± 6)
M' (counts.cm)	(2,06 ± 0,01) x 10^6	(1,89 ± 0,03) x 10^6
s (cm)	(8,9 ± 0,4)	(4,9 ± 0,3)
p (cm)	(45,8 ± 0,5)	(45,2 ± 0,8)

Table V - Global correlation for Setup II	
A	0.933
B	0.920
M'	0.699
s	0.583
p	0.518

Shielding optimization has accomplished a twofold reduction of the *FWHM*. The parameter exhibiting least correlation is the source position. This has been confirmed by placing the source at diverse positions. Hence the response to collimation can be considered homogeneous along the column length.

One other source of quantified information about the gain in collimation efficiency is the variation coefficient:

$$CV = \frac{\left[c_i(x) - C_x\right]^2}{c_i(x)} \tag{20}$$

the evolution of whose distributions is shown in Figures 10 and 11.
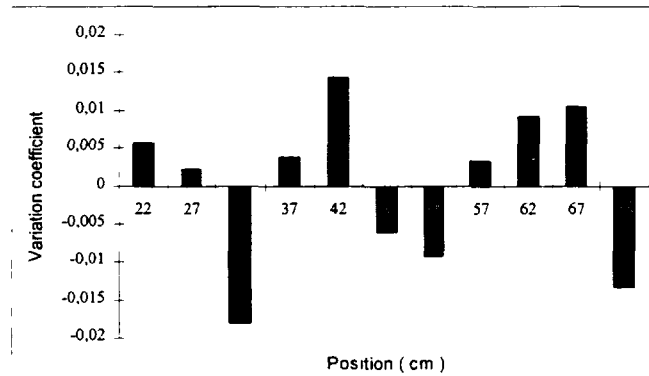

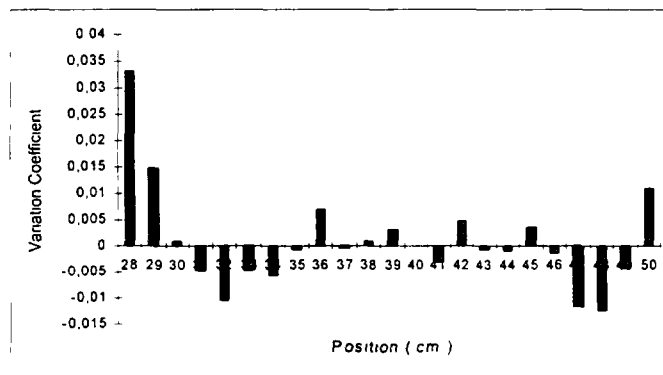Figure 10 - Variation coefficients for Setup I

Figure 11 - Variation coefficients for Setup II

Those positions exhibiting larger variations are situated near the column extremities. Hence they are least influential upon parameter determination via curve fitting, since they

256

correspond to the smaller count-rates. Given that count-rates follow the Poisson distribution, the error ε attributed at each position is:

$$\varepsilon_i = \frac{t_s}{\sqrt{c_i(x)}} \qquad (21)$$

showing that those positions with the lowest count-rates are more erratic, and consequently less weighted in the chi-square minimization scheme. The statistic t_s follows the "Student" t-distribution; all calculations having been performed at the 5% significance level. The rather low values of CV seem to qualify the models in Equations (14) and (18) for parameter determination and contaminant transport simulation.

4.4   The point source method for signal deconvolution

The strongly collimated signal in Setup II is still somewhat corrupted, even after exhaustive physical optimization. Hence, there is the need of somehow conceiving a mathematical filter to take charge of this residual deficiency. A method has been devised to abate both noise and imperfect resolution. Assuming linearity, the corrupted response $\hat{c}(x)$ is the superposition of the actual response $c(x)$ and the effect of imperfect collimation, besides noise effects. That is the same to say that $\hat{c}(x)$ results from the convolution of the desired $c(x)$ with a suitable filter $h(x)$:

$$\hat{c}(x,t) = \int_{x-\delta/2}^{x+\delta/2} c(\xi,t)\, h(x-\xi)\, d\xi \qquad (22)$$

Now, $h(x)$ is just the response of the physically collimated probe to a point source placed at position ξ, as determined in Section 4.3. Then the problem of defining the actual tracer distribution $c(x,t)$ from the known functions $\hat{c}(x,t)$ and $h(x)$ in Equation (22) becomes one of deconvolution. The above expression amounts to a weighting scheme h_i $(i=1,2,....N)$:

$$\hat{c}_i = \sum_{j=i-m}^{j=i+m} h_{i+j}\, c_j \qquad (23)$$

where $2m+1 = N$. What was missing at this point was only an efficient procedure to perform the iterative calculations required for arriving at c.

Savitzky and Golay have tackled this problem in the context of data smoothing and differentiation [6]. They assumed as smoothing function a $2m+1$ point filter in the form of a polynomial $f_i = \sum_{k=0}^{n} b_k i^k$ of degree $n < 2m+1$. This requires repetitively fitting the function f to $2m+1$ consecutive points. Then application of the least-squares criterion:

$$\frac{\partial}{\partial b_k}\left[\sum_{i=-m}^{m} (f_i - \hat{c}_i)^2\right] = 0 \qquad (24)$$

leads to $n+1$ simultaneous equations in the unknown coefficients b_k. The author's approach evaluates f_i at $i = 0$ and hence only expressions for b_0 are required at each i. This method speeds up convolution in the time domain for evenly spaced points. Later improvements turned it into a widely used procedure for piecewise smoothing in noise filtering operations, with minimum signal distortion. Gorry has cast f in the form of an orthogonal polynomial (Gram polynomial), enabling the convolution technique to be extended to cover all points in

the spectrum with any desired filter length [7]. Prior smoothing of the raw data has been accomplished also using this method.

In this way c could also be wrought out of Equation (22), since formally either c or h can be assumed as the filter function. The model parameters were determined by a compound convolution plus nonlinear least-squares search, which converges by successive trials to the minimization of the reduced chi-square, $\chi^2/\text{d.f.}$ The MINUIT code has been employed in these calculations [8].

The resulting distribution and its compliance with the proposed advection-dispersion tracer transport model is shown in Figure 12. As consistently done in this study, a statistical test has been applied to quantify the magnitude of the improvement. The quality of the fit as measured by the reduced chi-square, i.e.: χ^2 normalized by the number of degrees of freedom (d.f.) decreased from $\chi^2 = 35$ for the raw data to $\chi^2 = 1.4$ for the filtered/deconvoluted set. Although not evident from a visual inspection of Figure 12, this amounts to an impressive 25-fold amelioration, quite short of reaching the mark of $\chi^2 = 1$ which corresponds to a perfect fit.
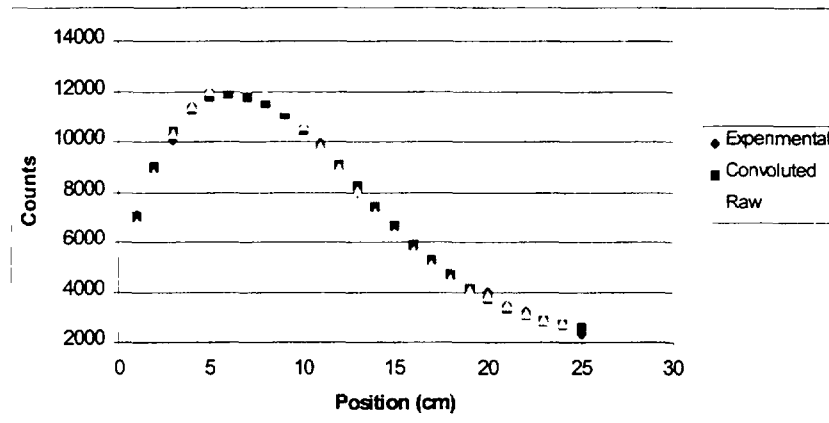

Figure 12 – Model fit to raw and filtered data

4.5 Results from column tests

The ^{137}Cs transport experiment in the column filled with the Goiânia soil has been carried for 206 days following tracer injection. Scans have been performed at 3 cm intervals, with a duration of 400 s. The obtained results and the quality of the fit to the model proposed are shown in Figures 13 and 14. Again, and confirming expectations a good fit was obtained.
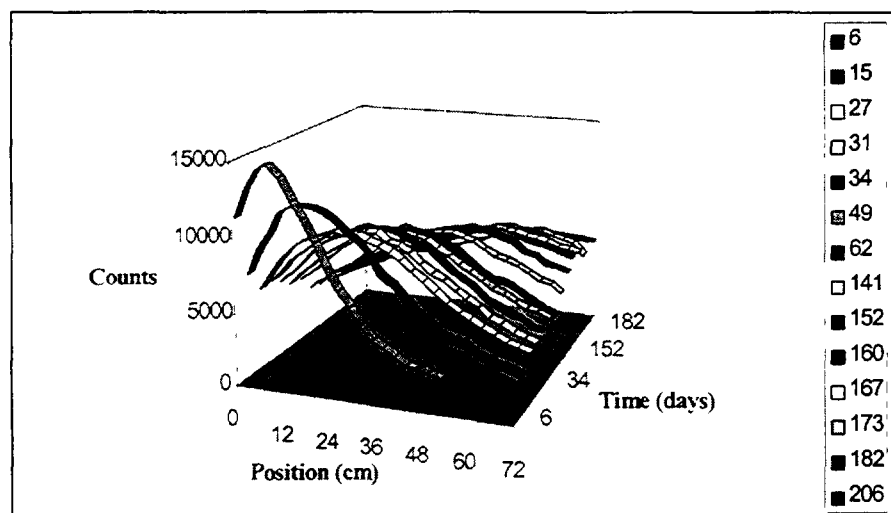

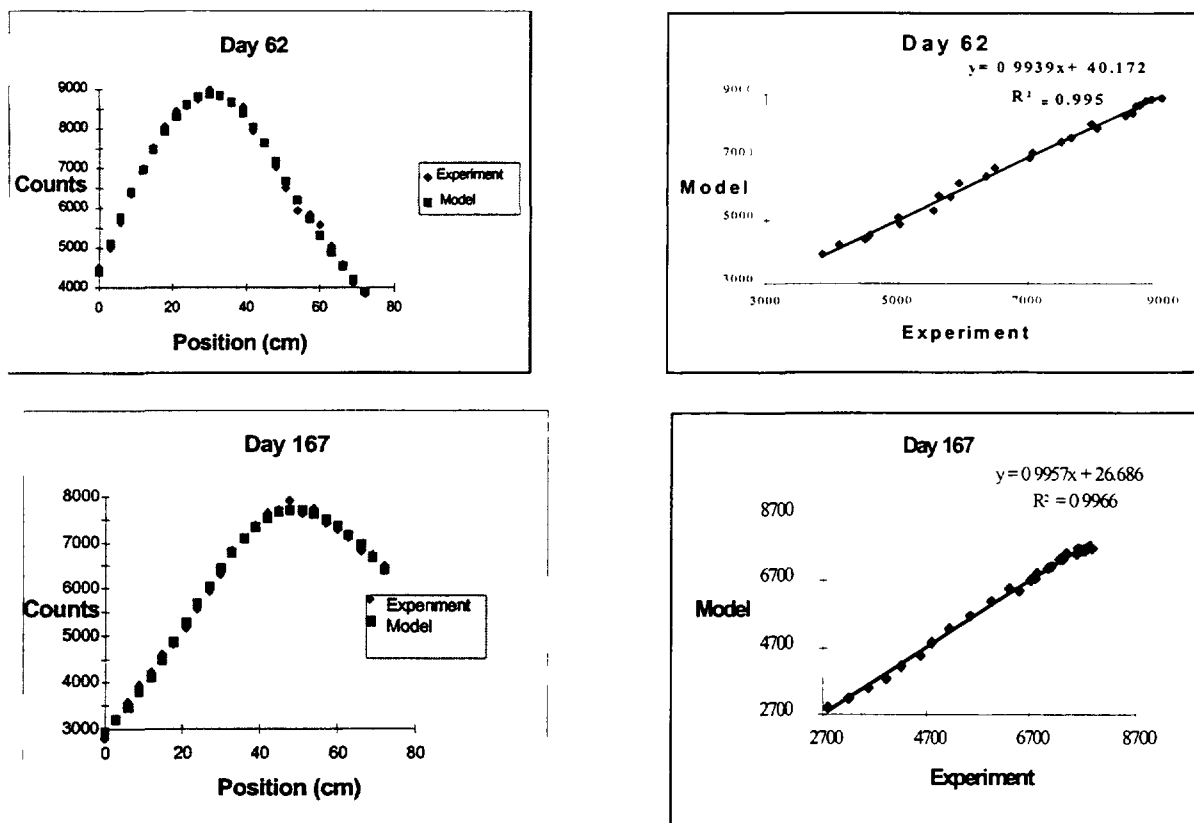Figure 13 - Evolution of ^{137}Cs distribution inside column

Figure 14 - Experimental and predicted ^{137}Cs distributions: after 62 days ($\chi^2 = 0.98$), and after 167 days ($\chi^2 = 0.44$)

5. CONCLUSIONS

Contaminant migration prediction is commonly based on transport parameters found in the literature often lacking a description of the conditions under which they were measured and how the measurement was performed. This may lead to significant errors. Test protocols should be made available. Besides that, it has been here shown that a great deal of improvement can be obtained by refining the equipment, and by relating the results to the theoretical fundamentals.

Measurement of K_d in a single batch test will probably fail to indicate the value to be found in nature since it is influenced by a set of physico-chemical variables, some of which are hardly reproducible in the laboratory. Hopefully, a better approximation will be attained by extrapolation of the results of batch tests with different values of V/m at the lower limit of the range allowed by the experimental technique.

Sampling at the exit of the column introduces distortions that can be easily corrected by a mathematical integration of the elution model. This procedure has effectively worked with the simple 1-D dispersion-advection model. It also allows determination of velocity and dispersion parameters based upon independent tests, thus decreasing errors stemming from correlation between a larger number of parameters simultaneously fitted to the model.

Probe collimation has a strong influence on tracer measurements in columns, although there is a practical limit to its mechanical improvement. Beyond this limit, noise can be filtered off with a suitable point filter without loss of information and a deconvolution technique can recover the actual tracer distribution from the filtered signal using a point source distribution. This procedure further enhances collimation.

The data thus far obtained for cesium and mercury transport parameters will allow more reliable safety assessment and impact evaluations. Work is planned to go on in this field, emphasizing the potential and limitations of simple expedite methods such as batch tests, i.e.: on the nature and the effect of the conditions influencing its accuracy. .

REFERENCES

[1] KLOTZ, D., Erfahrung mit Säulenversuchen zur Bestimmung der Schadstoff-migration, GSF Bericht 7/91, Gesellschaft für Strahlen und Umweltforschung, München (1991).
[2] SPOSITO, G., Derivation of Freundlich equation for ion exchange reactions in solids. Soil Sci. Am. J. 44 (1980) 652.
[3] LANG, H, WOLFRUM, C., 1992, Ermittlung experimenteller Daten in Batch-Versuchen zur Abschätzung des Ausbreitungsverzögerung radioaktiver Spalt- und Aktivierungs-produkte, Fachgespräch zu Fragen der Radionuklidmigration und Langzeitsicherheit des geplanten Endlagers Gorleben, B. & S., Braunschweig, 3.6.92.
[4] KLOTZ, D., LANG, H., MOSER, H., Experimentelle Untersuchungen zur Migration von Radionukliden der Elemente Cs, Sr, Ra, Mo, I und C im Deckgebirge des Enlagerortes Gorleben, GSF Bericht 15/88, Gesellschaft für Strahlen und Umweltforschung, München (1988).
[5] O'CONNOR, D.J., CONNOLLY, J.P., The effect of concentration of adsorbing solidson the partition coefficient, Water Res. 14 (1981) 1517.
[6] SAVITZKY, A., GOLAY, M.J.E., , Smoothing and differentiation of data by simplified least-squares procedures, Anal. Chem. 36 (1964) 1627.
[7] GORRY, P.A., General least-squares smoothing and differentiation by the convolution (Savitzky-Golay) method, Anal. Chem., 62: 1990, 570-573.
[8] LETERTRE, C., MINUIT Program Library, CERN Computer Center v.301 (1973).

PARTICIPANTS IN THE CO-ORDINATED RESEARCH PROJECT

Barrocu, G.

Dipartimento di Ingegneria del
Territorio Sezione Geologia Applicata
Universita di Cagliari, Piazza d'Armi, 099123 Cagliari, Italy
Fax: 0039-70275281; E-mail: barrocu@crs4.it

Buzek, F.

Czech Geological Survey
Geologicka 6, 152 00 Prague 5, Czech Republic
Fax: 00420-25818748; E-mail: buzek@cgu.cz

Chilton, J.

British Geological Survey
Crowmarsh Gifford, Wallingford, Oxfordshire, OX10 8BB
United Kingdom
Fax: 0044-1491692345; E-mail: j.chilton@bgs.ac.uk

Fórizs, I.

Hungarian Academy of Sciences
Budaörsi út 45, P.O. Box 132, H-1112 Budapest, Hungary
Fax: 0036-13193145; E-mail: forizs@sparc.core.hu

Fulin Liu

Beijing Research Institute of Uranium Geology
P.O. Box 9818-5, Beijing 100029, China
Fax: 0086-104917143

Garavito, F.

Instituto de Ciencias Nucleares y Energias Alternativas
Santa Fe de Bogota, Colombia
Fax: 00571-222073

Halas, S.

Maria Curie-Sklodowska University
Institute of Physics, Plac Marii Curie-Sklodowskiej 1
20-031 Lublin, Poland
Fax: 0048-8133669; E-mail: dudek@tytan.umcs.lublin.pl

Keqin Wei

Chinese Academy of Sciences
P.O. Box 1131, Guangzhou 510640, China
Fax: 0086-2085514130; E-mail: kqwei@ms.gzb.ac.cn

Moreira, R.

Comissno Nacional de Energia
Nuclear Centro de Desenvolvimento da Tecnologia Nuclear
Caixa Postal 941, 30161 Belo Horizonte, Brazil
Fax: 0055-314993249; E-mail: rubens@urano.cdtn.br

Qureshi, R.M.

Pakistan Institute of Nuclear Science & Technology
Environmental Research Lab - RIAD, P.O.
Nilore Islamabad, Pakistan
Fax: 0092-51429533; E-mail: pinstech@paknet1.ptc.pk

Robinson, B.

Institute of Geological & Nuclear Sciences
Private Bag 2000, Taupo, New Zealand
Fax: 0064-73748199; E-mail: b.robinson@gns.cri.nz

Shivanna, K.

Bhabha Atomic Research Centre
Isotope Division, Trombay, Bombay 400085, India
Fax: 0091-225560750; E-mail: isd@magnum.barct1.ernet.in

Tandia, A.A.

Department of Geology
Faculty of Sciences and Techniques, University CAD
Dakar, Senegal
Fax: 00221-8246318; E-mail: aztandia@ucad.refer.sn

Travi, Y.

University d'Avignon et des Pays de Vaucluse
Hydrogeology Laboratory, 33 rue Louis Pasteur,
84000 Avignon, France
Fax: 0033-490144489, E-mail: yves.travi@univ-avignon.fr

Vasu, K.N.

Centre for Water Resources & Management
Kunnamangalam, Kozhikode-kerala State, India
Fax: 0091-495357827

Vengosh, A.

Hydrological Service
PO Box 6381, Jerusalem 91063, Israel
Fax: 00972-25388704; E-mail: avnerv@vms.huji.ac.il

Zojer, H

Joanneum Research Institute of Hydrogeology and Geothermics
Elisabethstrasse 16/11, A-8010 Graz Austria
Fax: 0043-316876321; E-mail: monika.lohr@joanneum.ac.at

Gerardo-Abaya, J.

Isotope Hydrology
International Atomic Energy Agency, Wagramer Sstrasse 5
P.O. Box 100. Vienna, Austria
Fax: 00-431-20607; E-mail: J.Gerardo-Abaya@iaea.org